1127-21
1521

JOURNAL OF COLLOID SCIENCE

Editor-in-Chief
Victor K. La Mer, Columbia University, New York

Advisory Board

C. O. Beckmann
K. F. Bonhoeffer
J. A. Christiansen
M. L. Corrin
P. J. W. Debye
John T. Edsall
I. Fankuchen
John D. Ferry
Wilfried Heller
John G. Kirkwood
E. C. Lingafelter
L. G. Longsworth
S. G. Mason
J. Th. G. Overbeek
R. Ruyssen
E. K. Rideal
William Seifriz
Leo Shedlovsky
Theodore Shedlovsky
Robert Simha
R. H. Smellie
Jacinto Steinhardt
The Svedberg
Hugh S. Taylor
Arne Tiselius
Robert D. Vold
Bernard Vonnegut
Ralph W. G. Wyckoff
Bruno H. Zimm

VOLUME 9
1954

ACADEMIC PRESS INC.—PUBLISHERS
NEW YORK, N. Y.

ADSORPTION OF BOTH COMPONENTS FROM BINARY SOLUTION ON POROUS ADSORBENTS

Robert D. Hansen and Robert S. Hansen

Institute for Atomic Research and Department of Chemistry, Iowa State College, Ames, Iowa

Received August 6, 1953

ABSTRACT

The treatment of adsorption from binary liquid solution proposed by Kipling and Tester (4) is criticized for its application of a unimolecular adsorption mechanism to porous adsorbents. It is shown that results of Kipling and Tester and others for adsorption by porous adsorbents from solution can be interpreted in a more consistent way through a pore-filling mechanism. It is pointed out that adsorption from solution should be comparable to adsorption from saturated vapors only if the area of liquid-vapor interface in the latter case is negligible compared to the surface area of the adsorbent—a condition generally satisfied by porous adsorbents.

INTRODUCTION

Several attempts have been made to explain isotherms for adsorption from binary solution as composites of the individual isotherms of the two pure components.

The relation between the binary solution isotherm and the individual isotherms

$$\frac{n_0 \Delta x}{m} = n^s_1(1 - x) - n^s_2 x \qquad [1]$$

has been advanced by Ostwald and de Izaguirre (1) and Bartell and Sloan (2), where n_0 is the total number of moles in the original solution, n^s_1 and n^s_2 are, respectively, the number of moles of components 1 and 2 adsorbed per gram of adsorbent, and x is the mole fraction of component 1 in the solution after adsorption.

Bartell and Sloan assumed that the individual isotherms obeyed the Freundlich equation, thus obtaining the relation:

$$\frac{n_0 \Delta x}{m} = k_1 x^a (1 - x) - k_2 (1 - x)^b x. \qquad [2]$$

They evaluated the four constants by a series of successive approximations, thereby obtaining the individual isotherms. Later, Kipling and Tester (3) applied a similar treatment, assuming that the individual adsorption isotherms followed a Langmuir equation instead of a Freundlich equation.

The inadequacies of these two treatments have been discussed in a recent paper by Kipling and Tester (4).

Kipling and Tester obtained individual adsorption isotherms by measuring adsorption from the vapors in equilibrium with the binary solutions, using a steam-activated coconut charcoal adsorbent. They then proposed a method for describing their results. Following the treatment of Elton (5), they assumed that the surface of the adsorbent is covered at all times by a unimolecular layer of adsorbate. Thus they write:

$$n^s{}_1A_1 + n^s{}_2A_2 = A, \qquad [3]$$

where A_1 and A_2 are the areas occupied by 1 mole of components 1 and 2, and A is the total surface area of 1 gram of adsorbent. Equation [3] can also be rewritten as:

$$\frac{n^s{}_1}{(n^s{}_1)^0} + \frac{n^s{}_2}{(n^s{}_2)^0} = 1, \qquad [4]$$

where $(n^s{}_1)^0$ and $(n^s{}_2)^0$ are the amounts adsorbed from the vapors of the pure components. Using Eqs. [1] and [4] they obtained the individual isotherms, *i.e.*, $n^s{}_1$ and $n^s{}_2$ as functions of x, the mole fraction. The calculated individual isotherms agreed rather well with the individual isotherms obtained experimentally by adsorption from the vapor phase.

THEORY

The treatment of Kipling and Tester rests mainly upon the assumption that adsorption from binary solutions is unimolecular in character. They justify this assumption by noting that the isotherms for the pure vapors adsorbed separately on charcoal obey Langmuir's equation for unimolecular adsorption. There are several reasons for questioning strongly the validity of this treatment.

The adsorption of gases and vapors by charcoal, though fairly well represented by Langmuir's equation, has been shown rather conclusively to depend on a mechanism other than that proposed by Langmuir. Pierce, Wiley, and Smith (6) have stated that even at low relative pressures the assumption of monolayer adsorption is incorrect. Their reasons for assuming that capillary condensation occurs simultaneously with adsorption in the first layer are based on the following considerations: (1) excessively large surface areas are often computed on the basis of monolayer adsorption; (2) the pore diameters that must be assumed if adsorption is monomolecular are quite small; (3) volumes of adsorbates held by a given charcoal are constant. From the constancy of pore volume, they believe that capillary widths must be at least several molecular diameters, larger yet for steam-activated charcoals.

It has been demonstrated that adsorption from binary solution is not necessarily unimolecular, even on nonporous adsorbents. Recently Craig

(7) has shown the existence of multilayer adsorption in the system butyric acid-water on the nonporous adsorbent Graphon. In this case the adsorption of butyric acid actually exceeds the maximum amount that could be packed into a close-packed monolayer. Since indications are that monolayers contain solvent molecules as well as solute molecules, there is good evidence that all adsorption from binary solution is multimolecular in nature. Multilayer adsorption has been demonstrated from solutions of limited solubility by Hansen, Fu, and Bartell (8), using nonporous adsorbents. The presence of capillary condensation when water is adsorbed from solutions of water in the higher alcohols on silica gel has been shown by Bartell and Donahue (9). These facts would lead one to question the assumption that adsorption from binary solutions on porous adsorbents is unimolecular. Further doubts arise when one studies the molecular areas calculated by Kipling and Tester on the basis of unimolecular adsorption. They calculated molecular areas for benzene and ethyl alcohol of 27.1 and 17.9 square A., respectively. To explain this area for benzene it is necessary that the benzene be adsorbed edgewise; the value for ethyl alcohol is considerably smaller than the value of 21.6 square A. obtained from film balance studies on alcohols as reported by Adam (10). Edgewise adsorption of benzene seems energetically unfavorable compared to adsorption of benzene with the plane of the molecule parallel to the surface of the adsorbent.

What appears to us a more reasonable treatment and one more consistent with the known mechanism of vapor adsorption by porous adsorbents can be based on the assumption that the adsorption is constrained by the pore volume of the adsorbent. This can be expressed as:

$$n^s{}_1V_1 + n^s{}_2V_2 = V, \qquad [5]$$

where $n^s{}_1$ and $n^s{}_2$ have the same significance as before, V_1 and V_2 are the respective molar volumes of components 1 and 2, and V is the pore volume of the adsorbent. It should be noted that Eq. [5] can be rewritten in the form that is identical with Eq. [4], leading to the further result:

$$(n^s{}_1)^0V_1 = V. \qquad [6]$$

Thus, an analysis of a binary solution isotherm using Eqs. [1] and [4] will lead to individual isotherms which are identical with those calculated by the method of Kipling and Tester.

The volumes of liquid held by the adsorbent used by Kipling and Tester were 0.306, 0.311, and 0.309 cc. per gram for benzene, ethyl alcohol, and ethylene chloride, respectively. The variation from the average is within 1%. Tryhorn and Wyatt (11) studied adsorption from benzene-ethanol and benzene-acetone mixtures on charcoal. With their charcoal the volumes of liquid held were 0.162, 0.159, and 0.166 cc. per gram for benzene, ethyl alcohol, and acetone, respectively. The variation in this case is within

TABLE I

Adsorption from Ethanol-Benzene Solutions

Mole fraction of ethanol	Volume of ethanol adsorbed (*cc./g.*)	Volume of benzene adsorbed (*cc./g.*)	Total volume of adsorbate (*cc./g.*)
0	0	0.306	0.306
0.1	0.039	0.264	0.303
0.2	0.044	0.263	0.307
0.3	0.049	0.259	0.308
0.4	0.052	0.256	0.308
0.5	0.057	0.253	0.310
0.6	0.062	0.249	0.311
0.7	0.070	0.241	0.311
0.8	0.090	0.221	0.311
0.9	0.125	0.187	0.312
1.0	0.311	0	0.311

Calculated from isotherms of Kipling and Tester.

2.5% of the average. Tryhorn and Wyatt (12) obtained an average value of 0.16 cc. per gram for the pore volume from averaging the volume of adsorbate held by the four systems methyl alcohol-benzene to butyl alcohol-benzene. The constancy of these adsorbate volumes strongly indicates a pore-filling mechanism rather than a monolayer adsorption process.

In Table I are shown the total volumes of adsorbate for the system benzene-ethyl alcohol at one-tenth mole fraction intervals, taken from the isotherms of Kipling and Tester. It can be seen that the variation in total volume of adsorbate is within 1.5% of the average over the entire concentration range. This constancy of total volume of adsorbate over the entire range lends further support to the premise that the adsorption on charcoal occurs by a pore-filling mechanism.

With the method of analysis proposed here, once the pore volume has been determined for an adsorbent, individual isotherms can be calculated from the binary solution isotherm, using Eqs. [1] and [5]. This treatment, of course, leads to calculated individual isotherms substantially identical to those found by Kipling and Tester and was also found to represent well data of Tryhorn and Wyatt. The treatment of Kipling and Tester, even if applicable to porous adsorbents, cannot be used unless the values of the amounts adsorbed from the vapors of the pure liquids are known. To calculate the individual isotherms without these values, one must know the surrace area of the adsorbent and choose suitable values for the molecular areas occupied by the two components. In practice, this would undoubtedly be quite difficult.

In addition to the treatment already discussed, Kipling and Tester also proposed a kinetic treatment based on the same model of monolayer adsorption. This treatment gave the following equations for σ_1 and σ_2, the fractions of surface covered by components 1 and 2, respectively:

$$\sigma_1 = \frac{p_1}{p_1 + Kp_2}; \qquad \sigma_2 = \frac{p_2}{p_2 + p_1/K}. \qquad [7]$$

This treatment also gave results that agreed satisfactorily with experimental results.

Their kinetic treatment is quite similar to the Langmuir multicomponent treatment, as presented by Markham and Benton (13). In view of the fact that the separate gas isotherms obeyed Langmuir's equation, it is not surprising that the individual isotherms of adsorption from binary solution also fit the Langmuir multicomponent equations, although again it must be emphasized that this agreement in no way establishes a monolayer adsorption mechanism.

The limiting cases where this treatment fails to hold should be pointed out. Whenever the pore radii are the same order of magnitude as the molecular radii, the volume of adsorbate will cease to be constant due to incomplete filling of the pores. The steric effects of these small pore radii have been discussed in detail by Brunauer (14). When the pore radii are small, Eq. [5] no longer holds and this treatment breaks down.

It should be borne in mind that adsorption from saturated vapors differs from adsorption from solution in an important respect. In the adsorption from saturated vapors there is, in addition to the adsorption at the solid-liquid interface, adsorption at the liquid-vapor interface. Therefore, great caution must be exercised in comparing adsorption from solution with adsorption from saturated vapors. Only when the area of the liquid-vapor interface is neglibly small compared to the surface area of the adsorbent can the two modes of adsorption be considered the same. This condition is generally satisfied by porous adsorbents. However, when the pore radii became large, the liquid-vapor interface can no longer be neglected and the effects of the adsorption at this interface must be considered.

SUMMARY

The treatment of adsorption from binary liquid solution proposed by Kipling and Tester (4) is criticized for its application of a unimolecular adsorption mechanism to porous adsorbents.

It is shown that results of Kipling and Tester and others for adsorption by porous adsorbents from solution can be interpreted in a more consistent way through a pore-filling mechanism. In accord with this, total adsorption volumes are found to be constant in the systems discussed.

Equations are presented based on the pore-filling mechanism which are

formally equivalent to those presented by Kipling and Tester; these equations should be valid if pore diameters are suitably larger than molecular diameters of adsorbate components.

It is pointed out that adsorption from solution should be comparable to adsorption from saturated vapors only if the area of liquid-vapor interface in the latter case is negligible compared to the surface area of the adsorbent—a condition generally satisfied by porous adsorbents.

REFERENCES

1. OSTWALD, W., AND DE IZAGUIRRE, R., *Kolloid-Z.* **30**, 279 (1922).
2. BARTELL, F. E., AND SLOAN, C. K., *J. Am. Chem. Soc.* **51**, 1643 (1929).
3. KIPLING, J. J., AND TESTER, D. A., *Nature* **167**, 612 (1951).
4. KIPLING, J. J., AND TESTER, D. A., *J. Chem. Soc.* **1952**, 4123.
5. ELTON, G. A. H., *J. Chem. Soc.* **1951**, 2958.
6. PIERCE, C., WILEY, J. W., AND SMITH, R. N., *J. Phys. Chem.* **53**, 669 (1949).
7. CRAIG, R. P., Thesis, Iowa State College, Ames, 1952.
8. HANSEN, R. S., FU, Y., AND BARTELL, F. E., *J. Phys. Chem.* **53**, 769 (1949).
9. BARTELL, F. E., AND DONAHUE, D. J., *J. Phys. Chem.* **56**, 665 (1952).
10. ADAM N. K., The Physics and Chemistry of Surfaces, 3rd Ed. Oxford University Press, London, 1941.
11. TRYHORN, F. G., AND WYATT, W. F., *Trans. Faraday Soc.* **22**, 139 (1926).
12. TRYHORN, F. G., AND WYATT, W. F., *Trans. Faraday Soc.* **24**, 36 (1926).
13. MARKHAM, E. C., AND BENTON, A. F., *J. Am. Chem. Soc.* **53**, 497 (1931).
14. BRUNAUER, S., The Adsorption of Gases and Vapors, Vol. I. Princeton University Press, Princeton, New Jersey, 1945.

A COAXIAL CYLINDER VISCOMETER FOR THE STUDY OF FLUIDS UNDER HIGH VELOCITY GRADIENTS

Edward W. Merrill

Department of Chemical Engineering, Massachusetts Institute of Technology, Cambridge, Massachusetts

Received July 29, 1953; revised November 9, 1953

(*This paper is a revision of a paper received by the Journal of Colloid Science on July 29, 1953*)

ABSTRACT

A coaxial cylinder viscometer is described for the absolute measurement of shearing stress *vs.* velocity gradient up to high values of gradient. Principal features of construction are: bottomless cylindrical shearing surfaces, very small annular clearance, rigid mechanical alignment of the cylinders, and a pressure-feeding system. Several advantages are thereby achieved, not found together in other cylindrical viscometers: (1) versatility in testing a wide range of viscous fluids, including gels; (2) measurement of shearing stress and corresponding velocity gradient as essentially point values; (3) variability of velocity gradient up to high values; (4) good control of fluid temperatures; and (5) ease of introduction of fluids for test. Typical experimental results are presented for viscous Newtonian fluids, a commercial paint, and a varnish.

INTRODUCTION

The apparent viscosity η_a of any fluid is defined as the ratio τ/D, wherein τ is a point value of shearing stress and D the corresponding value of velocity gradient. As the apparent viscosity, η_a, of a non-Newtonian fluid is a variable function of τ and D, it cannot be specified unless τ or D is specified.

Falling ball and capillary viscometers subject a fluid under test to a flow pattern in which τ and D vary continuously. It is possible to interpret the flow of a non-Newtonian fluid in a capillary viscometer in terms of point values of τ and D (1), but the method entails extensive calculation. For the testing of *non-Newtonian* fluids, the usual types of coaxial cylinder viscometers, particularly those incorporating a torsion wire, have certain shortcomings: notably, considerable variation of D in the fluid under test, owing to the width of the cylindrical annulus containing the fluid, and virtual inoperability with gelled fluids. Another disadvantage of conventional instruments of this type is the low value of D obtainable within the range of Reynolds numbers associated with laminar flow. Many instruments in addition lack adequate means of controlling the temperature of the fluid under test.

Certain special instruments capable of providing high-velocity gradients have been designed to test specific fluids such as lubricating oil, paint, and printing ink (2, 3, 4). Their various constructional features, however, appear to preclude the testing of structurally unhomogeneous fluids such as some polymer solutions.

It is the purpose of this paper to describe a type of coaxial cylinder viscometer that permits the absolute measurement of τ and D as essentially point values. This viscometer, devised by the author, has several advantages not found together in any other cylindrical viscometer. The principal features of construction are bottomless cylindrical surfaces, very small annular clearances between the cylinders, rigid and precise coaxial alignment of the cylinders, and a closed, pressure-feeding system for introducing fluid for test.

The several advantages simultaneously achieved by these constructional features are:

1. Ability to test a wide variety of viscous and non-Newtonian fluids, including gels and pigmented fluids.
2. Establishment of a substantially constant velocity gradient and shearing stress.
3. Variability of the velocity gradient over a wide range and up to high values.
4. Good temperature control of the fluid under test.
5. Ease of introduction of fluids such as gels and highly viscous fluids.

Velocity gradients as high as 6700 reciprocal seconds have so far been explored, the practical limit being considerably higher, and viscosities as high as 9000 centipoises have been measured. The lower limit on the viscosity of fluids that may be tested appears to be of the order of magnitude of 50 centipoises.

DETAILS OF CONSTRUCTION

A cross-sectional plan of the viscometer is shown in Fig. 1. A ⅝-in. diameter steel drill rod, S, serves as the driving shaft for the instrument. The upper end is held in the chuck of a drill press (or other variable speed-driving mechanism), and the lower end rests on a lathe center-pin, P, suitably held in a frame so as to make the shaft exactly perpendicular. Securely fixed to the shaft is a concentrically machined frame, F, of the cross-sectional shape shown, the primary purpose of which is to form a seat for the outer ring OR of ball bearing B, so that this ring is exactly concentric with and perpendicular to the shaft S. A cylindrical brass ring, A, is machined so as to fit snugly and concentrically on the inner ring, IR, of the bearing B. The inner surface, M, of ring A is bored so as to be exactly vertical to and concentric with the shaft S. The diameter of cylindrical surface M on ring A is 2.502 in., and its height is 1.0 in.

A cylindrical cup, C, is bored so as to slide snugly without play on shaft S. The cup is milled out so as to provide a chamber, CW, to hold cooling water. The outer cylindrical surface, N, of the cup is 1.0 in. high and is machined so as to be exactly vertical to and concentric with the shaft S. The clearance between surfaces M and N is intended to be constant and very small. In the present instrument, the clearance is 0.00603 ± 0.0003 in. The outer cylindrical surface of the cup N is parallel to the axis of the instrument to within ± 0.0001 in., and its deviation from a true circle at any plane is ±0.0001 in. Surface M of the ring is parallel to the axis of the instrument to within ± 0.0002 in., and its deviation from a true circle at any plane is ±0.0002 in.

The cup C slides down shaft S and comes to rest on the frame F at such a level that the surfaces M and N exactly coincide.

A pin, V, on frame F cooperates with a hole, W, in the bottom of cup C so as to cause the cup C to rotate at the speed of the shaft S and frame F. The inner ring, IR, of bearing B and the ring A fitted thereon are restrained from rotating when the shaft is rotated, by a cord fastened to a hook K on ring A, which is led therefrom tangentially and horizontally to a pulley wheel of low friction, and thence vertically to a triple-beam balance secured on a frame overhead.

Details of Operation

Before any experimental measurements are made, the viscometer is rotated for a minute at high speed to distribute the lubricant (spindle oil) on the ball race. The speed-drag characteristics of the bearing, properly lubricated, are essentially constant at constant temperature. If the ball bearing becomes accidentally contaminated with foreign matter, it is

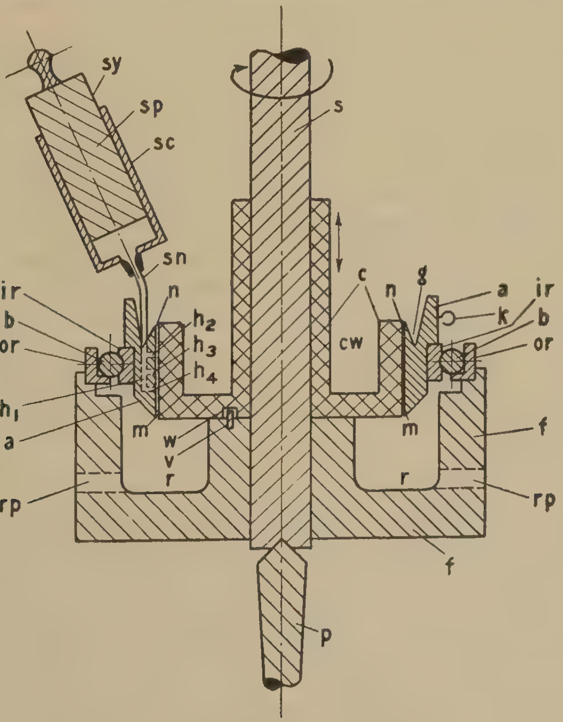

Fig. 1. Elevation of viscometer (drawn to scale).

thoroughly washed with benzene and again lubricated with a drop of spindle oil. One next rotates the instrument by means of the drill press at a number of different speeds, each speed constant and determined by the drill press belt arrangement, and records the force on the cord caused by the bearing drag for each speed, subsequently designated as F_D.

The fluid to be tested is now introduced into syringe SY (a small cylinder, SC, and piston, SP, with nozzle, SN). The syringe is mounted in a vertical hole, H_1, bored in ring A, which communicates with three small horizontal holes, H_2, H_3, and H_4, each 1/16 in. in diameter. By forcing the piston down into the syringe, the fluid to be tested is caused to flow through hole H_1 to H_2, H_3, and H_4 and then into the annulus formed by surfaces M and N. When fluid appears at the top of the annulus, the injection is stopped and the tests are made. The groove G in ring A is intended to receive excess fluid overflow.

One now rotates the instrument thus filled at successively greater or lesser rates of rotation and measures the gross force on the balance transmitted through the cord necessary to counterbalance the moment of torque on ring A. This force is subsequently designated as F_B.

In the determination of shearing stresses, a triple-beam balance of 2000-g. capacity has been found convenient.[1] A light cord running from the stationary ring of the viscometer is carried over a pulley wheel up to a hook under the platform of the balance. The friction in the cord and wheel is less than 0.5 g., and the balance itself (made by Central Scientific Company) is accurate to ±0.1 g., which is greater than the accuracy with which the bearing loss and the total force on the ring can be determined. The arm of the balance tends to wander slightly above and below the zero mark, but owing to its inertia this fluctuation is slow, and a consistent reading for nongelled fluids can be obtained to within at least ±2 g.

It has usually been found that a stable reading is attained within 3 sec. after start of rotation of the viscometer at a predetermined speed of rotation unless the fluid is thixotropic. The balance can be accurately adjusted within 5 sec. The results herein reported are based on readings which have been obtained in not less than 4 nor more than 8 sec. of operation at any speed.

The original data taken on a commercial enamel paint[2] are given in Table I and show a typical deviation of ±2 grams-force in the determination of gross scale reading F_B, and of ±1 gram-force in the determination

---

[1] A spring dynamometer was used in the testing of a glucose solution of 9100 c.p. viscosity, reported below, since the torque exceeded the capacity of the triple beam balances.

[2] As the gel structure of paint is destroyed virtually instantaneously upon shear, a stable reading of F_B is obtained at once. Paint exemplifies false-body rather than thixotropy.

TABLE I

Commercial Enamel Paint

(Data taken at 30.5° ± 0.2°C.)

Velocity gradient D[a]	F_B in grams—force					Bearing loss F_D[d]	Shearing stress τ[e]
	Run 1[b]	Run 2[c]	Run 3[b]	Run 4[c]	Avg.		
433	52	55	55	55	55	24	0.8
714	78	76	78	—	78	26	1.34
1220	110	113	110	110	110	31	2.04
1850	155	155	155	160	156	36	3.09
3210	248	245	245	—	246	43	5.23
3880	295	300	296	300	297	50	6.36
6690	470	472	470	470	470	70	10.3

[a] Found from rotational speeds by Eq. [1]; sec.$^{-1}$.

[b] Velocity gradient increased from 433 to 6690 sec.$^{-1}$.

[c] Velocity gradient decreased from 6690 to 433 sec.$^{-1}$.

[d] Bearing drag measured before and after 4 runs. Deviation ± 1 gram—force.

[e] Calculated from $F_{B\ \text{avg.}}$ by Eq. [4] in grams—force/sq. cm.

of bearing drag F_D for the empty instrument at a given rotational speed and under constant temperature.

During the course of a test, water at constant temperature is continuously supplied to the cup chamber, CW, through a tube (not shown) and is continuously removed through another tube (not shown) leading to an aspirator. In future models it is planned to design the ring A so that it too may carry a temperature-regulating water stream.

Cleaning the apparatus after a run is relatively simple. The cup C is pulled off shaft S and washed with a suitable solvent. With cup C removed, one can now wash and wipe clean the ring A. Because of its low hold-up, the feeding system (holes, H_1, H_2, H_3 and H_4) is easily cleaned by filling the syringe with a suitable solvent and forcing it through the feeding channels. The solvent and the excess fluid that leaks out of the annulus during test runs drop into the reservoir R formed in frame F, from which they run out through ports RP into a suitable collecting device.

PRINCIPAL CALCULATIONS—PHYSICAL CONSTANTS OF VISCOMETER

Calculation of Velocity Gradient D

In a coaxial cylinder viscometer the point velocity gradient D existing in a lamina of fluid at radius r is equal to $rd\omega/dr$.[3] Because in this viscometer the distance from inner to outer cylinders is so small a fraction of the radius of either, D is substantially constant from one cylindrical surface to the other and may be calculated as $r\Delta\omega/\Delta r$.

---

[3] Provided the fluid under shear is contained entirely between cylindrical surfaces of constant radii.

Thus

$$D = r_{avg.}(\omega_r - \omega_c)/(r_r - r_c) \qquad [1]$$

wherein: r_r = inside radius of ring;
r_c = outside radius of cup;
$r_{avg.} = (r_r + r_c)/2$;
ω_r = angular velocity of ring (zero for this viscometer);
ω_c = angular velocity of cup $= 2\pi(N)$;
N = revolutions per second (r.p.s.) of the shaft S.

In the instrument here described, $r_r = 1.251$ in. and $r_c = 1.245$ in.; thus $r_{avg.} = 1.248$ in. The quantity $r_r - r_c$ accurately measured was found to be 0.0060 ± 0.0003 in.

In the experiments hereafter reported, a standard series of fixed speeds of rotation of the shaft was used. These several rotational speeds and the corresponding velocity gradients obtained in the viscometer are given below:

N, in r.p.s.	0.333	0.548	0.938	1.425	2.47	2.98	5.14
D, sec.$^{-1}$	433	714	1220	1850	3210	3880	6690

Calculation of Shearing Stress

The average area A over which shear occurs is taken as the mean cylindrical area of height l radius $r_{avg.}$, bounded by ring surface M and cup surface N.

Thus

$$A = 2\pi r_{avg.} l. \qquad [2]$$

In the instrument described, $A = 50.5$ sq. cm.

Since the moment of torque at any radius from the axis is constant, the mean tangential force F resulting from fluid shear along the mean cylindrical surface A is calculated as:

$$F = (F_B - F_D)(r_0/r_{avg.}) \qquad [3]$$

Herein, F_B is the total force on the cord measured with the instrument filled, F_D is the bearing drag of the empty instrument at the same rotational speed, r_0 is the outer radius of the ring to which the cord is tangent, and $r_{avg.}$ is the mean radius of shear of the fluid, defined above. The ratio $r_0/r_{avg.}$ is numerically 1.30 for this instrument. The average shearing stress τ is now calculated as

$$\tau = F/A. \qquad [4]$$

Calculation of Viscosity

As A is measured in square centimeters and F has been reported in this paper as grams-force, dimensional consistency requires that the apparent viscosity η_a in *centipoises* be calculated as:

$$\eta_a = 98000\ \tau/D. \qquad [5]$$

TYPICAL EXPERIMENTAL RESULTS

Calibrating Fluids

To confirm the methods of calculation shown in the preceding section, three different calibrating fluids were tested by this viscometer, two aqueous solutions of sucrose of different concentrations and one glycerin solution. The glucose solutions were standardized on an Interchemical

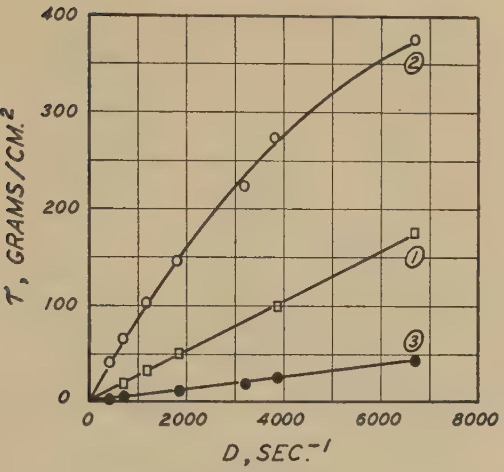

FIG. 2. τ-D diagrams for calibrating solutions.
Curve 1: Glucose-water, standard #1. 20.5° ± 0.2°C.
Curve 2: Glucose-water, standard #2. 20.5° ± 0.2°C.
Curve 3: Glycerol, 95.3% by weight. 17.0° ± 0.2°C.

Viscometer (5) at 400 r.p.m., corresponding to an *average* value of $D = 600$ sec.$^{-1}$, through the courtesy of the Dewey & Almy Chemical Company of Cambridge, Massachusetts.

The glucose solution of lower concentration, tested at 20.5° ± 0.2°C., behaves as a Newtonian fluid, as shown by the linear τ-D plot passing through the origin (curve 1 of Fig. 2). The value of apparent viscosity is found to be 2580 c.p., in fair agreement with the value obtained by standardization, 2370 c.p. The glucose solution of higher concentration, also tested at 20.5° ± 2°C., showed definitely pseudoplastic properties from the τ-D plot (curve 2 of Fig. 2). At a velocity gradient of 600 sec.$^{-1}$, the apparent viscosity η_a is found to be 9100 c.p., which is in fair agreement with the value obtained on the Interchemical Viscometer of 8950 c.p. for an *average* gradient in the latter instrument of 600 sec.$^{-1}$. The aqueous glycerol solution (96.3% glycerol by weight) tested at 17.0° ± 0.2°C. yielded a τ-D curve (curve 3 of Fig. 2) showing Newtonian behavior as expected and a viscosity of 672 c.p.

Paint and Varnish

In Figure 3, the τ-D diagrams of a commercial enamel paint and a commercial varnish are presented. Both determinations were made at 30.5° ± 0.2°C. The varnish (curve 2) shows substantially Newtonian behavior, having a constant viscosity of 113 centipoises and no yield point. The enamel (curve 1), on the other hand, shows a slight yield point upon extrapolation, perhaps 0.1 g./cm.², followed by a gentle curvature in the

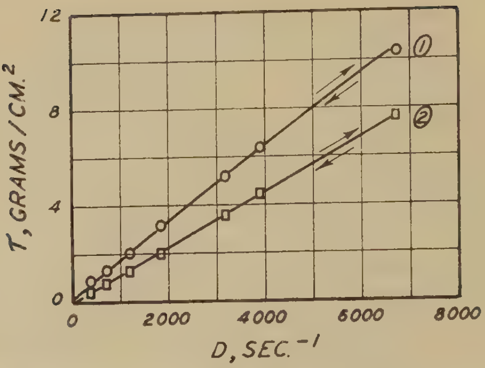

Fig. 3. τ-D diagrams for commercial paint and varnish samples at 30.5° ± 0.2°C.

Curve 1: Commercial enamel paint.
Curve 2: Commercial spar varnish.

τ-D plot. For both the enamel and the varnish, exactly the same τ D plots were obtained with increasing and decreasing velocity gradients.

In addition to the fluids described above, a number of solutions of synthetic rubber, including some highly gelled solutions, have been studied and will be described in a subsequent paper.

DISCUSSION

Heat Generation in the Fluid during Shear

In viscometers that subject the fluid to high-velocity gradients, temperature rise in the fluid (as a result of degradation of shearing work to heat) becomes a matter of concern. The temperature coefficient of viscosity of many fluids is so great that accidental rise in temperature of the fluid by a few degrees is sufficient to invalidate the results of a viscometric test.

To ascertain whether temperature rise during shear occurs to a significant extent in this viscometer, the following experiment was made. A fine duplex thermocouple wire was led down through a specially fitted syringe through hole H_1 and out through hole H_3 (as shown in Fig. 1) until the tip of this probe protruded perceptibly into the annulus of fluid shear (between ring A and cup C of Fig. 1). A viscous fluid (10% Buna-N by weight in aniline) was then introduced through the syringe into the viscometer, the cup of which was receiving cooling water at 21.0°C. Ambient air temperature was 21.0°C. When the temperature of fluid in the interface had reached 21.0°C., the viscometer was set in rotation at a speed corresponding to a velocity gradient of 6690 sec.$^{-1}$. The following data were obtained:

Time from Start (*sec.*)	Temperature of Fluid (°*C.*)	Change of Temperature (°*C.*)
5	21.0	0
30	22.2	+1.2
60	23.0	+2.0

The average net force required to restrain the ring of the viscometer during the test was 2500 g., corresponding to a shearing stress of 63 g./cm.^{2} on the fluid. The apparent viscosity of the fluid at this velocity gradient was determined to be 930 centipoises. Calculation of the rate of work input to the fluid and the corresponding rate of heat generation in the fluid showed that the temperature rise would be of the order of 1°C. per second if the fluid were considered as an adiabatic system.

The observed fact that the rate of temperature rise was approximately $\frac{1}{30}$th of that predicted for adiabatic operation clearly indicates that the shearing members of the viscometer (the cup and the ring) serve as effective isothermal reservoirs for heat. Not only is the mass of these parts very large compared with that of the fluid (some 300 g. *vs.* 0.75 g.) but the layer of fluid is so thin that rapid dissipation of heat by conduction is possible.

As the scale readings for all viscometric determinations are taken within a maximum of 8 sec. of the start of shear, it is believed that temperature control of the fluid in this viscometer is sufficiently precise. The variations in temperature noted in the experimental results presented above are not ascribable to heat generation during shear, but solely to the inadequacies of the thermostatic system used to control the water supply to the cup of the viscometer.

Effect of Surface Tension

In considering how a fluid, introduced into the bottomless annulus of the viscometer here described, can remain in the annulus during testing, it is reasonable to examine the role of surface forces. In normal operation of this viscometer, fluid that has flowed up out of the annulus forms a layer above the annulus that wets the upper surfaces both of the ring and the cup. It is, therefore, inconceivable that interfacial tension of significant magnitude is operative at the top of the annulus to hold liquid in the annulus in the manner of a column of fluid held in a capillary tube.

If one will assume that a perfectly uniform ring of fluid hangs from the bottom of the annulus, the minimum cross section of this ring occurring at the edge of the annulus, then following the principle underlying the pendant drop method of surface tension measurement, one may compute approximately the surface tension which the fluid must have in order to support the entire annular body of fluid against gravity, as:

$$2\sigma > l(r_r - r_c)\gamma \qquad [6]$$

wherein γ = specific weight, l = height of fluid annulus (here 2.54 cm.), and r_r and r_c are as previously defined and equal to 0.0153 cm. The weight of fluid in the pendant ring is neglected. Assuming a density of 1.0 ($\gamma = 980$) and using the values of l, r_r, and r_c given above, one finds $\sigma \geqslant 19$ dynes/cm.—a value lower than the surface tensions of most simple organic fluids and far lower than most aqueous solutions.

It is, therefore, at least theoretically possible that most liquids should remain in the annulus owing to surface tension in the pendant ring below when the cylinders are stationary. On the other hand, during operation of the viscometer, the continuous movement of the fluid hanging from the annulus and the disruption of its surface render the surface tension effect possibly negligible and surely indeterminable. During shear the loss of fluid from the annulus at a significant rate is more likely prevented solely by the fact that the gravitational force acting vertically on the fluid causes only a very slight velocity of descent, owing to the substantial viscosities of the fluids appropriate for testing in this instrument. This will be shown more fully below.

Deviations from Ideal Flow

The idealized case of radial slip of perfect, concentric, cylindrical laminas of fluid past each other that underlies the evaluation of Eq. [5] is never completely achieved in any viscometer. Certain deviations in the flow pattern from the ideal case occur in the viscometer here described that are worthy of note. These deviations are caused by: (1) the presence of the holes (H_2, H_3 and H_4 of Fig. 1) in the ring; (2) the possibility of new fluid issuing from these holes during testing; (3) the presence of excess fluid in the shape of ill-defined rings above and below the annular surfaces (M and N of Fig. 1); and (4) the vertical descent of fluid through the annulus under gravity.

The effect of the holes in the ring, and especially the effect of fluid issuing slowly therefrom, has not been fully verified. However, the experimental data pertaining to the paint tested (Table I and Fig. 3) suggest that these effects are negligible; for in some of the runs, fluid was supplied continuously during *the runs*, but in other runs fluid was supplied *before* and not during the run, but no difference in stress could be detected within the limits of accuracy previously discussed.

The presence of the excess fluid accumulating above the annulus formed by the cup and ring is believed to have a negligible effect on the evaluation of true shearing stress. In several experiments fluid was intentionally allowed to accumulate to a depth of about 1/16th of an inch; the torque then measured was substantially the same as at the outset of the experiment when fluid had just appeared at the top of the annulus. Visual examination of this supernatant layer of fluid during rotation revealed a gradual and slow change in radial velocity from the cup to the ring. It is supposed that the maximum velocity gradient established in this fluid, lacking the confinement imposed by the annular boundary surfaces, is relatively small compared with that in the annulus proper, and that the shearing force associated with this supernatant liquid is negligible, owing first to the low gradient in it and second to its relatively small shearing area with respect to the annular area of shear (Eq. [2]). The effect of fluid accumulation at the bottom of the annulus is believed to be even less important, since during rotation of the viscometer centrifugal force tends to drive the liquid against the sharp edge of the ring (Fig. 1) from which it appears to fall cleanly away.

The disturbance to flow occasioned by descent of the fluid under gravity deserves some attention. For the purpose of estimating the velocity of descent, a *Newtonian* fluid is assumed, having a viscosity η of 50 c.p. (0.5 poise), density 1.0, and corresponding specific weight γ of 980 dynes per cubic centimeter. As an approximation, it is assumed that the annulus of the viscometer may be replaced by two parallel vertical planes, separated by a distance D, D equal to $r_r - r_c$ or 0.0153 cm., and of height l, l being 2.54 cm. in this case. One may now compute [7] the maximum velocity of descent of the fluid, V_0, occurring midway between the boundary planes, as:

$$V_0 = \frac{\gamma D^2}{8\eta} \qquad [7]$$

From the values given above, V_0 is found to be 0.0574 cm. per second, and the *average* velocity of descent V, equal to $\frac{2}{3}V_0$, is 0.0383 cm. per second. At the *midplane* of the annulus, where the vertical velocity of an element of fluid is a maximum, the peripheral velocity of the same element at a low rotational speed of 0.333 r.p.s. (D = 433 sec.$^{-1}$) is approximately 3.3 cm. per second. This element of fluid thus will describe a helical path, the angle of whose pitch is $\sin^{-1}$ (0.0574/3.33) or about 1.0°. For all elements of fluid lying between the annular boundary walls the angle of descent during rotation of the viscometer is of the same order of magnitude, and the angle would evidently decrease at higher rotational speeds. It is tentatively assumed, therefore, that the error in the determination of shearing stress owing to vertical descent of the fluid is negligible.

Transition from Laminar to Turbulent Flow

Barr (6) proposes a modified Reynolds number for predicting onset of turbulent flow in an ideal coaxial cylinder viscometer in which the inner cylinder is rotated, the other being stationary, and in which the annular clearance is a small percentage of the radius of either cylinder. Translating Barr's equation into the nomenclature of this article, one finds that turbulent flow is predicted when

$$\frac{r_c(r_r - r_c)^3\rho^2N^2}{\eta^2} > 43 \qquad [8]$$

For the equation to be dimensionless, r_c and r_r are in centimeters, density ρ in grams per cubic centimeter, η in *poises*, and the rotational speed N in second^{-1}. Assuming an average density for all fluids of 1.0, one finds for the viscometer herein described that $N > 1950\ \eta$ for onset of turbulent flow.

Given a fluid of 50 c.p. viscosity (0.5 poise), it is seen that a mechanically unattainable value of 975 r.p.s. is predicted. The maximum rotational velocity employed in the tests reported was 5.14 r.p.s.

Barr's equation, equivalent to the square of a Reynolds number, is found to be reducible to:

$$\frac{DV_{\text{max.}}\rho}{\eta} > 592 \qquad [9]$$

in which D = clearance between surfaces $(r_r - r_c)$, and $V_{\text{max.}}$ = maximum linear velocity of fluid (next to rotating cup) = $2\pi r_c \times N$.

For the case of free, unidirectional flow of a fluid over a flat plate, onset of turbulence is predicted (7) for:

$$\frac{D'V'_{\text{max.}}\rho}{\eta} > 500 \qquad [10]$$

in which D' is thickness of layer and $V'_{\text{max.}}$ is velocity of free surface. As the coaxial cylinder viscometer may be reduced to this case in the limit, comparison of Eq. [9] with Eq. [10] verifies the correctness of Barr's equation at least in order of magnitude.

It is therefore concluded that under conditions of practicably obtainable speeds of rotation, with fluids having viscosities appropriate for testing in this viscometer, turbulent flow is not possible.

SUMMARY

1. A viscometer has been described by which it is possible to measure essentially point values of velocity gradient and shearing stress. Gradients of at least 6690 sec.$^{-1}$ may be obtained, and a fluid of 9000 c.p. viscosity has been measured. The viscometer is operable with any fluid, gelled or otherwise, which may be introduced through the pressure-feeding syringe, providing its viscosity is around 50 c.p. or greater.

2. Experimental data are presented for calibrating fluids, which confirm the validity of design of the viscometer.

3. Illustrative of the practical use of the viscometer, the experimentally determined flow characteristics of a commercial paint and a commercial varnish are presented.

4. Typical data are presented to indicate the over-all accuracy of determinations with the viscometer.

5. Temperature rise of the fluid during test, surface tension effects, flow patterns, and the Reynolds number criterion are discussed.

ACKNOWLEDGMENTS

The author wishes to express his gratitude for generous help and advice in the construction of this viscometer to Professor Harold H. Weber, Mr. Henry Chasen, and Mr. Harry Archibald; to Professor Warren K. Lewis for his critical review of the manuscript and his valuable suggestions; to Mr. H. H. Carter for preparation of the drawings; all of the Chemical Engineering Department of the Massachusetts Institute of Technology.

REFERENCES

1. ALFREY, T., Mechanical Behavior of High Polymers, p. 41. Interscience Publishers, New York, 1948.
2. A.S.T.M. Symposium on Methods of Measuring Viscosity at High Rates of Shear, *Tech. Pub. No.* **111** (1949–1950).
3. ASBECK, W. K., LAIDERMAN, D. D., AND VAN LOO, M., *J. Colloid Sci.* **7**, 306 (1952).
4. HULL, H. H., *J. Colloid Sci.* **7**, *316* (1952).
5. GREEN, H., *Ind. Eng. Chem., Anal. Ed.* **14**, 576 (1942).
6. BARR, G., A Monograph of Viscometry, p. 224. Oxford University Press, London, 1931.
7. ROUSE, H., AND HOWE, J. W., Basic Mechanics of Fluids, pp. 118, 129. John Wiley and Sons, New York, 1953.

ELECTROOSMOSIS AND STREAMING IN NATURAL AND SYNTHETIC FIBERS

G. J. Biefer[1] and S. G. Mason

Pulp and Paper Research Institute of Canada, McGill University, Montreal, Canada

Received June 9, 1953

LIST OF SYMBOLS

A = cross-sectional area of porous pad.
c = concentration wt./vol. of pad.
D = dielectric constant of flowing liquid.
E = applied electroosmotic potential.
F = volume rate of electroosmotic flow.
I = stream current.
K = permeability coefficient.
L = length (of pad, capillary, air bubble).
p = pressure drop causing flow.
Q = volume rate of viscous flow.
r = radius (of capillary, pore, fiber).
R = electrical resistance of pad.
u = velocity.
V = stream potential.
x = film thickness.
α = specific volume of solid.
δ = equivalent thickness of electrical double layer.
ζ = electrokinetic potential.
η = viscosity of flowing liquid.
λ = surface tension.
σ = surface area per unit mass of fibers.
ϕ = permeability.

INTRODUCTION

In an investigation of the electrokinetic properties of compressed pads of cotton fibers, Goring and Mason (1) found that the ratio of the electroosmotic function to the stream potential function, expressed as

$$\frac{\zeta_E}{\zeta_S} = \frac{F\eta L/ED}{V\eta L/pDR}, \qquad [1]$$

in which the symbols have their usual meanings in this connection, varied from 1.2 to 1.5 over a range of increasing pad concentrations. According

[1] Holder of a Fellowship under the National Research Council of Canada. Present Address: E. I. du Pont de Nemours and Co. Inc., Waynesboro, Virginia.

to the conventional theory of electrokinetic flow through porous plugs (2) or the alternative hypothesis advanced for the case of plugs of highly swollen fibers (8), the ratio should be unity.

Equation [1] has been confirmed experimentally by measurements on a clay diaphragm (4), single glass capillaries (5), and beds of powdered glass (6). Kanamaru (3), however, found a ratio of as low as 0.4 for pads of cellulose and cellulose acetate. All of the measurements cited above including those of reference (1) were made in the presence of dilute aqueous electrolytes. Rutgers and de Smet (7) have recently investigated streaming and electroosmosis of solutions of tetra-iso-amyl ammonium picrate in dioxane-water and benzene-acetone mixtures through single glass capillaries; ζ_E/ζ_S ranged from 0.9 to 2.3 and increased with the applied electroosmotic potential E.

In view of these discrepancies, it was considered to be of interest to determine whether the results with cotton were due to imperfections in the electrokinetic theory when applied to fibrous materials or were due to faulty experimental methods. A comparison was made of the electrokinetic effects of streaming and electroosmosis over a wide range of fiber concentrations for swelling (cellulose), slightly swelling (cellulose acetate) and nonswelling (glass) fibers. In the streaming measurements, the stream current function $I\eta L/pD$ rather than the stream potential function was determined since, as has been shown previously (8), it can be determined more conveniently and with less error. The precision of the measurements reported here is high for measurements of this type; ζ_E and ζ_S were found to be in excellent accord.

EXPERIMENTAL METHODS

Materials

The following materials were used:

1. Bleached unbeaten softwood sulfite pulp.
2. Cotton, from a roll of Parke-Davis absorbent cotton.
3. Cellulose acetate. The material (Canadian Celanese Ltd.) was 3 denier ($20\ \mu$ diameter) staple having an acetyl value of 54.
4. Glass fiber. Two types were used: Owens-Corning Aerocor $2.5\ \mu$ diameter staple, and a sample of $0.5\ \mu$ diameter staple obtained from Glass Fibers Inc., Toledo, Ohio.

The long-fibered samples were chopped in a Wiley mill and, in most cases, fines were removed by wet screening over a 150-mesh screen.

The High-Compression Stream Current and Electroosmotic Cell

The electrokinetic measurements were made in a compression-type cell with reversible electrodes similar in principle to that described by Goring and Mason (8) but designed to allow compression of the fiber pads to higher concentrations. A partial view of the cell is shown in Fig. 1. The body was of heavy-wall pyrex tubing of internal cross-sectional area 5.00 cm.^2. The reversible silver/silver chloride electrodes fitted snugly into the cell, and each was attached to a ½ in. O.D. heavy-wall pyrex tube with a liquid-tight seal. A series of 1/16 in. diameter holes drilled through each electrode permitted liquid to flow freely through the electrode to the annulus between the inner and outer glass tubes. Electrical connection was provided by a silver bus bar which was fused to the back of the electrode and run through the inner glass tube.

When assembled, each electrode mounting was inserted in the cell through a rubber stopper. The cell was clamped in a wooden frame between two parallel threaded steel tie rods with wing nuts. Brass plates which fitted over the steel rods could be brought against the bakelite inserts at the ends of the electrode mountings, and wing nuts could be tightened against the brass plates to apply pressure to the material between the electrodes.

The rugged construction of both cell and electrodes made it possible to apply relatively high compression to the material between the electrodes without danger of breakage.

The silver electrodes were chloridized at 3 ma./cm.^2 for 2½ hours, as previously described (8).

Pad Formation

Before forming a pad, the fiber was repeatedly washed in distilled water over a period of 24 hours. It was then soaked in a solution of 2.5×10^{-5} N KCl, the electrolyte used in all measurements.

To form the pad, the compression cell was clamped vertically, with the lower electrode in position. The suspension of fibers was formed into a pad by filtration through the electrode. The cell was then assembled, and the pad deaerated (1).

The solution used in each set of measurements was freshly prepared from deaerated distilled water. To establish sorption equilibrium of the electrolyte in the pad, the system was thoroughly flushed with the solution a number of times.

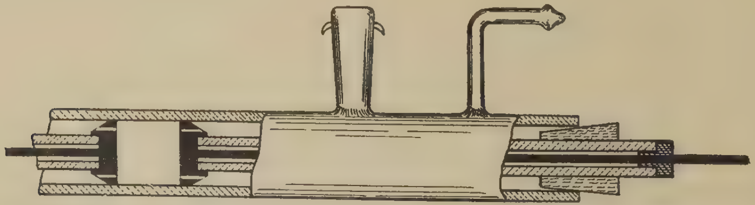

FIG. 1. Partial view of the high compression stream current and electroosmotic cell.

Having direct contact between the electrode face and the pad was a departure from earlier procedure. Goring and Mason (1) reported a decay of both stream potential and permeability with prolonged liquid flow through a pad when this was done, and had eliminated this effect by interposing several layers of plastic mesh between the electrode and the pad.

Two sources of error arise from the use of the mesh. Since the mesh is compressible, there is an uncertain correction to the measured pad length. Secondly, there is the equally indeterminate electrical resistance of the mesh space, which must be added to the resistance of the galvanometer when it is necessary to correct the stream current for leak-back through the pad.

In the present investigation decay was reduced by removing fines from the chopped fibers and was never significant.

Stream Current and Permeability Measurements

Stream current and permeability measurements were carried out as before (8), at an operating pressure of about 40 cm. of water. The measured stream current was corrected for the residual electrode polarization current. The current leak-back (8) was negligible, and no corrections for this effect were necessary. The constancy of the electrolyte concentration was checked by measuring the conductivity of the effluent solution in a flow-type conductance cell included in the liquid outlet line. The values of η and D used were those of water.

Electroosmotic Flow Measurements

For the electroosmotic flow a calibrated capillary (2.464 mm. I.D. × 33 cm. long) was connected in parallel with the cell and a potential difference applied across the electrodes; the rate of movement of an air bubble in the capillary gave $F_{\text{obs.}}$.

Several sources of error were eliminated by the use of reversible electrodes directly in contact with the pad. In the earlier measurements of Goring and Mason (1), the pad was held in a lucite cell between perforated lucite end pieces, and the potential was applied to platinum electrodes which were separated from the pad. E was calculated from the measured current and the pad resistance, the latter being measured separately by the insertion of auxiliary electrodes. Difficulties were encountered owing to evolution of gas at the electrodes.

In the present apparatus there was no evolution of gas at the reversible electrodes, and E was measured directly with a calibrated voltmeter. Electrode polarization at the end of each electroosmotic run was removed by reversing the potential for the same length of time, and then running 25–50 ml. of solution through the pad.

Goring and Mason (1) found a rather large "capillary electroosmosis," i.e., movement of the bubble without a pad in the cell, and corrected for this effect. In the cell used in the present experiments it was insignificant and no correction was necessary.

The electroosmotic leak-back through the pad, resulting from the appreciable resistance to flow in the capillary, was allowed for as follows. Using the quantity

$$\phi = Q\eta/p \qquad [2]$$

as a measure of liquid permeability where Q is the rate of viscous flow of a fluid of viscosity η, under a pressure head p, the true rate of electroosmotic flow was calculated from

$$F = F_{\text{obs.}}\ (1 + \phi_p/\phi_c) \qquad [3]$$

where the subscripts p and c designate the pad and capillary, respectively.

The quantity ϕ_p was obtained directly from the permeability measurements. For the capillary, this proved less practical. At ordinary operating pressures, turbulent flow occurred, yielding spuriously low values of ϕ_c. Viscous flow took place at $p < 2$ cm. water, where the accuracy of measurement was poor. In the initial treatment of the experimental data, ϕ_c was calculated from the Poiseuille equation, using the capillary dimensions and neglecting entrance and exit losses which calculation showed to be insignificant. It will be seen that this procedure led to erroneous results in certain instances.

RESULTS

Comparison of Electroosmotic and Stream Current Functions

Pads of various materials were compressed in stages between the electrodes. The quantities I, ϕ_p, and $F_{\text{obs.}}$ were determined at each pad concentration c; c was calculated from the pad length (measured by means of a travelling microscope), the cross-sectional area of the cell, and the subsequently measured dry weight of the pad.

Figure 2 shows a series of values of

$$\zeta_E/\zeta_S = \frac{F\eta L}{ED} \Big/ \frac{I\eta L}{pD} \qquad [4]$$

for various materials at different pad concentrations, using the Poiseuille value for ϕ_c in correcting $F_{\text{cbs.}}$.

The ratio ζ_E/ζ_S was close to unity except with the cotton and acetate pads, where it dropped significantly at low pad concentrations. The experimental values for acetate rayon, for which the discrepancy between the stream current and electroosmotic functions is greatest, are given in Table I.

A result of particular interest, which is discussed later, was obtained

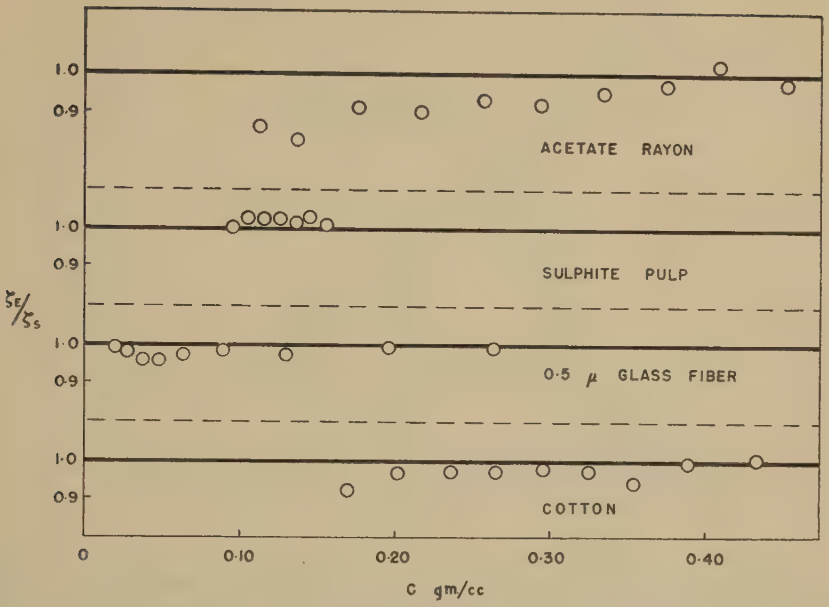

FIG. 2. ζ_E/ζ_S as a function of pad concentration (c) for various fibers, using the Poiseuille correction for ϕ_c.

TABLE I

Measurements of Stream Current and Electroosmotic Flow. Acetate Fibers in 2×10^{-5} *N KCl*

c (g./cc.)	ϕ_p (cc. × 10^8)	$F_{\text{obs.}}\eta L/ED$ (mv. cm.^{2})	$I\eta L/pD$ (mv. cm.^{2})	ζ_E/ζ_S[a]	ζ_E/ζ_S[b]
0.114	48	14.72	20.20	0.86	1.01
0.137	40.5	13.94	19.20	0.83	.95
0.176	30.8	14.20	17.30	0.91	1.00
0.216	23.6	12.70	15.40	0.90	.98
0.257	17.85	11.83	13.50	0.93	1.00
0.294	13.75	10.57	12.00	0.92	.97
0.334	10.50	9.54	10.40	0.95	.99
0.375	7.95	8.50	9.00	0.97	1.00
0.410	6.10	7.83	7.85	1.02	1.04
0.453	4.50	6.50	6.75	0.98	1.00

[a] Using Poiseuille value for ϕ_p.

[b] Corrected for bubble effect as described later.

with the 0.5-μ glass fibers. Here $F\eta L/ED$ and $I\eta L/pD$ showed good agreement (Fig. 3) at pad concentrations as low as 0.9 per cent by volume.

The cotton and acetate pads had higher permeabilities (ϕ_p) than the sulfite and glass pads at corresponding pad concentrations. This suggested

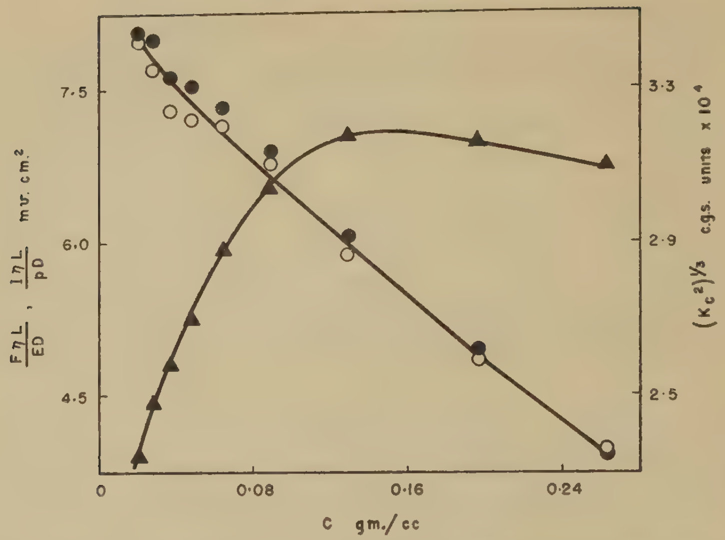

FIG. 3. Stream current (solid circles) and electroosmotic functions (open circles) for 0.5-μ glass wool. The triangular points are calculated from ϕ_p as described in *Discussion*.

an error in the correction for electroosmotic leak-back through the pad given by Eq. [3], since this correction increases with increasing ϕ_p .

In the electroosmotic measurements, the following additional effects were noted:

1. Values of $F_{\text{obs.}}$ varied with the bubble size in the capillary flowmeter. In a series of preliminary measurements carried out on the 2.5-μ glass fiber, a maximum was found at a bubble length of 3 mm.; this bubble length was employed in all the measurements reported above.

2. At all pad concentrations, $F\eta L/ED$ was found to increase with increasing E, and appeared to approach a plateau value. The measurements given above were made at potentials of 45 to 90 volts where F/E did not change with E.

The experiments described in the following sections indicate that these anomalies were due to an unexpected effect of the air bubble in the capillary flowmeter which yielded spuriously low values of F.

Influence of Bubble Length on F

To ascertain whether the low values of ζ_E/ζ_S at high pad permeabilities and the variation of $F\eta L/ED$ with bubble length were related effects, a series of measurements was made on a pad of acetate at three solid concentrations.

The results obtained appear in Fig. 4, which includes the observations on the 2.5-μ glass fiber. The horizontal lines represent the value of $I\eta L/pD$,

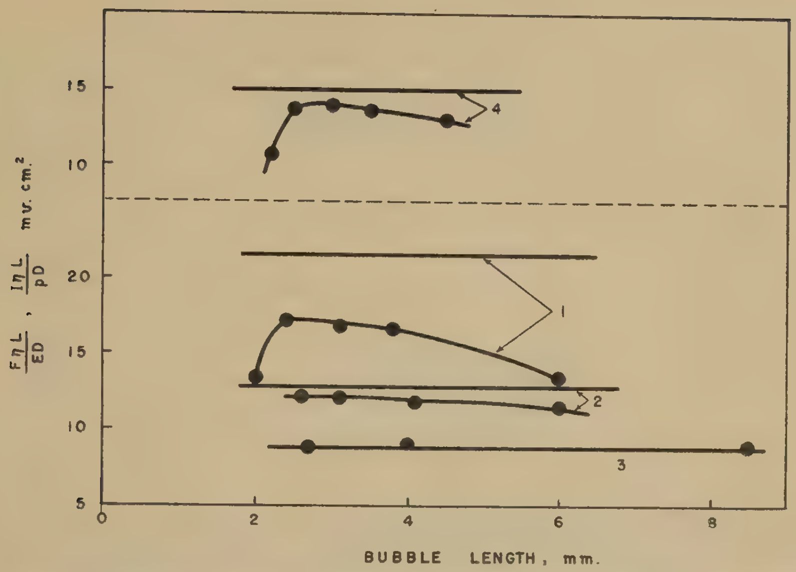

FIG. 4. Electroosmosis at various bubble lengths for an acetate pad at pad permeabilities ϕ_p of 80.1×10^{-8} (curve 1), 21.2×10^{-8} (curve 2), and 5.05×10^{-8} (curve 3) cc., and for a 2.5-μ glass fiber pad of $\phi_p = 26.5 \times 10^{-8}$ cc. (curve 4). The horizontal lines show the corresponding stream current functions.

and the points show the corresponding values of $F\eta L/ED$ at different bubble lengths.

It is seen that the two effects are found together, and that they are related to the permeability of the pad. At the highest ϕ_p , a maximum electroosmotic flow rate was found at a bubble length of 2.4 mm. $F\eta L/ED$ was 20–35% below $I\eta L/pD$. At the intermediate ϕ_p the dependence of electroosmotic flow rate on bubble length was greatly diminished, and $F\eta L/ED$ fell below $I\eta L/pD$ by 5–10%. At the lowest ϕ_p the electroosmotic flow rate was independent of bubble length from 2.7 to 8.5 mm., and $F\eta L/ED$ was equal to $I\eta L/pD$ within the experimental error.

The decrease of $F\eta L/ED$ occurring at bubble lengths less than 2.4 mm. is readily explained. The internal diameter of the capillary was 2.464 mm.; this was the shortest bubble length which still maintained "contact" with the walls of the horizontal capillary. At bubble lengths below 2.4 mm., there was a visible gap between the bottom of the bubble and the capillary wall. It is conceivable that flowing liquid could pass under the bubble, giving too low a value for F. Analytically, this is equivalent to decreasing the apparent permeability of the capillary used in Eq. [3].

The decrease in $F\eta L/ED$ at bubble lengths greater than 2.4 mm. is attributed to a real decrease in capillary permeability due to the bubble itself. Values of ϕ_c were calculated on this assumption from the data obtained

TABLE II

Calculated ϕ_c at Various Bubble Lengths for Acetate Fibers

$c = 0.070$ g./cc.
$\phi_p = 80.1 \times 10^{-8}$ cc.
$I\eta L/pD = 21.50$ mv.cm.^{2}

Bubble length (*mm.*)	Bubble velocity (*cm./sec.*)	ϕ_c (*cc.* × 10^8)	Calculated film thickness (x)	
			From Eq. [5] (μ)	From Eq. [7] (μ)
0	—	274[a]		
2.4	0.203	144	3.2	3.6
3.1	0.200	141	3.2	3.1
3.8	0.196	132	3.2	3.3
6.0	0.159	86	2.9	2.6

[a] Poiseuille value.

on the acetate pad of lowest concentration (Fig. 4), where the leak-back flow was largest. These are given in Table II, where it is seen that ϕ_c decreases with bubble length and is from ½ to ⅓ of the Poiseuille value.

Bubble Resistance

The pronounced effect of the air bubble on the permeability of the capillary was unexpected. It can be explained as follows.

From measurements of bubble velocity and liquid flow, Fairbrother and Stubbs (9) concluded that there is a film of liquid between the moving bubble and the walls of the capillary whose thickness x is given empirically by

$$x = \frac{r_c}{2}\sqrt{\frac{u\eta}{\lambda}} \qquad [5]$$

r_c being the radius of the capillary, u the bubble velocity, and λ the surface tension of the liquid, all in c.g.s. units. The existence of a film around a bubble moving through a capillary has also been demonstrated by electrical conductivity measurements (10).

The hydraulic resistance of the bubble can be calculated by assuming that it moves as a solid plug, i.e., that the velocity gradient is confined to the film around the bubble and is zero inside the bubble. This assumption appears to be justified by Garner's observation that in free sedimentation of fluid drops at low Reynolds numbers, the expected velocity gradients inside the drops are absent (12).

If we assume further that the bubble is cylindrical and that x/r_c is small, it is readily shown that at equilibrium flow

$$p_B = \frac{2Q\eta L_B}{\pi r_c^{\,3} x} \qquad [6]$$

where p_B is the pressure drop across the bubble and L_B is the length of the bubble.

Adding to Eq. [6] the pressure drop in the remainder of the capillary of length L_c calculated from the Poiseuille equation, the total pressure drop becomes

$$p = \frac{2Q\eta L_B}{\pi r_c^3 x} + \frac{8Q\eta L_c}{\pi r_c^4},$$

and the permeability is given by

$$\phi_c = \frac{\pi r_c^3}{2\left(\frac{L_B}{x} + \frac{4L_c}{r_c}\right)}. \qquad [7]$$

Substituting for x from Eq. [5], this becomes

$$\phi_c = \frac{\pi r_c^4}{4\left(L_B\sqrt{\frac{\lambda}{u\eta}} + 2L_c\right)}. \qquad [8]$$

It follows from Eq. [8] that ϕ_c (1) is lower than the Poiseuille value; (2) decreases with increasing bubble length; and (3) increases with increasing bubble velocity.

Values of the film thickness x calculated from values of ϕ_c using Eq. [7] have been included in Table II for comparison with those calculated from the measured bubble velocity using Fairbrother and Stubbs' empirical relation (Eq. [5]). Despite the indirect method of arriving at experimental values of ϕ_c, the agreement is remarkably good.

The reality of the bubble resistance was confirmed by a simple experiment. A reservoir of water was connected to a capillary tube 2 mm. I.D. inclined slightly from the horizontal. Water from the reservoir was blown into the capillary, and the time (t) taken, after release of pressure, for the meniscus to travel between two fixed points 40 cm. apart was measured. This was also done with air bubbles of various lengths in the capillary, in each case shifting the two reference marks upwards along the capillary by the length of the bubble, so that the effective hydrostatic head was at least as great as without a bubble. A typical set of measurements is shown in

TABLE III

Time of Descent at Fixed Inclination

Bubble length (*mm.*)	t (*sec.*)
0	18.1
5.0	22.9
8.0	30.3
14.5	50.4

TABLE IV

Time of Descent at Fixed Bubble Length

Time		$\frac{(t_b - t)}{t}$
Without bubble t (*sec.*)	With bubble t_b (*sec.*)	
73.4	159	1.16
54.7	112.3	1.07
53.0	110.5	1.09
37.6	75.7	1.01
33.1	61.8	.87
26.2	46.8	.79
17.9	29.3	.64
17.5	26.3	.50
15.6	23.0	.47

Table III. ϕ_c, which is proportional to t^{-1}, decreases with increasing bubble length.

Similar measurements were carried out at a bubble length of 7.5 mm., the inclination of the capillary being varied to change u. The results, arranged in increasing order of u in Table IV, show that the resistance of the bubble, expressed as $(t_b - t)/t$, decreases as the bubble velocity is increased.

Effect of Electroosmotic Potential

The increase in $F_{\text{obs.}}\ \eta L/ED$ to a constant value at higher potentials, mentioned earlier, occurred at all pad concentrations and all bubble lengths. The effect is illustrated in Table V for the highly permeable acetate pad, using a 3-mm. bubble.

It is clear from the foregoing considerations that this is caused by the increase in ϕ_c at increasing bubble velocities. Values of ϕ_c calculated as

TABLE V

Variation of Observed Electroosmotic Rate of Acetate Fibers with Applied Potential

$c = 0.070$ g./cc. $L_B = 3.0$ mm.
$\phi_p = 80.1 \times 10^{-8}$ cc. $I\eta L/pD = 21.55$ mv.cm.^{2}

E (*volts*)	u (*cm./sec.*)	$F_{\text{obs.}}\ \eta L/ED$ (*mv. cm.*^{2})	ϕ_c (*cc.* $\times 10^8$)	x	
				From Eq. [5] (μ)	From Eq. [7] (μ)
24.0	0.031	12.48	109	1.3	1.8
48.0	0.068	13.48	133	1.9	2.6
69.6	0.101	13.79	141	2.3	2.9
92.3	0.136	14.02	149	2.7	3.3
115.8	0.173	14.18	154	3.0	3.4
138.2	0.209	14.30	157	3.3	3.7

TABLE VI

Summary of Values of ζ_E/ζ_S for Various Fibers Corrected for Bubble Effect

Fiber	Range of c (g./cc.)	Number of c's	Mean ζ_E/ζ_S
Glass (0.5 μ)	0.02–0.26	9	0.975
Sulfite	0.09–0.16	7	1.010
Cotton	0.17–0.43	9	0.980
Acetate	0.11–0.45	10	0.994
Mean			0.990

before from the observed data in Table V yield film thicknesses which are in reasonable agreement with those calculated directly from the bubble velocity, using Eq. [5].

At very low F's ($<10^{-3}$ cc./sec.) the bubble moved erratically; this is further evidence of the influence of the bubble, since at these low velocities $x \rightarrow 0$, and the well-known Jamin effect of hysteresis in contact angle (11) becomes operative.

Correction for Bubble Effect

Values of ζ_E/ζ_S for the acetate pad, using electroosmotic functions corrected for the bubble effect by calculating ϕ_c from $F_{\text{obs.}}$ using Eq. [8], are given in the last column of Table I. This has also been done for the remaining pads of Fig. 2, and the data summarized in Table VI. The mean of 0.990 for $\zeta/_E\zeta_S$ is considered to show excellent agreement between the electroosmotic and stream current functions.

Electroosmotic Pressure

Since all the discrepancies in electroosmosis experiments are attributable to the air bubble, it was considered to be of interest to conduct some measurements without a bubble. This was done by eliminating the capillary bypass and substituting a differential manometer of 1 mm. I.D. Upon application of a potential across the electrodes, the electroosmotic flow caused a pressure to build up across the pad; this pressure increased until the equilibrium value p_E was reached at which the leak-back flow through the pad was equal, and opposite, to F.

Under these conditions, $F = \phi_p p_E/\eta$; and hence, the following relationship should apply:

$$\frac{p_E \phi_p L}{ED} = \frac{I\eta L}{pD}. \qquad [9]$$

The capillary manometer was used to minimize the volume of liquid transported in establishing equilibrium and thus reduce electrode polariza-

TABLE VII

Electroosmotic Pressure with Acetate Fibers

$c = 0.458$ g./cc.

$\phi_p = 3.87 \times 10^{-8}$ cc.

$I\eta L/pD = 5.35$ mv.cm.^{2}

E (volts)	p_E (cm. H_2O)	$p_E\phi_pL/ED$ (mv. cm.^{2})
137.6	4.84	5.75
114.0	4.00	5.70
91.3	3.15	5.65
69.0	2.48	5.85
45.4	1.61	5.80
22.7	0.80	5.75

tion; however, temperature fluctuations in the system caused the liquid in both manometric arms to move simultaneously, rendering it difficult to determine p_E with precision. Furthermore, it was found that on reversing the potential, p_E was substantially reduced; this may have been due to electrode polarization, changes in electrolyte concentration inside the pad, or a directional change in ϕ_p, but no cause could be definitely assigned.

A set of measurements on a pad of acetate on which the stream current function and ϕ_p were also determined is given in Table VII; $p_E\phi_pL/ED$ was constant over the range of potentials applied. However, it was 10% higher than $I\eta L/pD$. The results are too fragmentary to account for this difference, but it is probably related to the hysteresis in p_E on reversing the potential.

DISCUSSION

When proper corrections are made for leak-back, $\zeta_E/\zeta_S = 1$ for swelling and nonswelling systems. Discrepancies noted by other workers, e.g., Rutgers and de Smet (7), may have been caused by overlooking electroosmotic leak-back. The discrepancy (1) leading to the present investigation appears to have been caused by overlooking the leak-back through the capillary when correcting the capillary electroosmosis. When the data are recalculated to allow for this effect, which is superimposed upon the leak-back through the pad, ζ_E and ζ_S show much closer agreement. As noted earlier there was no capillary electroosmosis in the all-glass system used in the present experiments.

The experimental data given here cover a wide range of pore sizes through which flow occurs. The order of magnitude of the pore radius r_p in the fiber pads can be calculated from the Eq. [8]

$$r_p = \frac{2(1 - \alpha c)}{\sigma c}$$

TABLE VIII

Minimum and Maximum Dimensions in Glass and Acetate Pads

$\delta = 680$ A.

Fiber	r_f (μ)	c		r_p/r_f		r_p/δ	
		Max. (g./cc.)	Min. (g./cc.)	Max.	Min.	Max.	Min.
Glass	0.5	0.022	0.263	113	8.5	830	62
Acetate	10	0.114	0.453	7.8	1.20	1150	175

where α is the specific volume and σ the surface area per unit mass of fibers. For fibers of radius r_f, $\sigma = 2\alpha/r_f$ and

$$r_p = \frac{(1 - \alpha c)r_f}{\alpha c}. \qquad [10]$$

For 0.5-μ glass fiber and acetate pads the ratio r_p/r_f, calculated from Eq. [10], varied from 1.2 to 113 (Table VIII). Despite the low ionic strength, the equivalent double layer thickness δ was always small compared to r_p, so that no complications arise from interpenetration of the double layers.

In electrically induced flow (electroosmosis) the liquid phase moves as a "plug," the entire velocity gradient being concentrated at the solid surface in a layer of the same order of thickness as the diffuse electrical layer. In hydraulically induced flow (streaming), on the other hand, the gradient decreases linearly with distance from the wall, becoming zero towards the center of the channel. According to the conventional electrokinetic theory, ζ is the potential difference between the surface of zero liquid velocity and the bulk liquid. Whether or not this surface is coincident with the solid surface is a matter of speculation (13, 2). In any event, the equivalence of ζ_E and ζ_S is evidence that the surfaces of zero slip are the same for the two types of flow through the complex network of the fiber pads.

In this connection the results obtained with the 0.5-μ glass fibers are of interest. The maximum solid fraction to which the pad could be compressed was, unlike sulfite, cotton, and acetate pads, well below the range of applicability of the Kozeny-Carman equation (15). In the valid range of this equation a plot of $(Kc^2)^{1/3}$ against pad concentration c yields a straight line of *negative* slope (14, 1). K is the permeability coefficient calculated from

$$K = \frac{\phi_p L}{A}$$

where A is the cross-sectional area of the pad. The plot for glass fibers, shown in Fig. 3, passes through a maximum and has a *positive* slope at low c's.

The increase in absolute value of the slope at solid fractions less than 0.2 (0.5 g./cc. of glass) is well known (14, 15). An increase, but not a reversal in sign, of the slope is predictable from Emersleben's theoretical treatment of viscous flow in the direction of the axes through an assembly of parallel cylinders (16).

The behavior noted here is in agreement with an equation derived by Brinkman (17) from a consideration of the viscous force exerted by a flowing liquid on a swarm of separated spherical particles, as an extension of Stokes law for a single particle. In the notation used here, Brinkman's equation takes the form

$$K \doteq \frac{2\left[1 + \tfrac{3}{4}\,\alpha c\left(1 - \sqrt{\frac{8}{\alpha c} - 3}\right)\right]}{\sigma^2 \alpha c}. \qquad [11]$$

At solid fractions (αc) greater than 0.2 this equation yields numerical values of K substantially the same as the Kozeny-Carman equation (15). It is readily shown that Eq. [11] predicts a maximum in $(Kc^2)^{1/3}$ at $\alpha c \sim 0.13$ and a positive slope at lower solid fractions.

This is somewhat higher than the value observed in the present experiments ($\alpha c \sim 0.06$), but this difference may be attributable to differences in particle shape for the two cases.

Thus at low pad concentrations the conditions approach those of electrophoresis, *i.e.*, the electrically induced movement of free particles against the Stokes resistance. In view of the equality of $F\eta L/ED$ and $I\eta L/pD$, this is strong evidence of the equivalence of the electrophoretic function ($u\eta L/ED$, where u is the electrophoretic velocity in a field of strength E/L), the electroosmotic, and the stream current function, as is predicted from the conventional theory of electrokinetic phenomena (2).

SUMMARY

A critical comparison of the electroosmotic flow rate and stream current over a wide range of solid concentrations was made using softwood bleached sulfite, cotton, cellulose acetate, and glass fibers in the presence of 2.5×10^{-5} N KCl. ζ_E showed good agreement with ζ_S with the sulfite and glass fibers, but was lower than ζ_S for the cotton and acetate fibers. It was also found that the electroosmotic flow rate F was not directly proportional to the applied potential at low values of F. It was shown conclusively that the discrepancy was due to the unexpectedly large effect of the air bubble in the capillary flowmeter in resisting electroosmotic flow. When allowance is made for the bubble effect, F is independent of the applied potential and ζ_E and ζ_S agree within 1%. A series of measurements of electroosmotic pressures is reported.

With the glass fibers, agreement between ζ_E and ζ_S was obtained at solid

fractions as low as 0.009, in a region where the resistance to flow of fluid approaches the Stokes resistance of single particles. This is taken to be evidence of an equivalence of the electroosmotic, electrophoretic, and streaming functions.

REFERENCES

1. Goring, D. A. I., and Mason, S. G., *Can. J. Research* **28B**, 307 (1950).
2. Overbeek, J. Th. G., *in* H. R. Kruyt, Colloid Science, Vol. I., p. 194. Elsevier, Amsterdam, 1952.
3. Kanamaru, K., *Cellulose Ind.* **7**, 3 (1931). Cited from C. A. **25**, 3895 (1931).
4. Saxen, U., *Wied. Ann.* **47**, 66 (1892).
5. Rutgers, A. J., and de Smet, M., *Trans. Faraday Soc.* **43**, 102 (1947).
6. Overbeek, J. Th. G., and Wijga, P. W. O., *Rec. trav. chim.* **65**, 556 (1946).
7. Rutgers, A. J., and de Smet, M., *Trans. Faraday Soc.* **48**, 635 (1952).
8. Goring, D. A. I., and Mason, S. G., *Can. J. Research.* **28B**, 323 (1950).
9. Fairbrother, F., and Stubbs, A. E., *J. Chem. Soc.* **1935**, 527.
10. Marchessault, R. H., and Mason, S. G. To be published.
11. Bikerman, J. J., Surface Chemistry, p. 330. Academic Press, New York, 1947.
12. Garner, F. H., *Trans. Inst. Chem. Engrs.* (*London*) **28**, 88 (1950).
13. Overbeek, J. Th. G., *Advances in Colloid Science* **3**, 97 (1950).
14. Carroll, M., and Mason, S. G., *Can. J. Technol.* **30**, 321 (1952).
15. Sullivan, R. R., and Hertel, K. L., *Advances in Colloid Science* **1**, 37 (1942).
16. Emersleben, O., *Physik. Z.* **26**, 601 (1925).
17. Brinkman, H. C., *Appl. Sci. Research* **1A**, 27 (1947).

STREAMING DIELECTRIC DATA OF HYALURONIC ACID

B. Jacobson and T. C. Laurent

Karolinska Institutet, Biochemical Department, Stockholm, Sweden

Received June 11, 1953

Introduction

Owing to the difficulties of obtaining pure hyaluronic acid preparations, only slight attention has been paid to the physicochemical data of this substance (1, 2, 3). In spite of these purity difficulties we have made a streaming dielectric (4) investigation of hyaluronic acid. This was done primarily in order to throw light on the question of how to interpret dielectric data of macromolecular solutions rather than with the intention of describing the properties of hyaluronic acid as a macromolecular substance.

Experimental

We have investigated two preparations of sodium hyaluronate from human navel cord prepared by the chloroform-amylalcohol method according to Blix and Snellman (1). The first preparation (prep. A) contained 41.7% glucoseamine and 2.8% protein impurity (calculated as nonglucoseamine nitrogen × 6.25). In order to obtain the second preparation (prep. B) in the most viscous form possible, it was shaken with the chloroform-amylalcohol only four times, each time for about 12 hr. Otherwise, it had the same treatment as the first one. It contained 33.0% glucoseamine, 0.9% galactoseamine, and 13.1% protein impurities.

The intrinsic viscosity in m/15 phosphate buffer at pH 7.0 was 2.4 for prep. A and 49 for prep. B. If one uses the values of Blix and Snellman (1) for molecular length as a function of intrinsic viscosity one finds the molecular length to be about 1400 A. for prep. A and about 25,000 A. for prep. B. This value for prep. B, however, involves a very large extrapolation. The corresponding molecular weights would be about 64,000 and 1,300,000, calculated by the method of Blix and Snellman (1).

Solutions containing 0.1 g. sodium hyaluronate per milliliter solution were dialyzed at 4°C. three times with distilled water for about 4 hr. each time. The solutions were then diluted to the desired concentrations and measurements made immediately in the streaming dielectric apparatus previously described (4). The dielectric constant and the conductance of the solutions were studied at frequencies between 0.1 and 7 Mc. at 20°C.

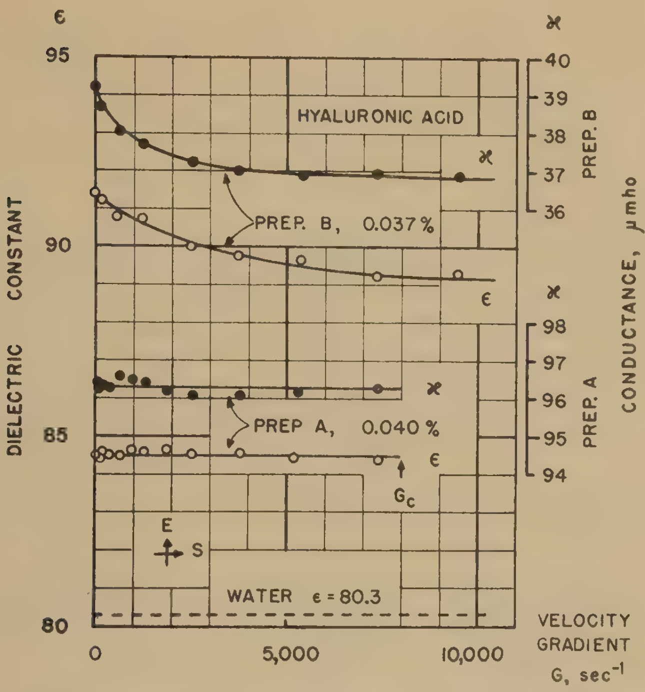

FIG. 1. Dielectric constant and conductance at 0.2 Mc. and 20°C. for sodium hyaluronate solutions. Electric field perpendicular to stream lines. Concentration in grams per 100 ml. solution. G_c is the critical velocity gradient for laminar flow.

During measurements the solutions were subjected to velocity gradients from 0 to 10,000 sec.$^{-1}$ when the electric field was perpendicular to the stream lines, and 0 to 3,600 sec.$^{-1}$ when the fields were mainly parallel.

RESULTS

Typical results are given in the adjoining figures. The dielectric increment per gram hyaluronic acid per liter was 11 for prep. A and 35 for prep. B at low frequencies and zero velocity gradient. The increment was a linear function of the concentration only at small concentrations. No streaming dielectric effect, viz., a change of dielectric constant or conductance with the velocity gradient, could be observed for any solution of prep. A. A small streaming dielectric effect was obtained for solutions of prep. B. These solutions were highly thixotropic. When the electric field was perpendicular to the stream lines, and thus also perpendicular to the orientation of the macromolecules, both the dielectric constant and the conductance decreased slightly with increasing velocity gradient at frequencies below 1 Mc. At high velocity gradients a saturation value is approached. When the electric field was mainly parallel to the stream lines the dielectric

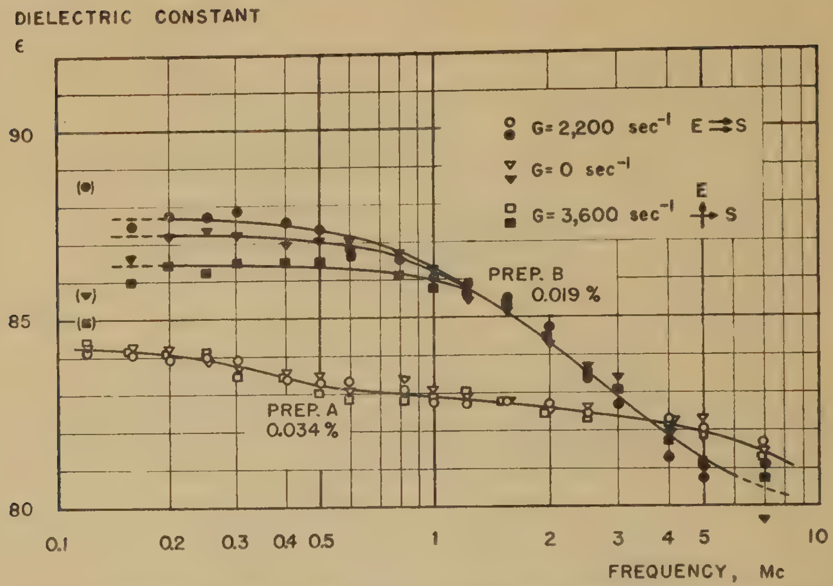

FIG. 2. Dispersion curves of sodium hyaluronate solutions. Measurements at zero velocity gradient (△▲), when electric field was perpendicular to stream lines (□■) or mainly parallel (○●). Temperature 20°C.

constant and the conductance of the solutions either were fairly constant or else increased slightly with the velocity gradient. However, owing to the nonideal electric field conditions (4) during the latter measurements, no large emphasis should be placed on the small increases noted. It is of interest to note, however, that no large decrease in dielectric constant was ever observed when the electric field was parallel to the stream lines. Both preparations for all concentrations studied (0.1 to 0.01 g. per 100 ml. solution) showed a dielectric dispersion in the megacycle range, as is illustrated in Fig. 2.

DISCUSSION

According to current opinion the dielectric properties of macromolecular solutions are considered to arise from rotations of the whole molecules with fixed electric moments. If interpreted in this way the dispersion in the megacycle range for hyaluronic acid should correspond to a relaxation of the rotation about the long axis, as that is the only possible movement for a relaxation time in the order of 10^{-6} sec. If the dielectric increment of the hyaluronic acid were due to such a rotation of the molecules, an increase in dielectric increment should be observed when the molecules were oriented perpendicular to the electric field (as opposed to having random orientation) and a decrease, when they were parallel to it. As this is not the case, it must be inferred that the dielectric properties of the hyaluronic acid solutions cannot be due to a rotation of the whole macromolecules. From that it also follows that molecular weights and axial ratios cannot be calculated from dielectric data according to the methods usually employed. Similar results have previously been obtained for sodium thymonucleate (4).

Therefore a new picture must be sought for the physical significance of the dielectric properties of macromolecular solutions. Recently Kirkwood and Shumaker (5) have proposed a new theory in which the fluctuation of the dipole moment due to mobile proton distribution is shown to be of importance for the dielectric increment of macromolecular solutions. Though their theory is not fully developed as far as the dielectric dispersion is concerned, it appears as though our streaming dielectric data could be partly explained through their picture of the dielectric process.

However, it seems to us that another hypothesis could be used to advantage in treating dielectric data as well as other physical properties of macromolecular solutions. According to this hypothesis, the surface of the macromolecules orders the water structure to form an ice-like structure surrounding the molecules. The ordering action of the surface is due to the fact that the hydrogen bonding positions on it (allowing bonding with the water) fit well into the structure of the ideal four coordinated water lattice. As ice has higher dielectric constant than water, the ice-like structure surrounding the macromolecules also has a high dielectric constant; this then principally accounts for the large dielectric increment observed in solutions of macromolecules with high asymmetry. The dielectric constant of such solutions according to this picture should be mainly independent of the orientation of the macromolecules; this has actually been shown to be the case. In discussing the physical significance of the dielectric increment it should also be mentioned, that a small contribution to it can be obtained from orientations of dipoles within the macromolecules or from dipole fluctuation, according to Kirkwood and Shumaker's theory (5).

The dispersion in the megacycle range of these solutions also fits well into this picture, as the ice-like structure would have a frequency of dispersion between that of water (10^{11} c.p.s.) and that of ice (10^4 c.p.s.). The streaming dielectric effect observed for thixotropic solutions might be due to a breakdown of the "crystallized" ice-like structure by the velocity gradient. The thixotropy could also be explained in the same way. A discussion on the further applicability of this hypothesis will be given elsewhere.

The strong interaction between the hyaluronic acid and the water structure, as described above, is of interest in view of the physiological importance of the acid with respect to the water content and permeability of tissues.

ACKNOWLEDGEMENTS

The authors would like to express their gratitude to Professor Wendell M. Latimer at the University of California for helpful discussions in connection with this work. To Dr. Sven Gardell and Dr. Lennart Roden at Karolinska Institutet we are indebted for invaluable help with the chemical analysis of the hyaluronic acid preparations.

REFERENCES

1. BLIX, G., AND SNELLMAN, O., *Arkiv Kemi, Mineral. Geol.* **19A,** No. 32 (1945).
2. BALAZS, E. A., AND LAURENT, T. C., *J. Polymer Sci.* **6,** 665 (1951).
3. JUNGNER, G., *Acta Chem. Scand.* **4,** 1154 (1950).
4. JACOBSON, B., *Rev. Sci. Instr.*, in press.
5. KIRKWOOD, J G , AND SHUMAKER, J. B., *Proc. Natl. Acad. Sci. U. S.* **38,** 855 (1952).

SIMPLE EXPERIMENT SHOWING THE EXISTENCE OF "LIQUID WATER" FILM ON THE ICE SURFACE[1]

U. Nakaya and A. Matsumoto

Snow, Ice & Permafrost Research Establishment, Corps of Engineers, Wilmette, Illinois, and Department of Physics, Hokkaido University, Sapporo, Japan

Received June 15, 1953

ABSTRACT

Two small ice spheres are suspended by thin cotton filaments. The top of one filament is displaced horizontally by a screw motion. The movable ice sphere is brought in contact with the stationary sphere, and then the screw is turned back. The normal cohesion is measured by the inclination of the filament when the spheres are separated. Sometimes the ice spheres showed a rotation before separation. The rotation took place more frequently in the range of temperatures near the freezing point, but it was observed once at −7.0°C., the lowest temperature when distilled water was used. When ice spheres made of 0.1% solution of NaCl were used, this rotation was very likely to occur and was observed quite often at −14°C. Successive rotations were sometimes observed in this case. These phenomena are explained by considering a model of the point of contact, which is composed of a solid ice bond and the surface films of a liquid-like nature. The relation between the strength of the ice bond and the area of contact is calculated by using Hertz's equation.

EXPERIMENTS

The regelation of ice has been a problem since the days of Faraday and Tyndall. Weyl (1), treating this problem from the standpoint of modern molecular physics, has strongly suggested the presence of liquid-water film on ice surface at temperature below 0°C. This liquid-water film is not supercooled water, but is in equilibrium with its vapor phase on one side and with the ice crystal on the other.

During the course of some experiments on the adhesive force between two ice particles, carried out in the cold chamber laboratory of the Low Temperature Institute, Hokkaido University, Sapporo, Japan, we found a phenomenon which seems to show the existence of this boundary layer. Two small ice spheres were suspended by very thin filaments. One filament could be moved by a screw motion so that the top of the filament was displaced horizontally. By this method, the normal adhesive force is measured by the inclination of the filament when the spheres are separated.

The ice sphere was made by freezing a drop of distilled water. A cotton

---

[1] Published by permission of the Office, Chief of Engineers, Dept. of the Army.

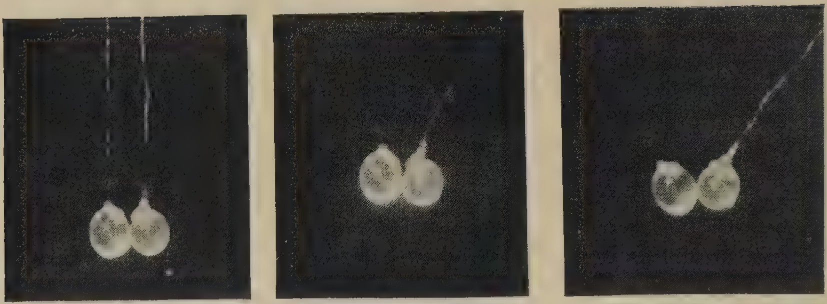

FIG. 1. Mean diameter of the ice ball = 1.45 mm. Temperature = −5.5°C. (*a*) Start of the experiment; (*b*) before rotation; (*c*) after rotation.

filament was used as the suspending material. The diameter of the ice spheres was varied between 1.5 and 4 mm. The experiment was carried out in a metal box with suitable windows for taking microphotographs and was observed through a horizontal microscope. The temperature in the box was varied between −0.5°C. and −16°C. The movable ice sphere was brought in contact with the stationary sphere by the screw motion device, but care was taken to avoid any appreciable pressure between the spheres. The effect of the duration of contact is an element to be studied, but in this series of experiments the time was chosen as 1 min. or a little less.

The two spheres usually separated at a certain angle θ of inclination of the filament. Sometimes, however, the ice spheres showed a rotation before separation, at an angle of ϕ. Two examples are shown in Figs. 1 and 2. In both cases, (*a*) shows the initial state, (*b*) the state just before the rotation, the inclination of the filament being ϕ, and (*c*) the state after rotation.

This rotation did not always occur, but it was not rare. For example, in one series of experiments, this rotation phenomenon was observed nine times in thirty-eight cases. The rotation took place more frequently in the range of temperature near the freezing point, but it was observed once at −7.0°C., the lowest temperature when distilled water was used. It some-

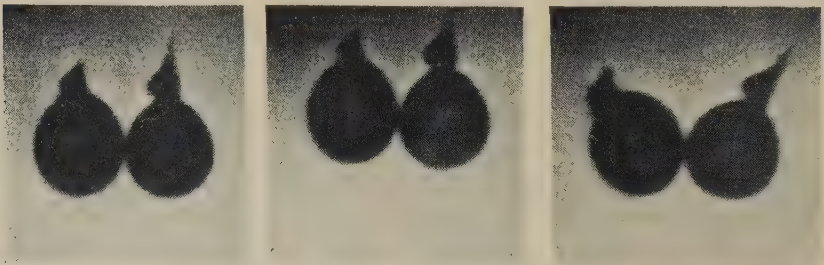

FIG. 2. Mean diameter of the ice ball = 1.95 mm. Temperature = −3.0°C. (*a*) Start of the experiment; (*b*) before rotation; (*c*) after rotation.

times happens, though seldom, that the spheres rotate two or three times in succession at the angles of ϕ_1, ϕ_2, and ϕ_3, and then separate at θ. This successive rotation takes place more often when NaCl solution of 0.1% is used, as described later. This phenomenon reminds us of Bowden's stick-slip motion in his friction experiment. The air in the measuring box

TABLE I

The Angles of Rotation and Separation for Ice Spheres of Distilled Water

No.	Temp. (°C.)	Radius a (mm.)	Length l (mm.)	ϕ Rotation	ϕ' (Obs.) after rotation	ϕ' (Calc.) after rotation	$\widehat{PP'}$ (mm.)	x (mm.)	θ Separation
1	−1.0	1.2	12.2	30°	27°	27.1°	0.57	0.16	>56°
2	−2.0	1.2	12.2	44	39	39.3	0.82	0.40	80
3	−5.4	0.7	16.3	33	31	31.5	0.38	0.20	>66
4	−3.0	1.2	16.4	35	32	30.5	0.67	0.28	43
5	−3.0	1.0	16.7	27	26	25.4	0.45	0.10	>67
6	−3.0	1.0	16.7	26	25	24.4	0.43	0.09	>66
7	−3.0	0.9	16.7	14	13	13.3	0.20	0.04	28
8	−3.0	0.9	16.7	6	5	5.7	0.08	0.03	>70
9	−3.0	0.9	16.7	47	44	44.0	0.69	0.35	>65
10	−3.0	0.9	16.7	29	27	27.5	0.42	0.17	66
11	−3.0	0.9	16.7	29	27	27.5	0.42	0.17	66
12	−3.0	0.9	16.7	43	40	40.3	0.63	0.35	65

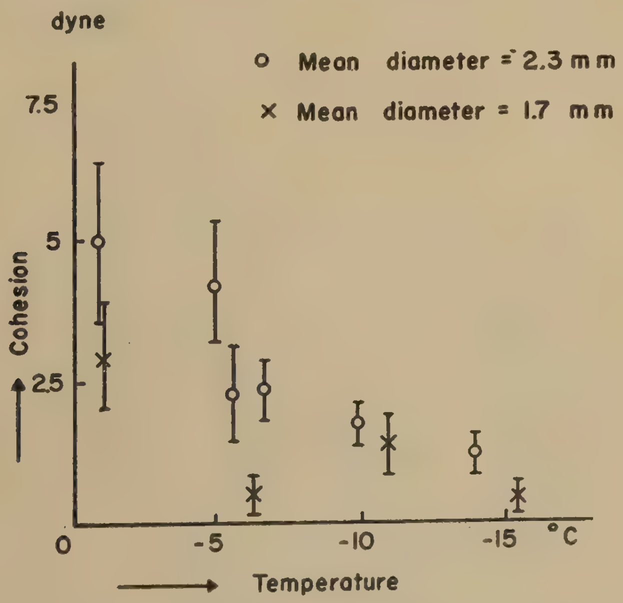

FIG. 3. The relation between normal cohesion and temperature.

must be considered as saturated at any time, because a considerable amount of frost crystals was in the box.

Some examples of ϕ and θ are shown in Table I, in which $>$ means that the spheres did not separate with this angle.

The normal cohesion was calculated from θ by Eq. [5], given in the next section, irrespective of the occurrence of rotation. Cohesion was studied as a function of temperature, keeping the time of contact and the initial pressure between the spheres roughly constant. The measured values showed a wide fluctuation, which is essentially the nature of this sort of phenomenon. The mean of the values is taken for each of the temperatures. Figure 3 shows the results for two series of the experiments. A vertical bar through each of the points shows its range of mean error. In this stage of the experiments, we can only say that the normal cohesion tends to decrease with decreasing temperature. Although it is qualitative, this tendency is quite evident.

DISCUSSION

Figure 4 shows the configuration at the moments before and after rotation of the sphere. The radius of the sphere is a, and the length of the fila-

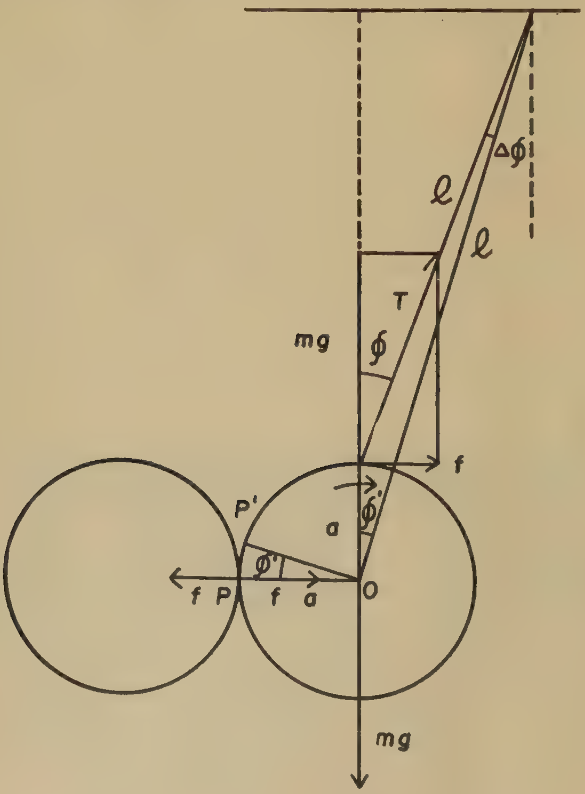

FIG. 4. Geometry of rotation of the sphere.

ment is l. When rotation takes place at the angle ϕ, the inclination of the filament changes to ϕ' after rotation. The tension of the filament T gives a horizontal component f, which causes a moment of rotation as well as the normal tensile stress at the point of contact P, the former being fa.

The moment of rotation is calculated from the geometry shown in Fig. 4.

$$\text{The moment of rotation} = mga \tan \phi. \qquad [1]$$

When the resistance at the point of contact is overcome by this moment of rotation, rotation of the sphere takes place. The angle of rotation is ϕ' and the initial point of contact P comes to P', as shown in the figure. ϕ and ϕ' are measured respectively on the microphotograph. ϕ'(obs.) in Table I shows this value.

ϕ' can be calculated from ϕ. Trigonometry shows that

$$\sin \phi' = \frac{l}{a + l} \sin \phi. \qquad [2]$$

ϕ' calculated by this equation is given in Table I as ϕ'(calc.). ϕ' is important because it is the angle of rotation of the ice sphere. The two values of the observed and the calculated are in good agreement. This shows that the sphere rotates to the amount of angle which is required by the mechanics.

The length of the arc PP', the sliding distance at the point of contact, is $a\phi'$, where ϕ' is measured in radians. For discussion of the problem of sliding at the point of contact, the geometry shown in Fig. 4 is not suffi-

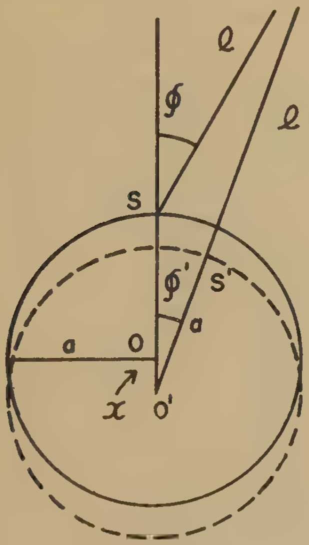

FIG. 5

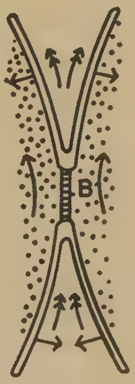

FIG. 6

FIG. 5. The displacement of the sphere by rotation.
FIG. 6. A model of point of contact.

cient, because it is only an approximation. The sphere moves down when it rotates, as shown in Fig. 5. The amount of displacement x is given by

$$x = l\Delta\phi \sin \phi - a(1 - \cos \phi), \qquad [3]$$

neglecting the second term. The length of the arc PP' and the value of x calculated by Eq. [3] are also given in Table I.

In order to explain this peculiar rotation of the sphere, a model is considered (Fig. 6). B indicates the supposed bridge of ice at the point of contact, and thick lines show the surface films of a liquid-like nature. It is believed that the liquid-like boundary layer will freeze when bounded by ice on both sides. So the infinitesimal portion of the film at the point of contact will be frozen, forming the ice bridge or bond B that has been assumed by many former investigators. If the adhesion of ice is chiefly due to this bridge or bond, which is a solid material, the spheres will not rotate but will separate at a certain critical inclination of the filament. The rotation must be due to another property of the boundary layer, conceivably the adhesion due to the liquid-like nature of the surface film. The fact that the sphere does not rotate until a critical moment of rotation is applied is explained by the existence of the solid bond. However, after this bond is broken, with the moment of rotation reaching $mga \tan \phi$, adhesion must be caused by surface tension of the film.

Rotation of the sphere can take place in two ways: (1) with the center of rotation fixed, or (2) with displacement of the center of rotation. In the latter case, if the displacement of the center of rotation is equal to the length of the arc traversed by a point on the surface, the locus of the point of contact is a cycloid and the motion is a pure roll. The stress given to the surface film will be normal to the film, as shown by the single arrows in Fig. 6. When the center of rotation is fixed, the moment of rotation will cause a tangential stress in the surface film, as shown by the double arrows in Fig. 6. In our experiments, the displacement of the center of rotation is x in Fig. 5, which is not equal to the length of the arc $\overset{\frown}{PP'}$. The difference between $\overset{\frown}{PP'}$ and x is equal to the displacement of the point of contact when the center of rotation is fixed. So $(\overset{\frown}{PP'} - x)$ will give a measure of the tangential strain in the surface film caused by this mode of rotation of the sphere. The values of $(\overset{\frown}{PP'} - x)$, obtained from the data in Table I, are given in Table II. As for the nature of this tangential strain, present data are not sufficient for further discussion.

The moment of rotation is calculated by Eq. [1], and the results tabulated in Table II. If the rotation starts by breaking the ice bond at the point of contact, the moment of rotation must be related to the contact area between two spheres. The contact area between two spherical surfaces can be calculated from Hertz's equation:

$$a = 1.1 \sqrt[3]{\frac{Fr}{2E}} \qquad [4]$$

in which a is the radius of contact circle, F the force at the point of contact, r the radius of curvature, and E Young's modulus. For a rough approximation, E is taken as 5×10^{10} dynes/cm^2., and F is assumed as 0.01 dyne. Supplementary experiments showed that the initial pressure between the two spheres caused a remarkable variation in cohesion; for example, an initial force of 0.1 dyne made the cohesion more than ten times larger. In this series of experiments, the initial force was made as small as possible, and we estimate it to have been about 0.01 dyne or less. So it is reasonable to assume F as 0.01 dyne. The contact area $A = \pi a^2$ is calculated and the result given in Table II.

The relation between the moment of rotation, which is considered to act primarily for breaking the ice bond, and the contact area is shown in Fig. 7. As the moment of rotation can be taken as a measure of the strength of the ice bond, Fig. 7 in effect shows the relation between the strength and size of the ice bond. The result is qualitatively in agreement with what is expected. The points are scattered over a wide range, chiefly owing to the fluctuation in F.

If we neglect the problem of rotation, the normal cohesion is roughly calculated from the angle of separation by the equation:

$$\text{Normal cohesion} = mg \tan \theta. \qquad [5]$$

TABLE II

The Moment of Rotation and the Contact Area

No.	$(\widehat{PP'} - x)$ (mm.)	$mga \tan \phi$ dyne-cm.	Contact area A (μ^2)
1	0.41	0.44	0.19
2	0.42	0.74	0.19
3	0.18	0.06	0.14
4	0.39	0.53	0.19
5	0.35	0.19	0.17
6	0.34	0.18	0.17
7	0.16	0.06	0.16
8	0.05	0.03	0.16
9	0.34	0.26	0.16
10	0.25	0.13	0.16
11	0.25	0.13	0.16
12	0.28	0.23	0.16

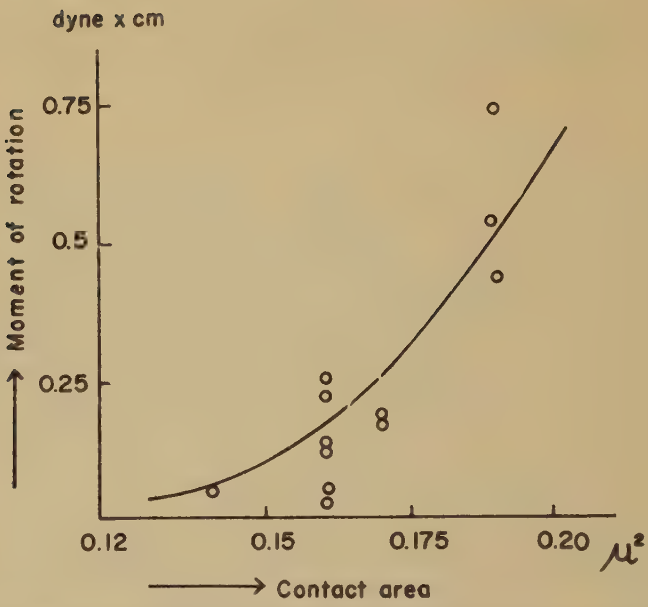

FIG. 7. The relation between the strength of the ice bond and the area of contact.

This normal cohesion decreases with decreasing temperature (Fig. 3). The individual value shows excessive fluctuation, which is considered to be mostly due to the slight variation in initial force between the two spheres. Most of the experiments were carried out with the initial condition such that the force acting at the point of contact was unmeasurably small, say 0.01 dyne or less. A slight increase in this force causes a remarkable increase

TABLE III

The Angles of Rotation and Separation for the Ice Spheres of 0.1% Solution of NaCl
Temperature = −14°C., l = 16.6 mm., a = 1.2 mm.

No.	Rotation and separation							Separation without rotation	
	ϕ_1	ϕ_1'	ϕ_2	ϕ_2'	ϕ_3	ϕ_3'	θ	No.	θ
2	5	4	37	35	65[a]	62	>65	1	39
3	24	23	—	—	68[a]	62	>68	5	42
4	39	36	65	62	—	—	>62	7	39
6	34	31	66	62	—	—	>62	8	>71
10	43	39	—	—	—	—	>65	9	53
14	26	24	—	—	67[a]	62	>67	11	55
15	43	39	—	—	—	—	>65	12	>71
16	27	25	—	—	—	—	51	13	>71
17	23	21	36	35	66[a]	62	>66		

[a] A slight shock is given to the box.

in cohesion. In one example, with minimum initial force, the cohesion was about 1 dyne at −5.5°C., the radius of the sphere being 0.7 mm. Under the same condition, when a force of 0.1 dyne was applied between the spheres by a negative inclination of the filament, the cohesion increased to more than 14 dynes, the limit of our measuring device.

Another conceivable cause of fluctuation in cohesion is the microcrystalline structure of ice. It is well known that the melting point of the boundary layer between component crystals is lower than that of pure ice. As a result, a large block of glacier ice is usually easily separated into its component crystals when it is kept at a temperature just below 0°C. In our experiment, the ice sphere is of microcrystalline structure, and the area of contact might be either a portion of the surface of a component crystal or partly a boundary layer between crystals. The cohesion would be very different for those two cases. So we cannot expect consistent cohesion values in ordinary ice, which is made of many component crystals.

Some experiments were carried out with ice spheres made of 0.1 % solution of NaCl. Several interesting phenomena were observed. Rotation of the sphere was very likely to occur, and was observed quite often at such low temperatures as −14°C. In seventeen experiments at −14°C., rotation took place in nine cases (Table III). Comparing angles of separation θ in Tables I and III, we see that cohesion is far stronger between ice spheres of 0.1 % solution of NaCl than between ice spheres of pure water; cohesion of the former even at −14°C. is higher than that of the latter at −1°C. or −3°C.

Another interesting phenomenon is repeated rotation, four examples of which are seen in Table III. The superscript *a* shows that the second or third rotation took place when a slight shock was given to the measuring box. With ice spheres of NaCl solution, the cohesion showed a marked tendency to increase after rotation. All the above phenomena suggest that some part of the impurity NaCl is concentrated on the surface during freezing, so that the surface layer has a more liquid-like nature than the surface of pure ice.

All the results obtained from this series of experiments may be explained by assuming the existence of a liquid film on the ice surface, and no other explanation seems to be adequate. Therefore, the authors consider that this experiment shows the existence of liquid-water film on the ice surface.

The experiments were carried out in the cold chamber of the Low Temperature Institute, Hokkaido University, Sapporo, while one of the authors (U. Nakaya) was in Sapporo. The authors wish to thank the authorities of the Low Temperature Institute for the use of their facilities.

REFERENCE

1. WEYL, W. A., *Surface Structure of Water and Some of Its Physical and Chemical Manifestations. J. Colloid Sci.* **6**, 389–405 (1951).

THE OBSERVATION OF FOAM DRAINAGE TRANSITIONS

Morton B. Epstein, John Ross, and Conrad W. Jakob

Colgate-Palmolive-Peet Company, Jersey City, New Jersey

Received June 30, 1953; revised October 26, 1953

Abstract

Apparatus and methods for observing foam drainage transition temperatures are described. Sharp and reversible transitions are observed in Duponol ME (long-chain sodium alcohol sulfates) systems containing unsulfated alcohol, and in Duponol ME systems in which the unsulfated alcohols are replaced with lauryl alcohol. The foam drainage transition temperatures agree with the corresponding film drainage transition temperatures.

Introduction

It has been known for some time that small amounts of organic polar compounds may lower markedly the drainage rate of detergent foams or single films (1, 2). This effect can be made to disappear by heating the system, and it has been shown for single films (2) that the disappearance occurs over a narrow range of temperature, generally of the order of 2°C. or less, which may be termed the film drainage transition temperature. The characteristics of the corresponding foam transitions as, *e.g.*, their sharpness and reversibility, have not previously been given detailed examination.

Experimental

It may be expected that a transition is a property of the composition of the solution with which the foam is in equilibrium and is independent of the distribution of bubble sizes or of the particular drainage conditions in the foam, *e.g.*, whether or not the draining solution is replenished. Entirely for reasons of experimental simplicity, the measurements have been made on uniform bubble-size foams being rewetted by a known constant input of solution. A single bubble size permits the reproduction of a given foam as desired, avoids segregation of bubbles according to size, and makes breakdown more evident when it occurs. Well-drained, low-density foams and foams showing breakdown have been avoided, as well as high-density foams (high flow rates) showing streaming of the bubbles.

Materials and Preparation of Solutions

The Duponol ME contained 88.1% mixed straight-chain alcohol sulfates (largely sodium lauryl sulfate), 6.1% alcohol insolubles (Na_2SO_4), 5.1% ether-soluble materials (largely unsulfated alcohols), and 0.2% moisture. Extracted Duponol ME was prepared by extraction with ethyl ether, raising the alcohol sulfate content to 92.8%. The lauryl alcohol was commercial material fractionated by distillation and had a purity of at least 99.3%, as estimated from freezing point analysis.

In all experiments, 0.25% solutions in distilled H_2O were used. Solutions of extracted Duponol ME to which 4.0% lauryl alcohol (alcohol sulfate basis) were added were prepared by dissolving the detergent and alcohol in a small amount of distilled water at approximately 80°C. and then diluting to the required volume with distilled water.

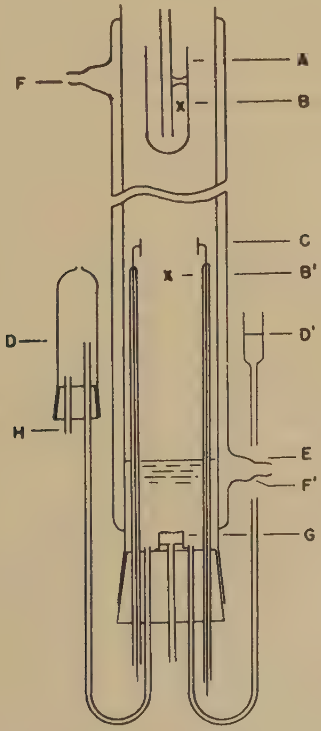

FIG. 1. Foam drainage apparatus. A, solution inlet with bubble trap; B and B' location of thermocouples; C, electrodes; D and D', reference level and auxiliary manometer; E, foam/solution interface; F, F' outlet to vacuum pump or to jacket supply; G, bubbler with air inlet; H, solution outlet with drop counter. Jacketed section of column 75 cm. long × 5 cm. internal diameter.

Foam Columns

Various columns have been used, a typical column being shown in Fig. 1. The inner tube is graduated in millimeters. The column is filled with foam by means of a bubbling device at the bottom. These devices have been of three kinds, including platinum spinnerets commonly used in spinning fibers; concentric tube bubblers, in which solution is flowed rapidly through an orifice concentric with an inner air orifice (3); and obstructed orifice types (4), in which a thin rod is used to obstruct partially a minute opening at the end of a narrow capillary. Bubbles ranging from 1 to 2 mm. are most conveniently produced by means of spinnerets; the other bubblers serve to produce smaller bubbles, ranging down to 0.1 mm., with rates of production of 1000 per second or greater. Generation of foam is halted when a suitable column of foam has been produced.

Solution is flowed into the foam at the top of the column by means of an overflow device which acts also as a bubble trap. The solution leaves through a constant level outlet having a drop counter. Auxiliary means for supplying air and solution at desired constant rates of flow and for altering the temperature of the input solution and the temperature of the jacket are conventional and are not shown. The jacket may be evacuated if desired. The output rate is followed by weighing of fractions and by photoelectric counting of the drops.

The pressure drop across the column of foam is taken as the difference in height between the level shown on an auxiliary manometer and the level of the foam/solution boundary.

Electrodes and Thermocouples

A pair of bright platinum electrodes can be inserted into the foam column from below. The resistance between the electrodes is measured by means of a 1000-cycle impedance bridge operated off balance. The output of the bridge is rectified, well filtered, and fed to a recording potentiometer. The initial capacitance of the foam is balanced out, and a decade resistance box in series with the electrodes serves in calibrating and in adjusting the range of the recorder. Four- and three-junction calibrated iron-constantan thermocouples can be inserted in the input device and in the foam. The output of the thermocouples is also fed to the recording potentiometer, which is a multiple-point instrument.

Film Drainage Transition Temperatures

Film drainage transition temperatures were determined by observing the descent of interference bands in a test tube film drainage apparatus (2).

DISCUSSION OF METHOD

Consider a tube partly filled with detergent solution and having an air/solution interface at a known reference level. Let foam be produced by any means, *e.g.*, by pouring a portion of the same liquid back into the column, by bubbling, or by mechanical agitation. Shortly after completion of foam generation, a foam/solution interface appears. It is obvious that since a certain amount of liquid now is in the foam, the foam/solution interface must be below the initial reference level. At any instant, the amount of solution displaced into the foam and the average foam density may be calculated from elementary considerations which are particularly simple if the columns are uniform cylinders.

These observations apply equally to foam columns through which a flow of solution is maintained, as the column in Fig. 1. If, with foam absent, solution is introduced at the top of the column at a steady rate, a reference level of the air/solution interface will be established by the orifice of the overflow tube, and the rate of flow out of the column will then equal the input. If foam is then generated until it fills the column to the level at which the rewetting solution is introduced, it will be found that the foam/solution interface is below the original (reference) level. Of necessity, the orifice defines a level of essentially unchanged (zero) pressure, and the amount of liquid in the foam is given by the lowering of the interface. The average foam density may be calculated exactly as before.

If the flow of solution into the column is halted, the output ceases almost immediately provided the column is of uniform cross section. Thereafter drainage proceeds in the normal manner described for a simple tube. The small amount of liquid collected upon halting the input is due mainly to the back pressure developed by the orifice; this pressure may be observed by means of the auxiliary manometer.

Internal foam collapse, foam transition, or any other source of change in the average foam density will result in a change in the level of the foam/solution interface, despite maintenance of constant input. Applications to the study of the rate of drainage of foam and other properties of foam are apparent.

The pressure drop across the complete column of foam does not reveal local changes in the foam. These may be studied by a variety of other means, including examination of optical properties (5), foam consistency (6), or electrical conductance. Of these only the last will be described. It has been established experimentally that the conductance of a foam, as may be expected, varies in a regular way and approximately linearly over a wide range of foam densities (1, 7, 8). With automatic recording, the measurement of resistance between electrodes immersed in a column of foam provides a versatile and flexible tool in the study of foam drainage.

Nonuniform columns are discussed below in connection with the observation of transition temperatures in such columns.

Hydrostatic pressure drop has been used previously as a measure of foam density by Schiebl (9) and Siehr (10).

The present approach regards a column of foam differently from a previous paper (1). One of the characteristics of a foam column is its capacity to alter in geometry according to the rate of solution flow. A column of foam swells when the flow through it is increased, the channels increasing particularly in their width. This increase is opposed by the buoyancy of the bubbles and by forces analogous to Bernoulli forces which arise from the streaming of liquid through narrow channels. In addition, the deformation of bubbles depends in part upon the size of the bubbles and the relative volume of liquid separating them. These effects are not inconsiderable, and it is evident that an adequate theory of foam drainage cannot ignore them.

Relative flow rates in thin, single films are noticeably of a very different order (fast:slow = 100:1) from the relative flow rates in a foam. As may be seen in Fig. 2, discussed below, this ratio in the foams reported is approximately 2:1.

The Foam-Air Interface

With certain exceptions, for systems in which the foam/solution interface is allowed to move freely with reference to an outlet in a fixed position, there is no change in the level of the foam/air interface whether the foam is being rewet or is draining freely. On the other hand, if the foam/liquid interface is kept at a constant level by manipulating the outlet level, then it is the level of the foam/air interface which reflects the changes in the average foam density. The principal exceptions include collapse of the foam at the top or a change in the total volume of the air in the bubbles due to change in temperature or to dissolving of gas by the solution.

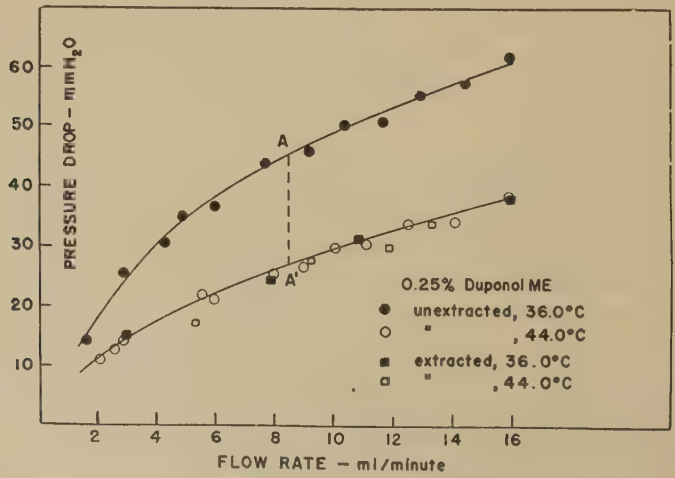

Fig. 2. Pressure drop (liquid held) *vs.* rate of flow. Bubble diameter, 1.5 mm.; column 50 cm. long × 2.5 cm. internal diameter. Reference level 42.6 cm. below solution inlet.

In the experiments described in this paper, appreciable expansion or contraction of the foam must occur during the course of the measurements. As shown by Fig. 1, the effective volume of the gas contained by the foam through which the solution flows is set by the volume included between the reference level and the level of the solution input. It is this volume which is constant throughout the experiment and not the mass of the gas.

Results and Discussion

In Fig. 2, the amount of liquid held in a column of foam, as given by the pressure drop across the foam, is presented for various steady rates of flow of 0.25% aqueous solution of Duponol ME. The two curves represent data obtained well above and below the transition temperature for the system. The marked difference in amount of liquid held, and therefore in the resistance to flow, illustrates the difference between "fast-" and "slow-" draining foams. Data are also presented for 0.25% aqueous solution of ether-extracted Duponol ME. It is apparent that this effect of the ether solubles upon drainage disappears above the transition temperature.

The two curves are divergent over the range examined. At sufficiently high densities, they may be expected to converge, but it has been found that mass turbulence of the whole foam sets in with very high flow rates.

Under the conditions of a uniform rate of input, transition from slow to fast drainage is accompanied by a loss of liquid equal to the difference along the ordinate representing the input, *i.e.*, between the points A and A' shown in Fig. 2. Any method of detecting such a shift in the drainage relation with change of temperature potentially is a method of measuring foam transition temperatures. In the experiments described in this paper, the temperature of the foam was altered at a uniform rate, either rising or falling, while the pressure drop across the foam, the resistance between electrodes immersed in the foam, or the rate of liquid output were observed with uniform or nonuniform columns as appropriate.

Isothermal Columns

Results for 0.25% aqueous solution of Duponol ME are given in Fig. 3, with pertinent details in the legend. The temperature of this jacket and the input liquid changed together, and since in addition the column was relatively narrow, it is termed isothermal. The thermocouple was located approximately midway between the electrodes and the input solution. It may be noted that with a narrow column, the tubes bearing the electrodes may occupy an appreciable volume and the column cannot be strictly regarded as having a uniform diameter.

It is apparent that a pronounced transition occurs in the foam density as shown by the pressure drop and resistance measurements. The transition is sharp and reversible. The abrupt change in the level of the foam/solution

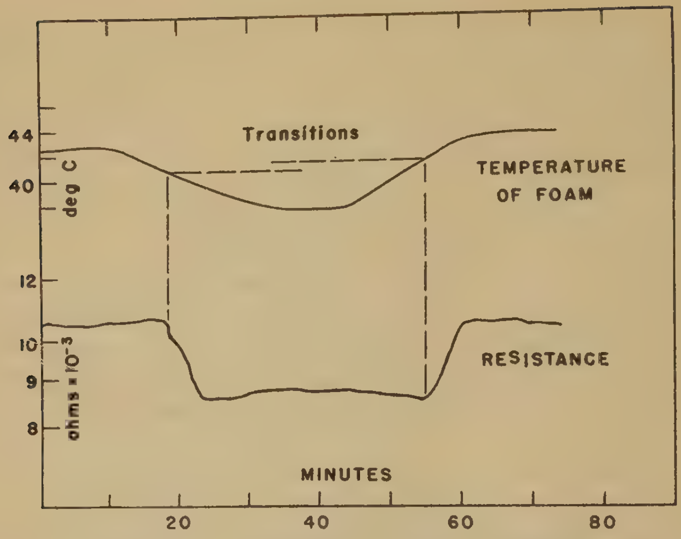

FIG. 3. Foam transitions in "isothermal" column. Bubble diameter, 1.0 mm.; column 50 cm. long × 2.5 cm. internal diameter. Thermocouple 6 cm.; electrodes 37 cm.; and reference level 42 cm. below solution inlet. Solution, 0.25% Duponol ME, not extracted; flow rate 9.75 ml. per minute.

interface often is apparent to the eye merely on watching the movement of the lower boundary of the foam. If it is assumed that the proper measure of the transition temperature is given by the onset of the transition, then the estimated values are: rising temperatures, 41.5°C.; falling temperatures, 40.6°C. Film drainage observations gave 41.5°C. as the transition temperature.

Adiabatic Columns

Results for 0.25% aqueous solution of ether-extracted Duponol ME plus 4.0% lauryl alcohol, alcohol sulfate basis, are given in Fig. 4 for rising temperatures and in Fig. 5 for falling temperatures. The column was wide and the jacket was evacuated to approximate adiabatic conditions at the walls. Thermocouples were located in the solution input device and at a short distance below the electrodes. Again, in each experiment there is a region over which a pronounced transition occurs in the average foam density, as shown by the pressure drop. Several of the details of the transition may be inferred from the resistance measurements, which reflect changes in the density of the foam at the level of the electrodes.

With rising temperatures, the transition is accompanied by an initial drop in resistance. This drop is a consequence of maintaining adiabatic conditions at the walls of the column. Under such conditions, the transition occurs first at the top of the column and then progresses downward. The

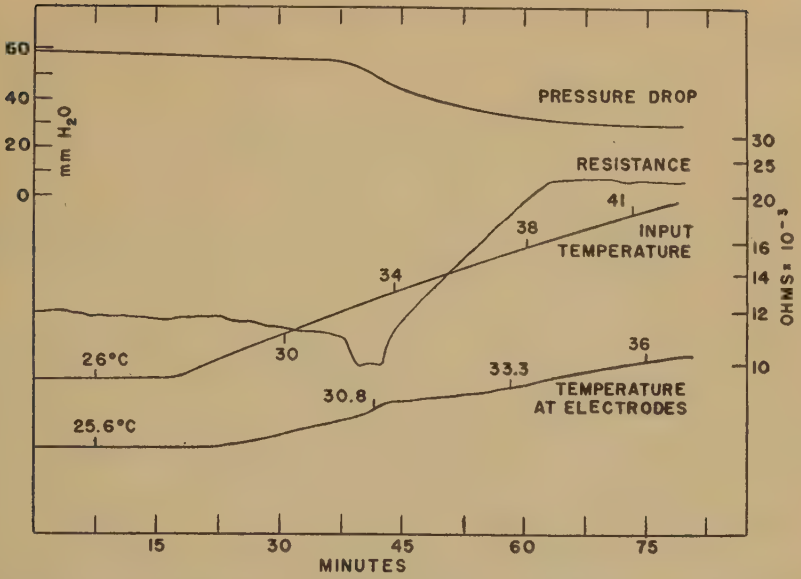

FIG. 4. Foam transition with "adiabatic" column, ascending temperature. Bubble diameter, 1.5 mm. Column as in Fig. 1. Temperatures measured in solution inlet and 2 cm. below electrodes. Electrodes and reference level 47 and 58 cm., respectively, below solution inlet. Solution 0.25% Duponol ME, ether-extracted, alcohol sulfate basis, plus 4% lauryl alcohol, alcohol sulfate basis; flow rate 18.3 ml. per minute.

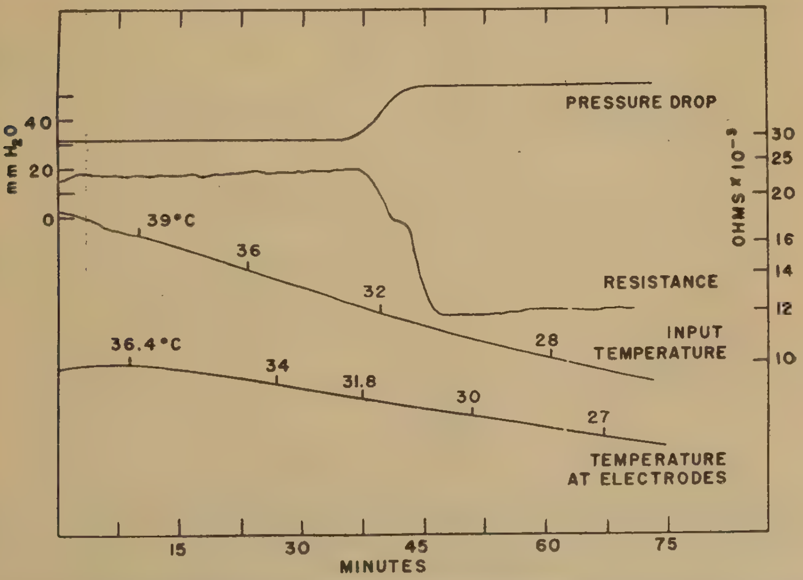

FIG. 5. Foam transition with "adiabatic" column, descending temperature. Details given in legend to Fig. 4.

excess solution shed by the section of the foam which has already become fast-draining accumulates as a flood which progresses in part below the boundary of the transition. When this excess sweeps past the electrodes, there is a drop in resistance; subsequently there is a much longer period during which the resistance rises as the foam loses liquid and reaches a steady and relatively drier condition.

With falling temperatures, the expected inverse effect was not observed. It may be that with a modification of the apparatus it would be possible to demonstrate a boundary which is somewhat drier than the foam on either side of the boundary.

The temperature of the foam near the electrodes faithfully reflects the varying rate at which solution flows by, as may be seen from the figures. Transition temperatures estimated from the breaks in the curves are: rising temperatures, 31°C.; falling temperatures, 31.5°C. Film drainage observations gave 33.0°C. as the transition temperature.

This apparent discrepancy arises for the reason outlined above, namely, that the flood progresses ahead of the region of the true transition, which is associated with an abrupt change in surface viscosity. With a column operated isothermally, there is no corresponding effect and the difference should diminish. The smaller the column, the smaller the difference due to lags should be, and a single film may be regarded as the limit of such a column. For this reason, and because of the economy of material that may

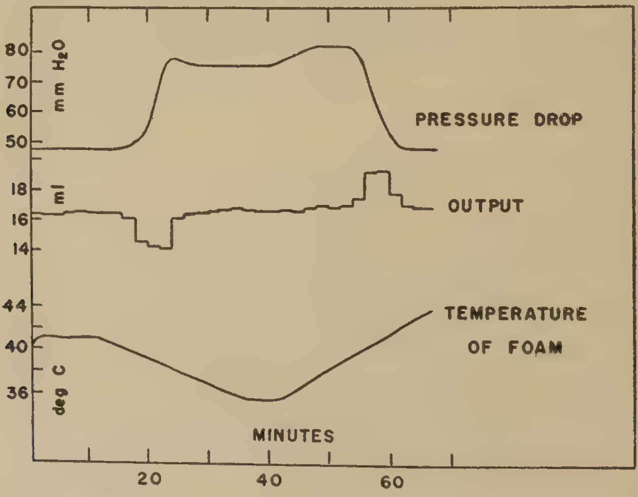

FIG. 6. Foam transitions in "isothermal" column of varying diameter. Bubble diameter, 1.5 mm., upper section of column, 59 cm. long × 2.2 cm. internal diameter; lower section of column, 34 cm. long × 0.9 cm. internal diameter. Thermocouple 8 cm. and reference level 64 cm. below solution inlet. Solution 0.25% Duponol ME, not extracted; rate of solution flow 8.2 ml. per minute.

be had with single films, extensive measurements preferably are made by observing the descent of interference bands in a test tube film drainage apparatus.

Columns of Varying Cross Section

In the preceding experiments with constant input of solution, a constant output is maintained, the solution lost or taken up by the foam during transition appearing as a change in the level of the foam/solution interface. If, however, the foam/solution interface is held at a constant level by manipulating the overflow tube, then the net loss or retention of solution during transition is superimposed on the otherwise steady output, and appears as a hump or trough on a plot of solution output against time. Alternatively, if the foam/solution interface lies within a narrow tube surmounted by a foam column of large cross section, no need remains for manipulating the overflow tube to keep the foam/solution interface at a constant level. An excess or deficiency in the output will be observed upon transition and may be computed roughly from the change in level of the interface and the difference in the cross-sectional areas of the tubes. An exact computation must take account of the difference in drainage relations in the two sections of the column.

An experiment based upon these considerations is presented in Fig. 6, (0.25% Duponol ME). The volume represented by the hump is 6.2 ml.; the volume of the trough is 7.6 ml.; the volume calculated from the change in pressure drop is 9.3 ml.

It will be noted that a small break occurs on reversal of the direction of temperature change. It may be noted also, on Fig. 2, that there is a definite alternation of the open circles about the curves. The upper points are obtained when the given rate is approached from above and the lower points when the given rate is approached from below. These effects derive chiefly from narrow column diameters and more particularly from a narrowing of the effective column diameter at the solution inlet.

We wish to acknowledge the interest and criticism of G. D. Miles, L. Shedlovsky, and A. Wilson throughout the course of this work.

REFERENCES

1. Miles, G. D., Shedlovsky, L., and Ross, J., *J. Phys. Chem.* **49,** 93 (1945).
2. Miles, G. D., Ross, J., and Shedlovsky, L., *J. Am. Oil Chemists' Soc.* **27,** 268 (1950).
3. Smith, C. S., *J. Appl. Phys.* **20,** 631 (1949).
4. Pattle, R. E., cited by F. B. Shepherd, *Ind. Chemist* **26,** 160 (1950).
5. Clark, N. O., and Blackman, M., *Trans. Faraday Soc.* **44,** 7 (1948).
6. Scott, G. V., and Thompson, W. E., *J. Am. Oil Chemists' Soc.* **29,** 386 (1952).
7. Clark, N. O., and Blackman, M., *Trans. Faraday Soc.* **44,** 13 (1948).
8. Clark, N. O., *J. Sci. Instr.* **23,** 256 (1946).
9. Schiebl, K., *Chem. Ztg.* **55,** 169 (1931).
10. Siehr, A., *Kolloid-Z.* **77,** 27 (1932).

THE STRUCTURE OF ALUMINUM STEARATE GREASE

D. Evans and J. B. Matthews

Thornton Research Centre, Thornton-le-Moors, Cheshire, England

Received August 14, 1952; revised August 13, 1953

Abstract

Measurements have been made of the viscosity changes with time which a commercial aluminum stearate grease undergoes, immediately after it has been heated to given temperatures and maintained at these temperatures under shear. When the equilibrium viscosity attained at any temperature is plotted against temperature, the curve obtained indicates the occurrence of a phase transformation in the grease, which is considered to be the transition from the paste to the jelly. It is concluded that the aluminum stearate grease is essentially a metastable jelly at temperatures below the transformation temperature, but transforms slowly to a paste on aging, the rate of transformation being accelerated by shear.

Introduction

Aluminum greases are different from the greases made from other metallic soaps in many respects, particularly with regard to structure, which is distinguished by the extreme fineness of the soap fibers contained in them (1, 2). The structure of aluminum soap-hydrocarbon systems has been the subject of intensive study during the past ten years (3, 4, 5, 6), but in general this work has been confined to systems containing low-viscosity hydrocarbons such as benzene. The gels or jellies formed in these light hydrocarbons possess unique rheological properties which make them suitable as flame-thrower fuels and as fillings for incendiary bombs, but they cannot be classed as greases, which are normally made from the soap and hydrocarbon oils with viscosities in the lubricating oil range. The work described in this paper was carried out on a commercially available aluminum stearate grease made from a high-viscosity oil.

Experimental

Material

The grease contained 5.5% commercial aluminum stearate in a high-viscosity mineral oil and was manufactured by heating these components to 140°C. to effect complete solution, cooling rapidly and milling. The aluminum stearate had a water content of 1.3%, a free acidity (acetone extraction) of 3.4%, an ash of 9.42%, and a water-soluble ash of 0.12%. The mineral oil was a once distilled oil of high viscosity (1100 secs. Redwood I at 140°F.).

Apparatus

The apparatus was a modified form of the McMichael viscometer. In its original form the apparatus was found to be unsuitable for use at temperatures above 20°C., owing to the crude method of temperature control. It was therefore modified according to the suggestions of Rice (7), *i.e.* by substituting the standard heating control by an oil jacket. The latter was fitted to the viscometer without any alterations to the original apparatus other than the removal of the contact switch. A new cup (diameter 3 cm.) was turned from solid brass to fit directly into the supporting oil jacket, through which oil was circulated from a thermostatically controlled oil-bath via heat-insulated copper tubes. The whole assembly was fitted with a lid, through which a central hole was drilled to take the torsion wire, and was efficiently lagged with asbestos and cotton wool. With these precautions it was possible to maintain a temperature of 100°C. (±0.5°C.).

Procedure

In order to obtain reproducible results it was necessary to control the experimental procedure, which was standardized as follows. The inner cylinder was removed from the viscometer, and oil at the predetermined temperature was circulated through the oil jacket for 10–20 minutes. Grease at room temperature was put in the rotating cup and stirred until its temperature was constant. This usually took about 25 minutes. The grease temperature was observed independently with a thermometer immersed in it, because when steady conditions were established there was always a difference between the temperature of the circulating oil and that finally attained by the grease. For example, at 90°C. the difference was 2.5°C. which remained constant to within the limits ±0.5°C. during a run of 300 minutes duration. When steady temperature conditions had been established, the thermometer was removed, and the inner cylinder, previously heated to the grease temperature, was inserted in the grease and suspended by the torsion wire.

Since grease is non-Newtonian in its rheological behavior, it was necessary to standardize the rate of shear in order to obtain significant results. The rate of rotation of the cup was fixed, therefore, at 30 r.p.m., which gave a constant mean rate of shear of slightly less than 2 sec.$^{-1}$. The only variable factor in these experiments, apart from temperature, was the height of immersion of the inner cylinder, which was deliberately varied in order to enable suitable scale deflections to be obtained over a range of viscosities.

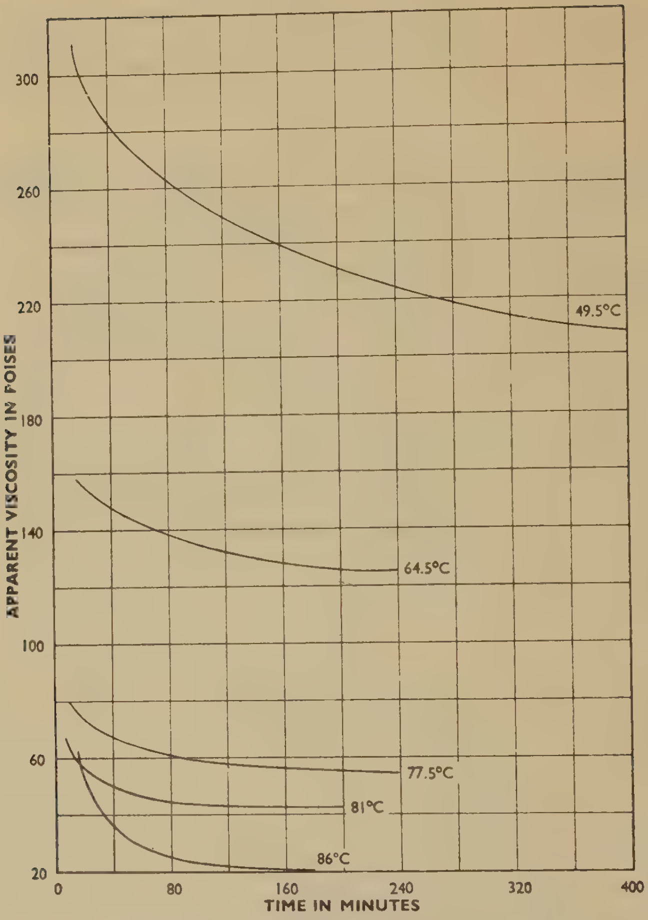

Fig. 1. Isothermal changes in apparent viscosity of aluminum stearate grease after being heated to various temperatures.

Results

The experimental observations are given in Figs. 1 and 2, in which "apparent viscosity" values are plotted against time. "Apparent viscosity" is recognized as being a loose, and sometimes misleading, conception, but its use is convenient for providing a suitable basis for comparison. Values of torque, the property measured, are not comparable in themselves since the height of immersion of the inner cylinder varies, but this variation is allowed for in the calculation of apparent viscosity. The latter, however, is not necessarily the real viscosity of the grease at the given rate of shear, since it is a "one-point" value and not calculated from the true gradient of the shear rate versus shearing stress curve. Zero time is defined as the

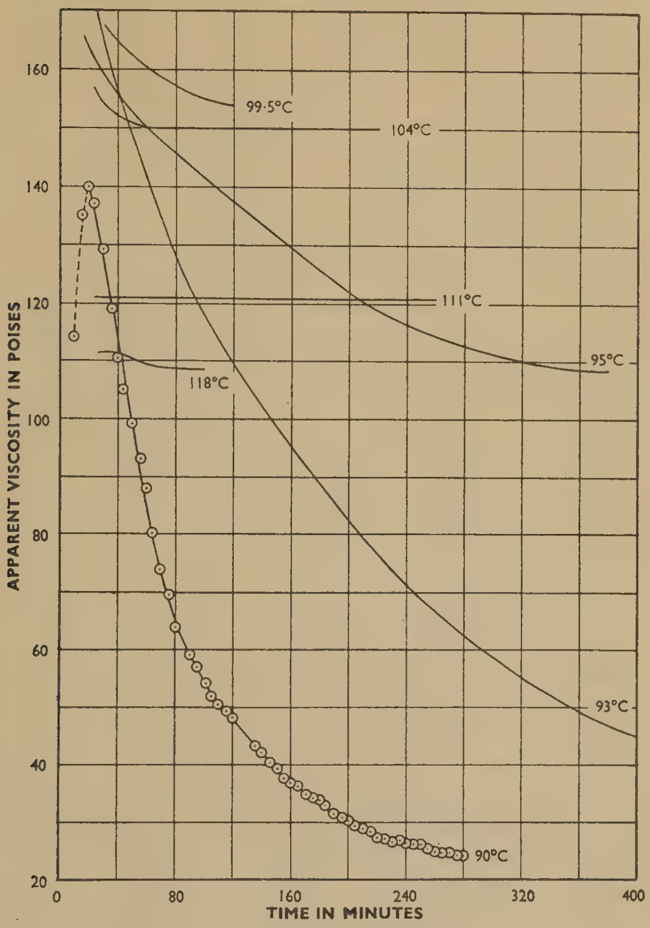

FIG. 2. Isothermal changes in apparent viscosity of aluminum stearate grease after being heated to various temperatures.

moment of introduction of the inner cylinder into the grease, and usually an initial rapid increase in apparent viscosity occurred, as shown in the 90°C. curve in Fig. 2. This initial increase, which for the sake of clarity has been omitted from the other curves, did not always occur, and tended to be erratic in nature. It is probably due to temperature fluctuations and to initial slip between the inner cylinder and the grease, and has therefore been ignored in the interpretation of the observed apparent viscosity changes.

The isothermal changes in apparent viscosity with time all follow the same course, although the extent of the changes occurring varies according to the temperature. At the highest temperatures the apparent viscosity,

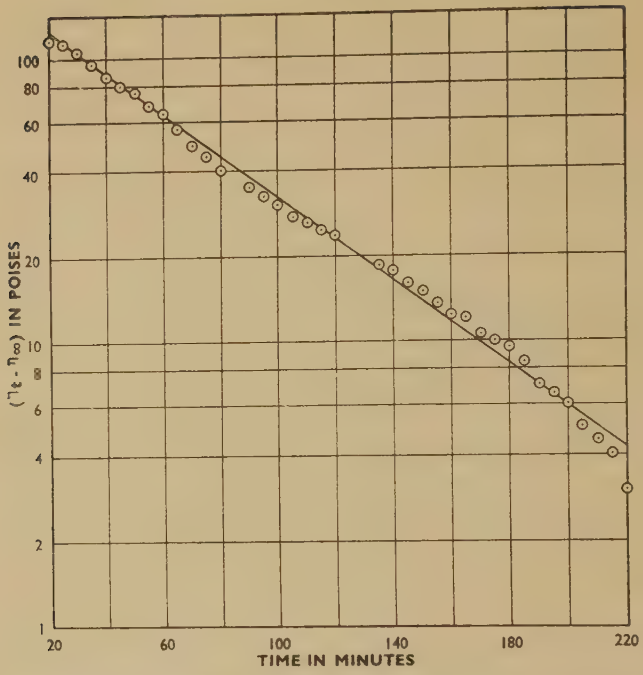

Fig. 3. The time dependence of the apparent viscosity change in aluminum stearate grease after being heated to 90°C.

after the initial fluctuations, is constant with respect to time. At other temperatures the fall in apparent viscosity with increasing time appears to follow an exponential law, as indicated by the linear relationship shown in Fig. 3.

The reproducibility of the measurements on different portions of the same sample of grease was found to be good. For example, at 90°C. two runs gave almost identical curves and equilibrium apparent viscosity values of 24 and 23.5 poises, and at 99°C. three runs gave similar curves and equilibrium apparent viscosity values of 150, 154 and 148.5 poises. However, results obtained with a different batch of grease were not identical with those shown in Figs. 1 and 2, although formally the apparent viscosity changes with respect to time were the same.

Figure 4 gives the viscosity-temperature relationships for the two batches of grease. For each grease there are two curves, one giving the initial apparent viscosity curve and the other the final apparent viscosity curve. The former was obtained by plotting as a function of temperature the initial apparent viscosity, which is defined as the apparent viscosity measured immediately after the initial fluctuations are over, and for the 90°C. curve in Fig. 2 is given by the apex of the curve. The latter was

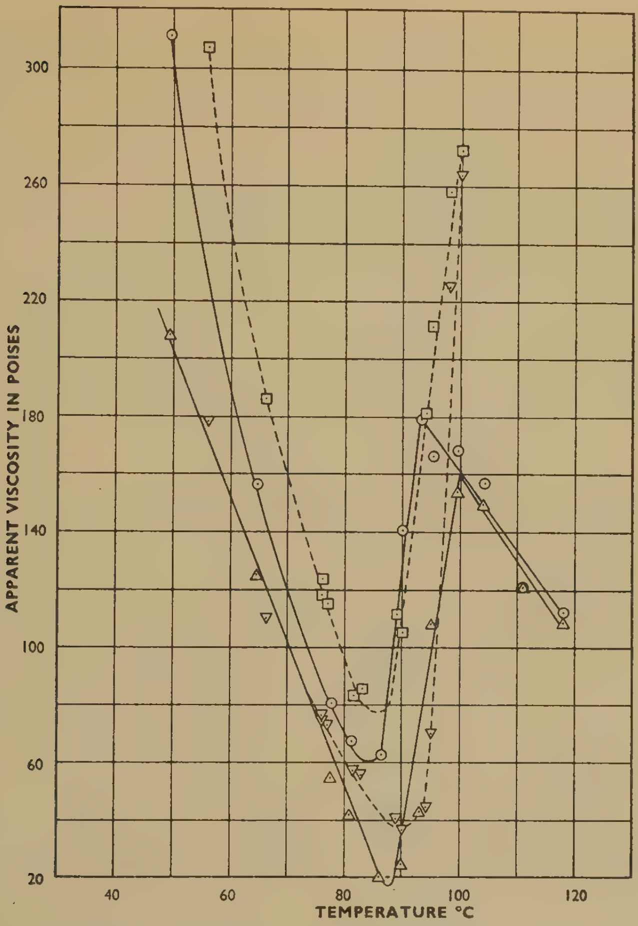

FIG. 4. The viscosity-temperature relationships for aluminum stearate grease. ⊙ and △ represent initial and equilibrium values for first sample of grease, and ⊡ and ▽, the same for the second sample.

obtained by plotting as a function of temperature the equilibrium apparent viscosity value, obtained by extrapolating the curves in Figs. 1 and 2.

DISCUSSION

The self-consistency of the results illustrated in Figs. 1, 2, 3, and 4, and the excellent agreement obtained for the equilibrium values of the two batches of grease below the temperature at which the first break occurs in the curves (the second batch was made and investigated seven years after the first) indicate fairly conclusively that the observed isothermal changes in apparent viscosity with increasing time are not due to plug flow, temperature variations, or other instrumental factors. A possible explanation is that the reduction of viscosity to a dynamic equilibrium value with increasing time is due to thixotropy. If we give the generally accepted meaning to the word thixotropy, this would imply that the apparent viscosity should recover, or tend to recover, its initial value when the shearing stress is removed, and also that the equilibrium apparent viscosity would be a function of the rate of shear causing the reduction. Both of these conclusions are contrary to the facts. Thus, after dynamic equilibrium conditions had been established in the viscometer at 90°C., the grease was left undisturbed in the viscometer for four days at 90°C., but during this quiescent period the apparent viscosity remained unchanged from the dynamic equilibrium value. Therefore, the change caused in the system by the applied shearing stress is not thixotropic but appears to be a permanent change in the structure of the grease. Again, according to the tabulated data the equilibrium state is independent of the rate of shear used in attaining it, although the time taken to reach this state is approximately inversely proportional to this rate of shear. This is also inconsistent with the view that the change is thixotropic.

Effect of Varying the Breakdown Rate of Shear on the Apparent Viscosity at 81°C.

Mean rate of shear (*sec.*$^{-1}$)	Time to attain equilibrium (*minutes*)	Equilibrium viscosity at "breakdown" rate of shear (*poises*)	Equilibrium viscosity at rate of shear of 1.8 sec.$^{-1}$ (*poises*)
1.2	230	52.0	42.5
1.8	150	43.0	43.0
2.4	105	34.0	42.0

On the other hand, the data are in agreement with the view that the original structure of the grease is unstable, and that the application of a shearing stress facilitates the transition from the unstable state to the stable state. This instability, however, does not appear to any significant extent above the critical temperature zone in which the breaks in the curves in Fig. 4 occur. It may be inferred, therefore, that the original structure of the grease is one which is stable above the critical temperature zone and metastable below it. In agreement with this view is the fact that in order to make a grease of maximum hardness it is necessary to chill the product rapidly from a temperature above the critical temperature zone. If the grease is slowly cooled with stirring through the critical temperature zone the product obtained is much more fluid, and similar in all respects

---

PLATE I. Photomicrographs of aluminum stearate grease viewed in transmitted ordinary light at an original magnification of 226×.
(*a*) Original grease; (*b*) after equilibration at 56° C. and cooling;
(*c*) after equilibration at 77° C. and cooling; (*d*) after equilibration at 94° C. and cooling;
(*e*) after equilibration at 105° C. and cooling; (*f*) same as (*e*) after milling.

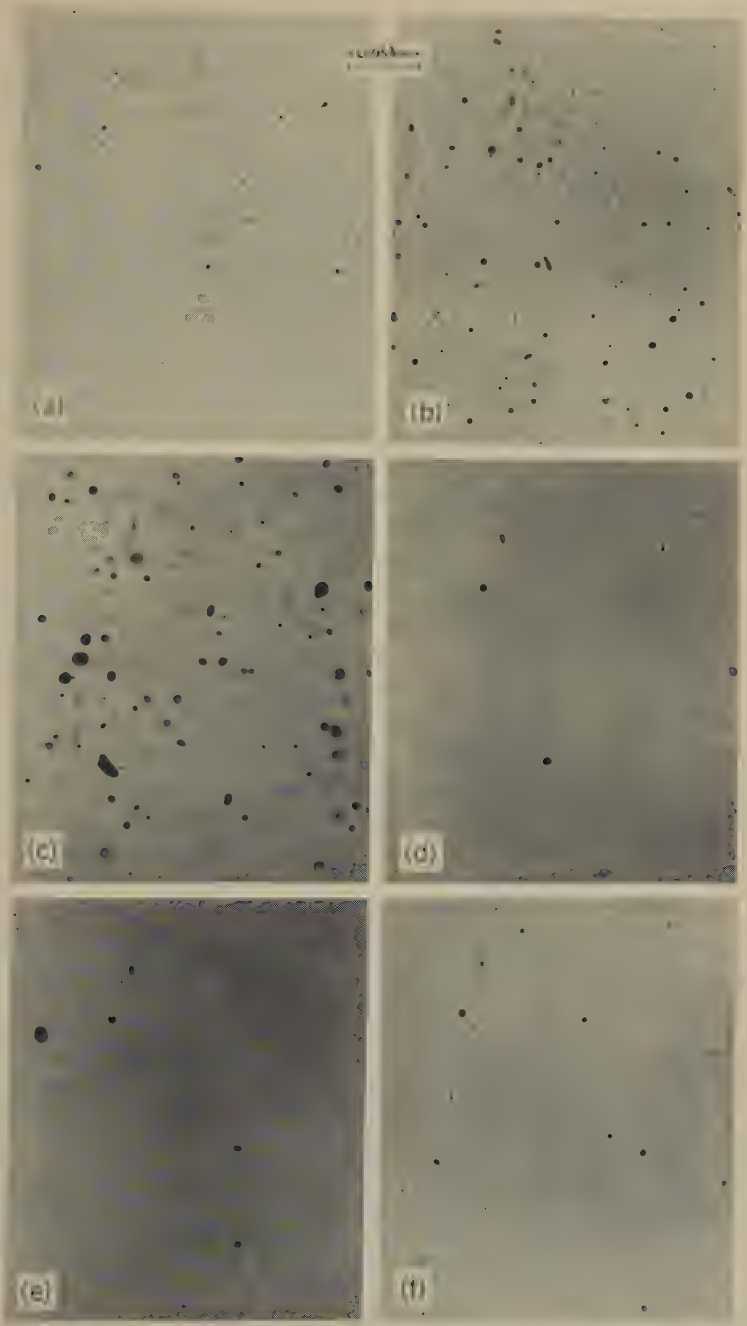

PLATE I

to the dynamically equilibrated grease obtained at temperatures below the critical zone in the experiments described in this paper.

Accordingly, the critical temperature zone can be ascribed to a phase transformation in the grease. The possibility exists that two phase transformations are involved, since there are two distinct breaks in the curves in Fig. 4. This is unlikely, since it would follow that the phase which is stable between the two critical temperatures would possess a very high and positive temperature coefficient of viscosity. It is more probable that only one phase transformation occurs, which would produce a true discontinuity in the curve, if the soap was a pure chemical compound. Commercial aluminum stearate, however, is an ill-defined chemical mixture, which may provide a spectrum of transformation temperatures resulting in a broad transformation temperature zone instead of a unique transformation temperature. In this connection it should be noted that even pure aluminum di-laurate shows a complex inhomogeneous behavior (8).

Micrographical evidence, illustrated in Plate I, shows that the two phases stable above and below the critical temperature zone are both isotropic, and the essential difference appears to be that the former is a homogeneous system, the latter, heterogeneous. The transformation can, therefore, be described as a transition from jelly to paste, adopting McBain's definition of a jelly as being a homogeneous isotropic phase. This transformation is presumably the same as the transition occurring at temperature T_2 according to Lawrence's scheme (9). No experimental evidence has been obtained in support of a critical temperature corresponding to Lawrence's temperature T_1 (jelly $\rightleftharpoons$ sol), but this may be due to the fact that, owing to the limitations of the apparatus, a sufficiently high temperature region was not explored. On the other hand Mysels (3) claims that the transition from jelly to sol for the aluminum di-laurate system is gradual and does not involve a critical temperature, which is in agreement with the observations of McBain and Working (4) on aluminum di-laurate, and of Gray and Alexander (6) on aluminum stearate–hydrocarbon systems.

It should be noted in Plate I that the original grease shows definite signs of heterogeneity, whereas freshly made grease, illustrated by *f* in Plate I, shows much less evidence of heterogeneity, and the product obtained by statically cooling the system after equilibrating at 105°C. shows practically none. This suggests that the transition from the jelly state to the paste state can occur when the grease ages in the absence of shear, as well as under conditions of shear. It also leads to the conclusion that the grease when freshly made is essentially a supercooled jelly, which slowly transforms on aging to a paste, this transformation being accelerated by shearing. Another notable feature of Plate I is that, as the equilibration temperature is increased, the size of the particles in the equilibrium state increases. It is possible that there is a continuous range of equilibrium paste states varying in particle size with temperature, and analogous to the "calotropic" jelly states of aluminum di-laurate.

The different initial-value curves (Fig. 4) obtained for the two samples of grease may be due to differences in composition of the greases. Another explanation may be minor differences in the composition of the soap or in the treatment to which it was subjected, either during its manufacture or during the manufacture of the grease from it (8). The data suggest that, in addition to the differences recorded in Fig. 4, there will also be marked differences above the transformation temperature zone between the equilibrium values as well as the initial values. Since the equilibrium curves are coincident below the transformation temperature zone it would appear that the grease in the paste state is much less sensitive to differences in soaps or composition than it is in the jelly state.

The curves shown in Fig. 4 are similar in form to those obtained by Moses and Puddington (10) by plotting the Goodeve thixotropy coefficient and the residual viscosity against temperature. The breaks in their curves, however, occur at temperatures lower than those shown in Fig. 4. The explanation for this may be a difference in the component oils, since independent evidence has been obtained by us showing that by changing the oils the transformation temperatures can be altered. Rager (11) has also obtained a curve which superficially resembles those given in Fig. 4, but his results were obtained by following the viscosity changes which occur during the dissolution of the soap, whereas Fig. 4 refers to results obtained with greases made from soap solutions. When this difference is taken into consideration, the differences between Rager's results and those described in this paper can be understood.

ACKNOWLEDGMENT

The authors wish to thank the Directors of the Shell Petroleum Co. Ltd. for permission to publish this work.

REFERENCES

1. FARRINGTON, B. B., AND DAVIS, W. N., *Ind. Eng. Chem.* **28,** 414 (1936).
2. FARRINGTON, B. B., AND BIRDSALL, D. H., *Oil and Gas J.* **45,** 268 (1947).
3. MYSELS, K. J., *J. Colloid Sci.* **2,** 375 (1947).
4. MCBAIN, J. W., AND WORKING, E. B., *J. Phys. & Colloid Chem.* **51,** 974 (1947).
5. SHEFFER, H., *Can. J. Research* **26** (6), 481 (1948).
6. GRAY, V. R., AND ALEXANDER, A. E., *J. Phys. & Colloid Chem.* **53,** 9 (1949).
7. RICE, W. A., *Ind. Eng. Chem., Anal. Ed.* **17,** 676 (1945).
8. MYSELS, K. J., AND MCBAIN, J. W., *J. Phys. & Colloid Chem.* **52,** 1471 (1948).
9. LAWRENCE, A. S. C., *J. Inst. Petroleum* **31,** 303 (1945).
10. MOSES, G. B., AND PUDDINGTON, I. E., *Can. J. Chem.* **29,** 996, (1951).
11. RAGER, R., *Rev. inst. français du pétrole et Ann. combustibles liquides* **5** (10), 311 (1950).

A NEW METHOD FOR THE MEASUREMENT OF AEROSOL ELECTRIFICATION

B. L. Hinkle,* Clyde Orr, Jr., and J. M. DallaValle

The Georgia Institute of Technology, Engineering Experiment Station, Atlanta, Georgia

Received June 8, 1953; revised September 29, 1953

ABSTRACT

Because of the importance of the electrical forces associated with aerosol particles, an electrification analysis apparatus permitting rapid evaluation of the amounts of negatively and positively charged particles in an aerosol by measurement of the lateral deflection of the aerosol stream in an electrical field has been developed. Results obtained thus far have been in excellent agreement with expectation and with the published data of other investigators. The principal advantages of the method presented are the rapidity and ease of obtaining data and the elimination of the need for numerous samples to give statistically accurate results. An equation is presented for the calculation of the average electron charge carried by particles.

INTRODUCTION

The electrical characteristics of certain aerosols have been examined by a number of investigators. DallaValle (1) has summarized the work of the early investigators, notably Knoblauch (2), Rudge (3) and Whitman (4), who showed that the charge acquired by an aerosol was dependent on the composition and size of the particles, the nature of the ducts through which the aerosol was conveyed, the conveying velocity, and the relative humidity. These studies were concerned chiefly with the net charge acquired by a dust cloud, however. Whytlaw-Gray and co-workers (5) presented information on the relative amounts of negatively and positively charged particles in smokes of ammonium chloride, stearic acid, magnesium oxide, and tobacco. Kunkel (7) published similar information on the electrification of quartz dusts, and Daniel and Brackett (8) have applied a scheme which determines the charge:mass ratio to the analysis of quartz dusts.

One point of agreement among the diverse studies is clear: the electrification of a freshly prepared aerosol is largely dependent on the method of formation. Violent reactions, such as the burning of magnesium ribbon, give rise to highly electrified particles, whereas volatilization at low temperatures results in only a small fraction of charged particles. Aerosols produced with a LaMer (9) generator, for example, are relatively uncharged. Wilson and LaMer (10) found that less than 25% of the particles comprising a glycerol aerosol were charged, even though radioactive sodium produced the nuclei for the formation of the glycerol particles. None of the particles carried as many as four electronic charges. White and Hill (11) found that aerosols produced with a LaMer generator contained particles either uncharged or carrying single electronic charges. Recently, LaMer *et al.* (12) found that dioctyl phthalate aerosols produced with a LaMer generator were almost devoid of charged particles. At present the data on aerosol electrification are still scanty, and more information on a variety of aerosol systems is needed.

---

* Present address, E. I. DuPont de Nemours & Co. (Inc.), Richmond, Virginia.

The chief obstacles to detailed studies of aerosol electrification have been the difficulties encountered in experimental methods and techniques. Whytlaw-Gray and Patterson (5) used an ultramicroscope cell containing horizontal electrodes and noted the action of the particles in the field of vision. Kunkel and Hansen (13) used a modification of the apparatus described by Hopper and Laby (14), who employed a photographic technique to measure the deflection of oil drops falling under gravity in a horizontal electric field. LaMer *et al.* (12) used a modified Millikan oil drop apparatus. Gillespie (15) used an instrument in which the charged particles were deposited on microscope slides and the neutral particles were collected in a thermal precipitator.

The technique reported here avoids many of the experimental difficulties which accompany photographing or observing discrete particles and permits rapid evaluation of the electrification of an aerosol, but it introduces certain new difficulties. These new limitations can be considerably minimized, however, and will be discussed in detail later.

Apparatus and Technique

The apparatus developed for the present work is designed to permit evaluation from the deflection of an aerosol stream. Since the aerosol stream serves as the sample, the necessity for obtaining numerous photographs in order to establish a precise sample average is removed, and the electrification of an aerosol may be determined in a single, brief experiment.

A schematic diagram of the main elements of the apparatus is given in Fig. 1. The aerosol stream passing through the electrification chamber was observed and photographed through a window which was located at an angle of 45 degrees with the forward path of the light beam. Since the intensity of scattered light is greatest in the near-forward direction, observation at an angle of 45 degrees with the direction of propagation of the incident beam was accomplished at some sacrifice in scattered light intensity. Background light was virtually eliminated by the 45-degree angle

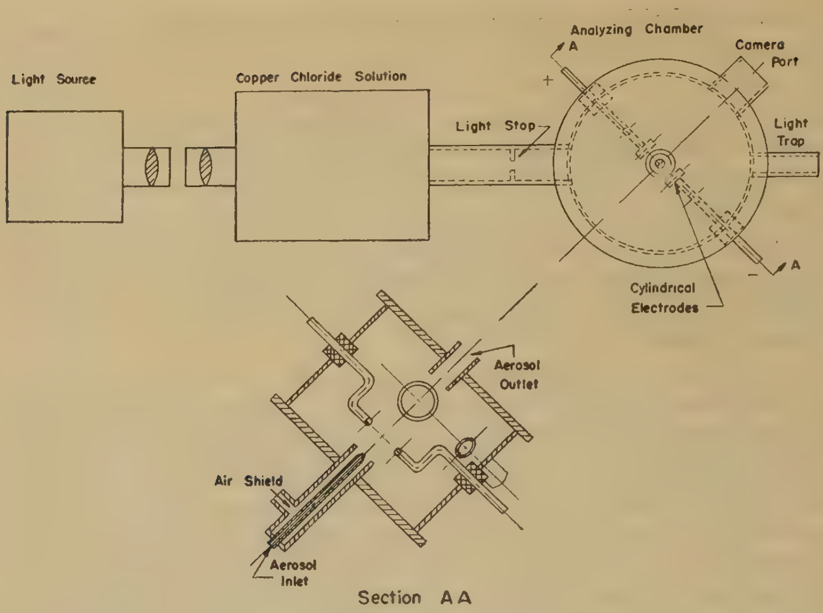

FIG. 1. Schematic diagram of aerosol electrification apparatus.

arrangement, however, and photographs showed excellent contrast between the image of the aerosol stream and the remainder of the film. A copper chloride solution was used to reduce the infrared intensity of the incident light, and a slit at the entrance to the electrification chamber controlled the size of the light beam. All surfaces within the chamber and ducts were painted with an optically black paint.

Previous investigators in the field of aerosol electrification have invariably used systems involving parallel plate electrodes. This construction generally requires dark-field illumination or observation at very acute angles, because small separation between the plates cannot be effected without having the edges of the plates project into the light path. The restrictions on observation angle were overcome by constructing cylindrical electrodes, located horizontally beneath the path of the incident light, and with axes at an angle of 90 degrees with the observational axis. With these modifications of electrode shape and location, a high-voltage gradient between the electrodes may be obtained without interference with the light beam.

The aerosol entered through a glass tube which tapered to, and terminated as, a slit 7.5 mm long and 0.2 mm. wide just below the plane of the electrodes. This central glass tube was, in turn, surrounded by another tube through which pure air could be drawn. In operation, the air velocity in the outer tube was synchronized with the aerosol velocity so that an aerosol stream having a width of very nearly 0.2 mm. passed through the

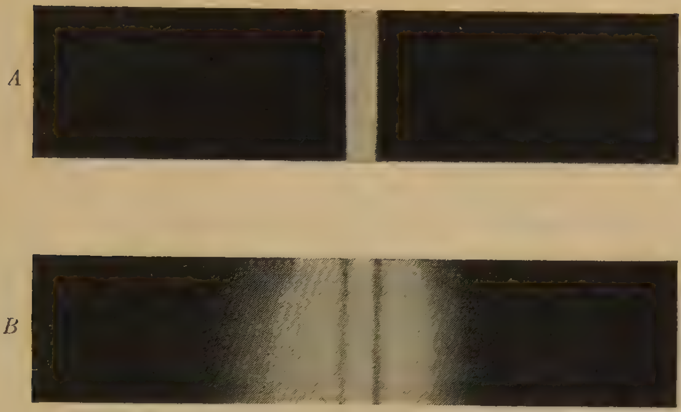

FIG. 2*A*. A stream of tobacco smoke in the absence of an electric field. *B*. A stream of tobacco smoke in an electric field of 5,000 volts per centimeter.

observational zone in the absence of an electrical field. This aerosol inlet tube was rotated so that the narrowest dimension of the stream was presented for observation or photographing. By this means an aerosol stream was obtained containing a sufficient number of particles to result in adequate exposure of the film negative even when the particles were dispersed in the electrical field. This flow system has an additional advantage over methods in which the settling of discrete particles under gravity is measured. In the present scheme, thermal forces on the movement of the particles are negligible in comparison to forces due to the velocity of the stream, whereas unequal radiative heating in some previous systems caused spurious measurements and necessitated excessive insulation.

The high-voltage source was controlled with a variable transformer so that the optimum dispersion of an electrified aerosol could be readily established. Maximum output was 20,000 volts, although it was seldom necessary to exceed 8,000 volts.

Photographic negatives of the aerosol stream, such as shown in Fig. 2, were taken with the camera located a suitable distance from the camera port to obtain proper magnification and focus. A desirable feature of the photographic elements was a copying attachment, which permitted replacement of the camera with a ground-glass plate for visual observation. During a test, the image of the aerosol stream was viewed through the ground-glass plate, and when a fine, steady stream was clearly visible, the camera was switched to replace the ground-glass plate, and photographs were taken, thus giving photographs showing the change in the flow pattern of the aerosol due to the electric field.

Photographic negatives were analyzed for optical density with a modified

Model B Beckman Spectrophotometer. Companion negatives showing the aerosol stream with and without the presence of an electric field were placed in a sample holder adapted for use with the spectrophotometer. The optical densities of the films were then obtained by traversing each negative. Results using different portions of the negatives were reproducible in all cases.

Three possible limitations of the apparatus construction and of the experimental procedure warrant discussion. First, there is a question regarding the possible electrification of aerosol particles because of their passage through the tubes from the aerosol reservoir to the electrification chamber and through the electric field within the chamber. The charging of particles through ducts appears to be a function of the velocity of the particles (1), and since this velocity was kept at an extremely low value (of the order of 1 cm. per second), it would be unlikely that the aerosols could become charged by passage through the tubes. The charging of particles by passage through an electric field takes place when corona discharge occurs, and calculations show that approximately double the voltage gradient used in this work would have been necessary to cause significant charging. These conclusions were justified by examining an aerosol formed by exposing titanium tetrachloride to a moist atmosphere. Measurements showed that this aerosol was uncharged both before and after passage through the tubes and the electric field.

The second question involves the possible effect of secondary light scattering, where the total light scattered by the aerosol stream might be less than the sum of the light scattered by the individual particles. According to Sinclair (16), particles scatter light essentially independently of one another when the distance between the particles is 10, or preferably 100, times the radius of the particle. In aerosols having a particle radius of 1 μ and a number concentration of 10^6 per cc., the volume available to each particle is 10^{-6} cc., the distance of particle separation is approximately the cube root of 10^{-6} or 10^{-2} cc., and thus the ratio of separation to radius is 10^{-2}: 10^{-4} or 100. For a 10-μ particle aerosol of the same concentration, the ratio is reduced to 10. In such an aerosol, some interference between the scattering of neighboring particles would be expected, but such high concentrations are seldom found in practice. With the exception of an elutriated clay aerosol with a median diameter of 3 to 5 μ, the aerosols used in this study exhibited median diameters of less than 1 μ. Since the concentration of the clay aerosol was of the order of 10^5 per cc., and concentrations of the other aerosols never exceeded 10^6 per cc., the assumption of independent scattering may be justified.

The third question concerns the photography. It has been shown that, to ensure an accurate analysis from film negatives, exposure conditions (light intensity and time) should be chosen so that the optical density of the negative is a linear function of the incident light. Proper choice of exposure was determined by calibration of the film according to the procedure recommended in a publication of the Eastman Kodak Company (17), and particular care was exercised to avoid any overexposure of the negatives showing aerosol streams dispersed in the electric field.

RESULTS

The behavior of a stream of tobacco smoke particles in the absence of an electric field is shown in Fig. 2*A*, and the flow pattern of the same aerosol in a horizontal field of 5,000 volts per centimeter is shown in Fig. 2*B*. The electrode and high-voltage source connections were such that the light area to the left of center in Fig. 2*B* represents positive particles, and that to the left, negative particles. The central line represents neutral particles. The relatively dark spaces between the central line and the light areas in Figure 2*B* suggests that the charged tobacco smoke particles at the outer boundaries of the dark spaces are carrying minimum charges. The charge will be shown later to correspond to a single electronic charge. No such dark spaces were evidenced by an aerosol containing clay particles when the range of particle size was great.

Figure 3 shows the results of optical analysis of the negatives corresponding to Figures 2*A* and 2*B*. In Fig. 3, the solid line presents the results of the optical scanning of Fig. 2*A*, *i.e.*, of tobacco smoke in the absence of an electric field, and the dotted line represents the results of the scanning of Fig. 2*B*, *i.e.*, of the same aerosol dispersed because of the presence of the field. Since it has been shown that secondary light scattering is negligible for the aerosols studied, and since care was exercised that the optical density of the negative for the aerosol in the presence of an electric field was a linear function of the number of particles causing the exposure, the areas under the broken curve of Fig. 3 may be taken as proportional to the number of particles scattering the light. If the total area under the dotted-line curve is fixed at unity, the area under the central peak of the curve represents the fraction of neutral particles in the sample; the area under the left peak, the negative fraction; and the area under the right peak, the positive fraction. The solid-line curve is not of great importance other than to serve as a guide. However, it is well to note that if no parts of either negative were overexposed or underexposed, the area under the solid-line curve should be equal to the area under the dotted-line curve.

Some of the results obtained with a number of aerosols are given in Table I. In addition to the agreement with Whytlaw-Gray and co-workers (5, 6) on the electrification of magnesium oxide, the results serve as verification of the work of others (10, 11, 12), who found that aerosols pro-

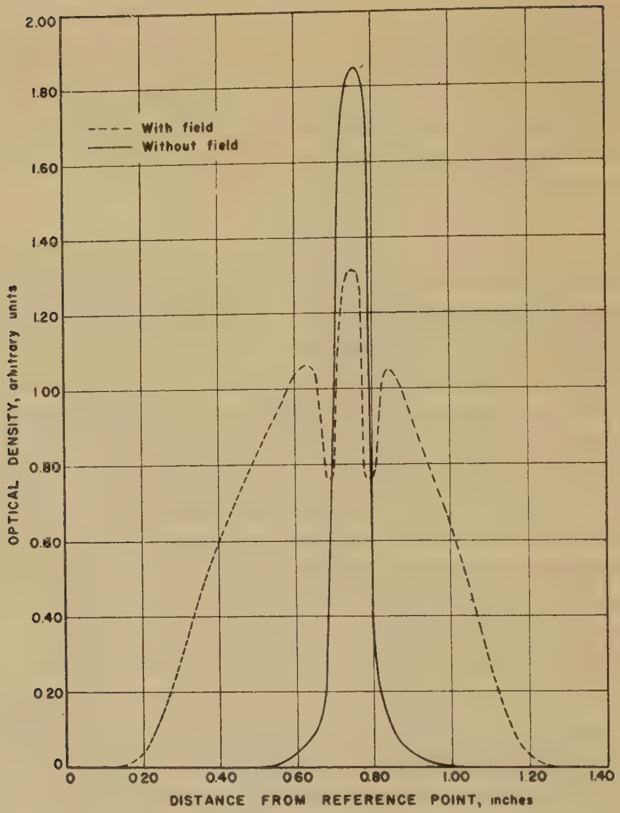

FIG. 3. Optical density curves from film negatives corresponding to Figs. 2*A* and 2*B*.

duced with the LaMer generator were only slightly charged. The importance of the method of generation on the electrification of an aerosol has been amply demonstrated. As shown in Table I, an ammonium chloride aerosol produced with a spark discharge type of LaMer generator contained less than 5% charged particles, whereas an aerosol made by atomizing an alcoholic solution of ammonium chloride contained over 70% charged particles. In the latter method, the high degree of electrification is not surprising, in view of the violent forces attending rupture of the liquid at the atomizer nozzle.

The values of positive and negative fractions reported in Table I represent the average values for a number of samples. Deviation from the average value rarely exceed 10%. Since the possible variation of electrification with time had not been determined, all measurements were made with freshly prepared aerosols.

TABLE I

Electrical Charge Data for Various Aerosols Soon after Generation

Aerosol	Method of formation	Approx. average diam. (μ)	Charge distribution		
			Positive (%)	Negative (%)	Neutral (%)
Tobacco	Burning	0.1–0.25	40	34	26
Magnesium oxide	Burning magnesium ribbon	0.8–1.5	44	42	14
Magnesium oxide	Burning magnesium ribbon	—	48[a]	43[a]	9[a]
Clay	Elutriation	3–5	47	44	9
Stearic acid	LaMer generator	0.2	2	2	96
Stearic acid	Low-temperature volatilization	—	3[a]	4[a]	93[a]
Ammonium chloride	LaMer generator	0.2	2	2	96
Ammonium chloride	Low-temperature volatilization	—	—	—	95[a]
Ammonium chloride	Dispersed from alcoholic solution by atomizer	0.8–1.5	40	40	20
Sugar	Dispersed from alcoholic solution by atomizer	0.8–1.5	40	39	21

[a] Data of Whytlaw-Gray and associates (5, 6).

In general, electrified aerosols were found to contain approximately equal amounts of positive and negative particles, with occasionally a slight excess of positive particles. This result is in agreement with the data of Whytlaw-Gray and Patterson (5), who ascribe the slight excess of positive particles to the greater mobility of negative ions.

Complete analysis of the charges associated with aerosol particles entails consideration of several factors. The amount of lateral deflection of a particle, in the system described, is a function of the mass of the particle, the charge, the field strength, and the flow rate of the aerosol stream through the electrification chamber. An analysis of the electric field between cylindrical electrodes has been summarized by Harnwell (18). If the boundary conditions imposed by the design of the apparatus and by the experimental technique are applied, an expression may be derived which relates the deflection of the particle passing through the field to the charge of the particle.

The electric forces on a particle in the field surrounding cylindrical electrodes arranged parallel to one another, as in this investigation, have also been discussed by Harnwell. Electrodes of infinite length were assumed in the theoretical analysis, however. The following derivation assumes that the finite length of the electrodes will not greatly affect the analysis and that the velocity of the particle will not be materially altered by the acceleration and deceleration effects of the electric field.

The force causing horizontal deflection of the particle is given by

$$F = \frac{q_L}{\pi K_o} \cdot \frac{q}{d} \cdot \cos \theta \qquad [1]$$

where q_L = charge per unit length of electrode,
q = charge on the particle,
d = distance from electrode to particle,
πK_o = conversion factor, and
θ = angle between the plate of the electrodes and the force vector between either electrode and the particle.

From the analysis of Harnwell,

$$\frac{q_L}{\pi K_o} = \frac{V}{\cos \mathrm{h}^{-1} c/2b} \qquad [2]$$

where V = potential difference,
c = separation between electrode centers, and
b = electrode radius.

From geometric considerations, Eq. [1] may be modified to give

$$F_x = \frac{Vcq}{2w} \cdot \frac{1}{(V_0t - y_0)^2 + (c/2)^2} \qquad [3]$$

where $w = \ln(c/2b + \tfrac{1}{2} \sqrt{(c/b)^2 - 4})$,
t = time
V_0 = vertical velocity of the particle, and
y_0 = vertical distance from the aerosol inlet to the plane of the electrodes.

If we assume that the viscous resistance $\left(6\pi\mu r \frac{dx}{dt}\right)$ force is much greater than the inertial resistance (ma) force and equate the viscous resistance to F_x,

$$6\pi\mu r \frac{dx}{dt} = \frac{Vcq}{[(2w)[(V_0t - y_0)^2 + (c/2)^2]} \qquad [4]$$

where μ = viscosity of the medium,
r = radius of the particle, and
x = horizontal deflection of the particle.

Integration of Eq. [4], together with application of the appropriate conversion factors, yields

$$x = \frac{(1.6 \times 10^{-12})Vq}{6\pi\mu r V_0 w} \left[\tan^{-1} \frac{2y_1}{c} + \tan^{-1} \frac{2y_0}{c}\right] \qquad [5]$$

where y_1 = vertical distance from electrodes to point of observation. The potential is measured in volts, the charge on the particle in electrons, and the other quantities in cgs units.

When the inertial resistance was considered, substitution of absolute numerical values showed that the term associated with the $m \frac{d^2x}{dt^2}$ force was negligible in comparison to the term associated with the $6\pi\mu r \frac{dx}{dt}$ force.

In the foregoing derivation, it should be noted that the amount of lateral deflection is also a function of the horizontal position of the particle in the aerosol stream, and that the equation is rigorous only when the width of the stream approaches the width of a single particle. Therefore, the aerosol stream's width was maintained as small as practicable (about 0.2 mm.).

The minimum deflection, determined from the width of the relatively dark space between the central stream and the charged particle area in Fig. 3, corresponds to tobacco smoke particles with a maximum diameter of the order of 0.6 μ, carrying charges of one electron. According to Eq. [5], optical scanning of a negative showing the electrification of an aerosol perfectly homogeneous with respect to particle size would give optical density curves exhibiting a series of maxima and minima in the charged particle area, each peak corresponding to a different multiple charge on the particle. Therefore, the departure from this predicted peaked curve to the relatively smooth curve of Fig. 3 indicated nonhomogeneity of particle size. Calculations by Eq. [5] may be based on a median particle size, thus permitting estimations of the fractions of particles carrying multiple charges, but the accuracy of the estimation depends upon the deviation of the distribution of particle sizes from the median value. For the tobacco smoke aerosols used in the present study, it was found that the deflection from the central stream to the peak of the curve in the charged particle area corresponded to singly charged particles from 0.1 μ to 0.25 μ in diameter. This result, in excellent agreement with the observations of Gibbs (19) and Sinclair (16) and with other observations on the size of tobacco

TABLE II

Electron Charge on Charged Aerosol Particles Soon after Generation

Aerosol	Method of formation	Average particle diameter (*microns*)	Average charge (*electrons*)
Tobacco smoke	Burning	0.1–0.25	1–2
Magnesium oxide	Burning	0.8–1.5	8–12
Clay	Elutriation	2–4	20–40
Stearic acid	LaMer generator	0.2	1
Ammonium chloride	LaMer generator	0.2	1
Ammonium chloride	Atomization of an alcoholic solution	0.8–1.5	12–15

smoke particles, is evidence that the relatively clear zone between neutral and charged particle areas on a film negative arises because the charged particles must carry at least a single electronic charge.

Equation [5] has been used to calculate the average charge carried by charged particles in several different aerosols. The results are summarized in Table II.

The multiple charges carried by magnesium oxide particles may be attributed to the violent reactions which occur during the combustion of magnesium ribbon. It is interesting to note that the average charge of clay particles is essentially the same value reported by Kunkel (7) for a quartz dust of corresponding particle size. The results showing that a single electronic charge is carried by the charged particles in aerosols formed with the LaMer generator confirms the work of others (11, 12).

The investigation is being continued to obtain electrification data on a number of aerosol systems and to clarify the effects of electrification on aerosol behavior.

REFERENCES

1. DALLAVALLE, J. M., Micormeritics. Pitman Publishing Co., New York and London, 1948.
2. KNOBLAUCH, O., *Z. physik. Chem.* **39,** 225 (1901).
3. RUDGE, W. A. D., *Phil. Mag.* **25,** 481 (1913).
4. WHITMAN, V. E., *Phys. Rev.* **28,** 1287 (1926).
5. WHYTLAW-GRAY, R., AND PATTERSON, H. S., Smoke. Edward Arnold and Co., London, 1932.
6. PATTERSON, H. S., WHYTLAW-GRAY, R., AND CAWOOD, W., *Proc. Roy. Soc. (London)* **124A,** 523 (1929).
7. KUNKEL, W. B., *J. Appl. Phys.* **21,** 820 (1950).
8. DANIEL, J. H., AND BRACKETT, F. S., *Arch. Ind. Hyg. and Occupational Med.* **3,** 505 (1951).
9. LAMER, V. K., *Proc. 1st Natl. Air Pollution Symposium.* Stanford Research Institute, Stanford, California, 1949.
10. WILSON, I. B., AND LAMER, V. K., *J. Ind. Hyg. Toxicol.* **30,** 265 (1948).
11. WHITE, L., AND HILL, D. G., *J. Colloid Sci.* **3,** 251 (1948).
12. LAMER, V. K., GOYER, G., GRUEN, RUTH, AND KRUGER, JOAN, United States Atomic Energy Commission NYO-514. Technical Information Service, Oak Ridge, Tennessee, June 30, 1952.
13. KUNKEL, W. B., AND HANSEN, J. W., *Rev. Sci. Instr.* **21,** 308 (1950).
14. HOPPER, V. D., AND LABY, T. H., *Proc. Roy. Soc. (London)* **178A,** 243 (1941).
15. GILLESPIE, T., Porton Technical Paper No. 289. Chemical Reference Experimental Establishment, Porton, Wiltshire, England, June, 1952.
16. SINCLAIR, D., Handbook on Aerosols, Chapters 7, 8. Summary Technical Report of Division 10, National Defense Research Committee. U. S. A. E. C., Washington, D. C., 1950.
17. *Kodak Materials for Spectrum Analysis.* Eastman Kodak Company, Rochester, New York.
18. HARNWELL, G. P., Principles of Electricity and Electromagnetism. McGraw-Hill Book Co., New York, 1938.
19. GIBBS, W. E., Clouds and Smokes. Blakiston Company, Philadelphia, 1924.

INTERPRETATION OF PLASTIC VISCOSITIES IN TERMS OF NEWTONIAN VISCOSITIES

Robert C. Harper, Jr., and Jacob Riseman

Research Division, International Resistance Co., Philadelphia, Pennsylvania

Received October 13, 1953

In the course of an investigation of the rheology of carbon black suspensions in petroleum oil, data were obtained which could be interpreted in a straightforward manner by analogy to solutions exhibiting Newtonian viscosity behavior.

Suspensions of four commercial channel blacks were prepared in a nondetergent petroleum oil by two passes of the mixed components through a 3-roll paint mill under identical mill clearance settings. Suspensions of 2.0 and 4.0 weight per cent carbon were prepared in this manner, and other concentrations reported were obtained by dilution with the petroleum oil. The carbons were used as received, without any conditioning treatment. Their ultimate particle diameters (mean), as determined by electron microscopy, were furnished by the suppliers.

A concentric cylinder viscometer in which the outer cylinder may be rotated at continuously variable velocities was employed to obtain the angular velocity *vs.* torque flow curve for each suspension. The inner cylinder was totally immersed to a predetermined depth and was suspended from a fixed support by straightened stainless steel wires whose torsion constants were determined by weight and pulley and by torsion pendulum experiments. Under the same total immersion conditions of the inner cylinder, the instrument was calibrated with N.B.S. standard viscosity liquids. Angular velocity determinations were made with the use of a Hasler-Tel tachometer (direct reading in r.p.m.) which was directly coupled to the drive shaft of the outer cylinder. A reproducibility of 0.5 r.p.m. could be obtained at any velocity employed. The deflection of the inner cylinder was measured by sighting through a telescope onto a dial attached to the shaft of this cylinder. This dial has 1000 divisions per revolution, and readings can easily be made to 0.5 division. The zero point was checked before and after each run, and it remained constant to within 0.5 division.

The outer cylinder was thermostated by a vigorously agitated water bath whose temperature was controlled to 30.00 ± 0.02°C. for all data reported here. A more complete description of the apparatus will appear in a future publication.

The petroleum oil exhibited a Newtonian viscosity of 0.630 ± 0.003 poise up to the highest velocity gradient (1200 sec.$^{-1}$) employed. The flow curve of each carbon suspension was typical of plastic or Bingham flow as characterized by the equation (1)

$$U = \frac{T(r_o^2 - r_i^2)}{4\pi h\omega r_o^2 r_i^2} - \frac{S_0}{\omega} \ln \frac{r_o}{r_i}$$

where U is the plastic viscosity, T the torque imparted to the inner cylinder at an angular velocity ω, h the depth of immersion of the inner cylinder, S_0 the yield stress, and r_o and r_i the radii of the outer and inner cylinders, respectively. For such a flow curve, the plastic viscosity and yield stress may be uniquely determined from the slope and extrapolated intercept, respectively, of the linear portion of the angular velocity *vs.* torque curve. Typical primary data are listed in Table I and depicted graphically in Fig. 1. From these representative data, it is clear that the plastic viscosity values are independent of the rate of shear over the range studied. The plastic viscosity and yield stress values for all runs are listed in Table II and are depicted graphically as functions of carbon concentration in Figs. 2 and 3.

TABLE I

Readings of Angular Velocity and Torque

2.0% Carbon A		1.0% Carbon C	
r.p.m.	*Div.*	*r.p.m.*	*Div.*
0	0.0	0.	0.0
16.0	129.0	27.0	54.0
44.0	236.5	86.5	159.5
73.5	333.5	146.0	261.0
101.0	420.0	201.0	356.5
130.5	508.5	259.0	454.5
156.0	584.0	316.0	551.5
185.5	669.0	374.0	649.0
215.5	754.0	435.0	752.0
245.0	837.0	405.0	700.0
273.5	916.0	348.0	603.0
302.5	997.0	289.0	503.0
287.5	956.0	230.0	402.0
260.0	877.0	172.0	303.0
229.5	792.5	116.0	208.0
201.0	712.0	59.0	110.0
172.5	630.5	16.0	33.0
144.0	546.5	0	0.0
116.5	465.0		
87.0	375.0		
59.0	286.0		
29.0	184.5		
0	0.0		

TABLE II

Values of Plastic Viscosity and Yield Stress

Carbon	Ultimate particle diameter (mean) (*mμ*)	Concentration (*wt.%*)	U (*poises*)	S_0 (*dynes/cm.*^{2})
A	9	1.0	0.84	225.
		2.0	1.17	1150.
		3.0	1.54	4350.
		4.0	2.11	10,900.
B	13	1.0	0.73	175.
		2.0	0.90_7	640.
		3.0	1.09	1620.
		4.0	1.33	3150.
C	18	1.0	0.70_7	130.
		2.0	0.81_3	470.
		3.0	0.94_5	800.
		4.0	1.09	1550.
D	23	1.0	0.65_8	60.
		2.0	0.70_3	155.
		3.0	0.77	390.
		4.0	0.85_5	625.

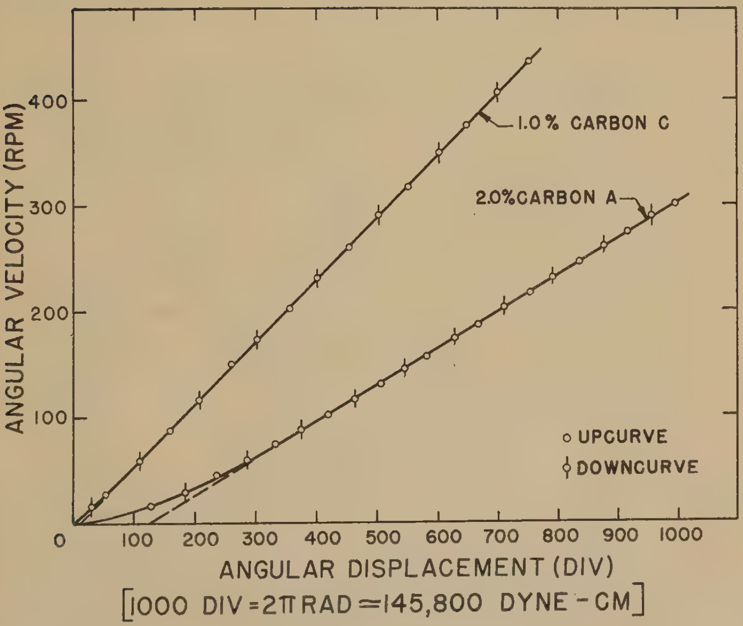

FIG. 1. Angular velocity *versus* angular displacement for two carbon-oil systems.

No simple correlation could be found for the changes in yield stress with concentration. Since the yield stress is a measure of the reticular structure formed by the solute, a rather complicated concentration dependence would be expected.

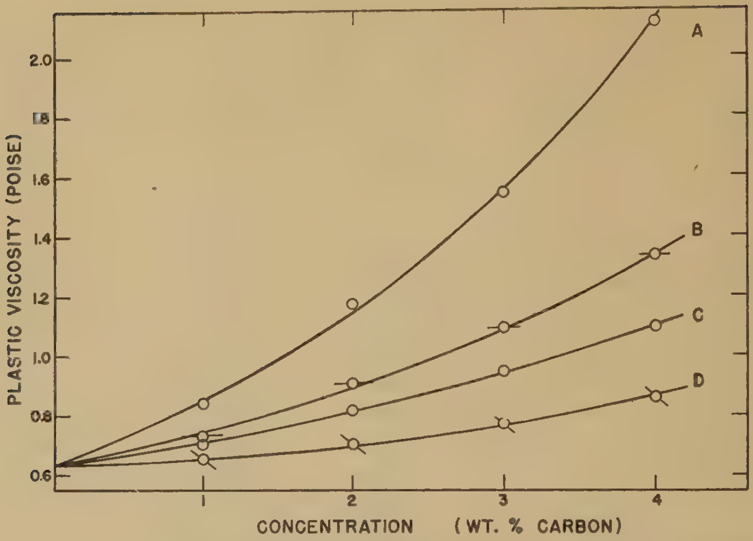

Fig. 2. Concentration dependence of the plastic viscosity for four channel blacks.

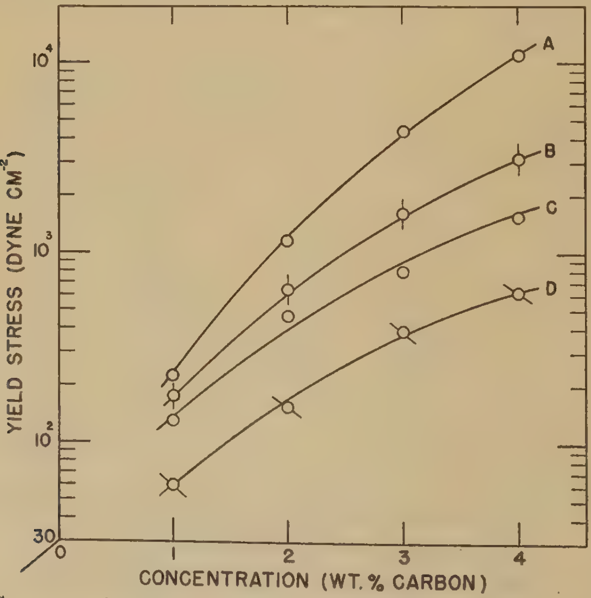

Fig. 3. Concentration dependence of the yield stress for four channel blacks.

In the case of the plastic viscosities, it was of interest to examine the hypothesis that, once the yield stress is exceeded, the excess dissipation of energy due to the presence of the solute is entirely analogous to the case of Newtonian solutions (or suspensions). For this purpose η_{sp}/c was plotted against concentration, and a straight line was obtained for each carbon, conforming to the Huggins' type of equation

$$\frac{\eta_{SP}}{c} = \frac{U - \eta_0}{\eta_0 c} = [\eta] + k'[\eta]^2 c$$

where U is the plastic viscosity of the suspension, η_0 the Newtonian viscosity of the medium, $[\eta]$ the intrinsic viscosity (or limiting viscosity number), k' the interaction coefficient, and c the solute concentration (conventionally expressed in units of grams of solute per 100 ml. of solution). $[\eta]$ is obtained as the ordinate intercept, and k' may then be evaluated from the slope. The linear plots are shown in Fig. 4 and the evaluated parameters are listed in Table III.

For calculation purposes, the densities of carbon and oil were taken to be 1.80 and 0.87 g./cm.^{3}, respectively, and ideal volume additivity was assumed. Values are also given for $\lim_{\phi \to 0} \left(\frac{\eta_{SP}}{\phi}\right)$, where ϕ is the volume fraction of solute. For Einsteinian spheres, the limiting value is 2.5. The higher values found indicate that the reticular or chainlike agglomeration

TABLE III

Intrinsic Viscosity and Interaction Coefficient for Four Channel Blacks

Carbon	Ultimate particle diameter (mean) (*mμ*)	$[\eta]$ (*100 ml./g.*)	k'	$\lim_{\phi \to 0} \left(\frac{\eta_{SP}}{\phi}\right)$
A	9	0.30	1.25 ± 0.25	55
B	13	0.15	2.15 ± 0.15	27
C	18	0.11	2.00 ± 0.20	21
D	23	0.03_2	2.00 ± 0.15	5.5

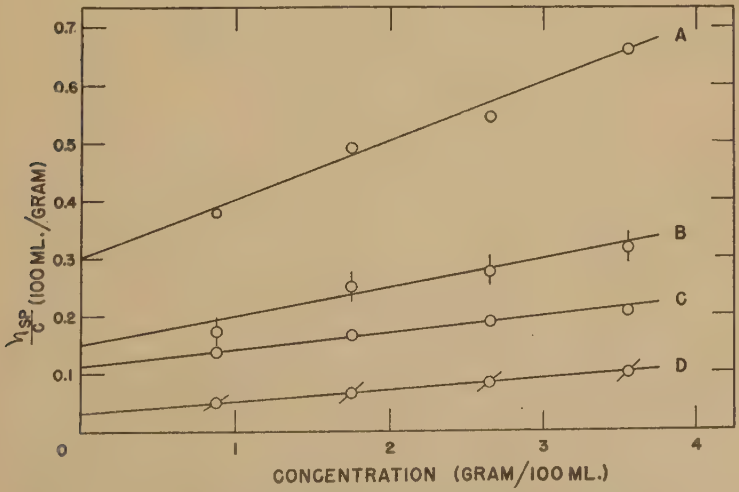

FIG. 4. Concentration dependence of η_{SP}/c for four channel blacks.

suggested by other workers (2–4) for carbon suspensions is a plausible explanation. Since a larger $[\eta]$ value is associated with a longer or higher "molecular weight" particle, the degree of agglomeration appears to increase as the ultimate particle diameter decreases. In accordance with this, the k' values appear reasonable. This dimensionless parameter has been associated with the relative stiffness or flexibility of the particles, reaching a value of about 0.5 for flexible, linear polymers and an upper value of about 5–6 for elongated rigid rods (5). The intermediate values found seem feasible in terms of a chainlike aggregation of the ultimate particles.

The linear concentration dependence of η_{SP}/c found implies that the original hypothesis was valid, at least for these systems over the range of concentration studied. After the shearing stress has exceeded the yield stress, the interference offered by the solute particles to the flow of the medium appears completely similar to cases of Newtonian flow. It would be difficult to explain why this should not be so unless a change in the applied shear stress is associated with a change in the extent of agglomeration or particle size.

References

1. Reiner, M., and Riwlin, R., *Kolloid-Z.* **43,** 1 (1927).
2. Bondi, A., and Penther, C. J., *J. Phys. Chem.* **57,** 72 (1953).
3. Voet, A., *J. Phys. & Colloid Chem.* **51,** 1037 (1947); *Am. Ink Maker* **26**(6), 31 (1949).
4. Amon, F. H., and Brown, O. J., Jr., *Am. Ink Maker* **19**(11), 25 (1941).
5. Eirich, F., and Riseman, J., *J. Polymer Sci.* **4,** 417 (1949).

Book Review

Low Temperature Physics, International Series in Pure and Applied Physics, by Charles F. Squire, Professor of Physics at the Rice Institute, Houston, Texas. McGraw-Hill Book Company, Inc., 1953. 244 and x pp. Price $6.50.

Before World War II there existed only about half a dozen laboratories in the world where liquid helium was available. At present there are about fifty such laboratories, and the study of the properties of matter in the temperature range from 0.001°K. to about 20°K. is recognized as one of the outstanding fields of research in physics. Professor Squire is to be congratulated on presenting the first postwar book devoted exclusively to this fascinating field.

Low temperature physics is concerned mainly with the properties of liquid helium, he phenomenon of superconductivity, and the production and measurement of temperatures below 1°K. by magnetic means. Professor Squire has dealt quite adequately with these main topics, as well as with gas liquefaction, thermometry, equations of tate, specific heats, and heat conductivity. He has maintained a nice balance in his reatment of theory and experiment. Theories are explained briefly without too much detail, and experiments are described with figures and the results either tabulated or plotted. In the appendix are tables of the vapor pressure of helium, hydrogen, and oxygen. This book should prove valuable both to students and to research workers n the field.

Mark W. Zemansky, New York, N. Y.

ERRATA

Volume 8, Number 4, August, 1953

In the paper entitled "Light Scattering by Solutions of Octyltrimethylammonium Octanesulfonate and Octyltrimethylammonium Decanesulfonate", by E. W. Anacker, please note the following:

1. Page 405, Equation (3) should read:

$$\Sigma R_i^2 = kH^2 + aH^2C_0^2 + nA^2 + gS^2 + 2bHAC_0 + 2dHC_0S + 2fAS - 2eH^2C_0 - 2dHA - 2hHS$$

2. After the term, " $e = \Sigma \frac{C_i}{\tau_i^2}$, " insert,

" $k = \Sigma\left(\frac{C_i}{\tau_i}\right)^2$ "

DETERMINATION OF SURFACE AREA AND PARTICLE SIZE OF SYNTHETIC LATEX BY ADSORPTION

I. LATICES CONTAINING FATTY ACID SOAPS

Samuel H. Maron, Max E. Elder, and I. N. Ulevitch

Physical Chemistry Laboratory, Department of Chemistry and Chemical Engineering, Case Institute of Technology, Cleveland, Ohio

Received September 11, 1953; revised February 15, 1954

ABSTRACT

A method is described for the determination of the surface area and average particle size of synthetic latices containing fatty acid soaps. The method involves the titration of a latex with soap until the critical micelle concentration of the soap in solution is attained. From the total amount of soap adsorbed per gram of polymer at this point, and the effective molecular surface area of the soap, the above quantities can be calculated. The particle size given by this method is a volume to surface average diameter.

Two techniques have been used to determine the titration end point, surface tension and conductance. Both methods give identical results. A scheme is also presented by which correction can be applied for the amount of unadsorbed soap in solution without assumption of the value of the critical micelle concentration of the soap used. In the soap titrations any free fatty acid present in the latices is completely displaced from the polymer surface by the added soap.

The effective molecular soap areas required in the calculation of particle size and area have been determined for laurate, myristate, oleate, palmitate, stearate, and OSR soaps. It is shown that these areas are valid from about room temperature to 50°C.

INTRODUCTION

In 1944 the authors developed a soap titration method for the determination of surface area and particle size of synthetic latices; this method has been used extensively in the Government Synthetic Rubber Program, and reference has been made to it in the literature (1–5). It is the purpose of this paper to present the theory and details of the method and to show its application to synthetic latices containing fatty acid soaps as the emulsifying agents. Subsequent papers in the series will describe the use of the method for latices containing rosin soaps, as well as some other emulsifiers.

PRINCIPLE OF METHOD

Synthetic latices are aqueous dispersions of spherical polymer particles stabilized by adsorbed emulsifying agents. In most instances these emulsifying agents are soaps, whose anions are adsorbed and impart to the latex particles a negative surface charge. The quantity of soap present in most latices is sufficient to cover only a fraction of the available surface, and hence the latex particles are capable of adsorbing more soap. Further, the relatively high surface tension of most latices indicates that practically all the soap initially present is adsorbed and that the concentration of unadsorbed soap is very low and insufficient to yield micelles. Finally, all the available evidence points to the fact that the soap is adsorbed in monomolecular form by the polymer and that it exists in this form on the surface even at aqueous phase concentrations exceeding those required for micelle formation. These facts suggest the possibility of employing soap adsorption for determination of average surface area and particle size of latices.

In the use of adsorption for surface area determination, as in the BET method, the usual practice is to determine the adsorption isotherm, and to find therefrom the quantity of adsorbate necessary to saturate the surface of the adsorbent with a monolayer. In the case of latex-soap systems this procedure is not feasible. However, it is possible to carry the adsorption process to a definite concentration of unadsorbed phase in solution at which point, in view of the equilibrium between the adsorbed and unadsorbed phases, a definite quantity of the adsorbate will be present on the substrate surface.

For systems containing soaps and other emulsifiers, such an end point for the adsorption process can be the concentration of adsorbate in solution at which micelle formation sets in. By determining then the amount of emulsifier adsorbed by the latex particles per unit weight of polymer at the point of micellization, and the *effective* surface area occupied by a molecule of the emulsifier on the polymer surface at this point, we should have all the information necessary for calculation of both surface area and average particle size.

Any given latex contains initially C_i moles of soap per liter and m_0 grams of polymer per liter. Since the amount of unadsorbed soap present in a latex is a negligible fraction of the total, the moles of soap initially held by a gram of the polymer is $S_i = C_i/m_0$. The problem then is to find how much more soap has to be added per gram of polymer in order to attain the critical micelle concentration (cmc) in solution, *i.e.*, $S_a = C_a/m$, where C_a is the concentration of added and adsorbed soap, and m is the concentration of polymer.

The quantity S_a can be determined either by surface tension or conductance measurements. When a given volume of latex of known concentration is titrated with standard soap solution, and the surface tension is measured after each addition of soap, a curve such as shown in Fig. 1 is obtained. This curve consists of two branches, AB, along which the

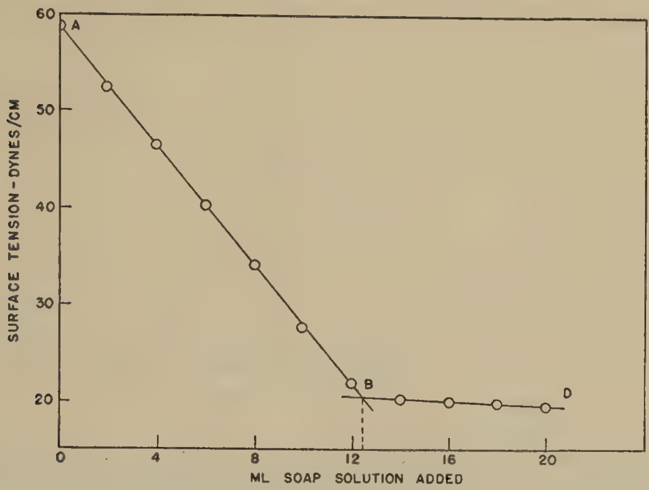

FIG. 1. Surface tension titration of a latex with soap at 50°C.

surface tension decreases rapidly with soap addition, and *BD*, along which soap addition produces very little change in surface tension. The point of intersection of the lines, *B*, gives the quantity of added soap at which micellization sets in in the aqueous phase, and is thus the sought titration end point. If we designate by V_0 the initial volume of latex taken for titration, V the volume of added soap necessary to reach point *B*, N its normality, and m_0 the initial polymer content of the latex in grams per liter, then at the cmc the concentration of added soap is

$$C = \left(\frac{V}{V_0 + V}\right) N \text{ moles per liter,} \qquad [1]$$

while that of the polymer is

$$m = \left(\frac{V_0}{V_0 + V}\right) m_0 \text{ grams per liter.} \qquad [2]$$

Instead of following the titration of a latex with soap by surface tension, we may do so by conductance. Figure 2 shows the type of plot which is obtained for $(L - L_0)$ as a function of the volume of added soap. L here is observed conductance (reciprocal of measured resistance) of the latex plus added soap solution, while L_0 is the initial conductance of the latex. It will be observed that $(L - L_0)$ rises from the origin along *AB*, and then breaks off at *B* to follow the linear curve *BD*. Here again point *B* corresponds to onset of soap micelle formation in the latex, and hence C and m can be obtained also, from the volume of titrating soap required to reach point *B* as determined by conductance measurements.

The values of C/m calculated from the breaks in either the conductance or surface tension titration curves do not yield S_a, but rather the moles

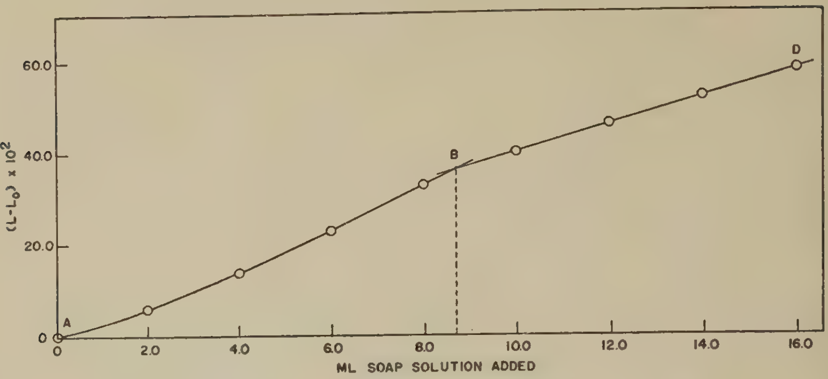

FIG. 2. Conductance titration of a latex with soap at 50°C.

of soap per gram of polymer which have to be added to a latex to bring about micellization of the soap in solution. To obtain S_a, a correction must be applied for this unadsorbed soap, and this correction, particularly with larger particle size latices, may amount to an appreciable fraction of the soap added. Furthermore, it is generally not valid to assume as the concentration of unadsorbed soap at the end point the cmc of the soap itself in aqueous solution, for most latices contain some electrolyte which modifies the cmc of the soap. Consequently, to make this correction we proceed as follows. The value of C obtained above must be equal to C_a, the concentration of added and adsorbed soap, and C_f, the concentration of unadsorbed soap in solution at the end point; *i.e.*, $C = C_a + C_f$. On division and multiplication of C_a in this equation by m we obtain

$$\begin{aligned} C &= \left(\frac{C_a}{m}\right)m + C_f \\ &= S_a\,m + C_f. \end{aligned} \qquad [3]$$

Now so long as the size of the polymer particles in a latex, or the nature of the adsorbing surface, or both, do not change, S_a should be constant. Similarly C_f, the cmc of the added soap in the given latex, should also be constant. Consequently a plot of several values of C corresponding to varying values of m should be linear, with slope equal to S_a and y-intercept equal to C_f. Figure 3 shows a typical plot obtained for C as a function of m. Its linearity establishes the validity of the above argument and permits the evaluation of both S_a and C_f from the titration data without the *a priori* assumption of a value for C_f.

In Figure 3 the solid points represent data obtained on a given latex by surface tension, and the open circles, by conductance. The fact that the data obtained by the two methods lie on the same straight line is evidence for the fact that the two methods yield identical results and that, where applicable, the two may be employed interchangeably.

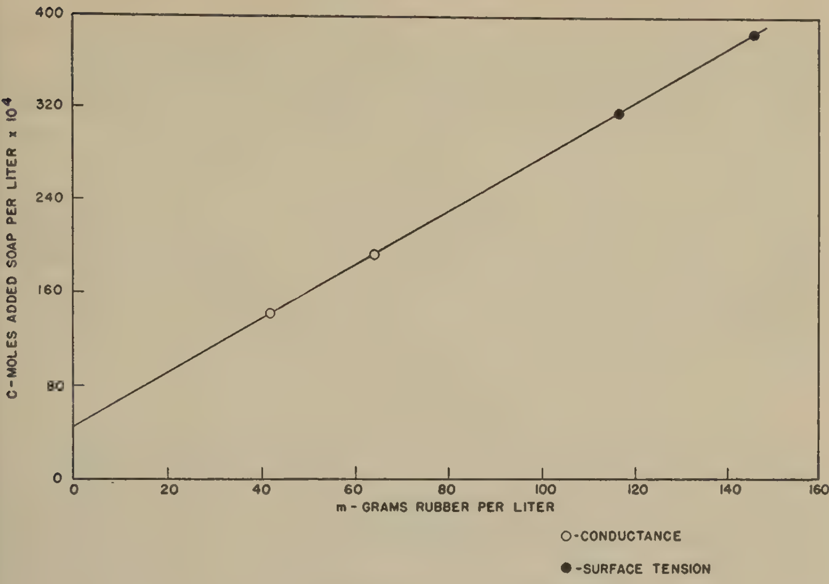

FIG. 3. Plot of C vs. m for latex.

From the values of S_a and S_i the average surface area per gram and the average particle size are readily calculable. Since the initial soap present in the latex may be different from the soap added, the areas per molecule of adsorbed soap may also be different. Therefore, let A_i be the effective area in A.^{2} per molecule of soap initially present in the latex, and A_a be the area per molecule of added soap. The surface area A in A.^{2} per gram of polymer follows then as

$$A = (S_i A_i + S_a A_a) N_0 \tag{4}$$

where N_0 is Avogadro's number. The volume of 1 g. of polymer in A.^{3} is

$$v = \frac{1 \times 10^{24}}{\rho} \tag{5}$$

where ρ is the density of the polymer, which may be taken to be the same as that of the polymer in bulk if the latices have been stripped of unreacted monomer. From Equations [4] and [5] we find for v/A

$$\frac{v}{A} = \frac{1 \times 10^{24}}{(S_i A_i + S_a A_a) N_0 \rho}. \tag{6}$$

However, since the polymer particles are spherical, we also have that for a sphere of diameter D_s, $v/A = D_s/6$. Substitution of this relation into Eq. [6] yields then for D_s, the average diameter of the latex particles in A.,

$$\begin{aligned} D_s &= \frac{6 \times 10^{24}}{(S_i A_i + S_a A_a) N_0 \rho} \\ &= \frac{9.961}{(S_i A_i + S_a A_a) \rho} \end{aligned} \tag{7}$$

Equations [4] and [7] are the relations employed to calculate surface area per gram and the particle size of the latices from adsorption data.

Since the particles in latices are generally not uniform in size, Eq. [7] yields a volume to surface type average diameter, *i.e.*,

$$D_s = \frac{\sum f_i D_i^3}{\sum f_i D_i^2} \qquad [8]$$

where f_i is the fraction of the total number of particles having diameter D_i. This average is to be distinguished from other types of averaging, such as number or weight (6).

EXPERIMENTAL

Determination of Initial Soap Content

The initial soap content of the latices and soap solutions used was determined by conductometric titration with HCl in 50% isopropanol-water as solvent (7). In each case the latices were analyzed also for fatty acid by similar means (7). To avoid at this stage possible complications by free fatty acid, any of the latter present in the latices was neutralized by addition of the requisite quantity of standard NaOH. Stock solutions of the neutralized latex were rechecked then for initial soap content by conductometric titration with HCl.

Determination of Initial Rubber Content of Latices

The initial rubber content of the stock solutions of latex was obtained by coagulation of the rubber in given volumes of latex with 99% isopropanol, washing with this solvent and water, drying of the polymer *in vacuo*, and weighing.

Determination of C and m

The procedures employed to determine these quantities were as follows:

a. Surface Tension Method. Twenty-five to fifty ml. of latex were placed in a 300- or 500-ml. flask; the flask was stoppered and immersed in a thermostat. When thermal equilibrium was established, a surface tension reading was taken. Next a given volume, say 1 or 2 ml., of standard soap solution was added, and the flask shaken with a rotary motion. After several minutes the surface of the latex was swept with a flattened glass rod or platinum foil, and the surface tension measured again. This procedure of soap addition, shaking, and surface tension measurement was repeated until enough soap was added to the latex sample to yield several points past break B in Fig. 1. The exact position of B was found by plotting as in Fig. 1 the observed corrected surface tensions versus the volumes of added soap. C and m were calculated then by Eq. [1] and [2].

All surface tension measurements were made with a duNouy ring tensiometer modified to permit measurements on samples immersed in a thermostat. In each instance at least three readings were taken and averaged. The averaged "pull" values were corrected to yield surface tensions by means of a calibration curve constructed from the correction equation given by Zuidema and Waters (8) and based on the work of Harkins and Jordan (9). It is these corrected surface tensions which are plotted in Fig. 1.

The above operations were repeated with several initial concentrations of rubber for a given latex to yield at least three values of C and m to be plotted as in Fig. 3. The slopes of such plots were taken then to obtain S_a.

b. The Conductance Method. The procedure here was very similar to the above, except that a conductivity cell replaced the Erlenmeyer flask, and a Wheatstone bridge the modified duNouy tensiometer. The cell employed is illustrated in Fig. 4. In this cell stirring was accomplished by alternate blowing and suction of the solution through one of the side arms. To avoid introduction of CO_2, the suction and blowing in of air was done through an ascarite tube. After introduction of 25–40 ml. of latex the cell was placed in the bath, brought to temperature, and a resistance reading taken. This gives $L_0 = 1/R_0$. Soap was then added in aliquot volumes, the solution mixed, allowed to reach equilibrium, and its resistance measured to yield L. The procedure was repeated until enough points were obtained to show a break such as B in Fig. 2.

In this work two a.-c. bridges were used, a portable 60-cycle Leeds and Northrup conductivity bridge, and a precision 1000-cycle Leeds and

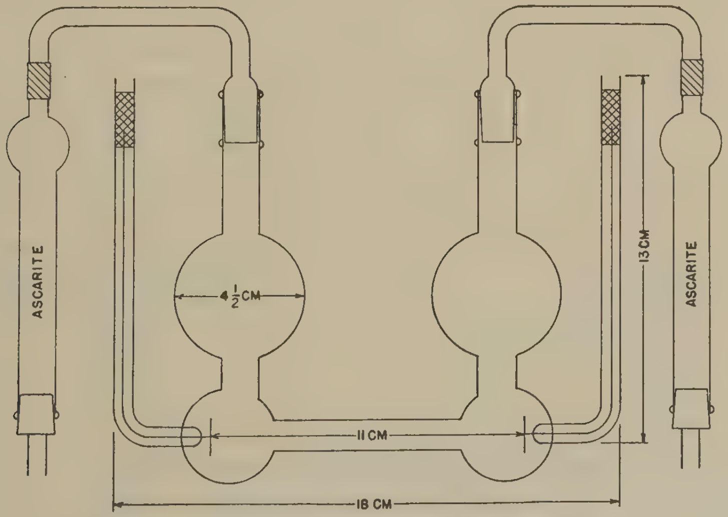

FIG. 4. Conductivity cell for latex-soap titrations.

Northrup Campbell-Shackelton assembly. For some solutions, where the conductance changes are pronounced, the former bridge does quite well, but in solutions where this is not the case, the more sensitive assembly must be used.

Of the two methods described, the one utilizing surface tension is somewhat faster and can be used in latices of any concentration. On the other hand, the conductance method may be applied satisfactorily only to latices of rubber contents up to 100–125 g. per liter. At higher rubber contents the changes in conductance on soap addition are generally too small to give sharp breaks at the saturation point.

Except where indicated, all measurements were made at 50°C. This temperature was chosen to permit the handling of fairly concentrated soap solutions, 0.05–0.25 N, for addition to latex without danger of gelation or curd segregation. The soap solutions were prepared and analyzed at 50°C., and were kept and added to latex at the same temperature.

The Effective Molecular Areas of Various Soaps

Before the surface areas and particle diameters of the latices studied can be calculated from the experimental data, the effective areas occupied on the polymer surfaces by the various soaps used must be known. The manner in which these molecular soap areas were arrived at will now be described.

In Table I are presented the results obtained on titration of nineteen latices with various soaps. The columns present in order the latex number, polymer composition, the nature of the initial soap, the initial soap content in equivalents per gram of polymer (S_i), and the values of S_a found on titration of the various latices with the indicated fatty acid soaps. The laurate, myristate, palmitate, stearate, and oleate soaps used for titration as well as for the preparation of the indicated latices were made from C.P. grade fatty acids obtained from the Amend Drug and Chemical Company in New York City. Potassium and sodium soaps were both used, since it was found that soaps containing these two cations gave identical results for S_a. The latices containing OSR soap were either regular or special plant products prepared with the standard fatty acid soap employed in the plants for the preparation of these latices. The OSR soap employed for titration was also the same standard product. In all instances any free fatty acid present in the latices was neutralized with NaOH or KOH prior to titration.

Inspection of the S_a values found on titration of a given latex with various soaps reveals that these differ with the nature of the titrating soap. This variation may be due to exchange of the titrating soap with the initial soap already present on the surface or to the fact that the different soaps occupy different effective areas on the polymer surface at the cmc.

TABLE I

Soap Titration Results for Various Latices

Latex no.	Type	Initial soap	S_i, equiv./g. × 10^4	S_a equiv./g. × 10^4					
				Oleate	Laurate	Myristate	Palmitate	Stearate	OSR
236	70:30 BD-St[a]	Laurate	2.82	2.98	2.00	2.60	—	—	—
238	70:30 BD-St	Laurate	1.14	—	3.30	—	—	—	—
235	70:30 BD-St	Myristate	2.51	—	1.49	2.09	—	—	—
240	70:30 BD-St	Oleate	1.53	3.76	—	3.37	—	—	4.01
19	70:30 BD-St	OSR	2.63	2.63	—	—	—	—	2.72
17	70:30 BD-St	OSR	2.25	2.37	—	—	—	—	2.41
205	70:30 BD-St	OSR	2.57	2.00	1.20	—	2.01	2.28	2.25
220	70:30 BD-St	OSR	2.36	2.08	1.54	1.62	—	—	2.37
211	70:30 BD-St	OSR	1.97	2.38	—	2.14	2.75	—	2.40
210	70:30 BD-St	OSR	2.17	1.96	1.33	—	2.40	2.53	2.05
14	70:30 BD-St	OSR	2.30	2.03	—	—	—	—	—
242	70:30 BD-St	Oleate	0.89	3.02	2.04	2.50	—	—	3.38
204	70:30 BD-St	OSR	2.03	1.99	1.30	1.50	2.10	2.21	—
242A	70:30 BD-St	Oleate	0.89	2.78	—	—	—	—	—
243	70:30 BD-St	Palmitate	0.83	2.69	—	—	3.24	—	—
250	50:50 BD-St	OSR	2.37	1.77	—	1.43	2.02	2.31	1.87
628	Polystyrene	Oleate	1.07	2.45	1.93	—	—	—	—
630	Polystyrene	Oleate	0.80	1.89	—	—	—	—	—
629	Polystyrene	Oleate	0.46	1.92	—	1.58	—	—	—

[a] BD—Butadiene; St—Styrene.

If exchange is present, then it is to be anticipated that the value of S_a observed will depend on the nature of the titrating soap as well as the soap initially present. On the other hand, if the various soaps occupy different areas and no exchange is present, then the relative values of S_a observed with various soaps should depend only on the soaps used for titration and be independent of the nature of the initial soap in the latex.

That the latter is the case is shown by the data in Table II. Here the columns list for each latex the ratio of S_a found for the given soap to that found with oleate. It will be observed that these ratios are fairly constant for a given soap and independent of the soap initially present in the latex. Consequently the variations in S_a observed are due to the fact that different soaps occupy different effective molecular areas on the polymer surface. Furthermore, the average values of the ratios give the effective molecular areas of the soaps relative to that of the oleate molecule, and as soon as the area of the latter molecule is found, the areas of the other soaps would follow.

The effective area occupied by the oleate molecule on the polymer surface was determined as follows. If we let A_0 be the oleate area, and k_i and k_a the respective areas of the soap initially present and added to the

TABLE II

Relative Molecular Areas of Various Soaps

(Oleate = 1.00)

Latex no.	Laurate	Myristate	Palmitate	Stearate	OSR
236	1.49	1.15	—	—	—
240	—	1.12	—	—	0.94
19	—	—	—	—	0.97
17	—	—	—	—	0.98
205	1.67	—	0.99	0.88	0.89
220	1.35	1.28	—	—	0.88
211	—	1.11	0.87	—	0.99
210	1.47	—	0.82	0.77	0.96
242	1.48	1.21	—	—	0.89
204	1.53	1.33	0.95	0.90	—
243	—	—	0.83	—	—
250	—	1.23	0.88	0.77	0.95
628	1.27	—	—	—	—
629	—	1.22	—	—	—
Average	1.47 ± 0.09	1.21 ± 0.06	0.89 ± 0.05	0.83 ± 0.06	0.94 ± 0.03

latex relative to that of the oleate, then $A_i = k_i A_0$, $A_a = k_a A_0$, and Eq. [7] becomes

$$D_s = \frac{9.961}{(S_i k_i A_0 + S_a k_a A_0)\rho}$$

from which $D_s A_0$ follows as

$$D_s A_0 = \frac{9.961}{(S_i k_i + S_a k_a)\rho} \qquad [9]$$

Using the data in Table I and the ratios in Table II, $D_s A_0$ values for eight latices were calculated by means of Eq. [9], and these are given in Table III. For any given latex $D_s A_0$ should be constant within experimental error and independent of the nature of the titrating soap. Such is the case. The average values of $D_s A_0$ for these latices are shown in column 7 of the table.

To resolve the product $D_s A_0$, D_s values for all the latices listed in Table III were obtained by electron microscopy in the manner already described (6), and these are given in column 8 of the table. Division of $D_s A_0$ by D_s yields the A_0 values shown in the last column of the table. These may be seen to be quite constant, and give 28.2 ± 1.4 A.^{2} for the effective area of the oleate molecule. From the value of A_0 for oleate and the relative molecular soap areas of Table II, we obtain finally the effective areas for the various fatty acid soaps used here. These are summarized in Table IV.

Table IV shows that for the saturated fatty acids the effective area

TABLE III

Effective Area of Oleate Molecule

Latex no.	Initial soap	$D_sA_0 \times 10^4$					D_s (A.) (E. M.)	A_0(A^2.)
		Titrating soap				Average		
		Laurate	Myristate	Oleate	OSR			
236	Laurate	1.53	1.49	1.52	—	1.51 ± 0.02	570	26.5
238	Laurate	1.66	—	—	—	1.66	630	26.3
240	Oleate	—	1.93	2.05	2.05	2.01 ± 0.05	700	28.7
235	Myristate	2.07	1.95	—	—	2.01 ± 0.06	720	27.9
220	OSR	2.42	(2.60)	2.52	2.44	2.46 ± 0.04	790	31.1
242A	Oleate	—	—	2.96	—	2.96	1100	26.9
630	Oleate	—	—	3.52	—	3.52	1270	27.7
629	Oleate	—	4.00	3.98	—	3.99 ± 0.01	1300	30.7
Average								28.2 ± 1.4 ± 5.0%

TABLE IV

Effective Molecular Areas of Fatty Acid Soaps

Soap	Relative area (Oleate = 1.00)	Molecular area (A^2.)
Laurate	1.47	41.4
Myristate	1.21	34.1
Oleate	1.00	28.2
OSR	0.94	26.5
Palmitate	0.89	25.1
Stearate	0.83	23.4

occupied by a soap molecule on the surface of the latex particle decreases as the number of carbon atoms in the straight chain increases. This means that at the cmc the higher molecular weight soaps are adsorbed in a more condensed layer than are the lower molecular weight soaps. The unsaturated oleate molecule occupies an area intermediate between the 14 carbon chain myristate and the 16 carbon chain palmitate. Again the OSR soap, which is a mixture of oleate, palmitate, and stearate, yields an effective area intermediate between oleate and the other two soaps, which is as expected.

Another important point indicated by these areas is that the soaps are adsorbed in a monolayer. The cross-sectional area of a straight-chain saturated fatty acid soap is *ca.* 21 $A.^2$. If the soaps were adsorbed in multilayers, the effective molecular areas of the various soaps would have to be below this figure. Actually, however, the stearate molecule gives an effective area which is very close to that for a condensed monolayer, while the other soaps show areas which indicate greater or lesser degrees of monolayer expansion at the micellization point.

Particle Diameters and Surface Areas of Various Latices

By combining the molecular soap areas given in Table IV with the titration data of Table I, the particle sizes and areas per gram of the various latices studied are readily calculable now through Eqs. [7] and [4]. The results of these calculations are summarized in Table V, where for comparison are given also the particle diameters and areas determined for eight of the latices by electron microscopy. The areas in Table V are expressed in square meters per gram, and are the values in A.^{2} yielded by Eq. [4] multiplied by 10^{-20}. The densities employed in Eq. [7] were 0.919 for the 70:30 BD-St polymer, 0.971 for the 50:50 BD-St rubber, and 1.05 for polystyrene. In the last column of the table is given also the percentage of the total polymer surface covered initially with soap. This percentage, P_i, is given in terms of the titration data by

$$P_i = 100 \left(\frac{S_i A_i}{S_i A_i + S_a A_a} \right). \qquad [10]$$

Inspection of the results presented in Table V reveals excellent concordance in the values of D_s obtained on titration of a given latex with various soaps. Further, the agreement in both D_s and A, as obtained by soap titration and electron microscopy, is quite satisfactory. Finally, perusal of the last column of the table shows that, depending on the initial soap content, latices may vary widely in the extent of surface coverage by soap. Actually,

TABLE V

Particle Diameters and Surface Areas of Various Latices

Latex no.	Initial soap	D_s(A.)								A(m.^{2}/g.)		P_i
		Titrating soap						Average, soap titration	Electron microscope	Soap titration	Electron microscope	
		Laurate	Myristate	Oleate	OSR	Palmitate	Stearate					
236	Laurate	540	530	540	—	—	—	537 ± 4	570	122.5	114.5	57.8
238	Laurate	590	—	—	—	—	—	590	630	110.7	103.6	25.7
235	Myristate	730	690	—	—	—	—	710 ± 20	720	91.5	90.7	56.5
240	Oleate	—	680	730	730	—	—	713 ± 22	700	91.7	93.3	28.4
19	OSR	—	—	750	770	—	—	760 ± 10	—	86.1	—	48.8
17	OSR	—	—	860	880	—	—	870 ± 10	—	75.3	—	47.8
205	OSR	920	810	870	850	910	890	875 ± 33	—	74.7	—	55.1
220	OSR	860	920	890	870	—	—	885 ± 20	790	73.1	82.6	51.0
211	OSR	—	870	910	940	900	980	920 ± 32	—	72.3	—	44.1
210	OSR	960	840	960	970	920	930	930 ± 33	—	70.9	—	49.4
14	OSR	—	—	920	970	—	—	945 ± 25	—	69.7	—	53.2
242	Oleate	990	980	980	950	—	—	975 ± 13	—	67.0	—	22.6
204	OSR	1010	1030	990	1050	1020	1030	1022 ± 15	—	64.0	—	50.7
242A	Oleate	—	—	1050	—	—	—	1050	1100	62.2	59.4	24.3
243	Palmitate	—	—	1120	—	1060	—	1090 ± 30	—	59.9	—	21.0
250	OSR	—	920	910	910	900	880	904 ± 11	—	68.8	—	55.4
628	Oleate	860	—	960	—	—	—	910 ± 50	—	63.1	—	28.9
630	Oleate	—	—	1250	—	—	—	1250	1270	45.7	45.0	29.7
629	Oleate	—	1420	1410	—	—	—	1415 ± 5	1300	40.4	44.0	19.4

the figures shown are the upper limits for this coverage for the given latices, since the free fatty acid in these latices has been neutralized. In the latices containing some unneutralized fatty acid the extent of surface coverage by soap is actually lower. These variations in the extent of surface coverage with soap are reflected in the variations observed in the stability of the various latices.

Effect of Free Fatty Acid

In all the experiments described heretofore any free fatty acid present in the latices has been converted to soap by addition of base. Since, however, most latices prepared with fatty acid soaps generally contain some free fatty acid, unless their pH has been adjusted to 10 or higher, it is of nterest to investigate what effect this free acid has on the soap titration method presented here.

To check this point, three of the latices which have already been studied, Nos. 14, 17, and 19, were retitrated with OSR soap without prior neutralization of the free fatty acid. The results obtained, as well as the corresponding ones for the neutralized latices, are summarized in Table VI. It will be observed that in all instances the value of S_a obtained with the unneutralized latices is larger than that for the neutralized ones. *However, in both titrations the sum of $S_i + S_a$ is essentially constant for a given latex.* This means that the free fatty acid, if adsorbed, is completely replaced on the polymer surface by the added soap and behaves in the soap titration as if it were not present in the system. Consequently, latices can be titrated directly without prior neutralization of the free fatty acid, provided that only the *initial soap present as such* is determined and used in the calculation of the particle size and surface area. The validity of this statement is borne out by the last item in Table VI, where the D_s values calculated from the $(S_i + S_a)$ values for the unneutralized and neutralized latices are compared. Within experimental error these are dentical.

Effect of Temperature

All the measurements described heretofore were made at 50°C. A question which arises is whether the effective surface areas determined at this

TABLE VI

Soap Titration of Latices with Unneutralized Fatty Acid

Quantity	Latex no. 14		Latex no. 17		Latex no. 19	
	Unneutral.	Neutral.	Unneutral.	Neutral.	Unneutral.	Neutral.
$S_i \times 10^4$	1.68	2.30	1.60	2.25	2.11	2.63
$S_a \times 10^4$	2.46	1.92	2.94	2.41	3.15	2.72
$(S_i + S_a) \times 10^4$	4.14	4.22	4.54	4.66	5.26	5.35
D_s(A.)	950	970	860	880	760	770

temperature are also valid at temperatures nearer to room temperature. To check this point a 70:30 BD-St latex containing initially 2.50×10^{-4} equivalents of OSR soap per gram of rubber was titrated with sodium oleate at 50°C. and 35°C. The results obtained for S_a at the two temperatures were, respectively, 2.05×10^{-4} and 2.00×10^{-4} equivalents per liter. These data, and the densities of the polymer at the two respective temperatures, 0.919 and 0.927 g. per cubic centimeter, yield $D_s = 861$ A. at 50°C. and $D_s = 863$ A. at 35°C. Consequently, the effective soap areas given in Table IV are applicable at 35°C. as well as at 50°C., and in all probability would be valid also for use at room temperature.

SIMPLIFIED PROCEDURE FOR SURFACE AREA AND PARTICLE SIZE

The method as described heretofore calls for the determination of several values of C at differing values of m, the construction of a C vs. m plot, and the evaluation of the slope of the curve to obtain the sought S_a. This procedure is rather lengthy and tedious when routine particle size and surface area determinations are run on a particular type of latex by titration with a single specific soap. Under such conditions it is generally found that the value of C_f for the system used is quite constant; and, once this value of C_f is determined, it is possible to reduce the measurements to a single titration as follows. Division of Eq. [3] by m and rearrangement yields for S_a

$$S_a = \frac{C - C_f}{m} \qquad [11]$$

and consequently a single determination of C and m is sufficient to yield S_a.

Table VII shows some data to illustrate how well this single titration procedure operates. In this case a particular type of latex has been titrated with sodium oleate at 50°C., and it has been found from C vs. m plots that C_f is essentially constant and equal to 33×10^{-4} mole per liter. This value of C_f was used then with some single titration data to obtain S_a by Eq. [11]. Table VII compares the results with those deduced graphically. The agreement may be seen to be satisfactory.

TABLE VII

Test of Simplified Procedure for Evaluation of S_a

Latex	m	$C \times 10^4$	$S_a \times 10^4$	
			Eq. [11]	Graphical
I	139.5	326	2.10	2.03
II	134.5	350	2.35	2.37
III	130.0	372	2.61	2.63

Discussion

The method described in this paper has been applied in our laboratory to hundreds of latices, and it has proved to be very reliable and reproducible, particularly when applied to latices of particle size below 2000 A. in diameter. In larger particle latices the initial soap contents and the amounts of additional soap required are low, and hence great care must be exercised in the determination of these. In such instances it is advisable to titrate larger samples of latex than indicated here.

The only serious difficulty encountered has been with latices which contain besides soap also electrolytes or other emulsifiers which titrate along with soap on addition of HCl during the conductometric determination of the initial soap content. Under such conditions it has been found necessary to isolate the soap from the latices prior to analysis. Generally the auxiliary emulsifiers found in some latices cause no trouble during the determination of S_a. In such titrations they behave like free fatty acid, and they are displaced from the surface of the latex particles by the more strongly adsorbed soap.

Acknowledgment

This work was performed as a part of the research project sponsored by the Reconstruction Finance Corporation, Office of Synthetic Rubber, in connection with the Government Synthetic Rubber Program.

References

1. Klevens, H. B., *J. Colloid Sci.* **2,** 365 (1947).
2. Borders, A. M., and Pierson, R. M., *Ind. Eng. Chem.* **40,** 1473 (1948).
3. Willson, E. A., Miller, J. R., and Rowe, E. H., *J. Phys. & Colloid Chem.* **53,** 357 (1949).
4. Maron, S. H., Madow, B. P., and Krieger, I. M., *J. Colloid Sci.* **6,** 584 (1951).
5. Morton, M., Salatiello, P. P., and Landfield, H., *J. Polymer Sci.* **8,** 279 (1952).
6. Maron, S. H., Moore, C., and Powell, A. S., *J. Appl. Phys.* **23,** 900 (1952).
7. Maron, S. H., Ulevitch, I. N., and Elder, M. E., *Anal. Chem.* **21,** 691 (1949); *ibid.* **24,** 1068 (1952).
8. Zuidema, H. H., and Waters, G. W., *Ind. Eng. Chem.* **13,** 312 (1941).
9. Harkins, W. D., and Jordan, H. F., *J. Am. Chem. Soc.* **52,** 1751 (1930).

DETERMINATION OF SURFACE AREA AND PARTICLE SIZE OF SYNTHETIC LATEX BY ADSORPTION

II. LATICES CONTAINING ROSIN ACID SOAPS

Samuel H. Maron, Max E. Elder, and Carl Moore

Physical Chemistry Laboratory, Department of Chemistry and Chemical Engineering, Case Institute of Technology, Cleveland, Ohio

Received September 17, 1953; revised February 13, 1954

Abstract

The soap titration method (1) for determination of synthetic latex particle size and specific surface area, applied before to latices containing fatty acid soaps, has been extended to include latices prepared with rosin soaps of various kinds. In this connection it was found that only conductance is a reliable means of following the titration, since surface tension measurements give curves from which it is difficult to ascertain the end point.

Effective molecular surface areas have been determined for the sodium and potassium soaps of K-wood rosin, Resin 731, Pexite 42, and Gum 42. The areas for the two soaps of a given rosin acid are identical. Furthermore, the areas remain constant between 25° and 50°C.

Free rosin acid in a latex does not interfere with the titration and behaves as if it were not present in the system. Hence it is not necessary to neutralize the free rosin acid prior to the addition of soap.

It was also found that fatty acid soaps can displace, at least partially, rosin soaps from the polymer surface. The reverse displacement, *i.e.*, of fatty acid by rosin soaps, does not occur. These observations indicate that fatty acid soaps are adsorbed more strongly by the polymer than are the rosin soaps.

Introduction

In the first paper of this series (1) was presented a detailed adsorption procedure for the determination of the particle size and surface area of synthetic latices. The method involves the titration of a latex of known polymer and soap content with a standard soap solution until the critical micelle concentration (cmc) is reached. From a knowledge of the amount and kind of soap adsorbed at the cmc, and the effective molecular area of the soap on the surface, the surface area of the particles per gram, A, and the average particle diameter, D_s, can be calculated by means of the equations

$$A = (S_i A_i + S_a A_a) N_0 \text{ in } A.^2 \quad [1]$$

$$D_s = \frac{9.961}{(S_i A_i + S_a A_a)\rho} \text{ in } A. \quad [2]$$

Here S_i is the initial soap content of the latex in equivalents per gram of polymer, S_a the equivalents of titrating soap adsorbed per gram of polymer at the cmc, A_i and A_a the effective molecular soap areas of the initial and added soap, respectively, and ρ is the density of the polymer. S_a is obtained by titrating several solutions of varying polymer content and ascertaining the concentrations of added soap C and polymer content m at the titration end point. Then

$$C = S_a m + C_f, \qquad [3]$$

where C_f is the cmc of the soap in the latex, a constant, and hence a plot of C vs. m is linear, and S_a follows from the slope of the line.

The first paper (1) dealt with the application of the method to the determination of the surface area and particle size of the polymer in latices containing fatty acid soaps as the emulsifying agents. The purpose of this paper is to show how the method may be extended to latices prepared with rosin acid soaps, and to present some results obtained on systems of this type.

Experimental

The rosin soaps used here were the sodium and potassium salts of K-wood rosin of the type normally used in the preparation of latices, and the following rosin soaps supplied through the courtesy of the Hercules Powder Company: Dresinate 731, 214, 87, 90, and 89. The properties of these dresinates have already been described (2). Dresinates 731 and 214 are, respectively, the sodium and potassium salts of Resin 731, Dresinates 87 and 90 are the sodium and potassium salts of Pexite 42, and Dresinate 89 is the potassium salt of Gum 42.

Solutions of the rosin soaps were prepared by dissolving approximately 60 g. of the particular dresinate in a liter of distilled water. Each solution was checked first for free rosin acid content by conductometric titration with base in 50% isopropanol (3a), and any free acid found was neutralized with NaOH or KOH, as required. Finally the soap content of each solution was determined by conductometric titration with acid (3a), and the solution diluted to approximately 0.1 *N*. The latter solutions were used then to titrate the latices.

The K-wood rosin soaps were prepared by dissolving the rosin in KOH and NaOH, adjusting the solutions until no free rosin was present, and then analyzing them for soap in the same manner as the dresinates.

The rosin soap latices used were mostly commercial products of regular or experimental production. The polymer, soap, and rosin acid contents of these latices were determined as described before (1, 3b). Any free rosin acid found was neutralized by the addition of the appropriate base. Except where otherwise indicated, all the results given here are for these neutralized latices.

Titration of the latices with soap was conducted by the same procedure as used with fatty acid soaps (1). The temperature was again 50°C., except where the effect of temperature was being investigated.

BEHAVIOR OF LATICES ON TITRATION WITH SOAP

It was shown before (1) that with fatty acid soaps both surface tension and conductance measurements constitute equally satisfactory means of determining the soap titration end point. However, this is not the case with rosin soaps. When a latex is titrated with a rosin soap and the titration is followed by measurement of surface tension, we obtain a plot such as shown in Fig. 1. Whereas in the case of fatty acid soaps the plot consists of two intersecting straight lines from which the end point can be ascertained unambiguously, with rosin soaps the branch *AB* is curved, and it thus becomes difficult to obtain the end point, which is actually at point *B*. Consequently *surface tension is not a satisfactory means of following the titration of latices with rosin soaps*. On the other hand, conductance works well here, as may be seen from Fig. 2, where a plot is given of $(L - L_0)$ vs. ml. of added soap. $(L - L_0)$ is the difference between the conductance at any stage of the titration and the conductance of the latex sample prior to addition of soap. For this reason only conductance was employed to follow the titration of latices with rosin soaps.

The shapes of the conductance titration curves which have been observed in this and prior work are not always those shown in Fig. 2. With latex samples of relatively high rubber content the conductance of the

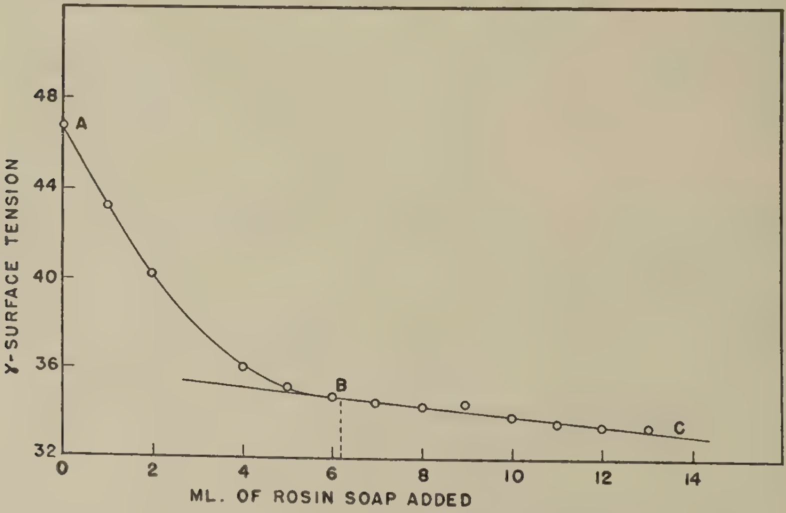

FIG. 1. Surface tension titration of latex with sodium soap of K-wood rosin at 50°C.

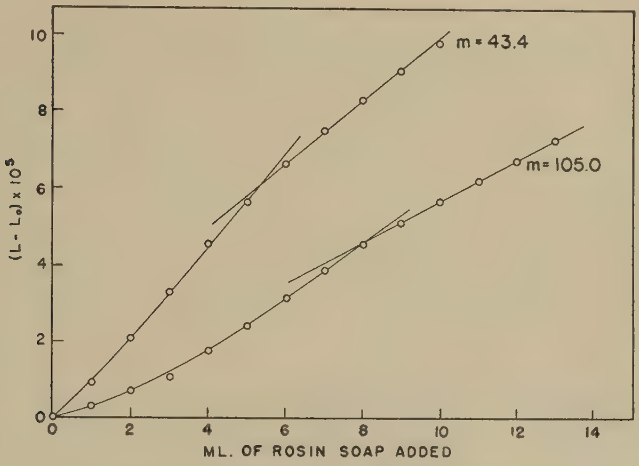

FIG. 2. Conductance titration of latex with sodium soap of K-wood rosin at 50°C.

latex–soap mixture may actually fall below that of the latex itself in the initial titration stages. However, we have found that the exact course of $(L - L_0)$ vs. ml. of added soap is unimportant so long as the break in the curve is observed. The sharpness of the break and the shape of the curve observed are functions of the relative conductances of the latex and soap solutions used. When these are close together, the break may not be sharp and may, in fact, be non-existent for some combinations of conductances. Under these conditions, a change in the rubber content of the latex solution used or the concentration of the soap solution employed for titration readily rectifies the situation and sharpens the end-point detection.

In Figure 3 is given a typical plot of C vs. m for a latex titrated with rosin soap. As found with fatty acid soaps and latices (1), the plot is linear in line with Eq. [3], and its slope yields S_a, the moles of added soap adsorbed per gram of polymer at the cmc.

Such straight lines for C vs. m plots have been observed not only with rosin latices titrated with rosin soaps but also on titration with rosin soaps of latices containing fatty soaps. However, when C vs. m plots were prepared from data obtained by titration of rosin latices with fatty acid soaps, the lines were no longer straight but concave downwards. This behavior was traced to exchange of added fatty acid soap for rosin soap adsorbed on the polymer surface. It indicates that fatty acid soaps are adsorbed more strongly than rosin soaps. Still, the exchange is not complete at the cmc, and hence it is not advisable for the purpose at hand to titrate rosin-containing latices with fatty soaps.

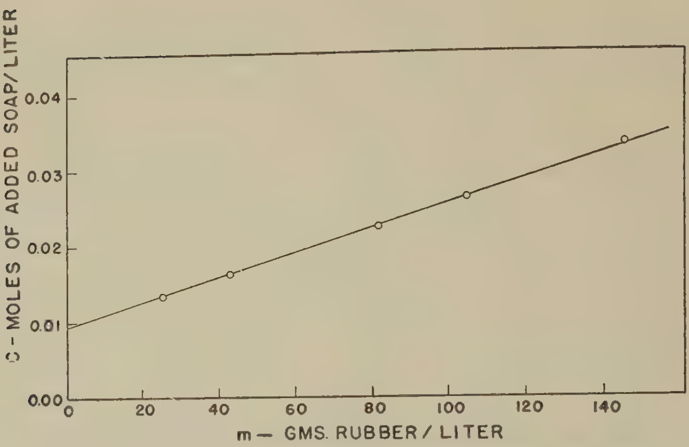

FIG. 3. Plot of C vs. m for latex titrated with sodium soap of K-wood rosin.

EFFECTIVE SURFACE AREAS OF ROSIN SOAP MOLECULES

The scheme employed for evaluation of the effective molecular areas of the dresinates involved the titration of several fatty acid soap latices first with oleate and then with the various rosin soaps. Since, as was pointed out above, rosin soaps do not displace fatty acid soaps from the polymer surface, then the amount of added oleate adsorbed per gram by a given latex at the cmc, $(S_a)_{\text{oleate}}$, is equivalent in effective surface coverage to the amount of added dresinate adsorbed by the same latex, $(S_a)_{\text{dresinate}}$. Consequently

$$A_{\text{dresinate}} (S_a)_{\text{dresinate}} = A_{\text{oleate}} (S_a)_{\text{oleate}} ,$$

where $A_{\text{dresinate}}$ and A_{oleate} are the effective molecular areas of the two soaps, and

$$A_{\text{dresinate}} = A_{\text{oleate}} \left[\frac{(S_a)_{\text{oleate}}}{(S_a)_{\text{dresinate}}} \right]. \qquad [4]$$

With the oleate area known as 28.2 A. (1), a determination of the S_a ratio is sufficient to yield $A_{\text{dresinate}}$.

In Table I are summarized the data obtained on titration of three fatty acid soap latices with oleate and the various dresinates. The latices contained 70:30 butadiene-styrene polymer and were prepared with OSR (standard Office of Synthetic Rubber) soap. The second column of the table lists the initial soap content of the latices, the third column S_a for the oleate, and the remaining columns give the found ratios for $(S_a)_{\text{oleate}}/(S_a)_{\text{dresinate}}$. It will be observed first that for a given rosin acid these ratios are essentially the same for the sodium and potassium soaps, and hence they depend only on the nature of the soap anion. Second, within a

TABLE I

Effective Molecular Areas of Rosin Soap Molecules

Latex no.	$S_i \times 10^4$ (OSR)	$S_a \times 10^4$ Oleate	S_a oleate/S_a dresinate			
			K-wood rosin	Resin 731	Pexite 42	Gum 42
1	2.16	2.03	1.25 (Na) —	1.48 (Na) 1.62 (K)	— 1.48 (K)	— 1.33 (K)
2	2.23	2.34	1.27 (Na) 1.29 (K)	1.57 (Na) 1.57 (K)	1.50 (Na) —	— 1.46 (K)
3	2.80	2.44	1.23 (Na) 1.21 (K)	1.60 (Na) 1.45 (K)	1.43 (Na) 1.46 (K)	— 1.35 (K)
Average			1.25 ± 0.02 ± 1.6%	1.55 ± 0.05 ± 3.2%	1.47 ± 0.02 ± 1.4%	1.38 ± 0.05 ± 3.6%
Effective molecular area (A.^{2})			35.2	43.7	41.5	38.9

TABLE II

Particle Diameters Calculated from Soap Areas

Titrating soap	D_s (A.)		
	Latex no. 1	Latex no. 2	Latex no. 3
leate	950	870	760
-wood rosin	950	880	750
esin 731	950	870	750
exite 42	950	880	750
um 42	930	890	750

mall percentage error the ratios, as expected, are constant for a given osin acid and independent of the latex used. Employing then the average alues of these ratios in Eq. [4], we obtain the effective surface areas iven at the bottom of the table for soaps of the four rosin acids in ques- ion.

As a check on these areas, there are given in Table II the particle sizes f the three latices calculated from the data given in Table I. The agree- nent among the results yielded by the four rosin soaps and oleate is ex- ellent.

PARTICLE SIZE AND SURFACE AREA OF SOME ROSIN SOAP LATICES

With the effective surface areas available, particle size and surface area eterminations were run on ten rosin soap latices, in which any free rosin cid present was neutralized with base prior to soap titration. In each

TABLE III

Particle Size and Surface Area of Some Rosin Soap Latices

Latex no.	Type[a]	Initial and added soap	$S_i \times 10^4$	$S_a \times 10^4$	D_s (A.)	A (m.²/g.)	P_i
301	50 BD-50 St	K-wood rosin	2.89	0.69	810	75.9	80.7
302	50 BD-50 St	K-wood rosin	2.26	1.56	760	80.0	59.2
303	50 BD-50 St	K-wood rosin	2.51	0.62	930	66.3	80.2
304	50 BD-50 St	K-wood rosin	2.73	0.48	910	68.0	85.0
305	50 BD-50 St	K-wood rosin	2.39	0.69	950	65.3	77.6
312	50-BD-50 St	K-wood rosin	2.41	0.71	930	66.1	77.2
311	50 BD-50 St	Dresinate 90	1.21	0.98	1130	54.7	55.3
319	50 BD-50 St	Dresinate 214	1.61	2.67	550	112.6	37.6
251	75 BD-25 St	Dresinate 731	2.24	1.79	620	106.0	55.6
604	75 Is-25 St	Dresinate 731	2.77	2.19	500	130.5	55.8

[a] BD—Butadiene; St—Styrene; Is—Isoprene.

instance the same soap was used for titration as was present in the latex initially. The results obtained are summarized in Table III. The values of D_s were calculated from S_i and S_a by means of Eq. [2] using $\rho = 0.971$ for the 50:50 BD-St polymers at 50°C., and $\rho = 0.919$ for the 75:25 BD-St and Is-St polymers. The area per gram, A, was calculated from Equation [1] and converted from A.^{2} to square meters by multiplication by 10^{-20}. Finally, P_i is the percentage of the total area initially covered by the soap and is given by

$$P_i = 100 \left(\frac{S_i A_i}{S_i A_i + S_a A_a} \right). \qquad [5]$$

Inspection of the table reveals that the K-wood rosin latices, which were all commercial Type III products, range in particle diameter from *ca.* 700–1000 A., and exhibit initial surface coverage with soap of 60–85%. The remaining latices, which were all experimental, show, on the other hand, considerably greater variation in particle size and initial surface coverages with soap ranging from 38 to 56%.

Effect of Free Rosin Acid

In the titration of latices containing fatty acid soaps as well as free fatty acid, it was observed that the free fatty acid is completely replaced from the polymer surface by the soap added during the titration (1). To ascertain whether rosin soap latices containing free rosin acid behave the same way, three such latices were titrated with and without neutralization of the free fatty acid with base. The results obtained are shown in Table IV. In this table S_{acid} represents the equivalents of free rosin acid per gram of polymer present in the latex, and $(S_i + S_a)$ is the total equivalents of *soap* adsorbed by a gram of the polymer at the cmc. It will be observed that for each latex the latter quantity is essentially constant. This means that free rosin acid, if adsorbed by the polymer, is completely

TABLE IV

Soap Titration of Latices with Unneutralized Rosin Acid

Latex no.	Initial and added soap	$S_{\text{acid}} \times 10^4$	$(S_i + S_a) \times 10^4$	D_s (A.)
4	K-wood rosin	0.00	3.01	970
		0.62	3.00	970
5	Dresinate 214	0.00	4.12	570
		1.55	4.00	590
6	Dresinate 731	0.00	4.83	490
		0.51	5.03	470

TABLE V

Effect of Temperature on Titration of Rosin Latices

Latex no.	Initial and added soap	$S_i \times 10^4$	Temp., °C.	$S_a \times 10^4$	D_s (A.)
302	K-wood rosin	2.26	50	1.56	763
			25	1.49	765
604	Dresinate 731	2.77	50	2.19	500
			25	2.14	496

displaced from the surface by the added soap, and hence the system behaves during the titration with rosin soap as if the free rosin acid were not present. Consequently, with rosin latices, as with the fatty soap ones, only the initial soap content of the latex need be considered in the titration for surface area and particle size determination. That this is true is evidenced further by the particle sizes of the latices given in the last column of Table IV, and calculated from the $(S_i + S_a)$ values. The agreement between the results for the neutralized and unneutralized latices is excellent and independent of the amount of rosin acid present.

Effect of Temperature

In Table V are shown data obtained on two rosin soap latices titrated at 50°C. and 25°C. Using the soap areas given in Table I and taking into consideration the changes in the polymer densities with temperature, we obtain the particle sizes given in the last column of the table. The fact that these are identical for each latex at the two temperatures indicates that the effective soap areas remain constant between 25° and 50°C. and that the values given in Table I for these areas may be used over this temperature interval.

Conclusions

The results presented in this paper show that the soap titration method for determination of synthetic latex particle size and specific surface area is applicable to latices containing rosin soaps as well as to those prepared with fatty acid soaps. The only difference found in the application of the method to rosin latices is that with these only conductance is a reliable means for ascertaining the titration end point, whereas with fatty acid soaps and latices both conductance and surface tension work equally well.

ACKNOWLEDGMENT

This work was performed as a part of the research project sponsored by the Reconstruction Finance Corporation, Office of Synthetic Rubber, in connection with the Government Synthetic Rubber Program.

REFERENCES

1. MARON, S. H., ELDER, M. E., AND ULEVITCH, I. N., *J. Colloid Sci.*, **9**, 89, (1954).
2. MARON, S. H., MADOW, B., AND BORNEMAN, E., *Rubber Age*, (*N. Y.*) April (1952).
3(a). MARON, S. H., ULEVITCH, I. N., AND ELDER, M. E., *Anal. Chem.* **21**, 691 (1949); (b). *ibid.* **24**, 1068 (1952).

ON THE SURFACE INACTIVATION OF PEPSIN

D. F. Cheesman and H. Schuller*

Department of Physiology, Bedford College, University of London

Received September 15, 1953

INTRODUCTION

It is still a matter of some obscurity whether an enzyme molecule, after having been unfolded at an interface, may still retain its activity, and whether, if unfolding does involve inactivation, the molecule may be restored to an active configuration by a simple process of desorption and refolding.

All enzymes cannot, of course, be supposed to behave similarly in this respect. Where the activity is due to a prosthetic group of nonprotein nature, the properties of which are determined by its immediate structural affinities, it is not excluded that this group and its mode of binding to the protein may be preserved during the unfolding process. Under these circumstances the activity may well be retained by the molecule in the unfolded state, even though it be altered quantitatively by steric factors. In cases, however, where an enzyme owes its activity to the mutual disposition of a number of centers on the molecular surface, which disposition is modified by the spreading process, it would seem improbable that activity could survive the unfolding, while any restoration of activity on desorption would be determined by the thermodynamic probability of the active configuration.

Evidence has been brought forward that certain enzymes, when spread as films at the air–water interface and transferred to media containing their specific substrates, continue to display activity. Such experiments have been carried out by Gorter (1) (1936); Langmuir and Schaefer (2, 3) (1938, 1939); Sobotka and Bloch (4) (1941); Mazia, Hayashi, and Yudowitch (5) (1947); Hayashi and Edison (6) (1950); and Kaplan (7) (1952). The earlier work has been reviewed by Rothen (8) (1947). With the single exception of Langmuir and Schaefer, none of these authors present sufficient data to enable the reader to decide whether or not the protein molecules had unfolded to the maximal extent before the enzymic activities were estimated. The last-named authors, after spreading pepsin under incompletely specified conditions, transferred the film after compression to metal slides, measured its thickness interferometrically, and estimated its enzymic activity by determining the rate at which it clotted milk. Although mean film thicknesses as low as 12 A. were recorded (as against the commonly accepted value of 9–10 A. for a fully extended polypeptide chain), it must be remarked that the most striking retention of activity by the films was observed with impure pepsin, where foreign protein, bound to the active centers of the enzyme, might have a stabilizing action upon their configuration. In their corresponding experiments with crystalline urease, Langmuir and Schaefer recorded film thicknesses of 7–43 A. There appears, however, to have been a rough positive correlation between the thicknesses of the films and their enzymic activities, and in no case did the activity exceed 2% of that of the corresponding amount of enzyme in bulk solution. In their later paper, Langmuir and Schaefer (1939) incline to the view that their pepsin films were inactive in the fully spread and adsorbed state but were re-endowed with activity after desorption from the slides by an unknown factor in the milk used for the estimations. As far as we can judge, however, their results are fully in keeping with the view that the active enzyme had never been in a state of complete unfolding.

---

* Present address: Technische Hochschule, Munich, Germany.

Hayashi and Edison (1950) and Kaplan (1952) dismiss as irrelevant the argument as to whether activity is retained by fully unfolded protein films. The former authors remark, for example: "Whether these molecules can be more completely spread is not the question; the point is that they are in a physically different state from the same molecules in solution." This approach to the problem, however, is attended by the difficulty that the "physically different state" of the autodigestible pepsin-albumin fibers of Hayashi and Edison and of the active catalase fibers of Kaplan is, as far as the individual molecules are concerned, rather poorly defined[1].

Thus, although ample evidence has been provided that enzyme molecules associated with a protein film at the air–water interface may retain their biochemical activity, no satisfactory data are available as to the degree to which this retention of activity is associated with incomplete unfolding. The investigation described in this paper was an attempt to provide such data in the case of a single enzyme, pepsin.

EXPERIMENTAL

Attempts were made to remove pepsin films from the surface of a Langmuir trough by suction. This method was highly successful at *p*H values in the region of 6, where the films showed low tensile strength at surface pressures of about 2 dynes per centimeter and could be withdrawn from the surface almost quantitatively, accompanied by only some 3 ml. of substrate. The activity of the enzyme thus removed was found to be very low, despite incomplete spreading, when tested on methemoglobin solutions at pH 1.8. We attributed this to mechanical inactivation in the region of the suction nozzle.

---

[1] After this paper had been submitted for publication, it was brought to our attention that Mazia and Hayashi (9) (1953) had recently established a loss of autodigestibility in fibers drawn from completely spread films of the pepsin–albumin complex. This finding is in full concord with our results, which nevertheless concern a different aspect of the problem, in that they derive from measurements of enzymic activity, rather than from observations of the lability of an enzyme–substrate complex.

A technique similar to that of Gorter (1936) was applied with some success. Films were spread at the surface of 0.01 N HCl in a polythene funnel. Below the surface was mounted a fine nylon net on a circular polythene frame. When the water level was lowered, the film was largely retained by the net, which was transferred in its entirety to a Petri dish containing methemoglobin substrate for the activity determination. The procedure had the disadvantages, however, that it was difficult to achieve a good fit between the net and the sides of the funnel and to prepare a series of nets with similar characteristics.

The method finally adopted was the following:

The rim of a porcelain Buchner funnel, internal diameter 15 cm., was ground flat. Both the rim and the interior, with the exception of the perforated plate, were rendered hydrophobic with a thin layer of pure paraffin wax. The funnel was carried by a filter flask, to the side tube of which a two-way tap was connected. By way of this tap, suction could be applied from a filter pump. Alternatively, the pressure in the flask could be brought to atmospheric, or to the value corresponding to the head of liquid in the funnel.

When an experiment was to be performed, a filter paper (Postlip 633A), fitting the funnel with not more than 1 mm. clearance, was inserted and about 500 ml. 0.01 N HCl was run through into the flask. The side tube was closed and the funnel filled to the brim with 0.01 N HCl. The surface was cleaned in the usual manner with paraffined glass barriers and suction. The level of liquid was then cautiously lowered to within 5 mm. of the surface of the filter paper, after which the side tube was closed and excess pressure was allowed to build up in the flask until not more than two drops of liquid passed through the funnel per minute. A pepsin solution (0.8 mg. per milliliter) was applied to the liquid surface with an Agla micrometer syringe in droplets of about 0.4 μl. The time at which half the requisite amount of protein had been applied was taken as zero spreading time. The rate of application was about 30 μl. per minute. When the desired period of spreading had almost elapsed, the pressure n the flask was reduced to atmospheric by opening the tap and the liquid was allowed to flow slowly through the funnel. The time when no free water surface remained in the funnel was recorded as the end of the spreading period. After 30 seconds, the paper was removed with blunt forceps and placed, with its upper face downwards, in a Petri dish of 15.4 cm. internal diameter containing a mixture (pH 1.8) of 25 ml. 2% (w./v.) bovine hemoglobin and 10 ml. 0.14 N HCl. This dish and its contents had been ncubated at 37°C. in an air incubator for 30 minutes. A stop clock was started and the dish was covered with a glass plate and returned to the incubator. At the end of a 30-minute period, the paper was removed from the dish with forceps, 5 ml. 2N trichloroacetic acid was added to the digestion mixture, and the solutions were rapidly mixed with a violent rotatory motion. The paper was returned to the dish and the mixing repeated. The paper was then drained and discarded. The suspension was filtered through Whatman No. 30 paper. 10 ml. of the clear filtrate was transferred o a 50-ml. measuring flask, made alkaline with 10 ml. N NaOH, and treated, during haking, with 3 ml. Folin-Ciocalteu phenol reagent (diluted three times). The flask was immediately made up to the mark and the contents mixed. The extinction coefficient was read after 3 minutes in the Spekker photoelectric absorptiometer (1-cm. cells, Ilford red filter No. 608).

Blank determinations were made at frequent intervals in precisely the manner described above, but in the absence of a pepsin film.

Values for the activity of unspread enzyme (activity at "zero spreading time") in amounts equal to those employed in the film experiments, were obtained by a similar procedure. In this case, however, the enzyme was added direct to the substrate from the syringe and thoroughly mixed before the insertion of the filter paper.

This procedure, although identical in principle with the standard method of Anson (10) (1939) for the estimation of pepsin, differs from the latter in that it employs far greater amounts of substrate protein. Deviations from the straight-line relationship between enzymic activity and extinction coefficient lay within the limits of error of the method, which were estimated at ± 2%. We therefore considered ourselves justified in treating the difference between the extinction coefficient and the reagent blank as a direct measure of the enzymic activity.

All reagents were of analytical grade. The hemoglobin was prepared from fresh ox blood by the method of Anson (1939). The 2% solution was made by dilution of the concentrated stock solution, the concentration of which was determined with an M.R.C. grey-wedge photometer. The water was distilled in an automatic apparatus with a tin delivery tube.

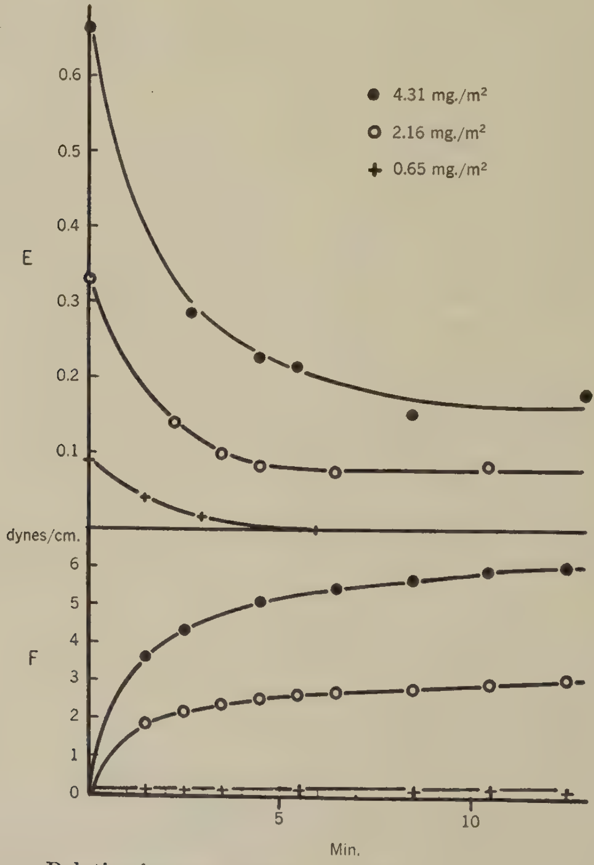

FIG. 1. *Above:* Relation between activity of pepsin films and time of spreading. *Below:* Relation between surface pressure of pepsin films and time of spreading at constant area.

Substrate: 0.01 N HCl. Temperature: 27–29°C.

The pepsin was the crystalline preparation supplied by Armour and Co. Solutions were made from material weighed out after drying overnight in a vacuum desiccator over P_2O_5. All concentrations recorded in the present account refer to material thus dried.

RESULTS

The investigation was made at a time of violent fluctuations in atmospheric temperature which, in view of the fact that we had made no provision for temperature control in our spreading experiments, led to considerable scatter in our earlier results. These were all, however, in qualitative agreement with the results recorded here, which were obtained during a period when the room temperature remained within the range 27–29°C.

Three typical relationships between enzyme activity and time of spreading, for widely different surface concentrations of enzyme, are shown in the upper part of Fig. 1. The lower part of the figure shows the results of parallel determinations of the increase in surface pressure with time, made concurrently in the Langmuir trough under conditions otherwise identical with those of the activity measurements. It will be observed that the activity of a film falls off rapidly as the surface pressure increases and tends to zero under conditions where spreading is most complete, *i.e.*, where the surface concentration of protein is sufficiently low to prevent the development of high surface pressures. The activity at zero time is taken as that of an equivalent amount of enzyme in bulk solution.

Figure 2 shows the force–area curve for pepsin fully spread on 0.01 *N* HCl as measured in the Langmuir trough. It is assumed here that complete

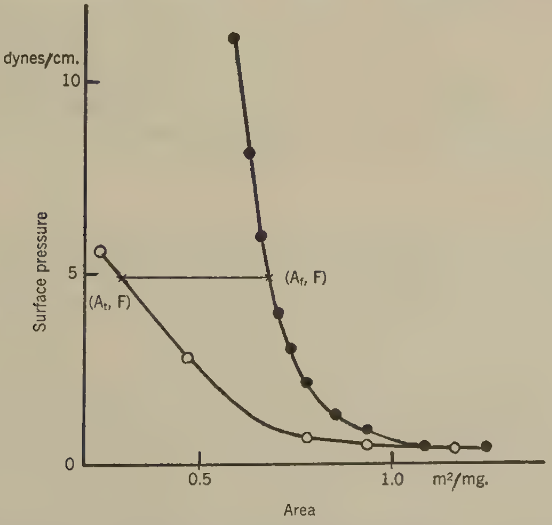

FIG. 2. Force–area curves for pepsin on 0.01 *N* HCl.

Dots: Protein spread from 60% *iso*propyl alcohol solution and compressed.

Circles: Protein spread from aqueous solution at constant area. Surface pressure recorded after 10 min.

unfolding is obtained after 5 minutes when the enzyme is spread on a large area from a solution, two weeks old, in 60% (*v*/*v*) *iso*propyl alcohol (*cf.* Ställberg and Teorell (11) (1939). The lower curve is a corresponding force–area isotherm obtained when different quantities of enzyme were spread from 0.08% aqueous solution on an area equal to that of the Buchner funnel, the pressures being recorded after a spreading time of 10 minutes. Each point represents a separate experiment.

Discussion

In the absence of all assumptions, save that the tendency of films to pass through the filter paper does not increase with their age, the results show conclusively that, as the unfolding of pepsin molecules approaches completion, so does their activity, as measured under the present conditions, decrease. The provision of an inadequate area for the spreading of a protein to its full extent, results in a film in which enzymic activity is partially retained.

It is still open to doubt whether the spreading is an all-or-nothing phenomenon or whether partially unfolded molecules, in which the topochemistry of the protein surface remains locally unaltered, can be incorporated in the uppermost layer of the film. It has become a matter of common experience to one of us (Cheesman, unpublished observations) that in work on the film potentials of difficultly spread proteins such as myosin, the potential is invariably found to be characteristic of the pressure, irrespective of the degree of spreading. Since the dipolar contributions of completely folded or partially folded molecules included in the film could scarcely be identical per unit area with those of the unfolded polypeptide chains, this constitutes good evidence not only that globular, or partially unfolded, molecules do not contribute to the film pressure to an extent readily measurable in a surface balance, but also that they occupy a position below the zone affecting the asymmetry potential, where their dipoles may be neutralized by ions in the substrate.

Let it therefore be tentatively assumed that the structure of the film is such that, after a short initial period, it consists of an upper layer of oriented polypeptide chains and bears on its lower surface an adsorbed layer of unaltered or partially altered molecules which contribute materially neither to the surface pressure nor to the film potential.

If we now consider the force–area curves in Fig. 2, it is clear that for an incompletely spread film represented on the lower curve by the point (A_t, F), corresponding to a total surface concentration of protein $c_t = 1/A_t$, the concentration c_f of unfolded protein will be given by the point (A_f, F) on the upper curve for fully spread protein, where $c_f = 1/A_f$.

The concentration c_a of adsorbed protein beneath the upper layer will be given by:

$$c_a = c_t - c_f.$$

TABLE I

Relationship between Activity of Films and Concentrations of Unfolded and Adsorbed Pepsin

c_t	c_f	c_a	Activity E
4.31	1.54	2.77	0.177
2.16	1.43	0.73	0.088
1.30	1.02	0.28	0.055
1.08	0.97	0.11	0.032
0.86	0.8(4)	(0)	0
0.65	0.6(6)	(0)	0

c_t = total surface concentration of protein, mg. per m.^{2}.
c_f = concentration of protein in unfolded layer, mg. per m.^{2}.
c_a = concentration of protein in adsorbed layer, mg. per m.^{2}.
E = activity of whole film, area 0.071 m.^{2}.
Time of spreading: 10 min.

If our reasoning is correct, and unfolded protein does not contribute to the activity of the film E, then

$$E = f\ (c_a)$$

and when $c_t = c_f$, $E = 0$.

The data in Table I have been calculated on the basis of the 10-minute values from the curves in Fig. 1 and others obtained with intermediate concentrations of protein in the same series of experiments. Although our surface balance was sensitive only within the limits ± 0.05 dyne per centimeter, it seems clear that the above relationship is approximately obeyed.

Now, if the adsorbed enzyme behaved during the activity determination in the manner of an enzyme in bulk solution, it would be expected that c_a would be directly proportional to E. This is clearly not the case. Inspection of the results suggests, indeed, a proportionality between E and $\sqrt{c_a}$. When these two quantities are plotted, as shown in Fig. 3, a rectilinear relationship appears to exist.

In subsidiary experiments, we have found that the filter papers bearing films retain their enzymic activity with surprising tenacity. In one case, for example, where the surface concentration of pepsin was 2 mg. per square meter, the paper was rocked in a Petri dish with 0.01 N HCl for 2 minutes before the activity determination, and despite this treatment, which required two additional passages through an air–water interface, it possessed 80% of the activity of a control paper treated in the usual manner.

If we suppose, then, that the active material remains almost entirely adsorbed during the activity determination, an explanation for the square root relation suggests itself. Let us imagine that a number of enzyme molecules are adsorbed on a roughly plane surface and tend to pack themselves in groups. Then irrespective of the number of active centers on each molecule, those molecules situated on the periphery of each group will obviously

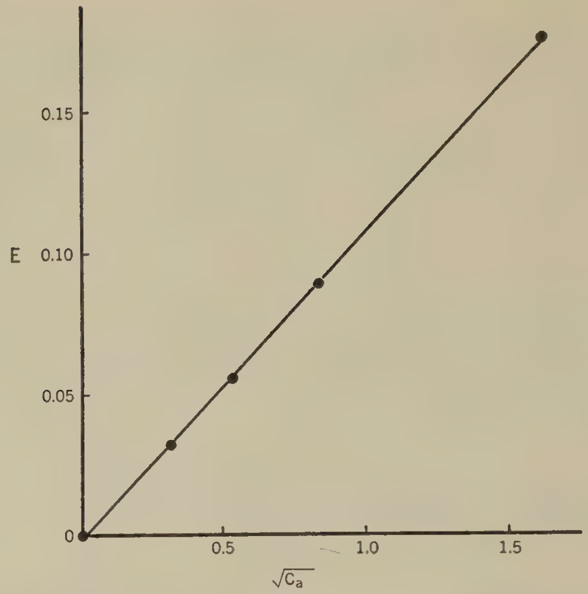

FIG. 3. Relation between enzymic activity of pepsin films (E) and the square root of the surface concentration of adsorbed, unspread protein ($\sqrt{c_a}$).

have more opportunity to display activity than those surrounded by other molecules. When the substrate molecule is large and must make two- or three-point contact with the active surface in order to undergo degradation, the activity will tend to be proportional to the sum of the circumferences of the groups rather than to the sum of the areas thereof.

Thus, for an ideal case where formation of circular groups of radius r does not result in the shielding of enzymically active centers:

$$E \propto \Sigma \pi r^2 \propto c_a;$$

whereas in the other extreme, where all but peripheral molecules are rendered inactive:

$$E \propto \Sigma 2\pi r \propto \sqrt{c_a}.$$

It may be significant that in experiments where a solution of denatured globin hydrochloride was used as substrate, enzymic activities of the order of 40% of the value for an equivalent quantity of unspread enzyme were consistently recorded with films of c_t = 2.2 mg. per milliliter and a spreading time of 10 minutes. Since this protein was by no means completely precipitated by trichloroacetic acid, it clearly contained much low-molecular polypeptide material, which may have had readier access to the adsorbed enzyme than the more intact molecules of methemoglobin. These experiments also served to show that it was improbable, even at high surface concentrations, that a large proportion of the enzyme passed through the filter paper. We cannot, however, exclude the possibility that the unspread protein consisted in part of molecules in solution below the film, which were retained in the paper or between the paper and the film. This would not inevitably affect the validity of our reasoning. If dissolved enzyme passed through the paper in significant amounts, which we were unable to detect, the square root relationship would be fortuitous.

Although these later speculations concerning the structure of pepsin films require further experimental study, we believe that our results suffice to cast considerable doubt on the earlier claims that unfolded pepsin molecules are either in themselves active, or readily desorbed in an active form when surrounded by a liquid medium.

Summary

1. A new method is described for the isolation of unimolecular films of protein.

2. This method has been applied to the study of films of pepsin. The results suggest that a fully unfolded pepsin film possesses no enzymic activity. There is no reason to suppose that a pepsin molecule, after having undergone complete unfolding at an air–water interface, can readily regain an active configuration.

Acknowledgment

One of us (H. S.) wishes to express his gratitude to the British Council for a bursary which made it possible for him to participate in this work.

References

1. Gorter, E., *Proc. Roy. Soc. (London)* **A,155,** 706 (1936).
2. Langmuir, I., and Schaefer, V. J., *J. Am. Chem. Soc.* **60,** 1351 (1938).
3. Langmuir, I., and Schaefer, V. J., *Chem. Revs.* **24,** 181 (1939).
4. Sobotka, H., and Bloch, E., *J. Phys. Chem.* **45,** 9 (1941).
5. Mazia, D., Hayashi, T., and Yudowitch, K., *Cold Spring Harbor Symposia Quant. Biol.* **12,** 122 (1947).
6. Hayashi, T., and Edison, G. R., *J. Colloid Sci.* **5,** 437 (1950).
7. Kaplan, J. G., *J. Colloid Sci.* **7,** 382 (1952).
8. Rothen, A., *in* "Advances in Protein Chemistry," Vol. III, p. 123. Academic Press, New York, 1947.
9. Mazia, D., and Hayashi, T., *Arch. Biochem. and Biophys.* **43,** 424 (1953).
10. Anson, M. L., *J. Gen. Physiol.* **22,** 79 (1939).
11. Ställberg, S., and Teorell, T., *Trans. Faraday Soc.* **35,** 1413 (1939).

THE RELATION BETWEEN THE SECOND IONIZATION POTENTIAL OF A METAL ION TO ITS INTERACTION WITH SERUM[1]

Newton Ressler,[2] Henry Uhl, and Albert J. Boyle

The Departments of Chemistry and Medicine, Wayne University, Detroit, Michigan

Received September 30, 1953; revised November 27, 1953

ABSTRACT

A correlation has been demonstrated between the ionization potentials of single-charged cations M^+ of a series of transition elements and the interaction of the corresponding double-charged cations M^{2+} with serum, measured by the smallest amount of cation which will cause clear serum to become turbid. Additive and antagonistic effects have been demonstrated. The ionization potential of cations has been discussed in relation to their chemical and binding properties. The second ionization potential of the metal atom M is parallel to the field strength of M^{2+}.

INTRODUCTION

The subject of this paper is the nature of the interactions of metal ions with intact human serum. A number of studies have been made on the binding of metal ions by serum proteins; these studies are mostly concerned with characterizing the proteins and protein groups in the blood which do the binding (1, 8).

In the present work an attempt is made to elucidate some of the factors involved in the interaction of serum proteins with cations by approaching the subject from a somewhat different point of view. This is done by comparing the effects upon serum proteins of a series of metal ions that can be related to each other on the basis of their physical properties. The salts chosen for this purpose are the chlorides of divalent manganese, iron, cobalt, nickel, copper, and zinc. With the exception of iron, these salts are generally stable in aqueous solution at a neutral pH. All of this series but nickel are naturally occurring in cells and are believed to be essential for life processes (9). However, the most important reason for the use of these ions is that they can be compared with each other on the basis of their electronic structure.

---

[1] This paper constitutes part of the Ph.D. dissertation of Newton Ressler (June, 1953). A preliminary report of this work was made to the American Chemical Society, 123rd meeting, Los Angeles, March, 1953. Supported by a grant-in-aid from the Michigan Heart Association and the Edwin S. George Foundation.

[2] Present address: Wayne County General Hospital, Department of Medicine, Eloise, Michigan.

Intact serum was utilized in order to study the final system which is a resultant of the interaction of the many serum components. It is felt that serum is of interest both from the standpoint of the nature of the unified system and from the standpoint of variations in the stability of this colloid in health and in disease. Studies of purified serum components will be included in a following report.

Experimental Methods

Determination of Turbidity-Producing Powers

Solutions of Mn^{2+}, Fe^{2+}, Co^{2+}, Ni^{2+}, Zn^{2+}, and Cu^{2+} chlorides were prepared. From 10 to 100 microequivalents of cation were added to and mixed with 2 ml. of serum in a test tube kept in a water bath at 37°C. The smallest amount of each cation which would cause a definite turbidity within two hours was determined visually against a serum blank. Each set of experiments was done on the same pooled serum sample, in order to cancel out variations between different serum supplies. Serum protein complexation appeared to inhibit the formation of zinc and copper hydroxides in the serum at pH 7.4. The serum's buffering capacity was sufficient to maintain the pH when the above cations were added.

Additive and Antagonistic Effects

To 2 ml. of serum, a preaddition of some of the above cations was made at room temperature to a concentration of 5 meq./l., which was too small a concentration to cause a turbidity. The sample of serum was then titrated with 0.01 N $CuCl_2$, and the amount necessary to produce a definite turbidity against a serum blank was determined after each preaddition.

The Nature of the Turbid Substance

The turbid substance was isolated by centrifugation. Emission spectrographic studies were made by the procedure of Boyle *et al.* (10). Protein determinations were done according to the method of Wolfson and Cohn (11). Cholesterol was determined by the method of Zlatkis, Zak, and Boyle (12).

Results

The Relation between the Turbidity-Producing Power of Cations in Serum to Their Second Ionization Potential

It was observed that clear, pooled human serum becomes turbid and cloudy a certain amount of time after a solution of Mn^{2+}, Fe^{2+}, Co^{2+}, Ni^{2+}, Zn^{2+}, or Cu^{2+} chlorides is added to it in appropriate amounts. The transition from a clear to a cloudy or turbid state is sufficiently abrupt and extensive to be easily followed with the naked eye.

In the case of Mn^{2+}, Co^{2+}, and Ni^{2+}, the turbidity could only be pro-

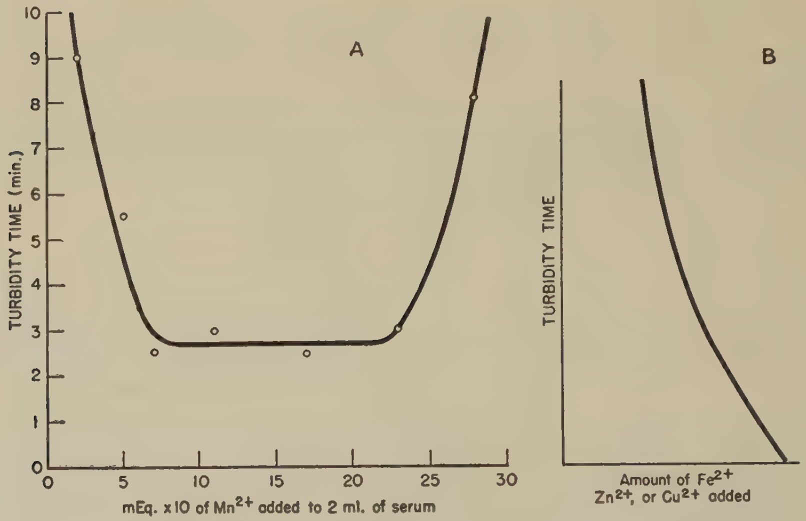

FIG. 1. Relation of time necessary for turbidity to develop after a cation addition, to the concentration of cation.

duced when the amount of cation added was in a certain critical range, and the serum would remain clear indefinitely if too much or too little were added. The relation between the amount of $MnCl_2$ added and the time necessary for the serum to become turbid after the addition is illustrated in Fig. 1*A*. The disappearance of turbidity that occurs when the maximum critical concentration is surpassed is not due to dilution, since the addition of distilled water does not clear the clouded serum. The curves obtained with Co^{2+} and Ni^{2+} were similar to that of Mn^{2+}. With Fe^{2+}, Zn^{2+}, and Cu^{2+} the shape of the time vs. turbidity curve is shown qualitatively in Fig. 1*B*.

The minimum critical concentration necessary for each of the above cations to produce a turbidity was determined and is plotted in Fig. 2*A* against the cation's second ionization potential. Figure 2*A* shows that a cation of greater second ionization potential can produce a turbidity in smaller concentration.

In order to test this relationship further, the time necessary to produce a turbidity was compared for each of the ions when they were all added to the serum in the same concentration. It is apparent from Fig. 2*B* that for a given concentration, a cation of greater ionization potential or field strength can cloud the serum more quickly.

THE INTERACTION OF DIFFERENT METAL IONS, AND CATION ANTAGONISM

In Figure 3 the ordinate represents the minimum critical concentration necessary for each cation to cause a turbidity by itself. The abscissa gives

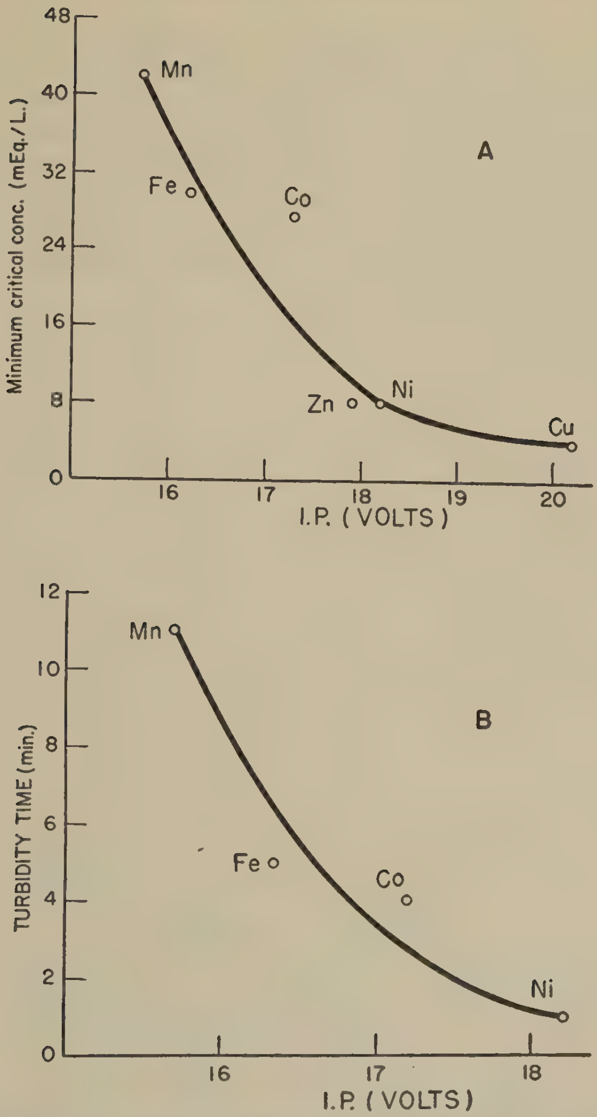

Fig. 2. In *A*, the smallest concentration of cation which will produce a turbidity is plotted against second ionization potential. In *B*, each cation was added to the serum in a concentration of 50 meq./l., and the turbidity time is plotted against second ionization potential.

the number of milliliters of a 0.01 N Cu^{2+} solution necessary to cloud the serum when added continuously after the preaddition.

When the preaddition cation has a greater turbidity-producing power, or lower minimum critical concentration, fewer Cu^{2+} ions are necessary to cloud the serum. This suggests that the turbidity-producing power of the preaddition and of the copper ions is additive. The extent of this additivity is brought out in Table I. The first row gives in milliequivalents per liter the concentration of each cation used as a preaddition (5 meq./l. in all cases), divided by the cation's minimum critical concentration. This ratio then represents the fraction of the preaddition cation present, necessary to cause a turbidity by itself. The second row shows the number of milliliters of $CuCl_2$ added after the preaddition, divided by the number of milliliters of $CuCl_2$ necessary to produce a cloud without a preaddition (1.88 ml.). The latter value is then the fraction of the Cu^{2+} ions present which cloud the serum alone. The sum of the two fractions was found to vary with the cations used from 1.06 to 1.15. The turbidity-producing powers of the preaddition and of the Cu^{2+} ions are thus nearly additive, but not perfectly so.

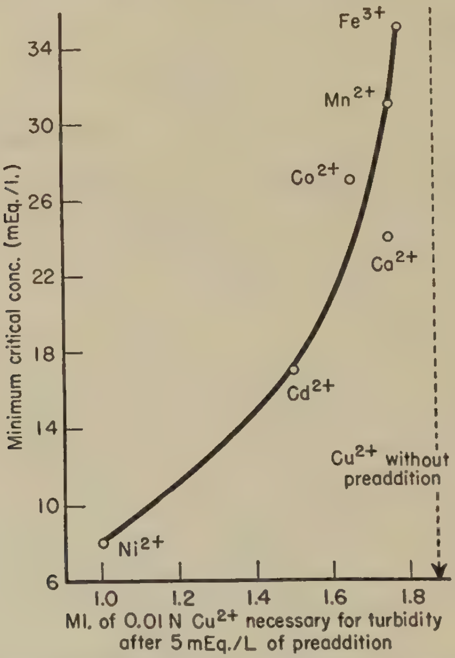

FIG. 3. The ordinate is the smallest concentration of each cation necessary to produce a turbidity by itself. The abscissa is the amount of Cu^{2+} necessary to cloud the serum after a 5 meq./l. preaddition of each cation to 2 ml. of serum.

It was next decided to investigate the effects of a preaddition when more than the maximum critical concentration was added. A sufficient preaddition of Ni^{2+}, Co^{2+}, or Mn^{2+} ions was made to the serum so that it would remain clear. The number of milliliters of 0.01 *N* $CuCl_2$ necessary

TABLE I

Additivity of Turbidity-Producing Powers

A. Cation	Fe^{3+}	Mn^{2+}	Co^{2+}	Ca^{2+}	Cd^{2+}	Ni^{2+}
B. Fractional minimum critical concentration of preaddition	0.14	0.16	0.18	0.21	0.30	0.62
C. Fractional minimum critical concentration of Cu^{2+}	0.94	0.93	0.88	0.93	0.80	0.53
D. Sum of *B* and *C*	1.08	1.09	1.06	1.14	1.10	1.15

to cloud the serum after the preaddition was determined. In Figure 4, the abscissa is the concentration of preaddition in the serum, while the ordinate is the milliliters of $CuCl_2$ necessary to cloud the serum. It is apparent that when enough cations are present to clear the serum, the turbidity formation by means of Cu^{2+} is inhibited; while only 1.88 ml. of the copper solution clouds the serum without a preaddition, 3.1 ml. are necessary in the presence of 500 meq./l. Co^{2+}. The height and slope of the curve is greatest for Ni, which has the largest second ionization potential (18.2 volts), and is the least for Mn, which has the lowest ionization potential (15.7 volts).

In the above work the preaddition ion has a lower ionization potential than the Cu^{2+} ion which was added afterwards. In the next experiment, the preaddition used (5 meq./l. of Ni^{2+}, Co^{2+}, and Cd^{2+}) had a greater

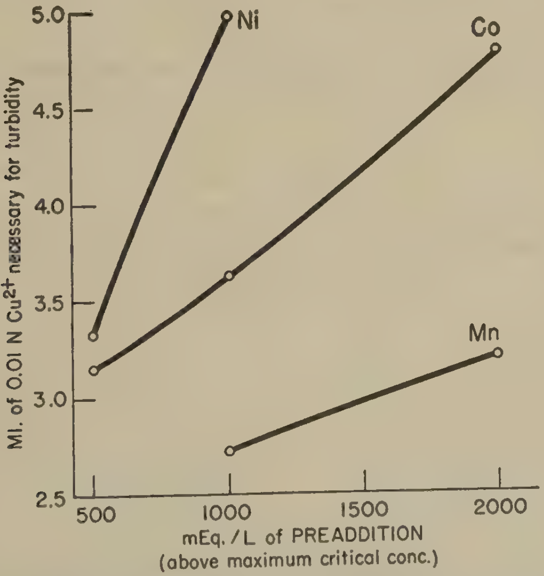

FIG. 4. The relation of the amount of Cu^{2+} necessary to cloud 2 ml. of serum (ordinate), to the concentration of preaddition cation (abscissa). The preaddition concentrations are too large for the serum to cloud, leaving it clear.

ionization potential than the metal ion added afterwards (100 meq./l. of Mn^{2+}). The preadditions of Ni^{2+}, Co^{2+}, or Cd^{2+} all have a stronger field than Mn^{2+}, and all inhibit the turbidity formation by it.

The reason for this antagonistic effect is not apparent, although similar phenomena have been observed previously. The coagulation effect of KCl and LiCl are also antagonistic upon a sulfur sol (13), and more of either salt is necessary for coagulation in the presence than in the absence of the other salt, within concentration limits.

THE NATURE OF THE SUBSTANCE PRODUCING THE TURBIDITY

The substance causing the serum to become turbid was isolated by centrifugation and decanting off the supernatant serum. The precipitate could be dissolved in dilute mineral acid. It was proved by the xanthoproteic and ninhydrin reactions to be a protein. Testing the turbid substance for cholesterol by the method of Zlatkis, Zak, and Boyle (12) shows that significant amounts of cholesterol are not present.

The turbidity-producing protein was isolated and studied qualitatively and quantitatively by means of an emission spectrograph (10). Besides Mn, which had been added, the protein contained Ca, Mg, and traces of Cu. The concentration of all of these elements was several times greater in the protein than in the supernatant serum.

The amount of cation per gram of turbid protein complex, produced by the addition to serum of various amounts of Cu^{2+} or Mn^{2+}, is presented in Table II. The Mn^{2+} was 267 and the Cu^{2+} was 3.7 times more concentrated in the centrifuged protein than in the supernatant serum. The copper content was fairly constant at 0.01 meq. of Cu^{2+} per gram of protein complex.

TABLE II

Cation Composition of Turbidity-Producing Protein

Meq. of cation added to 50 ml. of serum	Grams of isolated protein complex	Meq. of cation per gram protein complex	Meq. of cation per ml. of supernatant serum
A. Cu^{2+}			
0.46	0.428	0.0094	0.0035
0.54	1.126	0.013	
0.66	4.102	0.0096	
B. Mn^{2+}			
2.8	0.009	12.0	0.036
4.0	0.010	9.6	
5.8	0.008	17.5	
C. Mn^{2+}—After washing protein by centrifugation			
4	0.010	1.02	
4	0.008	0.81	
12	0.010	0.69	
12	0.009	1.06	

Since the concentration of Mn^{2+} was less constant, it was felt that all of the more loosely associated Mn^{2+} had not been washed out. Therefore, the determination of Mn^{2+} in the protein was repeated after it had been washed by means of centrifugation against distilled water, which was subsequently decanted. The results are given in Table II*C*.

After washing by centrifugation the concentration of Mn^{2+}, although still more variable than the Cu^{2+} content, was about 1 meq. per gram of complex, despite the amount of Mn^{2+} which had been added. The amount of precipitate appears to be independent of the amount of manganese added but increases with increasing additions of copper. This difference between Mn^{2+} and Cu^{2+} is consistent with the observation than an excess of Mn^{2+}, but not of Cu^{2+}, clears up the clouded serum. Copper is about nine times as effective in producing turbidity, and about one-tenth as concentrated in turbid protein as is manganese.

The turbid substance, when produced by 0.1 ml. of 0.25 N Ni^{2+} or 1.5 ml. of 0.01 N Cu^{2+} added to 2 ml. of serum, consists to a large degree of albumin and gamma globulin.

Discussion

One of the fundamental properties of a metal ion is its electric field strength or charge per unit area. For divalent cations, the smaller the size of the cation, the more concentrated will be the plus two charge and the more intense will be the electric field.

The comparative electric field strength of the divalent cations of Mn, Fe, Co, Ni, Cu, and Zn can be determined from their second ionization potentials. The electric field strength corresponds to the energy of attraction between the divalent cation and an electron.

$$M^{2+} + \text{electron} \rightleftarrows M^{1+} + \text{energy}$$

This energy is of the same magnitude, but opposite in sign, to the energy necessary to remove an electron from the monovalent cation, which is the second ionization potential. Consequently, this ionization potential is a measure of electric field strength.

All having the same charge of plus two, the cation of larger electric field (or second ionization potential) should have the smaller size. A comparison of ionic radii (14) to second ionization potentials of this series reveals that this is so. Fajans and Johnson (15) derived the apparent volume of a number of ions at infinite aqueous dilution. The values show that for the same series of cations, the forces of interaction between the cation and water increase with second ionization potential. It is generally found that the stability of complexes of these cations is greater when the electric field strength of the cation is larger (16). The correlation of a property measured in the gaseous state, the second ionization potential, with turbidity-producing power and other properties measured in solution suggests that cation electric field strength is a basic property relevant to all phases.

Although the reaction of a cation with such a complex medium as serum must involve a number of processes, the second ionization potential appears to be related to rate-determining steps.

It is probable that the ability of serum to remain clear when a cation is added in more than a critical amount involves a reversal of charge on the protein (19). Proteins consist of a number of polar groups and carry large dipole moments (17, 18). Since a correlation between cation field strength and protein interactions has been obtained, the binding appears to be primarily of a pole-dipole or pole-pole character.

The authors would like to express their appreciation to K. Fajans for the valuable suggestions he contributed towards this work.

Summary

A correlation has been demonstrated between the ionization potentials of single-charged cations M^+ of a series of transition elements and the interaction of the corresponding double-charged cations M^{2+} with serum. This relationship is measured by the smallest amount of cation which will cause clear serum to become turbid.

When two different M^{2+} ions are added to the sample of serum, the turbidity-producing effects are approximately additive when the cation of largest field strength is added last, but antagonistic when it is added first.

The turbid substance consists primarily of serum proteins and is shown by spectrographic analysis to combine with the M^{2+} cation in definite proportions.

The ionization potential of cations has been discussed in relation to their chemical and binding properties. The second ionization potential of the metal atom M is parallel to the field strength of M^{2+}.

References

1. Tullis, J. L., "Blood Cells and Plasma Proteins." Academic Press, Inc., New York, 1953.
2. Cohn, E. J., *Blood* **3,** 471 (1948).
3. Koechlin, B. A., *J. Am. Chem. Soc.* **74,** 2649 (1952).
4. Gurd, F. R. N., and Goodman, D. S., *J. Am. Chem. Soc.* **74,** 670 (1952).
5. Holmberg, C. G., and Laurell, C. B., *Acta Chem. Scand.* **1,** 1944 (1947).
6. Eisler, B., Rosdahl, K. G., and Theorell, H., *Biochem. Z.* **286,** 435 (1936).
7. Klotz, I. M., Faller, I. L., and Urquhart, J. M., *J. Phys. & Colloid Chem.* **54,** 18 (1950).
8. Tanford, C., *J. Am. Chem. Soc.* **74,** 211 (1952).
9. Underwood, E. J., *Nutrition Abstr. & Revs.* **9,** 515 (1939–40).
10. Boyle, A. J., Whitehead, T., Bird, E. S., Batchelor, T. M., Iseri, L. T., Jacobson, S. D., and Myers, G. B., *J. Lab. Clin. Med.* **34,** 625–630 (1949).

11. Wolfson, W. I., and Cohn, C., "Rapid Chemical Micromethods for the Analytical Fractionation of Serum Proteins." The Overbeck Co., Ann Arbor, Michigan, 1951.
12. Zlatkis, A., Zak, B., and Boyle, A. J., *J. Lab. Clin. Med.*, in press.
13. Svedberg, T., "Colloid Chemistry," pp. 264–268. The Chemical Catalog Company, New York, 1928.
14. Glasstone, S., "Textbook of Physical Chemistry," p. 383. D. Van Nostrand Company, Inc., New York, 1946.
15. Fajans, K., and Johnson, O., *J. Am. Chem. Soc.* **64**, 669 (1942).
16. Martell, A. E., and Calvin, M., "Chemistry of the Metal Chelate Compounds." Prentice Hall, Inc., New York, 1952.
17. Cohn, E. J., and Edsall, J. T., "Proteins, Amino Acids, and Peptides." Reinhold Publishing Corporation, New York, 1943.
18. Oncley, J., *Chem. Revs.* **30**, 433 (1942).
19. Kruit, H. R., "Colloid Science," Vol. II, p. 259. Elsevier Publishing Co., Inc., New York, 1949.

FLOW PROPERTIES OF SOME BUNA-N SOLUTIONS UNDER HIGH VELOCITY GRADIENTS

E. W. Merrill

Department of Chemical Engineering, Massachusetts Institute of Technology, Cambridge, Massachusetts

Received November 4, 1953; revised January 22, 1954

Abstract

With the use of a new coaxial cylinder viscometer, aniline solutions of milled Buna-N rubber have been examined for flow properties as influenced by temperature, concentration, and the addition of a nonsolvent, benzene. The results are presented in the form of curves of shearing stress (τ) versus velocity gradient (D), D ranging from 433 to 6690 sec.$^{-1}$.

Over the temperature range studied, the slope $[\partial \ln \eta_a/\partial(1/T)]_D$—wherein η_a is the apparent viscosity, defined as τ/D—is constant and independent of D. Empirical equations of the form $\tau = bD^s$ or the equivalent $\eta_a = bD^{s-1}$, for which the exponent s and the coefficient b were experimentally determined, fit the data accurately. It was found that s is virtually independent of temperature and solvent-diluent ratio, but decreases with increasing concentration, and that b increases with decrease in temperature, increase in concentration, and increase in the ratio of solvent to diluent.

Introduction

Several studies of concentrated polymer solutions have been published recently (1–3) in which the shearing stress imposed on the fluid was so low as to insure true Newtonian behavior. Conventional capillary, falling ball, and rotational viscometers were used for the most part. Working in an entirely different range and using the McKee worker-consistometer (4)—a high-pressure capillary instrument—Bestul and Belcher (5) investigated the flow properties of concentrated rubber solutions and even undiluted rubber at high shearing stresses and often at high-velocity gradients.

In the present study, the flow properties of moderately concentrated Buna-N solutions were examined over a range of velocity gradients intermediate between the two areas of exploration cited above, by means of a new type of coaxial cylinder viscometer (6). The effects on viscosity of temperature, concentration, and the addition of nonsolvents were investigated.

Experimental

For use in all the tests described below, a 135-g. batch of Buna-N type synthetic rubber (Hycar OR-25) was well broken down on a laboratory mill by 12 minutes of continuous milling through a tight nip at 120°–150°F.

The entire batch of milled rubber was at once shredded, put into aniline (a good solvent), and propeller-stirred until a uniform mix was obtained, having a concentration of rubber of 18.5% by weight. This master stock solution was later diluted as required with additional solvent (aniline) and for certain runs with a nonsolvent (benzene). To avoid solvent loss, the final sample was made by weighing into a bottle a determined amount of the stock solution (the concentration of which was exactly known by drying samples to constant weight), to which was added volumetrically aniline (and benzene) to obtain the concentration desired. The bottle was carefully sealed and then shaken in a bottle shaker for several hours until a homogeneous solution was obtained. The seal on the bottle was not broken until just before testing in the viscometer. Negligible solvent loss occurred by this method of preparation, as verified by evaporation to constant weight of a small portion of material taken from a bottle at the time of the viscosity test. Concentrations were determined with an accuracy of 1 part in 1000.

For a particular study, all the solutions were prepared at the same time. They were shaken for the same period of time under identical conditions. They were allowed to stand for the same length of time before viscosity testing; and finally, the viscosity testing of a complete series in a study took place within a consecutive period of not over 3 hours. The ages of the solutions at the time of test, reckoned from the date of milling of rubber and initial solution in aniline, were as follows: concentration studies, 3 days; solvent-diluent studies, 4 days; temperature studies, 8 days.

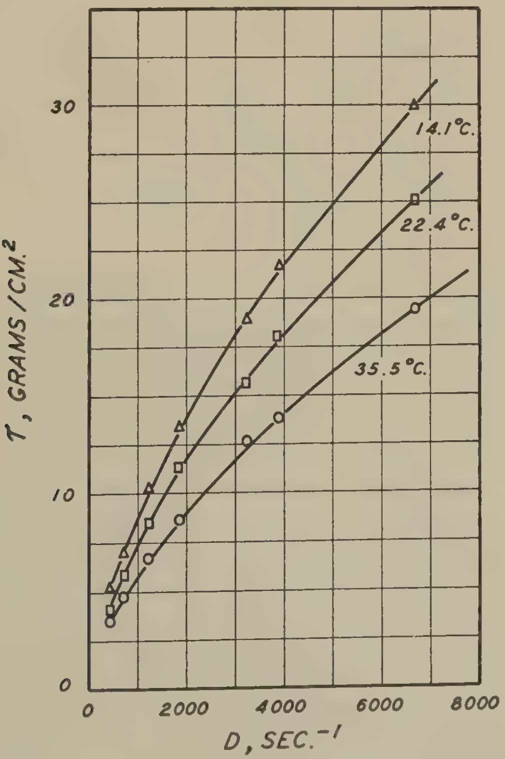

FIG. 1. τ–D curves for a solution of Buna-N (6.1%) in aniline (93.9%) at three different temperatures, 8 days old.

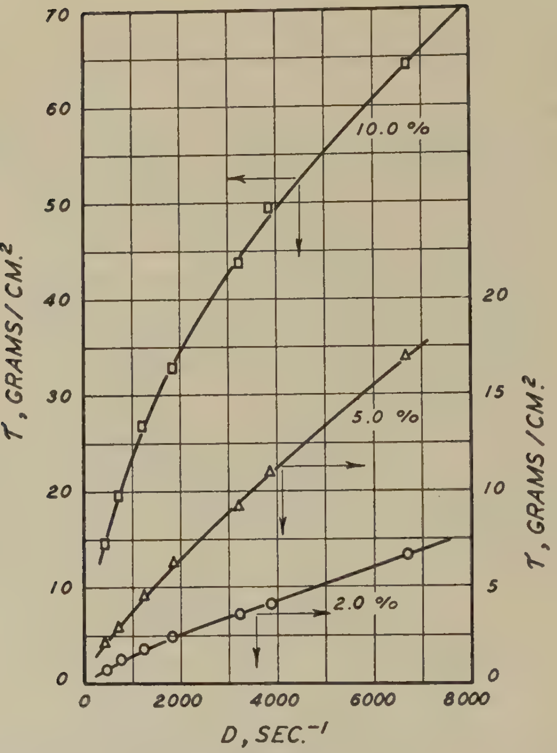

FIG. 2. τ–D curves for 2.0, 5.0, and 10.0% Buna-N solutions in aniline, measured at 20.5 ± 0.5°C., 3 days old.

VISCOMETRY

The coaxial cylinder viscometer used in these studies has been described fully in an earlier communication (6). This viscometer permits the measurement of velocity gradient and corresponding shearing stress as essentially point values and permits operation over a wide range of gradients. Control of the fluid temperature during test is good, and by reason of the design of the viscometer and its feeding system, solvent loss is minimized during test. The operation of this viscometer, the method of determining the point values of shearing stress, τ, and velocity gradient, D, and the calculation therefrom of apparent viscosity, η_a, as the point value of τ/D for a specified value of D, are presented in the paper cited.

The velocity gradients, D, to which each fluid was subjected, were obtained discontinuously but in sequence (either increasing or decreasing) and were fixed at these values[1] by reason of the fact that the viscometer was powered by a constant-speed motor operating through a predetermined sequence of pulley drives.

[1] Viz.: 433, 714, 1220, 1850, 3210, 3880, and 6690 sec.$^{-1}$.

In the testing of all these solutions, the value of τ determined for a particular gradient, D, was found to be almost independent of time or previous shearing history.

In general, the value of τ for a given D was slightly higher, as D was increased, than the value obtained as D was decreased. The difference in τ varied between zero and 2% of the higher value of τ. This indicates that the solutions studied were only very slightly thixotropic. Each point shown on the curves represents the arithmetic mean of four values of τ, two determined as the velocity gradients increased and two as the gradients decreased.

The decidedly non-Newtonian flow characteristics of these Buna-N solutions over the range of relatively high-velocity gradients studied are well shown in Figs. 1–3, wherein the experimentally obtained τ–D values are presented with respect to temperature, concentration, and solvent-diluent effects.

Figure 1 shows the τ–D curves for a 6.1% by weight solution of Buna-N in pure aniline, 8 days old, at three temperatures, namely, 14.1°, 22.4°, and 35.5°C.

The τ–D curves for three different 3-day-old concentrations of Buna-N

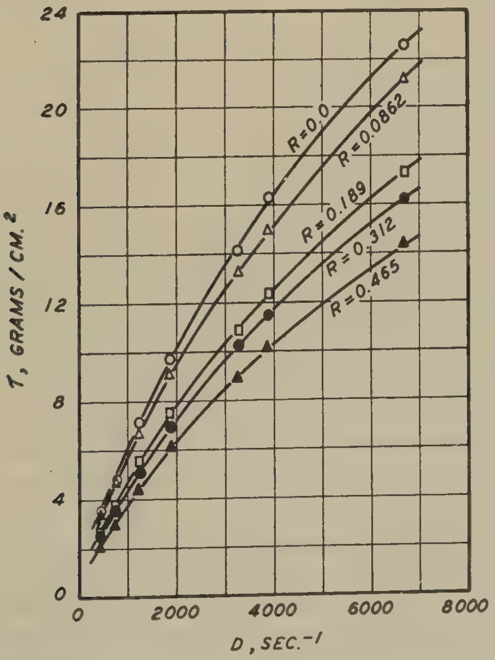

FIG. 3. τ–D curves for solutions of Buna-N (6.1%) in aniline diluted with benzene for various weight ratios (R) of benzene to aniline, measured at 22 ± 1°C., 4 days old.

in aniline (2.0%, 5.0%, and 10.0% by weight), all at 20.5 ± 0.5°C., are given in Fig. 2.

In Figure 3 the τ–D curves are shown for solutions of Buna-N of the same concentration (6.1% by weight) at essentially constant temperature, 22 ± 1°C., in which the ratio, R, of nonsolvent (benzene) to solvent (aniline) was varied from 0 to 0.465. These solutions were 4 days old at the time of the test. The substantial reduction in τ (and thus η_a) upon addition of benzene is evident, the percentage reduction being far higher than the small percentage increase in gram-moles of the solvent phase, owing to the replacement of aniline by benzene.[2]

DISCUSSION

Accuracy: The Effect of Solution Age

In a particular run on any sample, the precision of determination of τ was within ± 2% of the mean value reported. However, cross-comparison of the data shows that a greater deviation exists.

Consider, for example, the value of τ to be associated with a 6.1% solution in pure aniline at 20.5°C. and under a velocity gradient of 1850 sec.$^{-1}$.

a. By interpolation from a smooth curve drawn through the experimental values for 2.0, 5.0, and 10.0% solutions given in Fig. 2 (solutions 3 days old, tested at 20.5°C.), τ is found to equal 8.6 g./cm.^{2}.

b. According to Fig. 3 for 4-day-old solvent-diluent mixtures, the first curve for $R = 0$; *i.e.*, a 6.1% solution in pure aniline, shows that τ equals 9.75. (The actual temperature for this run was 21.0°C.)

c. Interpolation between the curves for 14.1° and 22.4°C. in Fig. 1 (6.1% solutions in aniline, 8 days old) gives a value for τ of 11.8.

The same trend of increase in τ with increase in solution age can be found for any other velocity gradient chosen. In view of the accuracy of the measurements of concentration and temperature, the increase of τ noted must be ascribed to some structural change in the solutions progressing with time. Whereas solutions of Buna-N in mediocre solvents (*e.g.*, ethylene dichloride) are noted for their tendency to increase in viscosity by progressive gelation with age, the gel structure is readily broken down under shear, and the solutions accordingly are observed to be highly thixotropic. Inasmuch as no significant thixotropy was noted in any of the solutions here reported, regardless of age, it is concluded that gelation did not occur.

The increase in τ (and thus in viscosity) was induced by a mechanism not materially affected by high shearing stresses. Either progressive dis-

---

[2] The weight ratio of benzene to aniline was varied from 0 to 0.465. Owing to the lower molecular weight of benzene (78) as compared with aniline (93), the replacement of aniline by benzene to a weight ratio of 0.465 slightly increased the total moles of solvent plus diluent per unit weight of dissolved rubber. For example, 6.1% rubber in pure aniline corresponds to 0.1655 gram-mole solvent per gram rubber, but 6.1% rubber in benzene-aniline having a weight ratio of 0.465 corresponds to 0.1755 gram-mole of solvent-diluent mixture per gram of rubber, an increase of the solvent phase of only 6%.

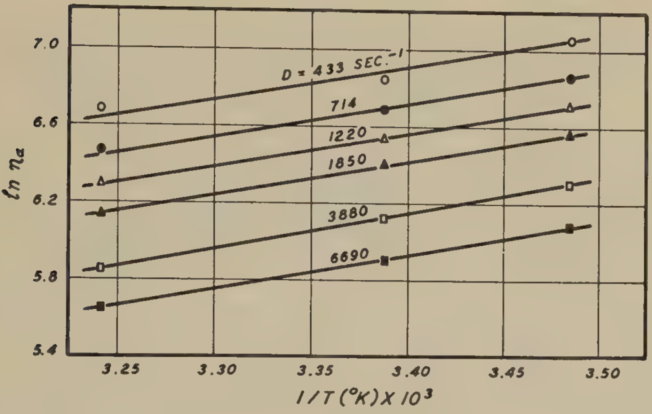

FIG. 4. ln η_a versus $1/T$ for several values of velocity gradient, based on Fig. 1.

persion in the solvent of originally aggregated polymer molecules occurred, or the solvent aniline, being a base, acted as a catalyst for a "vulcanization" of the polymer through oxygen cross-linkages. This unanticipated complication of aging does not vitiate the conclusions drawn below, as the data collected in each study were based on solutions of substantially identical histories.

Temperature Effects

It is well known that simple fluids and polymer solutions so dilute as to show Newtonian flow usually yield a linear relation between ln η_a and $1/T$, where T is the temperature in °K. Recently Ferry and his co-workers (1, 2) have shown that the same relation exists for concentrated high polymer solutions over limited temperature ranges, if the shearing stress be kept so low as to insure Newtonian flow.

Bestul and Belcher (5) have examined the temperature variation of viscosity under conditions of high shearing stresses, occurring, for example, in the flow of undiluted raw rubber. Using the hyperbolic sine equation of Eyring, they show that $[\partial \ln \eta_a/\partial(1/T)]_\tau$ for shearing stresses τ less than 10^5 dynes/cm.^{2} should be constant, and that $[\partial \ln \eta_a/\partial(1/T)]_D$ should be constant and equal to $[\partial \ln \eta_a/\partial(1/T)]_\tau$ provided the gradient D corresponds to a shearing stress τ of 10^5 dynes/cm.^{2} or less. Our results confirm the constancy of $[\partial \ln \eta_a/\partial(1/T)]_D$.[3] From the τ–D relations in Fig. 1, viscosity has been calculated (in centipoises), and the natural logarithm thereof has been plotted versus $1/T$ in Fig. 4. It will be seen that the slope $[\partial \ln \eta_a/\partial(1/T)]_D$ for several velocity gradients is nearly constant. It is found to be 1800 ± 50 (°K) for all curves except that corre-

[3] The highest value of τ measured in these studies was 64 g./cm.^{2} or 62,700 dynes/cm.^{2}, for 10% Buna-N in aniline at D = 6690 sec.$^{-1}$ (Fig. 2).

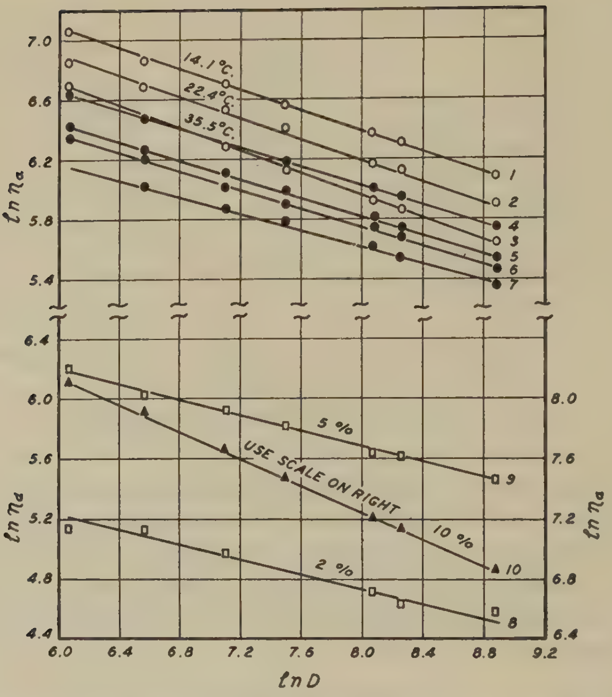

FIG. 5. Correlations: ln η_a versus ln D. Temperature runs (from Fig. 1): Curve 1, 14.1°C.; Curve 2, 22.4°C.; Curve 3, 35.5°C. Diluent runs (from Fig. 3): Curve 4, $R = 0.0862$; Curve 5, $R = 0.189$; Curve 6, $R = 0.312$; Curve 7, $R = 0.465$. Concentration runs (from Fig. 2): Curve 8, 2.0%; Curve 9, 5.0%; Curve 10, 10.0%.

sponding to $D = 433$ sec.$^{-1}$, which is uncertain because of the scatter of the experimental values. These results are of interest because they encompass a range of velocity gradients far higher than heretofore obtained with cylindrical viscometers, a range in which the flow of the polymer solution is markedly non-Newtonian.

Empirical Correlations[4]

For many pseudoplastic fluids, empirical equations of the form: $\tau = bD^s$ or the equivalent $\eta_a = bD^{s-1}$, $D > 0$, have been found applicable for the relatively low range of D ordinarily explored. If experimental values

---

[4] Attempts to correlate the data of the concentration studies by equations of the form ln η_a vs. $\sqrt{c}$ and η_a vs. c^2 failed. The equation of Doolittle (7), namely, $\ln \eta = \exp(-K/c^{0.25}) + \gamma$, was found applicable provided a different value of K was used for each velocity gradient. The Martin and the Baker equations, whose application to the correlation of viscosity-concentration data for polystyrene solutions is described by Weissberg, Simha, and Rothman (3), were also examined. As these equations require a precise evaluation of the intrinsic viscosity, which cannot be accurately determined from our data, we were unsuccessful in applying them.

TABLE I

Values of s and b in the Equations $\tau = bD^s$ *and* $\eta_a = bD^{s-1}$

Curve in Fig. 5	Temperature, °C.	Conc. by wt., %	R, wt. ratio Benz.: Aniline	s	b
1	14.1	6.1	0	0.65	9860
2	22.4			0.64	8880
3	35.5			0.625	7690
8	20.5 ± 0.5	2.0	0	0.80	565
9		5.0		0.745	2260
10		10.0		0.56	47100
4	22 ± 1	6.1	0.0862	0.68	5300
5			0.189	0.69	4070
6			0.312	0.69	3680
7			0.465	0.72	2600

of ln τ (or ln η_a) plotted against ln D yield a straight line, the relation is confirmed, and the exponent s is at once determinable as the slope. The coefficient b may then be calculated by using any pair of values of τ, D or η_a, D.

When the data for all runs in these studies are plotted as ln η_a versus ln D (Fig. 5), it is found that equations of the form cited above fit the data with remarkable accuracy over the range of D explored, 433 to 6690 sec.$^{-1}$. Table I presents the values of s determined from Fig. 5 and corresponding values of b computed from values of s and τ, D taken from Figs. 1–3.[5] It is concluded from these results that s is virtually independent of temperature and solvent-diluent ratio but decreases with increasing concentration. The coefficient b increases with decrease in temperature, increase in concentration, and increase in the ratio of solvent to diluent.

Summary

The flow properties of well-milled Buna-N rubber in a good solvent, aniline, have been presented by means of τ–D diagrams showing, respectively, the effects of temperature, concentration, and the addition of a diluent, benzene.

Pronounced decrease in viscosity is shown to occur when benzene is added.

The τ–D data of the temperature studies, replotted as ln η_a versus $1/T$, yield a family of straight lines for different values of velocity gradient, but the slopes of all lines are the same, as predicted from theory.

---

[5] The slope of any curve in Fig. 5 gives the value of $s - 1$, since the relation $\eta_a = bD^{s-1}$ is plotted logarithmically. The coefficient b is found from Figs. 1–3 by dividing any value of τ by the corresponding value of D^s, s being determined from Fig. 5 for the particular τ–D curve.

In all the studies shown, the data are well correlated with the empirical equations: $\tau = bD^s$ or $\eta_a = bD^{s-1}$. The variations of s and b with temperature, concentration, and diluent are examined.

The effect of solution aging on the accuracy of the data is considered.

ACKNOWLEDGMENTS

The author wishes to express his thanks to Mr. Herbert Viera and Mr. Carl Wolf for their painstaking efforts in helping to obtain the experimental data, to Professor Warren K. Lewis for his critical review of the manuscript, and to Mr. H. H. Carter for preparing the drawings—all of the Department of Chemical Engineering, Massachusetts Institute of Technology.

REFERENCES

1. FERRY, J. D., FOSTER, E. L., BROWNING, G. V., AND SAWYER, W. M., *J. Colloid Sci.* **6,** 377 (1951).
2. JOHNSON, M. F., EVANS, W. W., JORDAN. I., AND FERRY, J. D., *J. Colloid Sci.* **7,** 498 (1952).
3. WEISSBERG, S. G., SIMHA, R., AND ROTHMAN, S., *J. Research Natl. Bur. Standards* **47,** 298 (1951).
4. MCKEE, S. A., AND WHITE, H. S., *ASTM Bull.* **No. 153,** 90 (1948); *J. Research Natl. Bur. Standards* **46,** 18 (1951).
5. BESTUL, H. B., AND BELCHER, H. V., *J. Appl. Phys.* **24,** 696 (1953).
6. MERRILL, E. W., *J. Colloid Sci.* **9,** 7 (1954).
7. DOOLITTLE, H. K., *J. Appl. Phys.* **23,** 418 (1952).

THE EFFECT OF HYDROGEN ION CONCENTRATION ON THE VISCOSITY AND ELECTROPHORETIC MOBILITY OF SOLUTIONS OF SODIUM CARRAGEENATE

D. A. I. Goring

Maritime Regional Laboratory, National Research Council, Halifax,
Nova Scotia, Canada.

Received November 9, 1953; revised January 22, 1954

ABSTRACT

Between pH 3.5 and 11.6 the intrinsic viscosity, $[\eta]$, of sodium carrageenate in buffers of ionic strength 0.13 was constant to within ±2%. Below pH 3.5, $[\eta]$ decreased slightly. On heating solutions of the polysaccharide at 50°C. for 15 hours a decrease in $[\eta]$, $\Delta[\eta]$, was noted: $\Delta[\eta]$ was small and constant between pH 6 and pH 11.6. Below pH 6, $\Delta[\eta]$ increased appreciably as the pH decreased.

The electrophoretic mobility was 2.94×10^{-4} cm.^{2} sec.$^{-1}$ volt^{-1} and was constant to within ±3% from pH 2.0 to 10.0 in buffers of ionic strength of 0.05.

INTRODUCTION

The hydrocolloid extractible by water from the red seaweed, Irish moss (*Chondrus crispus*), is known as carrageenin. It is a polysaccharide and has been shown to consist largely of *d*-galacto-4-sulfate residues joined in the 1–3 position (1). Various ionizable cations are associated with the sulfate groups so that it may be prepared as the sodium (or other) carrageenate comparable with sodium alginate or pectate. About 30% of its composition is not definitely known. Because of its high intrinsic viscosity and gelling tendencies, this polysaccharide is widely used as an emulsifier and stabilizer in aqueous systems.

In the present investigation measurements of viscosity and electrophoretic mobility over a wide pH range have been made on a purified sample of carrageenin. All cations in the crude material were replaced with sodium by dialysis and a constant ionic strength, I, of buffer was used, since Rice (2) has shown that the viscosity varies widely with change in type and concentration of cations present in carrageenin solutions.

Hot water is used to extract the hydrocolloid. Thus it is important to determine the decrease in viscosity on heating the solution over a range of pH values.

EXPERIMENTAL

Materials

Irish moss was harvested at Prospect, Nova Scotia. Carrageenin was prepared by extracting the dry, ground seaweed with sodium acetate buffer ($pH = 6.0$: $I = 0.02$) at 60°C. for one hour. After centrifuging, the supernatant solution was poured into five volumes of absolute ethanol and the precipitated gel was dried with absolute ether. The crude polysaccharide was dissolved in and dialyzed against sodium acetate buffer ($pH = 5.5$: $I = 0.02$) to exchange all cations for sodium (3). After a final dialysis against distilled water to remove the acetate, the solution was freeze-dried and the white spongy product was stored at 4°C.

From pH 1.5 → 3.5, glycine–HCl buffers made up according to Miller and Golder (4) were used. Sodium acetate and phosphate buffers after the method of Green (5) were used from pH 3.8 → 5.5 and 6 → 8, respectively. For high pH values tribasic sodium phosphate was found satisfactory. The buffers used in viscosity determinations contained 0.08 M NaCl and the buffering salts increased I to 0.13. For electrophoresis, 0.03 M NaCl was used and the buffering salt increased I to 0.05.

Measurement of Intrinsic Viscosity

The specific viscosity, η_{sp}, was measured at 25°C. for a range of concentration, c, by means of Ubbelohde capillary viscometers. The design of Davis and Elliott (6) was used; this permitted successive dilutions without cleaning the viscometer. The mean shear rate for solvent flow computed by Kroepelin's (7) formula was 1100 sec.$^{-1}$.

As shown in Fig. 1, the graphs of η_{sp}/c vs. c were linear; this is in agreement with the results of Rice (2). The intrinsic viscosity $[\eta]$ was determined as usual from

$$[\eta] = \left(\frac{\eta_{sp}}{c}\right)_{c=0}. \qquad [1]$$

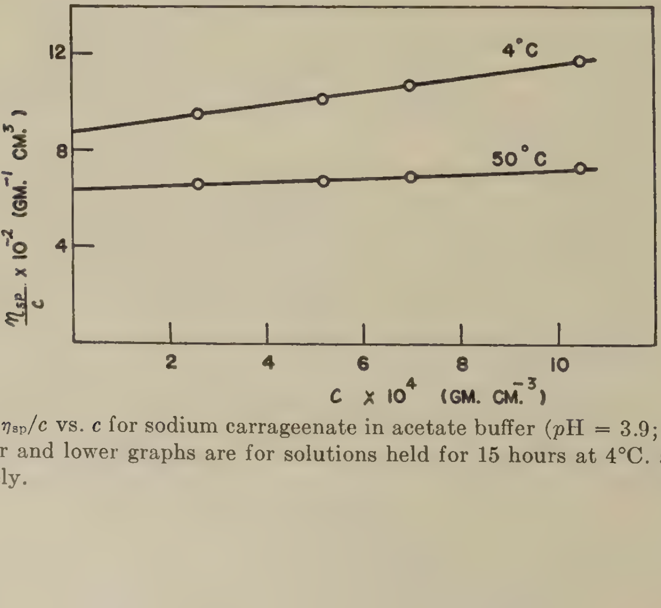

FIG. 1. η_{sp}/c vs. c for sodium carrageenate in acetate buffer ($pH = 3.9$; $I = 0.13$). The upper and lower graphs are for solutions held for 15 hours at 4°C. and 50°C., respectively.

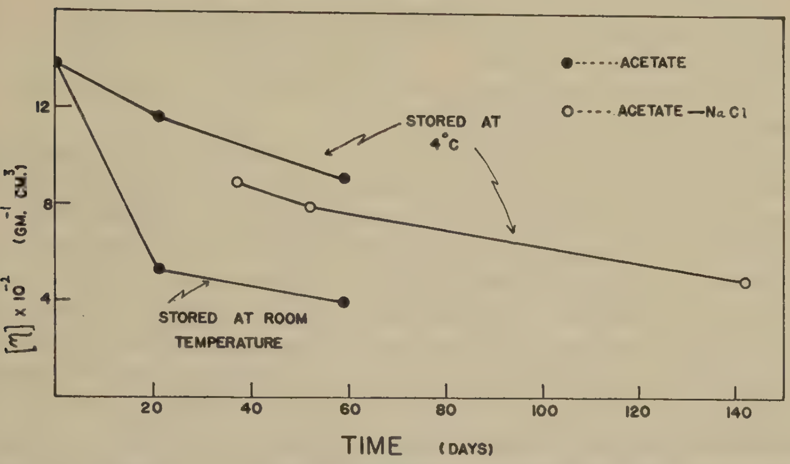

FIG. 2. Decrease of [η] on storage of the freeze-dried polysaccharide. The black circles are measurements in acetate buffer without NaCl (pH = 5.5; I = 0.05); the empty circles are measurements in the acetate buffer with NaCl (pH = 5.9; I = 0.13).

As shown in Fig. 2, the intrinsic viscosity of the sample decreased on storage in the dry state. This effect was more marked at room temperatures. Most of the viscosity determinations were made during a period of 15 days, and a small correction was made for this effect. However, the measurements in glycine–HCl buffer were made 90 days later and a larger correction was necessary.

At low pH values, η_{sp} was found to decrease slightly during the time of a run and a correction for this was made to the observed time of flow.

For studying the effect of heat, buffered solutions were held at 50°C. and at 4°C. for 15 hours. The decrease in intrinsic viscosity $\Delta[\eta]$ of the heated solution was then obtained from the graphs of η_{sp} vs. c as shown in Fig. 1.

Electrophoretic Measurements

Electrophoresis was observed in a Tiselius apparatus by the moving boundary method. The position of the boundary was recorded with the Longsworth scanning device. The mobility, U, was computed from

$$U = \frac{A\kappa\, dx/dt}{i}, \qquad [2]$$

where A was the area of cross section of the cell, κ the conductivity, dx/dt the velocity of the boundary, and i the current. The concentration was 0.5% sodium carrageenate and the current was 10 → 15 ma.

The usual technique was modified in the following ways.

a. Runs were done at 25°C. instead of 4°C. to decrease the tendency to gel.

b. The boundary was not moved with the compensator because under Poiseuille flow the solution stuck to the walls of the cell.

c. Solutions were not dialyzed, but the conductivity of the buffer was adjusted to equal that of the solution.

d. For computing the mobility of the ascending peak the conductivity of the solution below the peak was measured at the end of an experiment. This value was 10% lower than the conductivity of the main solution.

In Figure 3 a typical pair of patterns are given. The ascending peak was always considerably sharper than the descending. However, when the descending boundary was examined carefully for different positions of the knife-edge it was seen to be made up of a well-defined complex pattern of refractive index gradients sloping downward from the sides of the cell. The effect was qualitatively reproducible for several different preparations of sodium carrageenate. From results not given here in detail it was shown that the effect was not due to (*a*) boundary instability, (*b*) solution clinging to the sides of the cell, or (*c*) conductivity changes across the boundary. For different samples the asymmetry of the peaks was found to increase with increase in gelling tendency of concentrated solutions of the polysaccharide. However, for samples showing considerable variation in gel strength the electrophoretic mobility remained constant under constant buffer conditions.

As shown in Fig. 3, the pattern indicated a slight polydispersity. This effect was constant over the whole *p*H range and further separation was not obtained. Cook, Rose, and Colvin (8) have found two components in carrageenin but could not obtain an electrophoretic separation. In a current investigation (9) electrophoresis has been observed for a number of different fractions of carrageenin, and no clear separation was noted. There-

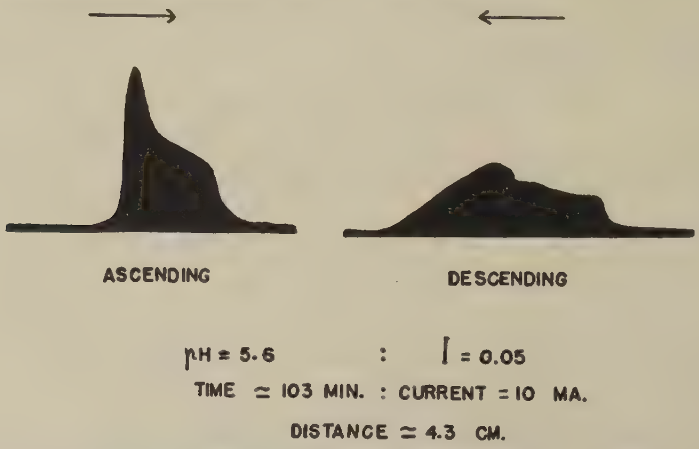

FIG. 3. Electrophoretic diagrams for sodium carrageenate in acetate buffer. At the end of the run the widths of the bases of the ascending and descending peaks were, respectively, 0.15 and 0.30 times the distance of migration.

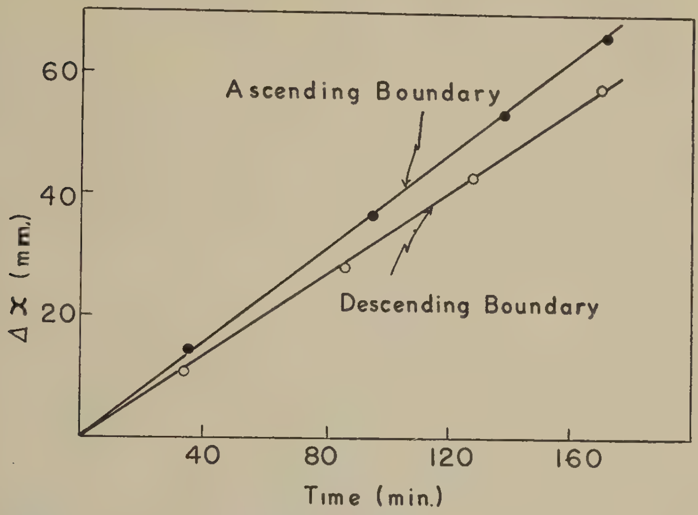

FIG. 4. Linear relationship between the distance of movement of the peak and time in electrophoresis of carrageenin.

fore, for the present work, the material was assumed to be electrophoretically monodisperse, and the spreading of the boundaries was attributed to the anomaly described above. The position of the boundary was taken to be halfway between the point at which the leading and trailing edges of the peak cut the base line.

The precision is indicated by the regularity of the linear graphs of the distance, x vs. the time, t, in Fig. 4. For all experiments dx/dt for the ascending peak was greater than for the descending peak. This anomaly was reduced by the use of the conductivity under the ascending boundary in computing its mobility. U was the mean of the values for the two peaks.

In contrast to the decrease in $[\eta]$ (see Fig. 2), U was unchanged on storage in the dry state. The independence of U and $[\eta]$ was more clearly illustrated by the data from another series of experiments. For a sample in which successive degradation had reduced $[\eta]$ by a factor of 38 the mobility was unchanged. Cook *et al.* (8) have reported a similar result in which U was constant for a threefold decrease in $[\eta]$. Thus no correction to U was necessary for the degradation shown in Fig. 2.

RESULTS

The variation of $[\eta]$ with change in *p*H is shown in Fig. 5. From *p*H 3.5 to 11.6 $[\eta]$ was constant to within ±2%. Below *p*H 3.5 a small decrease in intrinsic viscosity occurred.

In contrast, the decrease in $[\eta]$ on heating ($\Delta[\eta]$) was appreciable at *p*H 3.5, and the effect diminished up to *p*H 6.0. Above *p*H 6.0 a small constant value of $\Delta[\eta]$ was found which did not increase at high *p*H.

As shown in Fig. 6, the mean mobility was 2.94×10^{-4} cm.^{2} sec.$^{-1}$ volt^{-1} and was constant within ±3% over the *p*H range 2.0 to 10.0.

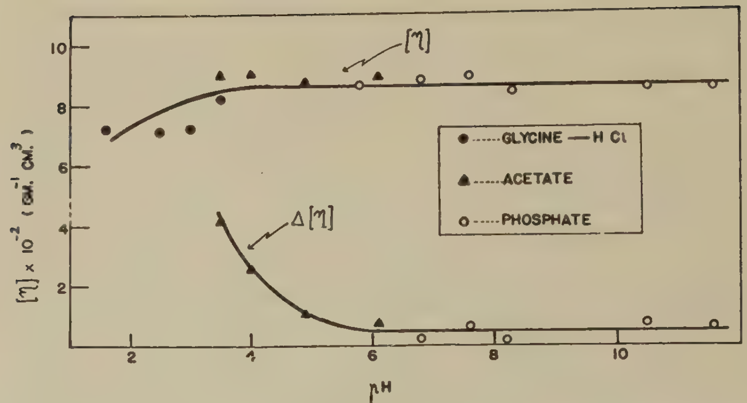

FIG. 5. Variation of [η] and $\Delta[\eta]$ with pH. The legend gives the buffers used over the different pH ranges.

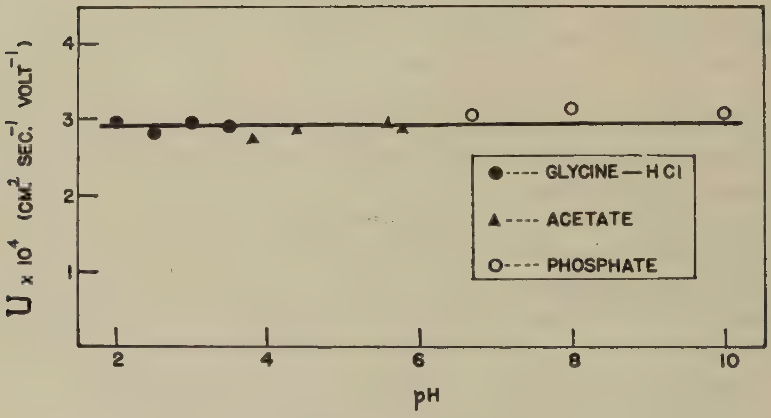

FIG. 6. *U vs.* pH. The legend gives the buffers used over the different pH ranges.

DISCUSSION

The decrease of [η] on storage shown in Fig. 2 was first noted in other samples of carrageenin prepared in the same way. The cause of this change is uncertain but it may be associated with the method of preparation. When the sodium acetate was dialyzed away in the final stages of preparation, some Na^+ ions associated with the polysaccharide would be removed. Thus the freeze-dried material would be a partially carrageenic acid. This acid is known to be unstable (10), and therefore an acid carrageenate might be expected to be easily degraded. However, the replacement of sodium ions by hydrogen could not have been extensive, because a 0.3% solution of the freeze-dried material in distilled water gave a pH of 5.02.

If the degradation on dry storage is a general property of the hydrocolloid, the absolute values recorded in previous comparative studies of viscosity (2, 11) in which this effect was not taken into account must be reconsidered.

The sensitivity of the molecule to acid is also shown in Fig. 5 by the sharp increase in $\Delta[\eta]$ at *p*H values below 6.0. This would be expected, since the glycosidic linkage is an acetal and therefore is hydrolyzed by mild acid treatment but is stable to alkali (12). The absence of a similar degradation at high *p*H shows that the unknown part of the molecule contains no bonds which are sensitive to alkali.

The absolute values of intrinsic viscosity shown in Figs. 1 and 5 were within the range of those reported by other workers. From the graphs of η_{sp} vs. c given by Rice (2), values of $[\eta]$ between 1000 and 1500 gm.$^{-1}$ cm.^{3} can be derived. Cook *et al.* (8) reported intrinsic viscosities of 340 to 1120 gm.$^{-1}$ cm.^{3} for different samples of carrageenin, while Masson and Caines (13) have obtained values from 70 to 350 gm.$^{-1}$ cm.^{3} for degraded preparations.

By a mild extraction and careful purification of the polysaccharide (9) it has been possible to obtain intrinsic viscosities as high as 2700 gm.$^{-1}$ cm.^{3} in acetate buffer (pH $= 5.5$; $I = 0.05$). It is evident that $[\eta]$ varies considerably from sample, to sample, indicating a wide range in the molecular size of the polysaccharide depending upon conditions of extraction and storage.

The constancy of $[\eta]$ between *p*H 3.5 and 11.6 shown in Fig. 5 suggests that for the buffer conditions used the molecular shape was unchanged in this range. Light-scattering data have indicated that the molecule is rodlike (14) and the recent viscometric study by Masson and Caines (13) confirmed this shape. From measurements of the rates of sedimentation and diffusion, Cook *et al.* (8) have reported axial ratios of 160 to 340 assuming no solvation. The molecule is believed to be branched (15), and therefore, the probable configuration is an extended branched structure with sulfate groups attached to the polysaccharide units of the chains. If the formal charge on the chains was decreased, the molecule would coil and a decrease in $[\eta]$ would result. Since $[\eta]$ was constant it is probable that the molecule remains completely ionized from *p*H 3.5 to 11.6. This is supported by the potentiometric titration of Dewar and Percival (16), who showed that the de-ionized polysaccharide from *Gigartina stellata* (a seaweed similar to *Chondrus crispus*) was a typical strong acid.

Below *p*H 3.5 the increased concentration of hydrogen ions would tend to cause association which would decrease the number of formal charges on the chains. Thus the molecule would coil and the viscosity would decrease as observed.

The constancy of U from *p*H 3.5 to 10.0 shown in Fig. 6 would be expected if the molecule was completely ionized in this range. Below *p*H

3.5, association and coiling would have opposing effects on the mobility. The decrease in charge would cause a decrease in U, whereas the change to a more spherical shape would cause U to increase (17). As shown in Fig. 6, U did not change significantly below pH 3.5, indicating that the mobility was equally sensitive to the change in shape as to a change in charge distribution.

Acknowledgment

The author wishes to thank Dr. E. G. Young for his interest and advice throughout the investigation.

References

1. Buchanan, J., Percival, E. E., and Percival, E. G. V., *J. Chem. Soc.* **1943,** 51.
2. Rice, F. A. H., *Can. J. Research* **B24,** 12 (1946).
3. Butler, M. R., *Biochem. J.* **28,** 759 (1934).
4. Miller, G. L., and Golder, R. H., *Arch. Biochem.* **29,** 420 (1950).
5. Green, A. A., *J. Am. Chem. Soc.* **55,** 2331 (1933).
6. Davis, W. E., and Elliott, J. H., *J. Colloid Sci.* **4,** 313 (1949).
7. Kroepelin, H., *Kolloid-Z.* **47,** 294 (1929).
8. Cook, W. H., Rose, R. C., and Colvin, J. R., *Biochim. et Biophys. Acta* **8,** 595 (1952).
9. Goring, D. A. I., unpublished data.
10. O'Neill, A. N., private communication.
11. Rose, R. C., *Can. J. Research* **F28,** 202 (1950).
12. Fieser, L. F., and Fieser, M., "Organic Chemistry," p. 216. D. C. Heath & Co., Boston, 1950.
13. Masson, C. R., and Caines, G. W., *Can. J. Chem.* **32,** 51 (1954).
14. Goring, D. A. I., *Can. J. Chem.* **31,** 1078 (1953).
15. Dillon, T., and O'Colla, P., *Proc. Roy. Irish Acad.* **B54,** 51 (1951).
16. Dewar, E. T., and Percival, E. G. V., *J. Chem. Soc.* **1947,** 1622.
17. Alexander, A. E., and Johnson, P., "Colloid Science," p. 308. Clarendon Press, Oxford, 1949.

A COMPARISON OF THE SOLUBILIZATION OF SEVERAL PARAFFIN HYDROCARBONS BY A POLYSOAP[1]

Lionel H. Layton[2] and Ulrich P. Strauss

School of Chemistry, Rutgers University, New Brunswick, New Jersey

Received August 6, 1953; revised January 29, 1954

Abstract

The solubilization of several paraffin hydrocarbons by a polysoap, prepared by the partial quaternization of poly-2-vinylpyridine with *n*-dodecyl bromide, was studied viscosimetrically in order to determine the influence of chain length and branching of the hydrocarbons. Isoöctane was solubilized to practically the same extent as *n*-octane, indicating that chain branching is of minor consequence. However, the solubility of the hydrocarbons decreased with increasing number of carbon atoms, though not as rapidly as with ordinary soaps. The solubility of hexadecane was still 40% that of hexane.

While a temperature increase speeded up the solubilization process, it did not affect the hydrocarbon solubility, and it caused only a very minor decrease in the reduced viscosity of the polysoap solutions, both in the absence and in the presence of solubilized hydrocarbon.

Introduction

The ability of soaps[3] to solubilize hydrocarbons and other water-insoluble compounds is now well established as being due to micelle formation by the soap molecules (1). An additional confirmation of this interpretation has recently been obtained through the observation that if micelles are "prefabricated" by chemically attaching soap molecules to polymer chains the resulting "polysoap" molecules solubilize hydrocarbons just as ordinary soaps do (2–5). However, no systematic study of the effect of the chain length of hydrocarbons on their solubilization by polysoaps has as yet been reported. The results of such a study, dealing with the normal paraffin hydrocarbons containing an even number of carbon atoms and ranging from hexane to hexadecane, are presented in this paper. In order to show the role of chain branching, 2,2,4-trimethylpentane is also included. Some exploratory experiments to determine the influence of temperature both on polysoap structure and on hydrocarbon solubilization are also described. In all these studies, the solubilization was determined by measuring its effect on the viscosity of a 2% polysoap solution.

---

[1] These results are contained in a thesis submitted by Lionel H. Layton in partial fulfillment of the requirements for the Ph.D. degree, Rutgers University, 1953.

[2] Now at Whiting Research Laboratory, Standard Oil Company of Indiana, Whiting, Indiana.

[3] This term is used here in its broader sense including both cationic and anionic detergents.

EXPERIMENTAL

Materials

Polysoap L1153, which consists of poly-2-vinylpyridine (D.P. ≈ 1000) 29.7% of whose pyridine nitrogens were quaternized with *n*-dodecyl bromide and 8.7% carried hydrogen bromide, has been described previously (5). The sample used for the comparison of the hydrocarbons at 25°C. was recovered from an aqueous solution of the original sample by removing the water with an air stream, followed by the usual purification procedure (2). Whereas the reduced viscosity of a 2% solution of the original sample had been 0.289, the corresponding value for the recovered sample was 0.283. A second recovery was necessary for the study of the temperature effects. The reduced viscosity of the twice-recovered sample was 0.271. The cause for these slight drops was not determined. The effect of recovery on the maximum amount of hydrocarbon which could be solubilized was found to be negligible.

The *n*-hexane and isoöctane were "pure grade, minimum purity 99 mole percent" Phillips Petroleum Company products. The other hydrocarbons were purchased from Eastman Kodak. The *n*-octane, *n*-decane, and *n*-tetradecane were "white label," the *n*-dodecane and *n*-hexadecane "yellow label" grade. All these hydrocarbons were redistilled at either atmospheric or reduced pressure. In the case of the dodecane and hexadecane only the fractions boiling between 90° and 91°C. at 9.5 mm. and between 144° and 145° C. at 8 mm., respectively, were collected.

Procedure

Sealed glass ampules containing the polysoap solution and the desired quantity of hydrocarbon were tumbled end over end in a constant temperature bath to attain equilibrium. Three days tumbling at 25°C. was found to be sufficient for the hydrocarbons containing ten or fewer carbon atoms. However, in order to save time, the ampules containing the hydrocarbons with twelve or more carbon atoms were first tumbled at higher temperatures (6, 7). This procedure could be advantageously employed since, as is shown below, the solubility of the paraffin hydrocarbons is at least as high at 45°C. as at 25°C.[4] Three days tumbling at 45°C. was found to be sufficient for dodecane and tetradecane. However, hexadecane, which showed an extremely low rate of solubilization at 25°C., needed a week of tumbling at 55°C. in order to produce saturated solutions, while less severe conditions were necessary to solubilize smaller amounts. Equilibrium was considered to be reached for undersaturated solutions when no more hydrocarbon was visible, for saturated solutions when further increasing the time and temperature of tumbling produced no further change in the viscosity of the solution. In all cases where higher temperatures were used to speed up the solubilization, the solutions were finally tumbled for at least two days at the temperature at which their viscosity was to be measured.

---

[4] The soundness of this procedure is further confirmed by the fact that the 25°C. viscosity values obtained with the decane solutions were the same whether the solutions were first heated to 45°C. or whether equilibrium was reached at 25°C. without heating.

The type of ampule used, the method of introducing hydrocarbon into the polysoap solution, and the way in which the solution was transferred from the ampule into the viscometer were varied depending on the vapor pressure of the hydrocarbon and the amount added, according to previously established procedures (3–5). Viscosities were measured in a Bingham viscometer (8) whose constants $(pt)o$ for water were 13,210 and 8845 gram seconds per square centimeter at 25° and 45°C., respectively.

RESULTS AND DISCUSSION

Solubilization of Paraffin Hydrocarbons at 25°C.

The effect of the solubilization of the hydrocarbons on the viscosity of a 2% polysoap solution is shown in Table I, where the reduced viscosity, η_{sp}/C (C = polysoap concentration in grams per 100 ml., and η_{sp} = specific viscosity with respect to water as the solvent), is given as a function of K, the hydrocarbon concentration in grams per 100 ml. of solution. Those K-values marked with asterisks represent saturated solutions containing a visible excess of hydrocarbon at the end of the tumbling period.

The data show the usual influence of aliphatic hydrocarbons on the reduced viscosity, which decreases uniformly with added solubilizate until saturation is reached, beyond which additional hydrocarbon has no further effect (3, 5). The viscosity depression has previously been found to depend only on the hydrocarbon to polysoap ratio, regardless of the polysoap concentration, and has therefore been explained as being due to a contraction of the polysoap molecules (3). Gram for gram, all the hydrocarbons seem to depress the viscosity by about the same amount, in contrast to some previous results obtained with a similar polysoap where n-dodecane caused a larger viscosity decrease than did isoöctane (3). Apparently the relative efficiency with which hydrocarbons depress the viscosity of polysoap solutions is very sensitive to small changes in the polysoap structure.

The hydrocarbon solubilities, K_s, expressed in grams per 100 ml. of polysoap solution, which are obtained in the usual manner from the breaks in the η_{sp}/C against K curves (3), are given in the fourth column of Table

TABLE I

Effect of Hydrocarbon Solubilization on the Reduced Viscosity of a 2% Polysoap Solution

n-Hexane		*n*-Octane		Isoöctane		*n*-Decane	
K	η_{sp}/C	K	η_{sp}/C	K	η_{sp}/C	K	η_{sp}/C
0.000	0.283	0.000	0.283	0.000	0.283	0.000	0.283
0.028	0.261	0.016	0.269	0.015	0.270	0.020	0.265
0.031	0.262	0.035	0.258	0.024	0.266	0.040	0.251
0.054	0.252	0.051	0.250	0.037	0.257	0.060	0.242
0.070	0.243	0.064	0.244	0.048	0.250	0.080	0.234
0.080	0.238	0.080	0.236	0.060	0.246	0.100	0.227
0.105	0.230	0.090	0.233	0.080	0.237	0.120*	0.225
0.120	0.227	0.110	0.226	0.090	0.233	0.200*	0.224
0.140	0.218	0.150*	0.220	0.110	0.226	0.200*	0.226
0.200*	0.212	0.180*	0.221	0.150*	0.219		
0.250*	0.213	0.200*	0.220	0.200*	0.218		
				0.250*	0.219		

n-Dodecane		*n*-Tetradecane		*n*-Hexadecane	
K	η_{sp}/C	K	η_{sp}/C	K	η_{sp}/C
0.000	0.283	0.000	0.283	0.000	0.283
0.020	0.262	0.020	0.266	0.010	0.269
0.030	0.258	0.020	0.265	0.010	0.272
0.040	0.252	0.030	0.259	0.025	0.262
0.050	0.246	0.040	0.250	0.050	0.256
0.060	0.243	0.050	0.248	Excess*	0.247
0.072	0.234	0.062	0.242	Excess*	0.250
0.100*	0.232	0.080*	0.237		
0.100*	0.232	0.090*	0.239		
0.150*	0.231	0.120*	0.237		

II. Since *n*-hexane and *n*-octane are slightly soluble in water (0.012 and 0.002 g. per 100 ml., respectively (9, 10)), their water solubilities are subtracted from the K_s-values to give the weight of hydrocarbon, S_g, actually solubilized by the polysoap per 100 ml. of solution. It is seen that to a very rough approximation S_g is inversely proportional to the number of carbon atoms of the hydrocarbon. A better empirical correlation is obtained on a volume basis. In Figure 1, S_v, the volume of hydrocarbon solubilized per 100 ml. of solution, is shown to be linear in the reciprocal of the molar volume of the hydrocarbon. Isoöctane is only very slightly more soluble than *n*-octane so that the effect of branching is practically negligible.

Possibly the most significant feature of these results is the relatively high solubility of the long-chain hydrocarbons in polysoap solutions as compared with their extremely low solubility in ordinary soap solutions.

TABLE II

Hydrocarbon Solubilities in a 2% Polysoap Solution at 25°C.

Hydrocarbon	Density	Molar volume	K_s	S_g	S_v
n-Hexane	0.655	131.6	0.158	0.146	0.223
Isoöctane	0.688	166.1	0.133	0.133	0.193
n-Octane	0.699	163.5	0.127	0.125	0.179
n-Decane	0.726	196.1	0.105	0.105	0.145
n-Dodecane	0.745	228.8	0.081	0.081	0.109
n-Tetradecane	0.759	261.5	0.073	0.073	0.096
n-Hexadecane	0.770	294.3	0.058	0.058	0.075

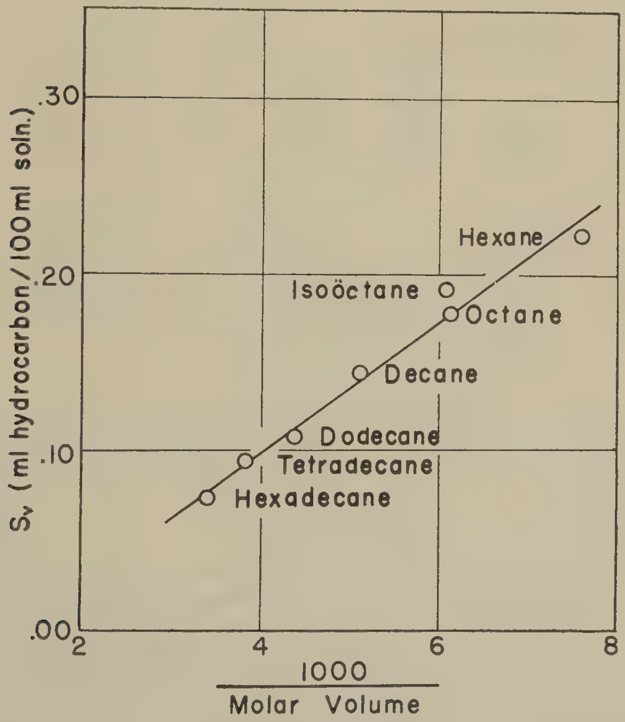

FIG. 1. Effect of molar volume on the solubilization of hydrocarbons in a 2% polysoap solution.

For instance, hexadecane was found to be completely insoluble in all the detergent solutions investigated by McBain and Richards (10); yet in the polysoap solution its solubility was still 40% that of hexane. This result is most likely due to the great number of soap molecules (in the present case 300 on the average) which are contained in a polysoap molecule, but the fact that the structure of polysoap molecules is less compact and probably more disordered (11, 12) than that of soap micelles may also play a role.

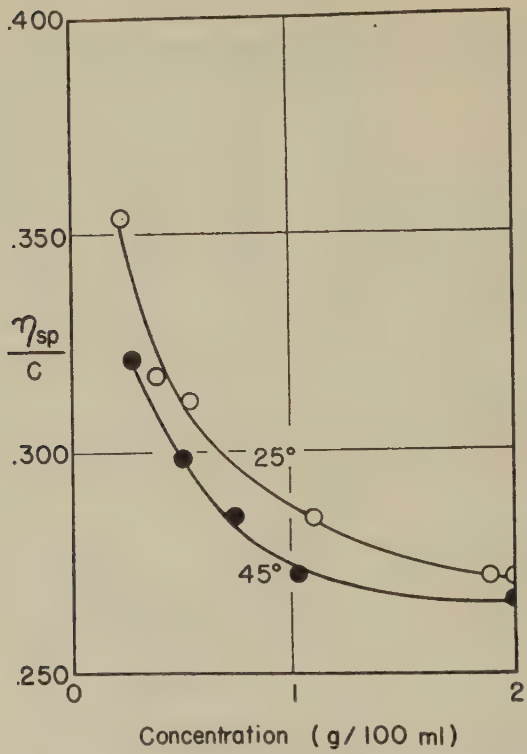

Fig. 2. Effect of temperature on the reduced viscosity of polysoap solutions.

Temperature Effects

That raising the temperature increases the rate of solubilization has already been mentioned. Since, as will be shown below, the structure of the polysoap molecules is only very little affected by a temperature rise, the high activation energy indicates some potential barrier which apparently makes it difficult for the hydrocarbon to penetrate to its solubilization locus in the polysoap molecule.

The influence of temperature on equilibrium properties is also of interest. Its effect on the reduced viscosity of the polysoap over a tenfold concentration range is shown in Fig. 2. The very small decrease, amounting to about 2–6% for a 20°C. temperature rise, indicates a slight contraction of the polysoap molecules. Now the configuration of a polysoap molecule is controlled mainly by three types of forces, namely the electrical repulsive forces between the ionized groups, the van der Waals attractive forces between the long hydrocarbon side chains, and the thermal forces. Since it can be shown that the direct effect of the temperature rise on the ionization and its secondary effect brought about by the

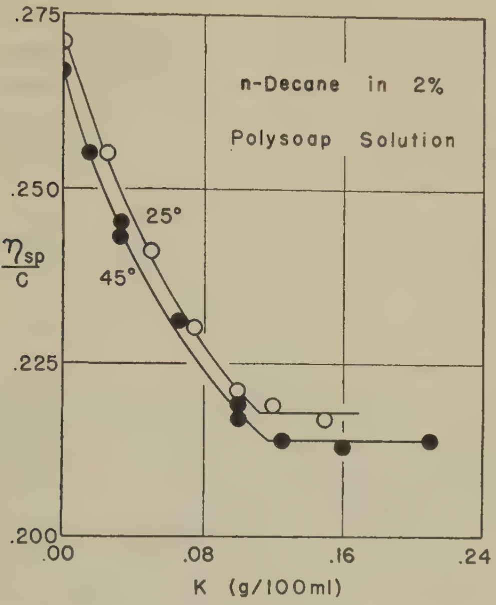

FIG. 3. Effect of *n*-decane solubilization on the reduced viscosity of a 2% polysoap solution at 25°C. and at 45°C.

TABLE III

Effect of Temperature on the Solubility of Paraffin Hydrocarbons in a 2% Polysoap Solution

Hydrocarbon	K_s at 25°C.	K_s at 45°C.
n-Octane	0.129 ± 0.008	0.138 ± 0.007
n-Decane	0.111 ± 0.007	0.119 ± 0.011
n-Tetradecane	0.072 ± 0.009	0.074 ± 0.006

lowering of the dielectric constant of water approximately cancel each other, its over-all effect on the electrical forces should be negligible. Since the van der Waals forces are also independent of temperature, the viscosity decrease is most likely due to the increased thermal forces. These forces tend to bring the polymer molecules to their unbiased random coil configuration, which is thereby shown to be even more compact than the configuration prevailing under the experimental conditions. This result in turn leads to the interesting conclusion that the electrical repulsions are somewhat stronger than the van der Waals attractions.

The slight depression of the reduced viscosity with increased temperature remains about the same upon solubilization of aliphatic hydrocarbons. This is illustrated in Fig. 3, where the effect of temperature on the reduced viscosity against decane concentration curve in a 2% polysoap solution is shown. Similar results have been obtained with octane and tetradecane.

The solubilities of the three hydrocarbons obtained from the breaks in the η_{sp}/C against K curves are given in Table III. The very slight solubility increases which are observed as a result of the temperature increase all fall within the limits of experimental accuracy and therefore cannot be assigned any significance.

Acknowledgment

This investigation was supported by research grants from the Office of Naval Research and the Rutgers Research Council.

References

1. Klevens, H. B., *Chem. Revs.* **47**, 1 (1950).
2. Strauss, U. P., and Jackson, E. G., *J. Polymer Sci.* **6**, 649 (1951).
3. Jackson, E. G., and Strauss, U. P., *J. Polymer Sci.* **7**, 473 (1951).
4. Layton, L. H., Jackson, E. G., and Strauss, U. P., *J. Polymer Sci.* **9**, 295 (1952).
5. Strauss, U. P., and Layton, L. H., *J. Phys. Chem.* **57**, 352 (1953).
6. Lambert, J. M., *J. Colloid Sci.* **2**, 479 (1947).
7. Lambert, J. M., and Busse, W. F., *J. Chem. Phys.* **16**, 847 (1948).
8. Bingham, E. C., "Fluidity and Plasticity," McGraw-Hill Book Co., New York, N. Y., 1922.
9. McBain, J. W., and Lissant, K. J., *J. Phys. & Colloid Chem.* **55**, 655 (1951).
10. McBain, J. W., and Richards, P. H., *Ind. Eng. Chem.* **38**, 642 (1946).
11. Klevens, H. B., *J. chim. phys.* **49**, 615 (1952).
12. Klevens, H. B., *Kolloid-Z.* **128**, 61 (1952).

HEMOLYSIS BY COLLOIDAL ELECTROLYTES[1, 2]

Sydney Ross and Arthur M. Silverstein[3]

Department of Chemistry, Rensselaer Polytechnic Institute, Troy, New York

Received February 10, 1954

Abstract

The hemolytic action was measured at 20°C. and at 37°C., of each of a homologous series of sodium alkyl sulfates (C_8 to C_{18}) and of each of a homologous series of benzyldimethylalkylammonium chlorides (C_8 to C_{18}) dissolved in water, and in *n*-propanol-water mixtures, containing 0.05 M phosphate buffer ($p\text{H} = 7.2$), made isotonic with sodium chloride. The results are examined for their bearing on a recent theory of the physical chemistry of hemolysis by surface-active agents, advanced by Pethica and Schulman. The effect of colloidal association on both hemolytic and bactericidal action of surface-active agents is discussed.

Introduction

A series of valuable investigations of the mechanism of hemolysis by colloidal electrolytes and other compounds was initiated by E. K. Rideal at Cambridge University and was subsequently carried forward by J. H. Schulman and his collaborators. A portion of their work dealt with the influence of the ionic group of the colloidal electrolyte. More recently they have studied the hemolytic reaction in terms of monolayer processes involving cholesterol and other lipids. Suggestive as this work has been, there are still many questions connected with the subject that it makes no claim to elucidate. The present study also includes the effect of molecular structure on hemolytic activity. By extending the range of conditions, it provides a wider foundation upon which to base postulates of mechanism.

Two homologous series of colloidal electrolytes, one anionic and the other cationic, have been used as hemolytic agents at different temperatures and also in the presence of added *n*-propanol at two different temperatures. The hemolytic effect of colloidal electrolytes is therefore recorded under the influence of four independent conditions, namely, ionic charge, size of

---

[1] Presented before the Division of Colloid Chemistry at the 125th National Meeting of the American Chemical Society, Kansas City, Missouri, March 24–April 1, 1954.

[2] This paper is based on a portion of a thesis submitted, by A. M. Silverstein, in partial fulfillment of the requirements for the degree of Doctor of Philosophy, to the Faculty of Rensselaer Polytechnic Institute.

[3] Present address, Division of Laboratories and Research, New York State Department of Health, Albany, N.Y.

alkyl group, temperature, and the presence of *n*-propanol. The data can then be systematically examined as a series of comparisons in which three conditions are constant and one is varied, or twelve different comparisons.

MATERIALS AND EXPERIMENTAL TECHNICS

1. Materials

The series of alkyldimethylbenzylammonium chlorides has been used previously in a study of their bactericidal effects and the method of synthesis and analytical data are already published (1). These materials were supplied by courtesy of the Sterling-Winthrop Research Laboratories. The trimethyldodecylammonium chloride is a sample generously provided by Dr. H. J. Harwood of the Armour Research Foundation. The pertinent information about this material has also been published previously (2).

The series of sodium alkyl sulfates (3) was kindly provided by Dr. Fred Karush of Children's Hospital, Philadelphia, Pennsylvania, with the exception of the 14-carbon member, which was kindly supplied by Mr. E. Barthel, Jackson Laboratory, E. I. du Pont de Nemours and Company. Dodecyltrimethylammonium bromide was also provided by Mr. Barthel.

All reagents employed in this study were made up and diluted in 0.05 *M* phosphate buffer at *p*H 7.2 made isotonic with sodium chloride.

The red cell suspension used is prepared as follows: sheep blood is drawn into citrate-glucose solution (4) to prevent clotting, stored at 3°–6°C., and used for no longer than one week. Each day a portion of the blood is centrifuged and the cells washed three times in isotonic salt solution by decantation. The washed, packed cells are then suspended in buffer to yield a 2.5%-by-volume suspension, and the suspension is then standardized exactly for hemoglobin content in a Coleman Junior Spectrophotometer at 545 mμ.

Ketene is prepared according to previously described methods (5), and bubbled through a chilled suspension of 5% sheep cells in isotonic $NaHCO_3$ solution. The bicarbonate is used in order to neutralize acetic acid formed during the acetylation of the primary amino groups of the protein moiety. After 15 minutes of treatment, the cells are washed three times in buffer by decantation and then adjusted to yield the standard 2.5% suspension. These acetylated cells are used in place of the normal, untreated cells for certain experiments.

2. Hemolysis Technics

The minimum concentration of each detergent necessary to hemolyze 50% of the standard cell suspension is determined as follows. Various dilutions of the detergent in isotonic buffer are prepared and brought to the required temperature. One-tenth of a milliliter of each dilution plus 0.2 ml. of buffer at the same temperature are pipetted into 10 × 75-mm. test tubes, and then 0.2 ml. of the standard red cell suspension is added. The mixture is allowed to react for 15 minutes in the water bath with shaking. At the end of this time, 1.0 ml. of cold 0.15 *M* NaCl solution is added and the mixture shaken and immediately centrifuged for 3 minutes to remove all unhemolyzed cells. The degree of hemolysis is then determined by reading in the spectrophotometer, which has been previously standardized to read directly the per cent hemolysis with the cell suspension used. That concentration of hemolytic agent just causing 50% hemolysis in the 15-minute interval is called the minimum hemolytic dose ($C_{H_{50}}$).

Experimental Results

The determination of hemolytic effectiveness for each member of each homologous series was done at each of two temperatures, 20.0°C. and 37.0°C., and then each determination repeated in the presence of 0.50 *M* *n*-propanol. In addition, for further comparison, the sample of trimethyldodecylammonium chloride was investigated under all the same conditions. The data are reported in Tables IA and IB and graphically in Figs. 1 and 2 as a series of twelve comparisons.

TABLE IA

The Hemolytic Activities ($C_{H_{50}}$) in Moles per Liter of a Homologous Series of Alkyldimethylbenzyl Ammonium Chlorides in the Presence and Absence of 0.5 M n-Propanol at 20°C. and 37°C.

Series member	No propanol		0.5 *M* *n*-Propanol	
	20°C.	37°C.	20°C.	37°C.
C_8	4.0×10^{-2}	1.7×10^{-2}	2.0×10^{-2}	3.0×10^{-2}
C_{10}	3.5×10^{-3}	1.1×10^{-3}	1.3×10^{-3}	3.5×10^{-4}
C_{12}	2.3×10^{-4}	1.5×10^{-4}	1.3×10^{-4}	4.5×10^{-5}
C_{14}	2.9×10^{-5}	3.9×10^{-5}	3.4×10^{-5}	2.3×10^{-5}
C_{16}	1.3×10^{-5}	1.6×10^{-5}	1.4×10^{-5}	1.3×10^{-5}
C_{18}	2.7×10^{-5}	3.0×10^{-5}	3.0×10^{-5}	2.5×10^{-5}

TABLE IB

The Hemolytic Activities ($C_{H_{50}}$) in Moles per Liter of a Homologous Series of Sodium Alkyl Sulfates in the Presence and Absence of 0.5 M n-Propanol at 20°C. and 37°C.

Series member	No propanol		0.5 *M* *n*-Propanol	
	20°C.	37°C.	20°C.	37°C.
C_8	1.8×10^{-2}	1.6×10^{-2}	1.7×10^{-2}	3.5×10^{-3}
C_{10}	9.7×10^{-4}	1.1×10^{-3}	1.1×10^{-3}	3.3×10^{-4}
C_{12}	5.9×10^{-5}	9.8×10^{-5}	6.1×10^{-5}	3.8×10^{-5}
C_{14}	2.7×10^{-5}	3.4×10^{-5}	3.7×10^{-5}	3.4×10^{-5}
C_{16}	3.2×10^{-5}	3.4×10^{-5}	4.7×10^{-5}	2.2×10^{-5}
C_{18}	6.3×10^{-5}	2.5×10^{-5}	6.8×10^{-5}	2.5×10^{-5}

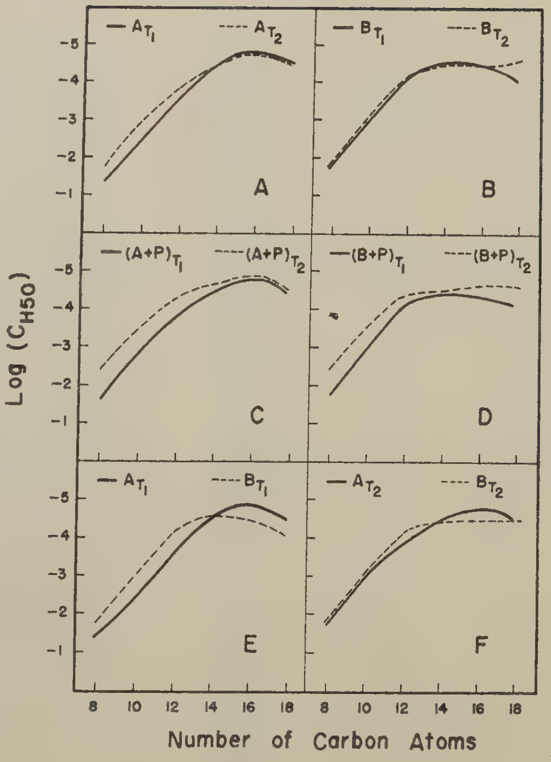

FIG. 1

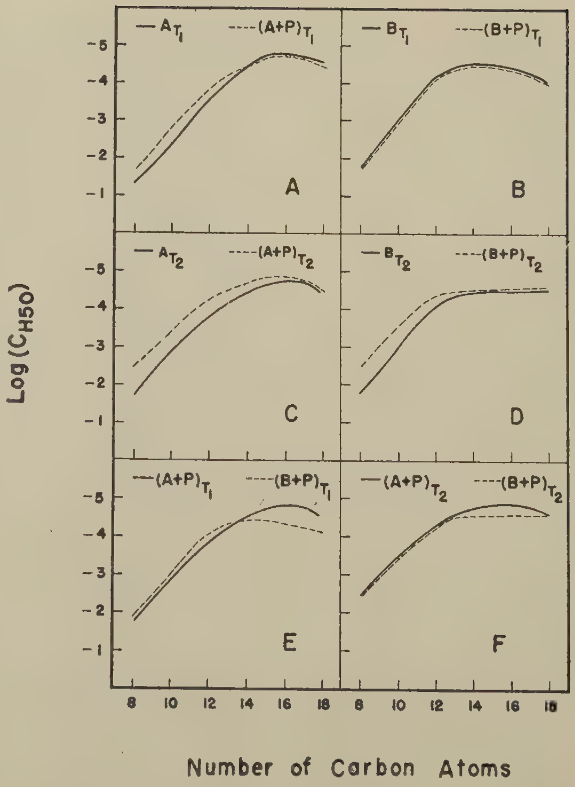

FIG. 2

FIGS. 1 and 2. The minimum hemolytic dose (C_{H50}) that will just cause 50% hemolysis of sheep erythrocytes in 15 mins. vs. the number of carbon atoms in the alkyl group of two homologous series, viz. benzyldimethylalkylammonium chlorides (A) and sodium alkyl sulfates (B). The presence of 0.50 *M* *n*-propanol is designated +P; T_1 = 20.0°C., T_2 = 37.0°C.

The determination of the hemolytic activity of dodecyltrimethylammonium bromide was done under the same conditions as are listed above and is compared with the results for the C_{12} members of the two series in Table II.

DISCUSSION

In Figures 1*A* and 1*B* the effect of temperature is shown on the hemolytic activities of the cationic and anionic detergents, respectively. The cationic series has a positive temperature coefficient for the lower members, becoming zero at the 14-carbon member and above. The anionic series has zero temperature coefficient throughout, save for the 18-carbon member, which exception may be attributed to the greater solubility of this relatively insoluble material at the higher temperature. Figure 1*B* agrees with the results of Ponder (6) that the activity of alkyl sulfates at 20°C. increases with chainlength and reaches a maximum at C_{14}. The maximum for the quaternary ammonium salts is at C_{16}.

The effect of the presence of 0.50 *M* propanol is to emphasize the temperature dependence of the hemolytic activity (Figs. 1*C* and 1*D*), especially notable for the alkyl sulfates, which previously had little or none. Comparisons of the effect of propanol at a single temperature (Figs. 2*A*, 2*B*, 2*C*, and 2*D*), shows that generally the propanol activates hemolysis by members of both series, the smaller chains more than the larger chains. The alkyl sulfates at 20°C., however, are not affected by the presence of 0.50 *M* propanol.

The remaining diagrams compare the two detergent series directly under the various conditions (Figs. 1*E*,1*F*, 2*E*, and 2*F*). The alkyl sulfates are less soluble than the corresponding homolog of the quaternary ammonium series, and the higher members of the alkyl sulfate series are not sufficiently soluble to demonstrate their full hemolytic capacity. This phenomenon is akin to the "Ferguson principle," in which the cut-off in activity is ascribed to a solubility effect (7). It is generally evident that the higher alkyl sulfates appear less active than the corresponding quaternary ammonium salts,

TABLE II

Comparison of Hemolytic Activities ($C_{H_{50}}$) in Moles per Liter of Dodecyl-Substituted Colloidal Electrolytes

$C_{12}H_{25}$	No propanol		0.5 *M* *n*-Propanol	
	20°C.	37°C.	20°C.	37°C.
$—SO_4^-$	5.9×10^{-5}	9.8×10^{-5}	6.1×10^{-5}	3.8×10^{-5}
$—C_6H_5CH_2—N^+(CH_3)_2$	2.3×10^{-4}	1.5×10^{-4}	1.3×10^{-4}	4.5×10^{-5}
$—N^+(CH_3)_3$	1.2×10^{-3}	1.2×10^{-3}	1.5×10^{-3}	3.6×10^{-4}

even though in general the alkyl sulfates are the more active hemolytic compounds. Schulman and Armstrong (8) have compared the hemolytic activities of a number of 12-carbon chain detergents and found the alkyl sulfate more active than trimethylammonium salt. We have also observed the same general result (Table II). The order of hemolytic activity

$$H(CH_2)_{12}—SO_4^- > —C_6H_5CH_2N^+(CH_3)_2 > —N^+(CH_3)_3$$

is preserved throughout all the various conditions employed in this study. These authors attribute the order of biological activity in part to a stereochemical or orientation effect of the ionic group, which can produce considerable differences in associating power between two ions or an ion and an induced dipole.

In a recent paper Pethica and Schulman (9) propose the view that hemolysis by saponin and ionic detergents is caused by interaction with the cholesterol portion of the red cell surface. This hypothesis emphasizes the interaction between the lipid portion of the cell membrane and the hydrophobic part of the detergent molecule. The results shown here and other well-known evidence for the increase of hemolytic activity with increasing size of alkyl group, show how important this interaction is. Similar results for an increase of *bactericidal* action of quaternary ammonium salts with increasing size of the alkyl group have also been interpreted as due to increasing hydrophobic interaction (1).

These considerations, however, need not deny the importance of the concomitant interionic attraction and the significance of the protein portion of the cell surface. It is well known that the protein molecule contains both positive and negative ionic groups. Interaction between proteins and detergents is also well known (10, 11) and has been reviewed by Valko (12) and by Putnam (13). An experimental fact that shows immediately the importance of the ionic group is the comparatively weak hemolytic action of nonionic detergents.

We have, moreover, observed that subhemolytic concentrations of sodium octyl sulfate will inhibit the hemolytic action of sodium hexadecyl sulfate. Thus 10^{-2} M sodium octyl sulfate produces a visible reduction in the rate of hemolysis by sodium hexadecyl sulfate, and a corresponding reduction in its hemolytic potency. This competition between the 8- and 16-carbon atom anions on the red cell surface is similar to that observed by Karush (14) between an anionic azo dye and sodium dodecyl sulfate on bovine serum albumin. The similarity is suggestive, since Karush interprets his results as competitive interaction between the organic anions for the oppositely charged sites on the protein molecule.

Perhaps the most direct evidence of the importance of the ionic groups on the erythrocyte surface as the primary site of hemolytic attack by ionic detergents is the effect of the acetylation of the amino groups on the erythrocyte surface by ketene. After thus reducing the number of surface cationic groups, the hemolytic activity of an anionic detergent is considerably lowered, while that of a cationic detergent is practically unimpaired. (These experiments are reported here for the first time.)

The connection of the biological action of quaternary ammonium salts (same salts as discussed in this paper) and their colloidal properties has been discussed by Ross, Kwartler, and Bailey (1). The increase of effectiveness with the number of carbon atoms is shown both in the hemolytic action and in the antibacterial action of these quaternary ammonium salts. The maximum action occurs at C_{16} for hemolysis and at C_{14} for the bactericidal effect. The presence of the maximum may be accounted for in the same way in both cases, namely, as a competition for detergent molecules between the cell surface and the colloidal micelle. Since micelle formation increases more rapidly than biological activity, as a function of the number of carbon atoms, the higher members of the series begin to show a declining hemolytic and bactericidal effect. Both in the hemolytic and in the bactericidal measurements, the concentrations used are in the same range as the critical micelle concentrations for C_{16} and C_{18}-alkyl groups, and it is precisely here that the effect of micelle formation influences the biological effectiveness. Low solubility of the detergents also influences biological effectiveness in the same way as does pronounced micelle formation and, for the alkyl sulfates, both low solubility (for the C_{18} member at 20°C.) and increased micelle formation contribute to produce the maximum.

For the lower member chains, micelles in the bulk solution should not affect the hemolytic action, as the critical micelle concentration is far greater than the concentrations at which hemolysis occurs. It is therefore not to be expected that any relation can be found between CMC and hemolytic action for these lower members. Flockhart and Ubbelohde (15) have measured, by electrical conductance, the CMC of sodium lauryl sulfate in water and in water-propanol mixtures. Examination of their results reveals that although the presence of propanol and differences in temperature cause relatively large variations in CMC, these variations are not paralleled by the variations of the hemolytic action. This is shown by the results reported in Table III.

Variation of temperature and the presence of *n*-propanol affect the hemolytic activity of detergents containing low-member chains in a manner that cannot be described as caused by their effect on micelle formation. It is only when the CMC is low, indicating a strong tendency to form micelles, that micelle formation can clearly be discerned as directly influencing the biological activity. Indirectly, the CMC may be taken as a measurement of surface activity, and the lack of correlation shown in Table III suggests mechanisms of hemolysis not related to the surface effects stressed by Pethica and Schulman.

TABLE III

Comparison of CMC[a] and Hemolytic Activity of Sodium Dodecyl Sulfate in the Presence and Absence of 0.5 M n-Propanol at 20°C. and 37°C.

Moles/liter	No propanol		0.5 *M* *n*-Propanol	
	20°C.	37°C.	20°C.	37°C.
$C_{H_{50}}$	5.9×10^{-5}	9.8×10^{-5}	6.1×10^{-5}	3.8×10^{-5}
CMC[a]	8.2×10^{-3}	8.0×10^{-3}	5.3×10^{-3}	5.6×10^{-3}

[a] The values for CMC are interpolated from Fig. 6 of the paper by Flockhart and Ubbelohde (15).

It has been pointed out by Love (16) that sodium dodecyl sulfate has unusual hemolytic action on human erythrocytes. A short initial period of rapid hemolysis is followed by an interruption of cell destruction that may last for many minutes before, finally, the disappearance of the remaining cells. This behavior is quite unlike the usual sigmoid curves found for kinetic hemolysis by complement, by butyl alcohol, or by distilled water, which show a period of lag before the onset of hemolysis. The following remarks by Love (16) have an important bearing on the present work.

"The relatively simple hemolytic action of . . . exposure to butyl alcohol is considerably modified in the case of sodium dodecyl sulfate, sodium oleate, and sodium taurocholate, all of which show an anti-hemolytic as well as hemolytic action. It is perhaps significant that the three compounds which have so far been found to have this additional effect are those which have a marked capacity for forming micelles. Their protective action may be a result of a tendency to aggregate with neighboring molecules when combined in large numbers with the cell surface."

During the course of the present work, hemolytic effects similar to those described by Love were observed. The magnitude of the instantaneous initial hemolysis is most pronounced with the higher members of the homologous series, both quaternary ammonium salts and alkyl sulfates, and is progressively less pronounced for the smaller alkyl groups. Below dodecyl the effect is imperceptible. This observation may be expected if Love's suggestion is true, namely that the unusual hemolytic action is characteristic of substances with a marked capacity for forming micelles. The tendency to form micelles decreases exponentially with a decrease in the size of the alkyl group (1).

It was also observed in the course of this work that the presence of small amounts of *n*-propanol down to 0.10 *M*, causes the disappearance of the unusual hemolytic effect obtained from the higher members of both series. The presence of such low concentrations of *n*-propanol affects the bulk CMC of the detergents only slightly (*cf.* Table III), but effects that may occur at the erythrocyte surface are not necessarily described by observations of bulk phenomena of detergent solutions in the absence of erythrocytes. The dielectric constant at the surface may be altered by n-propanol and surface aggregation greatly reduced as a consequence.

ACKNOWLEDGMENTS

A portion of the experimental work described in this paper was done in the laboratories of the Division of Laboratories and Research, New York State Department of Health, Albany, New York. The authors acknowledge the assistance of Dr. F. C. Nachod, Sterling-Winthrop Research Laboratories, who provoked a thorough discussion of the contents of the paper.

REFERENCES

1. ROSS, S., KWARTLER, C. E., AND BAILEY, J. H., *J. Colloid Sci.* **8,** 385 (1953).
2. CELLA, J. A., EGGENBERGER, D. N., NOEL, D. R., HARRIMAN, L. A., AND HARWOOD, H. J., *J. Am. Chem. Soc.* **74,** 2061 (1952).
3. KARUSH, F., AND SONENBERG, M., *J. Am. Chem. Soc.* **71,** 1369 (1949).
4. BUKANTZ, S. C., REIN, C. R., AND KENT, J. F., *J. Lab. Clin. Med.* **31,** 394 (1946).
5. HERRIOTT, R. M., *J. Gen. Physiol.* **18,** 69 (1934).
6. PONDER, E., *J. Gen. Physiol.* **30,** 15 (1946).
7. FERGUSON, J., *Proc. Roy. Soc. (London)* **127B,** 387 (1939).
8. SCHULMAN, J. H., AND ARMSTRONG, W. McD., "Surface Chemistry," pp. 273–279. Interscience Publishers, Inc., New York, 1949.
9. PETHICA, B. A., AND SCHULMAN, J. H., *Biochem. J.* **53,** 177 (1953).
10. PUTNAM, F. W., AND NEURATH, H. J., *J. Am. Chem. Soc.* **66**, 692, 1992 (1944).
11. SCHMIDT, K. H., *Z. physiol. Chem.* **277,** 117 (1942).
12. VALKO, E. I., *Ann. N. Y. Acad. Sci.* **46,** 451 (1946).
13. PUTNAM, F. W., "The Interactions of Proteins and Synthetic Detergents," (152 references). *Advances in Protein Chem.* **4,** 79–122, (1948).
14. KARUSH, F., *J. Am. Chem. Soc.* **72,** 2714 (1950).
15. FLOCKHART, B. D., AND UBBELOHDE, A. R., *J. Colloid Sci.* **8,** 428 (1953).
16. LOVE, L. H., *J. Cellular Comp. Physiol.* **36,** 133 (1950).

ANOTHER FORM OF ALPHA FERRIC OXIDE

F. A. Steele[1]

Central Research Department, Minnesota Mining and Manufacturing Company, St. Paul, Minnesota

Received August 13, 1953

INTRODUCTION

If a rather concentrated (30–50%) solution of ferric chloride be reacted with about 90% its stoichiometric equivalent of a base, such as sodium hydroxide or calcium carbonate, and if the resultant familiar slurry or gel of hydrous iron oxide and other reaction products be held for a sufficient time at a suitable temperature (about 1 hour at 300°C., 12 hours at 125°C., or 1½ years at room temperature), it changes to a precipitate of coarse (about 1 μ) spheroidal particles of surprising uniformity of size and shape. (Fig. 1). They have been called "K-particles," and the bulk material is called "K-Fe_2O_3." It is believed to be the most uniform nonangular particulate inorganic material to have been made by precipitation methods. It is with our studies of the nature of these particles and the mechanism of their formation that this paper has to do.

PROPERTIES OF K-Fe_2O_3

A sample of K-Fe_2O_3 made from materials of commercial purity (a selected ground limestone was the precipitant) contained about 96% Fe_2O_3, 1% SiO_2, 2.6% H_2O, 0.76% Cl, traces of CaO and Al_2O_3, and 3.3% L.O.I. at 1000°C. Some HCl was driven off on ignition and a trace of $FeCl_3$. The density was 4.66. In heating overnight at 240°C., the loss in weight was 1.8%, mostly water; the density became 4.86.

K-Fe_2O_3 is strikingly optically active. Between crossed Nichols or Polaroids, isogyres are clearly visible and when the microscope stage is rotated they weave in and out in the fashion characteristic of biaxial crystals. Incidentally, for many of these microscopic investigations a sulfur-selenium mount was preferred.

The particles are transparent. Had panchromatic film been used in preparing Fig. 1, they would have appeared clear-centered.

Considered as a pigment for the preparation of paints, oleoresinous

---

[1] Recently retired from the Minnesota Mining & Manufacturing Company. Present address: *744 E. Nevada Avenue, St. Paul 6, Minnesota.*

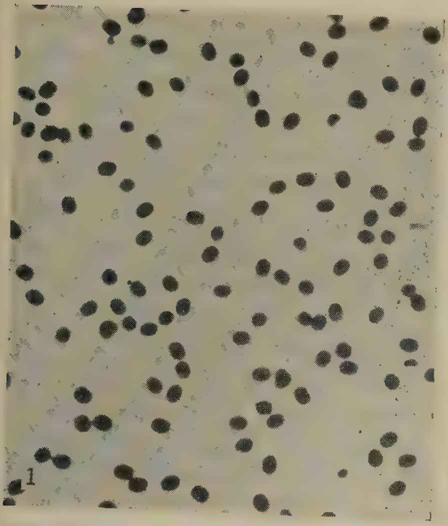

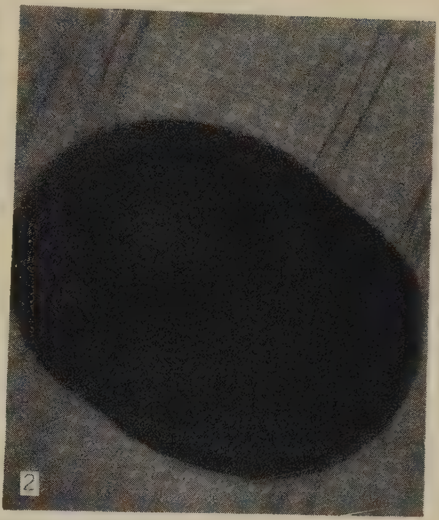

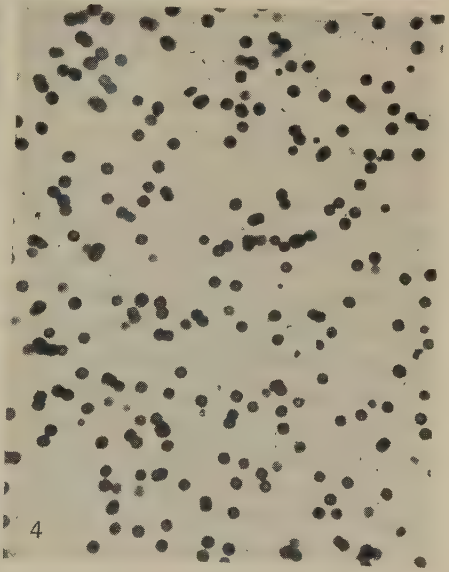

FIG. 1. Photomicrograph of K-Fe_2O_3; × 860.
FIG. 2. A single K-particle; 1 μ = 20 mm.
FIG. 3. Photomicrograph of K-Fe_2O_3 made with seed added; × 860.
FIG. 4. Photomicrograph of K-Fe_2O_3 made without seed added; × 860.

enamels, and the like, K-Fe_2O_3 has much better color, *i.e.*, higher chroma, than any other known iron oxide. This would in part be accounted for by the uniformity of particle size and shape and it is felt that more is involved. Heating for 16 hours at 240°C. grossly alters, darkens, the shade, although the particle size and shape as observed on the microscope is not affected. Neither is the primary particle size as estimated by X-ray diffraction line broadening. We have never been able completely to dehydrate a sample without a gross color change.

It would be most enlightening to determine the absorption and scattering spectra of these materials but time has not permitted. It could probably be accomplished by coating lacquers or enamels pigmented with them on glass sheet or cellophane, determining the reflectance over white and over black at various wavelengths, and applying the mathematics of Kubelka and Munk (1) and Steele (2).

K-particles are prolate spheroids with an average axial ratio of about 0.80. The particle in Fig. 2 appears to have an axial ratio of 0.74. The particles are rough, having a roughness factor, specific surface/geometric surface, of about 22. The roughness is unaffected by prolonged calcination below 300°C. The specific surface was determined by N_2 adsorption using the Branauer, Emmett, and Teller method (3, 4). The slowness with which adsorption equilibrium was reached suggested pores of the order of 16 A^2.

K-Fe_2O_3 gives an X-ray diffraction pattern of α-Fe_2O_3. The line broadening indicates a particle size of about 250 $Å^2$. The line broadening is more pronounced with a coarse, dark product than with a finer, lighter material.

EXPERIMENTAL

When the slurry of hydrous iron oxide described in the first sentence is heated in an autoclave to convert it to K-Fe_2O_3, the available iron all deposits on the particles in an hour or two if the temperature is suitable and after this has happened nothing further occurs; autoclaving for a much longer time has no effect. This suggests that seed or nuclei are present in the slurry and that it is the ratio of their concentration to the concentration of available iron that determines the particle size. It is also evident that seed do not continue to form during the autoclaving or the striking uniformity of particle size could not result.

It was found that K-Fe_2O_3 exhaustively pebble mill ground in water would behave as seed when thoroughly mixed into the slurry before autoclaving. The photomicrographs of products made with and without added seed show the effect clearly (Figs. 3 and 4). In this case 0.007 of the iron came from the added seed. The effect was less but still marked with 0.0007, barely detectable with 0.00007. A similarly ground pigment iron oxide, known to be hematitic, behaved the same way, as did particular types of Al_2O_3 and Cr_2O_3, perhaps because of the crystallographic similarity. Many other materials, such as very fine glass, silica, and SiC had no effect.

To study the rate at which the K-particles grow, 10 ml. portions of slurry were sealed in heavy walled glass tubes which were placed in capped steel nipples. In one nipple a glass tube containing a liquid (glycerine)

TABLE I[a]

Hours	$a(\mu)$	$b(\mu)$	b/a	$A(\mu^2)$	$V(\mu^3)$
3	0.7166	0.627	0.87	1.36	0.148
3.5	0.9415	0.771	0.82	2.14	0.293
4	0.946	0.794	0.84	2.23	0.312
5	1.183	0.927	0.78	3.21	0.532
6	1.398	1.100	0.79	4.51	0.886
6.5	1.350	1.087	0.81	4.33	0.836
7	1.525	1.298	0.85	5.81	1.34
7.5	1.598	1.279	0.80	6.01	1.37
8	1.702	1.323	0.78	6.58	1.56
8.5	1.758	1.398	0.80	7.22	1.80
9	1.906	1.500	0.79	8.19	2.25
9.5	1.829	1.460	0.80	7.84	2.04
10	2.046	1.608	0.79	9.74	2.77
10.5	2.233	1.735	0.78	11.31	3.52
11.25	2.393	1.879	0.78	13.17	4.42
12	2.306	1.810	0.79	12.22	3.95
21.5	2.343	1.856	0.79	12.76	4.15
			0.804 av.		

[a] a = major axis; b = minor axis; A = area; V = volume.

carried a thermocouple. The nipples were placed in a rack which kept them widely separated and the whole placed in a thermostatically controlled oven. Tubes were removed at intervals, the K-particles separated by centrifuge washing, and 1200× photomicrographs made and enlarged to 4800×. The time at which the thermocouple reached 125.5°C. was taken as zero. Tubes were removed every half hour for twelve hours. Figures 7 and 8 show the 3- and 12-hour samples. On each photomicrograph twenty-five or more particles were measured along both axes, the arithmetic means taken, and volume and area computed. Results are listed in Table I. Figure 5 shows volume plotted against time.

This experiment also showed that the particles grew from seed and that their shape remained substantially constant during their growth. Prior to this it had been suspected that the K-particles might result from the solidification of tactoid-like entities or that their shape (they were originally regarded as spheres) and size might be the result of the action of interfacial forces, as in some emulsions.

If the data in the last column of Table I be plotted as a function of the log of the volume against time, a straight line is obtained. The reaction kinetics implied by this fact are unique. The equation for the curve is log $V/V_0 = kt$, where k is a constant and t is the time. Differentiation of this equation gives $dV/dt = kV$. The rate of growth of the particles is proportional to their volume and, insofar as available data show, it is independent of the concentration of iron oxide in the slurry until that iron oxide is used

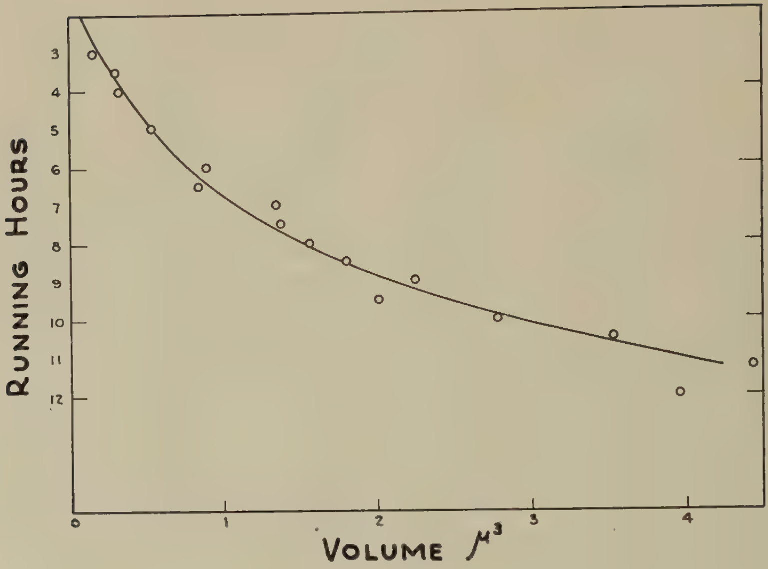

FIG. 5. Volume of a K-particle as a function of the time of autoclaving.

up, at which point the reaction stops. Although it would be interesting to speculate about the kind of force necessary to such a growth law, it would perhaps be well to leave it with the simple statement that ferromagnetic particles might act in such a manner. The particles do appear to be slightly ferromagnetic, although the B-H curve does not have a perceptible loop. α-Fe_2O_3 is regarded as slightly ferromagnetic as well as paramagnetic (5).

It having been established that the K-particles *could* grow from seed (ground K-Fe_2O_3, etc.), it was suspected that they *always did*. Since the particles continue to grow until the available iron is exhausted, it was supposed that each particle grew until the iron available to it was exhausted. If, then, there was no relative movement of the particles during growth, the final size of each one would depend upon the proximity of others and high uniformity would require uniform (not statistical) distribution of the seed in the slurry—a quite impossible situation. Incidentally, with a slurry of the type most commonly used the amount of iron needed to form a 2-μ particle would be contained in a spherical volume 7.17 μ in diameter. The fact of uniformity, then, seemed to indicate that there was some relative motion, as from convection, but many attempts to demonstrate the point, as by inhibiting convection by having the slurry in a tight bed of inert particulate material, were fruitless. It was then suggested that if there were an energy barrier at the particle surface which would prevent the capture of most of the needles (those not possessing some minimum kinetic energy) diffusing to it, so that the rate of diffusion would be large compared to the rate of capture, the uniform rate of growth and final size would be adequately explained. The same result would be expected if needles could be captured only if they had a preferred orientation. Since the needles are oriented in the K-particles, this is offered as an explanation.

When the 7-hour sample from the series in Table I was removed from the sealed tube it was diluted and centrifuged to remove the partially formed K-particles. The supernatant liquid, which was a clear sol, was studied on the electron microscope. Figure 6 shows the particles. They appear as needles 50 to 80 Å. wide by 800 to 1000 Å. long. These needles do not continue to grow but deposit on and constitute the growing K-particles. It takes about 2×10^5 such needles to make a 2-μ K-particle and the orientation cannot be random or the particles would not be optically active.

The size of these needles was reasonable confirmation of the particle size as estimated by X-ray diffraction line broadening, 250 Å.

The control of the particle size of K-Fe_2O_3 lies in the preparation, composition, and history of the slurry to be autoclaved, provided the autoclaving is carried to completion, as it always was except in the experiments just described. Precipitating on the alkaline side, *i.e.*, adding the $FeCl_3$ solution to the NaOH solution instead of the reverse (there is always violent agitation), precipitating at a higher temperature, autoclaving the slurry immediately rather than a few days or months later, and a lower excess $FeCl_3$, all give products composed of smaller K-particles. When such a material was made with a very small excess of $FeCl_3$, about 2%, the final product was so fine that it could not be resolved on the light microscope. An electronmicrograph (Fig. 9) shows that they are not K-particles at all. They appear to be more or less cubic with edges about 0.15 μ and less. A substantially identical electronmicrograph was prepared from the 2½ hour sample of Table I. The tiny crystals, which form first, remain as such if there is no iron oxide from which the K-particles can develop or if the temperature is lowered before they do. These, then, must be the seed from which the K-particles develop by the accretion of the needles. Some of the material of Figure 9 was tested as seed with positive results.

Figure 10 is from the 4-hour sample in Table I. All evidence of angularity is lost and the particles are spheroids about 0.6 $\mu \times 0.8\ \mu$. The specimen was prepared from the autoclaved slurry by washing on the centrifuge and a minute drop of the dilute suspension was placed at once on the coated grid and into the electron microscope. It had never been dry until it was subjected to the combined action of the vacuum and the electron beam in the 'scope. In this micrograph there are many needles adhering to the particles and a few in addition. It should be recognized that there is no reason for feeling that those needles were caught in the act of becoming parts of the K-particles. They were present in high concentration in the liquid and these few stuck to the particles while the rest were washed away.

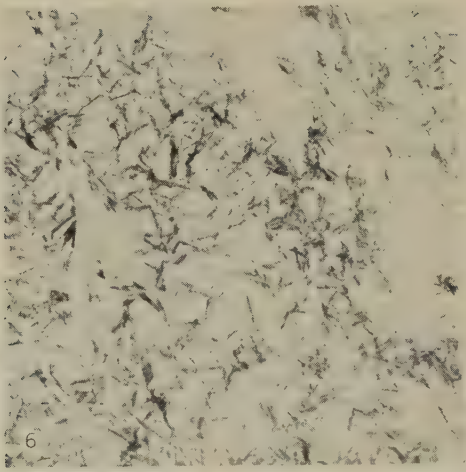

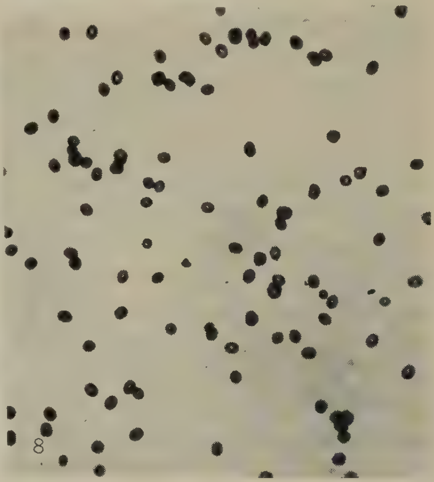

Fig. 6. Needles of α Fe_2O_3 from which K-particles are formed; $1\ \mu = 34$ mm.
Fig. 7. Slurry of hydrous iron oxide heated for 3 hours at 125.5 C.; × 860.
Fig. 8. Slurry of hydrous iron oxide heated for 12 hours at 125.5 C.; × 860.

These angular particles, which seem to be the seed which develop into K-particles, must be ionic crystals which grow from ions in solution. The nuclei from which they develop must be the entities, the concentration of which is controlled by the conditions obtaining during and subsequent to precipitation. It is their concentration, then, that determines the particle size of the final product. To check the point some dilute ferric chloride solution was dribbled into a slight excess of agitated dilute sodium hydroxide at an elevated temperature (80°C.), the precipitate thoroughly washed,

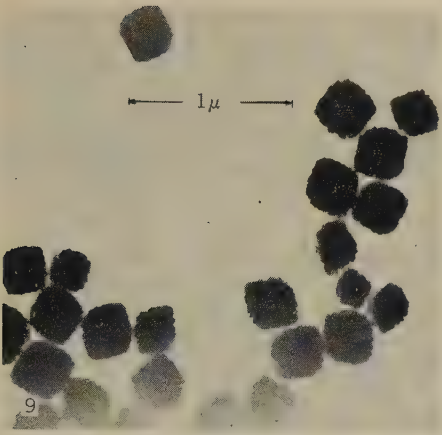

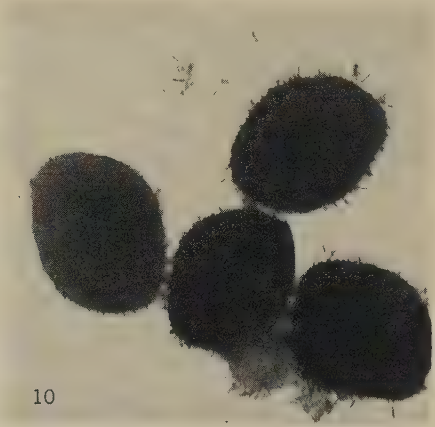

FIG. 9. Crystals of Fe_2O_3; 1 μ = 21 mm.

FIG. 10. Incompletely autoclaved sample with needles adhering; 1 μ = 26 mm.

and a minute amount very thoroughly incorporated into a slurry before autoclaving. It greatly reduced the particle size of the autoclave product, just as seed would have done. It seems that the nuclei are formed during precipitation and their concentration determines the concentration of the seed formed during the early stages of the autoclaving, which, in turn, determines the particle size of the final K-particles. The actual makeup of these nuclei can only be surmized, but that they are labile is evidenced by the fact that the slurries yield coarser and coarser autoclave products as they age, until they gradually level off and become constant after a few months.

The slurry made by the partial neutralization of ferric chloride contains all of the salt, alkali, or alkaline earth chloride ($MgCO_3$ and NH_4OH have also been used) that was formed in the reaction. It is of interest to consider the role of the salt. Its effect, if not its role, was studied rather roughly by altering the concentration and autoclaving. When a slurry is made more dilute in salts by alternate centrifuging, decanting and diluting it soon peptizes so that centrifuging is no longer effective. The concentration can be further reduced by dialysis and still further by electrodialysis but the first operation was sufficient to demonstrate the effect. The original concentration of $CaCl_2$, ordinarily determined on the mother liquor after autoclaving, is about 0.038 g./ml. When these slurries of lowered salt content were autoclaved, the products were still relatively normal with a concentration of 0.0044 g./ml. but became atypical at lower concentrations. The true role of the soluble salt is by no means clear but that it should be necessary for the agglomeration of the needles to form K-particles is not surprising.

Conclusions

If a solution of ferric chloride be partially neutralized and the slurry autoclaved, the product and the mechanism of its formation are truly remarkable. Much has been learned of both but still more remains to be learned. The writer hopes that someone will see fit to continue the problem.

Acknowledgments

The author appreciates the permission of the Minnesota Mining & Manufacturing Company to publish this paper subsequent to his retirement. Appreciated also are the suggestions and assistance of many members of the 3M staff, particularly, Mr. Alfred L. Nellesson, Dr. W. H. Pearlson, Dr. Harold M. Scholberg, and Mr. H. K. Smith. Dr. W. O. Milligan of Rice Institute offered valuable suggestions.

References

1. Kubelka, Paul, and Munk, Frank, *Z. tech. Phys.* **12,** 593 (1931).
2. Steele, F. A., *Paper Trade J.* **100,** 37–42 (1935).
3. Brunauer, Stephen; Emmett, P. H., and Teller, Edward, *J. Am. Chem. Soc.* **60,** 309 (1938).
4. Brunauer, Stephen; Emmett, P. H., and Teller, Edward, Symposium on New Methods for Particle Size Determination in the Subsieve Range. *A.S.T.M.* **1941,** 95–105.
5. Morin, F. J., *Phys. Review* **78,** 819–20 (1950).

ICE CRYSTALS FORMED SPONTANEOUSLY BY THE RAPID EXPANSION OF MOIST AIR

Vincent J. Schaefer[1, 2]

General Electric Research Laboratory, Schenectady, New York

Received January 4, 1954

The formation of large concentrations of ice crystals from aircraft propeller and wing induced vortices is of common occurrence, although these are not often noticed owing to the fleeting nature of the phenomenon.

During some of the early laboratory work of Project Cirrus, Vonnegut described (1) a few simple experiments illustrating the ease with which ice crystals may be formed under suitable conditions of rapid adiabatic expansive cooling. A short while later the writer made a brief investigation of this effect and more recently concluded a series of experiments designed to explore some of the quantitative relationships between moisture, pressure, and humidity. Several methods were used for conducting these experiments.

One of these consisted of a copper cylinder which could be capped, pressurized, the absolute humidity of the air controlled, and then the pressure released suddenly by a trigger device. A much simpler but equally effective method used a small, thin-walled glass bulb which after being pressurized could be broken suddenly with a falling weight. This latter method will be described in detail, since it produced results similar to that obtained with the more elaborate equipment.

THE GLASS SPHERE METHOD FOR PRODUCING LARGE NUMBERS OF ICE CRYSTALS

A ten-inch length of pyrex glass tubing 0.167 O.D., 0.075 I.D., was heated in cross flames until one end closed. This was then blown into a bulb of 0.225-in. diameter with walls about 0.015 in. thick. One and one-half inches of tubing was left attached to the glass sphere. A small brass rod was

---

[1] The research reported in this document was made possible through support extended the Research Laboratory of the General Electric Company by the Navy Department (Office of Naval Research) under Navy Contract Nonr-925 (00), NR 082-101.

[2] Present address: The Munitalp Foundation, R.D. 3, Schermerhorn Road, Schenectady, New York.

turned to make a slide fit in the bore of the tube. One end was turned to a diameter of 0.140 in. so that when placed against the end of the 1½ in. length of glass tube its small end did not project into the interior of the bulb but was flush with its inside surface. A small slot cut along the length of the brass rod with a jeweler's saw served as an air leak during pressurization and limited the flow down the tube after breakage. A copper tube with high pressure connections using about 2 in. of high-pressure plastic tubing was used to connect the air line to the small sphere. The bulb as used had a volume capacity of approximately 0.1 cm.^{3}.

Humidity under most conditions of the experiment was obtained by establishing equilibrium with respect to ice at a specific temperature. This was accomplished by injecting enough water into the bulb with a micropipet to coat the bulb's interior with a thin layer of water. This was then frozen.

For making a run at a specific temperature, a copper block was machined to accommodate the glass bulb in a suitable position for cooling, breaking, and permitting the pressurized air to escape into the surroundings without delay. The unit is shown as Fig. 1.

The copper block was fashioned as an integral part of the breaking mechanism and made small enough to be conveniently raised and lowered in a cold chamber. When operated a brass block 10 cm. × 2.5 cm. × 1.25 cm. having a hardened steel point projecting from its lower surface was raised 50 cm. to the top of two guide shafts and then suddenly released. Upon falling the steel point impinged upon the glass bulb and shattered it. The expanding air then shot rapidly outward from the cavity into the surrounding air of the cold chamber.

A cold chamber of 100 l. capacity was used in all experiments. It was operated at an equilibrium temperature of -14°C. ± 1°C. with a continuous supply of moist air feeding into it and forming a supercooled cloud (2). Under such conditions, ice crystals have a highly favorable environment for continuing growth, since at -14°C. the differential of the partial vapor pressures of ice and water reaches a maximum value.

The Results of Generating Ice Crystals by the Rapid Expansion of Moist Air

In the series of experiments to be described, six different pressures and three different temperatures were used. After the crystals were generated by the sudden expansion of the compressed air, the number formed in this manner was estimated by the procedure described by the writer (3) involving the rate of fall out of ice crystals being fed moisture at a constant rate.

An entirely different method was used in earlier experiments which gave similar values but was not as convenient and also required greater experi-

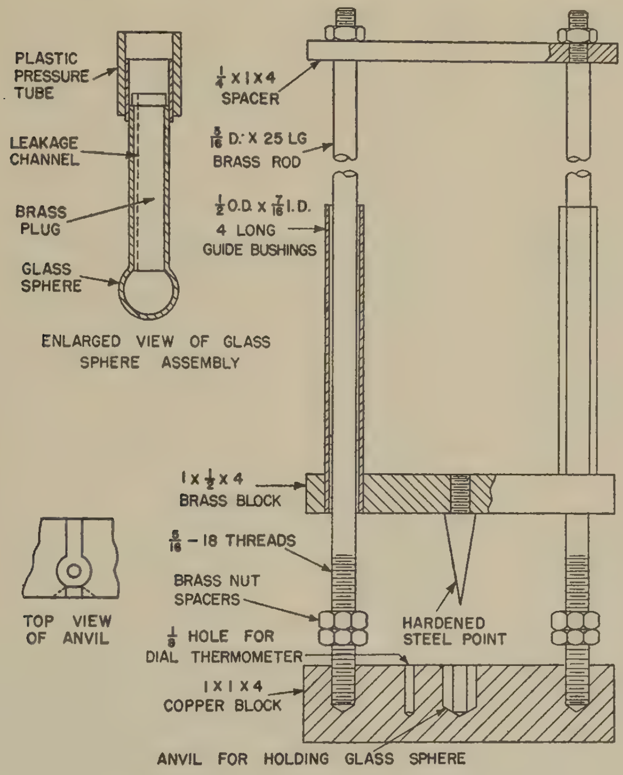

FIG. 1. Schematic diagram of sphere breaking apparatus.

mental skill and more equipment. This method utilized two cold chambers. The ice crystals were generated in the first chamber which had a volume of 50 l. Immediately following the generation of ice crystals by expansion, a known volume of the highly concentrated mass of crystals was rapidly transported from the 50-l. chamber to another having a capacity of 100 l. Both chambers contained supercooled clouds. The small but highly concentrated mass of crystals spreading through the second chamber became sufficiently diluted so that their concentration was low enough to prevent further evaporation of the smaller crystals and far enough apart to permit the concentration to be estimated. By measuring this concentration in the second chamber and knowing the fraction of the volume removed from the first chamber, it was possible to determine the initial concentration of crystals to a reasonable degree of accuracy.

It is important to realize that in all cases described the values given represent a low limit of the initial concentration. Evaporation, coagulation, melting, and other effects may have reduced the observed values by several orders of magnitude.

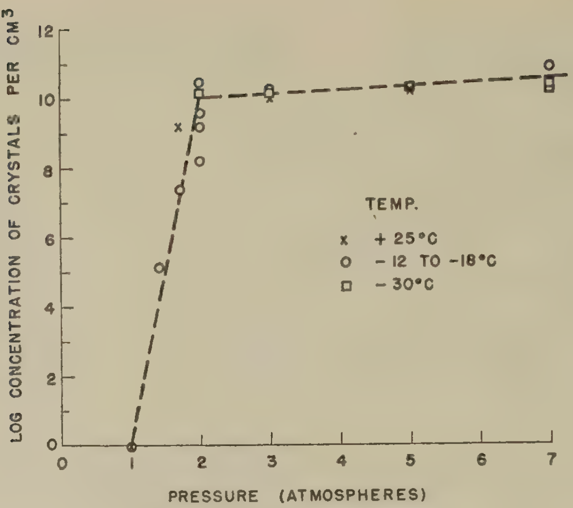

FIG. 2. The concentration of ice crystals formed spontaneously as related to pressure and temperature (moisture).

THE CONCENTRATION OF ICE CRYSTALS OBSERVED

As shown by Fig. 2, an upper limit to the number of ice crystals which may be produced by expansion cooling seems to lie in the range of 10^{11} per cubic centimeter. The actual value of the concentration of primary nuclei might be ten to one hundred or more times greater than this concentration for the reasons mentioned.

Even though this observed value of 10^{11} crystals per cubic centimeter represented the maximum number which could be formed by rapid adiabatic expansive cooling, the fact that it is possible to form such tremendous numbers of ice crystals in pure air is of great significance. It becomes obvious that a mechanism is involved which does not rely on foreign particle nuclei to serve as centers of formation. Of even greater significance is the sharp break which occurs in the curve shown in the figure. This indicates that a sharp discontinuity occurs in the physical relationships causing this phenomenon. Although it has not thus far been possible to firmly establish the physical mechanism responsible for the formation of such a tremendous initial concentration of ice crystal nuclei, other experiments give strong clues in this direction. The dry ice effect, originally reported by the writer (4) and more recently studied in detail with the continuous cloud chamber (5), suggests that the spontaneous formation of ice crystals occurs only when air contains moisture equivalent to water saturation at −39°C. and the air cools to at least that temperature. Under such conditions, submicroscopic ice crystals form in great number. If they are surrounded by air supersaturated with respect to ice, those which exceed a critical size continue to grow by the vapor diffusion process.

TABLE I

Data Obtained Under Several Conditions of Temperature and Pressure.

Pressure, p.s.i.	Bulb temp., °C.	Available moisture, g./cm.^{3} × 10^{-6}	Crystals formed, No. n/cm.^{3}
3	−18	0.923	2.7×10^3
6	−12	1.673	1.1×10^5
10	+25	23.063	1.5×10^9
10	−15	1.303	3.3×10^7
15	−15	1.303	1.5×10^9
15	−18	0.923	5.5×10^9
15	−19	0.863	1.6×10^8
15	−20	0.755	4.3×10^{10}
15	−30	0.203	1.4×10^{10}
30	+25	23.063	9.6×10^9
30	−12	1.673	2.3×10^{10}
30	−30	0.203	1.3×10^{10}
60	+25	23.063	5.8×10^{10}
60	−15	1.303	2.6×10^{10}
60	−30	0.203	2.0×10^{10}
60	−30	0.203	2.1×10^{10}
90	−17	1.063	1.4×10^{10}
90	−18	0.923	8.0×10^{10}
90	−20	0.755	3.0×10^{10}
90	−38	0.014	5.1×10^{10}

A study of Fig. 2 and Table I shows that the number of ice crystal nuclei which form spontaneously *and grow* as moist air is cooled rapidly by adiabatic expansion tend to reach a limiting value. Once this concentration is reached, a moisture increase of four orders of magnitude, a doubling of the pressure, or a decrease in temperature of more than 30°C. has little effect on raising this value. Thus at a pressure of 60 p.s.i., an increase in moisture of more than a hundredfold only doubles the number of crystals observed. Two runs with the same amount of moisture but with pressures of 15 and 90 p.s.i. gave values of 4.3×10^{10} and 3.0×10^{10} crystals per cubic centimeter respectively. Similarly, an initial temperature of −12°C. and 30 p.s.i. compared to −38°C. and 90 p.s.i. resulted in only doubling the concentration.

These effects are probably due to the following factors:

1. A critical reaction occurs.
2. The conditions necessary to produce this effect are pressures in excess of 10 p.s.i. above atmospheric pressure with the air containing enough moisture that when cooled below −39°C., supersaturation is sufficient to cause the spontaneous formation of submicroscopic water droplets in high concentration.
3. The number of ice crystals which form is dependent on the particles which survive by growing larger than a critical size during the expansion cycle (a few milliseconds) and which then enter an environment conducive to their continued growth. This latter condition is best achieved by sur-

rounding the experimental area with a supercooled cloud having a temperature colder than −10°C.

By several entirely different types of experiments which have been mentioned previously the existence of a critical phenomenon at −39°C. has been established. With the continuous cloud chamber it has been shown experimentally that not only do all pure water droplets freeze at −39°C. but that they may produce additional new crystals when the air is saturated with respect to water.

A simple calculation has been made using the highest value of ice crystal concentration observed in the current series of experiments to establish the probable size of the crystals which must form by this rapid expansion method. The calculation assumes that all of the moisture available is used in forming the crystals and that they are the survivors of the reaction which occurs at −39°C.

The experiment used a glass sphere cooled to −38°C. and lined with a thin layer of ice. The amount of moisture contained in the sphere was equivalent to 1.4×10^{-8} g. cm.$^{-3}$. The sphere was pressurized to 90 p.s.i. After the sphere was broken, the crystals passed into an environment containing a supercooled cloud at −22°C. Following the dilution and growth

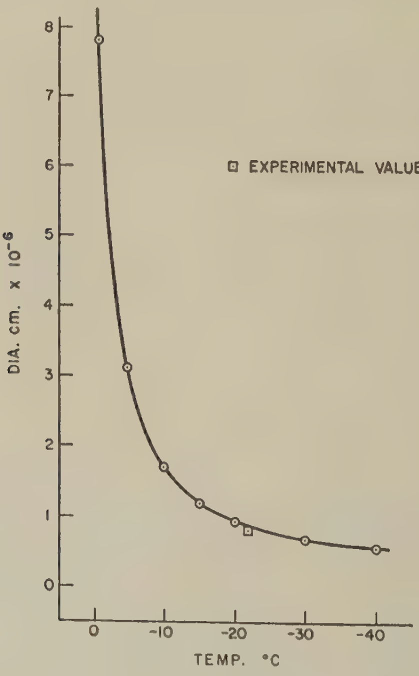

FIG. 3. The relationship of critical size of ice nuclei to temperature.

of the crystals, the number which formed was determined semiquantitatively to be 5 × 10^{10} per cubic centimeter. This number divided into the weight of available moisture indicates an amount of water per crystal of 2.8×10^{-19} g. By using Avogadro's number and the molecular weight of water, this value would indicate that the average number of molecules is 9300 per crystal. Assuming that the surviving particle would initially be spherical, this would indicate a diameter of 81 A.

In some of our earlier studies Langmuir calculated (6) the critical size limit of ice crystals which would survive under various physical conditions. This relationship is shown in Fig. 3. The nearly perfect agreement of the example cited with this curve may be fortuitous, but it indicates that the experimental results are of the right order of magnitude.

Although these experiments do not establish the size of the spontaneously formed primary ice nucleus, they show that the practical limit to the number of ice crystals which may be produced by rapid adiabatic expansion in a unit volume of moist air is governed by the number of those which grow larger than a critical size after the air is cooled below −39°C. This size is a function of temperature and moisture and approaches a limiting value of 50 A. (0.005 μ) diameter at −40°C.

Much work remains to be done in exploring these relationships. For example, it was discovered just at the conclusion of the experiments described in this paper that it was possible to produce ice crystals continuously by the rapid expansion of moist air from a high-pressure air source. Moist air under 90 p.s.i. pressure emerging from an orifice having a hole 100 μ in diameter formed a dense fog of ice crystals. These caused an optical effect indicating the particles to be less than 0.1 μ in diameter.

By using this continuous flow process for generating ice crystals, it should be feasible to study the complete range of ice crystal nucleation due to the rapid expansion cooling of moist air.

References

1. Vonnegut, B., "The Production of Ice Crystals by the Adiabatic Expansion of Gas," *J. Appl. Phys.* **19,** 959 (1948).
2. Schaefer, V. J., "The Production of Clouds Containing Supercooled Water Droplets or Ice Crystals Under Laboratory Conditions," *Bull. Am. Meteorol. Soc.* **29,** 175 (1948).
3. Schaefer, V. J. "The Measurement of High Concentrations of Ice Nuclei in a Small Parcel of Air." G. E. Research Laboratory Report RL1007.
4. Schaefer, V. J. "The Production of Ice Crystals in a Cloud of Supercooled Water Droplets," *Science*, **104,** 457 (1946).
5. Schaefer, V. J. "The Formation of Ice Crystals in Ordinary and Nuclei-Free Air," *Ind. Eng. Chem.* **44,** 1300 (1952).
6. Langmuir, I. "The Growth of Particles in Smokes and Clouds and the Production of Snow from Supercooled Clouds," *Proc. Am. Phil. Soc.* **92,** 167 (1948).

BOOK REVIEW

The Proteins. Chemistry, Biological Activity and Methods, (in two volumes, four parts). Edited by Hans Neurath and Kenneth Bailey. Academic Press, Inc., New York 10, N. Y., 1953. Volume 1, part A, viii + 548 pp. Price $12; part B (including index to both parts) 566 pp. Price $13.

This is, beyond question, the most authoritative, exhaustive, and useful monograph on the chemistry of the proteins that has ever appeared. It is difficult to believe that any of those for whom it is intended (advanced workers in proteins, and those with experience in related fields) will fail to acquire and make use of it. So thoroughly have most of the contributors done their work that the whole may be regarded as a critical and compendious key to a vast and growing literature, with few important gaps up to the end of 1951. Since no one individual can have followed critically the great volume of experimental observation and theoretical speculation about proteins that has appeared in recent years, it is safe to say that most protein investigators, like the reviewer, will be enlightened and stimulated by a careful perusal of these books.

The two parts under review comprise general treatments of the following subjects (consideration of specific proteins or classes of proteins is reserved to the two parts which are to follow): *Part A*. Isolation (J. F. Taylor); General Chemistry (P. Desnuelle); Amino Acid Composition (G. R. Tristram); Structure and Configuration of Amino Acids, Peptides, and Proteins (B. W. Low); Optical Properties (P. Doty and E. P. Gerduschek); Electrochemical Properties (R. A. Alberty). *Part B*. Size, Shape and Hydration (J. T. Edsall); Protein Interactions (I. M. Klotz); Denaturation (F. W. Putnam); Chemical Modification (F. W. Putnam); Relation of Chemical Structure to Biological Activity (R. R. Porter).

The topical organization just summarized serves to indicate the plan and the scope of the work. It will be noted that the organization favors experimental and theoretical approaches characteristic of recent years. Many particular topics which once would have merited chapters to themselves (titration curves, acidic and basic properties, for example) are now subheads in one or another of the above chapters. The parenthetical examples cited are treated, with only partial duplication, as parts of three separate chapters. Occasionally the arrangement is not obvious. Acidic and basic dissociations, for example, are most adequately treated in the chapters on Size, Shape, and Hydration of the Protein Molecule, and in Protein Interactions. The excellence of the index (in the second volume only), however, makes it simple and convenient to locate material.

Considerations of space preclude discussion of each separate contribution. All of the chapters achieve a high level of excellence, but this reviewer was especially impressed by the chapters on general chemistry (Desnuelle); amino acid composition (Tristram); X-ray evidence in structure (Low); size, shape, and hydration (Edsall); protein interactions (Klotz); and denaturation (Putnam).

It is no reflection on the book that the reviewer often felt a desire to engage in discussion with particular contributors on particular subjects. Few of the incentives to debate arose from a sense of error in fact or interpretation. A few exceptions to this statement follow. A very small number of omissions of significant work have been noted; in a few instances reporting work invalidating or making unnecessary certain speculations has not precluded a serious discussion of the same speculations some pages later; although the book does not lack frequent references to the fact that proteins previously judged on the basis of the solubility test to be pure have since been fractionated, several contributors tend to regard the solubility test of purity (*as usually performed and reported*) as the final criterion of purity *par excellence*; a number of contributors sometimes fail to distinguish sharply between unequivocal experimental fact and speculative inference at several removes from the data (the chapter on isolation, in fact, does not always cite explicitly the experimental evidence for some of the conclusions offered); the otherwise excellent and discerning chapter on denaturation is marred by what may be no more than verbal confusion between the thermodynamic ΔH for reversible protein denaturation, and the "thermodynamic analogue" ΔH^* for the activation step in denaturation kinetics; the same chapter includes a table of thermodynamic quantities for the reversible denaturation of three proteins, for one of which the results are obtained by combining data obtained under irreconcilably different conditions; there is also no explicit recognition that calculations of thermodynamic analogues, or energies of activation themselves, must take into account that reactions initiated and reversed by changes of pH must necessarily be mediated by different activated complexes when proceeding in opposite directions. Such recognition would serve to invalidate some of the results cited.

All these points are individual and constitute statistically insignificant exceptions to the general level of critical discernment. Such exceptions are presented against such a generally scholarly background of discussion that they are very unlikely to mislead or to be perpetuated in the literature.

The editors and publishers are to be thanked for providing so excellent a tool for the research worker in the field of proteins and to be congratulated on their unique success in so difficult an undertaking.

JACINTO STEINHARDT,
Cambridge, Massachusetts

ELECTRON MICROSCOPIC STUDY OF THE LOCUS OF A LATEX REACTION

Edward Crampsey, Manfred Gordon, and John W. Sharpe

The Royal Technical College, Glasgow C. 1, Scotland

Received August 20, 1953; revised January 29, 1954

The outstanding example of the study of reaction loci in an emulsion system was Harkins's work (1) in the field of emulsion polymerization. A simpler case presents itself for study when chemical reactions are carried out with preformed polymer emulsions (latices), as in the hydrochlorination of *poly*isoprene latex (2, 3). Here the reaction consists in the progressive conversion of the individual unsaturated isoprene units to their hydrochlorinated form:

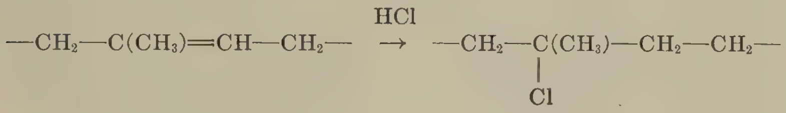

$$—CH_2—C(CH_3)=CH—CH_2— \xrightarrow{HCl} —CH_2—\underset{\underset{Cl}{|}}{C}(CH_3)—CH_2—CH_2—$$

the polymer particles preserving their identity throughout the reaction. The hydrochloric acid arrives at the site of reaction by a series of diffusion processes from the vapor phase and through the continuous aqueous phase. In principle there are still two loci at which the isoprene units may react with this reagent: in the bulk of the particle and at (or near) the interphase between the aqueous acid and the polymer particle. We were led by kinetic experiments (3) to conclude that the two loci do react at different rates and by different mechanisms, and it is the purpose of this report to provide quantitative evidence for this conclusion. At the same time we wish to put on record some observations connected with the electron microscopic technique used in the investigation.

The situation in the latex hydrochlorination reaction bears some resemblance to that in Smith's work (4) on emulsion polymerization "seeded" with preformed polymer particles. This proved that the polymerization took place in the preformed particles, after the relevant reagent (viz. the monomer) had arrived there by diffusion. However, no distinction has arisen in emulsion polymerization between the bulk locus and the surface locus of a particle of polymer. The technological importance of this new distinction in rubber chemistry is stressed below.

Our kinetic observations (3) suggested that a fast conversion of isoprene

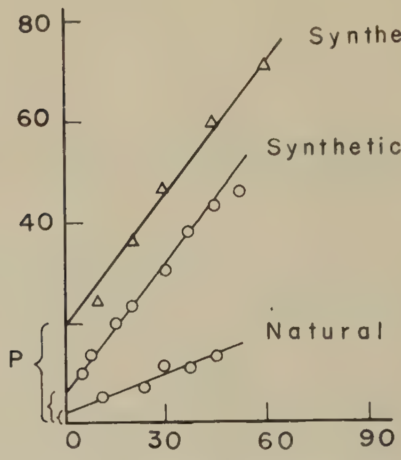

FIG. 1. Rate curves for the hydrochlorination of *poly*isoprene latices at 300° abs. and 2 atm. of HCl.

units near the polymer particle surface is responsible for observed abnormalities near the beginning of the rate curves. This is quantitatively confirmed by correlating the extent of the initial "jump" in the rate curves, measured by the intercepts P (Fig. 1), with measurements of the specific surface of the particles by means of electron micrographs (Figs. 2–4). Details of the preparation of the latices and of the kinetics and mechanism of the hydrochlorination in the bulk of the polymer particles, whose rate is measured by the slope of the straight lines in Fig. 1, have been published (3). The lines refer to natural (Hevea) latex and two synthetic *poly*isoprene latices. Two further synthetic latices are reported on in Table I, and the total range of average particle diameters studied is seen to be tenfold. The correct method of averaging n particles of diameters D_i so as to obtain a measure of the specific surface of a given latex, and thus of its total locus for the surface reaction, is to calculate the surface average diameter D defined thus:

$$\pi D^2 = \left(\sum_i \pi D_i^2\right)/n;$$

i.e.

$$D = \left[\left(\sum_i D_i^2\right)/n\right]^{1/2}. \qquad [1]$$

TABLE I

Surface Hydrochlorination Reaction (300° abs., 2 atm. of HCl)

P%	D (unshadowed), A.	D' (shadowed), A.	τ, A.	τ', A.	Latex
2.0	(4500)	—	15	—	Natural
6.25	1175	1400	12.5	14.7	Synthetic I
15	670	—	15	—	Synthetic III
20	467	700	17	24.9	Synthetic II
21	460	—	17.4	—	Synthetic V

The thickness τ of the outer shell of a sphere of diameter D, which comprises $P\%$ of the sphere by volume, may then be computed thus:

$$\tau = D(1 - 0.2155(100 - P)^{1/3})/2. \qquad [2]$$

The values of τ found for the one natural and four synthetic latices in Table I show very satisfactory constancy at 15 ± 2.5 Å. This confirms the kinetic inference that units privileged for fast reaction, react in the vicinity of the particle surface, *i.e.*, the interphase with the aqueous phase. The result can be expressed by saying that the extent of the fast initial hydrochlorination reaction is governed merely by the percentage P

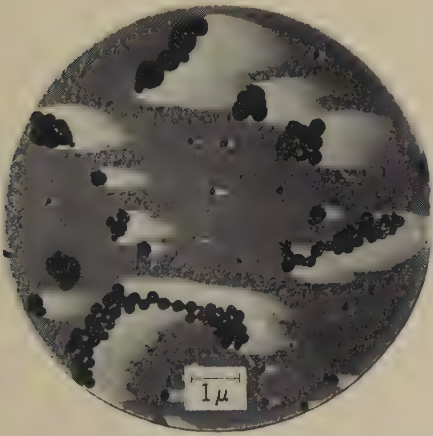

FIG. 2. Natural rubber hydrochloride latex

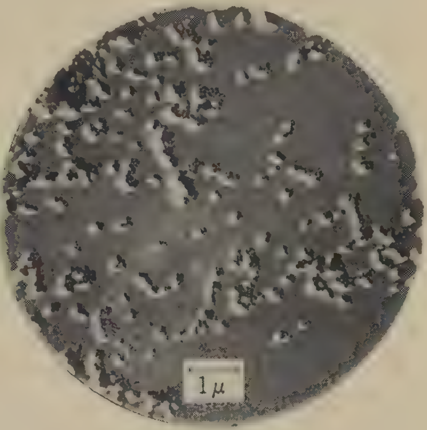

FIG. 3. Synthetic *poly*isoprene hydrochloride latex I.

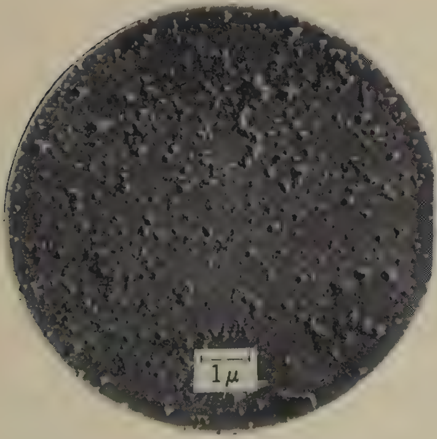

FIG. 4. Synthetic *poly*isoprene hydrochloride latex II.

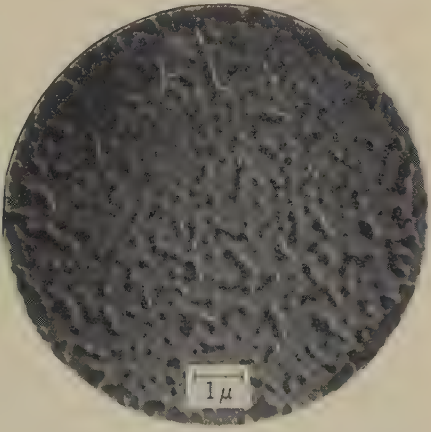

FIG. 5. Synthetic *poly*isoprene latex I.

All samples shadow-cast at approximate angle $\cot^{-1} 2.5$

of the polymer units which lies within $\tau = 15$ A. of the particle surfaces. This shows indirectly that the subsequent main reaction, corresponding to the linear rate plots (Fig. 1), occurs at the other possible reaction locus, namely, inside the bulk of the polymer particle. The kinetic evidence shows that the rate of the surface reaction, which is here too fast to be measured, must fall off rapidly with the progress of the surface reaction, and once the first four layers have reacted, the surface rate becomes negligible. This may be expressed by saying that the surface reaction has a very high reaction order. With natural rubber the thickness τ increases with temperature at constant HCl pressure. This, and other reasons, suggest that the falling off of the surface reaction is governed by a diffusion rate. If so, the rate of the surface reaction should be sensitive to prior crosslinking of the rubber. This has been investigated in vulcanization studies to be reported to the Third Rubber Technology Conference (London, 1954).

All latex samples (saturated with HCl in the case of hydrochlorinated samples) were prepared for examination in the electron microscope by diluting with distilled water and then placing a single drop of the dispersion on the standard collodion-covered specimen grids used in electron microscopy. The specimen was then allowed to dry in a desiccator. In some cases the samples were shadow-cast with gold/palladium alloy in order to enhance contrast.

Owing to their narrow size ranges, the synthetic latices (Figs. 3, 4) allowed sufficiently accurate values of the diameter D to be obtained by averaging a few particles chosen at random on the electron micrographs. In natural latex the particles are far from uniform in size (Fig. 2), but two different samples were found by van den Tempel (5) to agree closely in distribution curve and D, so that his value of $D = 4500$ A. was accepted.[1] All our micrographs were taken at a magnification of 8000×. Table I lists separately the surface average particle diameters D measured on non-shadow-cast specimens and those, denoted by D', measured on shadowed specimens of synthetic latices I and II. The maximum width of the shadow was taken as D', and this can be measured with somewhat higher precision than D, because of the higher definition of micrographs of shadowed specimens. The value of D' is seen to be larger than D by about 230 A. in both cases. The effect of shadow-casting in increasing the apparent particle size has been repeatedly noted by other workers, but its explanation is not quite certain. Kern and Kern (7), and Cosslett (8) independently explain the effect in terms of the surface charge of the particle producing the action of an electrostatic lens. The former authors imagine the lens to act on the electron beam in the microscope. A spuriously enlarged picture of the unshadowed particle is thus produced, while the shadowed particle, which allows its surface charge to leak away, gives a correct measure. Cosslett, however, considers the lens to affect the metal atoms in the shadowing process, in which case we must assume that the unshadowed particle gives the correct measure of the diameter. The chemical evidence based on our measurements of the intercepts P (Fig. 1) appears to support Cosslett's explanation, inasmuch as the "unshadowed" diameters D lead via Eq. [2] to noticeably more constant values of τ, when compared to the values τ' obtained via the same equation from the "shadowed" diameters D' (as shown in Table I).

---

[1] Rough estimates from our own micrographs led to somewhat lower values (2500–3000 A), while preliminary measurements by Cosslett quoted by Cockbain (6) are slightly in excess of van den Tempel's figure. In view of the limited relative accuracy of the small intercept P for natural latex ($2 \pm 0.5\%$), a full size analysis of our natural latex did not seem warranted.

Whatever the explanation of the effect, it is apparent from micrographs shown in Kern and Kern's paper that the effect is relatively more marked with smaller particles (such as bacteriophages). Our measurements confirm this and suggest in fact that

$$D' - D = 230 \text{ A.} \qquad [3]$$

The almost identical difference of 250 A. between shadowed and unshadowed particles was also observed by Kern and Kern on much larger (*poly*styrene) latex particles. The suggestion of the simple law of Eq. [3] may assist in the final theoretical explanation of the phenomenon.

Comparison of electron micrographs before and after hydrochlorination of our latices reveals several interesting features (*cf.* Figs. 3 and 5). The change from the rubbery amorphous to the glassy state (with or without embedded crystalline regions[2]) during hydrochlorination is reflected in a change of appearance of shadow-cast samples. Rubbery particles are flattened (Fig. 5) and appear disclike rather than spherical, owing to wetting of the collodion support by the deformable particle. The glassy particles are so stiff as not to be visibly flattened, and are thus much more useful for measuring the particle diameters. Although much irreversible aggregation occurs in drying out the rubbery samples, the ultimate particle size before the hydrochlorination reaction is seen to be essentially the same as after the reaction. This confirms that the particles preserve their identity during the reaction without dissolution or coagulation. (The volume change due to the actual reaction can, of course, be accurately computed from density data, but changes the diameter by only a few per cent.) The contrast in the micrographs, particularly in the case of unshadowed particles, increases considerably in the course of the reaction owing to the relatively high scattering power of the chlorine atoms introduced thereby. This suggests the usefulness of reactions like hydrohalogenation or halogenation of latices, after suitable stabilization against coagulation, when it is desired to study size distributions by electron microscopy.

---

[2] Electron diffraction experiments by the authors confirm that natural latex hydrochloride shows crystallinity (*cf.* van Veersen (9)), whereas synthetic *poly*isoprene hydrochloride is amorphous (*cf.* D'Ianni *et al.* (10)).

The demonstration here given of the occurrence of a polymer particle surface reaction locus, controllable by such variables as particle size and temperature, has colloid-chemical and technical importance. That the hydrochlorination reaction is not merely an isolated instance of this effect is suggested by similar rate curve "jumps" in the cyclization of Hevea latex (cf. ref. 3). Preliminary work suggests that in vulcanization of latex a surface locus can also be observed. In this reaction the technical effect would be expected to be particularly marked. For example, a lightly and uniformly cross-linked particle would give a useful prevulcanized latex. If, however, the reaction (interrupted after 1 per cent or so of conversion in practice) were found to be largely concentrated in the surface layer, as the present work shows the hydrochlorination reaction to be at such low conversions, one would obtain what might be described as an unvulcanized particle surrounded by a shell of ebonite, which would be technically useless. Differences in film strength of prevulcanized latices at constant combined sulfur are thought to be connected with the variability of the contribution of the surface locus from one vulcanization recipe to another.

The authors are indebted to Professor P. D. Ritchie for his kind interest in this work.

References

1. Harkins, W. D., *J. Am. Chem. Soc.* **69,** 1428 (1947).
2. Gordon, M., and Taylor, J. S., *J. Appl. Chem.* (London) **3,** 537 (1953).
3. Crampsey, E., Gordon, M., and Taylor, J. S., *J. Chem. Soc.* **1953,** p. 3925.
4. Smith, W. V., *J. Am. Chem. Soc.* **70,** 3695 (1948).
5. van den Tempel, M., *Trans. Inst. Rubber Ind.* **27,** 290 (1950).
6. Cockbain, E. G., *Trans. Inst. Rubber Ind.* **29,** 297 (1952).
7. Kern, S. F., and Kern, R. A., *J. Appl. Phys.* **21,** 705 (1950).
8. Cosslett, V. E., *Proc. Conf. Electron Microscopy*, Delft (1950).
9. van Veersen, J., *Proc. 2nd Rubber Technol. Conf.* **1948,** p. 87.
10. D'Ianni, J. D., Naples, F. J., Marsh, J. W., and Zarney, J. L., *Ind. Eng. Chem.* **38,** 1178 (1946).

THE PROPERTIES OF DETERGENT SOLUTIONS.
I. MOLECULAR WEIGHTS DETERMINED BY LIGHT-SCATTERING MEASUREMENTS

Eric Hutchinson

Department of Chemistry, Stanford University

Received February 8, 1954

Abstract

It is pointed out that all published results to date for light-scattering experiments on detergent solutions have been interpreted by a method which implicitly treats these solutions as being nonelectrolytes. Reasons are presented for believing that the molecular weight or degree of association is best determined by experiments in which a large excess of neutral salt is added to the detergent solution.

Debye has applied his treatment of light scattering to solutions of colloidal electrolytes (1), and similar applications have been made by Anacker (2) and Hutchinson (3). Hermans (4), Doscher and Mysels (5), and Hutchinson (6) have extended this treatment to take account of the fact that colloidal electrolytes are, in fact, electrolytes and that due attention must be paid to the question of gegenions and added salts in evaluating the so-called molecular weight of micelles from light-scattering data.

In particular Doscher and Mysels have deduced that

$$\frac{Hc_2^*}{\tau} = \frac{1}{M_2^*}(1 + p) \qquad [1]$$

where H = the conventional scattering constant;
c_2^* = the concentration of solute in grams per milliliter;
M_2^* = the micelle molecular weight;
τ = the absolute turbidity of the solution; and
p = the net charge on the micelle when the gegenions are univalent.

In the presence of excess electrolyte, p tends to zero, and Doscher and Mysels have concluded that, at the CMC of the colloidal electrolyte, the latter provides sufficient of its own simple ions for the condition $p \rightarrow 0$ to be satisfied and that, consequently, extrapolation of the Hc_2^*/τ curve to the CMC yields a close approximation to the true value of M_2^*. I propose to show that this is not so.

Debye's treatment (1) leads to the result

$$\frac{Hc_2^*}{\tau} = \frac{1}{RT}\frac{\partial \pi}{\partial c_2^*}, \qquad [2]$$

in which π is the osmotic pressure of the solution. In applying this to solutions of alkylammonium halides Debye has treated these as if the solute were a nonelectrolyte, writing,

$$\pi = RT\left(\frac{c_2^*}{M_2^*} + ac_2^{*2} + \cdots\right). \qquad [3]$$

I have recently shown (6) that for a solution of a pure colloidal electrolyte in the absence of salt,

$$\frac{Hc_2M_2}{2\tau} = g_1 + \frac{\partial g_1}{\partial \log c_2} \qquad [4]$$

where c_2 = the concentration of solute in gram formula weights per milliliter;

M_2 = the gram formula weight of the solute;

g_1 = the osmotic coefficient of the solvent.

The model for this derivation is that of a uni-univalent electrolyte in extremely dilute solution.

Dr. Marjorie Vold (7) has developed a treatment of micelle behavior on the basis of a model which essentially treates a micelle A_nG_n as a weak electrolyte,

$$A_nG_n \rightleftharpoons (A_nG_{n-1})^- + G^+ \rightleftharpoons (A_nG_{n-2})^= + 2G^+ \rightleftharpoons, \text{etc.}$$

This treatment embraces considerable generality as to the possible variations of the association factor r, and leads to the same model as the author's in dilute solution.

Dr. Vold has shown that all available osmotic data are consistent with the hypothesis that the micelles carry a fixed ratio of gegenions to colloidal electrolyte ions, and deduces that

$$g_1 + \frac{\partial g_1}{\partial \log c_2} = \tfrac{1}{2}(1 - r) + \tfrac{1}{2}\sum \frac{\partial c_i}{\partial c_2} \qquad [5]$$

where r = the ratio of gegenions per single colloidal electrolyte ion;

c_i = the concentration in moles per liter of the species $(A_nG_{n-i})^{-i}$;

c_2^1 = the concentration in moles per liter of the species AG.

The summation in Eq. [5] is to be carried out over all permissible values of r and i.

Assuming for simplicity that in a given solution n has only a single value (as seems justified by the apparent monodispersity of colloidal micelles (8)), we have, from Eqs. [4] and [5],

$$\frac{Hc_2M_2}{\tau} = (1 - r) + \frac{\partial c_n}{\partial c_2},$$

where c_n is the concentration of the unique colloidal ion now presumed to be formed in solution.

But $\partial c_n/\partial c_2^1 = 1/n$ where n is the association factor;

$$\therefore \frac{Hc_2M_2}{\tau} = (1 - r) + \frac{1}{n}. \tag{6}$$

This equation is almost identical with Eq. [1].

Dr. Vold's treatment implies that r remains constant under given conditions, and hence Hc_2M_2/τ should be constant. This is not observed to be the case, but, in view of the fact that the concentrations of the various species have been equated to their activities, this is not surprising.

Although the theory leading to Eq. [3] cannot be extended to cover cases in which added salt is present, except by making simplifying assumptions about the supposed ideality of the added salt in the absence of colloidal electrolyte, yet with reasonable accuracy Eq. [6] may still be applied. It may be anticipated that the effect of added salt is to cause $r \rightarrow 1$, *i.e.*, to make the micelle virtually uncharged. Then, and only then, does the Debye result give the correct value for n. It is noteworthy that in all cases reported the addition of salts brings the plot down to much more constant values.

From the results of conductance studies on pure colloidal electrolyte solutions (9) it may be deduced with certainty that, in the absence of added salts, r is appreciably less than unity, and that, in consequence, we have to deal with charged micelles. Consideration of osmotic coefficients and electrical conductance data suggests that with solutions for which $n \approx 100$ the value of r may lie between 90/100 and 99/100. It follows from this that at a concentration some ten times greater than the CMC the total ionic population is only very slightly greater than that at the CMC. If the nonconstancy of Eq. [6] for solutions containing no added salt is due to the dependence of the activities of the various species on ionic population, *e.g.*,

$$\frac{Hc_2M_2}{\tau} = \left\{\frac{1}{n} + (1 - r)\right\} (1 + ac_2 + bc_2^2 + \cdots),$$

it follows that the correct value of the quantity in the first brackets is obtained by extrapolation of Hc_2M_2/τ to zero concentration, and not to the CMC as suggested by Debye (1) and by Doscher and Mysels (5).

In the presence of added salts $r \rightarrow 1$, and thus the effect of ionic population on the activity of the micelle may be expected to be negligible, as appears to be the case. Alternatively, even if the micelle still bears a charge in the presence of added salt the ionic population is so little affected by the contribution due to the colloidal electrolyte that, over the range studied, no dependence of activity on the concentration of colloidal electrolyte will be perceptible.

It becomes obvious that the interpretation of these light-scattering data is far from simple. In Fig. 1 I have replotted Debye's data for dodecylamine hydrochloride (1). If we *assume* that $r = 1$ in 0.0457 M NaCl solu-

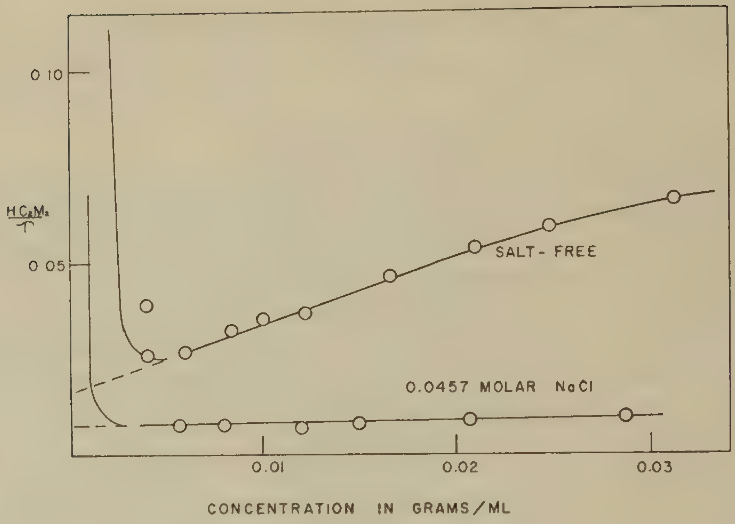

FIG. 1. Plot of Hc_2M_2/τ against concentration for dodecylamine hydrochloride, taken from the results of Debye (1).

tion, the value of n obtained is approximately 133. The extrapolated curve for pure dodecylamine hydrochloride gives a value of about 0.016 for the quantity $1/n + (1 - r)$. To interpret this one need not assume that n has changed. If n remains 133, a value of $r = 132/133$ corresponding to a micelle bearing a single charge would satisfy the result. It is therefore improper to assume that addition of salt necessarily changes the size of the micelle (1).

Clearly, since Eq. [6] contains two unknowns, we cannot obtain the size of a micelle from light-scattering data, any more than we can derive the size from freezing-point depression, except for uncharged micelles. All that we can do is to obtain a *minimum value for n*—a value which may be very much smaller than the true value.

Contrary to the idea that the addition of salt causes a change in the size of the micelle, it appears more reasonable, until further information becomes available, to assume that the effect of added salt is solely on the value of r. Some justification for this procedure may be adduced from experiments on solubilization. The solubilizing power of a micelle toward a nonpolar material may be expected to be more or less independent of the charge of the micelle. Harkins (10), has shown that in solutions of concentrations not more than about five times that of the CMC, the increased solubilizing power of potassium laurate due to added salt may be ascribed to the depression of the CMC and the consequent formation of more of the same micelles as were present before the salt was added. More convincing, however, is the evidence that experiments on the effects of added salts on the conductance of dodecylamine hydrochloride (9) show no signs of a change in the size of the micelle. The association factor of approximately 133 is in good accord with values obtained by diffusion and X-ray diffraction (8).

Similarly, unpublished data of the author for the effect of added salts on light scattering by sodium dodecyl sulfate solutions lead to an association factor of about 80, in good accord with diffusion and X-ray data (8).

It thus seems best to use light-scattering measurements to determine the size of micelles in fairly concentrated salt solutions, where the micelles are nearly uncharged, and to interpret the apparently smaller association in the absence of added salt in terms of the ionization of the micelle.

Some correlation of the light-scattering data with the results of conductance experiments may be made as follows. Above the CMC the solution may be considered to contain simple ions and charged micelles, and the specific conductance may be evaluated by the method suggested by van Rysselberghe (11). If we assume for simplicity that there is only one kind of micelle containing n units and possessing a charge m, and assume further that the concentration of solute in the aggregated form is $(c_2 - c_2^0)$, where c_2^0 is the CMC value, the specific conductance K of the solution is given by

$$K = \frac{c_2^0}{1000}(l_m + l_g) + \frac{(c_2 - c_2^0)}{1000n} ml_g + \frac{(c_2 - c_2^0)}{1000n} m^2 n^{-\frac{1}{3}} l_m \qquad [7]$$

where l_m = the equivalent conductance of the micelle-forming ion, and
l_g = the equivalent conductance of the gegenion.
writing $K^0 = (c_2^0/1000)(l_m + l_g)$, where K^0 is the specific conductance at the CMC,

$$K - K^0 = \frac{(c_2 - c_2^0)}{1000n}(ml_g + m^2 n^{-\frac{1}{3}} l_m). \qquad [8]$$

Hence,

$$\frac{K - K^0}{c_2 - c_2^0} = \frac{1}{1000n}\{ml_g + m^2 n^{-\frac{1}{3}} l_m\}. \qquad [9]$$

From the work of Ralston and Eggenberger (9) and Lottermoser and Puschel (12) the slopes of $K - K^0/c_2 - c_2^0$ may be obtained for dodecylamine hydrochloride and sodium dodecyl sulfate. Using the values of n obtained from light scattering in the presence of salt, viz., about 133 and 80, respectively, one may calculate that the charge m is about $+15$ for dodecylamine hydrochloride micelles and about -14 for sodium dodecyl sulfate micelles. Putting the appropriate values of $(1 - r)$, calculated from these values, into Eq. [6], we have

$$\frac{Hc_2 M_2}{\tau} = \frac{1}{133} + \frac{15}{133} \approx 0.11$$

for dodecylamine hydrochloride, and

$$\frac{Hc_2M_2}{\tau} = \frac{1}{80} + \frac{14}{80} \approx 0.18$$

for sodium dodecyl sulfate. It is noteworthy that although the Hc_2M_2/τ plots for these compounds do not yield constant values, particularly in the neighborhood of the CMC, as they should according to Eq. [6], yet the curve for sodium dodecyl sulfate (6) tends to a value of 0.2 in more concentrated solutions (concentrations some fifty times the CMC), and there is some indication that in the case of dodecylamine hydrochloride, where the results extend only to some fifteen times the CMC, a limiting value of Hc_2M_2/τ is reached, somewhere between 0.05 and 0.1.

The surprisingly good agreement which thus obtains between the light-scattering data and X-ray and diffusion data on the one hand, and between the light-scattering data and the conductance data on the other, supports the hypothesis that the size of the micelle is, in fact, unchanged by the addition of salt, and that the light-scattering data obtained in salt-free solutions give information on the charge rather than the size of the micelle.

REFERENCES

1. DEBYE, P., *J. Phys. & Colloid Chem.* **53,** 18 (1949).
2. ANACKER, E. W., *J. Colloid Sci.* **8,** 402 (1953).
3. HUTCHINSON, E., *Technical Report #1 O.N.R. Contract N6ONR 25130.*
4. HERMANS, J. J., *Rec. trav. chim.* **68,** 859 (1949).
5. DOSCHER, T. M., AND MYSELS, K. J., *J. Chem. Phys.* **19,** 254 (1951).
6. HUTCHINSON, E., *Technical Report #3 O.N.R. Contract N6ONR 25130.*
7. VOLD, M. J., *J. Colloid Sci.* **5,** 506 (1950).
8. PHILIPPOFF, W., *Discussions Faraday Soc. No.* **11,** 96 (1951).
9. RALSTON, A. W., AND EGGENBERGER, D. N., *J. Am. Chem. Soc.* **70,** 980 (1948).
10. HARKINS, W. D., *et al., J. Chem. Phys.* **15,** 496 (1947).
11. VAN RYSSELBERGHE, P., *J. Phys. Chem.* **43,** 1049, (1939).
12. LOTTERMOSER, A., AND PUSCHEL, F., *Kolloid-Z.* **63,** 175, (1933).

REACTION RATES IN POLYELECTROLYTE SOLUTIONS. I. THE DECOMPOSITION OF ETHYL DIAZOACETATE IN AQUEOUS POLYMETHACRYLIC ACID SOLUTION

M. Joseph[1] and H. Morawetz

Department of Chemistry, Polytechnic Institute of Brooklyn, Brooklyn 1, New York

Received February 8, 1954

INTRODUCTION

The large electrostatic forces between polyelectrolytes and their counter-ions give rise to a variety of effects which have been the subject of experimental and theoretical studies in recent years. As one would expect, the ionic activity coefficients are unusually small in dilute polyelectrolyte solutions, unless the counter-ions are shielded from the field of the polyion by addition of simple electrolyte. Kern (1) and Kagawa and Katsuura (2) calculated activity coefficients from potentiometric measurements, while Katchalsky and Lifson reported values obtained from dialysis equilibrium and proposed a theory to account for the observed effects (3).

Since the catalytic effect of hydrogen ion, hydroxyl ion, and other ions has been shown to depend on their concentration rather than activity (4), a measurement of the rate of a reaction catalyzed by a given ion in conjunction with a potentiometric activity measurement provides in principle a way of estimating the activity coefficient. The hydrolysis of ethyl diazoacetate was chosen for this study, since the reaction has been shown to be catalyzed by hydrogen ion and no other species (5, 6).

EXPERIMENTAL METHODS

A. Materials

Ethyl diazoacetate was prepared from glycine ethyl ester hydrochloride (Eastman) according to directions given in *Organic Syntheses* (7). It was purified by steam distillation under reduced pressure, extracted with ether, dried and distilled according to Fraenkel (5). The last traces of water had to be removed carefully, since otherwise a sealed capsule of the reagent tended to explode at the reaction temperature. The purity of the ethyl diazoacetate was determined by measuring the nitrogen evolved after complete decomposition in acetic acid solution. The values obtained were 99.8%, 99.6%, and 99.8% of theoretical, and subsequent checks showed that the reagent was stable on storage.

---

[1] Taken from the thesis of M. Joseph, submitted in partial fulfillment of the requirements for the M.S. degree at the Polytechnic Institute of Brooklyn, June 1953.

Polymethacrylic acid was prepared from glacial methacrylic acid (Rohm and Haas) distilled under reduced pressure to remove inhibitor. The polymerization was effected by heating 10 ml. of methacrylic acid in 40 ml. butanone with 29 mg. azo-bis-isobutyronitrile for 24 hours at 60°C. The polymeric acid was purified by dialysis and lyophilized.

Buffer solutions were prepared from analytical grade sodium acetate, sodium dihydrogen phosphate, and disodium hydrogen phosphate.

B. Determination of Reaction Rate

A sealed glass capsule containing a weighed amount of ethyl diazoacetate was introduced into the polymer or buffer solution thermostated at 65.5°C. The solution was saturated with nitrogen and connected to a water-jacketed gas buret consisting of ten calibrated glass bulbs and a 5-ml. tube graduated to 0.01 ml. When thermal equilibrium had been established, the capsule containing the reagent was broken by means of a glass lever, which could be manipulated without opening the system to the atmosphere. The solution was stirred rapidly by a magnetic stirrer, and the reaction was followed by measuring the nitrogen evolved at constant pressure. All runs conformed to a first-order decomposition of ethyl diazoacetate. The rate constant was calculated from $k = 2.303/(t_2 - t_1) \log (V_\infty - V_1)/(V_\infty - V_2)$, where V_1 and V_2 are nitrogen volumes at times t_1 and t_2 and V_∞ was calculated from the weight of the ethyl diazoacetate used.

C. Determination of pH

All *p*H and e.m.f. measurements were made on a Beckman Type G *p*H meter. Specially shielded glass and calomel electrodes for use outside of the *p*H meter were employed. The *p*H of polymethacrylic acid and buffer solutions at 65.5°C. was obtained from the relation $\epsilon - \epsilon_A = 0.0674\ (p\mathrm{H}_A - p\mathrm{H})$, where the subscript A refers to the e.m.f. and *p*H of 0.1 *N* half-neutralized acetic acid. The *p*H of the acetate buffer at 65.5°C. was taken as 0.06 unit higher than the value found at 25°C. (8).

RESULTS

Since it was the purpose of this investigation to derive activity coefficients in solutions containing highly charged polyions, the *p*H range had to be chosen so as to correspond to a substantial degree of ionization of the polymeric acid. At the reaction temperature of 65.5°C., rates of decomposition of ethyl diazoacetate were conveniently measurable up to 50% neutralization of 0.1 *N* polymethacrylic acid, corresponding to a *p*H of 6.81.

TABLE I

Decomposition of Ethyl Diazoacetate in Buffer Solutions at 65.5°C.

*p*H	Ionic strength	10^3k, min.$^{-1}$	$10^{-3}k/a_{H^+}$, liters mole^{-1} min.$^{-1}$
4.63	0.1	74	3.2
5.03	0.1	32	3.4
5.53	0.1	9.8	3.3
5.94	0.1	4.6	4.0
6.85	0.1	2.23	15.8
7.68	0.1	1.97	93
4.65	0.2	85	3.8
5.06	0.2	32	3.7
5.62	0.2	10.6	4.4
6.89	0.2	2.0	15.5
6.99	0.2	2.1	20.4

The results obtained in buffer solutions at ionic strengths of 0.1 and 0.2 are listed in Table I. The similarity of data obtained with the two buffer concentrations indicates a much smaller salt effect than that reported for ethyl diazoacetate decomposition in perchloric acid solution at 15°C. (9).

The ratio of the first-order rate constant and the hydrogen ion activity is constant up to about *p*H 5.5, but rises sharply at higher *p*H. (See Fig. 1.) This observation could be interpreted either as being due to water catalysis of the reaction or as a result of the hydrolysis of the ester group, followed by rapid decomposition of the unstable diazoacetate ion (10). The latter alternative is favored by the observation of slight *p*H drops

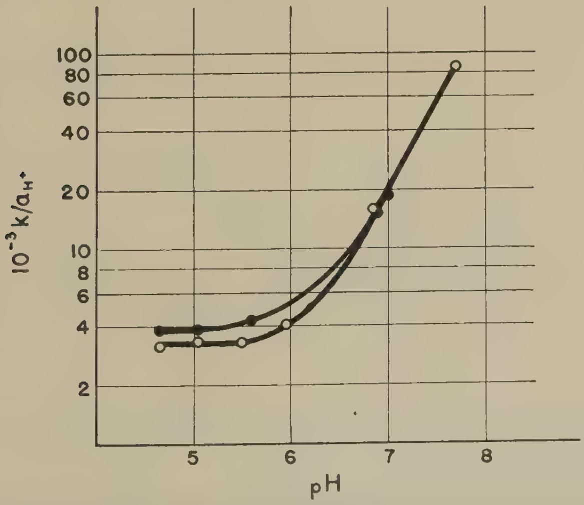

FIG. 1. Ratio of the rate constant and hydrogen ion activity in the decomposition of ethyl diazoacetate in buffer solutions at 65.5°C. –○– ionic strength 0.1; –●– ionic strength 0.2.

TABLE II

Decomposition of Ethyl Diazoacetate in Polymethacrylic Acid Solution at 65.5° C.

Normality of polymethacrylic acid	Degree of neutralization, %	pH	10^3k, *min.*$^{-1}$	$10^{-3}k/a_{H^+}$, *liters mole*$^{-1}$ *min.*$^{-1}$
0.1	0	4.26	115	2.1
0.1	2	4.42	60	1.6
0.1	6.7	5.21	16.0	2.6
0.1	20	5.81	5.8	3.7
0.1	33.3	6.23	3.0	5.1
0.1	50	6.81	0.96	6.1
0.033	0	4.31	62	0.79
0.033	5	5.31	11.3	2.3
0.033	10	5.69	6.2	3.0
0.033	50	6.80	1.21	7.6

during the reaction. This drop averaged 0.02 pH units for runs below pH 6.0 but rose to 0.06 pH units in runs at higher pH.

Reaction rates observed in polymethacrylic acid solutions of two concentrations and at various degrees of neutralization are summarized in Table II. The following points may be noted:

1. The ratio of rate constant to hydrogen ion activity rises uniformly with pH from 0 to 50% neutralization. (See Fig. 2.)
2. Ethyl diazoacetate is significantly more stable in unneutralized and 50% neutralized polymethacrylic acid than in buffers of equal pH.
3. For intermediate degrees of neutralization the reaction rates in 0.1 N polymethacrylic acid and buffers of the same pH are comparable, but those in 0.033 N polymethacrylic acid are slower.

A more detailed comparison of the reaction rates in unneutralized

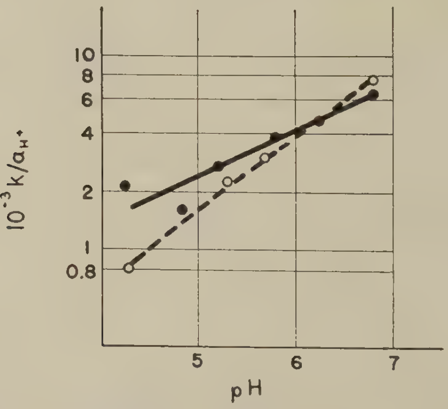

FIG. 2. Ratio of the rate constant and hydrogen ion activity in the decomposition of ethyl diazoacetate in polymethacrylic acid solutions at various degrees of neutralization. Temperature 65.5°C. -●- 0.1 N polymethacrylic acid. —○— 0.033 N polymethacrylic acid.

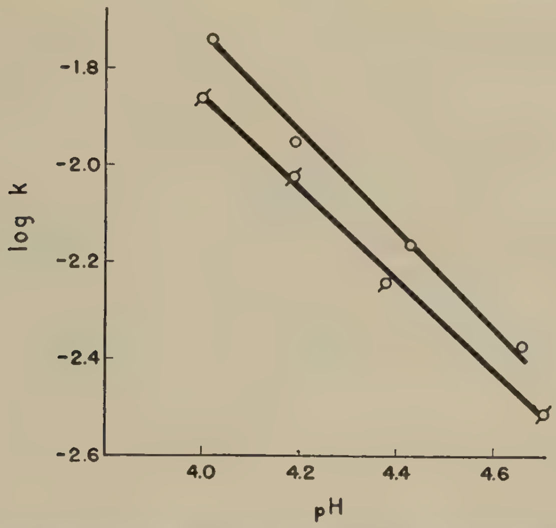

FIG. 3. Decomposition of ethyl diazoacetate in unneutralized polymethacrylic acid and in acetate buffer. Temperature 38.2°C. –○– acetate buffer, ionic strength 0.1; –⌀– polymethacrylic acid, 0.1 *N*, 0.033 *N*, 0.01 *N*, and 0.0033 *N*.

polymethacrylic acid solutions and buffers in the same *p*H range was carried out at 38.2°C. The results are plotted in Fig. 3, and it is seen that the rates are uniformly lower in the polymeric acid solutions.

DISCUSSION

A large body of experimental evidence indicates that the rate of acid-catalyzed reactions depends on the concentration, rather than on the activity, of hydrogen ions. Thus Dawson and Lowson (11) found the rate of ethyl acetate hydrolysis exactly proportional to the concentration of HCl between 0.002 and 0.2 molar, although the mean ionic activity coefficient falls in this range from 0.993 to 0.783. (Similar observations were made by LaMer and Miller (12) with respect to the decomposition of diacetone alcohol in presence of 0.02 *N* to 0.1 *N* hydroxide.) It follows that for a reaction catalyzed exclusively by hydrogen ion the reaction rate is given by

$$\text{Rate} = k_{H^+}C_{H^+} = k_{H^+}a_{H^+}/f_{\pm}$$

where k_{H^+} is the catalytic coefficient of hydrogen ions, C_{H^+} is their concentration, and $f_{\pm}$ the mean activity coefficients of the ions in solution.

The conclusion of Kern (1) and Katchalsky and Lifson (3) that activity coefficients in solutions of partially neutralized polyacrylic acid have unusually low values can hardly be questioned. Thus, Kern found an activity coefficient of 0.292 in half-neutralized 0.0625 *N* polyacrylic acid.

It was therefore expected that ethyl diazoacetate hydrolysis would be more rapid in the polyelectrolyte solution than in buffer of corresponding *p*H. The reverse was found in the present study, particularly with unneutralized polymeric acid and at a relatively high degree of neutralization.

The low rates in unneutralized polymethacrylic acid solution are probably due to the relative exclusion of the diazoacetic ester from the space occupied by the polymer molecules. This is not unexpected, since water is a solvent but the ester a precipitant for the polymeric acid. With the hydrogen ions concentrated in the neighborhood of the polyanion, the diazoacetic ester would be left in a region of relatively low acidity.

In buffer solution the rate of nitrogen evolution was found to be almost the same at *p*H 6.85 and 7.68. This is interpreted as due to two reactions

$$N_2CH\text{—}COOC_2H_5 + H_2O \xrightarrow{H^+} HOCH_2COOC_2H_5 + N_2 \qquad [1]$$

and

$$N_2CH\text{—}COOC_2H_5 + OH^- \rightarrow N_2CH\text{—}COO^- + C_2H_5OH \qquad [2a]$$

$$N_2CHCOO^- + H_2O \rightarrow HOCH_2COO^- + N_2 \qquad [2b]$$

where [2a] is the rate-determining step in the second mechanism (10). The relatively slow reaction velocity in half-neutralized polymethacrylic acid may be due to a difference in the relative catalysis of the two reactions by simple electrolyte and the polyelectrolyte. This is quite analogous to the specificity observed in the catalytic behavior of ion exchangers (13, 14).

Finally, it should be pointed out that the interpretation of *p*H measurements on polyelectrolyte solutions involves a considerable uncertainty of the liquid junction potential, which may differ considerably from that of the reference buffer solution. Theory and experimental data are at present inadequate to estimate the magnitude of this error.

REFERENCES

1. Kern, W., *Makromol. Chem.* **2,** 279 (1948).
2. Kagawa, I., and Katsuura, K., *J. Polymer Sci.* **9,** 405 (1952).
3. Katchalsky, A., and Lifson, S., *J. Polymer Sci.* **11,** 409 (1953).
4. Bell, R. P., "Acid-Base Catalysis," p. 25, 26. Oxford University Press, New York, 1941.
5. Fraenkel, W., *J. phys. Chem.* **60,** 202 (1907).
6. Roberts, J. D., Regan, C. M., and Allen, I., *J. Am. Chem. Soc.* **74,** 3679 (1952).
7. Womack, E. B., and Nelson, A. B., *Organic Syntheses* **24,** 56 (1944).
8. Kolthoff, I. M., *Rec. trav. chim.* **46,** 33 (1937).
9. Broensted, J. N., and Duus, H. C., *Z. physik. Chem.* **117,** 299 (1925).
10. King, C. V., and Bolinger, E. D., *J. Am. Chem. Soc.* **58,** 1533 (1936).
11. Dawson, H. M., and Lowson, W., *J. Chem. Soc.* **1928,** 2146.
12. LaMer, V. K., and Miller, M. L., *J. Am. Chem. Soc.* **57,** 2674 (1935).
13. Bernhard, S. A., and Hammett, L. P., *J. Am. Chem. Soc.* **75,** 1798, 5834 (1953).
14. Davies, C. W., and Thomas, G. G., *J. Chem. Soc.* 1607 (1952).

ULTRAVIOLET IRRADIATION OF DILUTE SOLUTIONS OF OVALBUMIN[1]

J. Gordin Kaplan, D. H. Andrews,[2] and M. J. Fraser[2]

Department of Physiology, Dalhousie University, Halifax, Nova Scotia

Received August 10, 1953; revised November 27, 1953.

Abstract

Evidence has been adduced showing that the action of ultraviolet radiation (largely 254 mμ) on 0.01% solutions of crystalline ovalbumin consists of two separable and fundamentally distinct processes: (1) a modification of the structure of the intact molecule involving neither the rupture of peptide linkages nor diminution of ability to form monomolecular films if spread from nonisoelectric solvent. This process is the "denaturation" of other authors; reasons for the avoidance of this term in the present paper have been presented. (2) An extensive fragmentation of the molecule leading to disappearance of ability to form films, and the appearance of base-binding groups as determined by formol titrations. Evidence has been presented for considering this fragmentation to be the result of rupture of peptide linkages (proteolysis). Associated with process (1) is a decrease in the ability of the films to form fibers upon complete collapse as well as an increase in the specific area of the films formed from the UV-modified protein. The action of ozone has been to cause structural modification but not proteolysis. The general sequence of events hypothesized in our previous studies of the effect of UV on albumin monolayers, similar to the hypothesis of Bernhart, has been confirmed.

Introduction

In our recent study of the effect of ultraviolet (UV) irradiation on monomolecular films of ovalbumin (1, hereafter referred to as I), the data suggested the existence of two distinct (and possibly consecutive) photochemical processes: (1) a nonproteolytic alteration (unfolding) of the structure of the already extended film molecules, resulting in increase in area of the film; (2) a proteolysis (yielding either small fragments possessing no surface activity, or larger fragments of altered physicochemical

---

[1] This research was supported by grants from the National Research Council (Ottawa) and the Defence Research Board. The senior author wishes to acknowledge his indebtedness to Professors F. R. Hayes, C. C. Coffin, W. Chute, and C. B. Weld for the loan of various items of equipment, and to Dr. A. D. McLaren for valuable criticism. He must make special mention of the almost excessive generosity of his colleagues Professors J. A. McCarter and J. G. Aldous, almost all of whose portable equipment was to be found at one time or another in the author's laboratory.

[2] Summer fellow, National Research Council (Ottawa).

properties) inferred from the subsequent progressive decrease in film area and from the changed character of the force-area curves obtained upon compression of the residual films (2). The present experiments have been undertaken to test the validity of this hypothesis by irradiating very dilute solutions of the soluble protein and studying the changes in molecular structure by surface-chemical and other standard procedures.

The present status of the question of the effect of UV on protein might fairly be characterized as confused, largely, as will be made clear below, because of the semantic cloud surrounding the indefinable, but frequently used term "denaturation."[3] The most commonly accepted definition, that of Neurath, Greenstein *et al.* (3), states: "denaturation is any non-proteolytic modification of the unique structure of a native protein, giving rise to definite changes in chemical, physical or biological properties."[4] Many workers have reported that UV causes "denaturation" in this sense (6, 7, see review by Arnow (8)).

On the other hand, other workers have shown that UV causes splitting of proteins into fragments of low molecular weight (9, 10, 11, 12). It also has been shown (13) that the action of UV is to cause *both* "denaturation" *and* molecular splitting. Work on model systems (see reviews by Giese (14) and McLaren (15)) and on protein films (16) has suggested the possibility that this "molecular splitting" might be a *proteolysis*, that is, *a rupture of peptide bonds*. However, a direct attempt to demonstrate UV-induced proteolysis (17) yielded negative results. Finally, to add further to the confusion, reviewers (18, 14, 15) have included proteolysis as part of the radiation-induced "denaturation," thus robbing this term of any meaning given it by the above definition.

We shall say that the protein has undergone a *nonproteolytic structural modification* when it is neither soluble nor capable of forming large, compressible monomolecular films at its isoelectric *p*H, in the absence either of direct evidence for the rupture of peptide linkages or for decrease in surface-activity at a *p*H removed from the isoelectric point (see 19); this italicized term and other suitable operational euphemisms (*e.g.*,

---

[3] Indefinable, in that even the most general definition (see above) describes "denaturation" in terms of the so-called "native" state; since the term "native" is incapable of independent definition (indeed, it is even more misleading than its opposite (4)), the term "denatured" can have no precise meaning—a conclusion to which many authors have been led (4, 5).

[4] Another serious objection to this definition is that it embraces structural changes in protein which are not considered to be "denaturative." For example, addition of oxygen to reduced hemoglobin certainly modifies the structure and properties of this conjugated protein; the change in *p*K value suggests that even the structure of the protein moiety has been altered. Further, addition of small amounts of acid or base to a protein solution ought *ipso facto* to constitute "denaturation," since change in its net charge reflects modification of its structure and leads to alteration of its properties.

"heat-treated") are intended as the equivalent of the "denaturation" of other authors. We shall say that the protein has undergone *proteolysis* when it can be demonstrated that an extensive molecular fragmentation has occurred accompanied by evidence for the release of one of the component groups of the peptide linkage (carboxyl groups.)

The purpose of this paper is to show that both nonproteolytic structural modification and proteolysis are involved in the action of UV on soluble ovalbumin, and thus provide a possible unification for the contradictory reports at present in the literature.

EXPERIMENTAL

1. Materials and Apparatus

The recrystallized ovalbumin used in I was made up as a 0.01% solution in unbuffered dilute HCl at *p*H 2.25 or 3.50 as explained below; optimal spreading into monomolecular films occurs in this range of protein concentration (20). Pyrex redistilled water was used throughout these experiments. No undissolved material was noted.

Surface pressure[5] and area measurements were made on 2 Langmuir-Adam surface troughs and balances, modified as described in I. The absolute precision and methods of handling, waxing, and cleaning these instruments have been described in detail in I. The troughs were mounted on a table resting on concrete piles to eliminate almost all extraneous vibration. The aqueous substratum in the troughs was dilute (1:10) McIlvaine's buffer at *p*H 4.8–4.9, the isoelectric point of ovalbumin. The protein solution was delivered to the interface by means of a micrometer syringe, using the method of Neurath (21). Surface tension measurements were made with a deNouy ring-type tensiometer (Central Scientific Company); attention has been called (22) to the inadequacy of this type of instrument in work with proteins, owing to molecular orientation phenomena as the ring is pulled through the interface. We have found this objection to be valid, but include certain of our data nevertheless, to indicate relative changes in surface activity rather than absolute values. Turbidity measurements were made with a Klett-Summerson photoelectric colorimeter.

---

[5] The surface pressure, F, may be shown to be related to the surface energies (or tensions) of the substratum and of the substratum plus film by the following equation (32):

$$F = \gamma_0 - \gamma_f ,$$

where γ_0 is the surface tension of the substratum, and γ_f is that of substratum plus film. This should not be confused with the spreading coefficient, F_S, which may be shown to obey the following relation (33):

$$F_S = \gamma_B - \gamma_A - \gamma_{AB} ,$$

where γ_B is the surface tension of the bottom phase, γ_A that of the top phase, and γ_{AB} the interfacial tension between them. F_S, which is the work of adhesion between A and B minus the work of cohesion, of phase A, is thermodynamically identical to the work of spreading multiplied by -1. Confusion between F and F_S has unfortunately penetrated the literature (15).

2. UV Irradiation

Irradiation was performed in an airtight tank saturated with water vapor to prevent evaporation; all solutions to be irradiated were placed in Petri dishes 3 cm. below the UV source, which was, unless otherwise specified, a "Sun-Kraft" quartz mercury vapor tube, described by the manufacturer as delivering 86% of its energy at the 2537 A. resonance line. Control solutions, to determine the effects of ozone, were placed next to the experimental dishes, shielded (but not sealed) from the radiation by a glass plate. Another unirradiated control was allowed to remain outside of the tank at room temperature during the course of the experiment.

3. Determination of Proteolysis

Fragmentation of the molecule was followed in the following manner. Two protein samples at *p*H 2.25 were placed in Petri dishes *a* and *b*; *a* was irradiated, while *b* was shielded. Aliquots were withdrawn at intervals and allowed to spread at the air/water interface as described permitting determination of specific area, or were used for surface tension measurements. Molecular splitting should be demonstrable as progressive loss in surface activity and film area. The *p*H of solutions *a* and *b* was checked electrometrically during the irradiation, but significant changes were not observed, thus eliminating the possibility of a large change in the isoelectric point of the protein during irradiation.

Direct evidence of proteolysis was obtained by means of formol titrations for free carboxyl groups. Another protein sample at *p*H 3.50 was placed in Petri dish *c* and irradiated as *a*. Another sample *d* served as control for ozone. Five-milliliter aliquots were withdrawn from dishes *c* and *d*, treated with neutralized formol (final concentration 10%) and titrated with standardized 10^{-3} N NaOH to a phenolphthalein end point. Because we discovered that the acidity of dilute HCl or of distilled water always increased upon intensive irradiation, it was necessary to irradiate a third dish, *e*, containing only the dilute HCl solvent, from which aliquots were withdrawn and treated exactly as those taken from *c*. Titration values for *c* were corrected for increase in acidity in *e*. The acidity of shielded solvent, *f*, was likewise determined by formol titration.

An unproved assumption is involved in connection with these titrations, namely, that the presence of the protein does not accelerate whatever process might be causing the change in acidity of the solvent alone. This assumption is not unreasonable, especially since the concentration of protein was little more than 10^{-6} M. Such dilute solutions are obviously not ideal for formol titrations, which are normally performed on much more concentrated protein; it was necessary for us to work with extremely dilute solutions to obtain maximum radiation effects and to avoid the danger of coagulation which we observed to occur with more concentrated solutions of protein, even at *p*H 3.50. Nevertheless, our results were consistent, as shown by a very low standard deviation on ten separate experiments (see below).

4. Nonproteolytic Structural Change

It was hoped that this could be detected by changes in the reducing activity of the protein in the absence of increase in free COOH groups. Nitroprusside, iodosobenzoic acid (23), and porphyrindin (24) tests were attempted, but these were all negative; these procedures are evidently useful only with protein concentrations of the order of 3–5%. A very successful method was finally devised, based on the fundamental observation of Bull (19) that heat-"denatured" protein, previously held to be nonspreading (21, 25), could be made to form films if it were spread from a solvent of sufficiently acid *p*H. Consequently, aliquots removed from *a* and *b* were treated in two different ways: (1) part was spread directly at the air/water interface as described; structurally modified albumin will spread at *p*H 2.25 (19); (2) part was dialyzed for 12 hours in the cold against constantly stirred isoelectric buffer (*p*H 4.9) before being allowed to spread at the air/water interface, as structurally modified protein will have coagulated and will be unable to form normal films. Any decrease in the area of the films spread from the dialyzed protein, as compared with that from undialyzed protein, would, in the absence of demonstrable increase in titratable COOH groups, testify to a nonproteolytic alteration in the structure of the intact molecule. This would be visible directly in the increased turbidity of the dialyzed solutions, owing to flocculation of the modified protein at its isoelectric point.

Ten complete experiments were run as described with a high degree of reproducibility.

5. *Operational Recapitulation*

Dishes *a*, irradiated, and *b*, unirradiated but in contact with ozone, etc., contained ovalbumin at *p*H 2.25. Aliquots withdrawn periodically were either used directly for surface procedures or were dialyzed against buffer at *p*H 4.9 in order to convert all modified protein, surface-active at *p*H 2.25, into non-surface-active, turbid aggregates. Dishes *c* and *d* contained irradiated and unirradiated protein, respectively, at *p*H 3.50; aliquots were withdrawn for formol titration. Dishes *e* and *f* contained solvent (*p*H 3.50) alone, and were used to detect the effect of irradiation and ozone, respectively, on the acidity of the solvent; titration values for aliquots from *c* and *d* were corrected for any increases in titer in aliquots from *e* and *f*, respectively.

RESULTS

1. *Undialyzed Sample*

The sequence of changes in specific area is shown in Fig. 1. Curve A, the undialyzed fraction, shows an initial slight but consistently observed increase in area; this demonstrates that the UV induces an additional asymmetry causing the molecule to spread to a larger area. We have reported a similar finding in the case of films irradiated on a saline substratum (I)[6]. Stallberg (26) has reported that heat-modified protein will spread to a slightly larger area than will the untreated control—a result quite like our own.

Thereafter, a sharp drop in area is observed, so that after 10 hours the protein has virtually lost its capacity to form films. Since structurally modified ovalbumin will spread under these conditions (19), the progressive decrease in area (noted likewise by Neurath (21)) must be due to a destruction of the molecule with appearance of small, soluble, nonspreading fragments.

Figure 2 shows the course of change in appearance of carboxyl groups.

---

[6] A second note by Dognon and Gougerot (29) contradicts this result in the case of what they call "albumins"; they did observe the area increase in the case of irradiated "globulins." Our next paper will contain an extended discussion of their results and interpretations, both of which differ from our own.

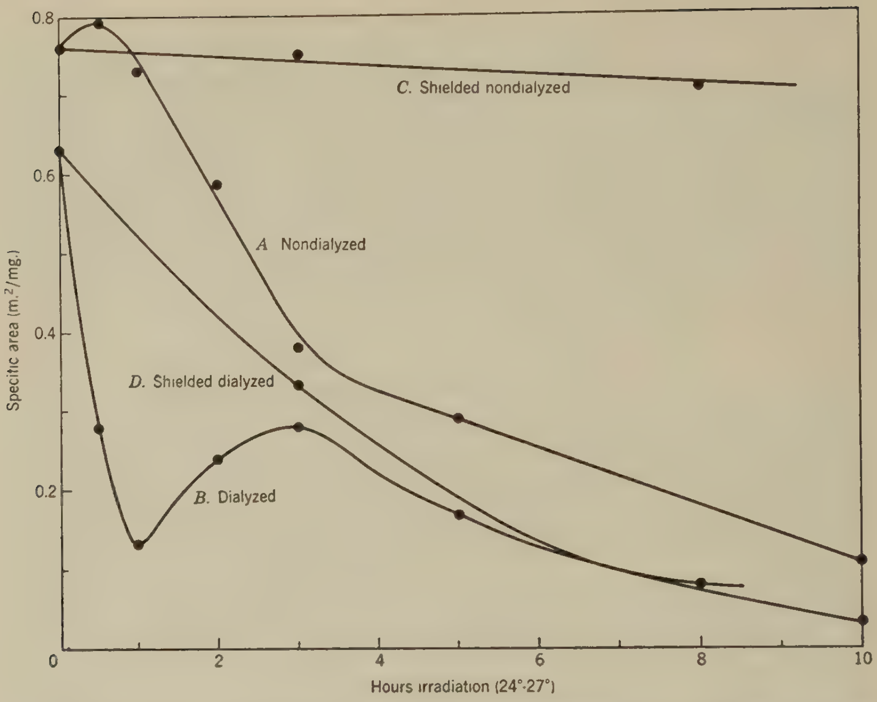

FIG. 1. Specific (extrapolated) area changes with duration of irradiation at room temperature. Curve *A*, nondialyzed, irradiated; *B*, dialyzed, irradiated; *C*, ozone control, nondialyzed; *D*, ozone control, dialyzed.

It will be noted that during the first hour of irradiation there is no detectable increase in these groups; thereafter, there is a marked increase in the amount of base required to titrate an aliquot to neutrality, leveling off at around 5 hours; the leveling off suggests that nonspecific, indirect photooxidations are not involved. Table I demonstrates that treatment of an ovalbumin solution in the boiling water bath does not significantly increase the amount of base required in the formol titration. It follows therefore that the observed increase in free COOH groups must be due, not to an unfolding of the protein molecule (assuming that heat and, initially, UV alter the configuration of the molecule in a qualitatively similar way), but rather to a rupture of peptide bonds. This confirms the evidence of Fig. 1*A*, which also suggests the occurrence of proteolysis. No increase in COOH groups was recorded for the protein solution allowed to remain, unirradiated, at room temperature.

The average corrected increase in base required for neutralization (*i.e.*, change in titer of protein solution minus change in titer of solvent alone) was 1.8 ± 0.1 ml. ($n = 10$) for periods of irradiation varying from

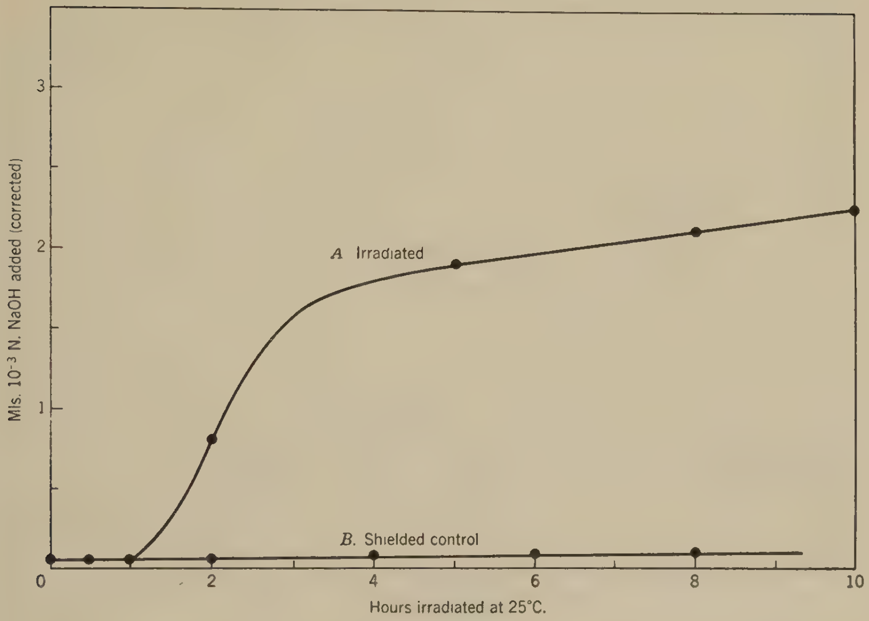

FIG. 2. Formol titrations of undialyzed irradiated and control (ozone) solutions. Curve *A*, irradiated; *B*, ozone control.

TABLE I

The Effect of Heat-Modification on Formol Titrations

Minutes in boiling water bath	ml. 10^{-3} N NaOH added (uncorrected)
0	2.5
30	2.7
	2.6
60	2.6
	2.6

10 to 24 hours. On the basis of a molecular weight for ovalbumin of 45,000, this corresponds to an increased uptake of 162 moles NaOH per mole of protein originally present—a surprisingly high figure. Assuming that there are 400 amino acid residues per molecule, approximately 2 acidic groups have appeared for every 5 residues present.

2. Dialyzed Sample

Figure 1, curve *B*, represents the change in area of the irradiated protein following dialysis against isoelectric buffer. There is, during the first hour, a very sharp *reduction* in area; the difference in area between the 1 hour dialyzed and undialyzed aliquots constitutes unequivocal evidence of a change in protein structure which prevents the molecule from spreading at the air/water interface at its isoelectric point. After 1 hour, there is

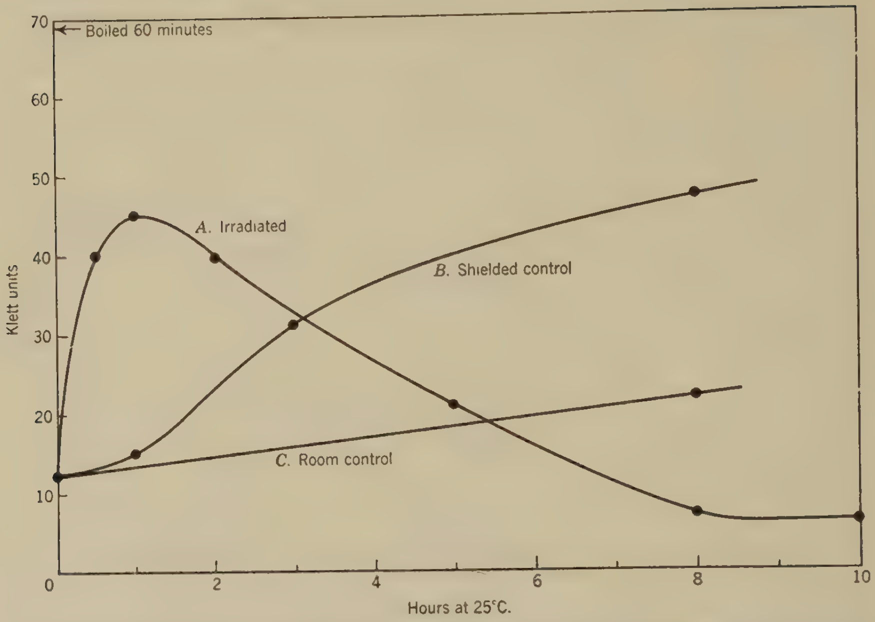

FIG. 3. Development of turbidity with irradiation at room temperature in dialyzed samples. Curve *A*, irradiated; *B*, ozone control; *C*, sample left at room temperature. Turbidity level developed upon dialysis of an aliquot heated for 60 minutes at 100°C. is shown.

a clear-cut rise in area of the films; this is followed by a progressive decrease in area, until at 10 hours only a very small film can be formed.

Figure 3, curve *A*, represents the turbidity changes in the dialyzed sample. Maximum turbidity is reached at 1 hour; after 2 hours there is a rapid fall in turbidity and at 8 hours the solution is less turbid than it was at zero hours. Figures 1*B* and 3 demonstrate the existence of two distinct processes, the first being a nonproteolytic alteration of molecular structure, resulting in insolubility at the isoelectric point with consequent inability to unfold into monolayers and increased turbidity, and the second a destruction of the molecule, the decrease in area and turbidity confirming the more direct evidence of proteolysis of Fig. 2.

3. Effect of Ozone

Figure 1, curve *C*, and Figure 2, curve *B*, show that ozone causes little appreciable proteolysis. Figure 1, curve *D*, and Figure 3, curve *B*, show that ozone is effective in modifying the structure of the protein so as to render it insoluble and nonspreading at its isoelectric point.

4. Changes in Other Properties

Qualitative changes in the appearance and tensile strength of the fibers formed upon complete collapse of the monolayers are described in Table

TABLE II

Appearance of Fibers with Duration of Irradiation; Results Identical for Room-Temperature and Cold-Room Irradiations

Duration, *hours*	Non dialyzed		Dialyzed	
	Irradiated	Ozone	Irradiated	Ozone
0	++++	++++	++++	++++
¼	+++		++	
½	++		±	
1	+	++++	−	+++
2*	−		−	
3	−	++	−	−
8	−	±	−	−
10	−		−	
Boiled ½ hr.	±		−	

* If three times usual volume is spread, no change in results.

++++ Tough thread running full width of trough, picked up in one piece.

+++ Noncontinuous thread; possible to pick up parts from trough.

++ Very fragile, slender, noncontinuous thread, impossible to pick up.

+ Only tiny "hairs" (3–5 mm.) visible.

± Very fragile thread sometimes, but not always, seen.

TABLE III

Change of Surface Tension with Irradiation; pH 2.25

Duration, *hours*	Room temperature, *dynes/cm.*
0	54.0
8	71.3
Solvent alone (unirradiated)	71.9

II; these changes are identical in character to those observed following irradiation of the monolayers (I). These findings seem to us to be very significant, despite the virtual impossibility of dealing with them quantitatively. Table II shows also that the ability of an ovalbumin film to form a solid thread or fiber is greatly diminished by prior modification of the soluble protein by heat, ozone, or UV, and is eliminated entirely by proteolysis. This is a regular and extremely reproducible phenomenon, whose significance we have discussed in a communication which has appeared elsewhere (27). Decrease in surface activity with irradiation is shown in Table III, which reveals that after 8 hours of irradiation the surface tension of the protein solution has reached the value of the solvent alone. This is closely parallel to the data of Dognon and Gougerot (28).

Changes in the compressibility of the films are represented graphically in Fig. 4; it should be emphasized that considerable variability with respect to this property is encountered. The undialyzed protein shows no real decrease in compressibility until between 5 and 8 hours, reaching a level within the range reported for irradiated films (Figs. 1 and 4), which likewise showed no real increase in slope until 8 hours irradiation.

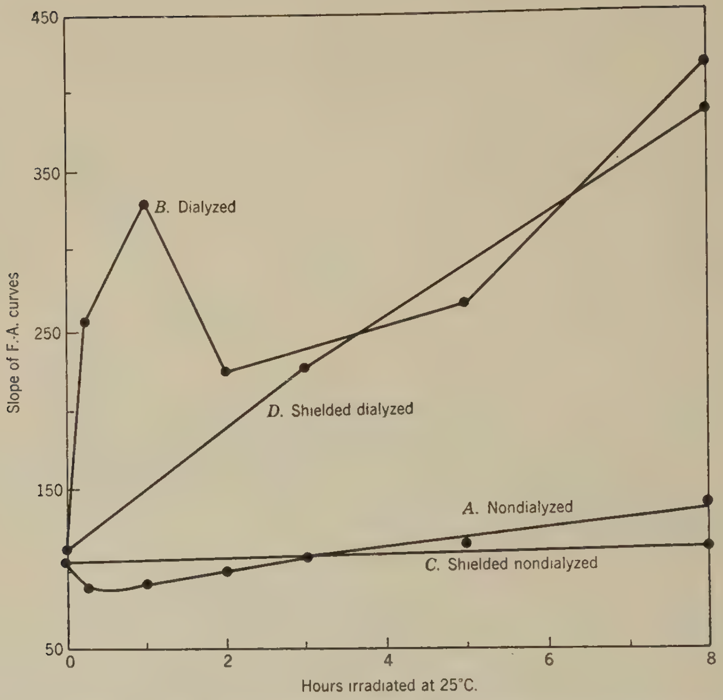

FIG. 4. Changes in film compressibility with irradiation at room temperature; same volume spread in all cases. Curve *A*, irradiated, nondialyzed; *B*, irradiated, dialyzed; *C*, ozone control, nondialyzed; *D*, ozone control, dialyzed.

The slopes of the films spread from dialyzed protein reflect quite a different situation, revealing two peaks (of minimum compressibility), the first early in the irradiation, between ½ and 2 hours, and the second at 8 hours or after. The ozone-modified protein after dialysis likewise yields a film which is of very low compressibility. One may hazard the guess that these very incompressible films, occurring when total film area is lowest, result from the presence at the interface of poorly spreading, incompressible aggregates formed by bringing to the isoelectric point the structurally modified protein or certain of its breakdown products.

The differences, reported in I, between the linearity (and collapse) points of irradiated and unirradiated films were not observed in these experiments.

DISCUSSION

The initial effect of UV radiation has been to alter the structure of ovalbumin so as to render it coagulable and nonspreading at *p*H 4.9, its isoelectric point, yet causing it to spread to an even larger specific area at *p*H 2.25; no increase in COOH groups was noted during this period. The criteria which we have proposed above for a nonproteolytic structural alteration have thus been satisfied. These changes in properties, as well as the change in appearance of the fibers formed on compression of the films, are also produced as a result of treatment of the protein with heat and (with the exception of the area increase, which has not been reported) with urea (see 27). The primary action of the absorbed UV energy has probably been the rupture of some secondary valence bond or bonds changing the protein to a condition similar to that brought about by the usual "denaturing" agents (3). The similarity of action of all these agents makes it uneconomical to invoke proteolysis as part of the primary UV process, although of course the possibility of the destruction of a very small number of peptide bonds, below the level of sensitivity of our method, cannot be gainsaid by our wholly negative evidence.

Positive evidence of proteolysis appeared after 1 hour of irradiation, as base-binding groups were discovered in the formol titrations. The large number of these groups seems to exclude the possibility that this be due to a nonspecific oxidation of aromatic residues, proposed by McLean and Giese (17). In any case, nonspecific oxidations could not account for the other secondary changes observed: decreasing coagulability at the isoelectric point, loss of ability to form films, and abolition of surface activity. These are changes characteristic of proteolysis, a process which produces small incoagulable and non-surface-active fragments; a possible shift in the isoelectric point of the protein produced by molecular unfolding with consequent exposure of acid or basic groups could not account for the abolition of surface activity noted at *p*H 2.25, nor, indeed, for most of the other effects noted.

Following the minimum in film area (Fig. 1, curve *B*) observed after dialysis of the 1-hour–irradiated protein, there was observed a secondary rise in area. That this was due to proteolysis is further strongly suggested by the analogous situation obtaining in a paper by Gorter (25), where nonspreading, "denatured" ovalbumin could be caused to form films of normal area by addition of a small amount of proteolytic enzyme to split the protein "into somewhat smaller particles."[7] Direct evidence of proteolysis in UV irradiated solutions of chymotrypsin has been found in the laboratory of McLaren (30), where both amino and carboxyl groups were successfully titrated.

We regard our data as confirmation of the essentials of the hypothesis of Bernhart (13), who irradiated solutions of ovalbumin and noted first an increase and then a decrease of isoelectric coagulable protein; he demonstrated that his clear filtrate contained dialyzable nitrogen. He stated that "the weights of egg albumin precipitated at the isoelectric point follow closely the theoretical values obtained from an equation which assumes that the denatured protein is formed by a first order process and that the isoelectric soluble derivatives are formed from the denatured protein by a first order process."

---

[7] Or possibly small non-film-forming fragments might aggregate into larger, surface-active units. This interpretation is favored by the curious fact that the secondary rise in area was not noted in several experiments in which the irradiation was carried out at 2°–5°C., despite the fact that spreading was thereafter performed at room temperature.

The possibility of some sort of indirect action through the irradiated medium, other than that due to ozone, has not been investigated. That photooxidation of the peptide bond may be involved in the secondary process (proteolysis) is strongly suggested by the data of many workers (see reference 15), but has not here been studied, nor have we eliminated the possibility of the action of trace amounts of photosensitizing contaminants (31); these processes would not upset the validity of our conclusions.

REFERENCES

1. KAPLAN, J. G., AND FRASER, M. J., *Biochim. et Biophys. Acta* **9,** 585 (1952).
2. KAPLAN, J. G., AND FRASER, M. J., *Proc. Nova Scotian Inst. Sci.* **23,** 91 (1950–1951).
3. NEURATH, H., GREENSTEIN, J. P., ERICKSON, J. O., AND PUTNAM, F. W., *Chem. Revs.* **34,** 157 (1944).
4. PHILLIPPI, G. T., On the nature of proteins. Thesis, Amsterdam, 1936.
5. LANGMUIR, I., *Cold Spring Harbor Symposia Quant. Biol.* **6,** 159 (1938).
6. BOVIE, W. T., *Science* **37,** 373 (1913).
7. CLARK, J. H., *J. Gen. Physiol.* **27,** 101 (1944).
8. ARNOW, L., *Physiol. Revs.* **16,** 671 (1936).
9. BECKER, J. P., AND SZENDRO, P., *Pflügers Arch. ges. Physiol.* **228,** 755 (1931).
10. SPIEGEL-ADOLF, M., *Biochem. J.* **28,** 372 (1934).
11. SVEDBERG, S., AND BROHULT, S., *Nature* **143,** 938 (1939).
12. SANIGAR, E. B., KREJCI, L. E., AND KRAEMER, E. O., *Biochem. J.* **33,** 1 (1939).
13. BERNHART, F. W., *J. Biol. Chem.* **128,** 289 (1939).
14. GIESE, A. C., *Physiol. Revs.* **30,** 431 (1950).
15. MCLAREN, A. D., *Advances in Enzymol.* **9,** 75 (1949).
16. MITCHELL, J. S., AND RIDEAL, E. K., *Proc. Roy. Soc.* (*London*) *A***167,** 342 (1938).
17. MCLEAN, D. J., AND GIESE, A. C., *J. Biol. Chem.* **187,** 543 (1950).
18. HAUROWITZ, F., "Chemistry and Biology of Proteins." Academic Press, New York, 1950.
19. BULL, H. B., *J. Biol. Chem.* **125,** 585 (1938).
20. BULL, H. B., *Advances in Protein Chem.* **3,** 95 (1947).
21. NEURATH, H., *J. Phys. Chem.* **40,** 361 (1936).
22. NEURATH, H., AND BULL, H. B., *Chem. Revs.* **23,** 391 (1938).
23. HELLERMAN, L., CHINARD, F. P., AND DIETZ, V. R., *J. Biol. Chem.* **147,** 443 (1943).
24. GREENSTEIN, J. P., AND EDSALL, J. T., *J. Biol. Chem.* **133,** 397 (1940).
25. GORTER, E., *Trans. Faraday Soc.* **33,** 1125 (1937).
26. STALLBERG, S., *Trans. Faraday Soc.* **35,** 1416 (1939).
27. KAPLAN, J. G., AND FRASER, M. J., *Nature* **171,** 559 (1953).
28. DOGNON, A., AND GOUGEROT, L., *Bull. soc. chim. biol.* **25,** 183 (1943).
29. DOGNON, A., AND GOUGEROT, L., *Bull. soc. chim. biol.* **27,** 240 (1945).
30. LEITNER, N. B., AND MCLAREN, A. D., Personal communication, 1950.
31. MITCHELL, J. S., RIDEAL, E. K., AND SCHULMAN, J. H., *Nature* **139,** 625 (1937).
32. ADAM, N. K., "Physics and Chemistry of Surfaces," 3rd ed. Oxford University Press, New York, 1941.
33. HARKINS, W. D., *in* "The Theory and Application of Colloidal Behavior" (R. H. Bogue, ed.). McGraw-Hill Book Co., New York, 1924.

VISCOSITY AND ELECTROVISCOUS EFFECT OF EMULSIONS

M. van der Waarden

Koninklijke/Shell-Laboratorium, Amsterdam, Holland

Received October 28, 1953; revised March 22, 1954

INTRODUCTION

The viscosities of dispersions of particles enveloped by a diffuse electric double layer exceed those of dispersions of uncharged particles (electroviscous effect). Von Smoluchowski (1), Krasny-Ergen (2), and Booth (3) have tried to derive a quantitative relation between this excess viscosity and the structure of the diffuse double layer. Experimental data of Booth and of Dobry (4) show that the effect predicted by von Smoluchowski is too high. Harmsen, *et al.* (5) conclude from experiments with a silver iodide sol that their results do not conflict with Booth's nor with von Smoluchowski's theory. They ascribe the electroviscous effect in their system to an interaction between the double layers of the particles, and leave the effect at very low volume concentrations (φ) of the particles out of consideration.

The present article describes measurements of viscosities of emulsions, *i.e.*, dispersions of spherical particles of different sizes. In addition, the particle diameters have been calculated from light-scattering measurements.

EXPERIMENTAL

The following materials were used:

The oil was a medicinal oil, molecular weight 320, viscosity at 20°C., 39 centipoises, density at 20°C., 0.87.

The emulsifier was a white, powdery mixture of sodium naphtha sulfonates obtained by treating an SO_2-extracted mineral oil with oleum. The technical product was freed from mineral oil and water and consisted mainly of alkylbenzene (naphthene) sulfonates with an average molecular weight of 475.

Distilled water.

The emulsifier was dissolved in the oil to concentrations of 5 to 35% wt. The densities of these solutions are a linear function of the weight percentage of emulsifier, corresponding with a density of the emulsifier of 1.10 at 20°C. To the clear, fluid oil-emulsifier system water was gradually added with stirring, giving successively clear-fluid, clear-gelated, turbid-plastic systems. Above a certain percentage of water the system becomes fluid again and can be easily diluted with water, yielding oil-in-water emulsions. The oil droplets are small to very small and only a minor part of those of the coarsest type are visible under a microscope. Emulsions of 10 % wt. made from oils containing 30 % wt. and more of emulsifier were centrifuged for half an hour at an acceleration of 25,000 *g*; no migration of emulsified oil was noticed. These facts warrant the conclusion that there are no significant differences in particle diameter, as was to be expected in view of the method of preparation. Schwarz's (6) reasoning that variations in droplet diameter decrease with the average particle size would point in the same direction.

The oil-in-water emulsions made by the method of phase inversion were diluted with water to varying oil concentrations after which the viscosities were measured at 20.00 ± 0.02°C. in B.S.I.-viscometers (British Standard Institution No. 188 (1937) (7). The viscometers used were such that corrections for kinetic energy, being $<0.5\,\%$, could be neglected.

Light-scattering measurements were made after diluting the emulsions with water to 1 % wt., and subsequently to 0.1–0.0005 % wt. with a 0.015 % wt. solution of emulsifier in water, which is the critical micelle concentration. It was used to prevent desorption of emulsifier from the water-oil interface, as this would lead to instability of the emulsions. Light scattering was measured[1] at different angles θ with the incident beam. Assuming the particles to be of equal size, their diameters were calculated with the aid of Rayleigh's equation for the scattering of spherical particles:

$$i_\theta = \frac{9\pi^2 NV^2}{2r^2\lambda^4}\left(\frac{n_1^2 - n_0^2}{n_1^2 + 2n_0^2}\right)^2 (1 + \cos^2\theta)\cdot I_0$$

where

i_θ = intensity of the scattered light in a direction which makes an angle θ with the incident beam;
I_0 = irradiance of incident light;
V = volume of a particle;
N = number of particles per cm.^{3};
r = distance between scattering volume and measuring device;
n_0 = refractive index of medium;
n_1 = refractive index of particle;
λ = wave length in medium.

After subtraction of the light scattered by the medium, the particle diameters were derived:

1. From the intensity i_{90} of the scattered light perpendicular to the

---

[1] The light-scattering measurements were made by Messrs. D. J. Coumou and W. Boog of this laboratory, who also carried out the calculations of the particle sizes.

incident light beam. For particles larger than 0.1 λ a correction P (90) was applied for deviation from the pure Rayleigh scattering (8). This correction can be found in the usual way from dissymmetry measurements.

2. From the intensity i_0 of the scattered light when $\theta = 0°$, found by extrapolation of the scattering in different directions θ.

The measurements were carried out in a light-scattering apparatus fitted with a photomultiplier cell. The incident beam was light of the blue mercury line ($\lambda_{vac} = 4358$A.).

RESULTS

1. Viscosity of the Emulsions

The relative viscosities η_r of the emulsions are recorded in Table I; the viscosity of the medium is assumed to be 1.015 centipoises, viz., the viscosity at 20°C. of a 0.015% wt. solution of emulsifier in distilled water (critical micelle concentration). From n_r we calculated $K = (\eta_r - 1)/\varphi$; φ = volume fraction of emulsified oil + emulsifier in the emulsion.

K as a function of φ is plotted in Fig. 1: for the sake of convenience as $\sqrt{K}$ versus φ. K-values for $\varphi \to 0$ are derived by extrapolation, giving values which lie between the reasonable limits recorded in Table I.

According to Einstein's relation (uncharged rigid spheres) $K_{\varphi \to 0} = 2.5$. The values found are higher, which points to an apparent increase in volume

TABLE I

Viscosity Data of the Emulsions

% wt. emulsifier in emulsified oil	% wt. emulsified oil in emulsion	Parts by vol. of emulsified oil in emulsion φ	η_r emulsion	K	$K_{\varphi \to 0}$	$V = \frac{K_{\varphi \to 0}}{2.5}$
5	5	0.0565	1.17	3.01	2.6–2.7	1.04–1.08
	10	0.112	1.40	3.57		
	20	0.222	2.12	5.04		
	30	0.328	3.52	7.70		
10	5	0.0559	1.21	3.77	3.0–3.1	1.20–1.24
	10	0.111	1.51	4.60		
	20	0.219	2.56	7.13		
	30	0.325	5.64	14.3		
17	5	0.0549	1.25	4.56	3.4–3.5	1.36–1.40
	10	0.109	1.68	6.23		
	20	0.216	3.94	13.6		
	30	0.321	22.15	66.1		
35	5	0.0531	1.35	6.59	4.8–5.0	1.92–2.00
	10	0.106	1.96	9.04		
	20	0.210	6.50	26.2		
	30	0.313	92.8	294		

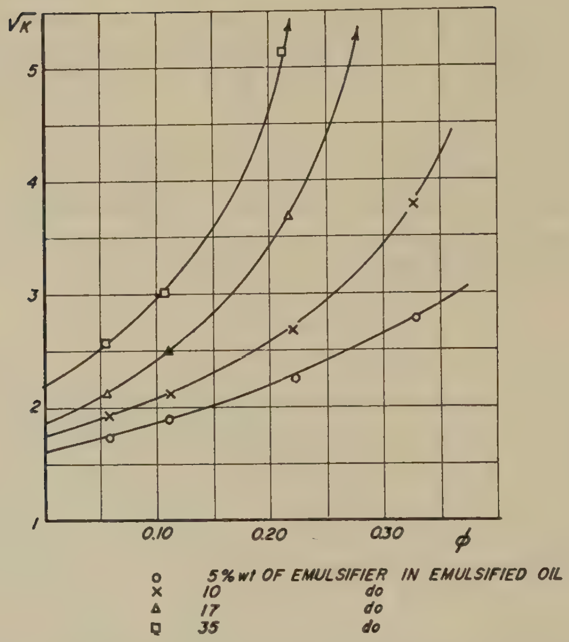

FIG. 1. Relation between $\sqrt{K}$ $\left(K = \frac{(\eta_r - 1)}{\varphi}\right)$ and φ (parts by volume of emulsified oil).

fraction of dispersed oil, *i.e.*, during flow the oil droplets behave as if their volume were V times the real volume. Maintaining Einstein's relation, this means that

$$\frac{\eta_r - 1}{V\varphi} = 2.5 \quad \text{and} \quad V = \frac{\eta_r - 1}{2.5\varphi} = \frac{K_{\varphi\to 0}}{2.5}$$

From the data mentioned in Table I it appears that $K_{\varphi\to 0}$ approaches 2.5 and V approaches 1 when the emulsifier content of the emulsified oil approaches zero.

2. Light-Scattering Measurements

The particle diameters calculated from the light-scattering measurements are represented in Fig. 2 as a function of the emulsifier content of the oil. The values calculated from i_{90} and i_0 agree fairly well.

No doubt the particles are not strictly of equal size. Heterodispersity leads to stronger scattering than corresponds with the volume average of the particles and hence the calculated diameters will be on the high side. As we assume that the (slight) heterodispersity increases with the average diameter (see *Experimental part*), only the data of emulsions with particles smaller than 500 A. are used for the following calculations.

Earlier work (9) had shown that emulsions of this type made by phase

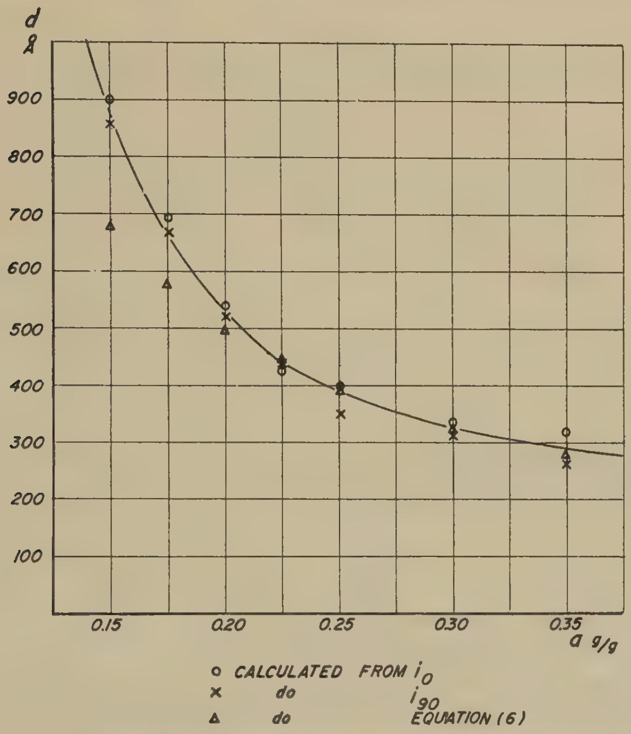

FIG. 2. Relation between particle diameter d derived from light-scattering measurements and emulsifier content a of emulsified oil.

inversion have practically all their emulsifier molecules in the oil-water interface. Starting from this knowledge and from the particle diameters derived from light-scattering measurements, we can calculate values for the surface area occupied by one emulsifier molecule at the oil-water interface.

Let 1 g. of emulsifiable oil with a density ρ_0 be divided into n spherical particles with equal radius r.

$$n = \frac{1/\rho_0}{4\pi r^3/3} = \frac{3}{4\pi r^3 \rho_0}. \qquad [1]$$

The total surface area of these particles is given by:

$$S = n 4\pi r^2 \qquad [2]$$

Substituting the n-value of [1] leads to:

$$S = \frac{3}{r\rho_0}. \qquad [3]$$

Each gram of emulsified oil contains a g. of emulsifier with molecular weight M or $(a/M) \times N$ molecules of emulsifier. (N = Avogadro's number.)

TABLE II

A. Surface Area S_s per Emulsifier Molecule in Oil-Water Interface. B. Particle Diameter d Calculated from S_s.

A				B		
a, g./g.	d, A.	ρ_0, g./cm.^{3}	S_s, A.^{2}	a, g./g.	ρ_0, g./cm.^{3}	d, A.
0.225	430	0.914	54	0.15	0.899	670
0.25	380	0.919	54	0.175	0.904	570
0.30	325	0.930	52	0.20	0.908	500
0.35	290	0.940	50			
				0.05	0.880	2050
				0.10	0.890	1020
				0.17	0.904	585
				0.35	0.940	275

Hence, the surface area occupied per molecule of emulsifier at the oil-water interface of the emulsion is given by

$$S_s = \frac{3M}{r\rho_0\, aN} = \frac{6M}{d\rho_0\, aN} \qquad [4]$$

where d = particle diameter. The S_s values calculated in this way ($M = 475$) are represented in Table IIA.

The calculated S_s values are fairly constant. By using the average value of 52 A.^{2} the particle diameters of emulsions with lower emulsifier contents (a = 0.15–0.175–0.20) of the oil can be calculated:

$$d = \frac{6M}{S_s N a\rho_0} = \frac{91}{a\rho_0}\ \text{A.} \qquad [5]$$

derived from [4].

These d values are shown in Table IIB. They are lower than the corresponding d values calculated from light scattering (Fig. 2). The difference increases with the average particle size; this is in agreement with the concept of increasing, yet small, heterodispersity.

The S_s value of 52 A.^{2} being probably a reliable characteristic value of the emulsions under investigation, it has been used for calculating in the same way the particle diameters of the emulsions whose viscosities were measured. The results are also recorded in Table IIB (a = 0.05–0.10–0.17–0.35).

DISCUSSION

If the apparent increase in droplet volume during flow is represented by an increase Δr of the radius r,

$$V = \frac{4\pi(r + \Delta r)^3/3}{4\pi r^3/3} \quad \text{or} \quad \Delta r = r(\sqrt[3]{V} - 1). \qquad [6]$$

This equation is used to calculate the Δr values of the emulsions under investigation (Table III).

TABLE III

Apparent Increase in Radius of Emulsion Droplets

a, g./g.	r (Table II), A.	V (Table I)	$\sqrt[3]{V} - 1$	Δr, A.
0.05	1025	1.04–1.08	0.014–0.028	14–28
0.10	510	1.20–1.24	0.062–0.073	31–37
0.17	293	1.36–1.40	0.108–0.118	32–35
0.35	138	1.92–2.00	0.242–0.260	33–36

Considering that the Δr value for $a = 0.05$ will be strongly influenced by small experimental errors, it can be concluded that the Δr values are independent of particle size. This means that during flow of the emulsions all oil droplets, irrespective of size, behave as if they were enveloped by a rigid layer of 30–35 A. thickness.

This conclusion has been drawn for very low concentrations of emulsion droplets where interaction between the particles is precluded.

The apparent increase of the radius of the spherical particles during flow can be ascribed to the presence of a charge on the surface of the oil droplets (electroviscous effect). The charge originates from the strongly ionized sodium sulfonate molecules in the oil-water interface, building up a negatively charged layer at the interface and a positively charged diffuse layer around the oil droplets. That Δr is independent of particle size becomes understandable considering that the density of the sulfonate molecules and hence the charge density on the surface of the oil droplets is equal for all emulsions (Table II).

The viscosity increase is much larger than follows from the theory of von Smoluchowski or of Booth (see ref. 5, page 76; $K = 2.50–2.58$ for $d =$ about 300 A.). It seems, therefore, not probable that the electroviscous effect found at very low emulsion concentrations is due to a distortion of the diffuse layer of counterions around the emulsion droplets. However, an appreciable attraction of the water molecules in the double layer may take place because of the high electric field strength (of the order of 10^5 to 10^6 volt cm^{-1}) occurring in the vicinity of the particle surface. Thus the apparent increase of the oil droplets radii may be caused by a strongly adsorbed layer of water molecules.

The diffuse layer of ions around colloid particles may increase light scattering of the dispersion (Hermans (10), Doscher and Mysels (11)). Hermans argues that the light scattering measured is that of the particles proper increased by that of the diffuse layer. The magnitude of this increase is determined by $b(v_j e_p / v_p e_j)$

where b = ratio of ion to particle influence per cm.^{3} of these compounds on the refractive index;

v = volume of ion and particle;

e = electric charge of ion and particle.

Assuming for the radii of sodium ion and particle 1 and 100 A., respectively, and one negative charge per 50 A.^{2} surface area of the oil drops, $v_je_p/v_pe_j = 0.0025$. Owing to the low polarizability of sodium ions their influence per cm.^{3} will not differ appreciably from that of the oil. Hence the value of b will be low, and the influence of the diffuse layer of sodium ions, negligible.

SUMMARY

From the viscosities of oil-in-water emulsions of varying particle size and concentration (prepared with the same oil and emulsifier) an apparent increase in oil concentration during flow was derived. The particle sizes were calculated from light-scattering data of these emulsions. Combination of these data makes it possible to calculate an apparent increase in particle diameter during flow in cases where interaction between oil droplets is precluded. This increase seems to be independent of particle size and is ascribed to the electric charge on the surface of the particles.

ACKNOWLEDGMENTS

The author is indebted to Professor Dr. J. Th. G. Overbeek and to Messrs. G. J. Harmsen and J. van Schooten for a valuable discussion and to the Management of the Koninklijke/Shell-Laboratorium, Amsterdam, for permission to publish this work.

REFERENCES

1. SMOLUCHOWSKI, M. v., *Kolloid-Z.* **18,** 194 (1916).
2. KRASNY-ERGEN, W., *Kolloid-Z.* **74,** 172 (1936).
3. BOOTH, F., *Proc. Roy. Soc.* (*London*) **A203,** 533 (1950).
4. DOBRY, A., *J. chim. phys.* **47,** 402 (1950); *ibid.* **48,** 28 (1951).
5. HARMSEN, G. J., VAN SCHOOTEN, J., AND OVERBEEK, J. Th. G., *J. Colloid Sci.* **8,** 64 (1953); *ibid.* **8,** 72 (1953).
6. SCHWARZ, N., *Proc. World Petroleum Congr. Proc. 3rd Congr., Hague,* **1951,** Section II, p. 641.
7. "Standard Methods for Testing Petroleum and Its Products." London, Institute of Petroleum. (7th Ed.) 1946.
8. DOTY, P., AND STEINER, R. F., *J. Chem. Phys.* **18,** 1211 (1950).
9. VAN DER WAARDEN, M., *J. Colloid Sci.* **7,** 140 (1952).
10. HERMANS, J. J., *Rec. trav. chim.* **68,** 859 (1949).
11. DOSCHER, T. M., AND MYSELS, K. J., *J. Chem. Phys.* **19,** 254 (1951).

ION RELEASE AS INFLUENCED BY THE MODE OF EXCHANGE

Lambert Wiklander and Erik Nilsson

Institute of Pedology, Royal Agricultural College, Uppsala, Sweden

Received April 6, 1953; revised December 1, 1953

Abstract

In this paper a simple theory of the continuous ion exchange supposed to occur in natural systems is discussed and some experimental data are presented. The release of adsorbed ions is calculated and compared with the corresponding release from the batch exchange of static systems. The experimental results were found to support the theory.

Introduction

Ion exchange in natural systems, *e.g.*, biological systems and soils, is generally a more or less continuous process of low rate which often fails to produce a final equilibrium state. Reactions of this type we find, for example, in the desorption of cations from soil colloids as part of the uptake of nutrients by plants. The replacing agent is primarily the hydrogen ions of carbonic acid slowly produced by the plant roots and living organisms. The capacity of the replacing hydrogen ions per unit time must obviously be low. Because of the nutrient absorption, caused both by the migration of ions and the flow of water from the soil into the roots, the concentration of replaced ions in solution is kept low. As a consequence of this mechanism the exchange will be slow and continuous. Part of the reactions involved in the loss of nutrients by leaching also belong to this type of exchange, since the sinking water contains carbonic acid and other electrolytes, leading to an ion exchange.

The uptake and leaching of nutrients have a disturbing effect on the distribution of the diffusible ions in the soil. As a matter of fact the active roots are far from being in contact with the whole soil surface, and the leaching water in many soils moves mainly in fissures, cracks, root holes, and other interstices. Because of these conditions, an ion diffusion, intimately associated with ion exchange, takes place, the latter being continuous and of low rate.

This process may be pictured as a repeated batch exchange taking place in an infinite number of steps, the amount of ions exchanged in each step being infinitesimal, owing to a low activity of the replacing ion. Further, the concentration in the solution of the ions replaced from the solid phase is often low, owing to a more or less complete removal of the ions from the exchange system or by some sort of inactivation (*e.g.*, complex formation) rendering the ions unable to take part in the equilibrium. An exchange of this kind consequently requires a special theoretical and experimental treatment.

The theory as presented here followed as a logical consequence of an investigation concerning the influence of the proportions of the exchanging ions and of the exchange of minute quantities on the ion distribution (1). It was briefly discussed in connection with a study of the release of plant nutrients in soil (2). In a recent paper (3) this exchange was further studied and given the name *continuous infinitesimal ion exchange*[1] to distinguish it from other categories of exchange such as the batch type and the dynamic exchange, taking place in static systems and columns, respectively.

In the continuous exchange we are interested in how far the exchange will proceed in a certain time, that is, the amount of ions released or the change in the composition of the adsorbed ions in this time. In the batch exchange, on the other hand, we study the ion distribution after a more or less momentary exchange caused by addition of electrolytes or by mixing exchangers of different composition.

THEORETICAL

A simple mathematical expression of the continuous exchange may be derived in the following way.

We assume an exchanger saturated with the ions A and B of the same valence, the total amount of the ions being A_T and B_T moles. By addition of a third ion, R moles of the adsorbed ions are replaced.

As has been shown in several papers from this Institute, ion-exchange reactions may be described by means of the Donnan equilibrium. The resulting distribution of the ions A and B between exchanger (e) and intermicellar solution (s) after the replacement can therefore be expressed as follows:

$$\frac{(A)_s}{(B)_s} = \frac{(A)_e}{(B)_e} \qquad [1]$$

where ( ) means activity of the respective ions.

Using the well-known relationship

$$(A) = f_A[A],$$

f_A being activity coefficient of A and [ ] concentration, we obtain

$$\frac{[A]_s}{[B]_s} = \alpha_{A,B}\frac{[A]_e}{[B]_e}, \qquad [2]$$

---

[1] In the following for the sake of brevity called only *continuous exchange*.

where $\alpha_{A,B}$ is the equilibrium quotient, related to the activity factors by

$$\alpha_{A,B} = \frac{f_{A(e)} \cdot f_{B(s)}}{f_{A(s)} \cdot f_{B(e)}}.$$

$\alpha_{A,B}$ is assumed to be constant.

Because A and B have the same valence and are present in the same liquid phase, their concentrations may be substituted with the corresponding moles (A_s, A_e, B_s, B_e), and the equilibrium is thus independent of the volume of the intermicellar and micellar solutions.

Using the equations:

$$\begin{aligned} A_T &= A_s + A_e \\ B_T &= B_s + B_e \\ R &= A_s + B_s \end{aligned}$$

Eq. [2] is transformed into the following expression, containing A_s as the only dependent variable:

$$\frac{A_s}{A_T - A_s} = \frac{\alpha_{A,B}(R - A_s)}{B_T - R + A_s}. \qquad [3]$$

If the exchange is very small, that is, $R \ll A_T + B_T$, and the conditions are fulfilled as stated below, it follows that $A_s \ll A_T$ and $(R - A_s) \ll B_T$. Equation [3] may thus be reduced to:

$$\frac{A_s}{A_T} = \frac{\alpha_{A,B}(R - A_s)}{B_T} \qquad [4]$$

or after transformation:

$$\Delta A_s = \frac{\alpha_{A,B} \cdot A_T}{B_T + \alpha_{A,B} \cdot A_T} \cdot \Delta R, \qquad [5]$$

where ΔA_s and ΔR mean the released amounts. The validity of [4] and [5] requires, however, that $\alpha_{A,B}$ be not very large ($\alpha_{A,B}$ not $\gg 1$) if the mole fraction of A is very small, that is, $A_T : B_T \rightarrow 0$, and that $\alpha_{A,B}$ be not very small ($\alpha_{A,B}$ not $\ll 1$) if the mole fraction of B is very small, that is, $B_T : A_T \rightarrow 0$.

If the exchange is a real continuous infinitesimal reaction, the conditions being $\Delta R \rightarrow dR$ and $\Delta A_s \rightarrow dA_s$, the exchange may be best described by the differential quotient

$$\frac{dA_s}{dR} \text{ or } \frac{-dA_e}{dR}.$$

The total amounts A_T and B_T of Eq. [5] have then to be substituted with the corresponding variables A_e and B_e. The resulting differential equation reads

$$-dA_e = \frac{\alpha_{A,B} \cdot A_e \cdot dR}{B_e + \alpha_{A,B} \cdot A_e}, \tag{6}$$

where $A_e = A_T - A_s$ and $B_e = B_T - R + A_s$.

For integration [6] is combined with the last two equations and can then be written

$$-dA_e = \frac{\alpha_{A,B} \cdot A_e \cdot dR}{\alpha_{A,B} \cdot A_e - A_e + A_T + B_T - R} \tag{7}$$

and after transformation

$$-dA_e[-A_e + A_T + B_T - R] = \alpha_{A,B} \cdot A_e \cdot dR + \alpha_{A,B} \cdot A_e \cdot dA_e$$

which gives

$$\frac{dA_e}{A_e} = \alpha_{A,B} \frac{-dA_e - dR}{A_T + B_T - A_e - R}. \tag{8}$$

Equation [8] can be integrated directly; thus

$$\ln A_e = \alpha_{A,B} \ln (A_T + B_T - A_e - R) + C \tag{9}$$

when $R = 0$, $A_e = A_T$, and $C = \ln A_T - \alpha_{A,B} \ln B_T$.

By substitution of C in [9] we obtain

$$\ln \frac{A_e}{A_T} = \alpha_{A,B} \ln \frac{A_T + B_T - A_e - R}{B_T},$$

or since $A_e = A_T - A_s$:

$$\frac{A_T - A_s}{A_T} = \left(\frac{B_T + A_s - R}{B_T}\right)^{\alpha_{A,B}}. \tag{10}$$

From Eq. [10] the release of the ion A by a continuous exchange can be calculated as a function of the total release R. From the relation

$$R = A_s + B_s$$

the release of the ion B is obtained.

Equation [10] can also be written in a form more convenient for calculation of the exchange isotherm. Thus,

$$\frac{A_e}{A_T} = \left(\frac{B_e}{B_T}\right)^{\alpha_{A,B}}. \tag{11}$$

Taking the logarithms of the function,

$$\log A_e = \log A_T + \alpha_{A,B} \log \frac{B_e}{B_T},$$

gives an equation of the first degree with α as the slope of the line. However, it must be kept in mind that the straight-line relationship is valid only as long as α is a constant. By several experiments it has been established that α has a tendency to vary with great changes in the ion proportion. The degree of this variation is dependent on the nature of the ions and the exchanger. It is of interest to note that in previous experiments (3) α proved to be rather constant for exchange performed as small successive replacements, supposed to resemble the continuous exchange.

The relationship between α, the relative release of A and B that is,

$$\frac{A_s:A_T}{B_s:B_T},$$

and the total release R has been discussed previously (1, 3).

The relationship proved to be:

$$\alpha_{A,B} \geqq \frac{A_s:A_T}{B_s:B_T} \geqq 1$$

if A has a lower adsorption affinity than B, and

$$\alpha_{A,B} \leqq \frac{A_s:A_T}{B_s:B_T} \leqq 1$$

if the opposite is true and

$$\lim_{R\to 0} \frac{A_s:A_T}{B_s:B_T} = \alpha_{A,B}.$$

In Figure 1 exchange isotherms are given for the continuous exchange as well as for the batch type of exchange, the former calculated from formula [11] and the latter from the Donnan equilibrium. The relative adsorption affinities of the ions A and B are varied by assuming α to be equal to 0.25, 1, and 4. Mole fraction of A is assumed to be 0.01.

From the figure the following conclusions can be drawn:

1. The desorption curves of the batch exchange are symmetric, whereas those of the continuous exchange are asymmetric.

2. When $\alpha_{A,B} = 1$, that is, the adsorption affinity of A and B being the same, the release is independent of the type of exchange and is proportional to the total release.

3. When $\alpha_{A,B} = 0.25$ (or more generally $\alpha_{A,B} < 1$), A being more firmly adsorbed than B, the continuous exchange releases less of A but more of B than does the batch exchange.

4. When $\alpha_{A,B} = 4$ (or more generally $\alpha_{A,B} > 1$), A being more weakly adsorbed than B, the continuous exchange releases more of A but less of B than does the batch exchange.

5. The continuous exchange compared with the batch exchange therefore

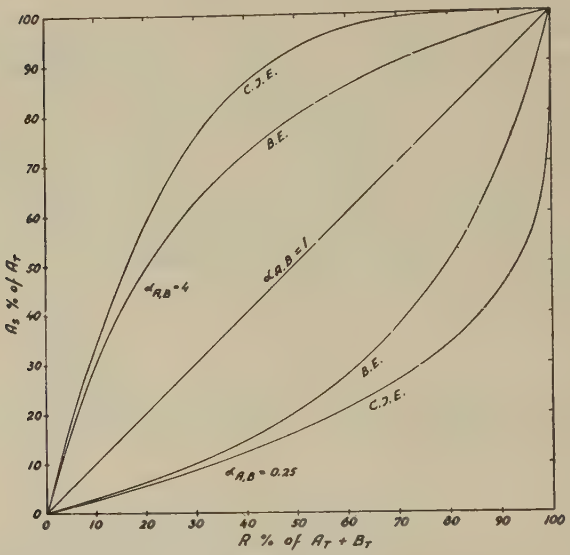

FIG. 1. Influence of the mode of exchange on the release of an ion A, combined with an ion B of the same valence, the equilibrium quotient ($\alpha_{A.B}$) assumed to be 0.25, 1, and 4 and the replacement (R) of $A + B$ to vary from 0 to 100%. B.E. and C.I.E. signify batch exchange and continuous exchange, respectively. A_s means amount of A replaced and A_T total amount adsorbed originally. Mole fraction of A = 0.01.

tends to decrease the release of the more firmly adsorbed ions and to favor the release of the more weakly adsorbed ions. This effect is the more pronounced the greater the difference between the adsorption affinities of the ions, that is, the greater or the smaller the α value, and the more dissimilar the mole fractions of the adsorbed ions. An ion present in a high proportion may be only little or practically not at all affected.

EXPERIMENTS

In our recent paper (3) some experimental results with the resinous cation exchanger Amberlite IR-100 saturated with either $Li^+ - K^+$, $Na^+ - K^+$, or $Na^+ - Cu^{2+}$ were presented to exemplify the ion-exchange theory discussed.

In further experiments, discussed below, the same exchanger was saturated with Li^+, K^+, and Mg^{2+} in two different proportions: (1) 5% Li^+, 90% K^+, and 5% Mg^{2+} and (2) 80% Li^+, 10% K^+, and 10% Mg^{2+}.

The batch exchange was accomplished by addition of increasing amounts of hydrochloric acid to a set of identical systems of the respective ion proportions. No real continuous exchange experiment has been carried out. From the theory it appeared that the continuous and the batch exchange curves approach each other and finally coincide as the percentage replacements decrease. Utilizing this fact a quasi-method for the continuous exchange has been applied.

In the experiments designed to resemble the conditions of the continuous exchange, small fractions of the adsorbed ions were successively replaced by addition of hydrochloric acid. Equilibrium having been established (two hours reaction time, shaking now and then), the free solution was thoroughly removed, new portion of acid added, etc. To increase the accuracy of the analyses successively replaced portions were combined, as given in the table, evaporated, and submitted to analysis. Li and K were determined by flame-photometer and Mg by the thiazol yellow method. The desorption curves of the "continuous" exchange were obtained by summation of the successively replaced quantities of the different ions and related to the sum of the released Li, K, and Mg.

System I: Li^+ 5 %, K^+ 90 %, and Mg^{2+} 5 %. The results are given in Table I and Fig. 2. This experiment deals with a system containing a small amount of the weakly adsorbed Li and the firmly adsorbed Mg and a large amount of the moderately adsorbed K.

System II: Li^+ 80 %, K^+ 10 %, and Mg^{2+} 10 %. The results are given in Fig. 3. This system deals with an exchanger saturated with a large amount of the

TABLE I

Replacement of Li^+, K^+, and Mg^{++} from Amberlite IR-100 by Addition of HCl

4 grams of exchanger saturated with 0.25 meq. Li^+, 4.50 meq. K^+, and 0.28 meq. Mg^{++}. Two different types of experiment, the first being of batch type and the second supposed to resemble continuous exchange. Solution volume 100 ml.

HCl added, *meq.*	Replaced, *meq.*				
	Li^+	$\alpha_{Li,K}$	K^+	Mg^{++}	$Li^+ + K^+ + Mg^{++}$
		Batch exchange			
1	0.077	3.20	0.55	Trace	0.63
3	0.13	3.35	1.14	0.0026	1.27
7	0.18	3.52	1.89	0.015	2.09
20	0.22	(4.45)	2.79	0.060	3.07
40	0.23	3.72	3.41	0.15	3.79
70	0.24	4.42	3.76	0.21	4.21
100	0.245	4.78	4.09	0.24	4.58
		"Continuous" exchange			
	Total		*Total*	*Total*	*Total*
5 × 0.1	0.063		0.43	Trace	0.49
10 × 0.1	0.12		0.91	0.0010	1.03
10 × 0.1	0.16		1.31	0.0019	1.47
20 × 0.1	0.21		1.90	0.0054	2.12
10 × 0.15+ 10 × 0.20	0.24		2.61	0.012	2.86
20 × 0.30	0.25		3.30	0.018	3.57
15 × 0.40	0.25		3.70	0.023	3.97
Σ replac. = 100					

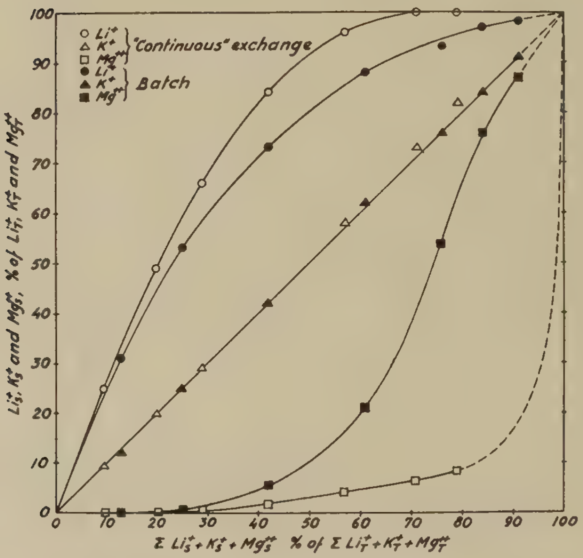

FIG. 2. Replacement of Li^+, K^+, and Mg^{++}. Mole fractions of Li^+ and Mg^{++} being small. Compare with Table I.

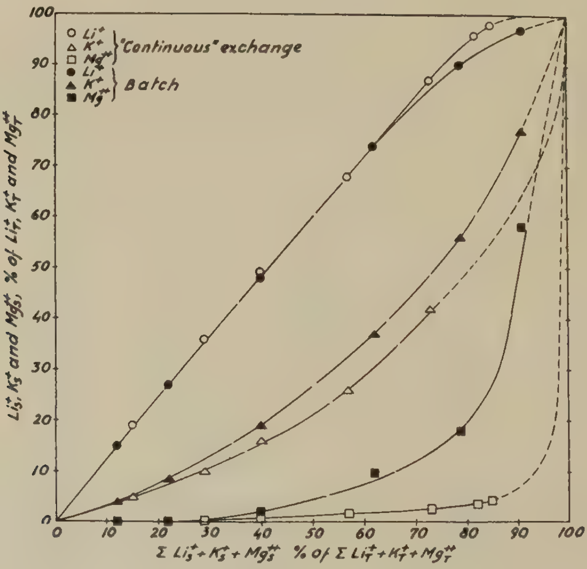

FIG. 3. Replacement of Li^+, K^+, and Mg^{++}. $Li_T^+ = 4.00$, $K_T^+ = 0.50$, and $Mg_T^{++} = 0.56$ meq.

weakly adsorbed Li and a small amount of the moderately adsorbed K and the firmly adsorbed Mg.

Discussion

System I. The results are qualitatively in good accordance with the theory. Thus, there is a marked difference between the percentage replacements of Li and Mg, respectively, in the batch exchange and the "continuous" exchange. While the weakly adsorbed Li shows a greater desorption by the "continuous" exchange than by the batch exchange, the opposite is true of the firmly adsorbed Mg. At a total desorption of 70 %, practically the entire amount of Li is released but only 6 % of Mg by the "continuous" exchange. The corresponding figures for the batch exchange are roughly 92 % of Li and 37 % of Mg. In addition to the effect of the mode of replacement, as discussed for ions of the same valence, the different concentration of the solutions, influencing the distribution of the mono- and bivalent ions (4), is also of importance in explaining the above results as to magnesium.

As could be expected, the release of potassium, representing the major part of the adsorbed ions, is not affected by the type of exchange as far as can be disclosed by an experiment of this kind. The equilibrium quotient, $\alpha_{Li/K}$ of the batch exchange has been calculated and proves to increase slowly with increasing degree of exchange (Table I).

This experiment shows conclusively and in accordance with the theory that a desorption taking place successively and in small quantities, in comparison with a larger desorption, tends to conserve the firmly adsorbed ions at the expense of the weakly adsorbed ions. This effect increases with the difference in concentration and in adsorption affinity of the ions in question. It is greater for ions of different valence than for ions of the same valence and comes to a maximum if the desorption is a real continuous infinitesimal exchange.

System II. Being the dominant ion, lithium behaves in this series the same way as potassium in the former, that is, no certain difference was found. On the other hand K and Mg, though being present at not less than 10 %, show a greater desorption in the batch exchange than in the "continuous" exchange. This is explained by the higher adsorption affinity of K and Mg than of Li. The release of Mg in the "continuous" exchange is markedly small, reaching only about 3 % at a total release of 80 %. The corresponding figure in the batch exchange amounts to 20 %. Owing to a higher degree of Mg saturation the difference between the Mg curves is less in system II than in system I. As a result of the greater competition between K and Mg than between Li and Mg, the Mg release in the batch as well as in the "continuous" exchange experiment is greater in system I than in system II.

Though these studies were carried out with a synthetic exchanger, the conclusions arrived at may have important bearings on several natural reactions. According to Clark and Washington (quoted by Rankama and Sahama (5)) the contents of sodium and potassium in the lithosphere amount to 2.83 % and 2.58 %, respectively, giving a ratio of 1.1. In the sea, however, the corresponding ratio is 27.8. The greater losses of sodium compared to those of potassium by leaching and the accumulation of sodium in the sea may be explained partly by the fixation of dissolved potassium as lattice component of clay minerals and partly by the continuous exchange taking place. As a matter of fact sodium is more weakly adsorbed than potassium by the soil material, thus making possible a dissimilar release of the two ions, strengthened by the continuous exchange. The loss of the important minor elements, present in the soil in very small quantities and being very firmly adsorbed, such as copper, cobalt, zinc, and molybdenum, may also be minimized by an ion exchange of the continuous type.

In a recent survey, Tompkins (6) discusses factors determining the ion selectivity of exchange resins, without, however, including the mode of exchange. As made clear by our study, this must also be considered as a significant selectivity factor. Calculation of the equilibrium quotient of the mass action law and of the relative adsorption affinities of ions from exchange data has been carried out by several investigators during the last years. By the present theory and experiments evidences are brought about that such a procedure is valid only if the results obtained are applied to systems where the exchange is performed in the same way. Thus, equilibrium quotients gained by batch exchange may not be directly applicable to natural systems with ion exchange of the continuous type unless the batch exchange comprises only a small portion of the adsorbed ions. With the use of the ordinary replacement method for determination of the relative adsorption affinities of soil-adsorbed ions *the percentage exchange should consequently be kept as small as possible.*

REFERENCES

1. WIKLANDER, L., *Acta Agr. Scand.* **1,** 190 (1951).
2. WIKLANDER, L., *Trans. Intern. Soc. Soil Sci., Dublin,* **1,** 189 (1952).
3. WIKLANDER, L., AND NILSSON, E., *Acta Agr. Scand.* **2,** 197 (1952).
4. WIKLANDER, L., *Ann. Roy. Agr. Coll. Sweden* (p. 107), **14,** 1 (1947).
5. RANKAMA, K., AND SAHAMA, TH. G., "Geochemistry." University of Chicago Press, Chicago, 1950.
6. TOMPKINS, E. R., *Analyst* **77,** 970 (1952).

THE RATE OF SPREAD OF LIQUID POOLS OVER HORIZONTAL SOLID SURFACES AND BETWEEN APPROACHING PARALLEL FLAT PLATES*

E. B. Bielak and E. W. J. Mardles

Royal Aircraft Establishment, Fairborough, England

Permission to publish has been granted by the Chief Scientist, British Ministry of Supply

Received June 1, 1953

Abstract

Some measurements have been made of the rate of radial spread of liquid pools on horizontal surfaces and between approaching parallel flat plates. Graphs giving the dimensions of the pools after different intervals of time and with different surface finishes have been prepared for several liquids on different kinds of surfaces; also derived graphs relating the rate of radial flow with film thickness, etc., have been included. Movement is complex and specific to the surface and chemical character of the liquid but it is possible to follow the effect of adsorbed surface films and to correlate movement with the periphery resistance (Jamin effect). With the use of binary mixtures of liquids, correlations have been found for rate of radial spread with several properties, such as the coefficient of friction, adhesion, contact angles, and swelling. Any increase in surface activity consequent upon molecular disaggregation is accompanied by a higher rate of movement, increased adhesion, etc. Some liquids are more sensitive to the roughening of surfaces than others. The effect of viscosity usually appears to be masked by surface effects, etc., but with liquids of low Jamin resistance, apart from the initial and later stages of spreading, an approximate relation between time and the radius of the pool can be obtained both for a liquid spreading on a horizontal surface and between approaching parallel plates.

When a small quantity of liquid, say 1 ml., is carefully pipetted on a clean and dust-free horizontal flat surface, it spreads relatively rapidly at first and then settles down to a state of slow movement. It is possible to make suitable measurements of the dimensions of the pool from time to time and so to follow the rate of spread.

These observations of the rate of radial spread of liquid pools, especially, for example, with lubricating oils for clocks, where it is important to know whether the lubricant will remain in or creep away from the pivots, are useful for comparing the flow behaviors of oils over and between surfaces of different kinds. Although the rates of spread of a pool in its various stages

---

* A paper read at the Annual Conference of the British Society of Rheology, Washington Singer Labs., Exeter, September, 1951.

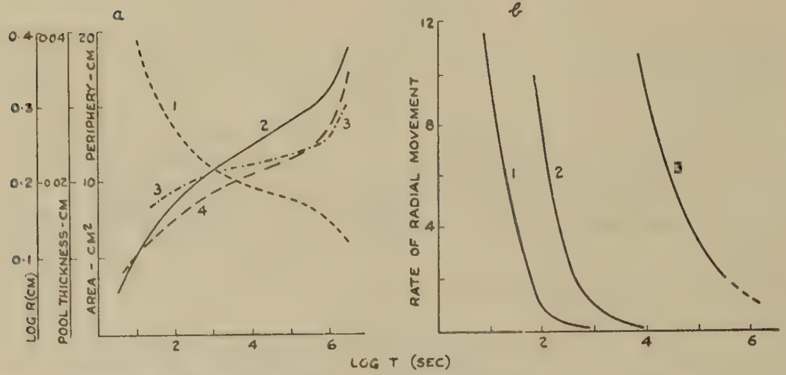

Fig. 1. Changes with log t (sec.) for a pool of clock oil, 0.2 ml. on glass. (*a*) Dimensions of pool: (1) pool thickness, (2) log radius, (3) periphery, (4) area. (*b*) Rate of radial spread: (1) cm. 10^{-3}/sec., (2) cm. 10^{-4}/sec., (3) cm. 10^{-6}/sec.

are highly specific to the kind of surface and its state of cleanliness, roughness, etc., it is possible to compare the rates of movement for different liquids under corresponding surface conditions.

From observations of the area of the pool after different intervals of time it is possible to prepare graphs relating time with film thickness, average radius of the pool, etc., and from these to obtain derived graphs relating film thickness or time and rate of radial spread.

In Figure 1*a* are shown, for example, the area, log radius, thickness, and periphery of a pool of 0.2 ml. of a proprietary clock oil on glass over a period of several weeks and in Fig. 1*b*, the rate of radial movement. From these results Fig. 2*a* was prepared relating the force acting in dynes with the rate of radial movement; the force was calculated from the thickness and density of the pool. It might appear surprising that with an oil of Newtonian flow rectilinear lines passing through the origin are not obtained. That this

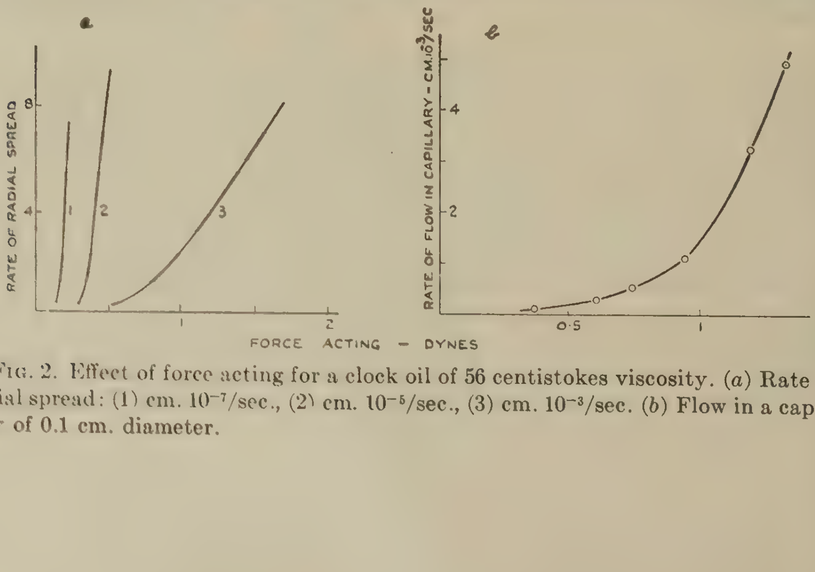

Fig. 2. Effect of force acting for a clock oil of 56 centistokes viscosity. (*a*) Rate of radial spread: (1) cm. 10^{-7}/sec., (2) cm. 10^{-5}/sec., (3) cm. 10^{-3}/sec. (*b*) Flow in a capillary of 0.1 cm. diameter.

behavior is general is demonstrated in Fig. 2*b*, where the rate of flow was measured for a length 2 cm. of the oil in a capillary of 0.1-cm. diameter, at various inclinations.

With the clock oil the movement of the pool practically ceased when the force decreased to about 0.1 dyne; if a Jamin resistance at the periphery of the pool, or of the menisci in the case of the capillary, is considered, the pool will cease to spread or the liquid to flow in the capillary when the force acting diminishes to that of the resistance. For mercury on glass or water on wax with high average Jamin resistances of about 150 and 25 dynes per centimeter, respectively, the pool quickly reaches equilibrium, the radius of the pool being in both cases about 1 cm. for a volume of 1 ml. On the other hand, with silicone fluid with a Jamin resistance of less than 0.05 dyne per centimeter the spreading of a pool can be followed over a period of weeks.

Dynamics of Flow

(*a*) *On a Horizontal Flat Surface.* Apart from surface tension effects the force at any time tending to enlarge the pool is a function of the film thickness and density of the liquid and the rate is inversely proportional to the viscosity. In Table I is given a selection of results obtained for the spreading of 1 ml. of silicone fluids of different viscosities on a polished aluminum plate.

The graphs relating values for log r and log t given in Table I are nearly linear, apart from the initial and later stages of spreading, and as a first approximation the maximum linear slope of the graphs can be represented by the general equation

$$\log r = \tfrac{1}{5}(\log c + \log t - \log \eta)$$

where c is a constant, t the time in seconds, and η the viscosity; or

$$r = \sqrt[5]{c\, t/\eta}. \qquad [1]$$

From Equation [1] by differentiation the rate of radial spread $dr/dt = c/5\eta r^4$, and since 1 ml. of liquid was used, $r^2 = 1/\pi h$, and the rate of spread is proportional to h^2/η, where h is pool height.

TABLE I

The Rate of Spreading of Pools of Silicone Fluid on Polished Aluminum, 1 ml. at 20°C.

	Log r, radius of pool in cm. Viscosity in centistokes					
Log t (sec.)	20	50	100	1000	4000	30,000
1.5	0.38	0.36	—	0.05	—	—
2	0.46	0.43	0.35	0.15	0.06	1.98
3	0.63	0.6	0.54	0.36	0.27	0.18
4	0.81	0.78	—	0.54	0.47	0.38
5	—	—	—	—	0.6	0.52
6	—	—	—	—	—	0.6

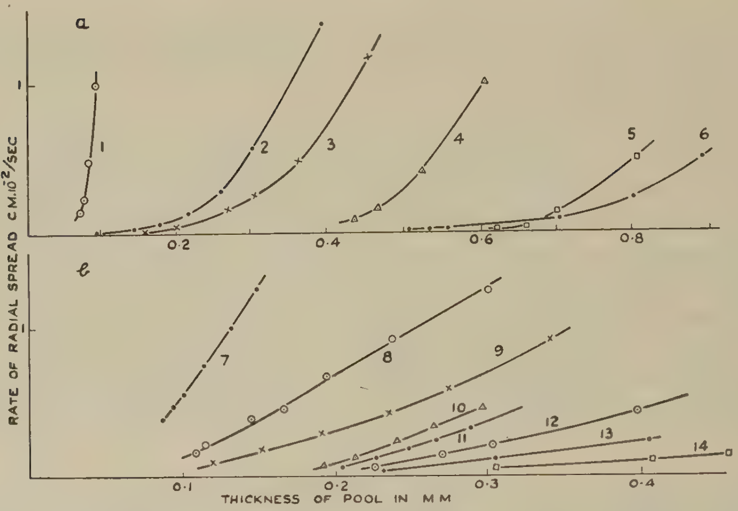

FIG. 3. The relation between rate of radial spread and pool thickness: (*a*) on aluminum; (*b*) on aluminum alloy: (1) iso-octane, (2) *n* hexyl alcohol, (3) *n* hexyl alcohol-amyl phthalate (50/50), (4) liquid paraffin (British Pharmacopoeia), (5) *n* octyl alcohol, (6) diamyl phthalate, (7) methyl alcohol, (8) ethyl alcohol, (9) *n* propyl alcohol, (10) *n* butyl alcohol, (11) iso butyl alcohol, (12) *n* amyl alcohol, (13) *n* hexyl alcohol, (14) benzyl alcohol.

Usually liquids tend to stop spreading or to creep slowly when the thickness of the film reaches a limiting value h_l; thus for the general case for silicones the rate of spreading is proportional to $(h^2 - h^2_l)/\eta$. If r_l is the radius of the pool corresponding to the limiting height h_l, then, apart from the initial and later stages of spreading, the time taken to spread from radius R_0 to radius R_1 is

$$t = c\pi^2 \eta r_l^4 \int_{R_0}^{R_1} \frac{r^4}{r_l^4 - r^4}\, dr.$$

In Figure 3 is shown a collection of results obtained for a variety of pure liquids spreading over metal surfaces, cleaned with a whiting-water paste, rinsed with hot distilled water, and polished with a degreased cotton lint. With most of the liquids examined the relation between rate of radial flow and pool thickness or the square of the pool thickness is expressed by a curvilinear graph which tends to cut the axis for values of h or h^2 some distance from the origin. The graphs for amyl and *n* octyl alcohol intersect, and for a mixture of equal volumes of *n* hexyl alcohol and amyl phthalate the flow behavior resembles far more that for the alcohol than for the ester. At the lower rates of flow the viscosities of the liquids obtained from the inverse of the slope of the graphs are usually different from the bulk viscosities and are different for different surfaces, as indicated by the graphs for *n* hexyl alcohol.

(*b*) *Between Approaching Parallel Flat Surfaces.* With the use of a known volume of liquid and a glass flat as one of the surfaces, the average distance between the plates can be calculated from the area of the pool at any time. Apart from surface tension effects the distance between the plates at any time is according to the approximate equation

$$d^4 = ct^{-1}f^{-1} \qquad [2]$$

where $c = 3\eta \cdot V^2/8\pi$, t is time, f the force acting, V the volume of liquid, and η the viscosity.

It has been found that the radial spread is not in accord with this approximate equation but has several curious features apparently associated with film rupture when the thickness of the film approaches 20 microns. The results are specific to the liquid and kind of surface (2).

In Figure 4 are given some results obtained for radial movement between glass and other surfaces for mineral oils and silicone fluid under different conditions. The relation between the logarithm of the radius of the pool and log t is usually curvilinear instead of being rectilinear, as would be expected from the relevant equation

$$r^8 = cft, \qquad [3]$$

where $c = 8V^2/3\eta\pi^3$.

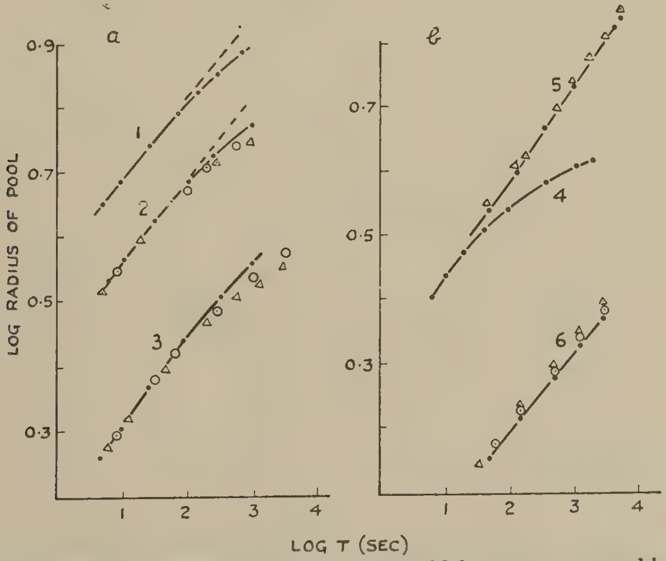

FIG. 4. The radial movement of 0.1 ml. of liquid between approaching parallel surfaces.

● glass/glass
○ glass/brass
△ glass/steel

(*a*) (1) Liquid paraffin (British Pharmacopoeia), load 12 kg., (2) liquid paraffin (B. P.), load 1 kg., (3) mineral lubricating oil, load 1 kg. (*b*) (4) White mineral oil, load 0.5 kg., (5) silicone fluid (50 centistokes), load 1 kg., (6) 0.05 ml. of silicone fluid (100 centistokes), load 10 g.

It will be seen that the mineral oils tend to spread more on the glass, whereas the silicone fluid spreads less on the glass than on the metals. It will also be seen that the mineral oils tend to give thicker films than the silicone fluid. These differences appear to be associated with surface wetting and rupture effects.

The Specific Nature of the Spread of Liquids

The movement of liquids over and between solid surfaces under small forces is complex and little understood, and there appears to be no simple or complete theory. One of us, E. W. J. Mardles (1), has shown that the rate of radial spread of several alcohols over a polished brass surface is quite different for that over aluminum, the rate of methyl alcohol being highest over aluminum but lowest over brass.

It has been observed that some liquid pools tend to wander from their original site or sometimes contract after a period of spreading. Bulkley and Snyder (2) using compounded oils found that the film adsorbed on the

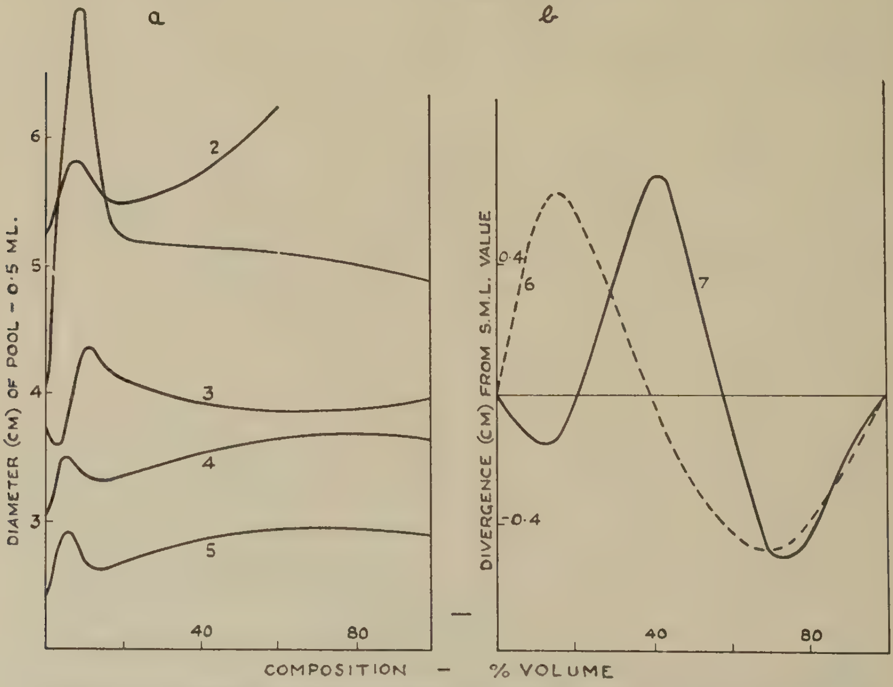

FIG. 5*a*. The variation with composition of the size of liquid pools of binary mixtures of liquid paraffin (British Pharmacopoeia) with: (1) oleic acid on glass, (2) anisole on steel, (3) anisole on brass, (4) cyclohexanone on steel, (5) cyclohexanone on brass.

FIG. 5*b*. The divergence of pool diameter from that given by a simple mixture law for *n* octyl alcohol and 2-diethyl hexyl sebacate: (6) on glass, (7) on steel.

solid surface tended to make the pool unstable so that it contracted into drops.

Similarly, Bigelow, Pickett, and Zisman (3) have shown that long-chain polar compounds with time are adsorbed from solution on solid surfaces to form oleophobic monolayers over which the solution will not spread. Woog (4) considered that in a clock oil an active constituent is necessary so that its molecules may adhere and form a barrier (epilame) preventing the saturated components of the oil from spreading and disappearing from between the bearing surfaces. Hardy (5) concluded that condensation of vapor on the surface adjacent to the liquid was a prelude to its spreading, and Goodeve (6) has described Admiralty researches on the creep of oils based on the view that oils which tend to dissolve a contaminating grease film spread whereas those which do not possess this capacity have a high contact angle and remain stationary.

The Spreading Behavior of Mixed Liquids

The spreading behavior of a mixture of liquids is usually quite different from that of the constituents; for example, with a binary mixture the graph relating the size of the pool, say for 0.5 ml. after a thousand seconds, with the composition often has an interesting shape sometimes with maxima

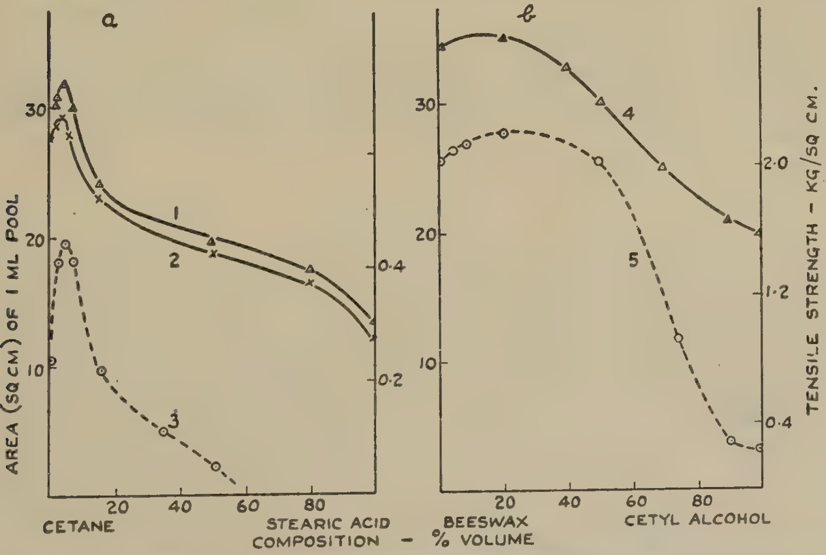

Fig. 6. The spread of binary mixtures of liquids and correlation with the adhesion strength after solidification. (*a*) Mixtures of cetane and stearic acid: (1) the spread on brass, (2) the spread on aluminum, (3) the adhesion (tensile) strength. (*b*) Mixtures of beeswax and cetyl alcohol: (4) the spread on brass, (5) the adhesion (tensile) strength.

and minima. Examples of such graphs are given in Fig. 5. The variation in the pool size appears to be associated with changes in surface activity due to molecular disaggregation. With the increased surface activity there is a corresponding decrease in the coefficient of friction (7), and an increase in the dispersive power for finely divided solids (8). With increased spreading there is also an interesting correlation with increased adhesion. When a small flat disc is allowed to sink into a pool of wax which subsequently solidifies, a measure of the adhesion of the wax can be found by observing the force required to detach the disc. In Fig. 6 are shown some results correlating the size of the pool and the adhesion strength of the joint under normal pull, for binary mixtures of cetane and stearic acid and of beeswax and cetyl alcohol.

We have already reported (9) that there is a correlation between the contact angles and area of spread of ethyl alcohol-chloroform and ethyl alcohol-water mixtures on a sodium stearate surface while the increases in spread coincide with swelling and solubility increases of the sodium stearate in the mixtures.

The Effect of Temperature on the Spreading Rate

Some tests were carried out with mineral oils at a variety of temperatures. The decrease of spread consequent on temperature reduction was not large despite the fact that a large increase in viscosity occurred and over a period of several days the amount of creep was greater than at room temperature. This is presumably due to the presence of an invisible ice film, although the tests were made in a desiccator. Some results are shown in Fig. 7.

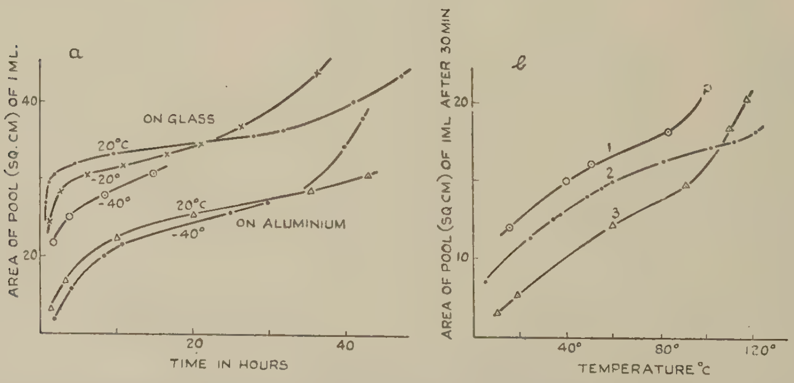

FIG. 7. The effect of temperature on the rate of spread of oils. (*a*) Light mineral oil (D.T.D. 44D) on glass and aluminum. (*b*) (1) Light mineral oil (D.T.D. 44D) on steel, (2) engine oil on aluminum, (3) liquid paraffin (British Pharmacopoeia) on steel.

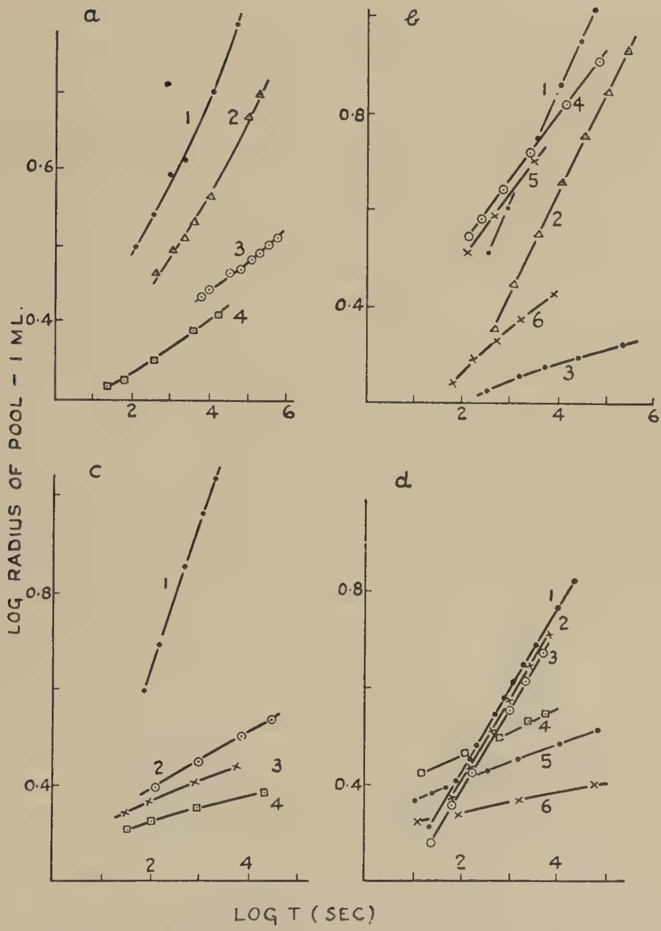

FIG. 8. The effect of surface finish on rate of spread. (*a*) Light mineral oil on glass: (1) with trace of oil on surface, (2) washed with benzene, (3) polished in water with whiting, (4) washed in soapy water and rinsed. (*b*) Liquid paraffin (British Pharmacopoeia) on glass and on aluminum: on glass (1) grit-blasted, (2) frosted, (3) polished; on aluminum (4) 300 emery paper, (5) 500 emery paper, (6) polished. (*c*) Pennsylvania oil (sp. gr. 0.865) on brass: (1) 500 emery paper, (2) polished; and clock oil (synthetic ester base) on brass: (3) 500 emery paper, (4) polished. (*d*) Silicone fluid (100 centistokes) on steel: (1) coarse emery, (2) 500 emery, (3) polished, and diamyl pthalate on aluminum, (4) 500 emery, (5) 300 emery, (6) polished.

The Effect of Surface Finish on the Rate of Spread

Unless otherwise stated the experiments recorded were made with surfaces cleaned with a whiting paste and water followed by water rinse and polishing with a cotton lint. Different results were obtained when hot soapy water was used or when the surfaces were washed with redistilled organic solvents. Some results illustrating these effects are given in Fig. 8; included are some results with roughened surfaces. It will be seen from the graphs that some liquids are more sensitive to roughness than others as regards their rate of spreading; the silicone fluid spread practically the same rate on rough steel as on the polished, whereas a Pennsylvanian oil after one hour's spreading had formed a pool on roughened brass seventeen times the area of that on polished brass.

REFERENCES

1. MARDLES, E. W. J., *Brit. J. Appl. Phys.*, Supplement No. **1,** 7 (1951).
2. BULKLEY, R., AND SNYDER, G. H. S., *J. Am. Chem. Soc.* **55,** 194 (1933).
3. BIGELOW, W. C., PICKETT, D. L., AND ZISMAN, W. A. J., *J. Colloid Sci.* **1,** 513 (1946).
4. WOOG, P., *Compt. rend.* **173,** 303 (1921); **181,** 772 (1925).
5. HARDY, W., *Proc. Roy. Soc.* (*London*) **A 100,** 573 (1922); *Phil. Mag.* **38,** 49 (1919).
6. GOODEVE, C., Essays in Rheology. Pitman, 1947.
7. BIELAK, E., MARDLES, E. W. J., AND TINGLE, E. D., *Brit. J. Appl. Phys.*, Supplement No. **1,** 58 (1951).
8. MARDLES, E. W. J., AND DE WAELE, A., *J. Colloid Sci.* **6,** 42 (1951).
9. MARDLES, E. W. J., AND CLARKE, E. B., *Trans. Faraday Soc.* **42,** B 295 (1946).

CRITICAL PHENOMENA IN AQUEOUS SOLUTIONS OF LONG-CHAIN QUATERNARY AMMONIUM SALTS

Irving Cohen, Clarence F. Hiskey and Gerald Oster

Department of Chemistry, Polytechnic Institute of Brooklyn, Brooklyn 2, New York

Received March 22, 1954

Abstract

Solutions of hyamine 1622 (di-isobutyl phenoxy ethoxy ethyl dimethyl benzyl ammonium chloride) at concentrations above the critical micelle concentration have been studied as a function of NaCl concentration and temperature. At a given temperature there is a critical NaCl concentration above which the system separates into two layers; the top layer is practically free of the quaternary ammonium salt and the bottom layer shows the characteristics of an oil. The volume of the bottom layer decreases with increasing NaCl concentration. Before the onset of the two-phase separation, the turbidity and the dissymmetry of light scattering increases with increasing NaCl concentration. Small temperature changes produce a marked change in the stability of the bottom layer. In the immediate neighborhood of the critical temperature the system exhibits a marked opalescence.

The experimental results can be explained in terms of current concepts of critical solution phenomena where NaCl alters the interactions between the micelles of the quaternary ammonium salt. The details of the interactions are given qualitatively by the theory of Verwey and Overbeek.

Introduction

Aggregation of soap molecules in aqueous media has been intensively investigated by a large variety of physical chemical methods. These efforts have, in the main, been concerned with critical micelle formation. In this region of critical micelle concentration there is considerable evidence to indicate that the size and shape of the micelle is independent of soap concentration and temperature. In fact, Vetter (1) suggests a second critical micelle concentration which delimits this region of constant size and shape. However, added electrolyte has a profound effect upon soap systems, even in the critical micelle concentration range. In addition to lowering the critical micelle concentration (2) light-scattering studies of Debye (3) of long-chain cationic soaps show that the molecular weight of the micellar aggregate increases with increasing KBr concentration.

X-ray studies (4, 5) indicate that for higher soap concentrations (generally greater than 6%), there occurs an increase in micelle size and a transformation of shape to a laminar or cylindrically shaped aggregate.

There has been a considerable amount of dispute (6) as to the possible equilibrium coexistence of spherical and laminar shaped micelles at higher soap concentrations.

The work to be reported in this paper is concerned, primarily, with interactions of micelles of like charge. For many soap systems, over a concentration range above the critical micelle concentration, a macroscopic two-phase system may be produced by the addition of a sufficient amount of electrolyte, such as NaCl, to the system. Two-phase systems of this type, composed of aggregates of anionic soaps, *i.e.*, alkali oleates, stearates, and palmitates, have been investigated by Bungenberg de Jong and associates (7). These systems have been classified by these workers as one of several forms of coacervation.

The qualitative mechanism of coacervation proposed by Bungenberg de Jong and co-workers involves a reduction of the electrostatic repulsion between micelles by the addition of electrolyte, accompanied by a partial desolvation of the micellar aggregate. Booij (7) suggests a mechanism for two-phase formation that involves rather special physical arguments. He proposes that the following micellar transformations will account for two-phase formation. In the region of critical micelle concentration the micelle is the Hartley sphere (8). With increasing soap concentration the spheres flatten out. The argument for this flattening out is related to decreased dissociation of the polar groups of the micelle and the necessity to accommodate an increasing number of polar heads on the periphery of the micelle. Added electrolyte, such as NaCl, further reduces dissociation, hence reducing the electrostatic repulsion of the polar heads of the associated soap molecules. This effect favors further growth of the flattened or platelike structure. This platelike structure promotes a loose intermicellar association due to van der Waals' attraction. With higher NaCl concentrations, relatively large micelle surface regions will be undissociated, and these undissociated spots form places where the micelles may be attached to each other. At still higher electrolyte concentrations, the number of points of attachment increases, and finally, the system contracts, no longer occupying the total volume of available liquid.

The very special arguments developed by the Bungenberg de Jong group involve the concept of a nonuniform charge density on the micelle periphery. In particular their thesis that solvation plays a decisive role in long-range interactions is untenable (9).

What we have attempted to do is to study macroscopic phase transition for one micellar system as a function of NaCl concentration and temperature. We propose to explain the data obtained in this study in terms of a single unifying physical mechanism, one that is readily applicable to all colloidal phenomena, *i.e.*, coagulation, peptization, gelation, thixotropy, etc. In particular we utilize the concept of the attraction of the micelles to each other by London-van der Waals' forces, balanced by the intermicellar repulsion due to their ionic double layers.

Theories for such interaction forces have been described for idealized models (10, 11, 12) and have been developed further in recent years by Verwey and Overbeek (13).

EXPERIMENTAL

Materials

Hyamine 1622 (di-isobutyl phenoxy ethoxy ethyl dimethyl benzyl ammonium chloride monohydrate) is a pure crystalline quaternary ammonium salt monohydrate.

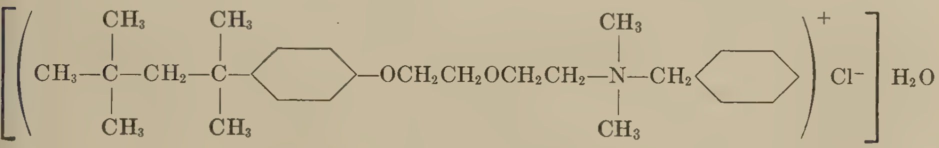

This substance, as obtained from Rohm and Haas, contains 1.5% H_2O as the only appreciable impurity.

The NaCl used in this study is Mallinckrodt C.P. grade. All solutions used, including the distilled H_2O, were filtered through a Bush, positive-pressure, ultrafine filter. A single pass through this filter was sufficient to insure dust-free solutions, sufficiently clarified for reproducible light-scattering measurements.

Analyses of hyamine and NaCl concentrations of the two-phase systems were made gravimetrically. Weighed aliquots of the two phases were evaporated in tared porcelain crucibles, with a final drying in a vacuum oven at 55° C. for six hours. Total solids were determined in this manner. The crucibles were then ignited to 800° C. with a final 10 minutes ignition at 950° C. The residue was weighed as NaCl. A preliminary ignition of hyamine at 800° C. showed a negligible inorganic residue, well within the experimental error of these gravimetric determinations. An analysis of a set of synthetic systems of this sort, as shown in Table I, indicates a relative accuracy of these determinations of approximately 0.5%.

Apparatus

The relative volumes of the two phases were measured in glass-stoppered 10-ml. graduated cylinders which could be conveniently placed into a thermostat rack. These cylinders were equilibrated for 48 hours in the thermostat with thorough shaking after 24 hours. The thermostat was maintained at constant temperature to ±0.2° C.

Light-scattering measurements were made with an Aminco high-sen-

TABLE I

Gravimetric Analyses of Hyamine—NaCl Mixtures

	Weight of Hyamine			Weight of NaCl		
No.	Known	Determined	% Relative Error	Known	Determined	% Relative Error
1	1.4687 g.	1.4670 g.	0.12	1.1804 g.	1.1776	0.24
2	0.9711	0.9761	0.51	1.3041	1.2966	0.58
3	1.6680	1.6639	0.30	0.7040	0.7015	0.35

sitivity photometer (14). The cells were matched cylindrical vials, 2.2 cm. in diameter and 6.0 cm. high, fitted with polythene stoppers.

One hundred milliliter, dust-free solutions of constant soap concentration and variable NaCl concentration were made up. Fifteen milliliter aliquots were placed in the cylindrical vials and the polythene stoppers were sealed to the vials with a high melting point wax. These sealed cells were equilibrated in a thermostat for 48 hours, with thorough shaking after 24 hours. During the light-scattering measurements, the solvent in the cylindrical cell holder was maintained at the thermostat temperature by circulating the thermostat liquid through a copper coil (painted black to minimize light reflections) surrounding the sealed cell containing the soap solution. This coil was so arranged that light intensity measurements could be made at angles from 0° (the transmitted beam) to 150° (Fig. 1).

Experiments of the following nature were performed. For the systems in which two phases are formed, the relative volumes of the phases as a function of NaCl concentration and temperature were measured. The soap and NaCl concentration of the phases was determined. Light-scattering measurements, intensity of scattering at an angle of 90°, and dissymmetry measurements were made on the homogeneous system in the range of NaCl concentration corresponding to the onset of two-phase formation.

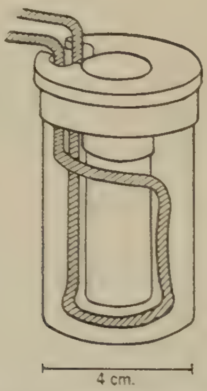

FIG. 1. Constant-temperature light-scattering cell.

TABLE II

Separation of 3.11% Hyamine Solution (0.070 M) into Two Phases with Addition of NaCl at 24.0°C.

Gross NaCl Conc.	Hyamine conc. top layer	Hyamine conc. bottom layer	NaCl conc. top layer	NaCl conc. bottom layer
0.296 *M*	3.11%	3.11%	0.296 *M*	0.296 *M*
0.306	0.28	5.33	0.329	0.300
0.318	0.19	8.00	0.349	0.296
0.352	0.07	15.89	0.399	0.297

After the two phases formed, light-scattering measurements were made on the soap-rich bottom layer.

Results

Aqueous hyamine-NaCl solutions equilibrated for 48 hours, at a fixed temperature, separate into two phases above a certain NaCl concentration. The quaternary ammonium soap is concentrated in the bottom layer. The ratio of the concentration (by weight) of the soap in the bottom layer to the concentration of the soap in the top layer increases with increasing NaCl concentration. For example; a 3.11 % soap solution, at 24.0° C., is homogeneous for an NaCl concentration of 0.30 *M*; for an over-all NaCl concentration of 0.32 *M*, the system is a two-phase system, the bottom layer occupying 27.5 % of the total solution volume, and the ratio of soap

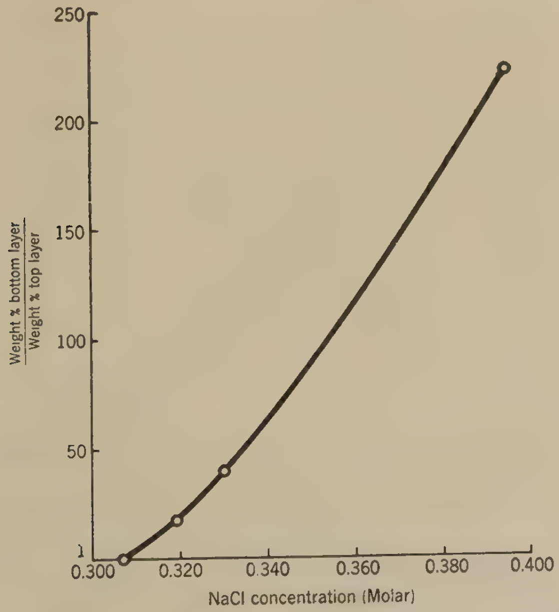

Fig. 2. Ratio of weight % hyamine in the bottom layer to weight % hyamine in top layer vs. NaCl concentration. Initial hyamine concentration 3.11%.

concentrations of the bottom layer to the top layer being 40:1; for an overall NaCl concentration of 0.37 M this ratio is 237:1. The soap concentration of the bottom layer, in the latter case, is 15.9% by weight, and this layer occupies 19.0% of the total solution volume (Table II and Fig. 2).

The formation of a two-phase system, for a fixed NaCl concentration, is strongly dependent upon temperature. A 3.65% soap solution is homogeneous, for an NaCl concentration of 0.283 M, at 24.8° C. At a lower temperature of 19.7° C. this system will be a two-phase system with the bottom layer occupying 78.0% of the available solution volume (Fig. 3). Because of the extreme slowness of the formation of two phases in the critical region, it was difficult to determine precisely the critical temperature for two-phase formation for this NaCl concentration. For a fixed higher

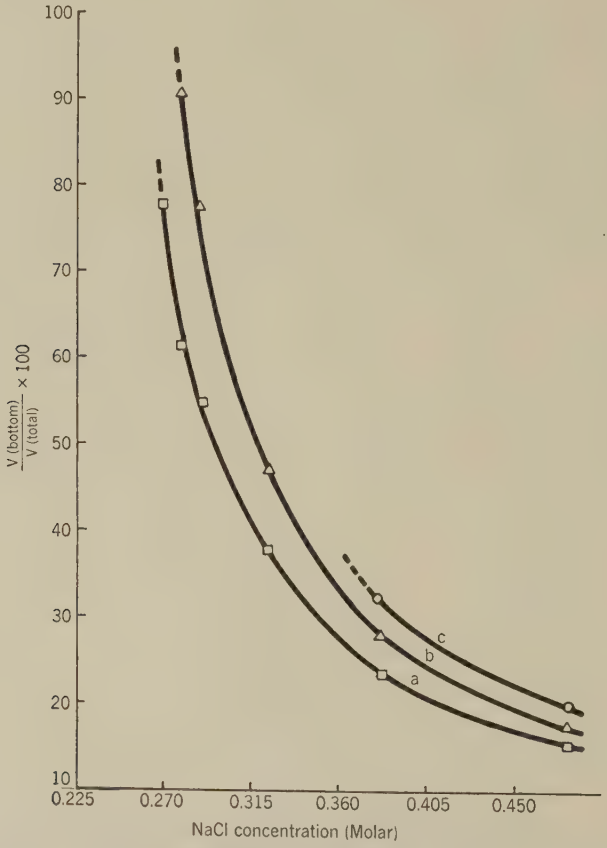

FIG. 3. Ratio of volume of soap-rich bottom layer to total volume ×100 vs. NaCl concentration at constant temperature.

(a) $T = 19.7°$C.; (b) $T = 24.8°$C.; (c) $T = 28.2°$C.
Initial hyamine concentration 4.15%.

NaCl concentration, however, the two phases form rapidly, and as seen in Fig. 3, the volume of the bottom phase increases markedly with increase in temperature.

At a fixed temperature onset of two-phase formation does not occur until the NaCl concentration exceeds a critical value. Thus (Fig. 3) for a fixed temperature of 24.8° C., this critical NaCl concentration lies between 0.270 *M* and 0.279 *M*. At this latter NaCl concentration the bottom layer occupies 90.8% of the available solution volume.

The onset of two-phase formation is characterized by a critical opalescence which extends through the entire system. Under examination in a phase-contrast microscope (Zeiss at 420 times magnification) systems exhibiting this opalescence appear to consist of spherical droplets of the order of 2 μ in diameter. These droplets coalesce to form larger droplets, which impart a grainy appearance to the solution and sediment slowly to form a homogeneous bottom phase.

For a soap system of constant soap concentration and at a fixed temperature, light-scattering measurements show an increase in scattering intensity, at a 90° angle, with increasing NaCl concentration. This is indicated by the solid curves of Fig. 4. At higher NaCl concentrations, above the critical NaCl concentration, where the system exists as a two-phase system, the

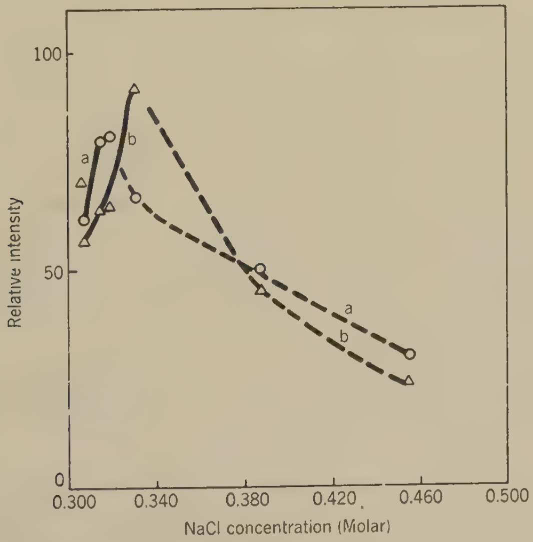

FIG. 4. Relative intensity of light scattering for $\lambda = 546\mu$ at an angle of 90° vs. NaCl concentration at constant temperature.

(*a*) $T = 28.0$°C.; (*b*) $T = 28.8$°C.

Homogeneous system—solid line.
Two-phase system (bottom layer)—dotted line.
Initial hyamine concentration 3.65%.

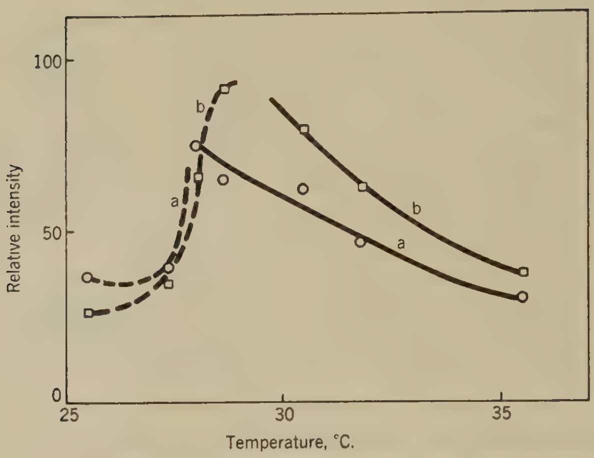

FIG. 5. Relative intensity of light scattering for λ = 546μ at an angle of 90° vs. temperature at constant NaCl concentration.

(*a*) NaCl = 0.318 *M*; (*b*) NaCl = 0.330 *M*.

Homogeneous system—solid line.

Two-phase system (bottom layer)—dotted line.

Initial hyamine concentration 3.65%.

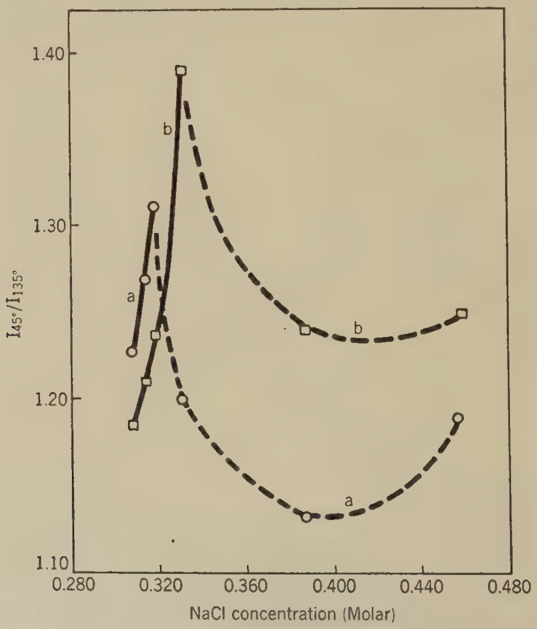

FIG. 6. Dissymmetry of scattering I_{45}/I_{135} for λ = 546μ vs. NaCl concentration at constant temperature.

(*a*) T = 28.0°C.; (*b*) T = 28.8°C.

Homogeneous system—solid line.

Two-phase system (bottom layer)—dotted line.

Initial hyamine concentration 3.65%.

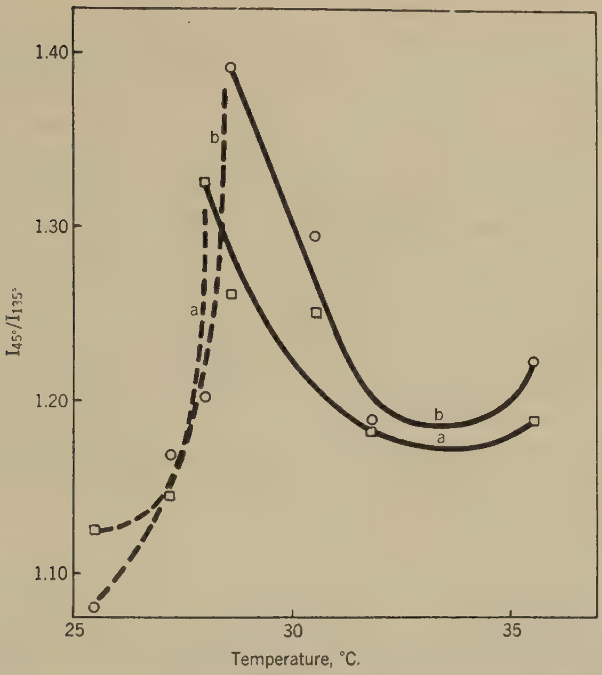

FIG. 7. Dissymmetry of scattering I_{45}/I_{135} for $\lambda = 546\mu$ vs. temperature at constant NaCl concentration.

(*a*) NaCl = 0.318 *M*; (*b*) NaCl = 0.330 *M*.
Homogeneous system—solid line.
Two-phase system (bottom layer)—dotted line.
Initial hyamine concentration 3.65%.

intensity of right-angle light scattering for the soap-rich layer decreases, as shown by the dotted curves of Fig. 4. Here a maximum in light scattering, for an equilibrated system, corresponds to the onset of two-phase formation.

Figure 5 shows the scattering changes for solutions of fixed NaCl concentration as a function of temperature. As the temperature of the homogeneous solution is lowered (solid line of Fig. 5), the scattering increases until it reaches a maximum at the onset of two-phase formation. With a further decrease in temperature the scattering decreases sharply (dotted line of Fig. 5).

The dissymmetry of scattering shows a qualitatively similar behavior, in that a maximum appears at the onset of two-phase formation, as seen in Figs. 6 and 7.

DISCUSSION

The system considered in the present paper differs qualitatively from the anionic soap systems investigated by Bungenberg de Jong *et al.* (7) in that:

1. The soap-rich layer, in our case, settled to the bottom of the vessel, while theirs rise to the top.

2. Lowering of the temperature, in our case, enhances two-phase formation, whereas in their system the effect was in the opposite direction.

We did find, however, in agreement with their results, that increasing electrolyte concentration favored both two-phase formation and the contraction of the soap-rich layer. It is important to note that the range of concentration of NaCl necessary for two-phase formation, with our cationic soap, was nearly one-tenth the amount of 1:1 electrolyte necessary for two-phase formation for the anionic soaps studied by Bungenberg de Jong and associates (7).

Since the concentration of the quaternary ammonium salt in this study was well above the critical micelle concentration, the particles whose interactions we are concerned with are the soap micelles. Addition of NaCl to a homogeneous system of such micelles will exert a dual effect. Firstly, the thickness of the ionic atmosphere surrounding the particles will be decreased according to the Debye-Hückel expression (for a 1:1 electrolyte in water at 25° C.):

$$\frac{1}{\mathrm{K}}=\frac{3}{\sqrt{c}}\ \text{Å},$$

where c is the NaCl concentration and a second factor is the growth of the micelle under the influence of added electrolyte to a homogeneous system (cf. Ref. 3). The dissymmetry light-scattering data (Fig. 6) seems to indicate that a rather striking aggregate growth takes place in the region of NaCl concentration corresponding to the onset of two-phase formation. Dissymmetry can most simply be interpreted if the system is sufficiently dilute, *i.e.*, where the interparticle interference disappears. A more detailed study of the light-scattering properties of these systems is now in progress and a mathematical analysis of the light scattering of nonideal systems of sphere is available (15).

Both factors, mentioned above, enhance aggregation of the micellar particles. Increasing the NaCl concentration decreases the ionic double layer repulsion, and increasing the size of the micelles increases the London-van der Waals' attraction of the particles (11). Hence the formation of very large aggregates of the particles will set in over a narrow range of NaCl concentration. Aggregates will strongly attract other aggregates by the enhanced London-van der Waals' forces, and groups of aggregates will attract other groups more strongly. This behavior is analogous to the condensation of a gas at its critical point, and in a manner quite similar to gas condensation, these soap systems exhibit critical opalescence.

Large groupings of the particles will settle to the bottom of the vessel. Once the soap-rich layer has formed, further addition of electrolyte will decrease the double layer thickness and permit the micelles to approach each other more closely. The effective radii of the micelles is given by $(r + 1/\kappa)$, and hence the volume of the soap-rich layer, which is proportional to the third power of this effective radius, will depend strongly on

NaCl concentration. More explicitly, the volume of this bottom layer will be proportional to

$$A + \frac{B}{c^{1/2}} + \frac{D}{c^{3/2}}$$

where A, B, D are constants and c is the concentration of NaCl. The curves of Fig. 3 seem to bear out this contention. Table II shows that for two-phase systems the NaCl concentration in the bottom layer is slightly less than that of the top layer, this difference increasing with increasing soap concentration in the bottom layer. As can be seen from the data, this difference in NaCl concentration in the two layers can be accounted for in terms of displacement of solvent by the soap, and no recourse to Donnan equilibrium need be made.

For a fixed NaCl concentration, a variation in temperature will have an enormous effect upon the interactions between the particles. For example, when the repulsive forces are weak the potential of force is proportional to $e^{-\kappa d}$ (ref. 6, p. 95), where d is the distance between particles. If we neglect the change in dielectric constant of the medium, since our temperature intervals are small, κ may be considered to be inversely proportional to the square root of the absolute temperature, and the repulsive forces will decrease sharply with a decrease in temperature. Hence we see that a decrease in temperature is equivalent to an increase in salt concentration. This is borne out by a comparison of Figs. 4 and 6 with Figs. 5 and 7. The same arguments are also applicable to explain the contraction of the soap-rich layer due to lowering of the temperature, which is equivalent to an increase in NaCl concentration.

REFERENCES

1. VETTER, R. J., *J. Phys. & Colloid Chem.* **51,** 262 (1947).
2. CORRIN, M. L., AND HAWKINS, W. D., *J. Am. Chem. Soc.* **69,** 683 (1947).
3. DEBYE, P., *Ann. N. Y. Acad. Sci.* **51** (Art 4), 357.
4. HARKINS, W. D., *J. Chem. Phys.* **16,** 156 (1948).
5. HESS, K., AND GUNDERMAN, J., *Ber.* **70,** 1800 (1937).
   HESS, K., KIESSIG, H., AND PHILIPPOFF, W., *Naturwiss.* **26,** 184 (1938); *ibid.* **27,** 593 (1939); *Kolloid-Z.* **88,** 40 (1939).
6. For review see: MCBAIN, J. W., "Colloid Science," pp. 255–267. D. C. Heath and Co., Boston, 1950.
7. For review see: BOOIJ, H. L., *in* "Colloid Science" (H. R. Kruyt, ed.), Vol. II, pp. 701–718. Elsevier Publishing Co., Amsterdam, 1949.
8. HARTLEY, G. S., "Aqueous Solutions of Paraffin-chain Salts." Hermann et Cie., Paris, 1936.
9. OSTER, G., *J. Gen. Physiol.* **33,** 445 (1950).
10. KALMAN, H., AND WILLSTÄTTER, M., *Naturwiss.* **20,** 952 (1932).
11. LANGMUIR, I., *J. Chem. Phys.* **6,** 873 (1938).
12. DERJAGUIN, B., *Acta Physiochim. U. R. S. S.* **10,** 333 (1939).
13. VERWEY, E. J. W., AND OVERBEEK, J. T. G., "Theory of the Stability of Lyophobic Colloids." Elsevier Publishing Co., Amsterdam, 1948.
14. OSTER, G., *Anal. Chem.* **25,** 1165 (1953).
15. OSTER, G., AND RILEY, D. P., *Acta Cryst.* **5,** 1 (1952).

A THEORY OF CRITICAL MICELLE CONCENTRATION OF COLLOIDAL ELECTROLYTE SOLUTIONS

Yuzuru Ooshika

Kobayasi Institute of Physical Research, Kokubunji, Tokyo, Japan

Received August 13, 1953; revised January 22, 1954

Abstract

A theory of the critical micelle concentration of colloidal electrolyte solutions and the effect of added alcohols is developed by using a lamellar model. The logarithm of the critical micelle concentration is approximately a linear function of the number of carbon atoms of the hydrocarbon chain, and the constants involved are of reasonable values. Debye's theory is shown to be incorrect. Since added alcohol molecules form a kind of mixed micelle, it is concluded that the logarithm of the ratio of the decrease of the critical micelle concentration by the addition of alcohol to the concentration of alcohol is a linear function of the number of carbon atoms of the alcohol chain. The agreement of the theory with experiment is quite satisfactory.

Introduction

The solutions of colloidal electrolytes, *e.g.*, soaps and reverse soaps, change their properties abruptly at a certain concentration. The osmotic pressure and the electrical conductivity become much lower than the values predicted by the theory of Debye-Hückel, and the viscosity and the turbidity are increased. At present, these phenomena are considered as due to the formation of thermodynamically stable and reversible colloidal particles, and this idea is supported by many investigators.

The shape and size of these particles, which are called "micelles," have not been uniquely determined. Hartley and his collaborators (1) have proposed a model called the spherical micelle; McBain (1) thought that there are two kinds of micelles, one a large lamellar micelle and the other a small spherical micelle; and Harkins and co-workers (2) have explained the X-ray diffraction patterns of soap solutions by his cylindrical micelle. These models are not fundamentally different from each other in the author's opinion, and hence it seems appropriate to adopt a view that several dozens of molecules aggregate into a micelle, directing their polar heads to water and arranging their long hydrocarbon tails side by side, that is, this model is cylinder-like in character. Recently, Debye and Anacker (3) said that the micelle particles should be regarded as rodlike, their constituent molecules being arranged perpendicular to the rod-axis, when the concentrations of added electrolytes are large. Since we are interested, in this paper, in the critical micelle concentration when the added electrolyte concentration is negligible, we will not consider this rodlike micelle.

On the other hand, as the soap concentration increases far above the critical micelle concentration, there appears in the X-ray diffraction pattern a maximum showing a long spacing, this being considered to be due to a certain interaction between the micelle particles, *i.e.*, an existence of very large aggregates like those proposed by McBain (1) and Philippoff (4). Because this pattern does not appear in the neighborhood of the critical concentration, this long-range interaction may be neglected, so far as the critical micelle concentration is concerned.

In the equilibrium state, there must be aggregates of various sizes and shapes, and the distribution of them is to be determined by statistical mechanics. But, if the size (aggregation number) of a micelle is several dozens, the mixing entropy of the micelle particles in the solution is negligible compared with that of monomers, and the critical micelle concentration may be regarded as the point where a kind of phase change occurs. Therefore the critical micelle concentration is not appreciably affected by the distribution of the micelle sizes. Meyer and Van der Wijk (5) have discussed this point in more detail, though such a treatment is not applicable if the ratio of long-chain ions and gegenions is not unity (6).

If the critical micelle concentration is the one at which a phase change occurs, why do not the aggregates become infinitely large? Debye (7) has suggested that the reason ties in the counterbalance of the van der Waals attractive energy of the hydrocarbon tails and the coulomb repulsive energy of the polar heads. But, in ordinary phase changes, it is due to the surface energy and not due to the additive van der Waals energy that the phase which has a low free energy tends to grow infinitely. Hence it is clear that we must add to the free energy the surface energy between the micelle particle and the water. Then the size should be determined by the counterbalance of the surface energy and the coulomb repulsive energy. The thermal energy of molecules and aggregates and the effect of the ionic atmosphere do not change the situation essentially, though the latter is important when we take account of the effect of added electrolytes, which will be discussed in detail in later papers.

THEORY OF CRITICAL MICELLE CONCENTRATION

Suppose that a micelle particle consists of n soap molecules in equilibrium with the solution. As previously described, we assume that we may consider the total system as divided into two phases, one the solution and the other the micelle phase. The coulomb repulsive energy of a micelle is proportional to $n^{3/2}$, when the charges are distributed on a plane with a constant surface density. The van der Waals attractive energy is proportional to n, because this attraction is of short-range character. The surface energy is proportional to $n^{\frac{1}{2}}$ as a first approximation, since in our model the area of the lateral surface is proportional to the square root of the volume and hence of the number of constituent molecules. As described in the introductory chapter, the effect of the ionic atmosphere causes no appreciable differences when added electrolytes are absent. The energy per micelle, *i.e.*, per n molecules, is, therefore, expressed as follows:

$$w = n^{3/2}w_e - nw_m + n^{\frac{1}{2}}w_s \qquad [1]$$

where w_e, w_m, and w_s are constants, determined by particular soaps.

Now we suppose that N_1 soap molecules are in the solution, N_2 are in the micelle phase, and the number of water molecules present in the solution is N_0. The free energy of mixing in the solution is

$$N_1 kT \log \frac{N_1}{N_1 + N_0} + N_0 kT \log \frac{N_0}{N_1 + N_0} \qquad [2]$$

where k is Boltzmann's constant and T the absolute temperature. Since the mixing entropy of the micelle particles in the solution is negligible as previously described, the part of the free energy concerned with the equilibrium between the micelle phase and the solution is

$$\begin{aligned} F &= N_1 kT \log \frac{N_1}{N_1 + N_0} + N_0 kT \log \frac{N_0}{N_1 + N_0} + N_2(w/n) \\ &= N_1 kT \log \frac{N_1}{N_1 + N_0} + N_0 kT \log \frac{N_0}{N_1 + N_0} \\ &\qquad + N_2(n^{\frac{1}{2}}w_e - w_m + n^{-\frac{1}{2}}w_s) \end{aligned} \qquad [3]$$

The critical micelle concentration, $c_0 = N_1/(N_1 + N_0) \simeq N_1/N_0$, and the size (the value of n) are determined by minimizing the total free energy, holding $N_1 + N_2$, and N_0 at constant values, respectively.

$$dF = \left(\frac{\partial F}{\partial N_1}\right)_{N_2,n} dN_1 + \left(\frac{\partial F}{\partial N_2}\right)_{N_1,n} dN_2 + \left(\frac{\partial E}{\partial n}\right)_{N_1,N_2} dn = 0 \qquad [4]$$

subject to the condition

$$dN_1 + dN_2 = 0.$$

Then

$$kT \log c_0 = w/n; \qquad [5]$$

$$n = w_s/w_e. \qquad [6]$$

Hence

$$kT \log c_0 = 2\sqrt{w_e w_s} - w_m. \qquad [7]$$

Debye (7), Nakagaki (8), and Halsey (9) have determined the aggregation number, n, and the former two also the critical micelle concentration by minimizing the energy per micelle, *i.e.*, energy per n molecules. But the thermodynamical condition determining the values of parameters involved in the equilibrium is the minimization of the free energy of the total system. Therefore, their method is incorrect. Further, it seems to be unreasonable that Debye's condition determining the critical concentration does not involve the surface energy, in spite of the fact that what holds a micelle in a definite size is just the counterbalance of the surface energy and the electrical energy, as described above.

EFFECT OF ADDED ALCOHOLS

When aliphatic chain alcohols are present in the solution, the critical micelle concentration decreases with increasing concentration of alcohol. This effect is considered to be due to the formation of mixed micelles consisting of the soap and alcohol molecules. Besides alcohols, dyes and other organic compounds penetrate into the micelles, which effect is known as solubilization. This phenomenon will be treated in detail in later papers. Suppose that there are n_1 soap molecules and n_2 alcohol molecules in a micelle particle, and that the alcohol molecules are arranged just like the soap molecules. Though alcohol molecules are not dissociated into ions like soap molecules, and though the interaction between their polar groups is as in a pair of planes with opposite uniform charges rather than as in a plane, we consider the interaction between the alcohol molecules and between the alcohol and soap molecules to be the same as that between the soap molecules. Then, if the constants of the electrostatic repulsive energy between the soap molecules and between the alcohol molecules are w_{e_1}, and w_{e_2}, respectively, the constant between the soap and the alcohol molecules will be $\sqrt{w_{e_1} w_{e_2}}$. Therefore, the total repulsive energy of a micelle particle is

$$(n_1 + n_2)^{3/2} \left(\frac{n_1 \sqrt{w_{e_1}} + n_2 \sqrt{w_{e_2}}}{n_1 + n_2} \right)^2, \qquad [8]$$

if we assume that the two sorts of molecules are randomly distributed. The error, due to the fact that the repulsive energy of the polar heads of alcohol molecules is not quite the same as that of the soap molecules, does not affect appreciably the determination of the critical micelle concentration; this will be shown later in the paper.

The van der Waals attractive energy between hydrocarbon chains is of short-range character, and, therefore, the total attractive energies between soap molecules and between alcohol molecules are expressed as

$$n_1^2 w_{m_1}/(n_1 + n_2),\ n_2^2 w_{m_2}/(n_1 + n_2), \qquad [9]$$

respectively. The random distribution of molecules is always assumed.

The attractive energy between two hydrocarbon chains is a function of their chain length (number of carbon atoms) and of additive character with respect to their carbon atom number. Hence, provided they are arranged side by side, it is proportional to the chain length of the shorter chain. Since we consider the case where the alcohol chains are shorter than the soap chains, the total attractive energy between the alcohol and the soap molecules in a micelle is

$$2n_1n_2w_{m_2}/(n_1 + n_2) \tag{10}$$

If the soap chain is the shorter, then w_{m_2} above is to be replaced by w_{m_1}.

Further, the surface energy of a micelle will be

$$(n_1 + n_2)^{\frac{1}{2}}\, w_s \tag{11}$$

when there is a small number of alcohol molecules, w_s being an appropriate mean value for the soap and the alcohol.

In addition to the above terms, there is the free energy of mixing of the soap and the alcohol molecules in a micelle particle. This is, as is well known,

$$kT\left[n_1 \log \frac{n_1}{n_1 + n_2} + n_2 \log \frac{n_2}{n_1 + n_2}\right].$$

Finally, the free energy per micelle is

$$\begin{aligned} w = {} & \frac{(n_1\sqrt{w_{e_1}} + n_2\sqrt{w_{e_2}})^2}{(n_1 + n_2)^{\frac{1}{2}}} - \frac{n_1^2 w_{m_1}}{n_1 + n_2} - \frac{n_2(2n_1 + n_2)w_{m_2}}{n_1 + n_2} \\ & + (n_1 + n_2)^{\frac{1}{2}} w_s + n_1 kT \log \frac{n_1}{n_1 + n_2} + n_2 kT \log \frac{n_2}{n_1 + n_2} \end{aligned} \tag{12}$$

If we put

$$\begin{aligned} & n_1 + n_2 = m, \qquad N_1 = N_m n_1\,, \qquad N_2 = N_m n_2\,, \\ & \eta_1 = N_1/(N_1 + N_2), \qquad \eta_2 = N_2/(N_1 + N_2). \end{aligned} \tag{13}$$

where N_m is the number of micelle particles, and N_1 and N_2 are the numbers of the soap and the alcohol molecules in the micelle phase, then the total free energy of the micelle phase is

$$\begin{aligned} W = N_m w = (N_1 + N_2)\{ & m^{\frac{1}{2}}(\eta_1\sqrt{w_{e_1}} + \eta_2\sqrt{w_{e_2}})^2 - \eta_1^2 w_{m_1} \\ & - (2\eta_1\eta_2 + \eta_2^2)w_{m_2} + m^{-\frac{1}{2}}w_s + kT(\eta_1 \log \eta_1 + \eta_2 \log \eta_2)\}. \end{aligned} \tag{14}$$

In this formula, the independent variables are N_1, N_2, and m. The chemical potential of the soap per molecule in the micelle phase is

$$\begin{aligned} \mu_1 = \left(\frac{\partial W}{\partial N_1}\right)_{N_2,m} = {} & m^{\frac{1}{2}}(\eta_1\sqrt{w_{e_1}} + \eta_2\sqrt{w_e})^2 - \eta_1^2 w_{m_1} - (2\eta_1\eta_2 + \eta_2^2)w_{m_2} \\ & + m^{-\frac{1}{2}}w_s + 2m^{\frac{1}{2}}(\eta_1\sqrt{w_{e_1}} + \eta_2\sqrt{w_{e_2}})(\eta_2\sqrt{w_{e_1}} - \eta_2\sqrt{w_{e_2}}) - 2\eta_1\eta_2 w_{m_1} \\ & - (2\eta_2^2 - 2\eta_1\eta_2 - 2\eta_2^2)\, w_{m_2} + kT \log \eta_1 = m^{\frac{1}{2}}\{(\eta_1\sqrt{w_{e_1}} + \eta_2\sqrt{w_{e_2}})^2 \end{aligned}$$

$$+ 2(\eta_1\sqrt{w_{e_1}} + \eta_2\sqrt{w_{e_2}})(\eta_2\sqrt{w_{e_1}} - \eta_2\sqrt{w_{e_2}})\} - (\eta_1^2 + 2\eta_1\eta_2)w_{m_1} - \eta_2^2 w_{m_2}$$
$$+ m^{-\frac{1}{2}}w_s + kT \log \eta_1 \tag{15}$$

That of the alcohol is

$$\mu_2 = \left(\frac{\partial W}{\partial N_2}\right)_{N_1,m} = m^{\frac{1}{2}}(\eta_1\sqrt{w_{e_1}} + \eta_2\sqrt{w_{e_2}})^2 - \eta_1^2 w_{m_1} - (2\eta_1\eta_2 + \eta_2^2)w_{m_2}$$
$$+ m^{-\frac{1}{2}}w_s + 2m^{\frac{1}{2}}(\eta_1\sqrt{w_{e_1}} + \eta_2\sqrt{w_{e_2}})(-\eta_1\sqrt{w_{e_1}} + \eta_1\sqrt{w_{e_2}}) + 2\eta_1^2 w_{m_1}$$
$$- (2\eta_1^2 - 2\eta_1\eta_2 + 2\eta_1\eta_2)w_{m_2} + kT \log \eta_2 = m^{\frac{1}{2}}\{(\eta_1\sqrt{w_{e_1}} + \eta_2\sqrt{w_{e_2}})^2$$
$$- 2(\eta_1\sqrt{w_{e_1}} + \eta_2\sqrt{w_{e_2}})(\eta_1\sqrt{w_{e_1}} - \eta_1\sqrt{w_{e_2}})\} + \eta_1^2 w_{m_1}$$
$$- (2\eta_1^2 + 2\eta_1\eta_2 + \eta_2^2)w_{m_2} + kT \log \eta_2 \, . \tag{16}$$

The critical micelle concentration can be determined by the following equations

$$\left.\begin{aligned} kT \log c_1 &= \mu_1 \\ kT \log c_2 &= \mu_2 \end{aligned}\right\} \tag{17}$$

where c_1 and c_2 are the critical micelle concentration and the concentration of the added alcohol in the solution, respectively. These are equivalent to the minimization of the free energy of the total system with respect to the distribution of molecules in the micelle phase and the solution.

The size of a micelle particle is determined by the minimization of the free energy of the total system, and therefore W above, with respect to m,

$$\left(\frac{\partial W}{\partial m}\right)_{N_1,N_2} = 0 \tag{18}$$

$$m = \frac{w_s}{(\eta_1\sqrt{w_{e_1}} + \eta_2\sqrt{w_{e_2}})^2} \tag{19}$$

Substituting this value of m into the equations for μ_1 and μ_1 ,

$$kT \log c_1 = 2\sqrt{w_{e_1}w_s} - w_{m_1} + \eta_2^2(w_{m_1} - w_{m_2}) + kT \log \eta_1$$

and, [20]

$$kT \log c_2 = 2\sqrt{w_{e_2}w_s} + (1 - \eta_2^2)w_{m_1} - (2 - \eta_2 + \eta_2^2)w_{m_2} + kT \log \eta_2$$

These equations determine the critical micelle concentration c_1 , when the. alcohol concentration c_2 is given. Ordinarily $c_1 \gg c_2$ and therefore $\eta_1 \gg \eta_2$ Then μ_1 and μ_2 may be expanded into powers of η_2 . We obtain

$$\begin{aligned} kT \log c_1 &= 2\sqrt{w_{e_1}w_s} - w_{m_1} + kT \log (1 - \eta_2) + 0(\eta_2^2) \\ &= kT \log c_{10} + kT \log (1 - \eta_2) + 0(\eta_2^2) \end{aligned} \tag{21}$$

$$kT \log c_2 = 2\sqrt{w_{e_2}w_s} + w_{m_1} - 2w_{m_2} + 0(\eta_2) + kT \log \eta_2 \tag{22}$$

where c_{10} is the critical micelle concentration when the added alcohol is absent. From these, by simple calculations, we obtain

$$\log \frac{c_{10} - c_1}{c_2} = \frac{2(\sqrt{w_{e_1}} - \sqrt{w_{e_2}})\sqrt{w_s} - 2w_{m_1}}{kT} + \frac{2w_{m_2}}{kT} \qquad [23]$$

COMPARISON WITH EXPERIMENTS

It is too difficult for the critical micelle concentration to be measured exactly. It is considered as a small concentration range rather than as a definite concentration.

1. When added alcohol is absent.

We use the data obtained by I. M. Kolthoff and W. Stricks (10) and by Harkins *et al.* (11). The present author plotted $\log_{10} c_0$ (c_0 by mole fraction) versus N_c (the number of carbon atoms of the hydrocarbon chain). Then he obtained the following equation with Na- and K-caprate, laurate, myristate, and palmitate,

$$\log_{10} c_0 = -0.50 - 0.25\, N_c \qquad [24]$$

That $\log_{10} c_0$ is a linear function of N_c is widely known. The coefficient of N_c is approximately constant, but the different homologous series have different constant terms. This proves to be due to the fact that the attraction between hydrocarbon chains does not change appreciably with the change of the polar group, but the electrostatic repulsion changes from compound to compound because of the variety of their sizes and the dissociation constants.

In Eq. [7], w_m is a linear function of N_c and w_e is the term due to the repulsion between the dissociable groups and, in order to know its exact value, the degree of dissociation and the size of the group must be known. However, if the total charge is constant and the surface density is uniform, the total electric energy is proportional to the square root of the total area. The number of the molecules, n in a micelle particle is proportional to the total charge, if the degree of dissociation is constant. Therefore, w_e is proportional to the square root of the total surface area and hence to N_c^{σ} ($\sigma = 0 \sim -1$). (If the hydrocarbon chains are exactly parallel to each other, w_e is proportional to N_c^0, and if they extend at a constant angle to each neighbor molecule, w_e is proportional to N_c^{-1}. In intermediate circumstances, w_e changes with N_c, as shown above.) Finally, as w_s is proportional to N_c, $\sqrt{w_e w_s}$ is proportional to

$$N_c^{(\sigma+1)/2}, \left(\frac{\sigma + 1}{2} = \tfrac{1}{2} \sim 0\right).$$

Therefore, $\sqrt{w_e w_s}$ changes with N_c much more slowly than w_m and its absolute value is also small if the degree of dissociation is not large. Hence we may treat this term as constant in Eq. [7]. Put

$$w_m/kT = \alpha + \beta N; \tag{25}$$

$$2\sqrt{w_e w_s/kT} = \gamma. \tag{26}$$

Then

$$\log c_0 = (\gamma - \alpha) - \beta N_c \tag{27}$$

Comparing this equation with the experimental formula above, we obtain

$$\left.\begin{aligned} \beta &= 0.25 \times 2.30 = 0.58 \\ \alpha - \gamma &= 0.50 \times 2.30 = 1.15- \end{aligned}\right\} \tag{28}$$

We can estimate the van der Waals energy per carbon atom from the evaporation heat of hydrocarbons (7). This value is 2.0 kT per carbon atom at room temperature. Comparing this with the value 0.58 of β, the agreement seems to be rather poor, but considering that the hydrocarbon chains in micelles are more irregularly arranged and the distances between them are increased by the repulsion of dissociable groups, the value 0.58 is considered to be quite reasonable. The attraction between the chain and the water molecules may, of course, have some influence.

Now, let us estimate the aggregation number of a micelle by using the values above. If we assume that the number of molecules on the lateral surface of a micelle is about $\sqrt{n}$,

$$w_s/kT = \frac{\beta}{2} N_c = 0.29\ N_c$$

$$w_s \simeq 1.2 \times 10^{-14}\ N_c \text{ erg}$$

Further, α is the contribution of carboxyl groups to the attractive energy divided by kT and we may estimate it about three times β, *i.e.*, 1.74, because they contain three heavy atoms, one carbon and two oxygens. Hence, from [28],

$$\gamma = 1.74 - 1.15 = 0.59;$$

$$w_e = (\gamma kT)^2/(4w_s) \simeq 1.5 \times 10^{-14}/N_c \text{ erg}.$$

Therefore

$$n = w_s/w_e \simeq 0.8\ N_c^2.$$

N_c varies from 8 to 14; n varies from about 50 to about 150. This is in good agreement with the values many investigators estimated. $\sqrt{w_e w_s}$ is comparatively insensitive to the dependence of w_e on N_c, but w_s/w_e is very sensitive to the latter, and we cannot estimate n exactly.

2. The effect of added alcohols.

Hertzfeld *et al.* (12) have obtained the following experimental formula for the effect of straight-chain alcohols upon the critical micelle concentration of dodecylammonium chloride (the number of carbon atoms of alcohols is from 3 to 10),

$$\log_{10}(\Delta C_\mu/\Delta C_a) = -3.7024 + 0.5017\, N_c \qquad [29]$$

where ΔC_μ is the decrease of the critical micelle concentration, ΔC_a is the concentration of the added alcohol, and N_c is the number of carbon atoms of the alcohol. We can write Eq. [23] as follows,

$$\begin{aligned}\log\,(\Delta C_\mu/\Delta C_a) &= \log\,(c_{10} - c_1)/c_2 \\ &= \frac{2(\sqrt{w_{e_1}} - \sqrt{w_{e_2}})\,\sqrt{w_s} - 2w_{m_1}}{kT} + \frac{2w_{m_2}}{kT} \\ &= \gamma_1 - \gamma_2 - 2(\alpha_1 + \beta N_{c_1}) + 2(\alpha_2 + \beta N_{c_2}) \\ &= 2\log c_{10} + 2\beta N_{c_2} - \gamma_1 - \gamma_2 + 2\alpha_2 \qquad [30]\end{aligned}$$

Now $(-\gamma_1 - \gamma_2 + 2\alpha_2)$ is small and we may neglect this term, and then, using $\log_{10} c_{10} = -1.886$ from the data in reference (12), and that $\beta = 0.58$, the value obtained above, we obtain also,

$$\log_{10}[(c_{10} - c_1)/c_2] = -3.772 - 0.50\, N_c\,. \qquad [31]$$

The agreement of theory with experiment is excellent.

References

1. McBain, J. W., "Colloid Science," D. C. Heath & Company, Boston, 1950.
2. Mattoon, R. W., Stearns, R. S., and Harkins, W. D., *J. Chem. Phys.* **16,** 644 (1948).
3. Debye, P., and Anacker, E. W., *J. Phys. & Colloid Chem.* **55,** 644 (1951).
4. Philippoff, W., *J. Colloid Sci.* **5,** 168 (1950).
5. Meyer and Van der Wijk, *Helv. Chim. Acta* **20,** 1321 (1937).
6. Vold, M., *J. Colloid Sci.,* **5,** 506 (1950).
7. Debye, P., *J. Phys. & Colloid Chem.* **53,** 1 (1949).
8. Nakagaki, M., *J. Chem. Soc. Japan (Pure Chem. Sect.)* **72,** 113 (1951).
9. Halsey, G. D., *J. Phys. Chem.* **57,** 87 (1953).
10. Kolthoff, I. M., and Stricks, W., *J. Phys. & Colloid Chem.* **52,** 1915 (1948).
11. Harkins, Corrin, and Roginsky, cf. reference 3.
12. Hertzfeld, S. H., Corrin, M. L., and Harkins, W. D., *J. Phys. & Colloid Chem.* **54,** 271 (1950).

DETERMINATION OF SURFACE AREA AND PARTICLE SIZE OF SYNTHETIC LATEX BY ADSORPTION. III. LATICES OF HIGH INITIAL SOAP CONTENT

Samuel H. Maron and Max E. Elder

Physical Chemistry Laboratory, Department of Chemistry and Chemical Engineering, Case Institute of Technology, Cleveland, Ohio

Received March 10, 1954

INTRODUCTION

The soap adsorption method for determination of synthetic latex particle size and specific surface area (1, 2) depends on the titration of a latex with soap solution until the critical micelle concentration (cmc) of the soap in solution is attained. Such a procedure can be employed only if the latex contains initially less soap than is required to reach this titration end point. If, however, the latex contains initially more soap than is necessary to attain the cmc, the method as presented heretofore is obviously inapplicable.

It appeared to us that the method may still be applicable to the latter situation if, instead of a soap solution, the latex were titrated with another latex unsaturated with soap, and the remaining capacity of which for adsorbing soap is known. It was anticipated that in such a titration the second latex will adsorb the excess soap present in the first; and, if the volumes of the two latices used were properly chosen, a mixture could be obtained in which both latices were covered with soap and in equilibrium with the cmc of free soap in the final solution.

Preliminary investigation showed that the end point of such a latex-latex titration can readily be determined, as before, by conductance measurements. Consequently a more extended study was undertaken to show that the results thus obtained are reliable. This was done by determining first the particle size of unsaturated latices in the usual manner, next adding an excess of soap, and then redetermining the particle size by titration with more of the same unsaturated latex. The results thus obtained with two rosin soap and two fatty acid soap latices, as well as the method of handling the requisite data, are described in this paper.

EXPERIMENTAL

The conductivity apparatus used in these experiments was the same as described before (1). The temperature throughout was 50°C.

The two fatty acid and the two rosin acid latices used were first analyzed for free acid content and then neutralized by the addition of the quantities of base required. Next the particle sizes of these latices were determined by soap titration in the usual manner. A part of each latex sample was then taken, and enough soap was added to it to give an appreciable excess above that required to yield the cmc. The soap added in each case was identical with that initially present in the latex. Definite volumes of the "soapy" latices were then titrated with samples of the latices from which they were derived, and the titrations followed by conductance to ascertain the position of the end point.

A typical plot of the data obtained during such a titration is shown in Fig. 1. The ordinate gives $(L - L_0)$, *i.e.*, the conductance of the mixture at each stage of the titration minus that of the latex taken, and the abscissa gives the milliliters of the unsaturated latex added. It will be observed that the plot shows a discontinuity, which was taken to be the volume of added latex at which both latices are in equilibrium with the cmc. Such titrations were repeated with each "soapy" latex at several initial dry rubber contents in order to obtain a plot from which the data required for particle size calculation could be obtained (see below).

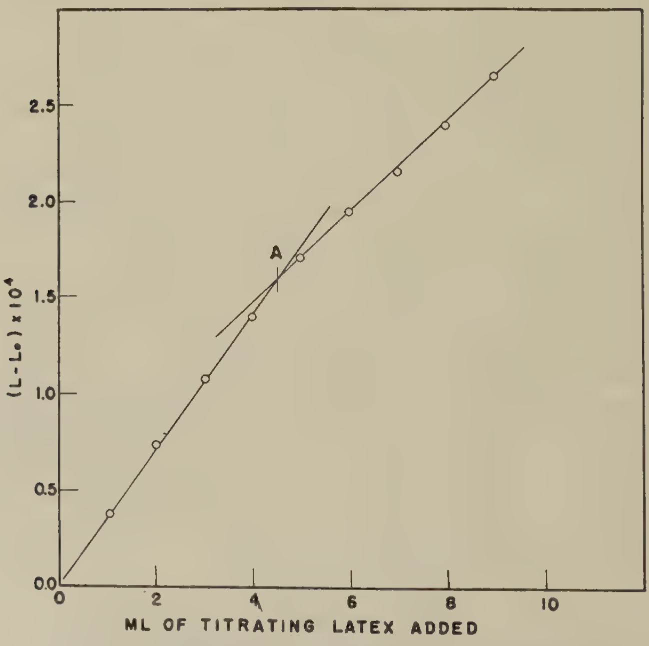

FIG. 1. Conductance titration of latex with latex.

Treatment of Data

In order to derive the equation relating the experimental quantities involved in the situation at hand, let:

S_{i_1} = moles of soap per gram of rubber present in the latex containing the excess soap (latex titrated).

S_{i_2} = moles of soap per gram of rubber present in the latex with insufficient soap for cmc (titrating latex).

m_1 = initial polymer content of latex (1), in grams per liter.

m_2 = ditto for latex (2).

V_1 = volume of latex (1) taken for titration, in milliliters.

V_2 = volume of latex (2) in milliliters at titration end point (point A in Fig. 1).

S_{t_1} = *total* moles of soap adsorbed per gram of rubber by latex (1) at cmc.

S_{t_2} = ditto for latex (2).

C_f = concentration of unadsorbed soap at titration end point (cmc).

w_1 = weight of polymer in V_1 of latex (1) taken for titration.

w_2 = weight of polymer in volume V_2 of latex (2) at titration end point.

From the above definitions

$$w_1 = m_1V_1/1000, \qquad [1]$$

and

$$w_2 = m_2V_2/1000. \qquad [2]$$

Further, the total quantity of soap, in moles, present in the system at the titration end point must be

$$S_{i_1}w_1 + S_{i_2}w_2.$$

This quantity of soap goes to cover the surfaces of the two latices, and to yield, say, x_f moles of unadsorbed soap. From the definitions given above it is apparent that the quantity of soap which is adsorbed by latex (1) is $C_{t_1}w_1$, whereas that by latex (2) is $C_{t_2}w_2$. Hence the total soap content of the system at the titration end point is also given by

$$S_{t_1}w_1 + S_{t_2}w_2 + x_f.$$

Equating these two expressions for total soap content we have that

$$S_{i_1}w_1 + S_{i_2}w_2 = S_{t_1}w_1 + S_{t_2}w_2 + x_f$$

or

$$S_{i_1}w_1 - (S_{t_2} - S_{i_2})w_2 = S_{t_1}w_1 + x_f. \qquad [3]$$

The quantity on the left in Eq. [3] represents the moles of soap unadsorbed from the system by latex (2). It can be converted to concentration in moles per liter on division by the total volume in liters, namely, $(V_1 + V_2)/1000$. If this division be performed, and substitutions be made for w_1 and w_2 from Eqs. [1] and [2], we get

$$C = \frac{S_{i_1} m_1 V_1 - (S_{t_2} - S_{i_2}) m_2 V_2}{V_1 + V_2} = S_{t_1} \left(\frac{m_1 V_1}{V_1 + V_2} \right) + \frac{1000 x_f}{V_1 + V_2} \qquad [4]$$

or

$$C = S_{i_1} m_1' - (S_{t_2} - S_{i_2}) m_2' = S_{t_1} m_1' + C_f, \qquad [5]$$

where

$$m_1' = m_1 V_1 / V_1 + V_2, \qquad [6]$$

$$m_2' = m_2 V_2 / V_1 + V_2, \qquad [7]$$

and

$$C_f = 1000\, x_f / (V_1 + V_2). \qquad [8]$$

m_1' is the rubber content of latex (1) at the end point, m_2' that of latex (2), and C_f is the critical micelle concentration of the soap in solution.

The value of C in Eq. [5] can readily be determined from measurements of S_{i_1}, S_{i_2}, S_{t_2}, m_1, m_2, V_1, and V_2. This quantity, according to the equation, should be a straight-line function of m_1'. Consequently, all that is required is a determination of C at several values of m_1', and a plot of C vs. m_1' should yield a straight line the slope of which is the sought S_{t_1}.

RESULTS AND CONCLUSIONS

Figure 2 shows a typical plot of C vs. m_1' obtained in the course of this work. In line with the above argument the plot is linear, and permits the evaluation of C_{t_1} from the latex-latex titrations. The values of C_{t_1} thus obtained are readily converted into particle size and specific surface area by means of Eqs. [7] and [4] of the first paper in the series.

A further confirmation of the validity of the latex-latex titration and an indication of the accuracy obtained compared with that obtained by ordinary soap titration are given by the data in Table I. In this table C_{t_1} values and particle diameters calculated from these are given for the four latices as obtained by soap and latex-latex titrations. It may be seen that the agreement among the results obtained by the two methods is excellent.

The technique of taking up excess soap by addition of latex suggests the possibility of reversing the usual soap titration procedure and of titrating a solution containing a known amount of soap with latex. Such a procedure was tried and gave good results. However, this technique restricts the range

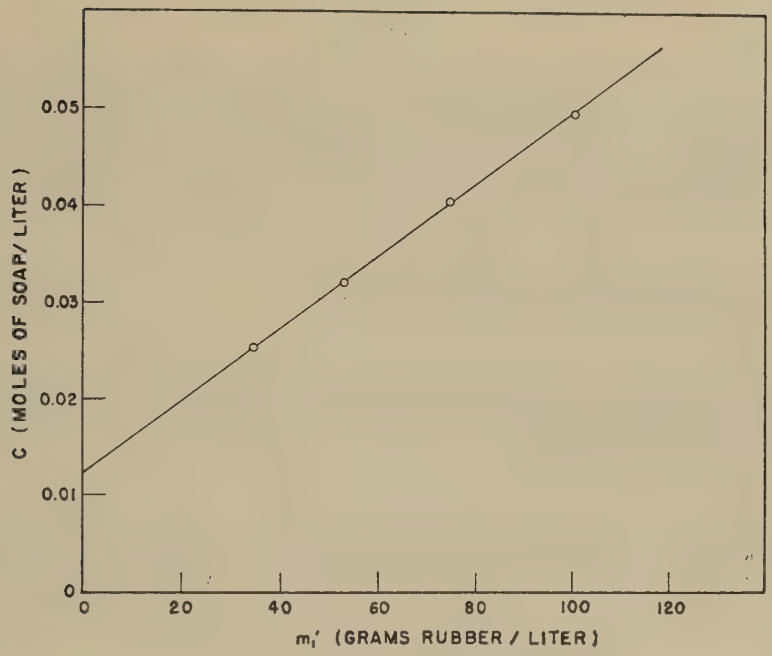

FIG. 2. Plot of C vs. m_1' for latex-latex titration.

TABLE I

Comparison of Latex-Latex and Latex-Soap Titration Results

Latex no.	Type[a]	Soap present and added	Latex titrated with	$C_{t_1} \times 10^4$	D_s (*A.*)
8	50/50 BD-St	K-wood rosin	Soap Latex	3.82 3.75	760 780
9	50/50 BD-St	K-wood rosin	Soap Latex	2.26 2.28	1290 1280
10	70/30 BD-St	OSR	Soap Latex	5.24 5.32	780 790
11	70/30 BD-St	OSR	Soap Latex	4.69 4.75	870 860

[a] BD—Butadiene; St—Styrene.

of latex concentrations which may conveniently be used in such titrations, and hence it is not recommended for routine use.

ACKNOWLEDGMENT

This work was performed as a part of the research project sponsored by the Reconstruction Finance Corporation, Office of Synthetic Rubber, in connection with the Government Synthetic Rubber Program.

SUMMARY

The soap titration method for determination of particle size and specific surface area of synthetic latices can be applied only to latices the initial soap content of which is less than that required to yield the critical micelle concentration of soap in solution. To handle latices the soap contents of which exceed the cmc, a procedure has been developed involving the titration of the latex with another the surface of which is still unsaturated by soap. The latter latex is used to take up the excess soap and to yield both latices in equilibrium with the cmc of the soap.

The end point of the titration can be determined, as before, by conductance. The end points are sharp, and the requisite data obtained permit a ready calculation of the latex particle size for both fatty and rosin soap latices. Further, the results obtained are in excellent agreement with those obtained by soap titration.

REFERENCES

1. MARON, S. H., ELDER, M. E., AND ULEVITCH, I. N., *J. Colloid Sci.* **9**, 89 (1954).
2. MARON, S. H., ELDER, M. E., AND MOORE, C., *J. Colloid Sci.* **9**, 104 (1954).

THE ANALYTICAL SOLUTION OF THE FICK EQUATION WITH A CONCENTRATION-DEPENDENT DIFFUSION COEFFICIENT IN ONE DIMENSION HAVING INFINITE VESSEL LIMITS[1]

Hiroshi Fujita

Department of Fisheries, Faculty of Agriculture, Kyoto University, Maizuru, Japan

INTRODUCTION

Even when the polydispersity effect may be ignored, the diffusion behavior of macromolecular substances in solutions is generally complicated because the concentration dependence of the diffusion coefficient makes the diffusion curve (concentration gradient vs. distance) more or less skew from the normal distribution curve corresponding to constant diffusion coefficient. The diffusion coefficient, D, for a dilute binary solution of a polymer is represented by an equation of the form:

$$D = \frac{RT}{N} \cdot \frac{(1 + B_1 C + B_2 C^2 + \cdots)}{f}, \qquad [1]$$

where R is the gas constant, T is the absolute temperature, N is Avogadro's number, f is the frictional coefficient of the diffusing molecule at a solution concentration C, and B_1, B_2, etc., are the constants relating directly to the coefficients in the virial expansion of the osmotic pressure. Equation [1] comprises two factors which produce a concentration dependence of the diffusion coefficient. The first factor, represented by the numerator of the equation, is a consequence from the thermodynamic interaction between the polymer molecule and the solvent, and may ordinarily be determined from osmotic or from light-scattering measurements. The second factor is the frictional coefficient for which the variation with concentration is a result of changes in molecular configuration and shape. Permeability to the solvent flow apparently gives rise to a concentration dependence of D. The relative degree of these two effects will vary characteristically for particular systems and experimental conditions. In some cases, however, either of these may predominate over the other in the degree of the effect, thus permitting one to obtain useful information as to the concentration dependence of the factor in question from diffusion measurements only.

The purpose of the present paper is to deal mathematically with a diffusion process in one dimension with infinite limits in both directions by assuming the frictional coefficient to be the only controlling factor for the concentration dependence of D. To make the analytical solution of the Fick diffusion equation possible, we shall deal only with such a simple case that the frictional coefficient, f, varies linearly with C, such that

---

[1] Presented at the XIIIth International Congress of Pure and Applied Chemistry, Stockholm, August, 1953, through the courtesy of Professor Nils Gralén of the Swedish Institute for Textile Research.

$$f = f_0(1 - \lambda C), \qquad [2]$$

where f_0 stands for the value of f at infinite dilution, and λ is a parameter. Combining Eqs. [1] and [2] and neglecting the effect of the polymer-solvent interaction, we have

$$D(C) = D(0)/(1 - \lambda C), \qquad [3]$$

with

$$D(0) = RT/Nf_0 .$$

Actual systems conforming to the above D-C relationship are not known, but this relationship may be realized in dilute aqueous solutions of polyelectrolytes. The reduced viscosity of polyelectrolytes in aqueous solutions is known to show a marked increase as the concentration is decreased. The reduced viscosity of a polymer solution, in general, gives a measure for the average volume occupied by the solute polymer molecule. On the other hand, the frictional coefficient of a polymer molecule in solution, at least at sufficiently low concentrations, is roughly proportional to one-third power of the average molecular space. Therefore, it may be expected that in the phase where the reduced viscosity increases markedly with dilution the frictional coefficient will also exhibit a marked decrease with increasing concentration. Equation [3] will then hold as a first approximation to the true form of the D-C relation governing such a region of concentration, and we may give for the parameter λ a meaning as a measure for the electrostatic interaction involved in the system. We may then expect that the concentration dependence of the diffusion coefficient for a dilute polyelectrolyte solution will become weak as simple electrolytes are added to the solution. A good illustration in accord with this expectation is found in the data of Gralén (1) for aqueous sodium chloride solutions of sodium cellulose glycollate. Rosen *et al.* (2) recently demonstrated with aqueous solutions of polyvinyl pyridinium bromide that in the phase where the reduced viscosity increases with increasing dilution the sedimentation rate decreases as a result of the expansion of molecular dimensions. Because the sedimentation rate is inversely proportional to the frictional coefficient, the finding of Rosen and co-workers may be accepted as suggesting the possibility that in the same phase of the viscosity vs. concentration relation the diffusion coefficient depends roughly on concentration as represented by Eq. [3].

MATHEMATICAL SOLUTION

In an ideal experiment for the measurement of the diffusion coefficient of a macromolecular substance in dilute solution, initially, a test solution of a known concentration, C_0, is placed in a tube called the diffusion cell and separated from the solvent or from the solution of a lower concentration, C_1, by a sharp interface. The interface is then rapidly removed without causing turbulence, and the subsequent changes in concentration at various points along the cell are followed by means of an appropriate optical technique. In such an experimental arrangement the medium through which the diffusion takes place must be regarded mathematically as of infinite limits in both directions.

Fix the co-ordinate origin on the initial interface and measure the distance, x, in the direction of diffusion. Since the diffusion here is one-dimensional, the Fick equation for diffusion is

$$\frac{\partial C}{\partial t} = \frac{\partial}{\partial x}\left[D(C)\frac{\partial C}{\partial x}\right], \qquad [4]$$

where C is the concentration of the diffusing substance at any point x and at any time t since the interface was removed, and $D(C)$ is the diffusion coefficient which, in this paper, takes the form given by Eq. [3]. Taking, for simplicity, $C_1 = 0$, the following conditions hold:

$$\begin{aligned} C &= 0 \qquad (t = 0, x > 0), \\ C &= C_0 \qquad (t = 0, x < 0). \end{aligned} \qquad [5]$$

On introducing the dimensionless variables defined by

$$\frac{C}{C_0} = \psi, \qquad \frac{x}{2\sqrt{D(0)t}} = \eta, \qquad \lambda C_0 = \epsilon, \qquad [6]$$

Eq. [4] reduces to an ordinary equation in η of the form:

$$\frac{d}{d\eta}\left[\left(\frac{1}{1-\epsilon\psi}\right)\frac{d\psi}{d\eta}\right] = -2\eta\frac{d\psi}{d\eta}, \qquad [7]$$

and the conditions [5] transform to

$$\psi \to 0 \qquad (\eta \to \infty), \qquad [8]$$

$$\psi \to 1 \qquad (\eta \to -\infty). \qquad [9]$$

In what follows, we shall assume that $0 < \epsilon < 1$, so that the present analysis is concerned only with a diffusion coefficient which increases monotonically with increasing concentration.

The substitutions defined by

$$(d\psi/d\eta)/(1 - \epsilon\psi) = -\varphi, \qquad [10]$$

$$1 - \epsilon\psi = z \qquad [11]$$

lead Eq. [7] to

$$\varphi z \frac{d^2\varphi}{dz^2} = -\frac{2}{\epsilon^2}. \qquad [12]$$

The first integral of this nonlinear differential equation of the second order is given by

$$z\frac{dZ}{dz} = \pm\left(\frac{1}{4}Z^2 - 2\alpha \ln Z + a\right)^{\frac{1}{2}} \qquad [13]$$

where

$$Z = \frac{\varphi}{\sqrt{z}}, \qquad \alpha = \frac{2}{\epsilon^2}, \qquad [14]$$

and a is an integration constant. Equation [7] is represented in terms of Z and z, giving

$$\sqrt{z}\frac{dZ}{dz} + \frac{1}{2\sqrt{z}}Z = -\frac{2}{\epsilon}\eta, \qquad [15]$$

which, on putting $\eta = 0$, gives

$$\left(z\frac{dZ}{dz}\right)_{\eta=0} = -\frac{Z_0}{2},$$

where Z_0 denotes the value of Z at $\eta = 0$. From Eq. [13] and this relation it follows that

$$a = 2\alpha \ln Z_0 . \qquad [16]$$

Hence, if the substitutions

$$\frac{Z}{Z_0} = y, \qquad \frac{8\alpha}{Z_0^2} = \beta \qquad [17]$$

are made, Eq. [13] becomes

$$z\frac{dy}{dz} = \pm\tfrac{1}{2}(y^2 - \beta \ln y)^{\frac{1}{2}}, \qquad [18]$$

whence

$$\tfrac{1}{2}\ln z + b_1 = \int^y (y^2 - \beta \ln y)^{-\frac{1}{2}}\, dy, \qquad [19]$$

$$\tfrac{1}{2}\ln z + b_2 = -\int^y (y^2 - \beta \ln y)^{-\frac{1}{2}}\, dy, \qquad [20]$$

b_1 and b_2 being integration constants corresponding, respectively, to the plus and minus solutions of Eq. [18].

If the condition [9] is combined properly with the subsequent transformations and relations given above, the following condition for y can be derived:

$$z \frac{dy}{dz} \rightarrow \infty \qquad (z \rightarrow 1 - \epsilon). \tag{21}$$

Similarly, we obtain from the condition [10]

$$z \frac{dy}{dz} \rightarrow -\infty \qquad (z \rightarrow 1). \tag{22}$$

It can also be shown that the following boundary conditions for y hold:

$$y \rightarrow 0 \qquad (z \rightarrow 1 - \epsilon), \tag{23}$$

$$y \rightarrow 0 \qquad (z \rightarrow 1). \tag{24}$$

Inspection of these four conditions together with Eq. [18] indicates that when the variable z moves from $1 - \epsilon$ to 1, the integral of Eq. [18] passes from the solution given by Eq. [19] to the solution corresponding to Eq. [20]. Consequently, it proves that the unknown constants b_1 and b_2 are to be determined, respectively, from the conditions [23] and [24]. With the values of b_1 and b_2 determined in this way, we obtain from Eqs. [19] and [20]

$$z = (1 - \epsilon) \exp \left[2 \int_0^y (y^2 - \beta \ln y)^{-\frac{1}{2}} \, dy \right] \tag{25}$$

where $(1 - \epsilon) < z < z_*$, and

$$z = \exp \left[-2 \int_0^y (y^2 - \beta \ln y)^{-\frac{1}{2}} \, dy \right] \tag{26}$$

where $z_* < z < 1$, and where z_* denotes the value of z at which the right-hand side of Eq. [18] changes its sign. If the value of y corresponding to z_* is denoted by y_*, it follows at once from Eqs. [25] and [26] that

$$1 - \epsilon = \exp \left[-4 \int_0^{y_*} (y^2 - \beta \ln y)^{-\frac{1}{2}} \, dy \right]. \tag{27}$$

Simultaneously, the following relation also follows:

$$z_* = (1 - \epsilon)^{\frac{1}{2}}. \tag{28}$$

Because at the branch point z_* the right-hand side of Eq. [18] necessarily vanishes,

$$y_*^2 = \beta \ln y_* . \tag{29}$$

Substituting this into Eq. [27], and putting

$$\frac{y}{y_*} = \theta, \tag{30}$$

$$\ln y_* = 1/2\mu, \tag{31}$$

we obtain the result

$$\epsilon = 1 - \exp\left[-4\int_0^1 (\theta^2 - 1 - \mu \ln \theta^2)^{-\frac{1}{2}}\, d\theta\right], \tag{32}$$

which gives μ as a function of the given parameter ϵ. Since μ is connected with a in Eq. [13] through Eqs. [31], [29], [17], and [16], Eq. [32] is a determinant equation for the unknown integration constant, a, in the first integral of Eq. [12].

Equations [25] and [26] can be expressed in terms of θ, giving

$$z = (1 - \epsilon) \exp\left[2\int_0^\theta (\theta^2 - 1 - \mu \ln \theta^2)^{-\frac{1}{2}}\, d\theta\right] \tag{33}$$

where

$$(1 - \epsilon) < z < \sqrt{1 - \epsilon},$$

$$z = \exp\left[-2\int_0^\theta (\theta^2 - 1 - \mu \ln \theta^2)^{-\frac{1}{2}}\, d\theta\right] \tag{34}$$

where

$$\sqrt{1 - \epsilon} < z < 1.$$

From these, on recalling Eq. [11], there results

$$\psi = \frac{1}{\epsilon}\{1 - (1 - \epsilon) \exp\,[2F(\theta)]\} \tag{35}$$

where

$$\frac{1 - \sqrt{1 - \epsilon}}{\epsilon} < \psi < 1,$$

$$\psi = \frac{1}{\epsilon}\{1 - \exp\,[-2F(\theta)]\} \tag{36}$$

where

$$0 < \psi < \frac{1 - \sqrt{1 - \epsilon}}{\epsilon},$$

and where $F(\theta)$ is a function of θ defined as

$$F(\theta) = \int_0^\theta (\theta^2 - 1 - \mu \ln \theta^2)^{-\frac{1}{2}}\, d\theta. \tag{37}$$

After some operations, it can be shown that Eq. [15] is rewritten in the form:

$$\eta = -\frac{1}{\sqrt{2\mu z}}\,[\theta \pm (\theta^2 - 1 - \mu \ln \theta^2)^{\frac{1}{2}}],$$

where the plus sign corresponds to ψ given by Eq. [35], and the minus sign, to ψ given by Eq. [36]. Substitution for z from Eqs. [33] and [34] leads the above equation for η to

$$\eta = -\frac{1}{\sqrt{2\mu(1-\epsilon)}}\, e^{-F(\theta)}[(\theta^2 - 1 - \mu \ln \theta^2)^{\frac{1}{2}} + \theta] \qquad [38]$$

where

$$\frac{1-\sqrt{1-\epsilon}}{\epsilon} < \psi < 1,$$

$$\eta = \frac{1}{\sqrt{2\mu}}\, e^{F(\theta)}[(\theta^2 - 1 - \mu \ln \theta^2)^{\frac{1}{2}} - \theta] \qquad [39]$$

where

$$0 < \psi < \frac{1-\sqrt{1-\epsilon}}{\epsilon}.$$

Equations [35], [36], [38], and [39] thus obtained provide the exact solution to the problem with θ as an intermediate parameter. The parametric constant, μ, involved in these equations is connected with the given parameter ϵ by Eq. [32]. Values of θ vary between 0 and 1.

The experimental information to be obtained with the diffusion cell is the plot of the concentration gradient against the distance along the cell. Since

$$\frac{\partial C}{\partial x} = \frac{C_0}{2\sqrt{D(0)t}} \cdot \frac{d\psi}{d\eta}$$

and $x = 2\sqrt{D(0)t}\cdot\eta$, only the relation between $d\psi/d\eta$ and η is important for theoretical purposes. The expression for $d\psi/d\eta$ is readily obtained from Eqs. [35]–[39], resulting in

$$\frac{d\psi}{d\eta} = -\frac{4(1-\epsilon)^{\frac{3}{2}}}{\epsilon\sqrt{2\mu}}\,\theta\cdot\exp\,[3F(\theta)] \qquad [40]$$

where

$$\frac{1-\sqrt{1-\epsilon}}{\epsilon} < \psi < 1,$$

$$\frac{d\psi}{d\eta} = -\frac{4}{\epsilon\sqrt{2\mu}}\,\theta\cdot\exp\,[-3F(\theta)] \qquad [41]$$

where

$$0 < \psi < \frac{1-\sqrt{1-\epsilon}}{\epsilon}.$$

The required plot between $d\psi/d\eta$ and η can be calculated in terms of Eqs. [40], [41], [38], and [39], with θ as an intermediate variable, if the value of μ for a given value of ϵ can be determined by solving the transcendental equation [32].

SOLUTION FOR SMALL VALUES OF ϵ

A number of recent works on diffusion for dilute polymer solutions have demonstrated a linear dependence of the diffusion coefficient on the concentration. In the nomenclature of the present paper, this relationship can be represented by

$$D = D(0)(1 + \epsilon\psi). \qquad [42]$$

On the other hand, for sufficiently small values of ϵ the diffusion coefficient of the present study may be expanded in powers of ϵ as follows:

$$D = D(0)\,[1 + \epsilon\psi + 0(\epsilon^2)]. \qquad [43]$$

Accordingly, to the degree of approximation which neglects terms higher than $0(\epsilon^2)$, our formal solution presented above should result in an approximate solution which is valid, at least to the same degree of approximation, for the diffusion coefficient having a linear dependence on concentration. The Fick equation with a linearly concentration-dependent diffusion coefficient cannot be integrated analytically under any initial or boundary condition of physical interest. It may be remarked, however, that several numerical solutions for this case subject to the same initial condition as adopted in this paper have recently been evaluated by Stokes (3).

For $\mu \gg 1$ the following approximation may be established:

$$\int_0^1 (\theta^2 - 1 - \mu \ln \theta^2)^{-\frac{1}{2}}\, d\theta \doteqdot \int_0^1 (-\mu \ln \theta^2)^{-\frac{1}{2}}\, d\theta = \left(\frac{\pi}{2\mu}\right)^{\frac{1}{2}}.$$

Hence, we find from Eq. [32]

$$\epsilon \rightarrow 4\left(\frac{\pi}{2\mu}\right)^{\frac{1}{2}} \qquad (\mu \rightarrow \infty),$$

which indicates that making $\epsilon \rightarrow 0$ is equivalent to making $\mu \rightarrow \infty$.

By making the change of variable:

$$\ln \theta = -\xi^2,$$

$F(\theta)$ proves to approach, when $\mu \rightarrow \infty$, the limiting form as

$$F(\theta) = \rho\,(1 - \operatorname{erf} \xi) + 0(\rho^3), \qquad [44]$$

where we have put

$$\rho = \left(\frac{\pi}{2\mu}\right)^{\frac{1}{2}}. \qquad [45]$$

Since $\theta = 1$ corresponds to $\xi = 0$, Eq. [44] gives

$$F(1) = \rho[1 + 0(\rho^2)]. \qquad [46]$$

Substituting this into Eq. [33] yields an expansion for ϵ in ρ as follows:

$$\epsilon = 4\rho - 8\rho^2 + 0(\rho^3). \qquad [47]$$

This provides a more accurate ϵ vs. ρ relation than that derived above for $\epsilon \ll 1$. By expressing Eq. [38] in terms of ξ, and expanding the resultant equation in powers of ρ, we obtain

$$\eta = -\xi\left[1 + \rho\left(1 + \operatorname{erf}\xi + \frac{1}{\sqrt{\pi}}\frac{e^{-\xi^2}}{\xi}\right) + 0(\rho^2)\right],$$

which inversely gives

$$\xi = -\eta\left[1 - \rho\left(1 - \operatorname{erf}\eta - \frac{1}{\sqrt{\pi}}\frac{e^{-\eta^2}}{\eta}\right) + 0(\rho^2)\right]. \qquad [48]$$

Following a similar procedure, there is obtained from Eq. [40] a series expansion of $d\psi/d\eta$ in ρ, resulting in

$$\frac{d\psi}{d\eta} = -\frac{e^{-\xi^2}}{\sqrt{\pi}}[1 - \rho(3\operatorname{erf}\xi + 1) + 0(\rho^2)],$$

which, on introducing Eq. [48], becomes

$$\frac{d\psi}{d\eta} = -\frac{e^{-\eta^2}}{\sqrt{\pi}}\left\{1 + \rho\left[2\eta^2 - 1 - (2\eta^2 - 3)\operatorname{erf}\eta - \frac{2\eta}{\sqrt{\pi}}e^{-\eta^2}\right] + 0(\rho^2)\right\}. \qquad [49]$$

Elimination of ρ with the aid of Eq. [47] leads to

$$\frac{d\psi}{d\eta} = -\frac{e^{-\eta^2}}{\sqrt{\pi}} + \epsilon\frac{e^{-\eta^2}}{2\sqrt{\pi}}\left[\frac{1}{2} - \eta^2 - \left(\frac{3}{2} - \eta^2\right)\operatorname{erf}\eta + \frac{\eta}{\sqrt{\pi}}e^{-\eta^2}\right] + 0(\epsilon^2). \qquad [50]$$

It is evident from the above deduction that this result is valid only for ψ when $(1 - \sqrt{1 - \epsilon})/\epsilon < \psi < 1$. It is shown, however, that a result identical with this can be derived when $0 < \psi < (1 - \sqrt{1 - \epsilon})/\epsilon$. Accordingly, Eq. [50] holds over the entire range of η from minus to plus infinity. The first term on the right-hand side of Eq. [50] represents the Gaussian distribution curve, whereas the second term multiplied by ϵ provides a main contribution to the skewness of the diffusion curve for $D(C)$ deviated slightly from a constant value. Equation [50] accords exactly with the result obtained recently by Kaneko (4) for the linearly concentration-dependent diffusion coefficient by the use of the method of successive approximations. Although he could provide only the first-order correction term with respect to ϵ, the second or higher correction terms are being calculated by the present author, the results of which will be published elsewhere.

DISCUSSION

As a numerical example, the case in which $\epsilon = 0.912$ was taken. This ϵ value corresponds to $\mu = 5.0$. The calculated ψ vs. η curve and $d\psi/d\eta$ vs. η curve are shown, respectively, in Figs. 1 and 2 as solid lines, whereas the curves for $\epsilon = 0$ (case of constant diffusion coefficient) are shown as dotted lines. The skewness of the $d\psi/d\eta$ vs. η curve from the corresponding normal distribution curve is seen to resemble rather fairly those which are found in many papers on diffusion of dilute polymer solutions. This resemblance, however, may not have a particular significance for practical purposes, because, owing to the great complexity of the general solution obtained, it is, at the moment, impossible to find an appropriate way of fitting the solution to given experimental data. Despite this defect, the results obtained seem to be of fair significance from the theoretical point of view, in that

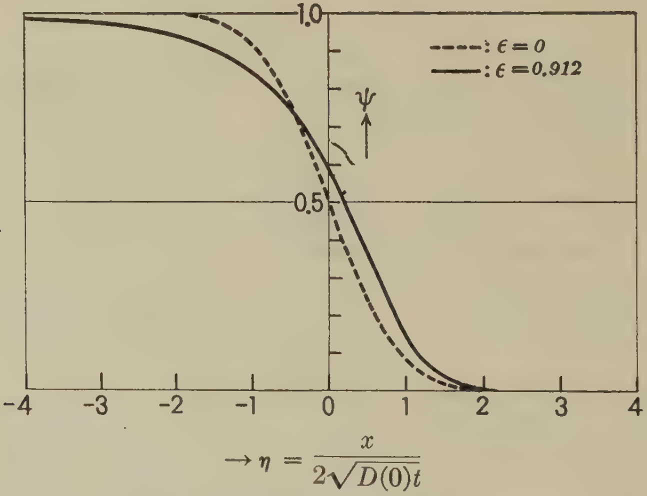

FIG. 1. Calculated concentration vs. distance curve.

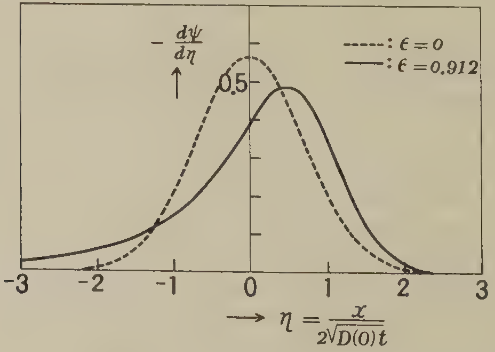

FIG. 2. Calculated concentration gradient vs. distance curve.

they represent the exact solution of a nonlinear diffusion equation. As far as the present author is aware, exact solutions for concentration-dependent diffusions in one dimension with infinite vessel limits have not been reported in the literature. This is the reason why we described the mathematical solution for Eq. [4] with $D(C)$ of the form of Eq. [3] in detail. Although the author, in a series of papers (5, 6, 7), presented exact solutions for the unidimensional diffusion equation having diffusion coefficients of three different types, they all are concerned only with the boundary conditions applicable to a semi-infinite medium. Consequently, no information is available from them as to the diffusion behavior of macromolecules in solutions having infinite limits in their both directions.

The Boltzmann-Matano method and/or its equivalent, the Beckmann-Rosenberg method (8), have been widely used to determine the diffusion coefficient vs. concentration relationship for a given solution of polymer from experimentally obtained diffusion curves. Although these methods, in principle, do not contain any approximation, they, when applied to actual experimental data, often lead to a peculiar D-C relationship in the vicinity of the ends of the concentration diagram, which generally makes it difficult to evaluate $D(0)$ with reliability. The rigorous check on this point is possible only when some mathematically exact curve for the concentration gradient vs. distance relation be found; this, however, has been impossible up to now owing to the reason mentioned above. Since such a mathematical solution has now been obtained, we are in a position to be able to attempt a rigorous checking for the reliability of the existing methods mentioned. This problem will be considered in a future work. In this connection, we note that with respect to the linearly concentration-dependent diffusion coefficient Kaneko (4) has examined the accuracy of the Beckmann-Rosenberg method using the approximate solution given by Eq. [50].

ACKNOWLEDGMENTS

The author expresses his cordial thanks to Professor Nils Gralén of the Swedish Institute for Textile Research, who kindly read this paper at the XIIIth International Congress of Pure and Applied Chemistry, Stockholm, August, 1953, and who recommended it for publication in this Journal. The author's thanks are also due members of the High Polymer Research Group of Kyoto University for helpful advice and criticism given for this work.

SUMMARY

The analytical solution for the one-dimensional Fick equation with a concentration-dependent diffusion coefficient of the form:

$$D(C) = D(0)/(1 - \lambda C),$$

where C is the concentration and λ is a parameter, is obtained under the initial condition that a solution and the solvent are initially separated by

a sharp interface in an infinitely long tube. It is supposed that this form of $D(C)$ may apply to describing the diffusion behavior of dilute polyelectrolyte solutions in the phase where the reduced viscosity increases markedly with increasing dilution. The mathematical analysis is carried out for the case of λ being positive, and the general solution obtained is discussed numerically. An approximate solution is derived from the general solution for the case of small values of λ. The skewness of the diffusion curve obtained has a good resemblance to experimental results associated with the diffusion coefficients increasing with increasing concentration. The theoretical significance of the exact solution obtained is discussed in relation to the check of the reliability of the Boltzmann-Matano method for evaluating the concentration dependence of the diffusion coefficient from given experimental data. Because of the complexity of the general solution, however, it is impossible to find an appropriate way of fitting the solution to experimental data.

REFERENCES

1. GRALÉN, N., "Sedimentation and Diffusion Measurements on Cellulose and Cellulose Derivatives." Dissertation, Uppsala, 1944.
2. ROSEN, B., KAMATH, P., AND EIRICH, F., *Discussion Faraday Soc.* **No. 11,** 135 (1951).
3. STOKES, R. H., *Trans. Faraday Soc.* **48,** 887 (1952).
4. KANEKO, K., AND SAINO, S., *J. Chem. Soc. Japan* (*Ind. Chem. Sect.*) **56,** 293 (1953).
5. FUJITA, H., *Textile Research J.* **22,** 757 (1952).
6. FUJITA, H., *Textile Research J.* **22,** 823 (1952).
7. FUJITA, H., *Textile Research J.* **24,** 234 (1954).
8. BECKMANN, C. O., AND ROSENBERG, J. L., *Ann. N. Y. Acad. Sci.* **46,** 329 (1945).

LETTER TO THE EDITORS

THE SURFACE PLASTICITY OF SODIUM MYRISTATE SOLUTIONS[1]

Certain solutions exhibit a higher viscosity at the surface than in the bulk liquid. Indeed, it has been shown that in many instances surfaces of soap solutions are plastic (2, 3), since they have a finite yield value and the viscosity is a function of the rate of shear. The purpose of this research was to investigate the nature of these plastic surfaces more fully. Solutions of pure sodium myristate, which have a marked surface plasticity under proper conditions, were employed.

In this investigation the surface viscosity and plasticity were measured by the oscillating disc method. Since the apparatus and technique employed were essentially those of Wilson and Ries (3), a detailed description is not warranted. All experiments were conducted with the bottom of the disc just touching the liquid surface. The torsion pendulum was suspended in a thermostated, glass-fronted box which served as a constant-temperature air bath. A slow stream of carbon dioxide-free air was continuously passed through the bath. The amplitude of oscillation was measured in arbitrary units by means of a cathetometer focused on a scale attached to the oscillating disc.

It has been shown (3) that if the logarithm of the amplitude is plotted as a function of the oscillation number a straight line results whose slope is a measure of the surface viscosity, provided the surface is not plastic. If the surface is plastic, a curved line concave downward results as a consequence of the fact that the viscosity increases as the rate of shear decreases.

The surface plasticity of sodium myristate solutions was found to be a function of temperature. For a given concentration, at a relatively low temperature, the solution is markedly surface plastic, as is shown by the curvature in the plot of logarithm amplitude versus oscillation number. With increasing temperature the plasticity decreased and finally disappeared completely. This transition from a measurably plastic to a nonplastic surface is quite sharp. A typical set of data for 0.002 *N* sodium myristate is shown in Fig. 1.

The transition temperature was found to be a function of sodium myristate concentration. For a 0.002 *N* solution the transition occurred between 46.0°C. and 47.0°C., and either an increase or a decrease in concentration resulted in a decrease in the transition temperature. A plot of transition

---

[1] This investigation is a joint undertaking of the Research Institute of the University of Oklahoma and the Office of Naval Research.

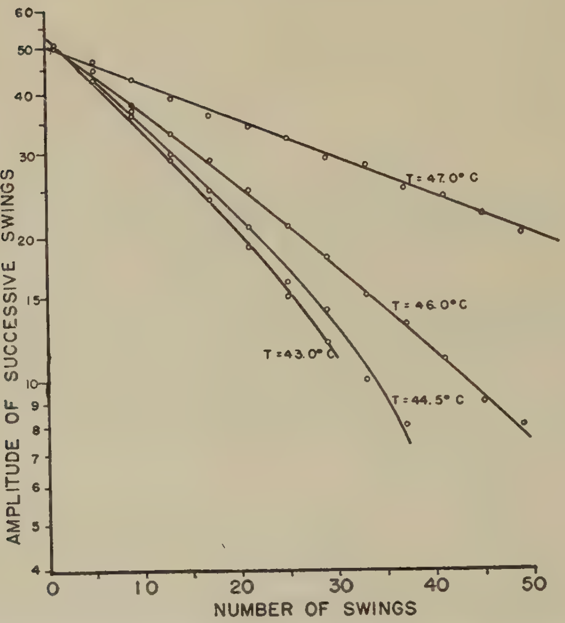

FIG. 1. Damping of torsion pendulum at the surface of 0.002 *N* sodium myristate solution.

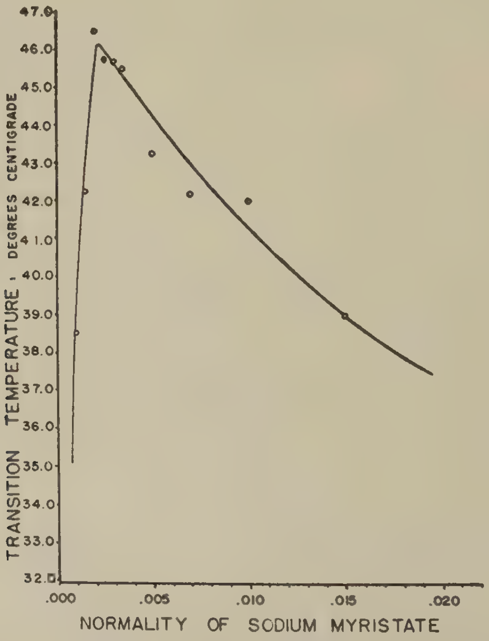

FIG. 2. Transition temperature versus concentration of sodium myristate.

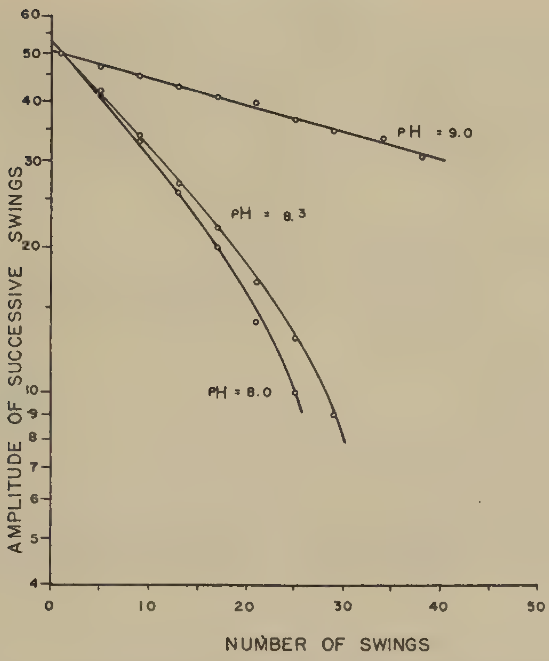

FIG. 3. Effect of pH on the plasticity of 0.001 N sodium myristate. Temperature = 34°C.

temperature as a function of sodium myristate concentration is shown in Fig. 2.

It was found that the surface plasticity was a function of pH. If the stoichiometric pH of a surface plastic solution is increased by the addition of sodium hydroxide a nonplastic surface results. This is shown in Fig. 3 for 0.001 N sodium myristate. At 34°C. the stoichiometric pH was 8.0. When the pH of the solution was increased to 9.0, the surface became nonplastic.

These results suggest that the surface plasticity of sodium myristate solutions can be attributed to hydrolysis products. When these solutions hydrolyze, the free fatty acid formed associates, at least partially, with unhydrolyzed ions to form acid soap. These hydrolysis products are surface active and concentrate at the solution interface where a plastic layer is formed. An increase in pH represses hydrolysis, and consequently the products are not available to form a plastic surface film. The maximum in the concentration versus transition temperature plot indicates that the nature of the surface is determined by the bulk concentration. Further experiments designed to elucidate the nature of these surfaces are in progress.

One of us (1) has recently reported that sodium laurate solutions exhibit no surface plasticity at 20°C. In view of the results presented here for sodium myristate it is possible that 20°C. is above the transition temperature for sodium laurate and that these surfaces would exhibit plasticity at lower temperatures. Indeed, the relationship between transition temperature and hydrocarbon chain length should be further investigated, and experiments with sodium laurate, sodium palmitate, and sodium stearate are contemplated for the future.

REFERENCES

1. BURCIK, E. J., *J. Colloid Sci.* **5**, 421 (1950).
2. PRESTON, W. C., AND RICHARDSON, A. S., *J. Phys. Chem.* **33**, 1142 (1929).
3. WILSON, R. E., AND RIES, E. D., *Colloid Symposium Monograph* **1**, 145 (1923).

School of Petroleum Engineering,
University of Oklahoma,
Norman, Oklahoma

EMIL J. BURCIK[2]
JAMES R. SEARS[3]
ALBERT TILLOTSON[4]

Received October 6, 1953

[2] Present address: School of Mineral Industries, The Pennsylvania State College, State College, Pennsylvania.

[3] Present address: Southern Production Company, Fort Worth, Texas.

[4] Present address: Oklahoma Medical Research Foundation, Oklahoma City, Oklahoma.

ON GEL FORMATION IN SOAPS

N. Pilpel

Chemistry Department, King's College, University of London, Strand, W.C.2

Received May 21, 1954

Abstract

Viscoelastic gels are formed by the addition of electrolytes to aqueous soap solutions. Equations have been derived that enable gel formation to be explained in terms of the conversion of the soap from the form of small, detached spherical micelles into long, interlinked cylindrical micelles.

The mechanism proposed reasonably explains the gel properties of the soaps of sodium oleate, elaidate, and oleylsulfate, and the influence on these properties of small amounts of long-chain alcohols, other soaps, and perfluoro-compounds.

Introduction

The work of numerous authors (1–10) on the physical properties of aqueous solutions of the soaps of long-chain fatty acids, sulfates, and sulfonates, and of quaternary ammonium compounds has clearly established that, except in very dilute solution, the molecules exist in the micellar state. The aggregation of the single molecules into micelles is detected by characteristic and sudden changes in such properties of the solutions as conductivity, surface tension, osmotic pressure, and viscosity, and generally takes place over a relatively small range of concentration of the soap.

Although the critical micelle concentration (c.m.c.) for a great many of the commoner soaps is now known with accuracy, the question of the actual sizes of the micelles, of their shapes, and, in particular, of their variation in size and shape, both at higher soap concentrations and on the addition of inorganic ions, is still a matter of considerable controversy.

McBain (8) had originally postulated small, highly conducting ionic micelles coexisting with a larger, weakly conducting neutral micelle, whereas, in contrast, Hartley and his collaborators (11) had envisaged an essentially spherical micelle, the size of which remained appreciably constant at all concentrations above the c.m.c. The observations by Hess and Gundermann of X-ray diffraction patterns from soap solutions led to the suggestion of a lamellar micelle composed of alternate layers of water and double amphipatic molecules, and McBain identified this with his neutral micelle. Later work of Harkins (12), Harkins and Mittelmann (13), and others, however, has shown that the X-ray patterns may be explained equally well in terms of cylindrical or rod-shaped micelles. The measurements of Debye and Anacker (14) clearly indicate the existence of asymmetrical micelles and lead to the postulation of a rod shape in which the molecules are oriented radially to the longitudinal axis.

In view of the considerable bulk of experimental data and of the numerous theories, many mutually conflicting, that have been advanced to explain these data in terms of a micellar model, it is not surprising to find that a rather cautious note is now being struck by the latest writers in the field. Philippoff (15) has shown that once the c.m.c. has been passed a number of different regions are encountered in aqueous soap solutions. These he designates: Region 1—electrolyte absent; Region 2—small amount of electrolyte present; Region 3—large amount of electrolyte present. The regions are distinguished by such properties as variation in relative viscosity with temperature, with rate of applied shear, and with change in concentration of the electrolyte. Further complexities are introduced, however, by the observation that the viscosity behavior is found to depend also on a number of other factors—nature of the soap, added ions, and concentration of both soap and electrolyte. Philippoff concludes that it is not possible to arrive at any satisfactory picture of the shapes or sizes of the micelles and, in fact, suggests that micelles of a variety of types coexist in metastable equilibrium in any particular soap solution at any particular concentration of soap and electrolyte.

Similar conclusions are arrived at by Schulman and Van den Berg (16). In a potassium oleate solution the X-ray bands corresponding to what they believe to be micelles with a lamellar structure disappear as the quantity of added electrolyte is increased until finally, when viscoelastic properties develop, only a diffuse scattering pattern is observed. This they ascribe to the presence of micellar aggregates of various sizes. Since the patterns for potassium oleate and potassium laurate systems are fundamentally different, they conclude that long-chain hydrocarbon polar compounds may aggregate or pack together in many different forms depending on the steric configurations of the molecules and on their environment, *e.g.*, oil, water, salts, temperature, concentration.

Discussion

In attempting to explain, in terms of a micellar model, the development of viscoelastic properties in soap solutions by the addition of electrolytes, it must be emphasized from the outset that such an explanation can, at best, be expected to be only rather approximate. All the evidence, both from the literature and from the present investigation, suggests that the development of viscoelastic properties takes place through a series of stages at any particular concentration of soap in the solution (provided it is above the c.m.c.) These stages, characterized presumably by the presence of micellar types of one kind or another, are not clearly defined but extend gradually one into the next. Since there is no reliable evidence for the actual micellar form preponderating at any one of these intermediate stages, it seems unlikely that any step-by-step treatment would be applicable to the problem of gel development. Nor is it possible to specify exactly the form and size of an original micelle type (postulated as existing at low concentrations of electrolyte) or of the final micelle type that occurs when gelling has occurred. Indeed, the evidence available points only to the likelihood of considerable variation in both, since their forms appear to depend on the nature of the soap, temperature, past history of the solution, etc.

Despite these formidable difficulties it is nevertheless considered of value to attempt an explanation of the present experimental results in terms of a micellar model. The aim is a treatment essentially quantitative in nature that is able satisfactorily to account for such qualitative observations as the effects of hydrocarbon chain length, addition of alcohols, fluoro-compounds, and ions on the mechanical properties of the gel systems produced. For the purpose the following simplifying assumptions are made.

Assumptions

At low concentrations of electrolyte and prior to the development of marked elastic and/or viscous properties, the soap molecules are assumed to exist in the form of relatively small, spherical micelles. The molecules are oriented radially with the polar heads outermost. On the evidence of the X-ray work of Harkins and Mittelmann (13) on the solubilization by soaps of long-chain alcohols and hydrocarbons, and of Phillips (17) on the energetics of the same process, the center of the spherical micelle is assumed to be completely oily. By this is meant that the hydrocarbon chains are coiled so that the whole of the center of the micelle consists of nonpolar groups; no water or electrolyte is present in this region. Under the influence of added electrolyte the spherical micelles first flatten, as proposed by Debye (18), and then pack together into long cylindrical rods in which the molecules are arranged radially to the axis with the polar heads outermost. The ends of the cylinders are assumed hemispherical, again with the polar heads outermost. Viscoelastic properties develop as a result of interlinking throughout the liquid of these long, rodlike micelles. In this way the gel structure is essentially similar to that now currently accepted for elastic solids such as rubber, gelatin, and various plastic materials (19).

Irrespective of the particular model assumed for the micelle, there are two main forces acting in it which serve to control its size and shape: van der Waals' attractive forces which act between neighboring $—CH_2—$ groups and thereby hold together the hydrophobic tails, and Coulombic repulsive forces which act between the polar heads and thereby tend to disrupt the micelle. Variation in both the van der Waals' and the Coulombic forces causes changes in the micellar shapes, and it is the influence on these two forces of the various factors outlined above that it is now proposed to examine in more detail.

Geometrical Considerations

Consider first the geometrical changes involved in the aggregation of n single soap molecules into a spherical micelle, followed by the flattening of the spheres into discs and the packing of X of them together to form a cylindrical micelle. If the fully extended hydrocarbon chain has a length L A. and its cross-sectional area is A A.^{2}, then the volume of the n molecules is $nAL\ A.^3$. If the center of the spherical micelle is assumed to be completely oily, its volume will also be nAL A.^{3}; its radius is given by

$$r = (3nAL/4\pi)^{1/3},$$

and its total surface area is

$$4\pi(3nAL/4\pi)^{2/3}. \qquad [1]$$

Since each molecule contains one polar head of cross-sectional area P A.^{2}, the total polar surface per spherical micelle is nP A.^{2}, and hence the total exposed hydrocarbon surface per spherical micelle is

$$4\pi(3nAL/4\pi)^{2/3} - nP. \qquad [2]$$

For X spherical micelles this becomes

$$4\pi X(3nAL/4\pi)^{2/3} - nXP. \qquad [3]$$

The volume of X spherical micelles is $nXAL$ A.^{3}, and this will also be the volume of the cylindrical micelle. If we assume the cylinder to have hemispherical ends, a radius R A., and a length (excluding the ends) of h A., it follows that

$$nXAL = \pi R^2h + ((4/3)\pi R^3. \qquad [4]$$

The total surface area is $4\pi R^2 + 2\pi Rh$, and hence the total exposed hydrocarbon surface per cylindrical micelle is

$$4\pi R^2 + 2\pi Rh - nXP. \qquad [5]$$

If we substitute for h from Eq. [4], this becomes

$$(4/3)\pi R^2 + nX[(2AL/R) - P]. \qquad [6]$$

Energy Considerations

Now consider the energy change associated with this conversion of X spherical micelles into one cylindrical micelle. If γ_{rw}, γ_{xw}, and γ_{rx} are, respectively, the surface energies in ergs/cm.^{2} between a hydrocarbon surface and water, a polar head surface and water, and a hydrocarbon and a polar surface, then, assuming the surface of a polar head in contact with the hydrocarbon surface also to be P A.^{2} and applying Eqs. [1]–[3], the total surface energy of the X spherical micelles is

$$[\{4\pi(3nAL/4\pi)^{2/3} - nP\}\gamma_{rw} + nP\gamma_{xw} + nP\gamma_{rx}]X \times 10^{-16} \text{ erg,}$$

which simplifies to

$$[4\pi(3nAL/4\pi)^{2/3}\gamma_{rw} + nP(\gamma_{xw} + \gamma_{rx} - \gamma_{rw})]X \times 10^{-16} \text{ erg.} \quad [7]$$

In a similar manner the total surface energy of the cylindrical micelle is

$$[\{(4/3)\pi R^2 + nX((2AL/R) - P)\}\gamma_{rw} + nXP(\gamma_{xw} + \gamma_{rx})] \times 10^{-16} \text{ erg,}$$

which simplifies to

$$[\{(4/3)\pi R^2 + 2nXAL/R\}\gamma_{rw} + nXP(\gamma_{xw} + \gamma_{rx} - \gamma_{rw})] \times 10^{-16} \text{ erg.} \quad [8]$$

Subtracting Eq. [7] from Eq. [8] gives the surface energy associated with the conversion as

$$\gamma_{rw}[(4/3)\pi R^2 + (2nXAL/R) - 4\pi X(3nAL/4\pi)^{2/3}] \times 10^{-16} \text{ erg.} \quad [9]$$

This energy change has come about solely as the result of the addition of electrolyte to the soap solution. Davies (20) has shown that Verwey and Overbeek's expression (21) for the energy of a diffuse double-layer system can be cast in the form

$$E = 6.1\sqrt{C}[\cosh(\psi e/2kT) - 1] \text{ ergs/cm.}^2, \quad [10]$$

where, as a first approximation, ψ is given by the Gouy Chapman expression

$$\psi = (2kT/e)\sinh^{-1}134/A_i\sqrt{C} \text{ millivolts.} \quad [11]$$

At room temperature $2kT/e$ has the value 51.2, A_i is the area per charge in A.^{2}, and C is the concentration of electrolyte in molarities. Substituting for ψ into Eq. [10] gives

$$E = 6.1\sqrt{C}[\cosh(\sinh^{-1}134/A\sqrt{C}) - 1]. \quad [12]$$

If C_s and C_c are, respectively, the electrolyte concentrations when spherical and cylindrical micelles exist, then the electrical energy change involved in the conversion is

$$6.1[\sqrt{C_c}\{\cosh(\sinh^{-1}134/A_c\sqrt{C_c}) - 1\}\{(4/3)\pi R^2 + 2nXAL/R\} \\ - \sqrt{C_s}\{\cosh(\sinh^{-1}134/A_s\sqrt{C_s}) - 1\}\{4\pi X(3nAL/4\pi)^{2/3}\}] \times 10^{-16} \text{ erg,}$$

where A_s and A_c are the appropriate surface areas per unit charge. It is now assumed that the surface energy change involved in going from X

spherical micelles to one cylindrical micelle will be of a similar order of magnitude to the electrical energy change in the same process. We may therefore write

$$\begin{aligned}&6.1[\sqrt{C_c}\{\cosh(\sinh^{-1}134/A_c\sqrt{C_c}) - 1\}\{(4/3)\pi R^2 + 2nXAL/R\}\\&\quad - \sqrt{C_s}\{\cosh(\sinh^{-1}134/A_s\sqrt{C_s}) - 1\}\{4\pi X(3nAL/4\pi)^{2/3}\}] \times 10^{-16}\\&\quad = K\gamma_{rw}[(4/3)\pi R^2 + (2nXAL/R) - 4\pi X(3nAL/4\pi)^{2/3}] \times 10^{-16}. \qquad [13]\end{aligned}$$

K is a factor which depends on the relative magnitudes of the electrical and surface energy changes. As a first approximation it will be assumed that $0.1 < K < 10$. Later it will be seen that when the appropriate values of the parameters have been substituted into Eq. [13] both the surface energy and the electrical energy of the one cylindrical micelle can be less than that of the X spherical micelles. This decrease in free energy shows that the cylindrical micelles will then be the favored form.

Equation [13] contains too many unknowns to be of much value on its own. A second relationship must therefore be sought which can be used in conjunction with it. The most likely line of approach seems to be offered by considerations of micelle stability.

The stability of a micelle has already been seen to depend on the relative magnitudes of the two forces—Coulombic and van der Waals'—which act in it, and it is thus necessary to derive a "stability of micelle" equation in terms of these two quantities which must also be satisfied if the process pictured is to have physical significance.

A micelle is stable provided that the work involved in introducing a further molecule into it, given by the expression $e\psi - W - kT$, is zero, *i.e.*,

$$e\psi - W - kT = 0,$$

where e is the electronic charge, ψ the surface potential, k Boltzmann's constant, T the absolute temperature, and W the van der Waals' energy per molecule. The conditions of stability for a spherical and cylindrical micelle are thus, respectively,

$$\begin{aligned}e\psi_s - W_s - kT &= 0,\\ e\psi_c - W_c - kT &= 0,\end{aligned} \qquad [14]$$

where the subscripts s and c refer to the spherical and cylindrical forms, respectively. The surface potentials in the two cases are given by the Gouy equation (Eq. [11]):

$$\begin{aligned}\psi_s &= (2kT/e)\sinh^{-1}134/A_s\sqrt{C_s}\\ \psi_c &= (2kT/e)\sinh^{-1}134/A_c\sqrt{C_c}\end{aligned} \qquad [15]$$

and combination of Eqs. [14] and [15] leads to

$$W_c/W_s = [2\sinh^{-1}(134/A_c\sqrt{C_c}) - 1]/[2\sinh^{-1}(134/A_s\sqrt{C_s}) - 1]. \qquad [16]$$

The left-hand side of Eq. [16] is the ratio of the average van der Waals' energy between molecules when these are in the form of cylindrical and spherical micelles, respectively. This ratio is not directly ascertainable by measurement. From the recent work of Reich (22), however, it may now be inferred that this ratio can be equated to the fraction of hydrocarbon surface which is covered when one type of molecular aggregate turns into another. Employing Eqs. [3] and [6], we may write

$$W_c/W_s = \frac{X[4\pi(3nAL/4\pi)^{\frac{2}{3}} - nP] - [(4/3)\pi R^2 + (2nXAL/R) - nXP]}{X[4\pi(3nAL/4\pi)^{\frac{2}{3}} - nP]} \qquad [17]$$

or

$$W_cW_s = 1 - [(4/3)\pi R^2 + nX((2AL/R) - P)]/X[4\pi(3nAL/4\pi)^{2/3} - nP], \qquad [18]$$

and combining Eqs. [16] and [18],

$$[2\sinh^{-1}(134/A_c\sqrt{\bar{C}_c}) - 1]/[2\sinh^{-1}(134/A_s\sqrt{\bar{C}_s}) - 1] = 1 - [(4/3)\pi R^2 + nX((2AL/R) - P)]/X[4\pi(3nAL/4\pi)^{2/3} - nP]. \qquad [19]$$

Equation [19] is what has been termed the "stability of micelle" equation. Used together with Eq. [13] it allows the following procedure to be adopted.

Of the parameters occurring in Eqs. [13] and [19] the following are known from the literature: $\gamma_{rw} = 52$ ergs/cm.^{2}, $P = 20$ A.^{2}, $A = 20$ A.^{2}, $L = 1.25$ A. per —CH$_2$— group. Since it has been postulated that the centers of both the spherical and cylindrical micelles are completely oily, it follows that both R and r must be less than $1.25N$, where N is the number of —CH$_2$— groups in the soap molecule. Equation [1] then requires that

$$n \ngtr 4\pi(1.25N)^2/3A.$$

The magnitudes of the remaining unknown parameters are restricted by several other considerations. Firstly, since it has been postulated that spherical micelles turn into cylindrical ones as the concentration of electrolyte is increased, it follows that C_c must be $> C_s$. Secondly, if Eq. [19] is put in the form $F = G + H/X$, it is seen that for X to be a positive number >1, G must be only slightly smaller than F, and the signs of $(F - G)$ and H must be the same. Thirdly, since A_c is unlikely to be greater than 150 A.^{2}, and since it is found experimentally that $C_c \ngtr 1.1$, F must be a positive quantity. Thus negative values of G will be inadmissible, since they would require X also to be a negative quantity. Finally, the values of n, X, and R which satisfy Eq. [19] with all the above restrictions in mind must still satisfy the requirements of Eq. [13]. This last restriction has been found of value in deciding between several possible combinations of cylinder dimensions for a particular soap system.

TABLE I

Variation in Area per Charge with Dimensions of Spherical Micelles

For spherical micelles area/charge, $A_s = 4\pi(3nAL/4\pi)^{\frac{2}{3}}/n$.

L	n	A_s	L	n	A_s	L	n	A_s
15	10	104	20	10	124	25	10	144
15	15	88	20	15	106	25	15	124
15	20	80	20	20	97	25	20	112
15	30	70	20	30	85	25	30	98
15	50	59	20	50	71	25	50	83
15	80	50	20	80	61	25	80	71

It has been found convenient, in working through the parameter combinations which satisfy both Eqs. [13] and [19], to prepare Tables I and II, which give the values of A_s and A_c for the various values of n, X, L, and R.

With the aid of these tables it is then possible to draw up a scheme which is illustrated briefly in Table III.

For any particular combination of n, X, L, and R the value of the right-hand side of Eq. [19] is expressed in the form $(G + H/X)$. Substituting in a value of X and taking the corresponding value of A_s and A_c from Tables I and II, respectively, we are then able to evaluate C_s from Eq. [19], C_c being the experimentally determined concentration of electrolyte which produces the viscoelastic gel. Only if C_c turns out to be $> C_s$ is it necessary to substitute for all the parameters to see if Eq. [13] is also satisfied. Provided both equations are satisfied, the parameter combination is "possible."

TABLE II

Variation in Area per Charge with Dimensions of Cylindrical Micelles

For cylindrical micelles area/charge, $A_c = [(4/3)\pi R^2 + 2nXAL/R]/nX$.

nX	L	R	A_c	nX	L	R	A_c	nX	L	R	A_c
100	15	15	49	200	20	10	82	400	25	8	126
100	20	15	63	200	25	10	102	400	15	6	100
100	25	15	76	200	15	8	76	400	20	6	134
100	15	10	64	200	20	8	101	400	25	6	167
100	20	10	84	200	25	8	126	800	15	15	41
100	25	10	104	200	15	6	101	800	20	15	55
100	15	8	78	200	20	6	134	800	25	15	68
100	20	8	103	200	25	6	167	800	15	10	61
100	25	8	128	400	15	15	42	800	20	10	81
100	15	6	102	400	20	15	56	800	25	10	101
100	20	6	135	400	25	15	69	800	15	8	75
100	25	6	168	400	15	10	61	800	20	8	100
200	15	15	45	400	20	10	81	800	25	8	125
200	20	15	58	400	25	10	101	800	15	6	100
200	25	15	71	400	15	8	76	800	20	6	134
200	15	10	62	400	20	8	101	800	25	6	167

TABLE III

Parameter Combinations Applied to Equations [13] and [19]

n	X	L	R	$(G + H/X)$	A_c	A_s	C_c	C_s	Remarks
33	3	20	15	$(0.46 - 0.46/X)$	63	82	0.25	0.40	Impossible (1)
20	5	20	10	$(0.22 - 0.27/X)$	84	97	0.25	0.24	Impossible (4)
20	5	20	8	$(-0.04 - 0.18/X)$	103	97	0.25	—	Impossible (2)
10	10	20	8	$(0.22 - 0.27/X)$	103	124	0.25	0.16	Impossible (4)
33	6	20	10	$(0.03 - 0.21/X)$	82	82	0.25	—	Impossible (3)
33	6	20	8	$(-0.32 - 0.14/X)$	101	82	0.25	—	Impossible (2)
20	10	20	9	$(0.21 - 0.26/X)$	82	97	0.25	0.24	*Possible*
20	10	20	8	$(-0.04 - 0.18/X)$	101	97	0.25	—	Impossible (2)
20	20	20	10	$(0.22 - 0.27/X)$	81	97	0.25	0.28	Impossible (1)
10	40	20	15	$(0.68 - 0.92/X)$	56	124	0.25	0.32	Impossible (1)
10	40	20	9	$(0.32 - 0.35/X)$	89	124	0.25	0.22	Impossible (4)
20	40	20	10	$(0.22 - 0.27/X)$	81	97	0.25	0.27	Impossible (1)

etc.

1. Because $C_c < C_s$.
2. Because $(F - G)$ and H have opposite signs.
3. Because C_s becomes negative.
4. Because Eq. [13] does not hold.

At this point it is necessary to consider in a little more detail what is meant by the quantity C_c. Strictly speaking the C occurring in the Gouy equation (Eq. [11]) refers to an ideal uni-univalent electrolyte, the concentration being sufficiently low for subsidiary anion adsorption onto the micelle to be negligible. Whereas these ideal conditions have clearly not been attainable in the present work, it is nevertheless logical to think that the results for the uni-univalent hydroxide and chloride will be more applicable to Eqs. [13] and [19] than will be those for the divalent carbonate or the trivalent phosphate. On the other hand, it has been noted that for all three soap systems now studied—oleate, oleylsulfate, and elaidate—the ratios of the molarities of univalent, divalent, and trivalent anions producing the viscoelastic maxima are proportional very nearly to 1.4/1.0/0.9. This is illustrated in Table IV.

This proportionality holds both for the sodium and for the potassium soaps; it has not been found explicable in terms of cation activities alone. Nevertheless it enables an "idealized" C_c to be calculated for the gels

TABLE IV

Electrolyte Concentrations Producing Viscoelastic Maxima

Anion	Na oleate *Molar*	K oleate *Molar*	Na oleylsulfate *Molar*	Na elaidate *Molar*
Cl'	0.48	1.1	0.25	0.34
CO_3''	0.38	0.8	0.16	0.25
Po_4'''	0.36	0.77	0.13	0.22

Mean values: Uni-/Di-/Trivalent::1.4/1.0/0.9.

produced by polyvalent anion electrolytes. Thus in the case of Na oleate, 0.38 M Na_2CO_3 produces the viscoelastic gel, but for the purpose of substitution into Eqs. [13] and [19] the value of C_c is taken as 0.53, *i.e.* $0.38 \times 1.4/1.0$. This procedure enables the results for all the different electrolytes to be reduced in effect to one. The errors are considered negligible in view of the semiquantitative nature of the analysis involved.

Taking C_c as 0.48, 0.34, and 0.25, respectively, for the Na oleate, elaidate, and oleylsulfate systems, and working through the scheme of Table III over the range $nX = 100$ to 800, it was found that only the values of the parameters shown in Table V satisfied, to the right order of magnitude assumed for K, both Eq. [13] and [19]. (The figure of about 10^{-12} erg for transforming 200 molecules in 10 spherical micelles into 1 cylindrical micelle implies that about 70 cal./gram-mole are involved in the conversion of one micelle type into the other. This is of the order expected for van der Waals' as opposed to chemical energy changes.)

The treatment outlined is not claimed to be more than semiquantitative in view of the several assumptions that have had to be made. Nor clearly is it an exhaustive one. Although isolated values of nX, *e.g.*, 2000, 5000, 10,000, did not yield satisfactory parameter combinations, it seems possible that, had the range been extended systematically, others might have been discovered. On the other hand, the results show that one important conclusion can be drawn: For the oleylsulfate and elaidate soap gels only a very limited number of cylindrical micelle types is possible; in the range considered, only one. For the oleate soaps, however, this number is increased, in the same range, to four. This conclusion of the existence of two different gel types—the one essentially homogeneous, consisting of only one type of cylinder, the other essentially nonhomogeneous and containing several different types of cylinders—leads very satisfactorily to an explanation of the following observed experimental facts:

1. The viscoelasticities of the oleylsulfate and the elaidate systems were very similar to each other but were markedly higher than those for the oleate systems. Measurements in the Weissenberg rheogoniometer

TABLE V

Satisfactory Parameter Combinations

Soap	n	X	L	R	*Equation [13]* L.H.S. $\times 10^{13}$, *ergs*	*Equation [13]* R.H.S. $\times 10^{12}$, *ergs*	K order of mag.
Na oleylsulfate	20	10	20	9	−5	−6	0.1
Na elaidate	20	10	20	9	−8	−6	0.1
Na oleate	20	5	20	10	−3	−7	0.1
	20	10	20	9	−11	−6	0.1
	10	20	20	8	−12	−20	0.1
	33	12	20	10	−34	−2	1

gave, for the former systems, a recoverable shear of the order of 20% and a relaxation time of the order of 0.02 sec., and for the latter systems a recoverable shear of the order of 4% and a relaxation time of the order of 0.002 sec. This considerable decrease in elastic properties could well be ascribed to the presence in the latter gels of weak links consisting either of short thin, or short fat, cylinders.

2. Under the influence of shearing forces or mechanical agitation a monodisperse, homogeneous gel would be expected to be more stable than a nonhomogeneous one. It was in fact found that the oleylsulfate systems were more stable to outside influence than were the oleate systems.

The picture of a relatively small, thin cylindrical micelle consisting of only a matter of hundreds of soap molecules differs from suggestions in the literature that the most probable form is one in which the cylinder has a radius equal to the length of the soap molecule and contains several thousand molecules. The observation that a temperature rise of only 5° is sufficient to destroy almost completely the elastic properties of all the soap gels supports the idea of small micelles, appreciably influenced by thermal Brownian collisions.

It is possible to evaluate the relative changes in the van der Waals' and the Coulombic energy terms in the conversion of 10 spherical micelles, each containing 20 molecules of Na oleylsulfate, into 1 cylindrical micelle of radius 9 A.

From Equation [17]

$$W_c/W_s = 1 - \frac{[(4/3)\pi(9)^2 + 200\{(2 \times 20 \times 20/9) - 20\}]}{10[4\pi(3 \times 20 \times 20 \times 20/4\pi)^{\frac{2}{3}} - 400]}$$

or

$$W_c/W_s \doteqdot 10.$$

This shows that the van der Waals' energy per molecule decreases by about 90% in going from spheres to cylinders.

The change in Coulombic energy involved in the conversion is obtained by considering Eq. [13]. From the left-hand side of Eq. [13] the total Coulombic energy of X spheres is

$$6.1\ [\sqrt{0.19}\{\cosh(\sinh^{-1}134/97\sqrt{0.19}) - 1\} \\ \{40\pi(3 \times 20 \times 20 \times 20/4\pi)^{2/3}\}] \times 10^{-16}$$

i.e., 12.1×10^{-12} erg, whereas of the one cylinder it is

$$6.1[\sqrt{0.25}\{\cosh(\sinh^{-1}134/90\sqrt{0.25}) - 1\}\{(4/3)\pi(9)^2 \\ + \frac{2 \times 20 \times 10 \times 20 \times 20}{9}\}] \times 10^{-16},$$

i.e., 11.6×10^{-12} erg. Hence in the same process the Coulombic energy decreases by about 5%. This decrease in both the van der Waals' and the

Coulombic energy in going from spheres to cylinders accounts for the greater stability of the cylindrical form at the electrolyte concentration producing gelling.

The micelle model proposed enables a number of other experimental observations to be logically explained. These are now discussed.

Flow Birefringence

It was found that at electrolyte concentrations producing maximum gelling, slight flow birefringence could be detected by subjecting the materials to shear in the standard form of coaxial cylinder apparatus. The effect, however, was too small to be measured quantitatively. Attempts to magnify it by increasing the rate of shear to large values only led to gel breakdown. No birefringence at lower electrolyte concentrations was detectable. This finding favored the view of a change from spherical to cylindrical micelles as the electrolyte concentration was increased.

Effect of Chain Length of Soap on Viscoelastic Properties

The soaps derived from octadecene combine a sufficiently high solubility in water with a carbon chain long enough for viscoelastic gels to be prepared. Unfortunately, it was not found possible to obtain the lower homologs in any state of purity, while the higher homologs, *e.g.*, erucic acid, are only very sparingly soluble in water. To explain the effect of chain length on gel properties in terms of the model adopted, it is therefore necessary to procede by inference. Experiments on Na tetradecyl and dodecyl sulfate showed that viscous, but nonelastic, and unstable gels are formed at approximately 0.4 and 0.6 M NaCl, respectively. An approximately 80%/20% mixture of oleic and hexadecenoic acids gives an elastic gel at approximately 0.65 M NaCl, whereas a similar mixture of oleic and erucic acids gives an elastic gel at approximately 0.35 M NaCl. Thus it is seen that the quantity of electrolyte for gelling, C_c, is increased as the chain length of the soap is decreased. If one assumes that C_c is approximately equal to 0.35 for Na dodecenyl sulfate, in which $L = 15$ A., it is found that in the range $nX = 100$ to 800 there is not a single combination of parameter dimensions that satisfies both Eqs. [13] and [19]. This means that cylindrical micelles, and hence elastic properties, cannot develop when the soap chain contains only 12 carbon atoms. For a chain of 20 carbon atoms, however, $L = 25$ A., and C_c will be less than 0.25; once again a limited number of cylindrical micelle types will be possible. A detailed analysis has not here been embarked upon, however.

The effect of chain length on elastic properties of the gels is illustrated by the results obtained on octadecene soap systems to which have been added small amounts of soaps possessing both longer and shorter carbon chains. One part in 10 of the appropriate saturated C-12 soap leads to a considerable diminution, while 1 part in 10 of the C-20 soap produces a slight increase in the elastic properties. As is to be expected, addition of the C-16 or C-18 soap has little effect. It is thus seen that, qualitatively at any rate, Schulman's conclusion (16) that in aqueous solutions elastic gels are produced only when the soap chains contain 16 or more carbon atoms is reasonably explained by the rather approximate treatment discussed above.

Effect of Addition of Long-Chain Alcohols

Following the pioneer work of Rideal and his co-workers, Schulman and Cockbain (23), Harkins and Mittelmann (13) and others have now clearly established that solubilization by soaps of long-chain alcohols takes place as a result of oriented penetration of the alcohol into the soap micelle. It gives rise to two effects. Firstly, owing to hydrogen bonding between the —OH and the —COOH polar heads, the water affinity of the latter groups is decreased, and in this way salting out of the complex micelle occurs at a lower concentration of electrolyte than that for the simple micelle. Secondly, since the alcohol molecules are not charged, their entry into the micelle leads to an increase in both A_s and A_c. The present investigation shows that the octadecene soaps solubilize a maximum of approximately one-tenth of their weight of oleyl alcohol. Using the subscript a to indicate a complex soap/alcohol micelle, it follows that for a spherical micelle containing 20 molecules of chain length $L = 20$ A., $A_s = 97$ A.^{2} and $A_{sa} = 107$ A.^{2}. When 10 of these micelles aggregate to form a cylinder of radius 9 A., we have $A_c = 90$ A.^{2} and $A_{ca} = 99$ A.^{2}. If the surface area of an —OH group is assumed to be the same as that of a —COOH group, it follows from Eq. [19] that

$$\frac{[2 \sinh^{-1}(134/A_c\sqrt{C_c}) - 1]}{[2 \sinh^{-1}(134/A_s\sqrt{C_s}) - 1]} = \frac{[2 \sinh^{-1}(134/A_{ca}\sqrt{C_{ca}}) - 1]}{[2 \sinh^{-1}(134/A_{sa}\sqrt{C_{sa}}) - 1]}$$

and by substituting in values for Na oleyl sulfate, $C_{ca} = 0.19$ M. The difference between this and the observed value of 0.14 M is due to hydrogen bonding effects. It is seen that the hydrogen bonding is quite small for this system.

In the analysis already outlined the replacement of $C_c = 0.25$ (no alcohol present) by $C_{ca} = 0.14$ (alcohol present) does not alter the fact that only a very limited number of cylindrical micelle types is possible. Hence, the presence of oleyl alcohol will not be expected appreciably to alter the elastic properties of the gels produced. This is found to be the case.

Applying exactly the same treatment to the Na oleate systems, however, it is found that the difference between $C_c = 0.48$ (no alcohol present) and $C_{ca} = 0.18$ (alcohol present) is much greater. This means that the presence of oleyl alcohol in this system should lead to a reduction in the number of different micelle types possible and should therefore produce an increase in elastic properties. Theoretically, since C_{ca} for Na oleate is nearly equal to C_{ca} for Na oleyl sulfate, one might expect the elastic properties of the two soaps containing oleyl alcohol to be equal. This was not found, the latter still being much higher. However, the presence of the oleyl alcohol did lead to some increase in the elasticities of the former systems, so that prediction and observation were in qualitative agreement at least.

When short-chain alcohols are added to soap systems, there must be a diminution in the radii of both the spherical and cylindrical micelles in order for the centers to remain completely oily. This has actually been confirmed experimentally (13). One would therefore expect elastic properties to be reduced. It was in fact found that 1 part in 10 of ethanol, propanol, or butanol almost completely destroyed the elasticity.

Effect of Perfluoro-Soaps

It has been seen that the micelle structure occurring in viscoelastic gels depends both on Coulombic forces, which may be influenced by addition of inorganic ions or alcohols, and on van der Waals' forces, which may be influenced by varying the chain length of the hydrophobic tails. An alternative method of altering the van der Waals' forces is by introducing $—CF_2—$ chains into the oily centers of the micelles.

It was found that addition of 1 part in 20 of perfluoro-hexanoate to oleate soaps produces almost exactly the same diminution in elastic properties as the same amount of laurate, while addition of 1 part in 20 of perfluorooctanoate or perfluorodecanoate has practically no effect. This shows that the van der Waals' forces in a $C_nF_{2n+1}COO'$ compound are almost exactly equal to those of the corresponding $C_{2n}H_{4n+2}COO'$ compound, and is therefore in agreement with the findings of Davies (24), who carried out surface potential measurements on these compounds. There are no data available for the dimensions of a $—CF_2—$ chain, and it is thus not possible to apply the above analysis to these results. Qualitatively, however, it appears that the $—CF_2—$ chains bind the hydrophobic portions of the micelle more firmly together than the corresponding $—CH_2—$ chains and thus increase the "strengths" of the cylinders.

ACKNOWLEDGMENTS

The author wishes to thank Professor Sir Eric Rideal, F.R.S., and Dr. J. T. Davies for constant interest and encouragement, and the Ministry of Supply for financial assistance.

SUMMARY

Viscoelastic gels are formed by the addition of electrolytes to aqueous soap solutions. The formation of such gels cannot be described by strictly thermodynamic reasoning owing to the number of factors involved and the

probable metastability of the systems themselves. By making a number of semiquantitative assumptions, however, equations may be derived which permit the explanation of gel formation in terms of the conversion of the soap from the form of small, detached spherical micelles into long, interlinked cylindrical micelles. One possible type of cylindrical micelle is thought to have a radius of about 9 A. and a length of about 200 A.

The mechanism proposed reasonably explains the gel properties of the soaps of sodium oleate, elaidate, and oleylsulfate, and the influence on these properties of small amounts of long-chain alcohols, other soaps, and perfluoro-compounds.

REFERENCES

1. KRAFFT, F., *Ber.* **29,** 1328 (1896).
2. DONNAN, F. G., AND POTTS, H. E., *Kolloid-Z.* **6,** 208 (1910).
3. MC BAIN, J. W., *Trans. Faraday Soc.* **9,** 99 (1913).
4. TARTAR, H. V., AND WRIGHT, K. A., *J. Am. Chem. Soc.* **61,** 539 (1939).
5. LOTTERMOSER, A., AND PUSCHEL, F., *Kolloid-Z.* **63,** 175 (1933).
6. HARTLEY, G. S., *Kolloid-Z.* **88,** 22 (1939).
7. HARTLEY, G. S., AND RUNNICLES, D. F., *Proc. Roy. Soc.* (*London*) **A168,** 420 (1938).
8. MC BAIN, J. W., "Colloid Science." Reinhold, New York, 1950.
9. HARKINS, W. D., *J. Am. Chem. Soc.* **69,** 1428 (1947).
10. KLEVENS, H. B., *J. Colloid Sci.* **2,** 301 (1947).
11. HARTLEY, G. S., "Aqueous Solutions of Paraffin Chain Salts." Hermann et Cie., Paris, 1936.
12. HARKINS, W. D., *J. Chem. Phys.* **16,** 156 (1948).
13. HARKINS, W. D., AND MITTELMANN, R., *J. Colloid Sci.* **4,** 367 (1949).
14. DEBYE, P., AND ANACKER, E. W., *J. Phys. & Colloid. Chem.* **55,** 644 (1951).
15. PHILIPPOFF, W., *Discussions Faraday Soc.* No. **11,** 96 (1951).
16. SCHULMAN, J. H., AND VAN DEN BERG, *Discussions Faraday Soc.* No. **11,** 147 (1951).
17. PHILLIPS, J. N., private communication.
18. DEBYE, P., *Ann. N. Y. Acad. Sci.* **51,** 573 (1949).
19. TRELOAR, L. R. G., "Physics of Rubber Elasticity." Clarendon Press, Oxford, 1949.
20. DAVIES, J. T., *Proc. Roy. Soc.* (*London*) **A208,** 224 (1951).
21. VERWEY, E. J. W., AND OVERBEEK, J. TH. G., "Stability of Lyophobic Colloids." Elsevier Publishing Co., New York, 1948.
22. REICH, I., private communication.
23. SCHULMAN, J. H., AND COCKBAIN, E. G., *Trans. Faraday Soc.* **36,** 651 (1940).
24. DAVIES, J. T., private communication.

SWELLING OF LATEX PARTICLES*

Maurice Morton, Samuel Kaizerman and Mary W. Altier

Rubber Research Laboratory, University of Akron, Akron, Ohio

Received November 17, 1953; revised April 2, 1954

Abstract

A theoretical relation has been derived for the equilibrium swelling of latex particles. The equilibrium solubility and rate of solution of solvents were measured on a series of polystyrene latex fractions of varying particle size. The solvents used were styrene, toluene, and chlorocyclohexane.

It was found, as predicted by theory, that the equilibrium amount of solvent imbibed by latex particles is a direct function of the particle diameter and an inverse function of the interfacial energy at the surface of the particles. The molecular weight of the polymer has no effect on the equilibrium swelling, within the range from 100,000 to several million molecular weight units. The rate of imbibition of these solvents appears to be extremely rapid, indicating that equilibrium solubility would appear to be maintained in most polymerization reactions.

The fact that a particular solvent is a "good" solvent for the polymer does not necessarily result in a greater swelling of the particles, since the solvent may show a higher interfacial energy against the aqueous phase.

The soap titration method is best for determining the average particle size of a latex for purposes of predicting equilibrium swelling.

Introduction

It is generally agreed that the emulsion polymerization of water-insoluble monomers proceeds largely within the latex particles. These polymer particles are generally capable of imbibing monomer, which is continually being converted to polymer. Hence, in any kinetic studies, the composition of the growing particles is of prime importance. Although it is well known that the polymer particles in a latex will absorb an equilibrium quantity of monomer, it has not been established whether such an equilibrium is reached or maintained during the course of polymerization. Harkins (1) has pointed out that the attainment of such an equilibrium would depend on the relative rates of polymerization and diffusion of the monomer from the free monomer phase to the particles. However, no data are available on these relative rates in any of the systems studied. Furthermore, in the case where an equilibrium quantity of solvent is absorbed by a latex, the factors governing this equilibrium have not been well established.

---

* Presented at the 122nd National Meeting of the American Chemical Society, Division of Polymer Chemistry, Atlantic City, New Jersey, September, 1952.

Certain approximate values for the equilibrium monomer-polymer ratio have been determined for several different systems, both in this laboratory (2) and elsewhere (3, 4), mostly in the course of kinetic studies. However, the variations which may be expected in the composition of these monomer-polymer particles and the parameters which control this composition have not been studied sufficiently. Smith (3) indicated what appeared to be a trend toward greater solubility of styrene in polystyrene latex of larger particle size. Harkins *et al.* (4) showed that the monomer-polymer ratio in a polystyrene latex decreased during the progress of a polymerization. A study of the factors governing this phenomenon has been made by Meehan (5). In the course of his investigation, Meehan found that the equilibrium solubility of monomer in the polymer particles was a minor function of the molecular weight of the polymer or the amount of emulsifier on the surface of the particles, but appeared to be very dependent on the size of the particles. However, the available data are insufficient for definite conclusions on these points.

THEORETICAL CONSIDERATIONS

It is obvious that the phenomenon of equilibrium swelling of a latex particle in the presence of free solvent is analogous to the equilibrium swelling of a polymer network and can be treated in a similar fashion to the treatment of swelling (6, 7). If no networks are present in the polymer particle, the restraining force which counterbalances the swelling force is simply the interfacial free energy between the latex particle and the aqueous phase. Hence, when the swollen particle is in equilibrium with free solvent, the following conditions exist:

$$\Delta \bar{F}_1 = \Delta \bar{F}_{m_1} + \Delta \bar{F}_t = 0 \qquad [1]$$

where $\Delta \bar{F}_1$ = partial molar free energy of the solvent;
$\Delta \bar{F}_{m_1}$ = osmotic contribution to $\Delta \bar{F}_1$;
$\Delta \bar{F}_t$ = interfacial free energy contribution to $\Delta \bar{F}_1$.

The evaluation of $\Delta \bar{F}_{m_1}$ can be carried out by the familiar Flory-Huggins expression, viz.:

$$\Delta \bar{F}_{m1} = RT\left[\ln(1 - v_2) + \left(1 - \frac{1}{n}\right)v_2 + \mu v_2^2\right]$$

where v_2 = volume fraction of the polymer in the swollen particle;
n = number average degree of polymerization;
μ = polymer-solvent interaction parameter.

The value of $\Delta \bar{F}_t$ can be deduced from a consideration of the increase in size of the interface as a function of the particle size and type of solvent. Thus, if r is the radius of the particle at swelling equilibrium, then let dr be the increase in radius caused by the imbibition of dn moles of solvent. The increase in surface area would then be $8\pi r dr$, and the increase in interfacial energy would be $8\pi r dr\gamma$, where γ is the value of the interfacial energy at swelling equilibrium. At the same time the increase in volume would be $4\pi r^2 dr$, which can also be written as dnM/ρ where M is the molecular weight of the solvent and ρ is its density. From this it follows that

$$8\pi r dr\gamma = \frac{2\,dnM\gamma}{\rho r} = \frac{2\,dnV_1\gamma}{r},$$

where V_1 = molar volume of solvent.

Hence the partial molar free energy contribution due to interfacial free energy can be expressed as

$$\Delta \bar{F}_t = \frac{2V_1\gamma}{r}. \qquad [2]$$

At equilibrium, therefore, it follows from Eq. [1] above that

$$\frac{2V_1\gamma}{rRT} = -\,[\ln(1 - v_2) + v_2 + \mu v_2^2] \qquad [3]$$

at high values of polymer molecular weight (n). Thus for a given polymer-solvent system, the swelling equilibrium of a latex particle should be a function only of its size, provided the interfacial energy is a constant quantity. Under such conditions, it should be possible to evaluate both μ and γ from a series of measurements, using the linear relation

$$-\frac{\ln(1 - v_2) + v_2}{v_2^2} = \mu + \gamma\,\frac{2V_1}{RTrv_2^2} \qquad [4]$$

With the above considerations in mind, a study was carried out of the equilibrium swelling of polystyrene latex particles by several solvents, as well as of the rate of swelling. In this study an attempt was made to maintain the interfacial tension (γ) at a constant value for any given solvent. Furthermore, to avoid complexities introduced by the distribution of particle sizes, the study was carried out on relatively homogeneous fractions of the latex obtained by fractional creaming.

Experimental Procedures

Materials

The materials used in preparing the polystryrene latex and in the fractionation and solubility work were as follows:

Distilled water, boiled to remove dissolved oxygen and stored under nitrogen.

Nitrogen, Linde high purity.

Styrene, Dow Chemical Co., distilled at reduced pressure to remove inhibitor.

Potassium laurate, prepared from Matheson lauric acid and recrystallized twice.
Potassium persulfate, reagent grade.
Sulfole mercaptan, as supplied by Phillips Petroleum Co.
Potassium chloride, reagent grade.
Diisopropylbenzenemonohydroperoxide, as supplied by Hercules Powder Co. and stated to contain 50% active peroxide.
Tetraethylenepentamine, as supplied by Carbide and Carbon Chemicals Corp., was distilled at 5 mm. pressure and the fraction of b.p. 174–178°C. was used.
Toluene, reagent grade.
Chlorocyclohexane, Eastman, b.p. 142–144°C.
Ammonium alginate, "Superloid" made by Kelco Co.

Preparation and Fractionation of Latex

Since substantial amounts of latex were required for this work, it was thought desirable to use the main fractions from latices specially prepared to yield an average particle size close to the desired size. The recipes used and the results obtained are shown in Table I. The term D_s refers to the average particle diameter obtained by soap titration, and D_w refers to that obtained by light scattering, as described below. Latex 106 was made for the purpose of obtaining a latex of the same particle size as Latex 102, but having a much lower molecular weight in the polymer, owing to the presence of the chain-transfer agent (Sulfole).

The above latices were subjected to fractional creaming by ammonium alginate, in order to obtain more homogeneous fractions. The fractionations were carried out in such a way as to remove the small particle size "tail" in the serum and the large particle size "head" in the cream. This made it posible to obtain a main fraction, representing between 20% and

TABLE I

Preparation of Polystyrene Latex

	Latex no.			
	103	102	106	104
Water	180	180	180	180
Styrene	30	100	100	100
Potassium laurate	5	5	5	1
Potassium persulfate	—	0.3	0.3	0.1
Sulfole mercaptan	—	—	0.3	
Potassium chloride	0.5	—	—	—
Diisopropylbenzenehydroperoxide	0.2	—	—	—
Tetraethylenepentamine	0.2	—	—	—
Temp. °C.	30	50	50	50
Avg. particle diam., D_s (A.)	290 550(D_w)	600	600	1600

50% of the original latex, and having a particle diameter close to the average diameter of the original latex. The amount of alginate required was determined for each latex and varied from 0.05% to 0.40% (based on latex weight). In each fractionation, the cream (bottom layer) was separated from the serum by centrifuging at 5000 r.p.m. for 1 hour, after which the serum could be easily decanted. For the creaming process, each latex was adjusted to a dry polymer content of about 10%.

In the case of Latex 102, in addition to obtaining a main fraction (having a particle diameter of ca. 800 A.), another smaller fraction was obtained (having a particle diameter of ca. 400 A.). This was done in order to obtain data on the effect of particle size on polymer molecular weight in the *same latex.*

Particle Size Determination

The particle size of the original latex was determined by the soap titration method of Maron *et al.* (8), whereas the particle size of the latex fractions was determined by means of light-scattering measurements with a Beckman Du spectrophotometer, using the method described by Maron and Ulevitch (9). The soap titration method, which measures the volume-to-surface ratio of the latex particles, ordinarily yields an average diameter of a polydisperse latex which is referred to as a volume-to-surface average (D_s). It is defined as

$$D_s = \frac{\Sigma n_i D_i^3}{\Sigma n_i D_i^2}.$$

The light-scattering method, on the other hand, yields a weight-average particle diameter (D_w) defined as

$$D_w = \left[\frac{\Sigma n_i D_i^6}{\Sigma n_i D_i^3}\right]^{\frac{1}{3}}.$$

Since the latex fractions were assumed to be relatively uniform with regard to particle size, the average diameter should be the same by any method of measurement. As a means of testing the monodispersity of the latex fractions, an attempt was made to measure the particle diameters by the soap titration method as well. However, it was found that the alginate apparently interferes with this method by occupying part of the surface of the particles, thus leading to low results in the calculation of surface area. This was indicated by the fact that a determination of the initial soap present in the latex fraction, by conductimetric titration (10), showed consistently higher results (moles soap per gram polymer) than found for the original unfractionated latex. Since the fractionation involves several dilutions of the latex, it might be expected that the soap content would be lower in the final fraction, owing to desorption from the surface of the particles. Hence it is strongly indicated that the alginate is interfering with the determination of soap content of the latex fraction, since ammonium alginate can react with the strong acids and bases used in this determination.

Under these conditions, it was impossible to determine the particle size of the latex fractions by soap titration. However, the fact that the creaming of the latex was quite sensitive to alginate concentration was an indication that relatively narrow fractions were obtained.

Interfacial Tension Measurements

Surface tension and interfacial tension measurements were done with the duNouy Tensiometer. The surface tension measurements on latex were required for establishing the extent to which the surface of the particles was covered with soap molecules. In this way a latex was considered "saturated" with soap when the minimum surface tension value was attained.

Measurements of the interfacial tension between the latex (aqueous phase) and the swelling solvent were carried out in an attempt to evaluate the interfacial energy (γ) at the surface of the swollen latex particles. Since these swollen particles generally contain a high proportion of polymer (up to 50% by weight), it was also necessary to determine the interfacial tension between the latex and appropriate polymer solutions. However, with high molecular weight polystyrene, it is not possible to obtain fluid solutions containing more than about 10% polymer. In order to test the effect of higher concentrations of polymer on the interfacial tension of the solution, it was necessary to prepare polystyrene of lower molecular weight, by bulk polymerization with benzoyl peroxide. This polymer yielded a fluid solution in styrene or toluene at a concentration as high as 40%. Neither the high nor the low molecular weight polymer showed any appreciable effect on the measured interfacial tension between the latex and the solvent; hence the values of γ used were those obtained for the given solvent.

Solubility Determination

The equilibrium solubility of the solvents in the latex was measured as follows:

Twenty-five milliliters of the latex (diluted to a polymer content of about 10%), together with an excess of solvent, was placed in a 40-ml. centrifuge tube. The tube was closed with a cork stopper and shaken for 1 hour, which was found to be ample for the attainment of equilibrium. Then a 4-in. hypodermic needle was inserted through the cork so as to reach almost to the bottom of the tube. The latter was centrifuged at 2000 r.p.m. for 30 minutes, resulting in a separation of the free solvent as the top layer. Then 10 ml. of the solvent-saturated latex was withdrawn through the needle by a hypodermic syringe, and transferred to a 100-ml. flask which was attached to a small distillation assembly. A few drops of acid were added to the latex (to prevent foaming), the latex frozen in a dry-ice mixture, the apparatus evacuated and sealed off. The solvent was then steam distilled over a steam bath, the solvent-water mixture being condensed in the receiver at ice-water temperature. The receiver was actually a long section of 7-mm. glass tubing, so that the amount of solvent could be read volumetrically. The solvent-water interface was quite sharp and the height of the solvent column could be read within 0.5 mm., representing 0.01 ml. Since the amount of solvent varied from 1 to 4 ml., this reading represented an accuracy of at least 1%. The distillation generally took about 4 hours, to ensure the collection of the last traces of solvent.

An important part of this work was the measurement of the swelling of latex particles whose surface was saturated with a monolayer of soap molecules. In order to do this, the above procedure was modified somewhat. First of all, the latex was titrated with soap, tensiometrically, to determine the amount of soap (potassium laurate) required to saturate the surface of the particles. Then the soap-saturated latex was saturated with the solvent as described above. However, as might be expected, the swollen particles should require additional soap to saturate the enlarged surface. Hence, an aliquot portion of the centrifuged latex was withdrawn through the needle and titrated with a soap solution to the minimum surface tension value. The correct amount of soap was then added to the whole sample of latex and the latter again shaken with excess solvent. This process was repeated until the surface tension values of the latex showed that no further addition of soap was required. This stepwise process was used in order to avoid having an excess of soap present at any time, since soap micelles might form and solubilize additional solvent. To minimize latex dilution, a 5% soap solution was used. Prior to use, the latex was neutralized to a *p*H of 10 to ensure that none of the soap was present as free fatty acid.

To determine the rate of solution of a solvent in the latex, 10 ml. of the latex (containing 1 g. polystyrene) was shaken in a graduated centrifuge tube with 3.5 ml. of the solvent, at about 160 strokes per minute, for varying periods of time. After each shaking period, the tube was centrifuged for 5 minutes at 2000 r.p.m. and the volume decrease of the solvent layer was noted. It was possible, at the beginning, to obtain a very sharp interface between the solvent and latex, so that the volume readings were accurate to within ±0.02 ml. However, after about 1 hour of shaking, the interface became progressively more diffuse, decreasing the accuracy of the reading to ±0.05 ml.

Molecular Weight Determination

The molecular weight of the polystyrene in each latex fraction was determined by measuring the intrinsic viscosity of the polymer in benzene at 30°C. The polymer was obtained by coagulating the latex in isopropanol. The viscosity measurements were carried out in a modified Ubbelohde viscometer, designed to permit several dilutions of the original benzene solution. In order to relate the intrinsic viscosity to the desired number-average molecular weight the following relation (11) was used:

$$\bar{M}_n = 178000\ [\eta]^{1.37}.$$

This equation applies to polystyrene obtained at low conversions in bulk polymerization, but is sufficiently accurate for the molecular weight differences encountered in this work.

RESULTS

Rate of Solution of Toluene in Polystyrene Latex

The rate at which toluene is imbibed by a polystyrene latex is shown in Table II. This solvent was chosen for this work since it is close to styrene in molecular size and structure. Furthermore, if the diffusion rate seriously affects the solution rate, then this should be more apparent for a relatively large molecule like toluene, which is bigger than that of most monomers encountered.

It can be seen that the saturation of the latex with toluene is virtually complete after the first half-hour of agitation. This agrees with the findings of Meehan (5) that butadiene can saturate a polybutadiene latex within a period of 20 minutes. The result is not surprising in view of the enormous surface area presented by the polymer particles toward the diffusing solvent molecules. Hence it appears that the diffusion rate of monomers into latex particles should not affect the rate of polymerization, since the particles can be kept in a saturated condition, except in some very extreme cases. For instance, from Table II it can be seen that a polystyrene latex particle can imbibe its own weight of toluene in about 10 minutes. A rate of polymerization sufficiently rapid to outstrip this rate of solution would not generally be encountered. Thus it can be assumed, in most cases, that latex particles are maintained in a state of equilibrium solubility with regard to any free monomer phase present, and that the monomer-polymer ratio in the particles during polymerization is represented by this equilibrium solubility, as long as a free monomer phase exists.

TABLE II

Rate of Solution of Toluene in Polystyrene Latex

(Latex fraction 102E, particle diam. 800 A., no added soap)

Time (*min.*)	Toluene absorbed (*ml./g. polystyrene*)	% Saturation of latex
5	1.00	61
10	1.25	76
15	1.40	85
20	1.55	94
90	1.65	100
210	1.65	100

Equilibrium Solubility in Polystyrene Latex

To determine the factors which govern the phenomenon of equilibrium solubility in a latex, three solvents were used, i.e., toluene, styrene, and chlorocyclohexane. The last solvent was chosen for the particular reason that it is a much "poorer" solvent than the other two, and should be expected to have a higher μ value. Its rating as a poor solvent was based on a comparison of the precipitation temperatures of polystyrene in toluene and chlorocyclohexane. Using a polystyrene of about 4.5 million molecular weight in a concentration in the vicinity of the theoretical critical volume fraction of polymer (12) (v_2 crit. $= \chi^{-1/2}$ where χ is the ratio of molar volumes of polymer to solvent), the precipitation temperature of the chlorocyclohexane was found to be about 260°K. compared to 160°K. for toluene, as determined by cooling experiments. Hence the chlorocyclohexane is a considerably poorer solvent than toluene.

The equilibrium solubility values found for the three solvents in latex fractions of different particle size are shown in Table III. The measured interfacial tension between the latex and the solvents was the same in all cases. The value obtained was 14 ± 1 dynes/cm. when the latex was "saturated" with soap and 19 dynes/cm. when no soap was added (Fraction 102E). The marked effect of added soap on the equilibrium swelling of the latex particles is shown very clearly in a comparison of the solubility of styrene in Latex Fraction 102E. Saturation of the particle surface with a layer of soap permits the particle to imbibe more than twice as much styrene as it would without added soap.

Fraction 106D was obtained from Latex 106, which was prepared specifically as a lower molecular weight polystyrene latex, in order to compare with Fraction 102E, which has a very similar particle size but a much higher molecular weight. The toluene solubility shows, as expected, that the polymer molecular weight is not a factor in the equilibrium solubility.

Fraction 102I represents a smaller particle size fraction obtained from the same original latex as Fraction 102E. It was used solely for a comparison of the molecular weight in large and small particles of the *same*

TABLE III

Equilibrium Solubility of Solvents in Polystyrene Latex

	Latex fraction no.					
	103B	102E	102E[a]	102I	104C	106D
Particle diameter (A.)	370	800	800	370	1730	840
Mol. wt. ($\bar{M}_n \times 10^{-6}$)	0.5	4.6	4.6	4.8	4.2	0.1
Solubility at 25°C. (g./g. polymer):						
Toluene	2.12	3.02	—	—	4.15	3.11
Styrene	1.81	2.93	1.50	—	4.60	—
Chlorocyclohexane	2.36	3.45	—	—	3.92	—

[a] Solubility measured with *no added soap*.

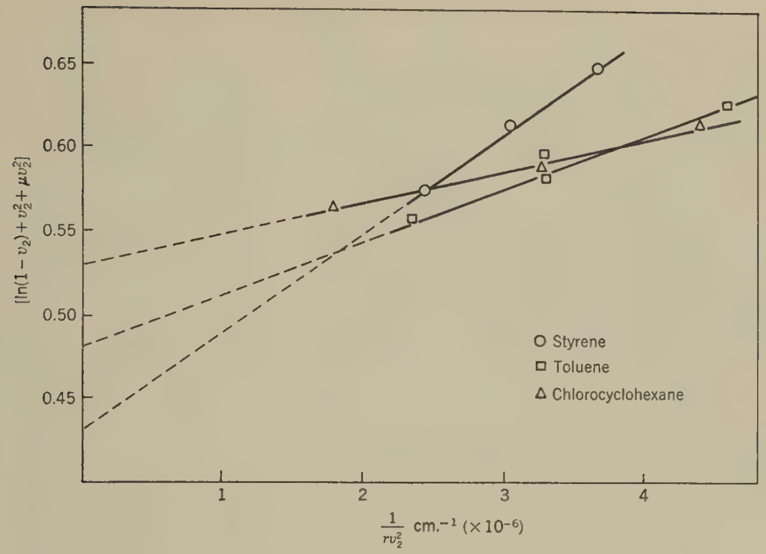

Fig. 1. Equilibrium swelling of polystyrene latex particles at 25°C.

latex. The data show no appreciable effect of particle size on molecular weight.

The equilibrium solubility data obtained for each solvent are shown plotted in Fig. 1 in accordance with Eq. [4]. This equation is, of course, based on the assumption that the interfacial free energy (γ) between the swollen particles and the aqueous phase is the same for all latex fractions and any given solvent, provided the surface of the particles is "saturated" with respect to soap. For the calculation of the volume fraction of polymer in the swollen particles (v_2) the specific gravity of polystyrene was taken as 1.06 at 25°C. and the volumes of polymer and solvent were considered as additive.

It can be seen from Fig. 1 that, for all three solvents, the experimental points lie on a straight line, as predicted by theory. From the slope and intercept of each line the following values can be obtained for the parameters μ and γ:

Solvent	μ	γ dynes/cm.)
Styrene	0.43	4.5
Toluene	0.48	3.5
Chlorocyclohexane	0.53	2.1

The value of μ for toluene can be compared with the one quoted in the literature (13) of 0.44. From this, and from the high value obtained for chlorocyclohexane, it can be inferred that the above μ values are somewhat high. However, the fact that any reasonable values at all can be obtained for this parameter on the basis of the assumption made supports the validity of Eq. [4]. The values for the interfacial free energy, γ, are all markedly lower than the measured value (*ca.* 14 dynes/cm.) and indicate that the measured value obtained from a plane interface does not represent the true interfacial energy at the surface of these very fine particles.

It is interesting to note the decreasing order of solvent power from styrene to chlorocyclohexane, which might have been predicted on the basis of available knowledge. This seems to be accompanied by a decrease in the interfacial free energy, so that the poorest solvent has the lowest value for interfacial free energy. Since polystyrene is a hydrocarbon polymer, it might be expected that a poorer solvent would be more hydrophilic and hence show a lower interfacial free energy. This opposing effect of μ and γ would help to explain why the poorer solvent, chlorocyclohexane, exerts a greater swelling effect on the smallest particles than does styrene. Obviously the higher surface-to-volume ratio in these smaller particles is the deciding factor. Conversely, for the largest particles, the smaller surface-to-volume ratio decreases the effect of the surface energy, and styrene, therefore, shows the highest swelling volume. The intermediate-size particles (800 A.) show a swelling volume which is not too different for all three solvents, apparently owing to a balance between the opposing effects of the μ and γ factors.

DISCUSSION

The experimental data show that, for any given solvent, the equilibrium solubility in latex particles is governed solely by the size of the particles and the interfacial energy between the particles and the aqueous medium. Thus the amount of solvent imbibed by the particles is a direct function of the particle size and an inverse function of the interfacial energy, in accordance with Eq. [3] as predicted by theory.

The swelling of a latex particle by different solvents depends not only on the type of solvent (μ factor) but on the effect of the solvent on the interfacial free energy of the particles (γ). Thus in the case of a hydrocarbon polymer such as polystyrene, a better solvent apparently shows a higher interfacial energy; hence the expected increase in swelling is not obtained in the case of the smaller particles, where the increased interfacial energy overrides the increased solvency effect. However, this relation between μ and γ may not hold for other polymers, especially those with polar functional groups.

It is interesting to consider the effect of Eq. [3] on the monomer-polymer ratio in latex particles during the course of an emulsion polymerization, since it can be assumed that the particles are maintained in a saturated or near-saturated condition as long as any free monomer phase exists. For any given system, the expression on the right side of Eq. [3] varies directly as the interfacial free energy (γ) of the particles and inversely as their radius

(r). During the course of a polymerization the particles increase in size, leading to an increase in γ, since the total amount of soap in the system is constant. If it is assumed that γ is thus directly proportional to the surface area of the particles, i.e., proportional to r^2, then the expression on the right side of Eq. [3] is directly proportional to r. Hence, over a period of polymerization when the conversion is doubled, the radius of the particle only increases by a factor of about 1.25, i.e., an increase of about 25%. Since the function $-[\ln(1 - v_2) + v_2 + \mu v_2^2]$ increases about two or three times as rapidly as v_2 (when $\mu \sim 0.45$), then, in the above case, v_2 can be expected to increase about 10% for a 100% increase in particle weight. This helps to explain why, during any given polymerization, the monomer-polymer ratio in the particles changes very little, as long as a free monomer phase exists.

It is also interesting to note the effect of particle size on molecular weight of the polymer formed. According to the Smith-Ewart (14) treatment of the kinetics of emulsion polymerization, the molecular weight of the polymer is dependent solely upon the rate of entry of free radicals from the aqueous phase into the polymer-monomer particles. On the basis of diffusion the rate of entry of such free radicals would be directly proportional to the radius of the particle. Hence a smaller particle would capture fewer free radicals, leading to the formation of a higher molecular-weight polymer. However, in any given latex, the interfacial free energy should be approximately the same (per unit area) for large or small particles. Hence the monomer-polymer ratio will be a direct function of particle radius, being smaller for smaller particles. Thus the rate of polymerization in the smaller particles will be less than that in the larger ones (lower monomer concentration). This will offset the slower rate of entry of free radicals into the smaller particles, leading to similar molecular weights in both large and small particles, as found.

Finally, some conclusions can be drawn concerning the effect of particle size heterogeneity on the solubility of solvents in a latex. It is obvious from the method of derivation of Eq. [3] that, for a polydisperse latex, the expression on the right side of Eq. [3] is proportional not to $1/r$ but to $\Sigma n_i r_i^2 / \Sigma n_i r_i^3$, where n_i represents the number of particles having radius r_i. Hence v_2 is a function of the particle diameter as expressed by D_s, i.e., a volume-to-surface average diameter. Hence the particle diameter, D_s, as determined by soap titration, should give the best measure on which to base conclusions concerning the equilibrium solubility of solvents in the latex.

ACKNOWLEDGMENT

This investigation was carried out under the sponsorship of the Office of Synthetic Rubber, Reconstruction Finance Corporation, in connection with the Government Synthetic Rubber Program.

REFERENCES

1. HARKINS, W. D., *J. Chem. Soc.* **69,** 1428 (1947).
2. MORTON, M., SALATIELLO, P. P., AND LANDFIELD, H., *J. Polymer Sci.* **8,** 215, 279 (1952).
3. SMITH, W. V., *J. Am. Chem. Soc.* **70,** 3695 (1948).
4. HERZFELD, S., ROGINSKY, A., CORRIN, M. L., AND HARKINS, W. D., *J. Polymer Sci.* **5,** 207 (1950).
5. MEEHAN, E. J., *J. Am. Chem. Soc.* **71,** 628 (1949).
6. FRENKEL, J., *Acta Physicochim. U. R. S. S.* **9,** 235 (1938).
7. GEE, G., *Trans. Faraday Soc.* **38,** 418 (1942).
8. MARON, S. H., private communication.
9. MARON, S. H., private communication.
10. MARON, S. H., private communication.
11. MAYO, F. R., GREGG, R. A., AND MATHESON, M. S., *J. Am. Chem. Soc.* **73,** 1691 (1951).
12. FLORY, P. J., *J. Am. Chem. Soc.* **73,** 1915 (1951).
13. HUGGINS, M. L., *Ann. N. Y. Acad. Sci.* **44,** 431 (1943).
14. SMITH, W. V., AND EWART, R. H., *J. Chem. Phys.* **16,** 592 (1948).

COLE-COLE'S CIRCULAR ARC RULE ON DYNAMIC PROPERTIES OF VISCOELASTIC MATERIALS

S. Takahashi

Electrotechnical Laboratory, Chiyoda-ku, Tokyo, Japan

Received March 5, 1954

I. Introduction

In 1950 Nolle (1) pointed out that the locus of his data for dynamic mechanical properties of Buna N in the complex compliance plane was a circular arc just as shown by Cole and Cole (2) in 1941 for various dielectrics in the plane of the complex dielectric constant. It was a remarkable advance in the phenomenological study of viscoelastic properties that Cole-Cole's useful experimental law was introduced into this new field. There has not, however, been further work to apply this rule to other data or to utilize this law for further discussions, simply because of the failure of Nolle's data for Buna N in the linearity test given by Cole-Cole.

The author has tested the validity of the circular arc rule on several series of dynamic mechanical data in the literature, and finds that this rule is also an excellent representation of these mechanical data. This paper presents these results.

II. Circular Arc Rule

Cole and Cole (2) found that the dielectric data for a large number of materials fall on circular arcs in the complex plane, as shown in Fig. 1. Each point along the arc corresponds to a different frequency. Points A and B at the left and right hands of the arc represent, respectively, the limiting values of the dielectric constant at the infinite frequency and at zero frequency, ϵ_∞ and ϵ_0. The arc is determined by these two values and by the parameter β, the geometrical significance of which is indicated.

Let the point P on the arc correspond to the angular frequency ω, and let the length of AP and PB be represented by u and v, respectively. The following relation (2) must hold, in general, for the linearity of the dielectric behavior:

$$\log (v/u) = \beta \log \omega\tau_m, \qquad [1]$$

when τ_m is the time constant for the most probable relaxation time. Therefore, the plot of log (v/u) against log ω should be linear, and the slope of the

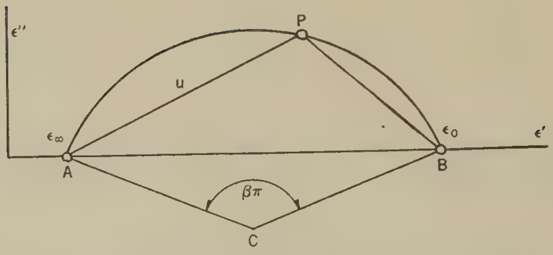

FIG. 1. Circular arc representation of dielectric data.

line should agree with the value of β obtained from the arc plot. They have shown also that the analytical expression of the complex dielectric constant $\dot{\epsilon}$, which satisfies the arc plot and the above relation, is as follows;

$$\dot{\epsilon} = \epsilon_\infty + \frac{\epsilon_0 - \epsilon_\infty}{1 + (j\omega\tau_m)^\beta}, \tag{2}$$

where $j = (-1)^{\frac{1}{2}}$.

This rule was introduced into the study of viscoelastic dynamic properties by Nolle (1). Figures 2*a*, *b*, and *c* are the transcriptions of his arc plots. The results, however, as mentioned by him, do not pass the linearity test (called the consistency test in his paper) of Eq. [1], that, the slope of the plot of log (v/u) against log ω is somewhat different from the value of β obtained from the arc plot. Therefore, Nolle thought that the Cole plot could not be taken as the basis for an analysis of the experimental results and gave up use of the circular arc rule for further discussion and for other data.

We notice, however, that the failure in linearity does not prove the unsuitability of the rule, but implies only nonlinear behavior of the material studied or the incorrectness of the experimental results. In this case the latter seems to be more probable than the former.

It is well known that the complex compliance $\dot{S}$, when it has linear characteristics, can be written most generally as follows:

$$\dot{S} = S_\infty + \int_0^\infty \frac{J(\tau)\,d\tau}{1 + j\omega\tau} - j\frac{1}{\omega\eta_0}, \tag{3}$$

where S_∞ is the real limiting value of $\dot{S}$ at infinite frequency, τ the retardation time, $J(\tau)$ the distribution function of retardation times, and η_0 the real limiting value of viscosity at zero frequency. When the circular arc rule is valid, the third term of the right-hand side of Eq. [3] is negligible and the second term must be

$$\int_0^\infty \frac{J(\tau)\,d\tau}{1 + j\omega\tau} = \frac{S_0 - S_\infty}{1 + (j\omega\tau_m)^\beta}. \tag{4}$$

The expression for $J(\tau)$, which satisfies the integral equation [4], is (2)

$$J(\tau) = \frac{1}{\pi\tau} \frac{(S_0 - S_\infty) \sin \beta\pi}{(\tau/\tau_m)^\beta + (\tau/\tau_m)^{-\beta} + 2 \cos \beta\pi}. \qquad [5]$$

III. Experimental Evidence

Blizard (3) has made measurements on three kinds of rubber over a fairly wide range of frequencies. Ferry and his co-workers (4) have made

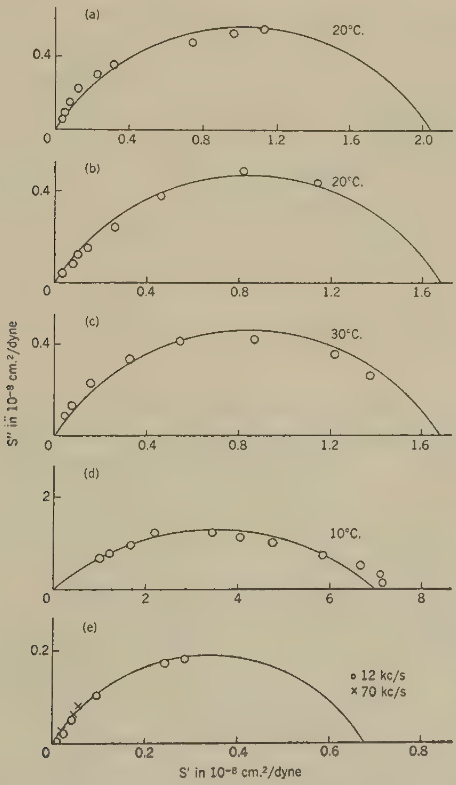

Fig. 2 (*a*) Compliance data for Buna N (Hycar OR-15, 100; ZnO, 5; butyl-8, 10 ml.; methyl ethyl ketone, 480; 20 minutes milling; solvent cast) plotted in the complex plane (transcribed from Nolle's report (1)).

(*b*) and (*c*) Compliance data for Buna N (Hycar OR-15, 100; P33 black, 50; S, 2; ZnO, 5; butyl-8, 10 ml.; methyl ethyl ketone, 480; benzoic acid, 2; 15 minutes milling; solvent cast) plotted in the complex plane (transcribed from Nolle's report (1)).

(*d*) Compliance data for natural rubber (crepe rubber, 100; ZnO, 3; diphenylguanidine, 1; 30 minutes at 147°C.) in the complex plane (based on Nolle's data (1)).

(*e*) Compliance data for Buna N (Hycar OR-15, 100; ZnO, 5; S, 2; stearic acid, 1.5; Thiuram M, 1; mercaptobenzothiazole, 0.5; 40 minutes at 153°C.). Locus in the complex plane when the frequency is fixed and the temperature is varied (based on Nolle's data (1)).

measurements on polyisobutylene at various frequencies and temperatures and have made clear that the mechanical properties of polyisobutylene are "thermorheologically simple" (5).

In general, the complex compliance $\dot{S}$ is the function of the two variables, the angular frequency ω and the absolute temperature T. If there exists a function $f(T)$ with which $\dot{S}$ can be expressed as the function of the single variable $x = \log \omega + f(T)$, the property is called "thermorheologically simple."

To check the rule, these data can be utilized as well as some of Nolle's data (1) which have not been tested. Though the circular arc rule holds originally only for the locus obtained when the frequency is varied and the temperature is fixed, it can be extended in the thermorheologically simple case to the locus obtained when the frequency is fixed and the temperature is varied. (In this case the linearity test is also applicable, taking $f(T)$ instead of $\log \omega$ as the horizontal axis.)

Since the data in the literature are expressed by the complex modulus

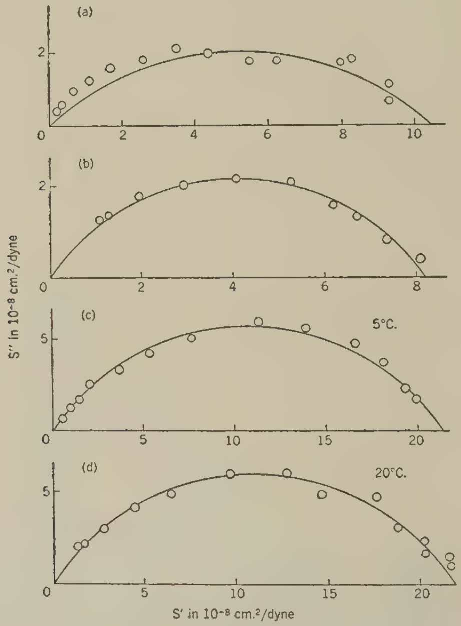

FIG. 3 (*a*) Compliance data for Hycar (Hycar OR-15, 100; P33, 50; ZnO, 5; benzoic acid, 2; butyl-8, 8) in the complex plane (based on Blizard's data (3)). The temperature of the sample is not described in the paper.

(*b*) Compliance data for crepe rubber (crepe, 100; ZnO, 5; S, 2; butyl-8, 8) in the complex plane (based on Blizard's data (3)). The temperature of the sample is not described in the paper.

(*c*) and (*d*) Compliance data for butyl rubber (GR-1 70, 100; ZnO, 5; S, 2; stearic acid, 1.5; Thiuram M, 1; mercaptobenzothiazole, 0.5) in the complex plane (based on Blizard's data (3)).

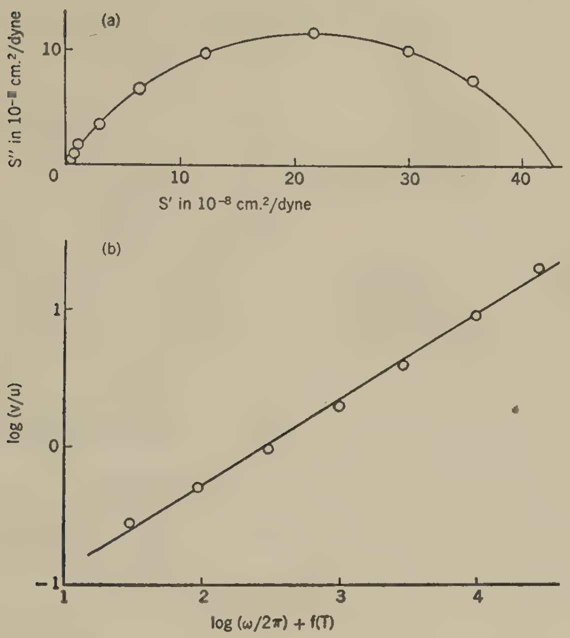

FIG. 4 (*a*) Compliance data for polyisobutylene (molecular weight 1.2×10^6). Locus in the complex plane when both the frequency and the temperature are varied (based on data of Ferry and his co-workers (4)).

(*b*) The plot of $\log (v/u)$ against $\log \omega + f(T)$ for polyisobutylene. In this case $\log \omega + f(T)$ must be taken as the abscissa, since both the frequency and the temperature are variables.

or the dynamic rigidity and the viscosity, these are transformed into data expressed by the complex compliance to be plotted in the complex plane. Results are as shown in Fig. 2*d* and *e*, 3, and 4*a*. All the loci examined here are fairly well represented by circular arcs.

Let us now examine the results by means of Eq. [1]. The plot of $\log (v/u)$ against $\log \omega + f(T)$ for polyisobutylene, for instance, the locus for which is shown in Fig. 4*a*, becomes a straight line as shown in Fig. 4*b*, and its slope satisfactorily coincides with the value of β obtained from the arc. Also the results based on Blizard's data pass this linearity test.

From the plot such as Fig. 4*b*, the time constant, or the most probable retardation time, is determined as the reciprocal of the angular frequency that makes $\log (v/u) = 0$. In Table I are given S_0, τ_m, β, and β', which is the slope of the frequency plot as in Fig. 4*b*, for the data plotted in Figs. 2–4.

Comparing the results with those for dielectric properties, we note the following facts:

1. S_∞ is far smaller than S_0. (For dielectric properties ϵ_∞ is usually comparable to ϵ_0.)

TABLE I

Constants Determining the Dynamic Compliance for Several Materials

Fig.	Reference	Materials[a]	Temp. °C.	S_0, 10^{-8} cm.²/dyne	β	β'	τ_m, sec.
2*a*	Nolle (1)	Buna N	20	2.04	0.67	0.53	3.7×10^{-3}
2*b*	Nolle (1)	Buna N	20	1.67	0.65	0.56	5.8×10^{-3}
2*c*	Nolle (1)	Buna N	30	1.67	0.65	0.54	1.4×10^{-3}
2*d*	Nolle (1)	Natural rubber	10	7.0	0.45	—[b]	—
2*e*	Nolle (1)	Buna N	—[c]	0.67	0.65	—	—
3*a*	Blizard (3)	Hycar	—[d]	10.4	0.51	0.51	6.5×10^{-2}
3*b*	Blizard (3)	Crepe rubber	—[d]	8.2	0.63	0.65	2.0×10^{-3}
3*c*	Blizard (3)	Butyl rubber	5	21.3	0.64	0.63	3.6×10^{-2}
3*d*	Blizard (3)	Butyl rubber	20	21.9	0.63	0.63	6.7×10^{-3}
4*a*	Ferry and others (4)	Polyisobutylene	—[e]	42.8	0.63	0.63	5.8×10^{-4}

[a] Details on the materials have been described in the legends for figures.

[b] In this case the plot of log (v/u) against log ω has not been linear, so that β' and τ_m have not been obtainable.

[c] The frequency was fixed and the temperature was varied.

[d] The temperature of the sample is not described in the paper.

[e] Both of the temperature and the frequency were varied. The value of τ_m in the table is for 25°C.

2. Both S_0 and β are almost invariable with temperature (thermorheologically simple). (For dielectric properties ϵ_0 decreases and β increases as the temperature increases.)

3. The value of β is near 0.6 and almost constant for several materials studied here.

It is also noticeable that the viscoelastic dynamic data are abundant in high frequency ranges, but so few in low frequency ranges that we can find only a few series of data in the literature from which complete arcs can be obtained.

IV. THE EFFECT OF PLASTIC DEFORMATION

When the third term of the right-hand side of Eq. [3] is not negligible, this masks the imaginary part of the second term at low frequencies. The plot in the complex plane, therefore, cannot be represented by a circular arc, even if the second term satisfies Eq. [4]. Figure 5*a* and the upper curve of Fig. 5*b* are examples of such plots. The former is based on Nolle's data (1) for unvulcanized Buna N, and the latter on those of Ferry and his co-workers (6) for concentrated solutions of polyvinylacetate. Though Ferry and his co-workers have mentioned that the circular arc rule is not valid for their data, it is not clear whether the effect of plastic deformation was taken into account.

Since the static viscosity has been given in this case, the intrinsic value of the imaginary part of the complex compliance not influenced by the plastic deformation can easily be obtained by subtracting $1/\omega\eta_0$ from the observed imaginary part of the complex compliance. The complex plane plot of such values is the middle curve of Fig. 5*b*, which also cannot be represented by a circular arc.

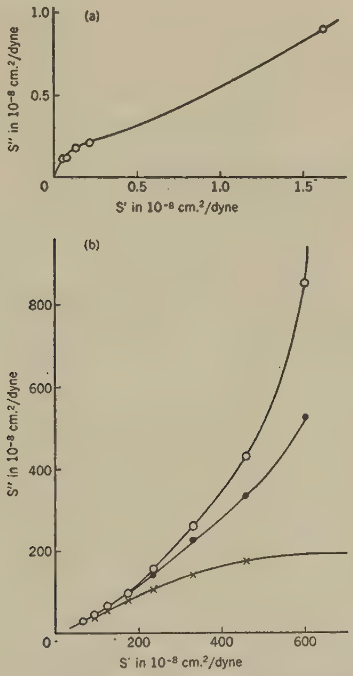

FIG. 5 (*a*) Compliance data for unvulcanized Buna N (Hycar OR-15; 20 minutes milling; cast as 20% solution in methyl ethyl ketone) in the complex plane (based on Nolle's data (1)).

(*b*) *Upper curve*: compliance data for concentrated solution of polyvinyl acetate in 1,2,3-trichloropropane in the complex plane (based on data of Ferry and his co-workers (6)). *Middle curve*: complex plane plot obtained by subtracting $1/\omega\eta_0$ from the observed imaginary part. *Bottom curve*: complex plane plot of $S' - jS''_{\text{cal}}$.

In such a case Cole-Cole's linearity test is not applicable, and if we want to examine the consistency of the experimental results with the linearity, the following Gross's general relation (7) will be the only aid

$$S''_{\text{cal}}(\omega) = \frac{2}{\pi}\int_0^\infty (S'(\mu) - S_\infty)\,\frac{\omega^2}{\omega^2 - \mu^2}\,d\mu. \qquad [6]$$

Putting the real part of the observed complex compliance into the integrand of the right-hand side of this relation, we can also get S''_{cal}, the imaginary part of the complex compliance not influenced by the plastic deformation, which must agree with the one obtained directly by subtracting $1/\omega\eta_0$ from the observed one, only if the properties have linear characteristics.

In practice, however, the integration is quite troublesome. The author has obtained the following approximate formula from the above relation, the deduction of which has been given elsewhere (8)

$$S''_{\mathrm{cal}}(x) = \sum_{1}^{4} A_n[S'(x + n) - S'(x - n)], \qquad [7]$$

where $A_1 = 0.468$, $A_2 = 0.077$, $A_3 = 0.030$, $A_4 = 0.016$, $x = \log_e(\omega_m/\omega)$, and ω_m is an arbitrary and constant angular frequency. This formula gives a good approximation, excluding the case of a sharp frequency dependence as given by Debye type dielectric properties.

S''_{cal} does not agree with $S''_{\mathrm{obs}} - (1/\omega\eta_0)$ for the data of Ferry and his co-workers. This means that the experimental results are influenced by some errors or some nonlinear mechanisms. It is, however, interesting that if we plot $S' - jS''_{\mathrm{cal}}$ instead of $S' - jS''_{\mathrm{obs}}$ in the complex plane, the locus becomes the bottom curve of Fig. 5*b*, which seems to be a part of a circular arc.

SUMMARY

The validity of the circular arc rule, found by Cole and Cole for dielectric properties and introduced by Nolle into the field of the dynamic studies of viscoelastic materials, has been tested on Nolle's, Blizard's, and Ferry's dynamic mechanical data in the literature. This rule is an excellent representation of the data examined here, excluding the failure of Nolle's data in the linearity test given by Cole and Cole. This failure, which made Nolle abandon the rule, never means directly the unsuitability of the rule. Some consideration has been given to the effect of plastic deformation and the linearity test of such data as do not satisfy the rule.

REFERENCES

1. NOLLE, A. W., *J. Polymer Sci.* **5**, 1 (1950).
2. COLE, K. S., AND COLE, R. H., *J. Chem. Phys.* **9**, 341 (1941).
3. BLIZARD, R. B., *J. Appl. Phys.* **22**, 730 (1951).
4. FERRY, J. D., FITZGERALD, E. R., JONSON, M. F., AND GRANDINE, L. D., *J. Appl. Phys.* **22**, 717 (1951).
5. SCHWARZL, F., AND STAVERMAN, A. J., *J. Appl. Phys.* **23**, 838 (1952).
6. FERRY, J. D., SAWYER, W. M., BROWNING, G. V., AND GROTH, A. H., JR., *J. Appl. Phys.* **21**, 513 (1950).
7. GROSS, B., *Phys. Rev.* **59**, 748 (1941).
8. TAKAHASHI, S., *J. Inst. Elec. Engrs. Japan* **73**, 579 (1953).

A SIMPLE METHOD FOR THE PRODUCTION OF HOMOGENEOUS WATER DROPS DOWN TO 1 MICRON RADIUS

Duncan C. Blanchard

Woods Hole Oceanographic Institution[1]

Received April 29, 1954; revised May 26, 1954

Abstract

A simple method for the production of homogeneous water drops down to 2 μ diameter is described. When bubbles of a given size burst at an air-water interface, the collapse of the bubble cavity produces an upward moving jet which quickly disintegrates into several small drops. Each of these drops, not necessarily all the same size, rises to a height which is remarkably constant from one bubble to the next. The drop size at each of these heights was found to be equally constant.

Photographs are shown of the drops produced and their remarkable uniformity in size. The size of the drops is a function of the bubble size.

Introduction

Those who have used hypodermic needles to produce water drops of a given size for calibration purposes know only too well the difficulty involved in producing drops $<$ about 1 mm. diameter. Surface tension considerations require that the bore diameter of the needle be many times less than that of the drop. At such small diameters high pressures are required to force the water through the bore, and, as solid materials in the water will clog the tube, the water must be filtered prior to using.

Drops down to 0.2 mm. diameter have been produced with hypodermic needles and microburets by passing a stream of air concentrically around the tip where the drops are being produced (1, 2). In the presence of the air stream the drops are blown free at a diameter far less than they would have in the absence of the air stream. However, even these techniques are inadequate to produce drops $<100\ \mu$ diameter. The production of homogeneous clouds of drops $<100\ \mu$ has been accomplished by utilizing the centrifugal forces associated with water on spinning discs. With an apparatus utilizing this principle, Walton and Prewett (3) produced monodisperse clouds from 15 μ to 3 mm. diameter. An improved model was capable of extending the lower limit to 6 μ (4). An entirely different method for the production of a

---

[1] This study was supported by the Office of Naval Research, Contract Nonr-798(00) (NR-085-001). Contribution No. 711 of the Woods Hole Oceanographic Institution, Woods Hole, Massachusetts.

monodisperse cloud, recently discussed by Vonnegut and Neubauer (5), produces streams of electrified uniform drops of about 0.1 mm. diameter by applying potentials of 5–10 kv. (a.c. or d.c.) to liquids in small capillaries. Under some conditions a smoke of particles of about 1 μ diameter can be produced. Drozin (10) has extended these electrical studies.

The present paper will describe a simple method for the production of homogeneous drops from about 500 down to at least 2 μ diameter. The experimental setup requires simply a stream of bubbles rising in a beaker of water. The realization that uniform drops could be systematically produced with such a simple apparatus came out of a photographic study (6) of the mechanism of the bursting of bubbles at an air-water interface (7). High-speed photographs conclusively showed that upon the collapse of a bubble a narrow jet rises rapidly from the bottom of the bubble cavity. Within a distance of perhaps one bubble diameter the jet proceeds to break up into five or six drops, all of which rise to characteristic heights. With the same bubble size these heights are systematically obtained, thus indicating the reproducibility of the various drop sizes at different levels.

These phenomena have been studied, in connection with different problems, by other investigators. Stuhlman (7) was interested in the problem of effervescence and was the first to suggest the jet mechanism as being responsible for the production of drops from breaking bubbles. Boyce (8), in connection with studies of the deposition of airborne salt particles on coastal plants, obtained data for the average diameter of drops ejected by bubbles in sea water as a function of bubble size. However, as neither Stuhlman nor Boyce studied the breaking bubble mechanism as a source of homogeneous drops, it was felt worth while to present the ideas contained in this paper.

Experimental Methods

The production of a steady stream of uniform bubbles of any diameter $>50\ \mu$ is easily accomplished by forcing air through fine tips produced by drawing out a length of glass capillary tubing. The size of the bubble is, of course, a function of the bore diameter. The smallest bubbles are produced from hairlike tips with an air pressure of approximately 30 p.s.i.

If the bubbles are allowed to rise in distilled water, they will break immediately on contact with the surface, providing the surface is clean. It is sometimes necessary to have the glass capillary tip near the surface to prevent the coalescence of bubbles as they rise through the water. However, if both these precautions are observed, a uniform and systematic breaking of the bubbles will occur. As each bubble breaks, the upward moving high velocity jet will form and break into a series of droplets. These droplets rise at speeds, estimated both from analysis of high-speed photographs and by computation, of several hundreds of cm. sec.$^{-1}$. The frictional retarding

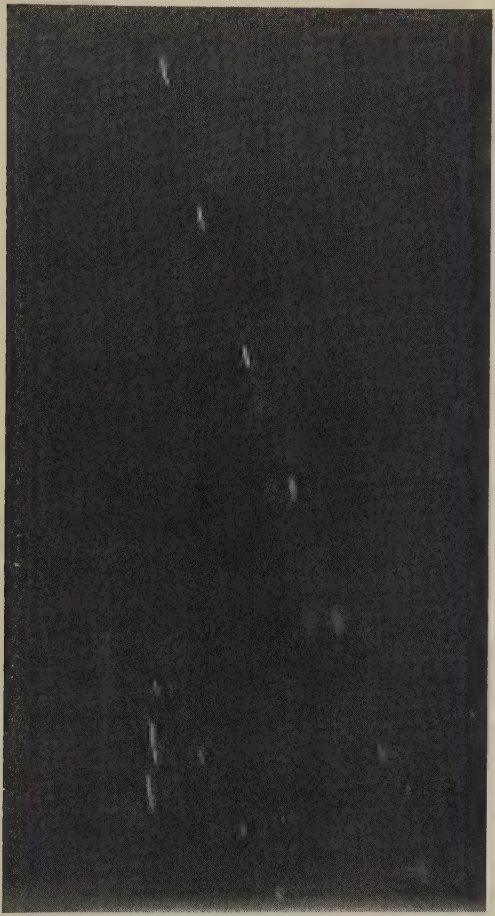

FIG. 1*a*. A photograph, taken at an exposure of 0.01 sec., of the homogeneous drops produced by the breaking of bubbles of approximately 450 μ diameter. The length of the streaks is a function of the fall velocity of the drops and this is directly related to the drop diameter. The water surface is slightly beneath the bottom of the photograph (see Fig. 1*b*). The vertical streak in the lower left center represents a drop moving rapidly upward from the bubble cavity.

force at such high speeds causes a rapid deceleration and loss of kinetic energy of the drops. For a given bubble diameter each of the drops will rise to a height which is remarkedly reproducible. If a slow drift of air exists over the water surface, the drops will fall at an angle to the vertical. This is illustrated in the photograph of Fig. 1*a*, where the bubbles are breaking in rapid succession so that six or more drops from the highest trajectory are simultaneously air-borne. This photograph was made at 0.01 sec. exposure with the aid of forward scattered light. With smaller bubbles and a higher rate of production one is able to produce drops at such a rate that 30 or more of the drops from the top trajectory are air-borne simultaneously.[2] This simple experiment, with the great uniformity of the settling rates of the drops formed, soon convinces one of the homogeneity of the drop diameters.

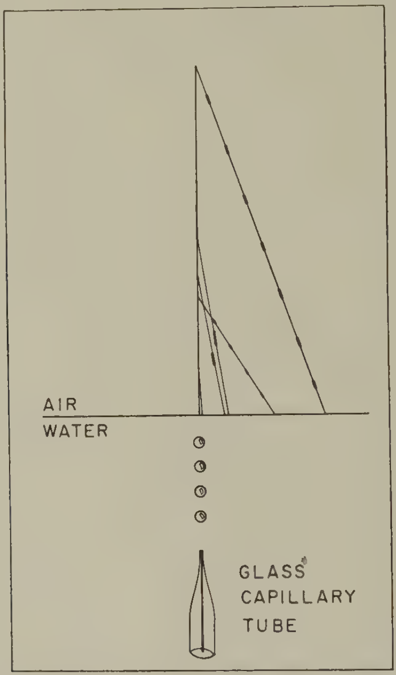

Fig. 1*b*. A drawing based on Fig. 1*a* to show the most probable trajectories of the drops. The heavy dashed lines represent the drops as shown in 1*a*, while the light solid lines indicate the trajectories.

Results

Figure 1*b* is a drawing, based on the photograph of Fig. 1*a*, to show the most probable trajectories of the drops. Note that the second and third trajectories from the top are represented in the actual photograph by single drops. These drops are sufficiently large and fall back to the surface at such a rate as to prevent more than one drop for each trajectory from being air-borne at any one time. The lowest trajectory on the drawing represents a fifth drop which did not happen to be air-borne during the brief exposure for the photograph. This drop is the largest of all the drops and even on its downward flight is discernible to the eye only as a streak of light.

---

[2] These drops are usually invisible to the unaided eye in normal daylight. They are best made visible by viewing against a black background and looking at an angle of about 140° as measured along a strong beam of light.

A crude estimate of the drop sizes represented by Fig. 1*a* can be obtained with a knowledge of their fall velocities and Stokes' law. The fall velocities were obtained by measuring the vertical component of the streaks, which represents the drops motion during the exposure, and dividing by the exposure time. With the fall velocities of the drops from the four different trajectories thus obtained, Stokes' law can be used, starting with the top trajectory, to obtain drop diameters of about 60, 75, 70, and 40 μ, respectively.

These diameter calculations have been mentioned only to indicate roughly the range of droplet sizes produced by a breaking bubble of the size used in the illustration (approx. 450 μ diam.). However, it might be well, for this and any future experiments, to qualify the use of Stokes' law. In the first place significant errors can be obtained with Stokes' law when it is applied to drops above about 70 μ diameter. With a diameter of 70 μ Stokes' law will give a fall velocity some 5% in excess of that actually obtained. Secondly, in the present case, one must assume that there is no effect on the fall velocity by updrafts created by the bursting bubbles. Although an updraft exists in a region within a few bubble diameters of the axis of the jet, its effect on the drop is negligible if a slight horizontal drift of the air serves to carry the drops far outside the updraft region (see Fig. 1*a*). In these regions the absence of any pronounced microturbulence in the air structure due to the jet updraft is indicated by the uniform settling velocities of the drops. It goes without saying that greater over-all accuracy is obtained in the foregoing considerations if evaporation of the drops in their trajectory is eliminated by enclosing the area and allowing the vapor pressure of the air to come into equilibrium with that of the water surface. Indeed, the writer has found this imperative for the study of small drops.

The homogeneity of the drops produced by the top trajectory of Fig. 1*a* is illustrated by Fig. 2. This is a photograph of the imprints of the drops on an ammonium chloride coated slide. The diameter of the imprints shown in Fig. 2 was several times the diameter of the drops. This is probably explained by the high solubility of NH_4Cl in water. Nevertheless, regardless of the ratio between the diameter of the imprints and the drops, the uniformity of the imprints testifies to the remarkable uniformity of the drop size from the top trajectory. The other trajectories produce their own uniform drops, but the upper one, being more readily accessible, was preferred as the source of uniform drops in the present study.

The drop diameters and the heights to which they are ejected is a function of bubble size and is dependent on whether the bubbles are breaking in sea or distilled water. Figure 3 is a graph of bubble size vs. the heights of the ejected drops. The solid lines are the results of measurements in distilled water by Stuhlman (7), who found six drops produced by the majority of bubbles. The dashed line represents some recent measurements of Boyce (8) in sea water. Note that he was concerned only with the top drop. A maximum ejected height is found in each case, with the drops from bubbles in sea water rising higher (for bubbles $>800\ \mu$) and reaching a maximum height at a greater bubble diameter than the same bubbles in distilled water.

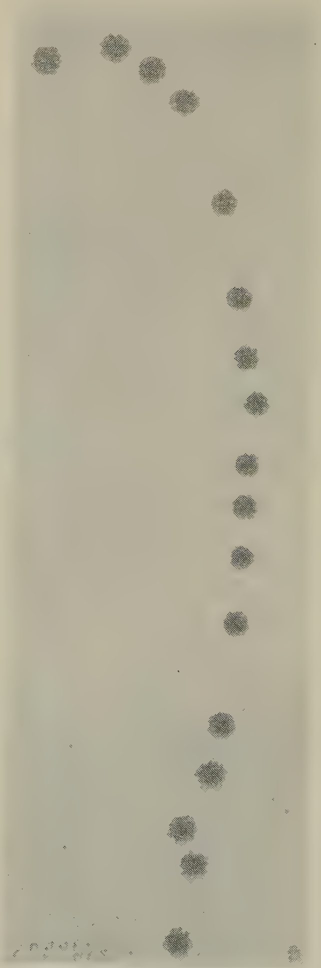

FIG. 2. Imprints of drops on an ammonium chloride coated slide. These drops represent those ejected to the greatest height when bubbles of 450 μ diameter break at an air-water interface. (See the top trajectory of Fig. 1*a* and 1*b*.)

Boyce (8) has presented experimental data on the diameters of the highest drop ejected by bursting bubbles in sea water as a function of bubble size. The data fit the linear equation $y = 51.5x - 3.95$ where x is the bubble diameter in millimeters and y is the drop diameter in microns. The data,

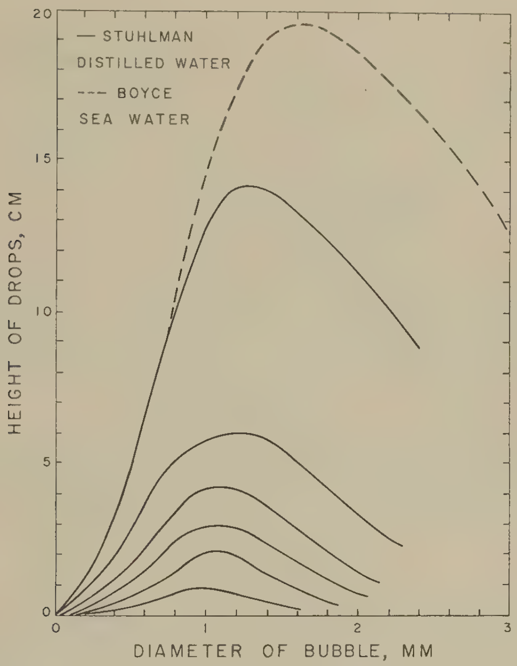

Fig. 3. The height of ejection of drops from breaking bubbles as a function of the bubble diameter. The solid lines were obtained by Stuhlman (7), who observed six drops produced when a bubble breaks in distilled water, and the single dashed line was obtained by Boyce (8). This latter measurement is for the maximum ejected height for drops produced by bubbles breaking in sea water.

however, represent the drop diameter at 83 % relative humidity and 21° C. To obtain the diameter when ejected from the bursting bubble one would have to compute the equilibrium size at the temperature and relative humidity (98 %) existing over the sea water at the time of ejection. These computations are easily done with the aid of graphs relating density, temperature, and saturation vapor pressure with chlorinity of the water (9). The above equation, although probably correct for large bubbles, cannot possibly hold for bubbles $<77\ \mu$ diameter, for below this size the equation predicts negative droplet diameters. Inasmuch as the writer has obtained droplets between 2 and 10 μ diameter from bubbles $<77\ \mu$, and as Boyce seemed little concerned with the small bubbles, it is justifiable to limit consideration of this equation to the larger bubbles.

In order to insure a continuous and rapid rate of production of homogeneous drops it is necessary, as was mentioned earlier, to maintain a clean water surface. This becomes more critical as the bubble diameter increases and especially so in the case of bubbling in sea water. Little difficulty is experienced, however, if the bubbles are $<$ about 600 μ and preferably breaking in distilled water. Fortunately, it is the smaller bubbles that are producing the drops in the size range that are beyond the limits of hypodermic needles, and it is in this size range that the bubble technique produces homogeneous drops with a high degree of accuracy.

References

1. Lane, W. R., *J. Sci. Instr.* **24,** 98 (1947).
2. Rasbash, D. J., *J. Sci. Instr.* **30,** 189 (1953).
3. Walton, W. H., and Prewett, W. C., *Proc. Phys. Soc.* (*London*) **62,** 341 (1949).
4. May, K. R., *J. Appl. Phys.* **20,** 932 (1949).
5. Vonnegut, B., and Neubauer, R. L., *J. Colloid Sci.* **7,** 616 (1952).
6. Woodcock, A. H., Kientzler, C. F., Arons, A. B., and Blanchard, D. C., *Nature* **172,** 1144 (1953).
7. Stuhlman, O., *Physics* (*J. Appl. Phys.*) **2,** 457 (1932).
8. Boyce, S. G., *Ecol. Monographs* **24,** 29 (1954).
9. Woodcock, A. H., *J. Marine Research* (*Sears Foundation*) **8,** 177 (1949).
10. Drozin, W. G., in press.

LIESEGANG RINGS IN INHOMOGENEOUS MEDIA. PARTIALLY COAGULATED GELATIN

Kurt H. Stern

Institute of Science and Technology, University of Arkansas, Fayetteville, Arkansas

Received April 26, 1954; revised June 2, 1954

Abstract

The formation of Liesegang rings has been studied in gelatin partially coagulated with methanol. The effect of inhomogeneities in the medium on ring formation is described. The diffusion equation is tested for the various media. The diffusion velocity is found to decrease with increasing methanol concentration.

Introduction

It has been well established that the general factors leading to the formation of periodic precipitates, or Liesegang rings, can be derived from a solution of Fick's diffusion law, under the assumption of proper boundary conditions (1). Such a solution predicts the general structure of Liesegang rings. However, since no rigorous solution of the equation has yet been worked out, a quantitative prediction of the ring distances to be expected in any given system cannot be made.

Previous workers in this field have used an essentially uniform medium of a colloid or water containing one of the reactants through which the other reactant was allowed to diffuse. In the present study an attempt was made to determine the effect of inhomogeneities in the medium on ring formation. One of the simplest methods of producing inhomogeneities, i.e., local variations in the density and viscosity of the medium, is to coagulate the gelatin partially by treatment with alcohol. The inhomogeneities produced are of two kinds, (*1*) gross disturbances, due to air bubbles or relatively large clumps of coagulated gelatin, and (*2*) a uniform distribution of fine particles of coagulated gelatin. The effect of both kinds of inhomogeneities is reported in this paper.

Experimental Part

Procedure

All measurements were carried out in 8 mm. diameter tubes, 25 cm. long. A 7 cm. length of 2 cm. tubing was fused to the end of each tube. This served as a silver nitrate reservoir.

TABLE I

Solution Compositions[a]

Tube No.	S (*ml.*)	H_2O (*ml.*)	CH_3OH (*ml.*)
		Series A	
I	5	5	0
II	5	4	1
III	5	3	2
IV	5	2	3
V	5	1	4
VI	5	0	5
		Series B	
I	5	5	0
II	5	4	1
III	5	3	2
IV	5	2.8	2.2
V	5	2.6	2.4
VI	5	2.4	2.6
VII	5	2.2	2.8
VIII	5	2	3
IX	5	1	4
X	5	0	5

[a] All solutions were prepared from a stock solution S made by dissolving 8 g. gelatin and 0.5 g. K_2CrO_4 in 100 g. water.

The gelatin used was of C.P. grade and chloride free. Two sets of solutions, A and B, were prepared. Set A contained gelatin with large-order inhomogeneities, and set B contained a uniform distribution of fine particles of coagulated gelatin. Concentrations of silver nitrate and potassium chromate were kept constant in both sets.

The composition of the solutions is shown in Table I.

In preparing the solutions in series B, air bubbles were carefully removed and the solutions were mixed thoroughly to assure their homogeneity. On the other hand, solutions in series A were not mixed well, and large air bubbles and clumps of coagulated gelatin were allowed to remain in the tubes. Both sets of tubes were placed in a refrigerator at 5°C. After the gelatin had set, 10 ml. of a 12% by weight solution of silver nitrate was poured into the reservoir on top of each tube. The concentrations used approximate the conditions for an infinite reservoir, since only 5% of the silver nitrate is required to react with all the potassium chromate in the tube. All tubes were kept in the refrigerator for 2000 hours. They were taken out only while measurements on them were made.

General Observations

Rings or periodic structures formed in all the tubes. However, after several weeks, rings in I and II of series A and B disintegrated partially, pro-

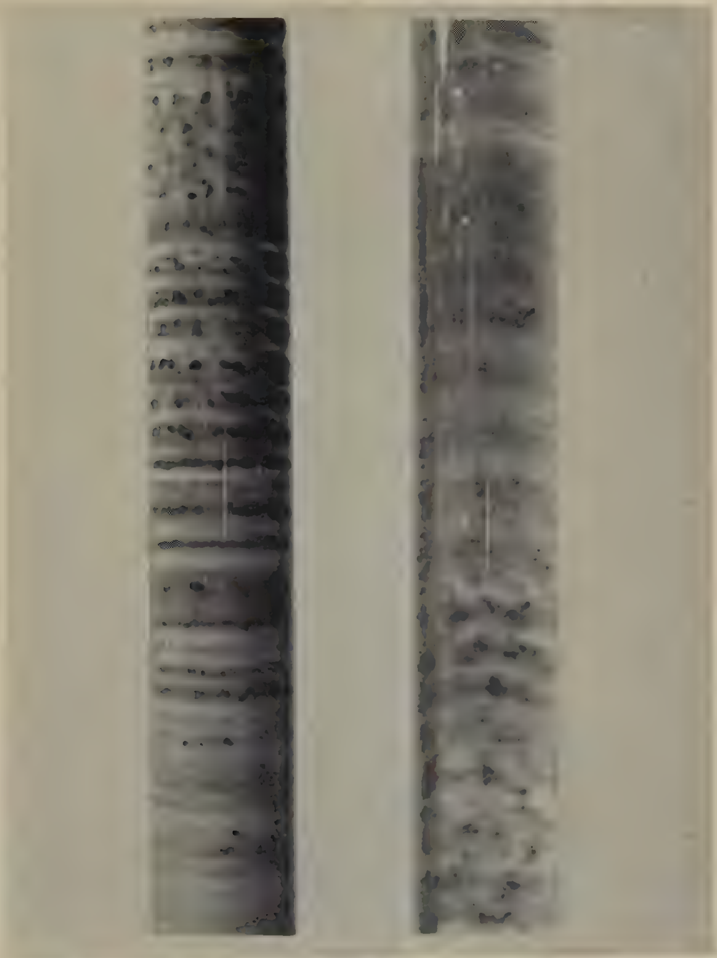

FIG. 1. Partially disintegrated Liesegang rings. (*Left*) Tube II, (*right*) Tube I.

ducing fuzzy bands consisting of small particles of silver or silver oxide (Fig. 1).[1] Rings formed in III A and B tended to become indistinct, and some reduction took place also (Fig. 2). In IV, V, and VI of A marbled structures formed, evidently owing to the disturbance of the diffusion front (Fig. 3). However, these marbled structures formed primarily in the top part of the tubes, whereas toward the bottom more or less regularly spaced rings were formed. Examination of the tubes under strong light showed that large-order inhomogeneities are evident only at the top of the tubes, while below the medium is similar to that of series B. Evidently coagulated gelatin mixed with air bubbles is of lower density and floated to the top of the tube before the gel set.

---

[1] The diffusion proceeded from top to bottom in all photographs.

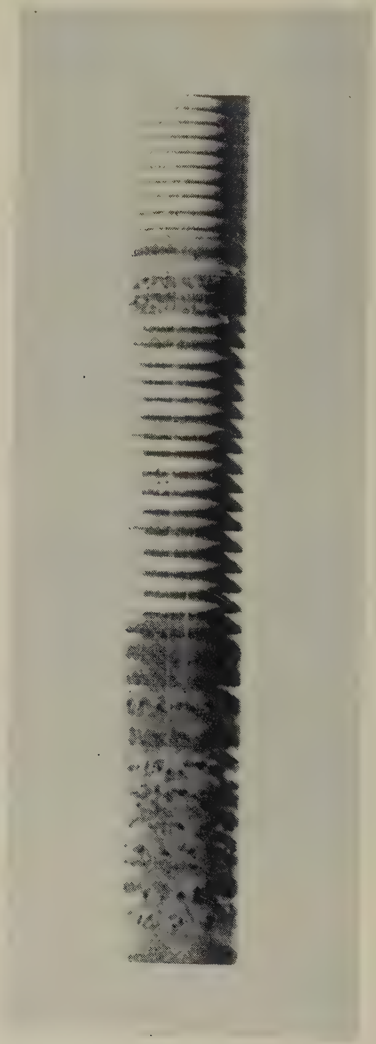

FIG. 2. Partially disintegrated Liesegang rings. Tube III.

In general the sharpness of the bands increased with increasing methanol content of the medium. Because of the marked difference in appearance between III A and IV A four solutions intermediate in concentration between these two were prepared in series B. Tube IV of B shows a slight amount of reduction, whereas no reduction is visible from V B on. At the same time

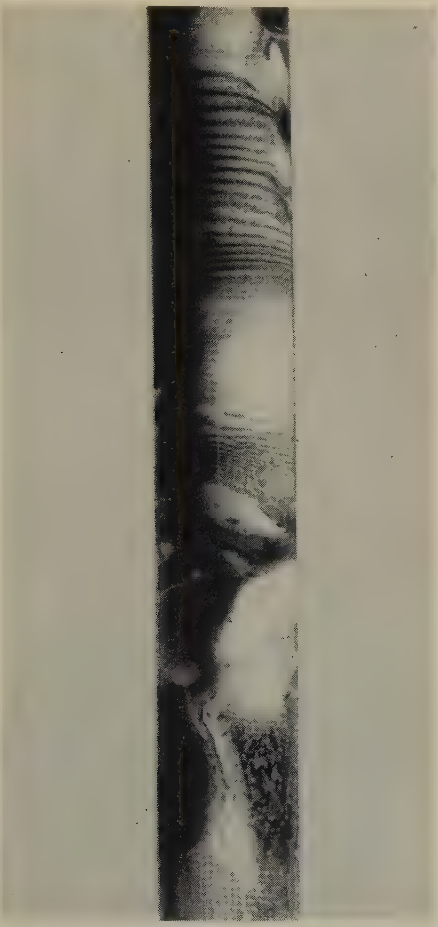

FIG. 3. Marbled diffusion structure.

the opacity of the medium, due to partially coagulated gelatin, increases markedly between IV B and V B. The sharp rings formed in VIII B are shown in Fig. 4. It can also be seen that the red color of the rings becomes lighter as the methanol concentration increases. The average thickness of the rings is 60 μ. All photographs were taken approximately 2000 hours after preparation of the solutions.

Tests of the Diffusion Equation

Measurements of series B were used in testing relationships derived from the diffusion equation. For this purpose measurements of distance x traveled by the diffusing silver nitrate were made at various times. The last ring formed was taken to be at the diffusion front. It has been shown (2) that

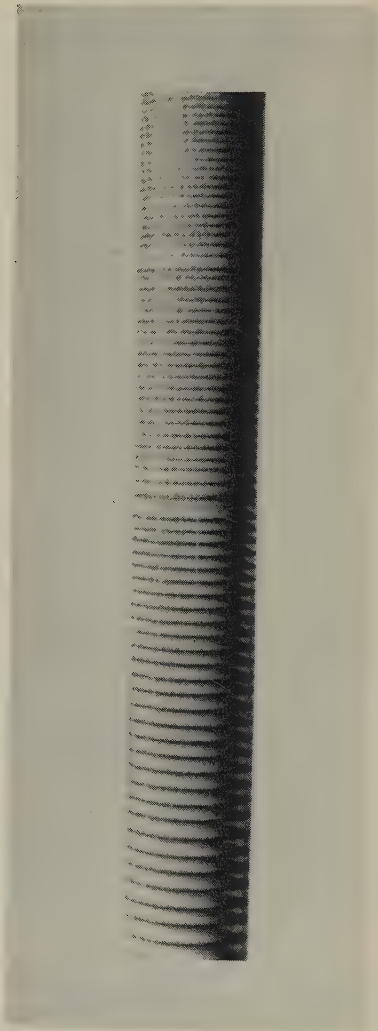

FIG. 4. Liesegang rings in 30% methanol system. Tube VIII.

TABLE II

Values of $x/\sqrt{t}$ *for Various Systems (in mm. hr.*$^{-\frac{1}{2}}$*)*

t (hours)	I	II	III	VIII	IX	X
10	5.69	5.06	4.44	4.44	4.12	3.80
118	5.07	4.42	4.15	3.87	3.50	3.24
506	4.72	4.14	3.78	3.56	3.34	3.11
991	4.62	4.00	3.66	3.49	3.28	3.09
1514	4.47	3.93	3.62	3.37	3.22	2.98

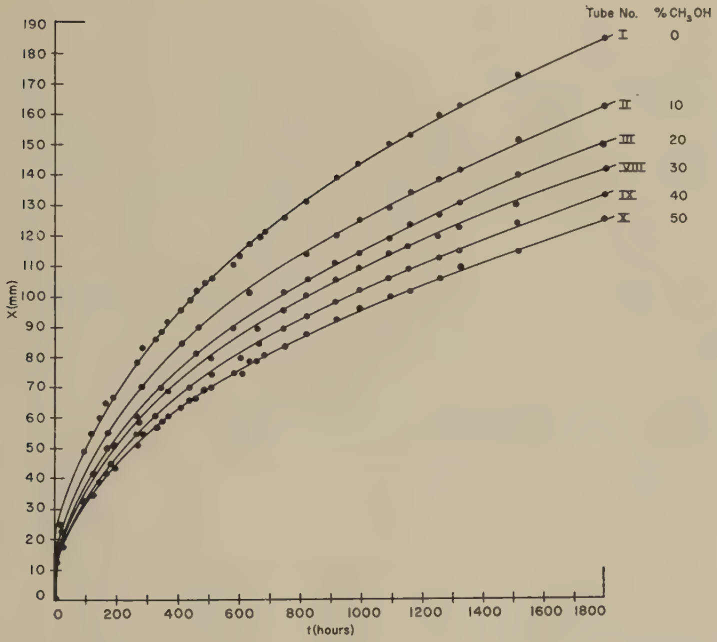

FIG. 5. Diffusion velocity for systems of different methanol concentrations.

the relationship $x/\sqrt{t}$ = constant can be derived from the diffusion equation. A selection of values obtained for this constant is given in Table II. It can be seen from these data that the initial diffusion rate is much higher than the final rate. This is also evident from a plot of distance against time shown in Fig. 5. From 1000 hours on, the diffusion rate decreases very slowly. The average rate for equal increments of methanol concentration is shown in Table III for the interval from 1000 to 1500 hours.

An attempt was also made to test the relation d_n/d_{n+1} = constant, where d_n is the distance between any two rings. It was found, however, that this ratio varied erratically in all the systems containing methanol, i.e., the rings were not evenly spaced, although the ratio rarely exceeds 1.05. Disintegration of the rings in I prevented measurements of the ratio in this system.

TABLE III

Diffusion Velocity as a Function of the Composition of the Medium

Tube No.	Vol. % CH$_3$OH	x/t (mm./hr.)
I	0	0.054
II	10	0.052
III	20	0.050
VIII	30	0.044
IX	40	0.042
X	50	0.036

DISCUSSION

The data obtained in series B can be used to test the validity of the diffusion equation. The values of $x/\sqrt{t}$ in Table II show that in the systems studied this constant decreases with increasing distance and time of diffusion. It was found, however, that the data could be fitted by the equation $x/t^{0.45}$ = constant over the entire range of x and t. The constancy of the quotient is shown in Table IV by some typical data for the tube VII. However, the value of this constant decreases with increasing methanol concentration in a manner similar to that of $x/\sqrt{t}$. This is evidently due to the decreases in diffusion rate with increasing coagulation of gelatin. The effect of this coagulation is one of increasing the average density and viscosity of the medium. The decrease in the exponent of t from its theoretical value of 0.5 to 0.45 may be attributed to the slight decrease of silver nitrate concentration in the reservoir as the diffusion proceeds.

TABLE IV

Test of the Equation $x/t^{0.45}$ = Constant (Data from Tube VII)

x (*m*)	t (*hr.*)	$x/t^{0.45}$
20	22	4.95
71	410	4.72
99	819	4.85
146	1946	4.84

An estimate can be made of the concentrations of the reactants present during the formation of any ring. The diffusion constant $D = 1 \times 10^{-5}$ cm.^{2} sec.$^{-1}$ for silver nitrate in water. If it is assumed that D is of the same order of magnitude in gelatin as in water, then the concentration of silver ion C can be determined if the concentration, C_0, in the reservoir is known (3). For the simple gelatin-water system (as in tube I) $C/C_0 = 0.04$ for all the rings in the tube. Since $C_0 = 0.75$ mole/liter, $C = 3.8 \times 10^{-2}$. On the assumption that the solubility product of silver chromate is the same in water as in gelatin, 10^{-12}, the concentration of chromate ions is 8×10^{-10} at the last ring formed. Since the chromate ion concentration in the gelatin far removed from the diffusion front must be near its initial value of 2×10^{-2}, it follows that a steep concentration gradient for the chromate ion exists near the diffusion front. This conclusion was also reached by Wagner in his derivation (4).

Unfortunately no data on diffusion constants and solubility products in partially coagulated gelatin are available. It is probable that the values would differ markedly from those for the gelatin-water system. If the same value of D were assumed in tube X as in I, the ratio C/C_0 would change from 0.04 to 0.2. This fivefold increase in concentration is unlikely, since the variation of C with x must be quite similar in all the tubes. Moreover, it is probable that the solubility product of silver chromate is decreased by the addition of methanol. This makes an increase in C very unlikely. If it is assumed that the major factor in the decrease of $x/\sqrt{t}$ from I to X is the decrease in D, it is possible to calculate the value of D required to satisfy the relation $C/C_0 = 0.04$, taking the average value of $x/\sqrt{t} = 3.0$ for tube X. The result is $D = 1.0$ mm.^{2} hr.$^{-1}$, or a 70 % decrease for a 50 % methanol system from the value for the 0 % case. This conclusion is at least qualitatively reasonable in view of the greater density and viscosity of coagulated gelatin.

It has been assumed in the above discussion that the effect of inhomogeneities on the diffusion velocity is a mechanical one, i.e., that any inert material dispersed in gelatin would produce the same effect as coagulated gelatin itself. This assumption remains to be tested experimentally.

The paucity of data on diffusion of electrolytes in gelatin prevents any rigorous treatment of Liesegang rings. For example, it is probable that, since D is a function of concentration (5), a change in D along the tube should be taken into account. If D is a variable, the diffusion equation becomes

$$\frac{\partial C}{\partial t} = \frac{\partial D}{\partial x}\left(D\,\frac{\partial C}{\partial x}\right) = D\,\frac{\partial^2 C}{\partial x^2} + \frac{\partial D}{\partial x}\cdot\frac{\partial C}{\partial x}.$$

The solution of this equation may be used to determine D (6, 7), if concentration is known as a function of distance

$$D = \frac{-\dfrac{1}{2}\displaystyle\int_{C_0}^{C} \lambda\, dC}{dC/d\lambda}$$

where $\lambda = x/\sqrt{t}$.

Such a refinement may be used to account for the increasing distance between rings as diffusion proceeds.

ACKNOWLEDGMENTS

The author wishes to express his gratitude for valuable discussions with Dr. Harold Shniad, of the Mathematics Department; and to Miss Ruth Rhoades, of the Institute of Science and Technology, for the preparation of the photographs; both of the University of Arkansas.

REFERENCES

1. STERN, K. H., *Chem. Revs.* **54**, 79 (1954).
2. SHEMYAKIN, F. M., *J. Gen. Chem.* (*U.S.S.R.*) **4**, 451 (1934).
3. DARKEN, L. S., AND GURRY, R. W., "Physical Chemistry of Metals," p. 444. McGraw-Hill Book Company, Inc., New York, 1953.
4. WAGNER, C., *J. Colloid Sci.* **5**, 85 (1950).
5. CLACK, B. W., *Proc. Phys. Soc.* (*London*) **36**, 313 (1924).
6. BOLTZMANN, L., *Ann. Physik* **53**, 960 (1894).
7. MATANO, C., *Japan. J. Phys.* (*Trans.*) **8**, 109 (1933).

VISCOSITIES OF DILUTE SOLUTIONS OF CELLULOSE ACETATE

W. R. Moore and J. Russell[1]

Department of Chemistry and Dyeing, Technical College, Bradford, England

Received December 1, 1953; revised March 5, 1954

INTRODUCTION

In a previous paper (1) we reported results of some viscosity studies on solutions of a secondary cellulose acetate. Viscometric measures of solvent power, applicable to more flexible polymers (2), to cellulose nitrate (3, 4), and to ethyl cellulose (5), were found not to apply. Acidic solvents and aniline gave the highest intrinsic viscosities, other basic solvents tended to give the lowest, and solvents of more neutral character gave intermediate values. Attention was mainly directed to results of initial phase separation studies, and factors which might affect the viscosities of solutions of cellulose acetate were considered only briefly. This paper presents some viscosity and initial phase separation results for a primary acetate obtained by nondegradative acetylation of the acetate previously studied. These are compared with those for the secondary acetate, and some of the factors which may be responsible for the variation of intrinsic viscosity with solvent and acetyl content are rather more fully discussed. A tentative interpretation of the variation with solvent type and acetyl content is advanced.

EXPERIMENTAL METHODS

The unfractionated acetate previously used ($\bar{m}_w$ = 49,000, acetic acid yield 53.7 %) was converted to the primary or triacetate by a nondegradative method (6) involving solution in pure pyridine and acetylation with acetic anhydride at room temperature for 10 days. After washing with water, the dry product had an acetic acid yield of 62.5 %. Number average degrees of polymerization of both acetates were determined osmotically at 25° ± 0.005°C., using chloroform as solvent for the primary and acetone for the secondary. Measurements were made by the dynamic method with a modified Meade-Fuoss osmometer using denitrated collodion membranes (7). No diffusion of solute was observed. Degrees of polymerization were obtained from the results of extrapolation of reduced osmotic pressure versus concentration plots to zero concentration. The degree of polymerization of the secondary acetate was 195, that of the primary being 218. The somewhat higher value for the primary might indicate some degree of association.

---

[1] Now at Department of Chemistry, Cornell University, Ithaca, New York.

The primary acetate was soluble only in solvents of acidic type. The following were used, all being purified and dried by appropriate methods and fractionally distilled just prior to use: *o*-cresol, *m*-cresol, methylene chloride, tetrachloroethane, and chloroform. Solutions were prepared by dissolving exactly 1 g. of acetate in about 50 ml. solvent with the aid of mechanical agitation, the resulting solution being diluted to 100 ml. These solutions were used for initial phase separation studies, less concentrated solutions used for viscosity measurements being obtained by careful dilution. All solutions were allowed to stand for 60 hours and filtered immediately prior to use.

Viscosities were determined at 25° ± 0.05°C., using Ostwald type capillary viscometers. Kinetic energy corrections were made where applicable. Determinations were made at concentrations within the range 0.05 to 0.5 g./100 ml. The flow time for each solution was determined at least three times, using a stop watch reading to 0.1 second. Such flow times differed by less than 0.2%. In duplicate experiments values of η_{sp} differed by less than 2%. *n*-Hexane and toluene, purified as previously described (1), were used as precipitants in initial phase separation. The volume of precipitant re-

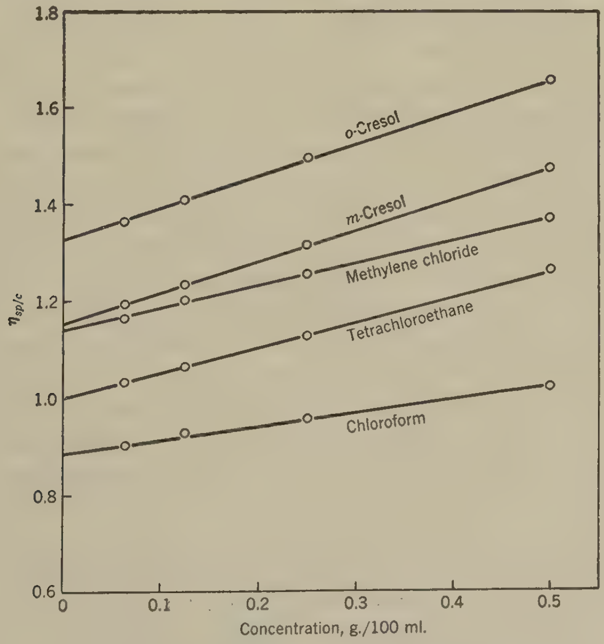

FIG. 1. Viscosities of solutions of primary acetate.

TABLE I

Viscosity Data and Volumes of Precipitants Required for Initial Phase Separation. Primary Acetate

Solvent	$[\eta]$	Initial slope	k'	Hexane, *ml.*	Toluene, *ml.*
Chloroform	0.88	0.28	0.36	1.00	1.9
Tetrachloroethane	1.00	0.53	0.53	1.90	2.5
Methylene chloride	1.14	0.42	0.32	1.70	2.5
m-Cresol	1.15	0.66	0.50	8.8	66.0
o-Cresol	1.32	0.64	0.37	8.05	41.0

quired to cause initial phase separation was obtained by running the precipitant from a microburet into 5 ml. of 1% solution with constant agitation at 25°C. End points were somewhat difficult to detect when chlorinated hydrocarbons were used as solvents.

Results

Viscosity results are illustrated in Fig. 1. Each point represents the mean of two or three separate determinations. The plots are linear, and intrinsic viscosities have been obtained by simple extrapolation to zero concentration. Intrinsic viscosities, initial slopes of η_{sp}/c versus c plots, and initial phase separation results are given in Table I.

Discussion

There is no obvious relationship between $[\eta]$ and the volume of either precipitant, though the initial slope tends to increase with these volumes. Because of solvation, however, good solvents of high molecular weight may lead to a real molecular weight of the dissolved polymer which is considerably greater than that of the dry polymer. If this is so, the molecular weight of the triacetate in each solvent is unknown, and instead of comparing initial slopes, which involve $[\eta]^2$, it may be better to compare values of initial slope/$[\eta]^2$, the Huggins's k' (2), values of which are given in Table I. They are not simply related to the volumes of precipitants. Calculations show that similar results are obtained if the Spurlin viscometric measure of solvent power (5) is used. If the volumes of precipitants are regarded as measures of solvent power, the variation of initial slope is similar to that reported by Frith (8). However, as we have previously pointed out (1) it is doubtful to what extent volumes of precipitants can be regarded as measures of solvent power. It is unlikely that complete correlation will be obtained between volumes of precipitants and thermodynamic measures of solvent power.

Comparison of values of $[\eta]$ with those obtained using the secondary acetate, given for convenience in Table II, shows that smaller values are obtained with the primary. The decrease in the cases of *o*- and *m*-cresol, the two solvents common to both acetates, is marked. Howlett *et al.* (9) found

TABLE II

Intrinsic Viscosities of Solutions of Secondary Acetate

Solvent	$[\eta]$
γ-Picoline	1.30
α-Picoline	1.37
Pyridine	1.46
Methyl acetate	1.48
Acetone	1.49
β-Picoline	1.55
Methyl formate	1.66
Dioxan	1.70
Nitromethane	1.73
m-Cresol	1.82
Acetic acid	1.83
p-Cresol	1.90
Aniline	1.95
o-Cresol	2.12

that the intrinsic viscosity of cellulose acetate in chloroform decreased markedly with increasing acetyl content. A smaller decrease was observed when acetone and pyridine were solvents.

Since the residue weight of the primary acetate is greater than that of the secondary, a given weight of polymer will contain proportionately fewer chains of primary than secondary. Other things being equal, this should lead to a lower viscosity at a given concentration, expressed in g./100 ml. The weights of the acetylated glucose units are 288 and 260 for primary and secondary, respectively, leading to a decrease of about 10% in η_{sp} and $[\eta]$. This might account for the variation of $[\eta]$ with acetyl content in acetone and pyridine but not for that in chloroform and the cresols.

The small range of values of $[\eta]$ for the secondary acetate in different solvents and the somewhat rigid nature of the chains makes any marked change in their configuration with solvent unlikely. Light scattering studies (10) suggest that chains of the secondary acetate are rather extended in methyl cellosolve (2-methoxymethanol) and acetone, neither of which can be regarded as good solvents thermodynamically, μ values being 0.49 and 0.43, respectively (11). The addition of appreciable amounts of nonsolvents has little effect on the intrinsic viscosities of solutions of the secondary acetate (9, 12). Appreciable changes in chain configuration, and hence of $[\eta]$, with solvent power in a thermodynamic sense seem unlikely. This may not be so for the primary acetate. Mandelkern and Flory (13) have suggested that appreciable coiling of cellulose tributyrate chains in solution is possible although only at somewhat elevated temperatures. The larger volumes of precipitants required for solutions of the primary acetate in the cresols make it unlikely, however, that the lower values of $[\eta]$ in these solvents can be attributed to changes in configuration with solvent power.

Other factors may be responsible for the variation of $[\eta]$ with solvent and acetyl content. Association of chains, persisting at low concentrations, is a possibility. This is known to occur in solutions of cellulose derivatives (14, 15, 16). Association favoring increased axial ratios of aggregates might lead to increased viscosity. The formation of aggregates with axial ratios similar to those of single chains should lead to lower viscosity. Wales and Swanson (15) found that the removal of aggregates, attributed to calcium bridges between sulfuric half-ester groups, resulted in a small decrease in the intrinsic viscosity of a high molecular weight fraction of secondary cellulose acetate in acetone. Removal of such aggregates from the unfractionated polymer appeared to have no effect on $[\eta]$. Doty *et al.* (16) found a secondary acetate to be associated in methyl cellosolve and in 10/23 and 10/20 acetone/methanol mixtures. A fraction of molecular weight 53,000 did not appear to be associated in acetone. Badgely and Mark (11), using fractions, obtained lower values of $[\eta]$ in methyl cellosolve than in acetone. Weissberg and Simha (12) found that $[\eta]$ for solutions of secondary acetate in acetone/methanol mixtures varied little for methanol contents up to 50%. Further additions of methanol resulted in a marked decrease.

These results suggest that association may, in certain cases, cause a decrease in $[\eta]$. Apart from the aggregation observed by Wales and Swanson which did not affect $[\eta]$ for the entire polymer, association does not appear to occur in acetone. Association in poorer solvent media may lead to low values of $[\eta]$ for the secondary acetate. We have suggested (17) that association might, in part, account for the downward curvature of η_{sp}/c versus c plots at low concentrations observed with pyridine and α- and γ-picolines as solvents. It seems unlikely that differences in degree of association could entirely account for the variations in $[\eta]$ with solvent or solvent type observed with the secondary acetate. Association of the primary acetate does not appear to have been studied, but the similar degrees of polymerization obtained osmotically for both acetates makes it unlikely that the low value of $[\eta]$ for the primary in chloroform can be entirely due to association. The larger volumes of precipitants required for initial phase separation of the primary acetate might suggest that the lower values of $[\eta]$ in the cresols are not due to association.

The number and size of solvating molecules may influence the axial ratio of the chains. Although there is strong evidence for solvation (18), the number of solvent molecules attached to each glucose residue is uncertain. Large numbers have been suggested, but it does not follow that all will be sufficiently firmly bound to the polymer to form part of a hydrodynamic unit. Dobry (19) suggests that only the first layer of solvent molecules is sufficiently firmly bound to contribute to the hydrodynamic volume of the chains. Calculations by Peterlin (20) give a hydrodynamic radius of 7 A. for cellulose acetate in acetone, suggesting that not many solvent molecules are firmly bound. Calculations leading to similar conclusions have been made by Kuhn (21). Whereas differences in size of solvating molecules may cause some variation of axial ratio with solvent, considerations of molecular volumes suggest, assuming only the first layer of solvent to be firmly bound, that this is unlikely completely to account for the variations of $[\eta]$ with solvent or solvent type.

Although a combination of association and solvation effects might lead to variations of $[\eta]$ in a range of solvents, an alternative suggestion, which takes solvation into account, may be tentatively advanced. This seems to account for the higher values of $[\eta]$ obtained with aniline and acidic solvents, for the lower values obtained with basic solvents, and for variations with acetyl content. It is based on suggested configurations of the cellulose chain and relates changes in $[\eta]$ to small changes in configuration of chains due to breaking of intramolecular hydrogen bonds.

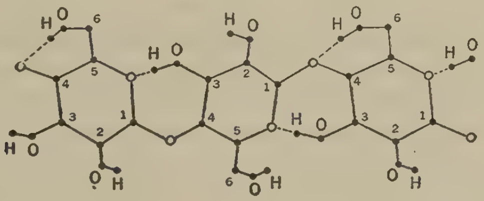

FIG. 2. A possible configuration of the cellulose chain.

Hermans (22) says that a possible configuration of the cellulose chain is a spatial one with a combined vertical and horizontal zigzag. Such a configuration is shown in Fig. 2, positions of atomic centers being shown. Hermans suggests that hydrogen bonds, indicated by broken lines, may be formed between the hydroxyl group in the 6-position and the bridge oxygen; also between the hydroxyl group in the 3-position and the ring oxygen of the neighboring glucose residue. Such bonds will give rise to additional ring systems impeding mutual rotation of adjacent glucose residues and to some extent stiffening the extended configuration of the chain. Robinson (23), using atomic models, has suggested that intramolecular hydrogen bonds can be formed by bonding each primary alcohol group to the nearest secondary alcohol group in the next ring. If such bonds are formed, they will restrict the flexing of the chain in the plane of the rings, though the model is more flexible normal to this plane.

In either of these configurations, the nature of the environment will determine whether or not the intramolecular hydrogen bonds are formed, as they will have to compete with a tendency to bond to solvent or other cellulose molecules. Acetylation will reduce the number of suggested hydrogen bonds in both cases. A secondary cellulose acetate will still, however, possess about one unacetylated hydroxyl group per cellobiose unit, and there is some evidence that those in the 6- and 3-positions may predominate (24). Even if this is not the case, the suggested stiffening in the Hermans configuration may persist to some extent. In the Robinson model, hydrogen bonding between a primary alcohol group and the hydroxyl oxygen of the nearest acetyl group in the next ring would seem to be possible and lead to some stiffening in the plane of the rings. In solutions of cellulose itself such intramolecular hydrogen bonds may be broken because of interaction of hydroxyl groups with solvent. Not all solvents for cellulose acetate seem, however, to interact with hydroxyl groups. Spurlin (25) has suggested that chlorinated hydrocarbons are bound to acetyl groups, and similar suggestions have been made by Clement (26). Marsden and Urquhart (27) postulate bonding between the hydroxyl group of phenol and acetyl groups of secondary cellulose acetate. There is considerable evidence (26, 28) that aniline and acidic solvents can form hydrogen bonds with acetyl groups. In such solvents the suggested intramolecular hydrogen bonding may persist, the stiffness and extended nature of the chains being unaffected.

Basic solvents, not possessing a hydrogen atom capable of taking part in hydrogen bonding, may interact with hydroxyl groups and break the intramolecular hydrogen bonds. Somewhat less extended configurations, due to decreased stiffness, may lead to lower values of $[\eta]$. Interaction with hydroxyls rather than with acetyl groups is also likely with the more neutral solvents which may be regarded as weakly basic. Clement (26) has suggested that both ketones and esters interact with hydroxyl groups of secondary cellulose acetate. Such interaction may occur to a lesser extent than in the case of more basic solvents so that a rather more extended configuration may lead to somewhat higher values of $[\eta]$. Errera *et al.* (29) have shown that the bond between alcoholic hydroxyls and pyridine is stronger than that between such hydroxyls and acetone.

Complete acetylation should result in the elimination of the suggested intramolecular hydrogen bonding and probably lead to less extended configurations in acidic solvents, resulting in lower values of $[\eta]$. The shape of the η_{sp}/c versus c plots is in agreement with this view. With the secondary acetate such plots often show upward curvature at concentrations above about 0.2 g./100 ml. (1), suggesting hydrodynamic interaction between extended chains (30). Plots for the primary acetate are linear up to a concentration above 0.5 g./100 ml.

The suggested interpretation of the variation of $[\eta]$ with solvent type may also account for the observed variations with acetyl content in different solvents. In those interacting only with hydroxyl groups the configuration of the chains may not be greatly affected by changes in acetyl content and, apart from the small effect, previously mentioned, arising from the variation of residue weight with acetyl content, $[\eta]$ should not be greatly affected. In solvents interacting only with acetyl groups a reduction in the number of hydroxyls should lead to decreasing stiffness of chains and to a decrease in [η] over and above that due to increasing molecular weight. Such a decrease is seen on comparing values of [η] for the two acetates in the cresols. Howlett *et al.* (9) found [η] for chloroform solutions to decrease with increasing acetyl content more markedly than when acetone or pyridine were used as solvents. They also found that [η] decreased with increasing acetyl content rather markedly in a mixture of methylene chloride and ethanol—a result only explained, on the basis of the foregoing suggestions, if the hydrogen bonding along the chains persists, to some extent at least, in the presence of the ethanol.

These suggestions would seem largely to account for the observed variations of [η] with solvent type and acetyl content. They do not account for differences within a group of solvents of similar acidic or basic type. Such variations may be due to small differences in the extent to which the suggested interactions between solvent and polymer occur. They might also reflect small differences in chain configuration with solvent power in a thermodynamic sense. Some degree of flexibility may be possible whether the chains are in the more exended form or not. Differences in degree of association and in the number and size of solvating molecules are also possible factors contributing to the variation of [η] in solvents of similar type.

ACKNOWLEDGMENTS

We wish to gratefully acknowledge a Courtaulds Research Scholarship to one of us (J. R.). We are indebted to Mr. J. Epstein for the osmotic pressure measurements and to Drs. C. H. Bamford and Conmar Robinson for helpful discussion on the subject of the configuration of cellulose.

SUMMARY

Viscosity and initial phase separation results for a primary cellulose acetate are presented and compared with those obtained with a secondary acetate of the same chain length. Possible factors leading to variations in intrinsic viscosity with solvent and acetyl content are discussed. A tentative interpretation, based on possible configurations of the cellulose chain involving intramolecular hydrogen bonding, is advanced to account for such variations with solvent type and acetyl content.

REFERENCES

1. MOORE, W. R., AND RUSSELL, J., *J. Colloid Sci.* **8**, 243 (1953).
2. HUGGINS, M. L., *in* "Cellulose and Cellulose Derivatives" (E. Ott. ed.), p. 943. Interscience Publishers, New York, 1943.
3. MOORE, W. R., *J. Polymer Sci.* **5**, 91 (1950).
4. MOORE, W. R., *J. Polymer Sci.* **7**, 175 (1951).
5. SPURLIN, H. M., MARTIN, A. F., AND TENNENT, H. G., *J. Polymer Sci.* **1**, 63 (1946).

6. Howlett, F., *Shirley Inst. Mem.* **18,** 241 (1941).
7. Fuoss, R., and Meade, D., *J. Phys. Chem.* **47,** 59 (1943).
8. Frith, E. M., *Trans. Faraday Soc.* **41,** 90 (1945).
9. Howlett, F., Minshall, E., and Urquhart, A. R., *Shirley Inst. Mem.* **18,** 251 (1941).
10. Doty, P., and Stein, R. S., *J. Am. Chem. Soc.* **68,** 159 (1946).
11. Badgely, W. J., and Mark, H., *J. Phys. & Colloid Chem.* **51,** 58 (1947).
12. Weissberg, S. G., and Simha, R., *J. Colloid Sci.* **2,** 305 (1947).
13. Mandelkern, L., and Flory, P. J., *J. Am. Chem. Soc.* **74,** 2517 (1952).
14. Steurer, E., *Z. physik. Chem.* **A190,** 1, 16 (1941).
15. Wales, M., and Swanson, D. L., *J. Phys. & Colloid Chem.* **55,** 203 (1951).
16. Doty, P., Wagner, H., and Singer, S., *J. Phys. & Colloid Chem.* **51,** 32 (1947).
17. Moore, W. R., and Russell, J., *J. Polymer Sci.* **9,** 472 (1952).
18. Howlett, F., and Urquhart, A. R., *Chemistry & Industry* **1951,** p. 82.
19. Dobry, A., *J. chim. phys.* **35,** 20 (1938).
20. Peterlin, A., *J. Polymer Sci.* **8,** 173 (1952).
21. Kuhn, H., *J. Colloid Sci.* **5,** 331 (1950).
22. Hermans, P. H., "Physics and Chemistry of Cellulose Fibres," p. 13. Elsevier, New York, 1949.
23. Robinson, Conmar, *Discussions Faraday Soc.* **16,** 125 (1954).
24. Gardner, T. S., and Purves, C. B., *J. Am. Chem. Soc.* **64,** 1539 (1942).
25. Spurlin, H. M., *in* "Cellulose and Cellulose Derivatives" (E. Ott, ed.), p. 868. Interscience Publishers, New York, 1943.
26. Clement, P., *Ann. chim.* **12,** 2, 420 (1947).
27. Marsden, R. J. B., and Urquhart, A. R., *J. Textile Inst.* **33,** T105 (1942).
28. Gordy, W., *J. Am. Chem. Soc.* **59,** 464 (1937); *ibid.* **60,** 605 (1938).
29. Errera, J., Gaspart, R., and Sack, H., *J. Chem. Phys.* **8,** 63 (1940).
30. Simha, R., *J. Colloid Sci.* **5,** 386 (1950).

DETERMINATION OF SURFACE AREA AND PARTICLE SIZE OF SYNTHETIC LATEX BY ADSORPTION.

IV. LATICES CONTAINING DAXAD 11

Samuel H. Maron and Max E. Elder

Physical Chemistry Laboratory, Department of Chemistry and Chemical Engineering, Case Institute of Technology, Cleveland, Ohio

Received April 5, 1954

INTRODUCTION

The soap titration method for measuring the surface area and particle size has thus far been shown to be applicable to latices emulsified with fatty acid and rosin acid soaps (1, 2). In preparing certain special latices it is a frequent practice to use auxiliary emulsifiers in connection with the above. One of these which has been employed very often is Daxad 11, a product reported to be a mixture of Na_2SO_4 and sodium salts of polymerized naphthalenesulfonic acids, and manufactured by the Dewey & Almy Chemical Company of Cambridge, Massachusetts.

In view of the presence of Daxad 11 in many special latices, it was deemed desirable to make a study of Daxad 11 in latex to ascertain (1) whether it is adsorbed by the rubber in latex; (2) its specific surface area in latex if adsorbed; (3) the relative strength of adsorption compared to fatty acid and rosin acid soaps; and (4) whether its presence in latex interferes in any way with the soap titration method for particle size determination.

The details of this study and the results obtained are presented in this paper.

EXPERIMENTAL

The latices used in this investigation were emulsified with fatty acid soap, Dresinate 731, and potassium soap of K-wood rosin. Each latex was analyzed first for fatty acid or rosin acid content, and any free acidity found was neutralized by addition of the requisite quantity of NaOH. Finally the soap contents and rubber contents of the latices were ascertained, and the latices diluted to stock solutions of 200 g. per liter of dry rubber.

A standard Daxad 11 solution was prepared by dissolving 30 g. of the powdered commercial product in distilled water to make a liter of solution.

Other concentrations required were obtained by dilution of this stock solution.

The absorption studies were conducted in every case by titration of the latices at 50° C. with either soap or Daxad 11 solutions using conductance to detect titration end points (1). All conductances were measured with a Leeds and Northrup precision AC Campbell-Shackelton bridge.

ADSORPTION OF DAXAD 11 BY POLYMER IN LATEX

Figure 1 shows a typical plot of the change in conductance, $(L - L_0)$, vs. the milliliters of added Daxad 11 solution observed on titration of a latex with Daxad. This plot shows a discontinuity of the same type as observed during soap titrations, and suggests that we are dealing here with adsorption of Daxad upon the rubber surface. That this is the case is further borne out by Fig. 2, where C, the concentration of Daxad 11 in the latex at the point of conductance break, is plotted against rubber content, m, at point of break for four latices. The linear plots are of the same type as found with soap solutions and indicate that the principles employed before (1, 2) with soap solutions apply equally well to Daxad; *i.e.*, the slope of the linear plots gives the amount of *added* Daxad 11 adsorbed per gram of rubber, while the y-intercept the value of C_f, the concentration of Daxad in solution at the critical miscellization concentration (c.m.c.).

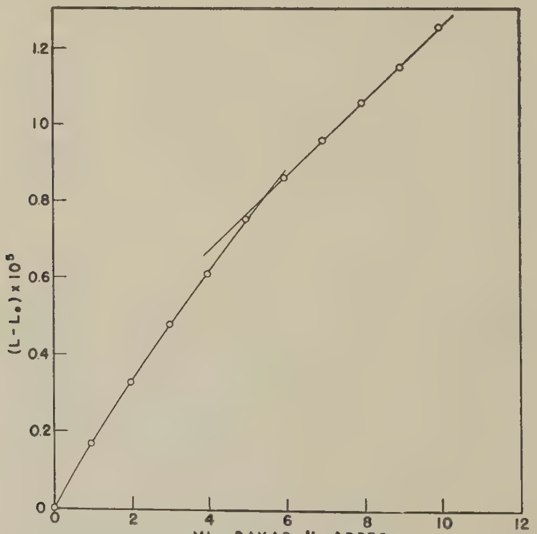

FIG. 1. Conductance titration of latex with Daxad 11 at 50°C.

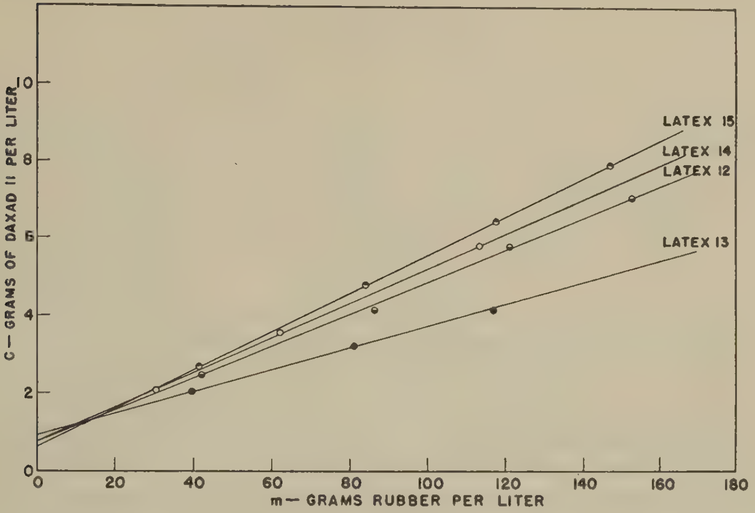

FIG. 2. Plot of C vs. m for Daxad 11 on various latices at 50°C.

THE EFFECTIVE SURFACE AREA OF DAXAD 11

After preliminary observations have shown that Daxad 11 is adsorbed by the rubber particles in latex, a series of experiments was initiated to ascertain the area occupied on the surface per gram of Daxad 11. For this purpose the areas available for adsorption were first determined in three latices by soap titration in the usual manner. Next fresh samples of these latices were titrated with Daxad solutions. In each case at least three rubber contents were used to define the C vs. m plots. The results obtained are summarized in Table I. In the table the fourth column gives the initial soap content of the latices in equivalents per gram polymer, the fifth column gives the additional soap adsorbed in the same units, and the sixth column gives the free surface area of the latices as evaluated from the data in column 5. The quantities in column 7 are the slopes of the C vs. m plots for the Daxad titrations, and represent the *grams* of Daxad 11 adsorbed per gram of polymer upon the areas shown in column 6. Since the molecular weight of Daxad 11 is not known, the best that can be done here is to calculate the effective surface area per gram of Daxad. This area, which is the ratio of the values in column 6 to those in 7, is presented in the last column of the table.

The effective specific surface areas obtained for the Daxad 11 may be seen to be essentially the same for all three latices, and to be equal to 11×10^{22} A^2. per gram of Daxad. This is about 2.2 times the area occupied on the polymer surface at the c.m.c. by a gram of sodium oleate. Some titrations made in this laboratory on solutions of Daxad 11 in water indicate

TABLE I

Effective Surface Area of Daxad 11

Latex no.	Soap present and added	$S_i \times 10^4$	$S_a \times 10^4$	Available area per g. polymer $10^{-21} \times A^2$	Daxad 11 adsorbed g./g. polymer	Effective area per g. Daxad 11 $10^{-22} \times A^2$
12	OSR	2.63	2.62	4.18	0.0414	10.1
13	K-wood rosin	2.26	1.56	3.30	0.0279	11.8
14	Dresinate 731	2.77	2.19	5.76	0.0500	11.5
					Average	11.1 ± 0.7

Note: Compositions of latices were as follows: No. 12—70/30 butadiene-styrene; No. 13—50/50 butadiene-styrene; No. 14—70/30 isoprene-styrene.

that the equivalent weight of Daxad may be about 3200. If we assume that this is also the molecular weight, then the effective surface area of a molecule of Daxad is about 600 A^2. compared to 28.2 A^2. for the oleate molecule.

In this connection it may be pointed out that similar studies made with duPont Aquarex D and General Aniline SA-178 (concentrated grade) gave as the effective surface area per gram of the former 6.80×10^{22} A^2., and 6.44×10^{22} A^2. for the latter.

TITRATION OF LATEX WITH SOAP IN PRESENCE OF DAXAD 11

Since Daxad 11 is adsorbed by the polymer in latex, it is of interest to ascertain the strength of this adsorption compared to soap, and to find out whether presence of Daxad 11 interferes in any way with the determination of latex particle size by soap titration. For these purposes six latices were titrated first conductometrically with the appropriate soaps to determine the moles of soap required for coverage of the total surface per gram of rubber at the c.m.c. Next, given amounts of Daxad 11 were added to fresh samples of the same latices, and the titrations repeated to see how much total soap is adsorbed per gram of rubber in presence of the Daxad 11.

The results thus obtained are summarized in Table II. Comparison of the data listed in column 6 observed in presence of Daxad and column 7 in absence of this emulsifier shows that essentially the same results are obtained whether Daxad 11 is present or not. This means that Daxad 11 in a latex does not interfere with the soap titration method for particle size determination. Further, the reason for this noninterference is that Daxad 11 is displaced from the polymer surface by both fatty and rosin soaps added during the titration. It must follow, therefore, that Daxad 11 is less strongly adsorbed by the polymer than either rosin or fatty acid soaps.

Although presence of Daxad in a latex causes no difficulty during the soap titration, it does interfere with the conductometric determination of the initial soap content of the latex. During the HCl titration in 50% isopropanol both the Daxad and soap react with the acid, and hence both

TABLE II

Adsorption of Soap by Latices Containing Daxad 11

Latex no.	Soap present	Soap added	Grams Daxad 11 added per liter	$S_a \times 10^4$	
				With Daxad	Without Daxad
12	OSR	Oleate	2.07	2.61	2.62
15	OSR	Oleate	2.07	2.03	2.05
13	K-wood rosin	K-wood rosin	1.07	1.49	1.56
16	K-wood rosin	K-wood rosin	1.07	2.81	2.88
14	Dresinate 731	Dresinate 731	2.61	2.21	2.19
17	Dresinate 731	Dresinate 731	2.61	3.89	3.81

Note: For compositions of latices 12, 13, 14 see Table I. No. 15—50/50 butadiene-styrene; No. 16—50/50 butadiene-styrene; No. 17—isoprene-styrene.

are included in the evaluation as soap. However, the error involved is small owing to the relatively small quantities of Daxad normally present in a latex, and owing to the high equivalent weight of the Daxad compared to soap. Thus, if a latex contains, say, 5 parts of soap and 1 part of Daxad per 100 parts of polymer, the error in the initial soap content introduced by the Daxad will be 1.8 %. If, further, the initial surface coverage of the polymer with soap is 50 %, then the error involved in the total adsorbed soap at the c.m.c. will be only 0.9 %, and this will be also the error in the surface area and particle size estimation.

THE CRITICAL MICELLE CONCENTRATION OF DAXAD 11

Conductance measurements at 50° C. on aqueous solutions of Daxad 11 showed that the commercial product micellizes at a critical concentration of 0.80 g. per liter. This value may be compared with the values of C_f found in the titrations of latex with Daxad 11, *i.e.*, the y-intercepts of plots such as shown in Fig. 2. The average of these is 0.77 g. per liter; this checks well with the result for the c.m.c. found in aqueous solution.

ACKNOWLEDGMENT

This work was performed as a part of the research project sponsored by the Reconstruction Finance Corporation, Office of Synthetic Rubber, in connection with the Government Synthetic Rubber Program.

SUMMARY

Daxad 11 is adsorbed by the polymer particles in both fatty acid and rosin soap latices. The amount of Daxad adsorbed is directly proportional to the surface area available for adsorption. At the critical micelle concentration of Daxad in solution the effective area occupied by the Daxad on the polymer surface is 11×10^{22} A^2. per gram, which is about 2.2 times the area occupied by a gram of sodium oleate.

Adsorbed Daxad 11 may be displaced completely from the polymer sur-

face by addition of both fatty and rosin acid soaps to the latices, and hence Daxad is adsorbed less strongly than the two types of soap. Further, this displacement permits the determination of surface area and particle size of the latices by the soap titration method without interference by the Daxad.

The c.m.c. of Daxad 11 at 50° C. has been found to be 0.80 g. per liter in aqueous solution, and 0.77 g. per liter in latex.

REFERENCES

1. MARON, S. H., ELDER, M. E., AND ULEVITCH, I. N., *J. Colloid Sci.* **9**, 89 (1954).
2. MARON, S. H., ELDER, M. E., AND MOORE, C., *J. Colloid Sci.* **9**, 104 (1954).

DETERMINATION OF SURFACE AREA AND PARTICLE SIZE OF SYNTHETIC LATEX BY ADSORPTION.

V. LATICES EMULSIFIED WITH LAURYLAMINE HYDROCHLORIDE

Samuel H. Maron and Max E. Elder

Physical Chemistry Laboratory, Department of Chemistry and Chemical Engineering,
Case Institute of Technology, Cleveland, Ohio

Received May 17, 1954

INTRODUCTION

Preceding papers in this series (1, 2, 3) described a method for the determination of the surface area and particle size of synthetic latices which involves titration of the latices with emulsifiers until the critical micelle concentration (c.m.c.) of the latter is attained in solution. Heretofore the method has been applied to latices stabilized by *anionic* emulsifiers such as fatty and rosin acid soaps and Daxad 11, and the titrating agents were also these substances. In every instance the latices involved were alkaline in character, and the dispersed polymer particles bore a negative charge.

It is a well-known fact that synthetic latices can be prepared as well with *cationic* emulsifiers. Such latices are generally acid, and the latex particles carry a positive charge due to adsorption of the emulsifier cation. Further, these latices are as a rule unstable on the alkaline side, and they tend to coagulate on addition of soap or soap-containing latex. It is therefore impossible to determine their surface area and particle size by titration with soap. However, it is still possible to apply the adsorption method provided we titrate the positive latex with a solution of a cationic emulsifying agent. It is the purpose of this paper to demonstrate this point by presenting results obtained on titration of latices emulsified with laurylamine hydrochloride with the latter substance.

The latices investigated here were supplied us by the B. F. Goodrich Company and the Government Laboratories operated by the University of Akron. They contained, besides the laurylamine hydrochloride, some $AlCl_3$ as well as possibly some free HCl. The latter substances introduced difficulty in analysis of the latices for initial amine content, and hence a new analytical procedure had to be developed to overcome the difficulties encountered.

TABLE I

Determination of Chloride in Amine Salt Solutions and in Latex by Titration with $AgNO_3$

Method	Milliequivalents chloride found in 25 ml. latex	Milliequivalents chloride found in 10 ml. amine soln.
Conductometric titration	1.578	0.978
Potentiometric titration	1.578	0.982

ANALYSIS OF LATICES FOR AMINE CONTENT

Determination of the amine contents of these latices by conductometric or potentiometric titration with NaOH was found to be unsatisfactory. Hence, it was found necessary to resort to another method of analysis to obtain the amine content. The scheme finally adopted involved first the determination of the total chloride content of the latices with $AgNO_3$, and next determination of the chloride not present as amine hydrochloride. The difference between the first and second of these determinations was taken to be the amine content of the latex. It was assumed throughout that the latices contained only amine hydrochloride, $AlCl_3$, and possibly free HCl.

The total chloride content of the latices can be determined either by conductometric or potentiometric titration of the latices in water with $AgNO_3$. Both methods yield results in satisfactory agreement, either in latex or in aqueous amine hydrochloride solutions, as may be seen from the results given in Table I. In the present study the conductometric method was used in the final analysis of the latices investigated. During such a

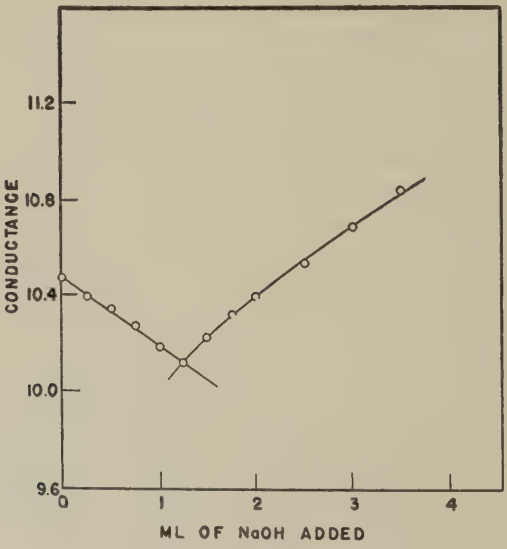

FIG. 1. Determination of free HCl content of latex.

TABLE II

Recovery of $AlCl_3$ in Positive Latex and Amine Solutions by Conductometric Titration with Base

System	Milliequivalents $AlCl_3$ Added	Milliequivalents $AlCl_3$ Recovered as HCl	% $AlCl_3$ recovered
Latex	0.182	0.167	92
Amine solution	0.182	0.172	95

titration no coagulation of rubber takes place when the latex is diluted with water prior to addition of the silver nitrate.

The chloride content of the latices due to any free HCl or $AlCl_3$ was determined by conductometric titrations of samples of the latices with standard NaOH (Fig. 1). Preliminary experiments have shown that $AlCl_3$ can be titrated with base with recovery of almost 3 equivalents of acid *as HCl* for every mole of $AlCl_3$ taken. To check how effective this recovery is in the presence of amine or in the latex, a definite quantity of $AlCl_3$ was added to previously analyzed amine hydrochloride solution and latex, and the samples analyzed for increase in HCl content as shown by conductometric NaOH titration. The results shown in Table II indicate that the recovery is better than 90%. Since the quantity of $AlCl_3$ present in the latices is small, the uncertainty introduced by the low result for $AlCl_3$ is also small, and in practically all cases does not introduce much uncertainty in the value for the amine content of the latices.

Electrode contamination and rubber coagulation do not take place during the above titration. These difficulties appear only during the subsequent amine liberation stage of the titration with base.

A summary of the analytical results obtained on the three latices used in this study by the methods described above is given in Table III.

PREPARATION OF AMINE HYDROCHLORIDE SOLUTIONS

To a given weight of laurylamine (Armour and Company product AM 1120) was added an approximately equivalent volume of 0.1 N HCl, and the mixture heated to effect solution. The resulting solution was analyzed to ascertain whether excess of amine or acid was present, and any excess found was neutralized by addition of the requisite quantity of HCl or amine. The

TABLE III

Summary of Analytical Results on Amine Latices

Latex	Source	Monomer ratio (BD:St)	Dry rubber content *(grams/liter)*	Total chloride content *(equiv./liter)*	Chloride recovered as HCl *(equiv./liter)*	Amine content *(equiv./liter)*
401	Goodrich	75:25	224	0.0870	0.0122	0.0748
402	Goodrich	75:25	236	0.0841	0.0018	0.0823
403	Gov't lab.	50:50	197	0.0631	0.0064	0.0567

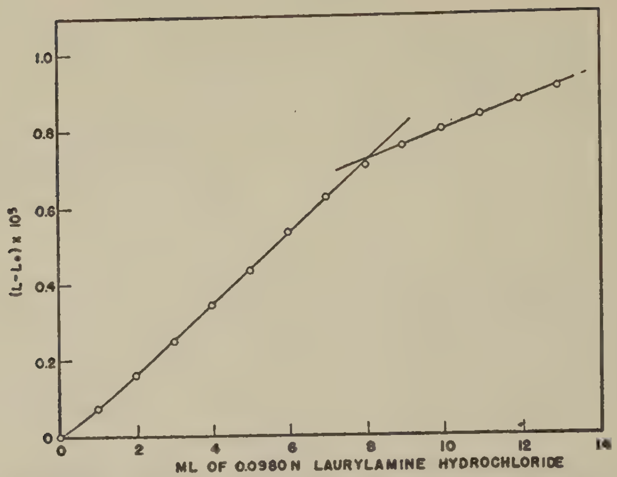

FIG. 2. Conductance titration of positive latex with laurylamine hydrochloride.

final solution was then analyzed for chloride content by both conductometric and potentiometric titration with $AgNO_3$. The results obtained by the two methods were identical within experimental error. An analysis for amine content by addition of chloroform and titration with NaOH using phenolphthalein as indicator (4) gave results which were 1.7% higher than the chloride analyses.

TITRATION OF LATEX WITH AMINE HYDROCHLORIDE

Titrations of the latices with laurylamine hydrochloride were carried out at 50° C. using the same procedure and conductance equipment described previously (1). The plot of conductance changes, $(L - L_0)$, vs. milliliters of added amine salt shown in Fig. 2 is typical of the titration results ob-

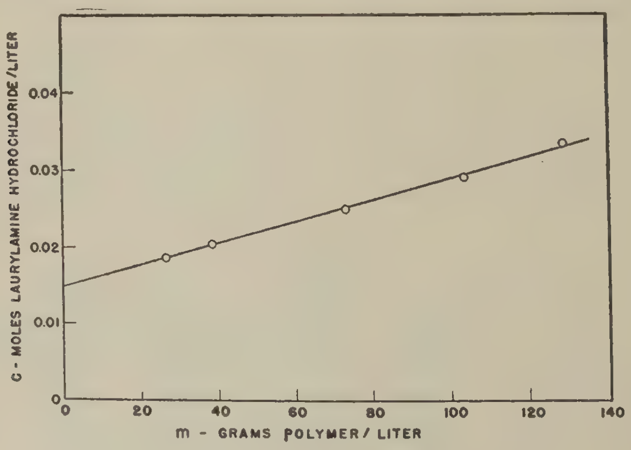

FIG. 3. Plot of C vs. m for latex 403 at 50°C.

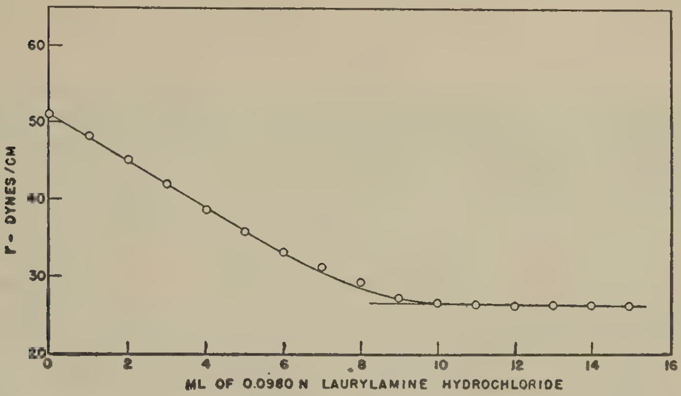

FIG. 4. Surface tension titration of positive latex with laurylamine hydrochloride.

tained. For each latex at least four different concentrations were run to arrive at a plot of C, the concentration of added amine salt at the end point vs. m, the concentration of polymer at the same point. Figure 3, an example of such plots, shows the expected linearity, and yields from the slope S_a, the moles of added amine adsorbed at the c.m.c., while the intercept gives C_f, the c.m.c of the amine in the latex.

Attempts were also made to determine the titration end points by surface tension rather than conductance measurements. Comparison of the resulting plot given in Fig. 4 with the conductance plot in Fig. 2 shows that end-point determination by conductance is more definite and satisfactory, and is to be preferred to observation of the surface tension changes attending titration.

RESULTS AND CONCLUSIONS

The results obtained on titration of the three latices are summarized in Table IV. In this table S_i is the initial amine content, S_a the moles of added amine adsorbed at the c.m.c., and S_t is the total number of moles of amine adsorbed at the c.m.c., all per gram of polymer. C_f is the concentration of amine in moles per liter present in solution at the c.m.c as determined from the y-intercepts of plots such as Fig. 3. In order to calculate from these data the specific area, A, and the average particle diameter, D_s, of the latices, the effective area of the laurylamine hydrochloride molecule is required. Since this quantity was not determined, we shall assume for it here

TABLE IV

Titration Results for Amine Hydrochloride Latices

Latex no.	$S_i \times 10^4$	$S_a \times 10^4$	$S_t \times 10^4$	C_f (moles/liter)	A (m.²/gram)	D_s (A.)	P_i
401	3.34	0.76	4.10	0.0150	64.2	1010	81.5
402	3.49	0.80	4.29	0.0137	67.1	970	81.4
403	2.88	1.40	4.28	0.0150	67.0	920	67.3

a value of 26 A^2. as reported by Harkins and co-workers (5) on the basis of X-ray measurements on amine hydrochloride solutions. Using this value for the molecular amine area, we obtain the results given in columns 6 and 7 for the area per gram and the particle diameter. The last column gives P_i, the percentage of the total surface initially covered by amine in the various latices.

From the results presented in this paper it is evident that the adsorption method can be extended to latices prepared with cationic emulsifiers. The assumption of the amine area in no way modifies this conclusion, for error in this area affects only the numerical values of A and D_s, but not their relative values. In fact, when the effective area of an emulsifier is unknown, the results can be expressed in terms of S_t without conversion to A or D_s. The actual area is then directly proportional to S_t, while the particle diameter is inversely proportional to this quantity.

Acknowledgment

This work was performed as a part of the research project sponsored by the Reconstruction Finance Corporation, Office of Synthetic Rubber, in connection with the Government Synthetic Rubber Program.

Summary

The adsorption method for determination of specific surface area and particle size of fatty and rosin soap latices has been extended to latices emulsified with a cationic protective agent such as laurylamine hydrochloride. The procedure involves titration of the latex with standard solutions of the amine hydrochloride and detection of the end point by conductance measurements. Surface tension was also tried as a means of end-point detection, but it is not as satisfactory as conductance.

An analytical method has also been developed for determination of the amine content of latices in presence of free HCl and $AlCl_3$. The method involves the determination of the total chloride content of the latices by potentiometric or conductometric titration with $AgNO_3$, and then the chloride content due to free HCl and $AlCl_3$ by conductometric titration with NaOH. The amine content follows as the difference between the two analyses.

With these methods, the specific surface areas and particle diameters of three amine latices were determined. In calculating these quantities a value of 26 A^2. was employed for the area occupied on the polymer surface by a molecule of laurylamine hydrochloride at the critical micelle concentration.

References

1. Maron, S. H., Elder, M. E., and Ulevitch, I. N., *J. Colloid Sci.* **9**, 84 (1954).
2. Maron, S. H., Elder, M. E., and Moore, C., *J. Colloid Sci.* **9**, 104 (1954).
3. Maron, S. H., and Elder, M. E., *J. Colloid Sci.* **9**, 347 (1954).
4. Tyler, W. P., and Kurtz, D. M., private communication.
5. Harkins, W. D., Mattoon, R. W., and Corrin, M. L., *J. Am. Chem. Soc.* **68**, 220 (1946).

SOME CONSIDERATIONS ON THE INTERACTIONS BETWEEN PARTICLES IN THE PRESENCE OF A WALL-FLOCCULATION[1] AND ADHESION AS INFLUENCED BY THE CUMULATIVE NET WEIGHT OF THE PARTICLES[2]

Max Bender[3]

Chemistry Department, New York University, New York, New York

Received June 14, 1954

ABSTRACT

Experiments with aqueous zinc sulfide suspensions illustrate that the height of the suspension can be an important factor influencing the degree of adhesion of the particles which have settled to the glass container bottom. In alkaline medium where zeta potential measurements and shallow cell microscopic observations show relatively strong repulsion between individual particles and glass and between particles themselves, there being no flocculation, it was observed that much adhesion of particles to the container bottom developed after settling, if the suspension was relatively tall. On the other hand, in the acid medium, where the zeta potential measurements and shallow cell observations show attraction between glass and individual particles but still slight repulsion between particles themselves and therefore no flocculation normally, the effect of increased suspension height was to decrease the adhesion at the glass bottom while bringing about flocculation.

INTRODUCTION

For a suspension, originally nonflocculated, when the total number of particles settling into the neighborhood of the container bottom is no greater than that corresponding to a layer one particle high on the bottom, it is expected that the degree of adhesion to the bottom will be directly dependent on the balance of electrostatic and nonelectrostatic repulsion-attraction forces between the particles and the glass surface and also individual particle characteristics, such as Brownian movement, weight, size, and shape (3, 7, reference in footnote 2).

But if the total number of particles corresponds to a heavier sediment, whether due to increased height of the suspension or greater particle concentration, it may become necessary to reckon with still another factor in order to understand the adhesion. This is the cumulative net weight of the particles one on top of another, and it can bring about not only adhesion results quite different and opposite to those expected but also flocculation.

---

[1] Flocculation (coagulation) is defined in all this work as the grouping together of the majority of the "individual" particles of a suspension, which are mostly microscopic (1–10 μ) and submicroscopic (<1 μ) in size, to become macroscopic (>100 μ) in size.

[2] The data cited are from Bender, M., "Brownian Movement—Electrical Charge—Flocculation," Ph.D. Dissertation, New York University (1948). See also reference (2).

[3] American Cyanamid Company, Bound Brook, N. J.

This is important to consider in connection with suspensions in general. Also it should be useful in ore flotation research, where one may be studying the relationship between the degree of particle adherence at the bottom of a container, the zeta potential, and the degree of flocculation, in various electrolyte media and interpreting this in terms of the tendency of the particles to "float." Papers by Bankoff (1), Kellogg (6), Taggart *et al.* (8), and Sun (7) are interesting in this connection.

The following experiments with sphalerite particles in alkaline and in acidic media are illustrative of the importance of the "cumulative weight" factor.

EXPERIMENTAL

Sphalerite suspension was prepared by first dry-grinding the mineral in a "Diamonite" mortar and pestle, then pasting with a small amount of distilled water and letting this down with more water to 0.025% solids by weight. This "master" suspension was then diluted 50:50, respectively, with $0.002M$ Na_2CO_3 and $0.002M$ H_2SO_4 to give the preparations now under consideration. Most of the particles were between 0.1 and 0.5 μ in radius. Neither suspension was flocculated when first prepared, the degree of dispersion appearing to be the same as judged by comparative settling rates and examination with the microscope.

Five different suspension heights were considered for each of the two preparations. The lowest was less than 35 μ and consisted of the "shallow cell" which is prepared by placing a microscope cover glass over a drop of the suspension on a glass slide. Here the extent of the adhesion was deduced on the basis of microscopically observing whether the particles were in Brownian movement, since adhering particles do not exhibit this activity (2). The next lowest height was about 1 mm. and corresponded to droplets of the suspensions positioned on glass slides with no cover glasses. The other heights, namely 2.5, 4.0 and 5.0 cm., respectively, were the suspension heights in 50 cc. beakers and also 10 cc. vials, 6 cm. high. Degree of adhesion for all experiments outside the shallow cells was judged visually after drawing off the preparation, lightly rinsing the surface, and drying over a flame. All suspensions were well shaken before any settling-adherence studies were made. Note that prior to use, the glassware was first washed with soap and water and rinsed, then treated with chromic acid solution, followed by thorough rinsing with distilled water and finally alcohol.

TABLE I

Adhesion of Sphalerite to Glass in 0.001M Na_2CO_3 and in 0.001M H_2SO_4 as a Function of Suspension Height

Expt. No.	Height of suspension	Period of settling	Degree of adhesion	
			In 0.001M Na_2CO_3	In 0.001M H_2SO_4
1	$<35\mu$	1–2 min.	Practically none	Practically all the particles
2[a]	About 1 mm.	20 min.	Some deposit	More deposit than in Na_2CO_3
3	2.5 cm. (beaker)	3 hrs.	Much	Quite small visually
4	4.0 cm. (vial)	Several hours	Much	Visually little or none
5	5.0 cm. (vial)	20 min.	Much	Visually little or none
		2 weeks	Very dense adhering compact cake	Granular loose cake coming readily off the bottom

[a] Droplets taken from preparations of No. 5 after shaking after the 20-minute settling. No. 2 was repeated by first placing single drops of 0.002M Na_2CO_3 and of 0.002M H_2SO_4 on the slides and to these solutions adding one drop of the 0.025% "master" suspension. Now the adhesion was about the same from the acid as from the alkaline media.

The experiments which were made are summarized in Table I. These data illustrate very well that the degree of adhesion can vary extremely, depending on the height of the suspension. The periods of settling (prior to examination of the container bottoms for adhesion) were of sufficient duration to allow most all the particles of the suspensions to settle fairly close to each other at the bottom. With further passage of time the degree of adhesion changes but little except for the taller alkaline suspensions where the cake becomes more firmly packed and adhering. In Experiment No. 5, the extreme of two weeks caused the alkaline cake to become so dense that vigorous shaking was required to resuspend it. However, the original degree of dispersion was obtained, although, as described below, this was not quite so with the acid sediment.

Flocculation was not evident at all for the alkaline suspensions. The acid ones, however, although not flocculated when first prepared, became so when a sufficient number of the particles (in the case of the taller suspensions) settled into close proximity in the vicinity of the bottom of the container. This could be seen for instance in Experiment 5, when the vials were carefully inverted after standing for about 20 minutes. The acid sediment was granular and flocculated, its coarseness relative to the alkaline sediment (which went readily back into suspension in the form of a cloud of fine particles) being very obvious.

Nevertheless, whatever flocculation was observed was not completely of

TABLE II

Electric Charge of Sphalerite Particles and Glass Surface in Alkali and Acid

	Sphalerite		Glass	
	C.V.[a]	ζ[b]	C.V.[a]	ζ[b]
$0.001M$ Na_2CO_3	−2.11	−27.5	−2.95	−38.3
$0.001M$ H_2SO_4	−1.12	−14.6	−0.38	−4.9

[a] Cataphoretic velocity in microns/sec./volt/cm.

[b] Zeta potential in millivolts. Calculated from C.V. by the Helmholtz-Smoluchowski equation.

permanent nature because the floccules could be broken up again into individual particles by shaking. This was true for acid suspension settling for 20 minutes as well as for suspension settling for two weeks. Actually, the original degree of dispersion was not quite obtained on shaking, this being more true in the situation of the two weeks settling. For instance, although most all the floccules were broken up on shaking, it could be seen visually and by microscope that these individual particles so obtained were on the whole somewhat coarser than originally.

Discussion

An explanation of how the height of the suspension can have such pronounced effect on the adhesion in either the alkaline or the acid medium and also on the flocculation in acid medium, may be sought with the aid of theoretical considerations such as have been made by Hamaker (5) and Verwey and Overbeek (9) applied to the electrokinetics in the present systems. Table II gives these data for the particles and the glass surface as obtained with a Northrup-Kunitz cataphoresis cell (2).

The appreciable repulsion between particles and glass in the alkaline medium is the reason for there being no adhesion of particles in the alkaline shallow cell. In the acid shallow cell, however, with the glass almost at the isoelectric point,[4] there is adhesion.

Flocculation was absent in the alkaline medium owing to the high mutual repulsion between the particles. In the acid medium with the particle charge being less negative and the repulsion between particles accordingly less, there was flocculation but only in the taller suspensions after they had been allowed to settle. These floccules could be broken up by vigorous shaking, although not quite to the original degree of dispersion, indicating some strong attraction by virtue of the particles' penetrating into a minimum energy field.

This difference in flocculation in the acid medium depending only on the suspension height must be explained in terms of the greater cumulative net weight of particle on particle in the taller suspensions. With the increased force due to gravity, the particles can penetrate the comparatively low repulsion barriers of each other, the breakthrough being so rapid that they attach at random, that is, at first sight so to speak, thus giving the flocculated loose structure observed.

---

[4] With greater acidity the charge of the glass becomes positive. For instance, at $0.002M$ H_2SO_4 the zeta potential is +16.6 millivolts.

Meanwhile the adhesion to the bottom (or the cohesion with other floccules) becomes practically nil, because any area of contact of the voluminous and irregular shaped floccules with the glass (or other floccules) is so small compared to the over-all floccule surface and weight that they do not hang on in the face of any degree of disturbance such as inverting the container or rinsing (see Ehrenberg (4); von Buzágh (3), p. 166–7; Hamaker (5); Verwey and Overbeek (9), p. 15, 17; and Sun (7)).

In the tall alkaline suspensions despite the higher zeta potentials in the system there is also penetration of the repulsion barriers owing to the cumulative net weight of the particles. But now, with the stronger repulsion between particles and particles and glass bottom, this action is quite slow compared to that in the acid medium. The particles, being in Brownian movement, move about and slide over each other and over the glass bottom as they are forced closer with settling. There is time to squirm and fit into crevices before the attraction forces prevail so that a compact sedimentation cake in close contact and strongly adhering to the container bottom eventually results.[5] It is interesting that the alkaline sedimentation cake, unlike the acid floccules, does revert to the original degree of dispersion on shaking, thus showing that the repulsion barriers have not yet been too strongly overstepped. Continued settling as in Experiment 5 (two weeks) brings the particles more into the field of minimum energy, as is evident from the more compact cake more difficult to redisperse. Evidently, centrifuging would probably bring the particles so close to each other that there would no longer be reversibility of dispersion (see Hamaker (5)).

It is thus seen that the height of a suspension may have much to do with the adhesion of particles at the bottom and also any flocculation. Explanation is given. These possibilities should be carefully considered in connection with adhesion and flocculation studies in general.

REFERENCES

1. BANKOFF, S. G., *Am. Inst. Mining Met. Engrs., Tech. Publ. No.* **1391** (1942).
2. BENDER, M., AND MOUQUIN, H., *J. Phys. Chem.* **56**, 272 (1952).

---

[5] With a still higher repulsion barrier, the formation of this compact adhering sedimentation cake is at least delayed. This was shown by adding one drop of Tergitol penetrant surface active agent (Carbide and Carbon Chemical Corporation) per 25 cc. suspension and allowing to sediment at 2.5 cm. height. No adhesion occurred. In the acid medium with the same concentration of agent and the same height there was a slight deposit, but this was very small compared to the original acid suspension.

3. Buzágh, A. von, "Colloid Systems." Technical Press, Ltd., London, 1937.
4. Ehrenberg, P., "Bodenkolloide," p. 83ff. Dresden, 1918.
5. Hamaker, H. C., *Rec. trav. chim.* **55**, 1015 (1936).
6. Kellogg, H. H., *Am. Inst. Mining Met. Engrs., Tech. Publ. No.* **1841** (1945).
7. Sun, S., *Am. Inst. Mining Met. Engrs., Tech. Publ. No.* **1580** (1943).
8. Taggart, A. F., Taylor, T. C., and Knoll, A. F., *Trans. Am. Inst. Mining Met. Engrs.* **87**, 217 (1930); or *Am. Inst. Mining Met. Engrs., Tech. Publ. No.* **312** (1930).
9. Verwey, E. J. W., and Overbeek, J. Th. G., "Theory of the Stability of Lyophobic Colloids." Elsevier, Amsterdam, 1948.

LETTER TO THE EDITOR

FACTORS LIMITING THE SOLUBILITY OF NONIONIC DETERGENTS IN WATER

In a recent Letter to the Editor of this Journal, M. H. J. Weiden and L. B. Norton (1) described temperature-phase diagrams for aqueous solutions of "Triton" X-100 and "Thiosolve" 8139. These two nonionic detergents,[1] both of which contain an ethylene oxide polymer unit as a major substituent in the surface-active molecules, were completely miscible in water at room temperature but separated into two phases, the heavier phase being detergent rich, above 60°C. The important observation reported by Weiden and Norton is that aromatic liquids in amounts of the order of 1–10 g./l. of detergent solution lowered the temperature at which phase separation occurred by 5–50°C. In several cases separation could be produced in aqueous mixtures at room temperature, starting with aromatic compounds and detergents that were normally miscible with water, by themselves, at room temperature.

Although nonionic detergents based on ethylene oxide have been used commercially for many years, little or no attention has been given to this unusual effect of aromatic compounds, at least as far as the scientific literature is concerned. Undoubtedly many industrial chemists have encountered some manifestations of this effect while working with these detergents, but these results remain unpublished. It is the purpose of this note to present some pertinent observations, based on our previous experience with these nonionic detergents, that could not be readily interpreted until Weiden and Norton presented their work. These observations will consist of three parts:

1. A presentation of further data in support of the generality of the observations of Weiden and Norton.
2. A suggestion that pH is an important factor affecting the solubility of nonionic detergents that was not examined by Weiden and Norton.
3. A review of some industrial applications utilizing the indicated methods for decreasing the solubility of these nonionic detergents.

GENERAL OBSERVATIONS

An initial observation established that aqueous solutions of a variety of nonionic surface-active agents based on ethylene oxide polymers had the same general behavior when mixed with catechol and similar phenols. As an example, it was observed that "Agent L," made by condensation of 28 g. technical 1-hexadecanol with 83 g. ethylene oxide in the presence of 0.3 g. Na at 175°C. for 4 hours, was completely miscible with water at room temperature. Addition of a 20% aqueous solution of catechol to a 20% solution of "Agent L" in water at room temperature immediately changed the solution into a turbid mixture from which two layers promptly separated.

---

[1] Commercial products from Rohm & Haas Co., Philadelphia, and Geary Chemical Corp., New York, respectively.

In a similar room temperature experiment, equal parts of a 20% aqueous solution of "Agent L" and a 12% aqueous solution of sodium *o*-chlorophenolate were mixed to form a homogeneous solution. Addition of a small amount of dilute sulfuric acid acidified the solution, thereby liberating the free phenol and producing a phase separation similar to that produced by catechol. The composition of the oily phase that separated corresponded to approximately 25% *o*-chlorophenol, 60% "Agent L," and 15% water.

It was also observed that a 20% aqueous solution of catechol would cause phase separation at room temperature when added to a 20% aqueous solution of "Tween" 20 (Atlas Powder Company, described as a sorbitan monolaurate polyoxyalkylene derivative), or a 5% aqueous solution of "Agent M," a condensation product made by the same general procedure as "Agent L," but having a ratio of 1 mole octadecanol to 16.3 moles of ethylene oxide.

pH EFFECTS

There is a significant difference between the two experiments described above in which phase separation of "Agent L" solutions occurred. The catechol solution alone produced this separation, whereas the mixture of "Agent L" and *o*-$NaOC_6H_4Cl$ in water separated only on acidification. This difference between phenols and alkali phenolates was observed consistently in our work. Weiden and Norton do not report the *p*H of the aqueous solutions for which they present temperature-phase diagrams. It seems likely that the boundary between one and two phases, as given by them, would be quite sensitive to *p*H, at least in the case of the phenol-water-"Triton" X-100 system (their Diagram 3).

No explanation has been proposed for the difference in effect between free phenols and their salts. It has been definitely established that the effect is observed consistently. For example, for detergent solutions at any given initial *p*H, the strongly acidic *o*- or *p*-nitrophenols are poorer coagulants for nonionic detergents than the less acidic *m*-nitrophenol or C_6H_5OH itself. The more weakly acidic phenols of course have a greater concentration of free phenol at any given *p*H.

INDUSTRIAL APPLICATIONS

Many industrial processes rely on controlled methods for converting water-soluble detergents and surface-active agents to insoluble forms. For example, the rubber latex industry relies heavily on coagulation techniques such as acidification of soap-stabilized latexes (2). An important feature of the commercial processes for emulsion polymerization of synthetic rubbers is the coagulation step, accomplished with salt and acid for the soap-stabilized GR-S dispersions (3) or by freeze-coagulation of rosin-soap stabilized neoprene dispersions (4). The stability of latexes or dispersions stabilized with nonionic surface-active agents containing the ethylene oxide polymer unit is such that these systems resist the conventional methods of coagulation. This has led to the proposal that heat be used for coagulation of such systems (5, 6, 7, 8). This is unsatisfactory for many latex systems. The coagulating effect of phenols on nonionic surface-active agents was recognized as having considerable commercial interest when it was first discovered by Bächle (9).

Examples of the use of this process can be selected from our investigations:

1. Standard neoprene latex (10) was made acid-stable by addition of "Agent L" in amounts that gave a final proportion of 3 parts nonionic agent per 100 parts of neoprene, as well as the usual 4.5 parts of anionic surface-active agent. The latex was then sensitized with 5.3 parts of an aqueous solution made from 4 parts water, 0.8 part catechol, and 0.5 part tetraethanolammonium hydroxide. Strong, smooth neoprene films 0.015 in. thick were produced by dipping a form first in a mixture of equal parts of ethanol and acetic acid, and then in the latex. If the sensitizing solution had not been added, no film would form on dipping.

2. A 50:50 mixture of butadiene and styrene was emulsified in an aqueous solution of "Agent L" containing potassium persulfate as a polymerization catalyst. The latex that formed on polymerization contained 10 parts "Agent L" per 100 parts of water. It could not be coagulated by addition of half its weight of 37% aqueous HCl. In contrast, one-third its weight of 40% aqueous catechol coagulated the latex completely.

3. A similar neoprene latex was made by emulsion polymerization of chloroprene under conditions giving a final latex containing 4 parts "Agent L" per 100 parts water, with a *p*H of approximately 2. This latex could not be coagulated by acids or electrolytes. Instant coagulation occurred at the interface between the latex and an aqueous solution containing 10–20% of phenol, catechol, resorcinol, or pyrogallol. The following phenols, which were added to the latex as aqueous solutions of the sodium salts because of the poor solubility of the free phenols, caused coagulation of the latex on addition of acid to adjust the pH to 2: *o*-cresol, *p*-cresol, hexyl resorcinol, resorcinol monomethyl ether, *o*-fluorophenol, *o*-chlorophenol, *p*-chlorophenol, *p*-bromophenol, *m*-nitrophenol, and 1-naphthol.

REFERENCES

1. WEIDEN, M. H. J., AND NORTON, L. B., *J. Colloid Sci.* **8**, 606 (1953).
2. NOBLE, R. J., "Latex in Industry," *Rubber Age*, New York (1953), p. 348.

3. Soday, F. J., *Trans. Am. Inst. Chem. Engrs.* **42,** 647 (1946).
4. Youker, M. A., *Chem. Eng. Progr.* **43,** 391 (1947).
5. Ogilby, S. R., U. S. Patent 2,215,562 (1940).
6. Ogilby, S. R., U. S. Patent 2,215,563 (1940).
7. Johnson, C. S., U. S. Patent 2,215,553 (1940).
8. Bächle, O., and Sinn, G., U. S. Patent Application Serial No. 362,608 (Published by Alien Property Custodian), 1943.
9. Bächle, O., German Patent No. 735,666 (1943).
10. Andersen, D. E., and Arnold, R., *Ind. Eng. Chem.* **45,** 2727 (1953).

H. K. Livingston

Jackson Laboratory,
E. I. duPont de Nemours and Co.,
Wilmington, Delaware

Received May 7, 1954

BOOK REVIEW

Current Chemical Papers is a new publication of the Chemical Society of London, published at £2.10s.0d per annum ($7.50) post free or, for copies sent by air mail to addresses outside Europe, £4.5s.0d per annum ($12.75). There will be no Index.

This publication is a monthly classified world list of new papers in pure chemistry, containing the titles, with authors' names and references to the original Journal, of relevant papers published in journals received during the previous month. Although the titles of papers will be expanded, where necessary, by the addition of a few words, *Current Chemical Papers* is intended to inform research workers of papers more rapidly than would be possible in a journal publishing full abstracts.

Readers of this journal would find this new service of more value to them if the Editors would classify papers under the separate headings of the type: (*a*) Colloids and Surface Chemistry, (*b*) Polymers and Polyelectrolytes, rather than distributing the papers belonging to these categories under such overloaded titles as ''Equilibrium Properties and Thermodynamics'' and ''Structure in Condensed Phases.''

Victor K. La Mer, New York, New York

The Proteins. Chemistry, Biological Activity and Methods. Edited by Kenneth Bailey and Hans Neurath. Academic Press, Inc., New York 10, N. Y. Volume 2, part A, x + 661 pp. Price $14.

This is the third volume (although called Volume II, Part A) of the most useful compendium on the subject which has appeared to date. Unlike the preceding two volumes (Parts A and B of Volume I) the arrangement of material here is by groups of individual proteins rather than by broad topics or groups of properties. There is surprisingly little duplication of material already presented in the earlier volumes. The very fact that this is so is noteworthy as an indication that protein studies of a theoretical nature (organic and physical chemistry) have tended to concentrate on and develop a rather small group of phenomena out of the whole range of remarkably diverse and biologically significant properties which characterize the proteins. The present book also serves to remind one again of the limitation of material to a relatively small group of proteins in the most highly developed physicochemical work.

The present volume has chapters on Nucleo-proteins and Viruses (R. Markham and J. D. Smith); Oxidizing Enzymes (T. P. Singer and E. B. Kearney); Respiratory Proteins (F. Haurowitz and R. L. Hardin); Toxic Proteins (W. E. Van Heyningen); Milk Proteins (T. L. McMeekin); Egg Proteins (R. C. Warner); Seed Proteins (S. Brohult and E. Sandgren); Proteins and Protein Metabolism in Plants (F. C. Steward and J. F. Thompson); and Protein Hormones (C. H. Li). Although they differ considerably in emphasis and organization, all of the chapters are excellent. They provide very complete summaries of the literature to the end of 1951 in a fully digested form that is easy to use. There is very little tendency, however, to be merely encyclopedic. With few exceptions work is not merely cited but discussed in a significant context. If often one would wish the discussion had been more complete, one must also recognize the limitations of space in a work that is so exhaustive. The omission in some chapters of a few uncritical references to obsolete earlier work might have permitted more adequate discussion of more recent and more significant results.

It is probably to be expected that the present volume is richer in biological aspects and considerations than the earlier volumes.

The prospective purchaser of Part A alone is warned that it contains no index. Indices to both parts are to be contained in Part B to be published this summer.

Jacinto Steinhardt, Cambridge, Mass.

ERRATA

Supplement 1, in the article, "The Penetration of Ions into Charged Films," by J. T. Davies and Sir Eric Rideal:

p. 4, paragraph 3, sentence 1, should read, "Figure 5 (6) shows the relation between . . . ."

p. 5, in the legend for Fig. 5, omit refs. (6, 7)

p. 8, ref. 6 should read, "6. Czeczowiczka, N., Ph.D. Thesis, Birmingham University (1953)."

SOLUBILIZATION BY POTASSIUM LAURATE SOLUTIONS CONTAINING LAURIC ACID[1]

Samuel Spring[2] and Edgar Howard, Jr.

Department of Chemistry, Temple University, Philadelphia 22, Pennsylvania

Received July 9, 1954

ABSTRACT

Studies have been made of the solubilization of benzene by potassium laurate solutions containing lauric acid, with moderate quantities of 1-butanol present to improve solubilities. Up to a concentration of about 25% lauric acid relative to potassium laurate, the influence of increasing acid content is a regular increase in solubilization of benzene. This increase is substantially greater than that produced by an equimolar increase in butanol concentration. At a potassium laurate–lauric acid ratio of about 3/1 to 4/1 a sharp change in properties occurs; beyond this transition region increased lauric acid content causes a great reduction in the solubilization of benzene, an increase in viscosity, and a sharp decrease in the influence of butanol as a co-solubilizer. Observations in this transition region are interpreted as indicating a change from a spherical to a rodlike micellar structure.

INTRODUCTION

References to the influence of fatty acids on solubilization by soap solutions are limited in number. Thus, McBain and Richards (1) reported that oleic acid is solubilized by soap solutions to a somewhat greater extent than the equivalent hydrocarbon. Acid soaps were found by Ekwall (2) to dissolve in more concentrated soap solutions. Rather general statements have been made by Winsor (3) and Klevens (4) that fatty acids should act similarly to alcohols to increase the solubilizing capacities of soap solutions because of the hydrogen bonding tendencies exhibited by both materials. The most specific data available are the work of McBain and Lissant (5), who showed that the solubilization of hydrocarbons by 0.25 M potassium laurate solutions is markedly increased when 5% lauric acid is added.

The present investigation covers a much larger range of lauric acid concentration than that of McBain and Lissant. To do this required the addition of substantial quantities of a co-solubilizer, butanol being chosen for this purpose.

---

[1] Abstracted from the dissertation submitted by Samuel Spring to the Temple University Graduate Council in partial fulfillment of the requirements for the Ph.D. degree, June, 1952.

[2] Present address: Pennsylvania Salt Mfg. Co., Whitemarsh Research Laboratories, P. O. Box 4388, Phila. 18, Pa.

One reason for initiating this work was to determine whether enhanced solubilization by potassium laurate in the presence of lauric acid is associated with acid soap formation, which might provide unusual micellar properties. Acid soaps of composition KL·HL, KL·2HL, 2KL·HL (6) and 3KL·HL (7) have been reported; the first two ratios would require very high concentrations of alcohol to form homogeneous systems at near ambient temperatures and were not given further consideration.

EXPERIMENTAL

1. Materials

Lauric acid was Eastman Kodak White Label Grade; m.p. 44.5–45.5°C. All samples assayed to 100 ± 0.1 % lauric acid by titration with standard 0.1 *N* alkali. Potassium hydroxide was Baker and Adamson Reagent. Distilled water was used for all experiments. 1-Butanol was Merck Reagent Grade; b.p. 116–118°C. Benzene was Merck Reagent Grade (thiophene free).

2. Preparation of Samples

Samples were prepared in 250-ml. Erlenmeyer flasks with ground-glass stoppers. Lauric acid was weighed (±0.01 g.) into the flask. The calculated quantity of standard 0.5 *N* KOH and the desired quantity of water were added from burets. The samples were heated to 70° ± 2°C. to yield homogeneous systems and then were cooled to room temperature. Concentrations are expressed as molalities; i.e., moles of lauric acid or potassium laurate, or mixtures of the two, per 1000 g. of solvent.

3. Solubilization Measurements

Samples were maintained in a constant-temperature bath at 30.5° ± 0.1°C. In one type of experiment, a specified volume of butanol (cosolubilizer) was added, and benzene was introduced in increments of 0.25 ml. Another portion was introduced as soon as the first was solubilized, When this no longer occurred, as evidenced by the presence of turbidity, the sample was agitated by shaking every 15 minutes. The last increment of benzene was in contact with the solution for at least 24 hours with manual shaking every 15 minutes for the last 2 hours.

In another type of experiment, 10.0 ml. of benzene was added and then 1-butanol was introduced in 0.25-ml. increments until the system was almost clear. The butanol was then added in 0.10-ml. increments at intervals of at least 2 hours until a clear system was obtained.

4. Viscosity Measurements

Measurements were made with an Ostwald-Fenske Viscosimeter (No. 200). Since relative values are of the greatest interest, data are expressed

TABLE I

Solubilization of Benzene by 0.5 Molal Potassium Laurate-Lauric Acid Mixtures Containing Butanol. T = 30.5°C.

Lauric acid neutralized (%)	Molar ratio $\frac{KL}{HL}$	Benzene solubilized (ml. per 100 g. of sample[a])		
		6.3 ml. Butanol[b]	7.1 ml. Butanol	8.0 ml. Butanol
66.7	2.0	0.0	0.2	0.8
71.7	2.5	0.9	1.1	2.0
74.5	2.9	1.5	1.9	2.5
77.0	3.4	2.2	2.3	9.5
80.0	4.0	—	8.5	—
82.0	4.6	8.6	8.9	9.7
85.0	5.7	—	8.8	—
87.2	6.8	8.2	8.7	9.4
92.2	11.3	7.6	8.2	8.8
100.0[c]	—	6.2	7.0	7.5

[a] Per 100 g. of sample including the specified quantity of butanol.

[b] Milliliters of butanol per 100 g. of 0.5 molal potassium laurate-lauric acid mixture.

[c] The value for the solution without any butanol is 3.2 ml. of benzene.

in seconds. Each recorded value represents the average of five readings. A constant-temperature bath at 30.0° ± 0.1°C. was used, and the sample was given 1 hour to reach bath temperature.

RESULTS

1. Solubilization of Benzene by Lauric Acid-Potassium Laurate Solutions

The volume of benzene solubilized by 0.50 molal potassium laurate-lauric acid mixtures, as a function of percentage of lauric acid neutralized, was determined for systems containing various quantities of 1-butanol. These data are presented in Table I and Fig. 1. The benzene was solubilized fairly rapidly until just before the saturation point when 1–2 hours were required to solubilize the last increment of benzene. After saturation, a definite turbidity resulted and emulsified benzene floated to the top of the solution.

The sharpness of the increase in solubilization of benzene in the region of 75%–82% lauric acid neutralized is quite striking. The curve for the system containing 8.0 ml. of butanol approaches its region of maximum change sooner than the curves for 6.3 and 7.1 ml. of butanol; this occurs at 75%–77%. The data are replotted in Fig. 2 as a function of the potassium laurate-lauric acid molar ratio.

Since solubilization is a function of concentration of soap, it is possible that these data are influenced by the changing soap concentration as the percentage of lauric acid neutralized increases. Consequently, this work

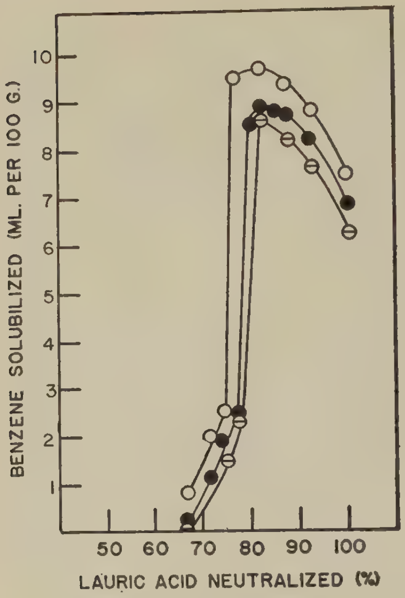

FIG. 1

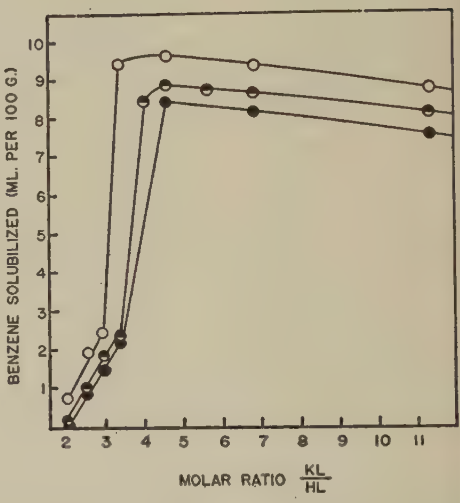

FIG. 2

FIG. 1. Solubilization of benzene by 0.5 molal potassium laurate-lauric acid mixtures in butanol-water solution at 30°C. Lower curve, 6.3 ml. butanol per 100 g. of 0.5 molal KL-HL mixture; middle curve, 7.1 ml.; upper curve, 8.0 ml.

FIG. 2. Solubilization of benzene by 0.5 molal potassium laurate-lauric acid mixtures in butanol-water solution at 30°C. (molar ratio plot). Lower curve, 6.3 ml. butanol; middle curve, 7.1 ml; upper curve, 8.0 ml.

was repeated with solutions having a fixed soap concentration to which quantities of lauric acid were added. The data obtained are given in Table II and Fig. 3.

It may be observed that these data are substantially in agreement with the data presented in Figs. 1 and 2.

In addition, the solubilization value for the system without butanol is given for 100% neutralized lauric acid (Table I). However, the solubilization process for this system was rather different. The benzene floated about as tiny particles which gradually disappeared as the saturation point approached.

2. Viscosity of Solutions of Lauric Acid in Potassium Laurate

Values for the viscosity of systems similar to those investigated for solubilization characteristics are given in Fig. 4. It may be seen that a pronounced break in the curve occurs in the region of 77%–78% lauric acid neutralized. The viscosity decreases less rapidly with increased

TABLE II

Solubilization of Benzene by Potassium Laurate (KL) Solutions Containing Lauric Acid (HL) in the Presence of Butanol. T = 30°C.

HL neutralized (%)	Free HL (g. per 8.0 g. of KL)	Molar ratio $\frac{KL}{HL}$	Benzene solubilized by 0.4 molal KL (ml. per 100 g. of sample[a])
100.0	0.0	—	8.0
94.3	0.5	16.0	9.0
88.9	1.0	8.0	10.1
84.3	1.5	5.3	10.7
80.0	2.0	4.0	11.2
76.2	2.5	3.2	2.7
72.7	3.0	2.7	1.7
69.6	3.5	2.3	0.7

HL neutralized (%)	Free HL (g. per 10.0 g. of KL)	Molar ratio $\frac{KL}{HL}$	Benzene solubilized by 0.5 molal KL (ml. per 100 g. of sample[b])
87.0	1.5	6.7	10.6
83.5	2.0	5.0	11.1
80.0	2.5	4.0	3.5
76.9	3.0	3.3	2.0

[a] Including 8.3 ml. of 1-butanol per 100 g. of sample.

[b] Including 7.4 ml. of 1-butanol per 100 g. of sample.

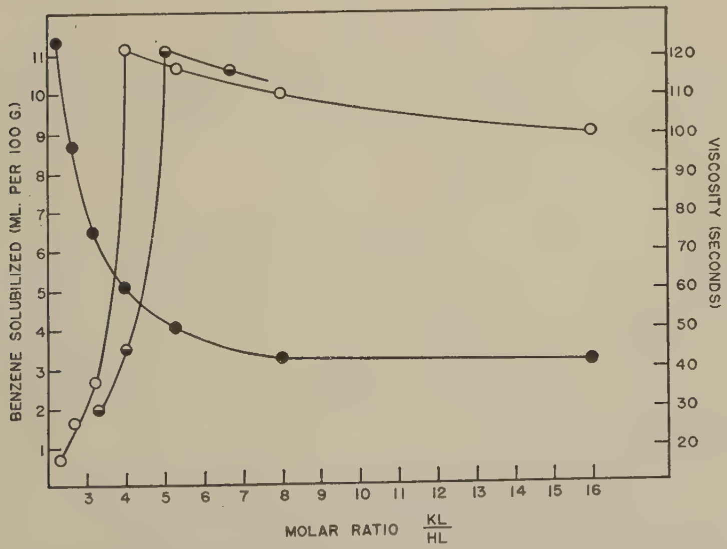

FIG. 3. Solubilization of benzene in butanol-water solution at 30°C. by potassium laurate-lauric acid mixtures having fixed soap concentration. ◒, 0.5 molal KL solution containing 7.4 ml. butanol per 100 g. of sample; ○, 0.4 molal KL solution containing 8.3 ml. butanol; ●, viscosities of solutions containing 8.3 ml. butanol.

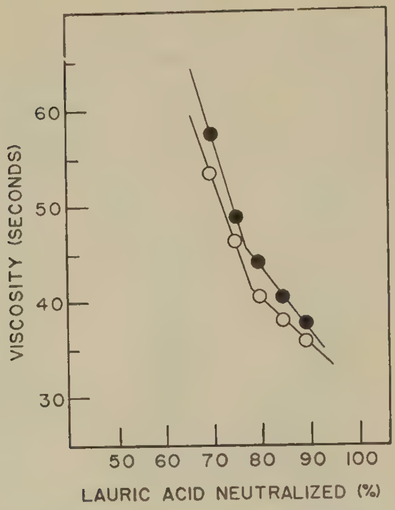

FIG. 4. Viscosities of systems described in Fig. 1: lower curve, 7.1 ml. butanol; upper curve, 8.0 ml. butanol.

neutralization past the points of inflection. The inflection points correspond very closely to the points at which the sharp alteration in solubilization is observed in Fig. 1.

The viscosities of the systems of fixed potassium laurate content with increasing quantities of free lauric acid are given in Fig. 3. Sharp inflection points similar to those observed in Fig. 4 were not obtained. However, the region of rapidly changing viscosity corresponds closely with the region of rapidly changing solubilization.

3. *Minimum Butanol Required for Solubilization of Fixed Quantity of Benzene*

In this experiment, a fixed amount of benzene was used and the volume of butanol required to yield an optically clear system was determined. The data are given in Table III and Fig. 5.

The sharply defined transition region that was obtained is demonstrated by Fig. 5. The minimum in the curve occurs at 72% lauric acid neutralized by potassium hydroxide.

The viscosities of this system are given in Fig. 6. The curve of Fig. 5 is inserted as a dotted line. It may be observed that the viscosity curve does not exhibit a minimum, as does the solubilization curve, but there is a rapid rise in viscosity below 72% neutralization (the minimum in the solubilization curve). For purposes of comparison, viscosities are also given for the equivalent system containing the same amount of butanol, but without solubilized benzene. It may be observed that the curves are

TABLE III

Butanol Required to Solubilize 10.0 ml. of Benzene in 100 ml. of 0.5 Molal Potassium Laurate-Lauric Acid Mixtures. T = 30°C.

0.477N KOH (ml.)	H_2O (ml.)	Lauric acid neutralized (%)	Butanol (ml.)
104.8	0.0	100.0	13.9
100.0	0.0	95.4	12.6
90.0	10.0	85.9	11.7
85.0	15.0	81.2	11.0
80.0	20.0	76.4	9.1
77.5	22.5	74.0	8.9
75.0	25.0	71.6	6.8
72.5	27.5	69.3	7.8
70.0	30.0	66.8	8.5
65.0	35.0	62.1	10.0
60.0	40.0	57.2	10.9
55.0	45.0	52.6	12.0

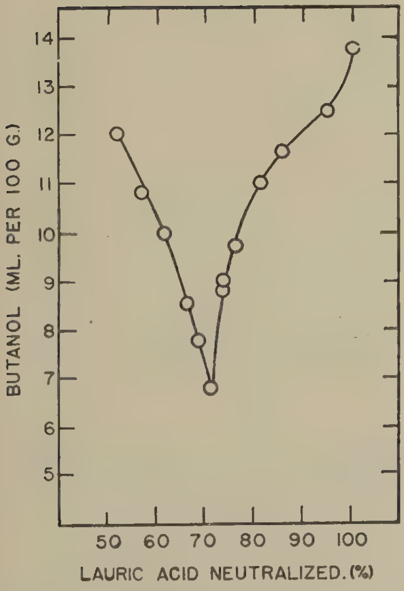

FIG. 5

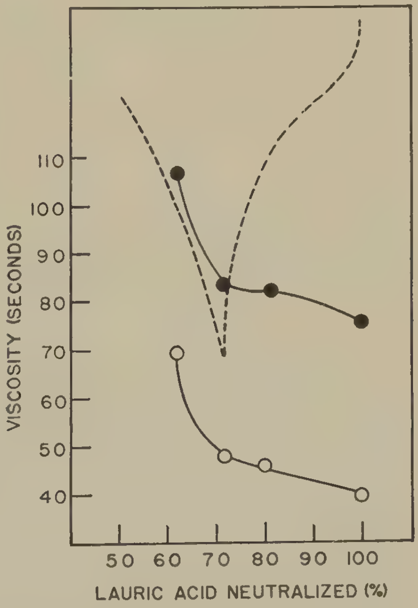

FIG. 6

FIG. 5. Minimum butanol required to solubilize a fixed quantity of benzene (10 ml.) in 100 ml. of 0.5 molal potassium laurate-lauric acid mixtures at 30°C.

FIG. 6. Viscosity of the benzene- and butanol-containing system described in Fig. 5 (●). Viscosity of the same system in the absence of benzene (○). The curve of Fig. 5 is inserted as a dotted line.

similar in form, but the systems containing solubilized benzene are considerably more viscous.

Discussion

1. The Influence of Fatty Acid and Alcohol on Soap Micelles

The thermodynamic stability of soap micelles is considered to be due to the reduction in interfacial free energy as the hydrocarbon portion of the soap molecule leaves its aqueous environment and obtains a hydrocarbon environment within the micelle.

The increase in solubilization of a hydrocarbon by the addition of an alcohol to a soap solution is attributed to an increase in the size of the micelles and hence of the hydrocarbon environment that is available. The increase in solibilization of benzene by potassium laurate with increase in lauric acid content, which takes place up to about 25% free fatty acid content, may also be attributed to increased size of the soap micelles.

Alcohols in soap solutions are considered to be introduced into the micelles with their polar groups contiguous to the polar groups of the soap molecules and the hydrocarbon portions parallel to the hydrocarbon portions of the soap molecules. Klevens (4) and Winsor (3) state that increased solubilization due to fatty acids would be the consequence of a similar structure.

Quantitatively, the influence of the free fatty acid is considerably greater than that of the alcohol. Thus, Fig. 1 shows that an increment of butanol of 0.01 mole changes solubilization in the range of 75%–100% neutralization by about 0.7 ml. of benzene, whereas difference of 0.01 mole of lauric acid has about four times this effect. This difference is even more striking in Fig. 5. Here, 0.0125 mole of lauric acid cause a reduction of 0.0889 mole in the butanol required for solubilization of 10 ml. of benzene. Thus, the lauric acid has four to seven times as much influence on solubilization of benzene as butanol, on a molar basis.

The influence of lauric acid in increasing the viscosity of potassium laurate solutions is greater than that of butanol (Figs. 4 and 6). In both instances this is probably due to the formation of larger micelles.

Although these data cannot be used to draw firm conclusions, they do indicate elements of difference in the behavior of butanol and lauric acid when these are added to potassium laurate. As the amount of free lauric acid is decreased by neutralization with potassium hydroxide, the amount of butanol required to solubilize a fixed amount of benzene passes through a minimum. On one side of the minimum, the butanol required is a direct function of the lauric acid concentration; on the other side, the relationship is reversed. This is hardly compatible with the general concept that the alcohol and fatty acid have similar positions in the micelles.

2. The Formation of Different Micellar Species

In the systems containing more than 25% lauric acid, the sharp reduction in solubilization of benzene (Fig. 1) and the sharp increase in viscosity (Figs. 3 and 4) indicate a change in the micellar structure. Further evidence for a relatively abrupt change in micellar structure is provided by the data on the minimum quantity of butanol required to solubilize a fixed quantity of benzene (Fig. 5). These yield sharp minima at about 25% free lauric acid concentration, the same region as that at which the other data show rapid changes in physical properties.

For the systems with more lauric acid, it might be inferred from the rather sharp increase in viscosity that the dissymmetry of the micelles is becoming greater. The formation of dissymmetrical micelles would have a greater influence on viscosity than moderate increase in size. Thus, it may be conjectured that the influence of additional free fatty acid past the transition region is to increase the size of the micelles and, particularly, to increase one axis of the micelles more rapidly than the other.

It is pertinent that Hess (8) has found that the micelles in a potassium laurate solution, originally symmetrical, become quite dissymmetrical on addition of excess potassium hydroxide. This was indicated by X-ray diffraction measurements and a sharp increase in viscosity.

One interpretation of the phenomena observed at the transition point would be that rodlike micelles are becoming longer and more dissymmetrical as more lauric acid is incorporated in the soap micelle. Another would be that a spherical micelle (of low viscosity and uniform solubilization characteristics) is transformed into a rodlike micelle, which then becomes longer as more lauric acid is added. The abruptness of the transition region would tend to favor the latter concept.

The changes in micellar properties at the transition region might make this a good system for the study of the size and shape of micelles. The components of the system on both sides of the transition region are identical with the exception of a small difference in free fatty acid content. This should offer considerable advantage over a system such as was used by Debye and Anacker (9) in which the soap solution had to be swamped with electrolyte in order to obtain dissymmetry of the micelles. Studies of this system might help to answer the questions concerning abrupt or gradual alteration of the size or shape of the micelles as the conditions of a soap system are changed.

3. Acid-Soap Ratios at the Transition Region

Because the composition at the transition region approximates the ratio of 3 moles of potassium laurate to 1 mole of lauric acid, corresponding to the insoluble acid soap $3NaL \cdot HL$ reported as a product of hydrolysis of sodium laurate solution (7), the constancy of the transition region is of interest.

The limited data obtained thus far indicate poor conformance to exact stoichiometric ratios. Thus, the point of rapidly changing solubilization varied from a ratio of potassium laurate to lauric acid of about 3/1 to about 4/1 when the butanol content was reduced by about 25% (Fig. 2). Similarly this ratio varied from 3.5/1 to 4.5/1 with increase of the potassium laurate concentration by 10% (Fig. 3).

SUMMARY

Data have been obtained for the solubilization of benzene by potassium laurate solutions containing lauric acid in the presence of moderate quantities of 1-butanol. Up to a concentration of about 25% lauric acid relative to potassium laurate, the influence of increasing acid content is a regular increase in solubilization. This increase is considerably greater than that obtained by equimolar increase in butanol concentration. Furthermore, the addition of lauric acid causes a substantially greater increase in viscosity than the addition of equimolar quantities of butanol.

At a potassium laurate-lauric acid ratio of about 3/1 to 4/1 a sharp change occurs in a number of properties which might be interpreted as due to a change in micellar species. Beyond this transition region, increased free lauric acid content causes an extremely sharp reduction in solubilization, a sharp increase in viscosity, and an extremely sharp alteration of the influence of butanol as a co-solubilizer for benzene. Limited data, however, indicate the lack of precise stoichiometry in this range.

The quantity of butanol required to solubilize a fixed quantity of benzene decreases and then increases sharply with increasing addition of lauric acid to potassium laurate. The results suggest that fatty acid and alcohol may have different effects upon the constitution of soap micelles, contrary to previous reports in the literature.

The data appear to be compatible with the hypothesis that two types of micelles exist. It appears that at potassium laurate-lauric acid ratios greater than 4.5/1, the micelles change in size and shape to a limited extent as the lauric acid concentration is increased, whereas at ratios less than 3/1, the changes are quite pronounced. The change in viscosity in the latter region indicates that the dissymmetry of the micelles increases progressively with increase in lauric acid concentration. This may be more readily interpreted as a transition from a spherical to a rodlike micellar model.

ACKNOWLEDGMENT

The authors wish to thank the Pennsylvania Salt Manufacturing Company, Whitemarsh Research Laboratories, for permission to use their facilities during part of this investigation.

References

1. McBain, J. W., and Richards, P. H., *Ind. Eng. Chem.* **38,** 642 (1946).
2. Ekwall, P., *Kolloid-Z.* **80,** 77 (1937).
3. Winsor, P. A., *Trans. Faraday Soc.* **44,** 376 (1948).
4. Klevens, H. B., *Chem. Revs.* **47,** 4 (1950).
5. McBain, J. W., and Lissant, K. J., *J. Phys. & Colloid Chem.* **55,** 655 (1951).
6. McBain, J. W., and John, L. M., *J. Am. Oil Chemists' Soc.* **25,** 141 (1948).
7. Ekwall, P., and Lindblad, L. G., *Kolloid-Z.* **94,** 42 (1941).
8. Hess, K., *Fette u. Seifen* **49,** 81 (1942).
9. Debye, P., and Anacker, E. W., *J. Colloid Sci.* **3,** 410 (1948).

DETERMINATION OF SURFACE AREA AND PARTICLE SIZE OF SYNTHETIC LATEX BY ADSORPTION

VI. CRITICAL MICELLE CONCENTRATIONS OF VARIOUS EMULSIFIERS IN LATEX

Samuel H. Maron, Max E. Elder, and Irwin N. Ulevitch

Physical Chemistry Laboratory, Department of Chemistry and Chemical Engineering,
Case Institute of Technology, Cleveland, Ohio

Received July 9, 1954

Introduction

The adsorption method for determination of surface area and particle size of synthetic latices, as presented in preceding papers in this series (1, 2), involves titration of several concentrations of a latex with an emulsifier until the critical micelle concentration (cmc) of the emulsifier in the latex is reached. Then the concentration C of added emulsifier required to attain the cmc is plotted vs. the polymer content of the latex at the cmc, m, in line with the equation

$$C = S_a m + C_f, \qquad [1]$$

where S_a is the moles of added soap adsorbed per gram of polymer, and C_f is the cmc of the emulsifier in the latex. The slopes of the linear plots thus obtained yield S_a, while the y-intercepts C_f.

It is the intent of this paper to summarize the values of C_f obtained in this manner with 19 emulsifiers at 50°C., and to compare them with cmc values for some of the emulsifiers observed at the same temperature in aqueous solution.

Experimental

The manner of determining C_f has been described before (1). The cmc's of the emulsifiers in aqueous solution were obtained by conductance using a Leeds and Northrup Campbell-Shackelton conductivity bridge and the special cells employed for latex titration (1). To determine the cmc a definite volume of water was placed in the cell, emulsifier solution added in aliquot volumes, and the conductance measured at 50°C. after each addition. In this manner a curve such as Fig. 1 is obtained, from which the cmc follows as the concentration at the break in the curve.

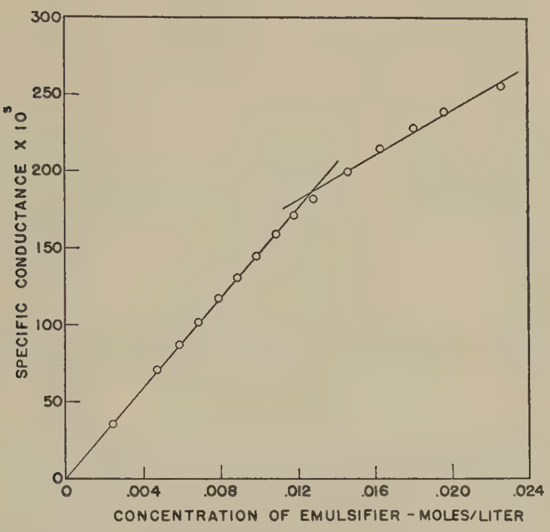

FIG. 1. Determination of cmc by conductance at 50°C.

TABLE I

Comparison of C_f and cmc Values of Emulsifiers at 50°C.

Substance	No. of determinations	C_f, *moles/liter*	*cmc, moles/liter*
Na Laurate	12	0.0211 ± 0.0007	0.0215
Na Myristate	13	0.0066 ± 0.0009	0.0075
Na Palmitate	8	0.0021 ± 0.0003	0.0021
Na Stearate	5	0.0018 ± 0.0002	0.0018
K Stearate	5	0.0018 ± 0.0003	—
Na Oleate	28	0.0033 ± 0.0006	0.0035
Na OSR	14	0.0028 ± 0.0006	0.0023
K K-Wood Rosin	27	0.0118 ± 0.0013	0.0122
Na Resin 731 (Dresinate 731)	11	0.0121 ± 0.0004	0.0122
K Resin 731 (Dresinate 214)	7	0.0104 ± 0.0011	—
Na Pexite 42 (Dresinate 87)	2	0.0110 ± 0.0006	—
K Pexite 42 (Dresinate 90)	4	0.0127 ± 0.0005	—
Na Resin 61	3	0.0089 ± 0.0000	—
K Resin 61	1	0.0105	—
K Gum 42 (Dresinate 89)	3	0.0113 ± 0.0004	—
Laurylamine Hydrochloride	3	0.0146 ± 0.0005	0.0130
Daxad 11	4	0.80 ± 0.12*	0.80*
Aquarex D	2	2.9 ± 0.1*	3.0*
SA-178	3	2.13 ± 0.10	1.9

* In grams per liter.

RESULTS AND DISCUSSION

In Table I are summarized the values of C_f observed during many titrations with a number of emulsifiers, as well as the cmc's for some of these measured in aqueous solution. Inspection of the data shows that in general the *average* of the C_f values observed for a given emulsifier agrees quite well with the cmc of the emulsifier as measured in water. However, with each emulsifier in latex there are observed deviations from the average which are sometimes quite pronounced, and which depend on the electrolyte content of the latex, the extent of monomer removal, and the presence of other substances which may modify the cmc without affecting S_a. For this reason it is not advisable to assume *a priori* the cmc of an emulsifier in a latex, and thereby reduce the determination of S_a in Eq. [1] to a single titration. Our experience indicates that the preferred procedure is still to make several titrations and to plot the observed C's vs. m in order to obtain S_a from the slope of the resulting straight lines. The method can be reduced to a single titration only when sufficient data have been accumulated for a given emulsifier in a given latex system to show what the value of C_f is in the particular system. With C_f thus defined, the simplified procedure described in the first paper of the series (1) is capable then of giving reliable results for surface area and particle size.

ACKNOWLEDGMENT

This work was performed as part of the research project sponsored by the Reconstruction Finance Corporation, Office of Synthetic Rubber, in connection with the Government Synthetic Rubber Program.

SUMMARY

In the determination of surface area and particle size of synthetic latex by adsorption of emulsifiers, one of the quantities deduced is the cmc of the emulsifier in the latex C_f. This paper presents a summary of the values of C_f thus observed for 19 emulsifiers of various types, and compares some of these with the cmc values found for the emulsifiers in water. In general the averages of the C_f values are in good agreement with the cmc values found in aqueous solution. However, some latices may show considerable deviations of C_f from the average, and hence it is not advisable to assume the cmc of an emulsifier in water to be identical with C_f of the emulsifier in a latex.

REFERENCES

1. MARON, S. H., ELDER, M. E., AND ULEVITCH, I. N., *J. Colloid Sci.* **9,** 89 (1954).
2. MARON, S. H., AND ELDER, M. E., *J. Colloid Sci.* **9,** 104 (1954).

ROLE OF LATTICE HYDROXYLS OF KAOLINITE IN PHOSPHATE FIXATION AND THEIR REPLACEMENT BY FLUORIDE[1]

Luis A. Romo[2]

University of Wisconsin, Madison, Wisconsin

Received December 22, 1953; revised March 15, 1954

ABSTRACT

This investigation was made with the purpose of studying the role that lattice hydroxyls play on phosphate fixation, and the effect of fluoride ions on the surface lattice hydroxyls of kaolinite.

The results obtained by means of quantitative infrared spectroscopy show that phosphate ions do not replace surface lattice hydroxyls of kaolinite. Accordingly, titration of excess alkalinity produced when kaolinite is placed in contact with fluoride solutions and direct infrared spectroscopic analysis of hydroxyl content show that lattice hydroxyls are replaced by fluoride. In fact, in a case where the fluoride solution was 0.40 *N* it was found that 22% of the lattice hydroxyls were replaced by fluoride ions.

X-ray powder photographs of untreated and fluorinated kaolinite show that the "*d*" spacings and the intensities have remained the same, indicating that the crystal structure of kaolinite has not been altered.

INTRODUCTION

The property of phosphate fixation by kaolinite has been investigated quite extensively. Thus Mattson (9) in his studies on the "laws of soil colloidal behavior" states that the phosphate fixing capacity of kaolinite is due to replacement of lattice hydroxyls by phosphate ions. Stout (10) studied this problem further and arrived at similar conclusions. Such a view has been accepted by various investigators (2, 3, 4, etc.).

The results of systematic studies made by the author on the chemistry of the kaolinite phosphate system made it difficult to accept such a view, which is untenable if one analyzes the structure of kaolinite and remembers that the ion size of the hydroxyl is quite different from that of the phosphate ion.

Equilibrium experiments designed to measure release of hydroxyl ions in kaolinite suspensions treated with phosphate at various concentrations failed to show any evidence that supports the findings of Mattson (9) and Stout (10). Accordingly, investigations were made to show that the surface lattice hydroxyls of kaolinite are not replaced by PO_4^{-3}, and that such hydroxyls can be replaced only by anions such as the fluoride, which has the following characteristics: (1) it is similar to hydroxyl in ion size, (2) it forms, presumably, stronger bonds with the octahedral aluminums in the structure because of its high electronegativity, and (3) it has a high hydrogen bonding capacity which holds the kaolin unit together.

---

[1] Taken in part from the dissertation submitted by Luis A. Romo in partial fulfillment of the requirements of the degree of Doctor of Philosophy to the Graduate Faculty of the University of Wisconsin, March, 1953.

[2] Present address: Division of Geochemistry, The Pennsylvania State University, State College, Pennsylvania.

MATERIALS

1. Preparation of Phosphated Kaolinite

Samples of 0.200 g. of $<2\ \mu$ fraction of kaolinite were poured into 20-ml. test tubes. To each tube in sets of three there was added 15 ml. of KH_2PO_4 solutions of 0.10, 0.25, 0.50, 0.75, and 1.00 molar strengths, respectively (suspension *p*H 4.3). The contents in each one of the tubes were shaken intermittently until a uniform suspension was obtained. Then they were digested on the hot plate at a temperature of 90°C. for a period of 10 days. Following this, the liquid phase was separated by centrifuging. The colloidal silicates were then washed once with 0.002 *N* H_2SO_4, three times with 90% ethyl alcohol, and once with acetone. Finally, they were dried at 50°C. and collected in small vials which were placed into a vacuum desiccator containing silica gel at a pressure of $<50\ \mu$ of Hg.

2. Preparation of Fluorinated Kaolinite

Samples of 1.00g. of kaolinite were saturated with NH_4^+ using 1 *N* NH_4Cl as the saturating solution. The excess of salt was washed out once with water, and three times with 90% ethyl alcohol by centrifuging. The samples were then transferred to 400 ml. Erlenmeyer flasks in sets of two each with 0.10, 0.20, and 0.40 *N* NH_4F solutions, respectively. The volumes were adjusted to 50 ml. with the corresponding standard ammonium fluoride solutions. They were left in contact with the fluoride at room temperature, for a period of 40 days with periodic shaking. After discarding the liquid phase, the remaining colloidal silicates were washed once with 0.002 *N* H_2SO_4, three times with 90% ethyl alcohol, and once with acetone. Finally the samples were dried at 50°C. and transferred to small vials which were placed in the same vacuum desiccator at a pressure of $<50\ \mu$ of Hg.

METHODS AND RESULTS

1. Measurement of Alkalinity Produced in Suspensions by Fluoride Treatment

As soon as kaolinite was placed in contact with the fluoride solutions as indicated above, it was observed that the suspensions became alkaline. Similar observations have been reported by Dickman and Bray (5). As in-

TABLE I

The Exchange of Lattice Hydroxyls in Kaolinite by Fluoride Ions

Normality of NH_4F used	HCl needed for neutralization meq./1.00 g.	Percentage of total hydroxyls exchanged[a]
0.10	1.45	9.35
0.20	2.46	11.83
0.40	3.56	22.91

[a] Percentages of lattice hydroxyls displaced by fluoride ions are based on the total hydroxyl content of 26.4%.

dicator, 10 drops of bromthymol blue were added to each flask. The color of the suspensions corresponded to a *p*H of 7.0. The alkalinity was measured every three or four days by titrating the contents in each one of the flasks back to neutrality with standarized 0.1 *N* HCl for a period of 40 days. After that time, alkalinity continued to appear but at a very reduced rate. The experimental results are presented in Table I.

2. Measurement of Variations in Hydroxyl Content of Kaolinite Treated with Phosphate by Integration of Areas of Infrared Absorption Bands

The phosphated kaolinite samples were left in the desiccator for three days, then the desiccator interior was brought to atmospheric pressure, and samples of kaolinite of 0.005 g. were taken from the vials with a stainless steel spatula and mixed immediately with a mulling agent, nujol oil, which gives only three absorption bands which do not interfere with those of kaolinite. Following this, each one of the samples was transferred to a sodium chloride plate (20 mm. × 12 mm. × 3 mm.) which was covered with another plate of the same size. The covering plate was worked around to obtain a uniform spreading and the formation of a very thin film. The plates were then mounted on a metallic holder which was set in place in the Baird Associates' recording infrared spectrophotometer. The spectra were recorded from 2 to 16 μ with the same instrumental adjustments. Every one of the spectrograms showed the presence of a sharp absorption band at 2.72 μ corresponding to unbonded hydroxyls. There were also recorded absorption bands at 9.2, 9.6, 9.9, 10.6 to 11.3, 12.6, 13.3, and 14.5 μ, respectively. These absorption bands are characteristic of kaolinite (1, 6, 8).

A relative estimation of hydroxyl content was obtained as a ratio of the areas of the hydroxyl band occurring at 2.72 μ and the absorption band characteristic of kaolinite which occurs at 10.6 to 11.3 μ. Previously, it was found that the area of this band remains constant regardless of treatment. The areas were integrated graphically. The average ratio of areas obtained was 0.162 ± 0.005, where the average deviation of 0.005 was also the deviation found within the triplicate runs of the same sample. Therefore, it was concluded that the hydroxyl content had remained unaltered regardless of phosphate treatment.

3. Direct Measurement of Hydroxyl Content of Kaolinite Treated with Phosphate and Fluoride

The hydroxyl content of kaolinite treated with phosphate and fluoride as indicated above was determined by means of infrared spectroscopy using a direct method of analysis. To accomplish this, pressed potassium bromide discs were prepared by mixing weighed amounts of kaolinite with constant amounts of potassium bromide. Ordinarily, potassium bromide contains occluded water and some impurities which are detectable in the infrared spectrum. Therefore, samples of potassium bromide were fused in porcelain crucibles in a furnace at 800°C. for two hours. After cooling, the crystalline cake was ground in an agate mortar. Then the powder was transferred to small vials and dried for two hours in a vacuum oven at 160°C. and a pressure of <50 mm. of Hg. The vials were kept in a vacuum desiccator at a pressure of <50 μ of Hg. The infrared spectrum of the baked KBr showed a small absorption band at 2.93 μ (Fig. 1*A*).

To prepare the discs it was found that a concentration of 3 mg. of kaolinite is adequate, thus samples approximating such weight were weighed out and poured into small vials which were placed immediately in the desiccator. The potassium bromide powder was added with a powder pipet; a glass pellet containing iron powder inside was included in the vial, and each one of the samples was ground and mixed in an electric vibrator for one hour. Then, each sample was transferred to a hardened steel mold and pressed immediately in a hydraulic press at 45 tons per square inch for ten minutes. Just before pressing, the mold was evacuated for two minutes in order to remove trapped air. The pressed potassium bromide discs had the following characteristics: diameter 18.75 mm., thickness 1.055 ± 0.045 mm., total weight 0.8055 ± 0.0200 g., and a content of kaolinite of 0.0030 ± 0.0003.

To record the infrared spectra each one of the discs was mounted immediately on a metallic holder which was set in place in the spectrophotometer. The apparatus was set to scan slow and the zero line and percentage of maximum transmittancy were adjusted with the blank (potassium bromide disc containing untreated kaolinite). The infrared spectra for all the samples were recorded in duplicate using the same adjustments.

The absorbance of kaolinite in the hydroxyl region was calculated using the base line method. According to Beer's law, we have that $A = \log(p_0/p)$, where A is the absorbance, p_0 is the incident radiant power, and p is the transmitted radiant power. But since the discs contain a mixture of potassium bromide and kaolinite which have different absorbances in the hydroxyl stretching region, we have that $A_{\text{true}} = A_{\text{sample}} - A_{\text{KBr}}$.

In the spectra shown in Fig. 1 it was found that the hydroxyl region is characterized by two overlapped bands at $\lambda_1 = 2.72$ μ and $\lambda_2 = 2.93$ μ, with λ_1 corresponding to unbonded hydroxyls characteristic of kaolinite

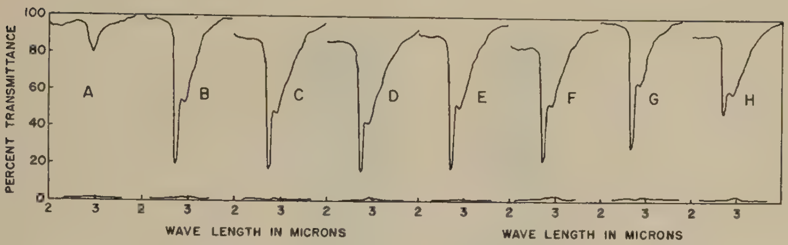

FIG. 1. The infrared spectra of kaolinite in the hydroxyl region showing variations in hydroxyl content after phosphate and fluoride treatment. *A*, KBr; *B*, KBr + untreated kaolinite; *C*, *D*, and *E* same as *B* but kaolinite treated with KH_2PO_4 solutions as follows: 0.50 *M*, 0.75 *M*, and 1.00 *M*, respectively; similarly, *F*, *G*, and *H* were treated with 0.10 *N*, 0.20 *N*, and 0.40 *N* NH_4F solutions, respectively.

TABLE II

The Absorbances of Hydroxyl in Kaolinite as Affected by Treatment with Phosphate and Fluoride

Treatment of kaolinite	Absorbance at λ_1[a]	Unbonded OH^-, %[b]	Absorbance at λ_2[c]
Blank	0.721	100	0.192
0.50 *M* KH_2PO_4	0.758	105	0.206
0.75	0.750	104	0.235
1.00	0.720	100	0.185
0.10 *N* NH_4F	0.642	88	0.185
0.20	0.589	82	0.129
0.40	0.565	78	0.274

[a] The absorbance of KBr at λ_1 is zero; therefore, the absorbances calculated at λ_1 needed no correction.

[b] Since A_{true} is proportional to concentration and assuming that scattering is the same regardless of treatment, the percentages of hydroxyl content with respect to the hydroxyl content of the blank were calculated as shown above.

[c] Absorbance of KBr at λ_2 is 0.08; thus the absorbances reported at λ_2 are the values resulting from subtracting 0.08.

and λ_2 corresponding to bonded hydroxyls which are characteristic of water. Therefore, absorbances were calculated at λ_1 and λ_2, respectively.

The results presented in Table II indicate that the surface lattice hydroxyls are not exchanged by phosphate ions. It is important to point out that such conclusion was obtained by indirect and direct infrared spectroscopic analysis.

The absorbances calculated at λ_2 vary somewhat. Such variations are due to the error in weight of KBr in the discs, which is of the order of ±20%. However, such an error in other respects is not important, *i.e.*, in scattering, for the refractive index of KBr is 1.559 and the average refractive index of kaolinite is 1.558 (7).

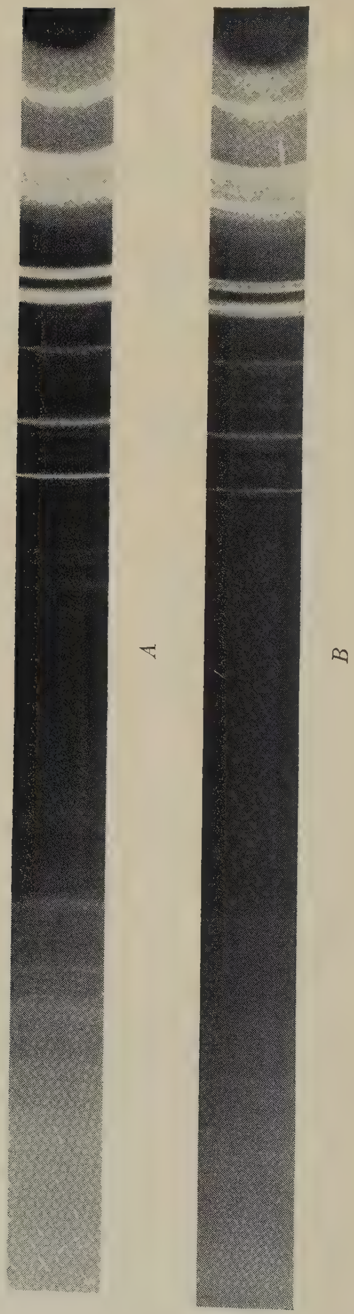

FIG. 2. X-ray powder photographs of kaolinite. (FeKa radiation) *A*, pure; *B*, 22% of lattice hydroxyls replaced by fluoride.

4. X-ray Diffraction Patterns of Pure and Fluorinated Kaolinite

Powder patterns of both pure and fluorinated kaolinite were taken with an X-ray Straumanis camera of 18 cm. in diameter under very similar conditions of specimen preparation, time of exposure, and photographic processing. The powder patterns shown in Fig. 2 indicate that the crystal lattice has remained the same regardless of fluorination. Slight differences in line intensities are due most probably to variations in the orientation of the particles in the rods.

DISCUSSION

The results obtained in this investigation show that the surface lattice hydroxyls are not replaced by phosphate ions as has been maintained by various investigators. The data presented in Tables I and II show that the hydroxyl content of kaolinite remains constant regardless of phosphate treatment.

If anionic replacement is to take place at the surface atomic planes of a crystal structure without its disruption, at least three requirements must be fulfilled: (1) the size of the substituting anion must be similar to that of the anion to be replaced or it must have the ability to deform itself considerably as to satisfy the spatial requirement, (2) the bond formed by the substituting anion must be stronger, and (3) electrical neutrality must be maintained. Clearly, the phosphate ion (most probably $H_2PO_4^-$ and/or HPO_4^{--}) does not meet with the requirements indicated, thus making impossible the exchange of lattice hydroxyl by phosphate ions.

The relative estimation of the hydroxyl content by means of ratios of integrated areas of the (OH):(10.6–11.3) μ absorption bands show that the hydroxyl content remains constant regardless of phosphate treatment. However, this information was not taken as conclusive because of the uncertainty involved in determining the constancy of the area of absorption band occurring at 10.6 to 11.3 μ as affected by phosphate treatment. Accordingly, this problem was investigated further by means of pressed potassium bromide discs which permitted a direct measurement of hydroxyl content. In this case, the error due to scattering is practically eliminated both because of the negligible difference in refractive indices between kaolinite and KBr, and the particle size which was $<<2$ μ. The information obtained by this method confirmed the fact that phosphate ions do not replace lattice hydroxyls in kaolinite (Fig. 1*C*, *D*, *E*).

Replacement of lattice hydroxyls by fluoride ions was shown to take place by means of titration of the excess alkalinity. But since it was suspected that the increase in alkalinity of the suspensions might be due to hydrolysis reactions which might have resulted in complex ion formation, it was decided to check these results (Table I) by means of direct infrared spectroscopic analysis. The results presented in Table II and Fig. 1*F*, *G*, *H* indicate that the fluoride does replace the surface lattice hydroxyls.

The close agreement obtained between the results arrived at by titration and infrared spectroscopic analysis indicates that the alkalinity measured by titration is due to actual displacement of hydroxyls from the lattice by fluoride ions.

Finally, if fluorides have taken the positions of the surface hydroxyls in the lattice, one must expect constancy in the interplanar spacings. Furthermore, since the number of electrons in the hydroxyl and fluoride are the same, the intensities of the diffraction lines of both pure and fluorinated kaolinite must be the same. In fact, in a sample of kaolinite where 22% of the lattice hydroxyls had been replaced by fluorides (Fig. 1*H*) it was found that the *d* spacings and the intensities of the diffraction lines remained the same (Fig. 2), thus adding further evidence to the fact that fluoride displaces hydroxyls from the surface lattice layers of kaolinite.

ACKNOWLEDGMENT

The author wishes to express his gratitude to Professor E. Truog for his interest during the course of this investigation.

REFERENCES

1. ADLER, H., *Am. Petroleum Inst.*, *Project* **49**, 1–72 (1950).
2. BARBIER, G., AND CHABANNES, J., *Compt. rend.* **226**, 749–751 (1948).
3. BLACK, C. A., *Soil Sci. Soc. Am. Proc.* **7**, 123–133 (1942).
4. CHATERJEE, B., AND DATTA, S., *J. Soil Sci.* **2**, 224–233 (1951).
5. DICKMAN, S. R., AND BRAY, R. H., *Soil Sci.* **52**, 263–273 (1941).
6. HUNT, M., WISHERD, M. P., AND BONHAM, L. C., *Anal. Chem.* **22**, 1478–1497 (1950).
7. JASMUND, K., "Die Silicatischen Tonminerale," p. 43. Verlag Chemie, Weinheim, 1951.
8. KELLER, D. W., AND PICKETT, E. E., *Am. Petroleum Inst.*, *Project* **49**, 123–140 (1950).
9. MATTSON, SANTE, *Soil Sci.* **32**, 342–365 (1932).
10. STOUT, R. P., *Soil Sci. Soc. Am. Proc.* **4**, 177–182 (1939).

CORRELATION BETWEEN OPTICAL AND DYNAMIC METHODS OF MEASURING SIZE OF WATER DROPS IN A CLOUD

Y. G. Naik

Gujarat College, Ahmedabad

Received January 5, 1954; revised June 1, 1954

Abstract

A comparison of the theory of the diffraction rings observed in a cloud by transmitted light is made with the Mie theory. The values of the radii determined experimentally on the bases of the two theories are compared with those obtained from the dynamic method using Stokes' and Cunningham's equations. It was found that the diffraction theory gives larger values of the radii for drops below 3 μ, whereas the Mie theory gives values of radii which agree with those obtained from Cunningham's equation for drops of radii varying from 1 to 5 μ.

Introduction

The determination of the size of water drops in a cloud is an important problem in meteorology. Of the many methods available for this purpose, the corona method based on the diffraction of light and the dynamic method based on the Stokes-Cunningham (1) equation are the best, as they involve rapid and simple measurements. The radii of water drops in a given cloud, determined by use of both the above methods, do not agree over the whole range of drop sizes. The corona method gives uniformly higher values of the radii than those obtained from the Stokes-Cunningham equation, especially for drops of radii >3 μ. The Mie theory (2), however, explains satisfactorily all optical phenomena like transmission, scattering, polarization, and dispersion of light passing through a cloud of spherical particles, and hence it can be used to estimate the drop sizes in a cloud and correlate other optical and dynamic methods.

The Diffraction Theory of the Corona

If one looks at a bright source of light through a cloud of particles, a series of concentric spectrum colored rings are seen around the source. In monochromatic light, the coronas consist of alternate bright and dark rings around the source. According to the diffraction theory (vide Humphrey (3)), the water drops serve as spherical obstacles in the path of light and give minima of intensity at such angles in the forward direction that

$$\alpha \sin \theta_n = \pi(n + 0.22)$$

where α is a parameter of the size of the drops and is equal to $2\pi r/\lambda$, r is the radius of the drops, λ is the wavelength of light, and θ_n is the angle subtended by a dark diffraction ring of order n. According to Wilson (4) this theory holds good for $\alpha > 30$ i. e., $\theta < 10°$.

Distinct diffraction rings could be observed in a cloud of water drops having radii $>1\ \mu$. A number of workers, for example, Wilson (4), Kamtz (5), Mitra (6) and Ray (7), have, however, pointed out that the diffraction theory of the corona gives larger values of the radii than those determined by the dynamic method for drops smaller than $3\ \mu$. Still however, the well-defined circular coronas observed in all artificial clouds in the laboratory indicate that the angular apertures of the diffraction dark rings even for drops smaller than $3\ \mu$ should give a reliable measure of their radii. As has been shown later, the Mie theory seems to provide a correct estimate of the size of the drops from the diffraction rings for the whole range of sizes of water drops in a cloud or a fog.

The Dynamic Method

By measuring the steady rate of fall of spherical particles, a measure of the radius can be obtained from the following Stokes-Cunningham equation:

$$X = 6\pi\eta r v \left(1 + \frac{Al}{r}\right)^{-1}$$

where X is the force maintaining the velocity and is the effective weight of the drop, η is the coefficient of viscosity of the medium, r is the radius of the drop, v is the uniform velocity of fall that the particle attains, A is a constant, and l is the mean free path of the molecules of the medium. According to Cunningham (1), the value of A is 1.63 and l, the mean free path of air molecule, is 0.9×10^{-5}. This formula has been used in the present investigation to estimate independently the size of the water drops in a cloud. The constant Al for the experimental range of sizes of the water drops was evaluated by a series of separate experiments and was found to be nearly the same as that given by Cunningham (1).

Mie theory and corona. The general theory of the scattering of light by spherical particles of any size and any refractive index was worked out by Mie (2), and this has been successfully applied by Blumer (8), Jöbst (9), Mecke (10), Paranjpe, Naik, and Vaidya (11), La Mer and Sinclair (12), La Mer and Barnes (13), Johnson and La Mer (13a), and Van de Hulst (14) in explaining the selective scattering of light in different directions by spherical particles. The transmission of light by a cloud of particles was also explained on the basis of the Mie theory by Stratton and Houghton (15), Sinclair (16), Ruedy (17), and La Mer, Inn, and Wilson (18). The colors of the corona have also been explained by Ruedy (17) and Naik (19) on the basis of this theory. It is, therefore, possible to explain the diffraction ring formation with the help of the Mie theory. The only handicap in the

TABLE I

Angles of First Minima of Intensity of Light Scattered or Diffracted by Water Drops

(Refractive index = 1.33)

$\alpha = \frac{2\pi r}{\lambda}$	θ, Angles of first minima		*Source of Mie theory values
	Mie theory	Diffraction theory	
3	80°	—	*a*
3.6	70°	—	*a*
3.83	—	90°	—
4	60°	73° 18′	*a*
4.8	50°	53°	*a*
5	50°?	50°	*e*
6	40°?	39° 42′	*e*
7	30°	33° 12′	*c*
8	50°?	28° 37′	*e*
9	20°	25° 12′	*c*
10	15°	22° 32′	*a*
12	12° 50′	18° 37′	*d*
15	30°?	14° 48′	*e*
20	9°	11° 3′	*a*
25	10°?	8° 49′	*a*
30	7° 15′	7° 21′	*d*
35	7°	6° 17′	*a*
40	5°	5° 33′	*a*

* *a*. Gumprecht, Neng-Lun Sung, Jin H. Chin, and Sliepcevich (20). *b*. Lowan's tables (21). *c*. Paranjpe, Naik, and Vaidya (11). *d*. Paranjpe and Lajme (22). *e*. Values which are according to (*a*) but which are anomalous or represent second-order minima.

application of this theory to this problem is the lack of sufficient evaluated data of the scattering functions, especially by particles of radii larger than the wavelength of light, and at small intervals of angles of scattering. More data of the scattering functions for larger water drops are now available from several sources and can be used to explain the coronas. The diffraction dark rings in monochromatic light represent the minima of the intensity of scattered light in the forward direction. It is, therefore, necessary to obtain the angles of minimum intensity of scattered light by different sizes of the drops. An attempt was made by Paranjpe and Lajme (22) in this direction for a few values of α only. The angles of first minima of scattered light for different values of the parameter α for water drops are given in Table I along with the corresponding values of angles calculated from the diffraction formula stated above. The sources of the intensity values of scattered light are indicated in the last column of this table. The angles of the first minima are expressed as "180 − γ," where γ is the angle of scattering, the direction of incidence being considered as 0°.

The above results are represented graphically in Fig. 1 given below. The Mie theory curve in this figure helps us to estimate α and hence the radius of the water drops by observing the angular aperture of the first dark corona. The values of θ for $\alpha = 8$ and 25 do not fit in the curve and probably represent higher order minima. For $\alpha = 15$, the minima should lie near about 10°, but the calculations, which are available for only integral values of angles, do not show any such minima. For $\alpha = 5$, 6, and 25, it is likely that correct angles of first minima are less than the actual angles indicated in the tables. It would be worth while evaluating the intensity functions near about these angles for different α's, to test the validity of the Mie theory over the whole range of drop sizes.

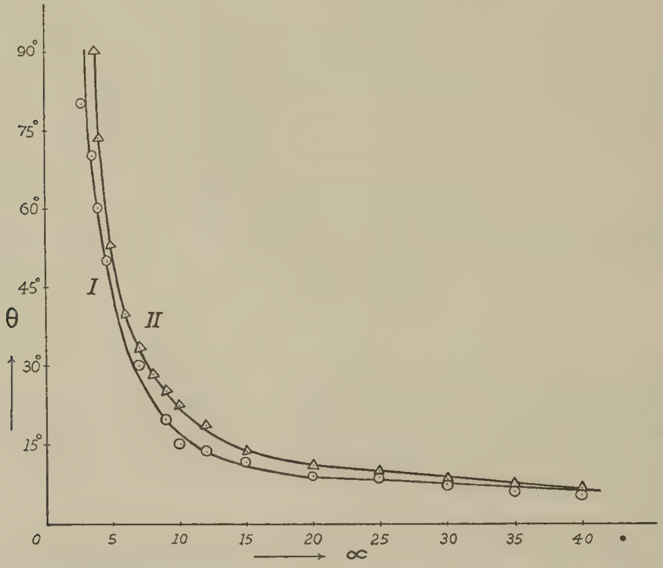

FIG. 1. Angles of first minima of scattered light by water drops: I. Mie theory curve; II. diffraction theory curve.

It must be noted that the values of the intensity functions are available at intervals of 1° for the range from 0° to 10°, whereas for angles $>10°$, they are available at large intervals of angle only. It is, therefore, likely that the actual values of the angles of the minima, especially for smaller α values, may be slightly different from those obtained from the available data. Still, however, the smooth curve of Fig. 1 shows that the deviations from these values of θ cannot be very large. In fact the Mie theory curve in the figure indicates that the two optical theories give nearly identical values of the angles of the first minima for $\alpha > 30$, but the values differ for $\alpha < 30$. Thus for values smaller than 3 μ, the radii of drops according to the Mie theory are uniformly smaller than the diffraction theory. The diffraction theory curve terminates at $\alpha = 3.83$ as θ, the angle of first minima, attains the value 90°, while the Mie theory curve shows that θ increases to 180° as α decreases to zero. This difference incidentally agrees with the conclusions of Wilson (4), Kamtz (5), and others that the diffraction theory gives uniformly higher values of radii for drops smaller than 3 μ.

It is reasonable to accept the as Mie theory correct for all values of radii as well as refractive index of the material of the drops. The Mie theory curve given above can serve as a standard guide to estimate the size of water drops in a cloud from a knowledge of the angle of the first dark ring seen in a water cloud, or from a knowledge of the angle of the first minimum of intensity of scattered light in the forward direction.

It is, however, desirable to compare the values of the radii of given drops in a cloud determined by these optical methods with those obtained by a dynamic method based on the Stokes-Cunningham equation.

Experimental

The following arrangement was made to observe the diffraction rings in a cloud and to determine the velocity of fall of the cloud drops. A large cloud chamber of pyrex glass of 20 l. capacity was set up to produce an artificial water cloud on dust or smoke nuclei. The details and working of this type of apparatus were given in earlier papers by Paranjpe, Naik, and Mirchandani (23) and Paranjpe, Naik, and Vaidya (11). After a cloud was formed by sudden expansion, the angular aperture of the first diffraction dark ring was instantly determined. The rate of settling of the cloud was next determined by observing the well-defined top of the cloud. Attempts were made to measure the velocity of individual drops by means of a microscope, but it was found too large to be measured accurately over a small distance of the eye-piece scale. It was also observed that the rate of fall of the cloud in the initial stages of the cloud formation was disturbed by the turbulence set up by sudden expansion. This appeared to subside within a short time and invariably before the cloud top reached the middle of the flask. The rate of settling of the cloud was, therefore, determined only after the cloud top reached the middle of the flask. The velocities measured after this limit were found to be very nearly constant for a given size of drops. It may be noted that the top of the cloud remained horizontal till it reached very nearly the bottom of the flask, and at the same time the size of the dark diffraction ring remained the same.

Before using Cunningham's equation, it was thought necessary to determine the constant Al independently for the present range of drop sizes. This is possible by comparing the values of radii determined by this method with those of the corona method, especially for radii >3 μ, for which the diffraction theory and the Mie theory give nearly identical values of radii.

TABLE II

Size of Water Drops Determined by Different Methods

(Refractive index = 1.33)

Angular aperture of the first dark ring θ	Velocity of fall, v, *cm./sec.*	Radius of drops, μ			
		Diffraction theory	Mie theory	Stokes' equation	Cunningham's equation
4° 6′	0.31	5.0	5.0	5.0	5.0
4° 40′	0.25	4.4	4.5	4.6	4.5
5°	0.21	4.1	4.1	4.1	4.0
6° 3′	0.15	3.4	3.4	3.6	3.5
7° 35′	0.09	2.7	2.63	2.8	2.7
8° 30′	0.06	2.4	2.3	2.4	2.3
9° 20′	0.04	2.2	1.8	1.9	1.8
10° 7′	0.03	2.0	1.62	1.7	1.6
12° 30′	0.02	1.7	1.2	1.4	1.2
14° 9′	0.01	1.5	1.04	1.2	1.08

From a large set of measurements on water clouds having drop sizes ranging from 3 to 7 μ, the constant Al was found to be 1.54×10^{-5} instead of 1.467×10^{-5} as given by Cunningham (1).

Four independent values of the radii of drops of a given cloud were obtained by using (1) the diffraction theory, (2) the Mie theory, (3) Stokes' uncorrected equation, and (4) Cunningham's equation. The results obtained for a typical set of clouds having radii of drops varying from 1 to 5 μ are given in Table II. The values of the angular aperture θ of the first dark diffraction ring and the velocity of fall of the cloud drops are given in the first two columns of this table.

It can be seen that all the methods give nearly equal values of the radii for drops >3 μ. Below this size, the values of the radii according to the uncorrected Stokes' law are intermediate between the diffraction and Mie theory values. The values obtained from Cunningham's equation agree fairly well with Mie theory values for the whole range of radii from 1 to 5 μ.

The diffraction theory is not suitable for drops smaller than 3 μ, and hence the Mie theory can be used to get a reliable estimate of the radii of drops below this size in view of the close agreement of the Mie theory results with those of the dynamic theory of Cunningham.

CONCLUSIONS

It is seen from the above results that the diffraction theory of the corona holds good only for radii of drops in a cloud >3 μ and gives uniformly higher values below this size. The Mie theory not only explains the formation of the corona but holds good for any size of drops. The results obtained from the Mie theory for water drops agree very closely with those obtained from the Stokes-Cunningham equation. It is, therefore, possible to use the

Mie theory curve given above to get a correct estimate of the size of water drops of any size either by observing the corona or by estimating the angle of the first minimum intensity of scattered monochromatic light.

As the corona method is very rapid and simple in operation, the Mie theory curve given here will serve as a useful aid in a rapid estimation of the size of water drops in a cloud.

My thanks are due to Shri N. H. Sahijwany for valuable help in the experimental work.

References

1. Cunningham, E., *Proc. Roy. Soc. (London)* **A83,** 357 (1910).
2. Mie, G., *Ann. Physik* **25,** 377 (1908).
3. Humphreys, W. J., "Physics of the Air," pp. 528. Philadelphia, 1923.
4. Wilson, J. G., *Proc. Cambridge Phil. Soc.* **32,** 493 (1936).
5. Kamtz, P., "Meteorologische Optik" (Pernter-Exner), pp. 495 (1922).
6. Mitra, M. N., *Indian J. Phys.* **3,** 175 (1928).
7. Ray, R., *Proc. Indian Assoc. Cultivation Sci.* **A7,** 1, (1921); *ibid.* **8,** 23 (1923).
8. Blumer, H., *Z. Physik* **32,** 119 (1925); *ibid.* **38,** 304 (1926).
9. Jöbst, C., *Ann. Physik* **78,** 157 (1925).
10. Mecke, R., *Ann. Physik* **61,** 471 (1920); *ibid.* **62,** 623 (1920); *ibid.* **65,** 257 (1921).
11. Paranjpe, G. R., Naik, Y. G., and Vaidya, P. B., *Proc. Indian Acad. Sci.* **A9,** 333, 352 (1939).
12. La Mer, V. K., and Sinclair, D., Progress Report on the Verification of Mie's Theory. OSRD Report, 1857 (1943). *Chem. Revs.* **44,** 245 (1949), and Atomic Energy Handbook on Aerosols. Washington, D. C., 1950.
13. La Mer, V. K., and Barnes, J., *J. Colloid Sci.* **1,** 71, 79 (1946).

13a. Johnson, I., and La Mer, V. K., *J. Am. Chem. Soc.* **69,** 1184 (1947).

14. Hulst, H. C. Van de, "Optics of Spherical Particles," Dissertation, Utrecht, Holland, 1946.
15. Stratton, J. A., and Houghton, H. G., *Phys. Rev.* **38,** 159 (1931).
16. Sinclair, D., *J. Opt. Soc. Amer.* **37,** 475, (1947).
17. Ruedy, R., *Can. J. Research* **A21,** 79, 99 (1943); *ibid.* **A22,** 53 (1944).
18. La Mer, V. K., Inn, C. Y., and Wilson, J. G., *J. Colloid Sci.* **5,** 471 (1950).
19. Naik, Y. G., *Science and Culture (India)* **15,** 485 (1950).
20. Gumprecht, R. O., Neng-Lun Sung, Jin H. Chin, and Sliepcevich, C. M., *J. Opt. Soc. Amer.* **42,** 226 (1952).
21. Lowan, N. A., Tables of Scattering Functions for Spherical Particles. National Bureau of Standards, Washington, D. C., 1949.
22. Paranjpe, G. R., and Lajme, S. S., *J. Univ. Bombay III,* **8,** 3 (1939); **9,** 38 (1940).
23. Paranjpe, G. R., Naik, Y. G., and Mirchandani, H. D., *J. Univ. Bombay II,* **1,** 1 (1932).

THE ELECTRIC CHARGE ON MACROSCOPIC GLASS SURFACE[1]

Max Bender[2]

Chemistry Department, New York University, New York, New York

Received June 14, 1954

ABSTRACT—SUMMARY

1. The zeta-potential of walls with which colloidal suspensions may be in contact, may be of great importance in the study of phenomena pertaining to these suspensions, and therefore it is desirable to be able to measure the electrokinetics at such walls. The method discussed in this paper involves the deduction of the magnitude of the electroosmotic currents in a closed cell, whose walls are made of the material in question, *i.e.*, glass, from the hydrodynamics occurring in the cell when an electric potential is applied.

2. Data illustrating changes in the hydrodynamics of a glass rectangular cell with *p*H are presented. It is seen that the relationship between cell height and particle velocity, which is a curve markedly parabolic in shape when the medium is alkaline or even neutral, approaches a straight line when the charge on the glass surface decreases and the electroosmotic currents become minimized.

3. Actual electric charge data (electroosmotic flow and zeta-potential) are given for the plane glass surface in contact with the electrolyte solution. The charge is negative in alkaline (Na_2CO_3) solutions. It decreases with decreasing alkalinity, becoming positive in acid (H_2SO_4) medium.

INTRODUCTION

Although one recognizes that electrokinetic phenomena play a very important part in coagulation and adsorption, the reaction occurring between given dispersions and the surfaces of substrates with which they are in contact is often overlooked, and even not understood. Usually, attention is focused only on the particles of the suspension to the neglect of the substrate, so that considerations pertaining to the system are not complete.

In order to interpret many phenomena correctly, it is necessary to have a knowledge of the zeta-potential of the walls in contact with the suspensions, and, therefore, the technique for estimating the charge on a plane glass surface is here considered. It is readily seen that the adherence of particles to a surface, *i.e.*, "slime coating" in mineralogical work or particle adhesion studies as carried out by A. von Buzágh (4), definitely depends on the electrokinetic nature of the substrate as well as on the nature of the particles of the suspension.

---

[1] The data cited in this paper are from Bender, "Brownian Movement—Electrical Charge—Flocculation," Ph.D. Dissertation, New York University (1949). See also Bender and Mouquin, *J. Phys. Chem.* **56**, 272 (1952).

[2] Present address: American Cyanamid Company, Bound Brook, New Jersey.

An important illustration of the effect of nearby walls on the properties of suspended particles is in Brownian movement studies, where often reported changes in pedesis, especially the actual cessation of activity, have really been due more to "wall effects"[3] than (as claimed) to subsidence of kinetic energy forces in the suspension itself. This has recently been demonstrated by Bender and Mouquin (3), where for a given case of actual Brownian movement stoppage due to electrolyte addition it was found that the charge of the glass cell wall had reversed itself and become positive while the particles remained negative so that electrostatic forces became operative to cause particle adhesion and prevent visual display of Brownian movement. Tables II and III (and Figs. 7 and 8) are taken from this work to show the electrokinetic changes. It is of interest that these and other results indicate that the differences in Brownian intensity observed by Henri (6) upon the addition of alkali or acid, could have been due to an appreciable extent to "wall effects."

EXPERIMENTAL PRINCIPLES AND TECHNIQUE

A glass cataphoresis cell is used, but the electroosmotic currents are measured as well as the cataphoretic velocity of the particles in suspension, and from this the electric charge of the plane glass[4] surface may be obtained. This technique has specifically been used by Tuorila (13) who followed the changes in zeta-potential of the glass surfaces in a rectangular cell, which were respectively in contact with varying concentrations of the electrolytes LiCl, NaCl, KCl, CsCl, HCl, HNO_3, KNO_3, and $AgNO_3$. The zeta-potential decreased in negativity with increasing amounts of these electrolytes but never became positive except in the case of the acids, when it became weakly so.

The electroosmosis is evaluated indirectly, it being necessary to interpret it from the velocities of suspended particles at different levels in the cell. Upon algebraic addition of the "true cataphoretic velocity" with the particle velocity at the cell surface, the liquid velocity at the surface is obtained.

"True cataphoretic velocity" occurs at two levels in the cell as dictated

---

[3] Usually the observation cells were shallow, having a height of 35μ and less, having been being prepared by placing a cover-glass on a drop of suspension on a microscope slide.

[4] Conceivably, electrokinetic properties of surfaces other than glass could be estimated equally as well in a cell made of that material, provided the optics are satisfactory for employment of a microscope to observe the particles.

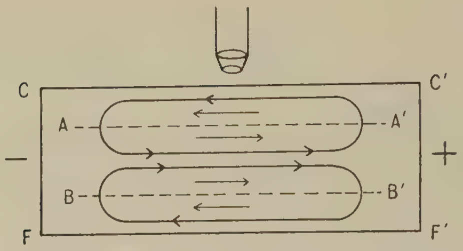

FIG. 1. Liquid currents due to electroendosmosis in a cataphoresis cell.

by the hydrodynamics of the system which is represented diagrammatically in Fig. 1. When a potential of the indicated sign is applied, the liquid circulates in the cell in the direction designated by the arrows if the surfaces *CC′* and *FF′* are negatively charged. Meanwhile the particles in suspension and under the influence of the applied e.m.f. will be affected by this flow throughout the cell except at the levels *AA′* and *BB′*, which are passive regions because they are between the layers of liquid coming and going. It is at *AA′* and *BB′* that the particles exhibit "true cataphoretic velocity."[5] The mathematical theory and the method of arriving at the position of the true cataphoretic layers are described for cylindrical as well as rectangular cells by Mooney (11), Mattson (8, 9), and Abramson (1), who follow the principles of von Smoluchowski.

Electroosmotic velocities thus calculated may be used as is (in μ/sec./volt/cm.) to give an indication of the state of the surface, or they may be converted to zeta-potentials by the Helmholtz-Smoluchowski equation,—see Henry (7) and Sumner and Henry (12):

$$\zeta_{\text{E.O.}} = \frac{4\pi\eta\,(\text{E.O.V.})}{\epsilon} \qquad [1]$$

which has been pointed out by Smoluchowski to be similar to the equation linking the zeta-potential with the cataphoretic velocity, *i.e.*:

$$\zeta_{\text{C}} = \frac{4\pi\eta(\text{C.V.})}{\epsilon}\,. \qquad [2]$$

In these equations $\zeta_{\text{E.O.}}$ and ζ_{C} are the zeta-potentials derived from electroosmotic and cataphoretic data, respectively, E.O.V. and C.V. are the electroosmotic and cataphoretic velocities per unit potential gradient, η is the viscosity, and ϵ the dielectric constant of the liquid medium.

---

[5] However, the measurements must be made sufficiently well removed from the sides and ends of the cell, owing to the complicating effects of the electroosmotic currents in these localities. For instance, see Viscontini, "Remarks on Smoluchowski's Equation for the Velocity of Electroosmosis in a Rectangular Cell," *J. Chim. Phys.* **41**, 225 (1944).

It is seen from Eqs. [1] and [2] that the ratio of E.O.V. to C.V. in a cataphoresis cell, where the surface properties of the walls and the suspended particles are the same, should be unity. Mooney (11), who worked with a suspension of oil drops in an oil-coated cylindrical cell, seems to have been the first to check this ratio. However, van der Grinten (5) did not obtain this result for glass particles in a glass cell. Actually, there has been an appreciable amount of work by various authors in the evaluation of this ratio for glass and also for coated (protein) surfaces, and in measurements of the electric potential of the macroscopic cell surfaces; resumés and references to this work are given by Abramson (1) and Abramson, Moyer, and Gorin (2). Most of the work, especially the coated surface investigations, showed the velocity of electroosmotic flow to be the same as the cataphoretic velocity of the particles. An actual comparison where there was agreement between the electroosmosis in a cataphoresis cell and that in a Quincke capillary has been obtained by Monaghan and White (10).

A rectangular modified Northrup-Kunitz cell was used for the present measurements. This affords a plane glass surface over which variations in the electric charge can be studied when the electrolyte solutions in contact with it are changed. Suspensions used for following the electroosmotic flow (besides introducing the electrolyte) were prepared from ground sphalerite mineral and contained 0.0125% by weight of this material. Dark field microscopy was employed, since the average diameter of the particles was well under 1 μ. Measurements were made at room temperature; however, the values obtained were adjusted to 25°C. through multiplication by the ratios of the viscosities of water at the corresponding temperatures.

RESULTS AND DISCUSSION

The data in Table I illustrate the hydrodynamics of the rectangular cataphoresis cell for different *p*H's. Sodium carbonate was used for alkalinity and sulfuric acid for acidity. Figures 2–6 are plots of these data. The parabolic shapes of the curves bear out the hydrodynamic theory of the cataphoresis cell. In an acid medium the particle velocity parabola becomes appreciably flattened out, indicating less electroosmotic flow, this being due to the great decrease in negativity of the glass.

Table II gives the electroosmosis at the glass surfaces of the cell for the five electrolyte solutions in Table I and also for 0.002 M H_2SO_4. This flow is calculated from the particle velocity at the cell surface and the true cataphoretic velocity by algebraic addition. Corresponding values of

TABLE I

Velocity[a] of Particles in Cell at Different Levels and Different pH's

Height in cell (μ)	pH				
	10.1 (0.001 *M*) (Na_2CO_3)	8.9 (0.0001 *M*) (Na_2CO_3)	6.6 (dist. H_2O)	4.3 (0.00006 *M*) (H_2SO_4)	2.9 (0.001 *M*) (H_2SO_4)
826	—	+1.27	+1.44	—	—
818	—	+1.45	+1.22	+0.29	−0.83
801	+0.46	—	+1.15	−0.37	−0.93
785	+0.55	—	+0.83	+0.03	−0.91
743	−1.00	−1.23	−0.30	−0.94	−1.00
661 (true C.V.)	−2.07	−2.04	−1.29	−1.90	−1.08
537	−3.33	−3.08	−2.57	−2.83	−1.65
413	−4.03	−3.44	−2.99	−3.14	−1.67
289	−3.32	−3.61	−2.62	−3.03	−1.48
165 (true C.V.)	−2.15	−2.14	−1.73	−2.29	−1.17
83	−1.15	−0.97	−0.77	−1.21	−0.90
41	−0.51	−0.09	−0.32	−0.64	−0.81
25	+0.33	+1.01	+0.39	−0.63	−0.74
8	+0.83	+1.23	+0.91	+0.48	−0.73
0	+0.84	+1.44	+0.96	+0.34	−0.65

[a] In μ/sec./volt/cm. The actual sign of charge of the particles is indicated in front of the true C.V. values. Signs opposite to this at other locations in the cell denote that the particles are travelling in opposite direction because of the electroosmotic currents.

$\zeta_{E.O.}$ were calculated by means of Eq. [1], (*i.e.*, at 25°C. $4\pi\eta/\epsilon$ equals 13.0), and are listed with the electroosmotic values. For comparison, the true cataphoretic velocity of sphalerite in each of these electrolyte media (and even in more acidic solution) is given. Figure 7 is a plot of the (velocity) data. Note how the glass surface readily becomes positively charged with increasing acid while the sphalerite particle charge does not even cross the isoelectric line.

Table III and Fig. 8 illustrate how the conditions can be altered in a cell so that particles originally in suspension and repelled by the walls, become attracted to them and adhere, thereby ceasing their Brownian activity. The data show, in six progressive steps, the changes occurring in the electrokinetic properties of the glass cell surface and the sphalerite particles, when acid solution is added to replace the alkaline solution in which the particles were first suspended. Both the glass wall charge and particle charge decrease in negativity as the suspension becomes more acid. But the wall charge decreases so much faster that it becomes positive by the time there is 50% of acid (0.002 *M*) and 50% of alkali (0.001 *M*). Meanwhile the particles remain negative even up to 100% acid solution, so that their tendency to adhere to the glass walls is understood.

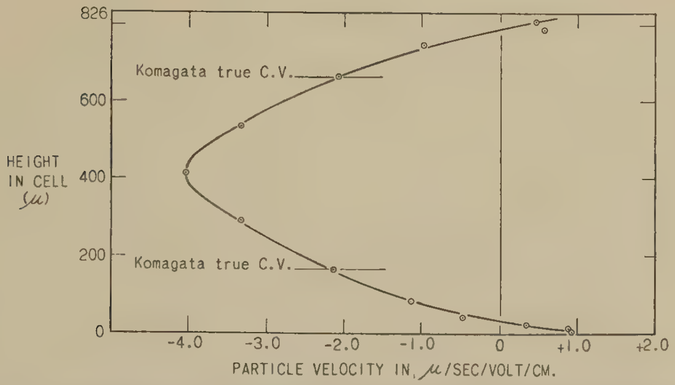

FIG. 2. Particle velocity at different cell levels 0.001 *M* Na_2CO_3; *p*H = 10.1.

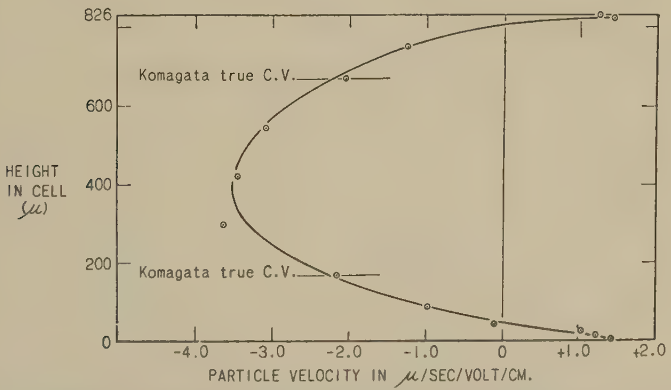

FIG. 3. Particle velocity at different cell levels 0.0001 *M* Na_2CO_3; *p*H = 8.9.

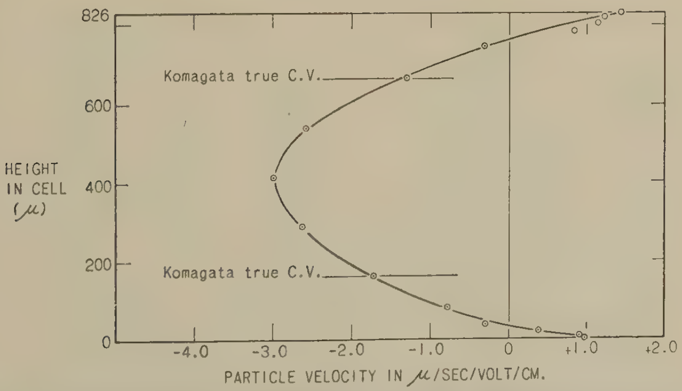

FIG. 4. Particle velocity at different cell levels distilled H_2O; *p*H = 6.6.

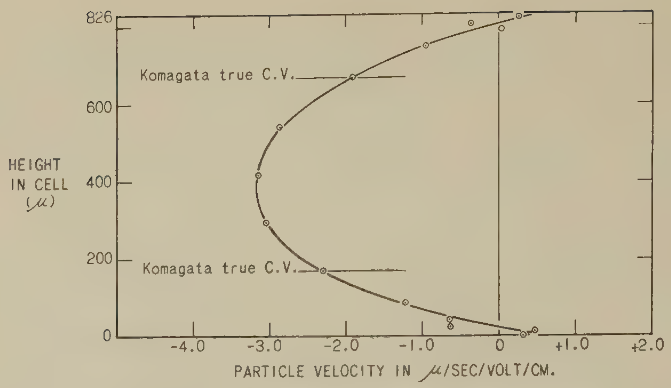

FIG. 5. Particle velocity at different cell levels 0.00006 *M* H_2SO_4; *p*H = 4.3.

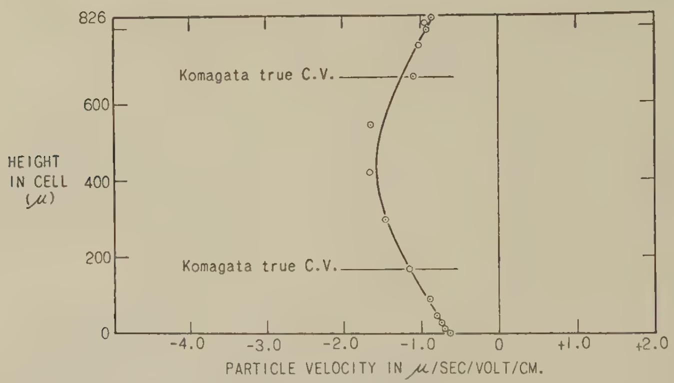

FIG. 6. Particle velocity at different cell levels 0.001 *M* H_2SO_4; *p*H = 2.9.

TABLE II

Electroosmosis[a] *and Zeta-Potential*[b] *at Plane Glass Surface at Different pH's*

*p*H	Electrolyte and concentration	E.O.V.[d]	$\zeta_{E.O.}$	C.V.[c] avg. of sphalerite
10.1	0.001 *M* Na_2CO_3	−2.95	−38.3	−2.11
8.9	0.0001 *M* Na_2CO_3	−3.54	−46.0	−2.09
6.6	Distilled water	−2.71	−35.2	−1.51
4.3	0.00006 *M* H_2SO_4	−2.48	−32.2	−2.10
2.9	0.001 *M* H_2SO_4	−0.38	− 4.9	−1.12
2.6	0.002 *M* H_2SO_4	+1.28	+16.6	−0.08
2.2	0.01 *M* H_2SO_4	—	—	−0.44
1.4	0.1 *M* H_2SO_4	—	—	(0)

[a] In μ/sec./volt/cm. at 25°C.; + or − sign means that the glass is charged that way.

[b] In millivolts.

[c] In μ/sec./volt/cm. at 25°C.

[d] This value is probably approximate.

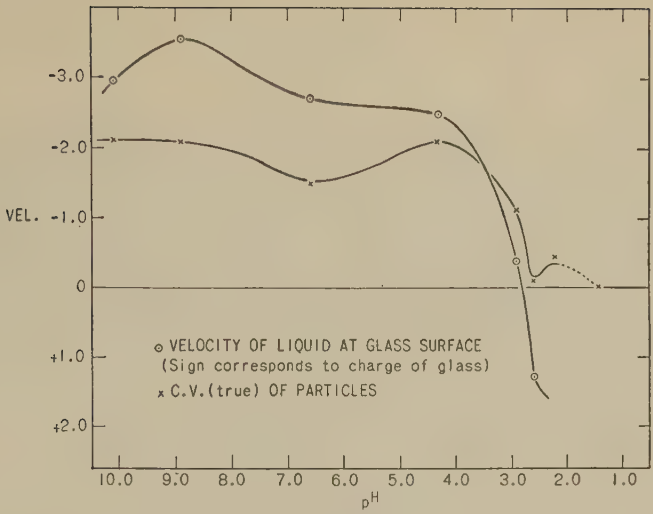

FIG. 7. Velocity of liquid at glass surface and C.V. (true) of particles vs. pH.

TABLE III

Changes in Electroosmosis and Zeta-Potential at Plane Glass Surface as 0.002 M H_2SO_4 is Added to 0.001 M Na_2CO_3

	% H_2SO_4	Molarity H_2SO_4	Molarity Na_2CO_3	Molarity Na_2SO_4	E.O.V.^{a,b}	$\zeta_{E.O.}^{c}$	C.V.^{a} avg. of sphalerite
1	0	0	0	0	−2.95	−38.3	−2.11
2	20.0	0	0.000400	0.000400	−3.98	−51.7	−2.31
3	33.3	0	0	0.000667	−1.12	−14.6	−1.86
4	50.0	0.000500	0	0.000500	+0.83	+10.8	−0.76
5	66.7	0.001000	0	0.000333	+1.09	+14.2	−1.49
6	100.0	0.002000	0	0	+1.28	+16.6	−0.08

[a] In μ/sec./volt/cm.

[b] Positive or negative sign means that the glass is charged that way.

[c] In millivolts.

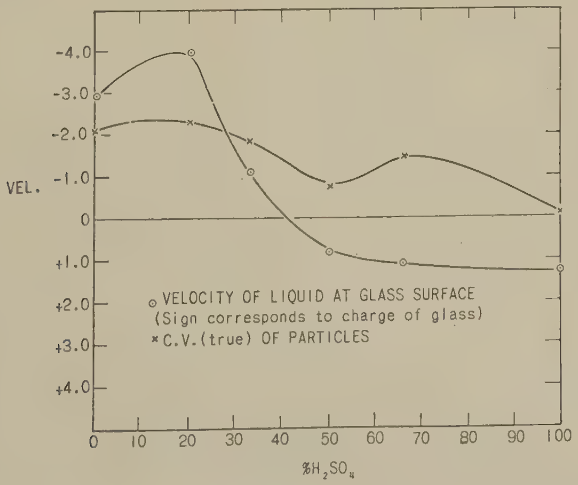

FIG. 8. Liquid velocity at the surface and particle C.V. (true) for different mixtures of 0.001 M Na_2CO_3 and 0.002 M H_2SO_4.

References

1 Abramson, H. A., "Electrokinetic Phenomena and Their Application to Biology and Medicine." The Chemical Catalog Company, Inc., New York, 1934.

2. Abramson, H. A., Moyer, L. S., and Gorin, M. H., "Electrophoresis of Proteins and the Chemistry of Cell Surfaces." Reinhold Publishing Corporation, New York, 1942.

3. Bender M., and Mouquin, H., *J. Phys. Chem.* **56,** 272, 1952. See also Bender, M., Ph.D. Dissertation, New York University, 1949.

4. von Buzágh, A., "Colloid Systems" (English translation). The Technical Press, Ltd., London, 1937.

5. Grinten, van der, K., *J. Chim. Phys.* **23,** 209 (1926).

6. Henri, V., *Compt. rend.* **147,** 62 (1908).

7. Henry, D. C., *Proc. Roy. Soc.* (*London*) **A133,** 106 (1931).

8. Mattson, S., *J. Phys. Chem.* **32,** 1532 (1928).

9. Mattson, S., *J. Phys. Chem.* **37,** 223 (1933).

10. Monaghan, Betty, and White, H. L., *J. Phys. Chem.* **39,** 935 (1935).

11. Mooney, M., *Phys. Rev.* **23,** 396 (1924).

12. Sumner, C. G., and Henry, D. C., *Proc. Roy. Soc.* (*London*) **A133,** 130 (1931);

13. Tuorila, P., *Kolloidchem. Beih.* **27,** 44 (1928).

THE SOLUBILITY OF THE PHOSPHATES OF STRONTIUM, BARIUM, AND MAGNESIUM AND THEIR RELATION TO THE PROBLEM OF CALCIFICATION[1]

L. Emmett Holt, Jr., Jerry A. Pierce, and Charlotte N. Kajdi

From the Departments of Pediatrics, Johns Hopkins University, Baltimore, and New York University College of Medicine, New York City

Received June 23, 1954

INTRODUCTION

The conditions controlling the deposition and solution of the mineral matter of tooth and bone have been the subject of many studies carried out during the past half century. These studies have attempted to define the nature of the solid phases at equilibrium and the solubility product constants of the ions participating in their formation. As knowledge has accumulated it has become clear that a simple interpretation of calcification in terms of solubility is no longer tenable. Phenomena of delayed equilibrium—of supersaturation—are concerned as well as adsorption of various ions upon an underlying crystal lattice.

A confusing feature has been the effect of bivalent metal ions other than calcium upon calcification. Experimentally rickets has been produced by the administration of strontium (1–3), beryllium (3, 4), manganese (5), and iron (6). Magnesium (7) in particular seems to exercise an unfavorable effect on calcification. Holt and Shipley (8) and Shelling, Kramer, and Orent (9) noted its untoward effect on calcification *in vitro*. Kajdi (10) and Stein (11) observed definite decalcifying effects *in vivo* and employed magnesium salts therapeutically in conditions of hyperostosis. The presence of an abnormally high proportion of magnesium in carious teeth observed by Howe (12) has occasioned speculation as to the role of this element in the pathological process. The decalcifying action of strontium was used therapeutically by Park and Nachlas (13) in an attempt to soften bones and correct rachitic deformities. A decalcifying action of strontium on teeth has been observed by Schmidt (13a).

The mechanism by which these various metals exert their unfavorable effects on calcification has not up to the present time been studied. Several possibilities exist. (1) It is possible that certain of these metals are capable of forming insoluble phosphates and carbonates which cause precipitation of these essential anions in the intestine resulting in failure of absorption and loss to the body. In such a case the anion deficiency would probably be revealed by blood analysis. (2) Insoluble phosphates of the metals in question could conceivably be carried through the blood in colloidal form; under such conditions blood analysis might reveal no deficit in inorganic phosphate, although the material presented to the osteoblasts for calcification might be unsuitable for use—either because of the presence of the strange metal or because of the unavailability of the phosphate. (3) It is possible that the action of the metal is produced as the result of an antagonistic effect of its ions on the activity of the ions normally concerned in the formation of bone salts. This could be due to the high valency of the cation or to some specific ion effect. (4) Lastly, the metal may exert some poisonous action on the enzyme systems of the osteoblasts themselves and thus interfere with the production of normal bone matrix for calcification.

---

[1] This work was commenced in collaboration with the late Dr. David H. Shelling, who participated in some of the preliminary orientation experiments.

It is obvious that no intelligent discussion of these various possibilities can be attempted without a knowledge of the solubilities of the carbonates and, more particularly, of the phosphates of the metals concerned. Data on the carbonates are available, but modern data on the phosphates are almost completely lacking, an exception being the solubility of secondary magnesium phosphate, which was studied by Tabor and Hastings (14) and by Greenwald (15). It was with a view to supplying this deficiency that the present experiments were undertaken. We were primarily interested in determining the solubilities of the orthophosphates of magnesium and strontium. Barium, although of limited biological interest, was included in the study because of the possibility that its behavior might throw some light on the anomalous behavior of calcium in the system under study.

EXPERIMENTAL METHODS

The system employed to study the solubilities of these salts was similar to that used by Holt, LaMer, and Chown (16) in their studies of the calcium phosphates. The titration curve of phosphoric acid with the hydroxide of the metal in question was first explored at 38°C. to determine the regions in which stable precipitates formed. Various points on the curve were then selected for further study, the appropriate quantities of acid and base being mixed together and shaken continuously at 38°C. for periods varying from 1 to 10 weeks, at the end of which time the precipitate was separated, the solution analyzed for *p*H, phosphorus, and the metal cation, and the precipitate for the latter two components. From the ratio, metal/phosphorus in the solid phase, which was determined directly and also calculated from the difference of the analytical figures on the solution from the quantity originally introduced, the nature of the solid phase at equilibrium was determined. Ion products were calculated for the ions forming the precipitate in question.

pH determinations were made with a quinhydrone electrode.

Phosphorus was determined by the method of Fiske and Subbarow (17).

Strontium was determined as $SrSO_4$ by a method devised by one of us (C. N. K.) as follows: To an aliquot portion of the filtrate or of a solution of the precipitate in HCl were added 1 to 2 cc. 20% H_2SO_4. A volume of alcohol equal to the volume of the resulting solution was added, the mixture stirred and allowed to settle overnight. The strontium sulfate was filtered in a permanent porcelain filter crucible and washed with 50% alcohol containing a little acid and finally with unacidified 50% alcohol until free of acid. It was then dried in an oven, ignited in a muffle furnace for 20 to 30 minutes, cooled and weighed. Weight of $SrSO_4 \times 0.477 =$ weight of strontium in the aliquot. This method was checked with known solutions of strontium salts.

Magnesium was determined as $Mg_2P_2O_7$ as follows: To a 10-cc. aliquot of solution or of precipitate dissolved in HCl were added 2 cc. 27% NH_4Cl and 2 cc. of a 10% solution of $(NH_4)_2HPO_4$. The solution was stirred, although frequently no precipitate occurred at this point. One third of the volume of 10% NH_4OH was then added, the solution stirred vigorously and allowed to cool. The resulting precipitate was allowed to settle overnight, filtered on an ash-free Whatman filter paper, and washed with 5% NH_4OH several times. The filter paper and precipitate were dried, ashed, and finally ignited in a weighed porcelain crucible in an electric furnace with the door closed for about 6 hours. After cooling it was weighed. On igniting the $MgNH_4PO_4$ is converted to the pyrophosphate, $Mg_2P_2O_7$. Weight of $Mg_2P_2O_7 \times 0.2184 =$ weight of Mg in aliquot. The magnesium and barium analytical procedures were checked against known solutions.

Barium was determined as $BaSO_4$ as follows: An aliquot of solution or of precipitate dissolved in HCl was heated to boiling, and to the hot solution was added an excess of 20% H_2SO_4. The solution was digested on the steam bath at least 2 hours, filtered through a weighed porcelain permanent filter, and washed with hot water containing a little H_2SO_4 and then with a little water to extract the acid. The filter was dried, placed in an electric furnace for ½ hour, cooled, and weighed. Weight of $BaSO_4 \times 0.5884 =$ Ba in sample.

Preparation of Solutions. The solutions were prepared as follows: To 20 cc. 0.1 M H_3PO_4 the appropriate amount of base was added and the volume made up to 200 cc. with distilled water. In most instances the solutions were mixed in the cold and then put into a water bath where they were continuously shaken for periods of 10 to 43 days. In some instances the solutions were heated before being mixed—a maneuver which apparently did not affect the final result.

Standardization of Solutions Used in Titration Curves. 0.1 M H_3PO_4 was standardized against 0.1 N NaOH solution. Saturated lime water was used for the $Ca(OH)_2$ solution, which was standardized against 0.1 N HCl. Solutions of $Sr(OH)_2$ and $Ba(OH)_2$ were likewise prepared in concentrations of approximately 0.02 M, which were standardized against 0.1 N HCl.

In the case of magnesium it was found impractical to use $Mg(OH)_2$ because of its limited solubility. Preparations were therefore made using weighed amounts of a partially hydrated magnesia containing by analysis 77.7% MgO. This was added in powdered form to the H_3PO_4 and water and shaken for 12 to 30 days.

Calculation of H_2PO_4', HPO_4'', and PO_4''' Ion Concentrations. These were calculated from measurements of pH and total phosphate, using the formulas derived by Holt, LaMer, and Chown (16), the following values being taken for the dissociation constants of phosphoric acid: $pK' = 2.11 - 0.5\sqrt{\mu}$; $pK'_2 = 7.15 - 1.25\sqrt{\mu}$, and $pK'_3 = 12.66 - 2.25\sqrt{\mu}$.

TITRATION CURVES OF PHOSPHORIC ACID

Since the titration curves of H_3PO_4 with these metal hydroxides present certain unusual features, and since certain deductions can be drawn from these alone, they will be discussed in detail. It will be recalled that the titration curve of H_2PO_4 with a base forming no precipitate, such as NaOH, shows two breaks—one at pH 4.5 and another at pH 8.5. The first break corresponds to the neutralization of the first equivalent of acid when the solution, containing almost exclusively primary phosphate, is unbuffered. The second corresponds to the neutralization of the second equivalent of acid when the solution, containing then almost exclusively secondary phosphate, is again unbuffered (see Fig. 1). The titration curve with a base forming an insoluble phosphate deviates from the above at the point where precipitate first makes its appearance, following thence a more or less horizontal course. This plateau indicates buffering of the solution due to the formation of precipitate; increments of alkali instead of raising the pH merely result in the formation of more solid phase. When no more precipitate can be formed, the addition of alkali again raises the pH and the curve turns upward to *rejoin* the NaOH curve.

The *area* between such a curve and the titration curve when no precipitate forms (like the NaOH curve) measures the buffering due to the formation of precipitate. The *abscissa*—e.g., the horizontal distance from the NaOH curve to the curve with the precipitate-forming base at any pH—measures the solubility of the precipitate at that pH; it measures the extent to which phosphate can be precipitated regardless of the nature of the solid phase. Some information can also be deduced from the *level of the plateau* as to the nature and solubility of the solid phase. It is obvious that a plateau appearing at a pH above 4.5 cannot be due to the precipitation of

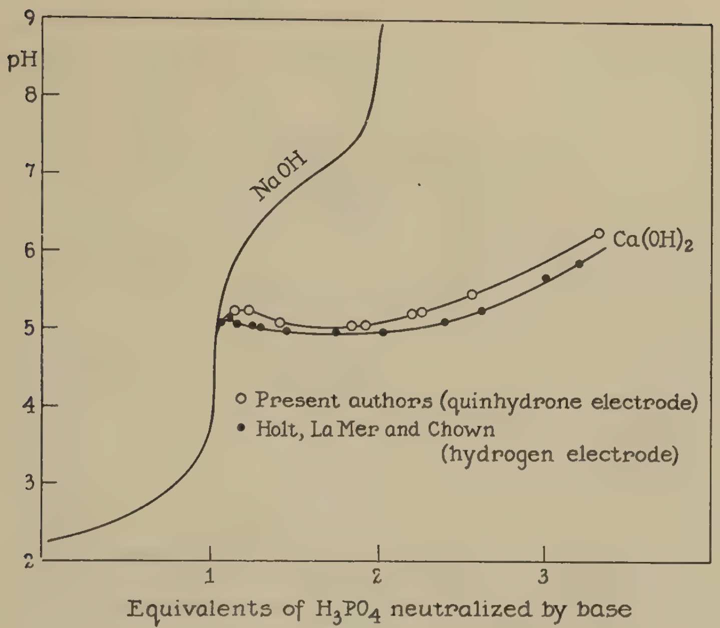

FIG. 1. Titration curve of phosphoric acid with calcium hydroxide.

primary phosphate and likewise that one appearing at a *p*H above 8.5 cannot be due to secondary phosphate. Between these *p*H levels, a plateau may be due either to secondary or tertiary phosphate, since both ions are increased by increases of *p*H in this range. If more than a single plateau appears, one can be reasonably sure of the presence of more than one solid phase. In comparing the plateaus of different curves, given the fact that the solid phase is similar, the lower plateau will obviously indicate the more insoluble salt.

THE CALCIUM CURVE

Since the earlier work of Holt, LaMer, and Chown (16) has been criticized (18) on the ground that the phenomenon of electrode poisoning which they encountered might have interfered with the accuracy of their *p*H determinations, it was decided to repeat the $Ca(OH)_2$ titration curve at 38°C. using the quinhydrone electrode. As may be seen from Fig. 1, the curve closely approximates that of the original authors.

THE MAGNESIUM CURVE AND THE SOLUBILITY OF THE MAGNESIUM PHOSPHATES

The curve obtained with $Mg(OH)_2$ is shown in Fig. 2. It will be noted that it begins to deviate from the NaOH curve after the first equivalent has been neutralized, this deviation being, however, very slight between

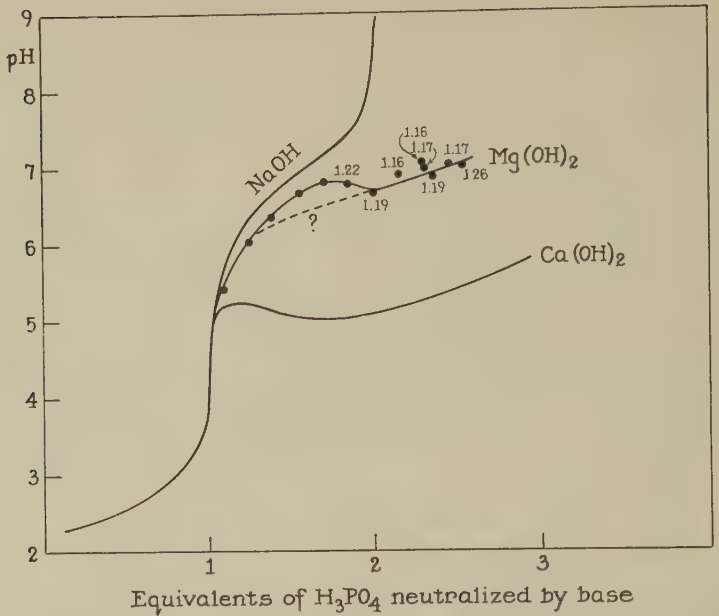

FIG. 2. Titration curve of phosphoric acid with magnesium hydroxide. The numbers attached to the points on the $Mg(OH)_2$ curve refer to the Mg/P ratio of the precipitate. Theoretical ratio for $MgHPO_4$ is 0.77; that for $Mg_3(PO_4)_2$ is 1.17.

1.0 and 1.5 equivalents. No visible precipitate made its appearance in this region, and we are inclined to attribute this slight deviation to the formation of minute colloidal particles of invisible precipitate. A similar phenomenon was noted in the case of $Ca(OH)_2$ by Holt, LaMer, and Chown before the first precipitate made its appearance. After 1.5 equivalents have been neutralized, the curve deviates sharply from the NaOH curve, this being accompanied by the appearance of a precipitate. In the neighborhood of the second equivalent the curve takes a reverse turn, the *p*H actually becoming more acid despite the addition of more alkali. Beyond 2.25 equivalents a definite plateau at *p*H 7.0 becomes established.

The downward deviation of the curve between 1.7 and 2.0 equivalents perplexed us considerably. Our first thought was that some unstable phase might be developing in the region of 2.0 equivalents, and we attempted by a more prolonged experiment to eliminate this negative hump. A time experiment in which solutions with 2.0 equivalents neutralized were equilibrated as long as 10 weeks (see Table I) indicated that, although the solution continued to lose magnesium and phosphorus at a very slow rate, this point on the *p*H curve was essentially correct. We are therefore inclined to believe that an unstable equilibrium is represented by the entire portion of the curve between 1.0 and 2.0 equivalents. Quite possibly a curve at true

TABLE I

Solubility of Magnesium Phosphate at 38°C.

Serial no.	Time equilibrated	Equivalents Mg (OH)$_2$ added	Mg/P ratio of ppt.	Analysis of solution			Calculated values for solution						
				*p*H	Mg (*moles* × *10*^{3})	P (*moles* × *10*^{3})	μ	$\sqrt{\mu}$	p[Mg$^{\cdot\cdot}$]	p[HPO$_4^{\cdot\cdot}$]	p[PO$_4^{\prime\prime\prime}$]	p[Mg$^{\cdot\cdot}$] + p[HPO$_4^{\prime\prime}$]	3[pMg$^{\cdot\cdot}$] + 2p[PO$_4^{\prime\prime\prime}$]
				Titration Curve Experiment									
M 11	12 days	1.85	1.22	6.76	6.23	7.47	0.0205	0.143	2.2055	2.547	8.1266	4.75	22.87
M 12	12 days	2.01	1.19	6.62	4.69	6.34	0.0154	0.124	2.329	2.725	8.485	5.05	23.96
M 13	12 days	2.16	1.16	6.89	4.79	5.66	0.0161	0.127	2.320	2.604	8.0839	4.92	23.13
M 14	12 days	2.32	1.16	7.00	4.54	5.25	0.0156	0.125	2.343	2.578	7.9578	4.92	22.94
M 15	30 days	2.32	1.17	6.97	4.46	4.94	0.0150	0.122	2.351	2.621	8.0358	4.97	23.12
M 16	30 days	2.37	1.19	6.83	3.23	3.66	0.0104	0.102	2.491	2.843	8.4428	5.33	24.36
M 17	12 days	2.47	1.17	7.00	3.21	3.71	0.0111	0.106	2.4935	2.7215	8.1415	5.22	23.76
M 18	30 days	2.54	1.26	6.99	2.30	2.72	0.0079	0.089	2.638	2.891	8.3612	5.53	24.64
				Time Experiment									
MT 1	5 min.	2.0	7.23	6.69	8.66	9.98	0.0276	0.166	2.0625	2.450	8.0538	4.51	22.30
MT 2	1 hr.	2.0	1.24	6.69	6.67	7.74	0.0212	0.146	2.176	2.573	8.2148	4.75	22.96
MT 3	29 days	2.0	1.18	6.61	5.82	7.36	0.0187	0.136	2.235	2.661	8.4085	4.90	23.52
MT 4	6 weeks	2.0	1.20	6.59	5.31	6.87	0.0170	0.131	2.275	2.706	8.4822	4.98	23.79
MT 5	8 weeks	2.0	1.17	6.62	5.46	6.87	0.0175	0.132	2.263	2.684	8.4268	4.95	23.64
MT 6	10 weeks	2.0	1.15	6.72	4.72	6.27	0.0159	0.126	2.326	2.662	8.3188	4.99	23.62

equilibrium would follow the course indicated by the dotted line. The delay in equilibrium here can conceivably be attributed to the fact that we are dealing (as shown below) with a salt composed of five ions whose precipitation, being a reaction either of a high order or a phenomenon of consecutive reactions, might be expected to be a slow one;[2] it may also be related to the fact that instead of starting with a true solution we introduced our magnesium as a solid phase; when the concentrations are such that the tendency to form the phosphate precipitate is small, it is possible that the minute nuclei of precipitate may protect some of the $Mg(OH)_2$ from interacting with the phosphate ions.

Analyses of the solid phase and calculations of the magnesium and phosphorus of the solid phase by difference checked quite accurately, Mg/P ratios being found throughout closely approximating 1.17, which is the theoretical ratio for the tertiary phosphate $Mg_3(PO_4)_2$. At no point on the curve were ratios suggesting the presence of secondary phosphates found. Calculations of the ion product $3pMg^{\cdot\cdot} + 2pPO_4'''$ are shown for the original titration curve and for the time experiment at 2.0 equivalents in Table I. It is apparent from the data in the time experiment that deposition of the tertiary salt is continuing, at least up to 10 weeks of continuous shaking, and that the ion product continues to decrease for at least a month. It should also be noted, however, that the ionic strength of the solution is also steadily diminishing; hence it is probable that the conditions in the shorter experiments, although not approaching equilibrium in respect to time, are actually not far distant from equilibrium at any point. On this account it has seemed justifiable to include these data in the graph in which pK_{sp} for $Mg_3(PO_4)_2$ is plotted as a function of the ionic strength of the solution (Fig. 5). Extrapolation of the experimental data indicates a pK_{sp} for $Mg_3(PO_4)_2$ at infinite dilution of 27.7 at 38°C. The influence of ionic strength of the solution on the K_{sp} is indicated by the equation $pK_{sp} = 27.2 - 29\sqrt{\mu}$. A comparison of these data with those obtained on the K_{sp} of tertiary calcium phosphate indicates that the magnesium salt is far more soluble. At infinite dilution the pK_{sp} of the calcium salt is approximately 32 in contrast to 27.2 for magnesium, and extrapolation of our data for ionic strengths comparable to that of blood serum indicates that in this range the pK_{sp} for the magnesium salt would be far below 20, in contrast to figures between 27 and 28 which have been obtained for the calcium salt. The far greater solubility of the magnesium salt is further attested to by the fact that the plateau on the titration curve caused by its precipitation occurs at a pH 7 instead of at a pH 5. One must conclude that such unfavorable influences as Mg ion may exert upon calcification are not attributable to the formation of an insoluble phosphate of magnesium in the body. The concentrations of magnesium would have to be many times that of the calcium before such a precipitate could be formed.

---

[2] See Holt, LaMer, and Chown, *loc. cit.* This question is further discussed by Rathje, W., *Ber. Deut. Chem. Ges.* **74B**, 546 (1941).

As has been mentioned, two papers in the literature deal with the solubility of $MgHPO_4$, that of Tabor and Hastings (14) indicating that this has a value for $pK_{sp}MgHPO_4$ of 4.46 at $\mu = 0.16$, and that of Greenwald indicating a value of 4.225 at $\mu = 0.12$ to 0.16. It may be noted that the ion products $[Mg^{\cdot\cdot}] \times [HPO_4'']$ in our studies were in general in the same range as in the studies of these authors, particularly when the solutions were equilibrated for a short time, although in the long-term equilibration experiments the figures tended to approach a pK_{sp} of 5.0. Yet in spite of this the final precipitates found by us at equilibrium conformed to the elementary composition of tertiary rather than of secondary phosphate. This raises the question as to whether the ion products reported by the previous authors actually represent conditions of equilibrium with secondary phosphate. It appears that Tabor and Hastings started with a solid phase consisting of $MgHPO_4$. Nevertheless they equilibrated for only 24 to 48 hours, and since they did not report analyses of the solid phase at the termination of their experiments, it may well be that its composition had changed, some $MgHPO_4$ going into solution and perhaps a more basic salt being deposited. Calculations which we have made of the ion product $[Mg^{\cdot\cdot}]^3 \times [PO_4''']^2$ in the solutions of Tabor and Hastings suggest that these may have been in equilibrium with the solid phase $Mg_3(PO_4)_2$. Greenwald (15) likewise failed to analyze the solid phase at the termination of his experiments. He was, however, cautious in his assumption that this was secondary phosphate, for he refers to the "apparent solubility product" of $MgHPO_4$. In view of these considerations it would seem that further work is needed to establish the true solubility product of secondary magnesium phosphate.

The Barium Curve and the Solubility of the Barium Phosphates

Although the data on barium are of comparatively little biological importance, they will be considered next because barium presents a somewhat simpler case than that of strontium. The titration curve of H_3PO_4 with $Ba(OH)_2$ is shown in Fig. 3 with the curves for NaOH and $Ca(OH)_2$ at 38°C. included for comparison. The barium curve, as may be seen, exhibits two plateaus; the first one between pH 4.7 and 4.8 appears very promptly after the first equivalent of H_3PO_4 has been neutralized. Between 1.6 and 1.9 equivalents the curve rises rapidly, but as it approaches the second equivalent it again flattens out, forming a second plateau at a level of pH 7.2 to 7.3. The two plateaus suggest the formation of two precipitates—a suggestion confirmed by the analytical data and by gross inspection of the solid phase. Analyses and indirect calculations of the Ba/P ratio of the solid phase show that between the first and second equivalents the pre-

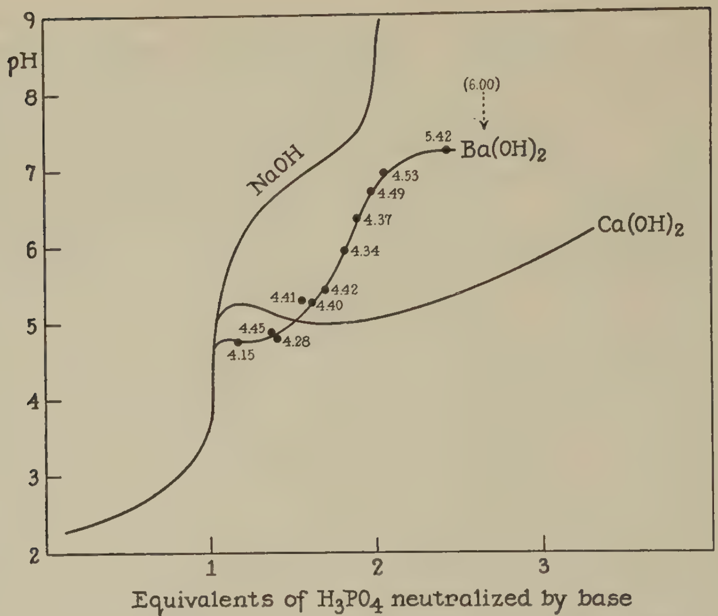

FIG. 3. Titration curve of phosphoric acid with barium hydroxide. The numbers attached to the points on the $Ba(OH)_2$ curve refer to the Ba/P ratio of the precipitate. Theoretical ratio for $BaHPO_4$ is 4.43; for $Ba_3(PO_4)_2$ is 6.64.

cipitate has a Ba/P ratio closely approximating 4.43, the ratio characteristic of secondary phosphate, whereas beyond the second equivalent a limited amount of data indicates a higher ratio and the presence of a more basic salt, presumably the tertiary phosphate. The precipitate obtained between 1 and 2 equivalents is grossly crystalline, whereas after 2 equivalents it is increasingly amorphous. It thus appears that the first plateau results from the deposition of the secondary salt and the second plateau, from the precipitation of the tertiary salt.

A comparison of the barium with the calcium curve indicates that the plateau caused by the deposition of secondary phosphate occurs at a lower *p*H in the case of barium (e.g., *p*H 4.7) than in the case of calcium (*p*H 5.1). From this one can deduce that the solubility of $BaHPO_4$ is less than that of $CaHPO_4$. Our analytical data and calculations of the K_{sp} for $BaHPO_4$ (shown in Table II) bear this out. The reverse relation seems to hold in the case of the tertiary salt. The second plateau in the case of barium occurs at a *p*H of 7.2 to 7.3, in striking contrast to that formed by the deposition of $Ca_3(PO_4)_2$ (approximately *p*H 5.0). The conclusion that the tertiary barium salt is therefore much more soluble than the corresponding calcium salt is also supported by the analyses of the one solution (B 14) which could be regarded as in equilibrium with this solid phase. The pK_{sp} for $Ba_3(PO_4)_2$

TABLE II

Solubility of Barium Phosphate at 38°C.

Serial no.	Time equilibrated *(days)*	Equivalents $Ba(OH)_2$ added	Ba/P ratio of ppt.	Analysis of solution			Calculated values for solution						
				*p*H	Ba *(moles* × *10³)*	P *(moles* × *10³)*	μ	$\sqrt{\mu}$	p[Ba$^{\cdot\cdot}$]	p[HPO$_4''$]	p[PO$_4'''$]	p[Ba$^{\cdot\cdot}$] + p[HPO$_4''$]	3p[Ba$^{\cdot\cdot}$] + 2p[PO$_4'''$]
B 3	12	1.15	4.15	4.76	4.24	8.39	0.0127	0.113	2.37	4.31	11.96	6.68	31.05
B 4	12	1.38	4.45	4.84	3.21	6.34	0.0097	0.0983	2.49	4.39	11.99	6.88	31.45
B 5	12	1.43	4.28	4.79	2.87	5.60	0.0086	0.0926	2.54	4.50	12.16	7.04	31.94
B 6	12	1.55	4.41	5.28	2.46	4.63	0.0074	0.0857	2.61	4.11	11.29	6.71	30.41
B 7	12	1.64	4.40	5.23	1.56	3.38	0.0049	0.0699	2.81	4.31	11.58	7.12	31.59
B 8	12	1.70	4.42	5.41	1.79	3.30	0.0044	0.0667	2.75	4.15	11.25	6.89	30.73
B 9	12	1.82	4.34	5.94	0.877	1.61	0.0027	0.0521	3.06	3.97	10.57	7.02	30.31
B 10	12	1.89	4.37	6.33	0.702	1.15	0.0022	0.0473	3.15	3.77	9.994	6.92	29.45
B 11	12	1.965	4.49	6.69	0.513	0.789	0.0018	0.0419	3.29	3.65	9.530	6.94	28.93
B 12	12	2.05	4.53	6.95	0.291	0.388	0.0010	0.0318	3.54	3.80	9.437	7.34	29.48
B 13	12	2.45	5.42	7.25	0.258	0.198	0.0008	0.0281	3.59	3.94	9.289	7.53	29.34
B 14	12	2.67	6.00	—	—	Trace only	—	—	—	—	—	—	—

at $\mu = 0.008$ is found to be 29.34, in contrast to the pK_{sp} for $Ca_3(PO_4)_2$) which indicates a pK_{sp} in the neighborhood of 32.0 at this ionic strength.

If we compare the abscissa between the NaOH and the $Ba(OH)_2$ curves with that between the NaOH and $Ca(OH)_2$ curves at various pH's, we can see at a glance the extent to which Ba can compete with Ca for the available phosphate. Between pH 4.7 and 5.0 barium forms the more insoluble salt, whereas above this pH calcium forms by far the more insoluble salt. Consequently under biological conditions in the body it would appear that barium is unable to compete successfully with calcium for the body phosphate. The toxic effects of this metal must be otherwise explained.

THE STRONTIUM CURVE AND THE SOLUBILITY OF THE STRONTIUM PHOSPHATES

The titration curve of H_3PO_4 with strontium hydroxide is shown in Fig. 4. It will be noted that this begins to deviate from the NaOH curve less promptly after the first equivalent has been neutralized than does the curve for calcium or that of barium hydroxide. A plateau is encountered in the vicinity of pH 5.4 between 1.1 and 1.4 equivalents. Analysis of the solid phase at these points reveals an Sr/P ratio characteristic of secondary strontium phosphate. Beyond 1.4 equivalents the curve rises again, tending

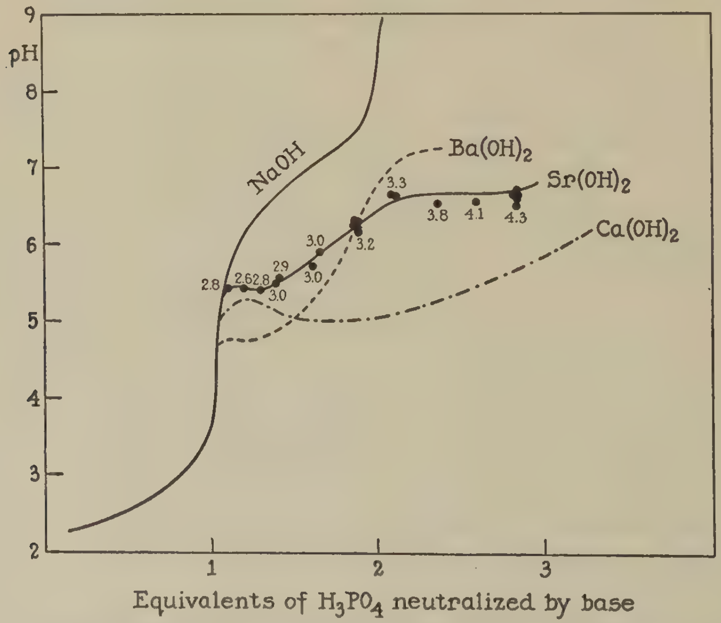

FIG. 4. Titration curve of phosphoric acid with strontium hydroxide. The numbers attached to the points on the $Sr(OH)_2$ curve refer to the Sr/P ratio of the final precipitate. Theoretical ratio for $SrHPO_4$ is 2.82; for $Sr_3(PO_4)_2$ is 4.23.

TABLE III

Solubility of Strontium Phosphate at 38°C. (Titration Curve Experiment)

Serial no.	Time equilibrated (*days*)	Equivalents of $Sr(OH)_2$ added	Sr/P ratio of ppt.	Analysis of solution			Calculated values for solution						
				*p*H	Sr (*moles* × 10^3)	P (*moles* × 10^3)	μ	$\sqrt{\mu}$	p[$Sr^{\cdot\cdot}$]	p[HPO_4'']	p[PO_4''']	p[$Sr^{\cdot\cdot}$] + p[HPO_4'']	3p[$Sr^{\cdot\cdot}$] + 2p[PO_4''']
S 4	12	1.127	2.84	5.43	4.09	7.75	0.0123	0.111	2.389	3.703	10.684	6.09	28.58
S 5	12	1.219	2.57	5.43	3.64	6.57	0.0108	0.104	2.439	3.783	10.779	6.22	28.98
S 6	12	1.312	2.84	5.41	3.24	6.15	0.0098	0.099	2.489	3.837	10.865	6.33	29.20
S 7	12	1.409	2.54	5.50	3.23	5.49	0.0094	0.097	2.491	3.803	10.744	6.29	29.06
S 8	12	1.420	2.93	5.57	2.67	5.32	0.0083	0.091	2.574	3.756	10.642	6.33	29.01
S 9	30	1.420	2.99	5.54	2.84	5.24	0.0085	0.092	2.547	3.789	10.702	6.34	29.01
S 10	12	1.640	2.96	5.73	1.84	3.51	0.0057	0.075	2.736	3.801	10.562	6.54	29.33
S 11	30	1.657	2.96	5.90	1.90	3.46	0.0059	0.077	2.721	3.645	10.233	6.37	28.63
S 12	12	1.872	3.01	6.30	1.15	2.04	0.0038	0.061	2.938	3.532	9.754	6.47	28.32
S 13	30	1.890	2.98	6.28	1.12	1.85	0.0035	0.060	2.733	3.592	9.839	6.54	28.53
S 14	12	2.102	3.28	6.66	1.07	1.43	0.0034	0.059	2.972	3.403	9.270	6.37	27.46
S 15	12	2.13	3.31	6.63	1.12	1.73	0.0038	0.061	2.951	3.339	9.231	6.29	27.33
S 16	30	2.37	3.79	6.54	1.09	1.36	0.0033	0.058	2.963	3.516	9.506	6.48	27.90
S 17	30	2.60	4.10	6.56	1.12	1.36	0.0034	0.058	2.949	3.500	9.469	6.45	27.79
S 18	12	2.82	4.15	7.01	0.66	0.754	0.0022	0.047	3.179	3.466	9.011	6.65	27.56

TABLE IV

Solubility of Strontium Phosphate at 38°C. (Time Experiment)

Serial no.	Time equilibrated (*days*)	Equivalents $Sr(OH)_2$ added	Sr/P ratio of ppt.	Analysis of solution			Calculated values for solution						
				pH	Sr (*moles* × *10*^{3})	P (*moles* × *10*^{3})	μ	$\sqrt{\mu}$	$p[Sr^{\cdot\cdot}]$	$p[HPO_4'']$	$p[PO_4''']$	$p[Sr^{\cdot\cdot}] + p[HPO_4'']$	$3p[Sr^{\cdot\cdot}] + 2p[PO_4''']$
ST 1	7	1.89	3.21	6.29	1.42	2.31	0.0045	0.067	2.847	3.480	9.701	6.33	27.94
ST 2	15	1.89	3.165	6.29	0.985	1.74	0.0032	0.057	3.007	3.613	9.855	6.62	28.73
ST 3	21	1.89	3.16	6.20	1.03	1.85	0.0033	0.057	2.987	3.666	9.996	6.65	28.95
ST 4	28	1.89	3.12	6.17	1.116	1.86	0.0035	0.059	2.952	3.688	10.044	6.64	28.95
ST 5	39	1.89	3.215	6.22	1.147	2.03	0.0037	0.061	2.940	3.604	9.907	6.54	28.63
ST 6	43	1.89	3.155	6.19	1.116	1.92	0.0035	0.059	2.952	3.658	9.993	6.61	28.84
ST 7	7	2.85	4.40	6.63	0.594	0.838	0.0019	0.044	3.227	3.670	9.599	6.90	28.88
ST 8	15	2.85	4.28	6.59	0.539	0.651	0.0016	0.040	3.269	3.814	9.793	7.08	29.39
ST 9	21	2.85	4.29	6.65	0.544	0.720	0.0017	0.042	3.264	3.723	9.639	6.99	29.07
ST 10	28	2.85	4.32	6.49	0.583	0.854	0.0018	0.043	3.234	3.771	9.844	7.01	29.39
ST 11	39	2.85	4.28	6.69	0.572	0.764	0.0018	0.043	3.243	3.667	9.543	6.91	29.81
ST 12	43	2.85	4.24	6.62	0.550	0.772	0.0017	0.042	3.259	3.715	9.661	6.97	29.10

to form a second plateau between 2.0 and 3.0 equivalents. Between 1.4 and 2.0 equivalents a negligible increase in the Sr/P ratio of the solid phase occurred (2.9 to 3.0 as compared with a theoretical ratio of 2.82 for $SrHPO_4$). Beyond 2.0 equivalents, however, the Sr/P ratio of the solid phase increased steadily, finally exceeding the theoretical ratio (4.24) for the tertiary salt.

An explanation of the gradually increasing basicity of the solid phase was sought. One possibility was that this represented a delayed equilibrium, in which case more prolonged equilibration would tend to eliminate it and produce a more uniform solid phase. Consequently further observations were made on solutions equilibrated for periods up to 43 days instead of 10 days as in the original series. A time experiment was run, two series of identically prepared solutions being made, one member of each of which was terminated at intervals for analysis. The results shown in Table IV indicate no appreciable change in the composition of the solution after the tenth day. Microscopic examination of the solid phase at equilibrium was carried out for us by Dr. J. D. H. Donnay of the Department of Geology, Johns Hopkins University. Precipitates obtained between 1 and 2 equivalents were definitely crystalline, being transparent prismatic to acicular crystals belonging to the triclinic or possibly monoclinic systems, but definitely not orthorhombic. This description coincides with that of Schulten (19) for strontium brushite ($SrHPO_4 \cdot 2H_2O$). The failure of the precipitate to lose water until heated in the electric furnace and the weight loss on such heating which would result in the formation of pyrophosphate indicated, on the other hand, that we were dealing with an anhydrous salt. The frankly crystalline structure of the precipitate tended to disappear beyond the second equivalent, a completely amorphous solid phase being noted at 2.7 equivalents. Although in the absence of X-ray analysis the nature of the solid must remain incompletely defined, it would appear to us that the increasing basicity of the precipitate could be explained by adsorption of Sr ions upon the crystal lattice of secondary phosphate—a process which had been observed by Logan and Taylor (20) in the case of calcium phosphate. Whether a strontium apatite occurs at any point can not be stated.

Regardless of the nature of the solid phase in these strontium experiments, it is clear from the comparison of the plateaus of the titration curves that the phosphates of strontium are more soluble than those of calcium, and Sr would hence have to be present in biological fluids in higher concentrations if it were to compete successfully with Ca for available phosphate.

Data on the solubility products of the secondary and tertiary phosphates of the alkaline earth metals as a function of the ionic strength of the solution are given in Figs. 5 and 6. The ion products for the tertiary barium and

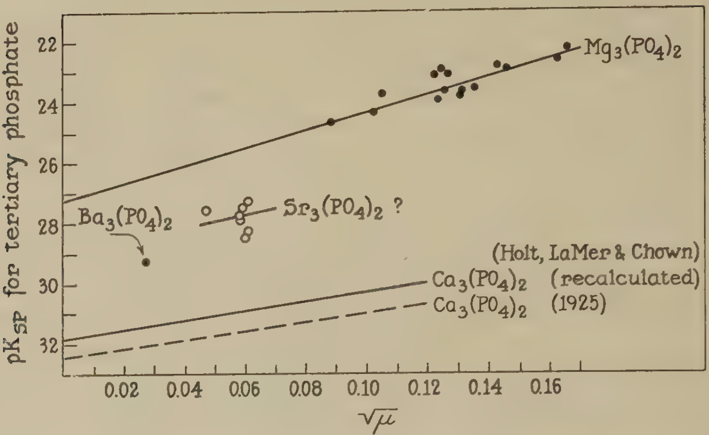

FIG. 5. Relation between the solubility products of the tertiary phosphates of calcium, strontium, barium, and magnesium.

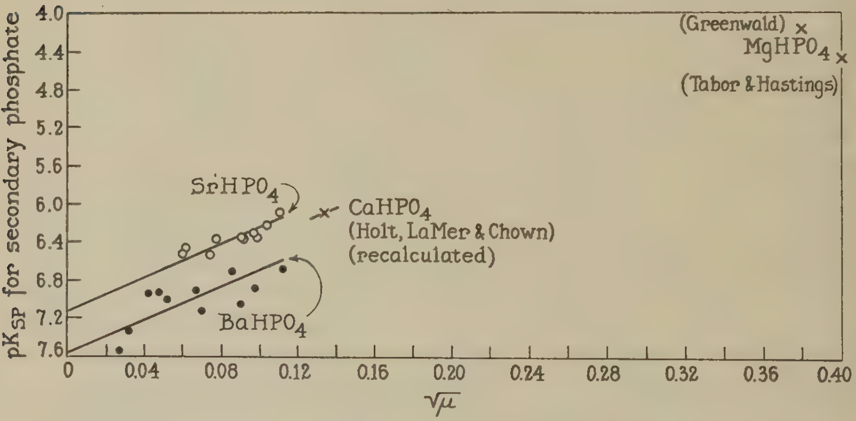

FIG. 6. Relation between the solubility products of the secondary phosphates of calcium, strontium, barium, and magnesium.

strontium salts must be regarded as "apparent" solubility products in view of the questionable nature of the solid phase at equilibrium.

DISCUSSION

The data presented indicate that the tertiary phosphates of the alkaline earth metals studied are considerably more soluble than the corresponding calcium salt. If, as is now generally believed, the solubility of the tertiary phosphate is at least a limiting factor, even if not the only one, concerned in the deposition of the apatite complex known as bone salt, it would appear that these other metals could compete successfully with calcium only at concentrations well above those attained by calcium in biological fluids. There is no evidence that such concentrations are approached in conditions in which Sr or Ba has been given. In the case of Mg, too, rises in extracellular concentration are possible only to a limited extent, and it does not appear that these could compete successfully with calcium in processes of extracellular calcification.

The possibility that secondary phosphate occurs as an *initial phase in the deposition of calcium* has been mentioned repeatedly in the literature, notably by Kramer and his co-workers (21). Direct evidence of crystalline secondary phosphate in calcifying tissues has not been obtained, only apatite structures being found. It is also difficult to reconcile this hypothesis with the observations of Shear and Kramer (22) that serum is undersaturated with respect to $CaHPO_4$. However, even if it were true that deposition of $CaHPO_4$ occurred as a transitory phenomenon, as has been claimed, it does not appear from our data here presented that strontium or magnesium could by the formation of their secondary phosphates interfere with the deposition of the calcium salt. Such interference could occur only in the case of barium, which forms a highly insoluble secondary phosphate.

It would appear to us that the antagonistic effects of magnesium and strontium upon calcification are more readily explained by competition of these metals in the metal complex of the enzyme systems of cells concerned with calcification than by any direct effects on the equilibria concerned with the deposition of bone salt. Sobel *et al.* (23) likewise came to the conclusion that the decalcifying action of strontium could not be explained in terms of solubility phenomena.

It may be pointed out that our data on the solubility of the magnesium phosphates may be of significance quite apart from the problem of calcification. This element, as is well known, occurs in high concentration in intracellular fluids, as do various types of phosphates. The formation of $Mg_3(PO_4)_2$ may well prove to be a limiting factor in determining the concentration of free Mg ion in tissues.

SUMMARY

1. By means of titration curves of phosphoric acid with alkaline earth bases, the solubility of the orthophosphates of magnesium, strontium, and barium has been studied and related to that of the corresponding calcium salts.

2. The solid phase formed by the interaction of H_3PO_4 and $Mg(OH)_2$ at 38°C. was found to be the tertiary phosphate $Mg_3(PO_4)_2$ throughout the range studied, no evidence being found of the formation of the secondary phosphate $MgHPO_4$. The solubility product for tertiary magnesium phosphate was found to be $pK_{sp} = 27.2 - 29\sqrt{\mu}$.

3. The solid phase formed by the interaction of H_3PO_4 and $Ba(OH)_2$ at 38°C. was the secondary phosphate throughout the greater part of the range studied, some evidence of a more basic solid phase being obtained

when more than 2 equivalents of acid were neutralized by base. The $pK_{sp}BaHPO_4$ was found to be $7.56 - 8.4\sqrt{\mu}$. Assuming that the more basic precipitate encountered was the tertiary phosphate, the apparent $pK_{sp}Ba_3(PO_4)_2$ was found to be 29.34 at $\mu = 0.0008$.

4. Analysis of the solid phase at equilibrium formed by the interaction of H_3PO_4 and $Sr(OH)_2$ at 38°C. showed this phase to be $SrHPO_4$ between 1.1 and 1.85 equivalents, after which a steadily increasing Sr/P ratio was obtained. The solubility product for $SrHPO_4$ was found to be pK_{sp} $7.06 - 8.1\sqrt{\mu}$. The apparent solubility product for $Sr_3(PO_4)_2$, if we assume that this was present in the more basic precipitates, was $pK_{sp} = 27.8$ at $\mu = 0.0035$.

5. The decalcifying action of alkaline earth minerals is discussed in relation to the above data.

The authors wish to thank Prof. Victor K. LaMer for his kindness in reading and criticizing this manuscript.

REFERENCES

1. SHIPLEY, P. G., PARK, E. A., MCCOLLUM, E. V., AND SIMMONDS, N., *Bull. Johns Hopkins Hosp.* **33,** 216 (1922).
2. LEHNERT, F., *Beitr. pathol. Anat. u. allgem. Pathol.* **47,** 215 (1910).
3. SOBEL, A. E., GOLDFARB, A. R., AND KRAMER, B., *Proc. Soc. Exptl. Biol. Med.* **31,** 869 (1934).
4. GARCIA, I., *Compt. rend. soc. biol.* **119,** 109 (1935.)
5. BLUMBERG, H., SHELLING, D. H., AND JACKSON, D. A., *J. Nutrition* **16,** 317 (1938).
6. MCCOLLUM, E. V., SIMMONDS, N., SHIPLEY, P. G., AND PARK, E. A., Quoted by Eliot, M. M., and Park, E. A., in Brennemann's Pediatrics (I. McQuarrie, ed.) Vol. 1, Chap. 36, p. 6. Prior, Hagerstown, 1948.
7. WALTNER, K., *Biochem. Z.* **188,** 381 (1927).
8. SHIPLEY P. G., AND HOLT, L. E., JR., *Bull. Johns Hopkins Hosp.*, **41,** 437 (1927).
9. SHELLING, D. H., KRAMER, B., AND ORENT, E. R., *J. Biol. Chem.* **77,** 157 (1928).
10. KAJDI, L., Personal communication.
11. STEIN, I., *Surg. Clin. North Amer.* **33,** 1745 (1953).
12. HOWE, P. S., *Dental Cosmos* **68,** 1021 (1926).
13. PARK, E. A., AND NACHLAS, I. W., Personal communication.

13a. SCHMIDT, H. J., *Deut. zahnärztl. Z.* **4,** 1363 (1951).

14. TABOR, H., AND HASTINGS, A. B., *J. Biol. Chem.* **148,** 627 (1943).
15. GREENWALD, I., *J. Biol. Chem.* **161,** 697 (1945).
16. HOLT, L. E., JR., LAMER, V. K., AND CHOWN, H. B., *J. Biol. Chem.* **64,** 509 (1925).
17. FISKE, C. H., AND SUBBAROW, Y., *J. Biol. Chem.* **66,** 375 (1925).
18. HODGE, H. C., Communication to Conference on Structure, Composition and Growth of Mineralized Tissue, held by New York Academy of Science, Jan. 23, 1954.
19. DE SCHULTEN, A., *Bull. soc. ind. minerale* **26,** 11, 15 (1903).
20. LOGAN, M. A., AND TAYLOR, H. L., *J. Biol. Chem.* **119,** 293 (1937).
21. SHEAR, M. J., AND KRAMER, B., *J. Biol. Chem.* **79,** 109, 161 (1928).
22. SHEAR, M. J., AND KRAMER, B., *J. Biol. Chem.* **86,** 677 (1930).
23. SOBEL, A. E., COHEN, J., AND KRAMER, B., *Biochem. J.* **29,** 2640 (1953).

LIMITED COALESCENCE OF OIL DROPLETS IN COARSE OIL-IN-WATER EMULSIONS

R. M. Wiley

Physical Research Laboratory, The Dow Chemical Company, Midland, Michigan

Received July 2, 1954

ABSTRACT

Coalescence of emulsion droplets, at a rate which decreases to zero as the droplets approach a limiting size and relatively uniform size distribution, a little-known but widely occurring phenomenon termed "limited coalescence," is investigated.

An explanation of the phenomenon, on the basis of the Gibbs-Kelvin relation between the radius of droplet curvature and the adsorption of emulsifier particles, is proposed.

A relation between the limiting size of emulsion droplets, the amount and particle size of emulsifier, and the volume of the emulsified phase is derived on the assumption of mono-layer adsorption of emulsifier particles. Experiments confirming this relation are described.

INTRODUCTION

The first and only clear description of "limited coalescence" in the literature is by W. B. Hardy (1) in 1928. Since Hardy's remark also authorizes a rather broad (and for present purposes convenient) use of the terms "colloid" and "emulsion," we quote it in full:

"A definition of the colloid state which certainly had a vogue was in terms of the size of the units. An emulsion which turned up fortuitously during the course of some work on lubricants must be held to have disposed finally of a definition of that kind. It was a stable emulsion whose droplets were uniformly three millimeters in diameter. By shaking it violently, the droplets could be broken but, on standing, they reverted slowly to standard size—three millimeters in diameter."

Although this is apparently the only description of the phenomenon itself, there are many references to similar or related phenomena in the colloid literature.

Berkman and Egloff (2) quote Wright (3) to the effect that oil field emulsions, upon aging, commonly become coarser and more uniform in drop size.

King and Mukherjee (4) report that in emulsions prepared with high molecular weight colloids, such as gelatin, the droplets become larger and more stable upon standing for several days.

The common occurrence of "limited coalescence" during the preparation of emulsions with finely divided solids may be inferred from the fact, first reported by Pickering (5), that the size of the droplets does not depend on the intensity of agitation, but on other factors such as the amount and particle size of the emulsifier.

Bennister, King, and Thomas, in an excellent general survey of solid emulsifiers (6), report a limiting size (Hardy's "standard size") as "a minimum size of oil droplets thus stabilized which cannot be reduced by mechanical means." In view of the coarseness of their emulsions—"often so coarse as to be visible to the naked dye"—it must be presumed that the droplets were broken by the mechanical means (homogenization), but quickly coalesced to the limiting size. The same process probably occurs following the homogenization of milk and explains the uniformity of drop size thus obtained.

Similar phenomena occur during the coagulation of hydrophobic colloids (7, 8, 9), although the mechanism (10) and the factors affecting the limiting size of the aggregates may be different.

The behavior of foam bubbles also bears a close resemblance to this phenomenon. Berkman and Egloff (2), for example, report (p. 140) that "Elastic forms of large size bubbles are considered more stable than those of small size bubbles; this is not in line with other colloid systems."

An increase of bubble size with time, in the case of flotation foams, is reported by Gaudin (11).

PRELIMINARY EXPERIMENTS

The present work originated in a study of the problem of bead size control in suspension polymerization and involved preparation of coarse emulsions of monomers in aqueous colloids ("granulating agents"). Since the monomer-polymer droplets in these systems were so coarse as to be easily visible to the naked eye, the process of coalescence could be readily observed upon stopping the agitation. Among the bewildering variety of events which occurred during such simultaneous creaming and coalescence, the phenomenon described by Hardy was observed, sometimes with astonishing speed and with the production of beautifully uniform droplets.

Such observations prompted a more detailed investigation, the preliminary stages of which involved rather crude trial-and-error testing of a wide variety of recipes, with visual observation of results. The following conclusions were drawn from this preliminary work.

1. The oil-to-water ratio in the recipe is not important, provided that at high ratios (e.g., two-to-one by volume) the oil is added slowly to the water phase, with agitation insufficient to break the emulsion.

2. The nature of the oil phase is of minor importance in most cases, provided that it does not contain surface-active groups or impurities and that its viscosity is of the same order of magnitude as that of the aqueous phase. With extremely viscous oils subdivision to the required droplet

size can be obtained only by adding a thickening agent to the aqueous phase.

3. The intensity and duration of the initial agitation have no effect, provided that both exceed certain minimum values. Agitation apparently serves not only to break up the oil phase into droplets smaller than the limiting size, but to promote adsorption of the colloid by intensifying colloid-to-interface collisions. Mild agitation during coalescence frequently speeds up the process, without affecting the limiting size.

4. The phenomenon occurs only when at least one of the ingredients in the recipe is a water-dispersible colloid or finely divided solid of very high molecular weight. It occurs with inorganic colloidal salts or hydroxides, clay, raw starch, sulfonated cross-linked organic high polymers, alginate and certain emulsion polymer particles. It does not occur with soaps and low molecular weight surface-active agents used alone. With colloids of intermediate molecular weight such as gelatin, linear organic polyelectrolytes, polyvinyl alcohol, and methyl cellulose, it occurs only slowly and indistinctly.

5. In most cases a "promoter" or a combination of promoters is necessary. Such substances promote adsorption of the colloid at the oil-water interface. They apparently act either by depressing the thickness of the diffuse electrical double layer around the colloid particles, or by partly coating them with an organic material which is attracted to the oil phase, or both. From another point of view, the promoter serves to adjust the "hydrophobic hydrophilic balance" (12) of the emulsifier particles. The theory of promoter action in froth flotation, as discussed by Gaudin (11), appears to apply equally well to the case of solid emulsifiers.

An extremely wide variety of such agents, known variously as "flocculating agents," "extenders," "collectors," "sensitizing agents," "protective colloids," etc. (14–17), may be employed, and are frequently effective in such low concentrations that unknown and variable impurities may interfere with reproducibility of results unless a strong promoter is deliberately added to the recipe. Gelatin, being amphoteric, is particularly effective with a wide variety of colloids, at about 10 p.p.m. in the aqueous phase. In some cases, both an inorganic electrolyte and an organic promoter seem to be necessary.

6. The limiting size of the oil droplets is directly proportional to the product of oil phase volume and colloid particle size, and inversely proportional to the weight of colloid employed in the recipe. It is usually independent of the amount of promoter employed, within the range required to promote "Limited Coalescence."

7. Any distinction between "limited coalesence" and other types of coalescence, flocculation, etc., appears to be somewhat arbitrary. For present purposes, the term is used to designate coalescence of emulsion

droplets which ceases within a few seconds or minutes, rather than hours or days, and which results in stable droplets having a size range of less than three to one, rather than ten (or more) to one, as in ordinary (18) emulsions.

8. The coalescence of oil droplets resembles the process of coalescence of air bubbles at an interface, as described by Hardy (19)—it occurs suddenly, after the elapse of a certain contact time, which depends on the nature of the interfacial film. With oil droplets in a given recipe this contact time increases with increasing droplet radius. "Limited coalescence" occurs when this contact time increases, over a narrow range of drop sizes, from a few seconds to many hours. Under a range of conditions, a wide variety of coalescence speeds and final drop size distributions are obtained, differing only quantitatively from "limited coalescence." Suspensions may coalesce "very much like a foam, which slowly breaks down and disappears" (20), or may break "suddenly, after an induction period" (reference 6, p. 228).

THEORY

On the basis of existing theories of emulsification (12), the increasing stability of oil droplets with increasing drop size during coalescence indicates that the emulsifier particles are much more strongly attracted to the larger droplets. Such theories, however, provide no explanation of why this should occur, nor of why it occurs only in the case of very high molecular weight, or particle weight, emulsifiers.

A very simple explanation is obtained if one considers the attachment of the emulsifier particles to the oil drops as an adsorption phenomenon, obeying Eq. [1], the well-known Kelvin-Gibbs relation:

$$\mathrm{Ln}\,\frac{Sr}{S} = \frac{2\sigma M}{dRTr}, \qquad [1]$$

where Sr = escaping tendency of particle from surface of radius r (r is negative for concave surfaces).
S = escaping tendency from flat surface.
σ = interfacial tension.
M = molecular weight of particle.
d = density of particle at the surface.
RT = gas constant and temperature.

Although this relation has recently (1951) been verified by V. K. LaMer and Ruth Gruen (21) in a study of the vapor pressures of volatile solvents in nonvolatile aerosol droplets, these authors point out that "The general acceptance which equation (1) enjoys rests on the cogency of the Kelvin-Gibbs (22) derivation, and on the success of further theories based upon it."

Acceptance of the equation in the present connection, which involves a rather unconventional extension to cases in which the kinetic units are colloidal particles rather than molecules, and the attachment of the particle to the surface is generally called "adhesion" rather than "adsorption," rests on a similar basis.

Qualitatively, Eq. [1] appears to fit the facts very nicely. It predicts not only a decrease in escaping tendency of the emulsifier particles with increasing radius of the oil droplets, and therefore the greater stability of the larger droplets, but also the increased magnitude of this effect with increasing "molecular" weight of the particle.

This equation is applicable only where electric double-layer effects can be neglected. An equation derived by Knapp (8) includes such effects, but reduces to [1] under the conditions of limited coalescence—small electric charge and/or large radius.

The variation of Sr/S with r, in the case of low molecular weight materials ($M = 100$), becomes appreciable only when r is less than about 10^{-5} cm. (23); that is, when M/r is greater than 10^7. Since the other factors on the right side of Eq. [1] usually vary only over a small range compared to M and r, one would expect that at values of M/r much greater than 10^7 the dependence of escaping tendency on radius would become increasingly strong. Thus, with $r = 1$ cm., a strong dependence of escaping tendency on r would be expected only with colloids having M much greater than 10^7. This seems to explain the fact that in the visible range of drop sizes, limited coalescence requires colloids of very high molecular weight.

The fact that "limited coalescence" is not generally obtained by the use of colloids composed of flexible, linear macromolecules is undoubtedly due to the fact that the molecular weight of the "kinetic unit" in such molecules is relatively low and independent of the size of the molecule. With colloids and/or surface-active agents having "kinetic units" of low molecular weight, the phenomenon would be expected to occur only with very small droplets. The process described by Bhatnagar (24), of producing emulsions of uniform droplet size by violent agitation of a concentrated emulsion, might be explained on this basis.

Thus, in a recipe containing a completely adsorbed colloid in amount insufficient to coat all the surface area produced by the agitation, coalescence proceeds until this area becomes equal to the sum of the cross-sectional areas of the colloid particles present. The sharpness of the size distribution of the resulting droplets is dependent on the rate of change of escaping tendency of the colloid with radius of curvature.

In this case, the geometry of the situation requires a very simple relationship between the limiting diameter (D) of oil droplets, the volume (V) of oil in the recipe, and the particle diameter (h) and weight (w) of colloid employed. This is derived as follows:

If there are N oil droplets of diameter D in the resulting emulsion, their volume will be:

$$\text{(a)} \qquad V = \frac{N\pi D^3}{6}; \qquad N = \frac{6V}{\pi D^3}.$$

The total oil-water interfacial area A will be:

$$\text{(b)} \qquad A = N\pi D^2 = \frac{6V}{D}.$$

Assuming cubic packing of n colloid particles of diameter h, the area covered, nh^2, is equal to A, or

$$\text{(c)} \qquad nh^2 = \frac{6V}{D}; \qquad D = \frac{6V}{nh^2}.$$

If w and d are the dry weight and density of the colloid particles, and k is the ratio of volume of the wet colloid on the droplet surface to its volume in the dry state, then

$$\text{(d)} \qquad k = \frac{1/6n\pi h^3}{w/d}, \quad \text{or} \quad n = \frac{6wk}{\pi h^3 d},$$

This, with (c) gives:

$$D = \frac{\pi d}{k} \frac{Vh}{w}. \qquad [2]$$

This equation applies only when the colloid is completely adsorbed at the interface.

If the amount of promoter or the intensity of agitation is insufficient to cause complete adsorption of the colloid, limited coalescence may occur but the drop size becomes very sensitive to the nature of the oil phase as well as to the amount of promoter, traces of impurities, etc., and is difficult to reproduce. For these reasons, the present study has been largely restricted to the simpler conditions, under which Eq. [2] should hold.

Experimental

As a test of Eq. [2], the limiting diameters of oil droplets obtained from several recipes employing colloid particles of known diameter, were compared with the theoretical diameters predicted by the equation.

To obtain spherical colloid particles of known diameter, a sample of Dowex 50 (25) ion-exchange resin beads (finer than 400 mesh, acid form) was fractionated by repeated sedimentation and decantation in 25% ethyl alcohol into four fractions. The range of particle sizes and the average particle size, as estimated by examination at 300 power under a microscope with micrometer eyepiece, are listed in Table I.

Emulsions were prepared from each of these fractions by placing in a test tube 7 ml. of distilled water containing 0.4% $CaCl_2$, the amounts of gelatin (Baker and Adamson, Code 1797) and Dowex shown in Table II, and 5 ml. of styrene monomer. The pH of the emulsions were not measured. After vigorous shaking by hand, the tubes were allowed to stand for about

TABLE I

Particle Size of Dowex 50 Fractions

Fraction number	Particle size, *microns*	
	Range	Average
1	4.8–18	9
2	9.0–20	13.5
3	13.5–30	20
4	22–45	31

TABLE II

Measured vs. Theoretical Oil Drop Diameters Obtained with Dowex 50 Fractions

Colloid added		Promoter % in aqueous phase		Measured oil drop diam. (*mm.*)	Theoretical oil drop diam. (*mm.*)	Remarks	
Fraction	Wt. (grams)	$CaCl_2$	Gelatin			Drop size uniformity	Adsorption of Dowex
1	0.084	0.4	0.001	3	2.0	Fair	Complete
2	0.127	0.4	0.001	2.5	2.0	Fair	Complete
3	0.188	0.4	0.001	2.0	2.0	Fair	Complete
4	0.290	0.4	0.001	1.8	2.0	Fair	Complete
1	0.168	0.4	0.001	2.5	1.0	Fair	Incomplete
2	0.255	0.4	0.001	1.5	1.0	Fair	Incomplete
3	0.376	0.4	0.001	1.4	1.0	Poor	Incomplete
4	0.580	0.4	0.001	1.0	1.0	Poor	Incomplete
1	0.168	0.4	0.0016	1.4	1.0	Good	Incomplete
2	0.255	0.4	0.0016	1.2	1.0	Fair	Incomplete
3	0.376	0.4	0.0016	0.8	1.0	Poor	Complete
4	0.580	0.4	0.0016	0.8	1.0	Poor	Complete
1	0.168	0.4	0.0024	1.1	1.0	Good	Complete
2	0.255	0.4	0.0024	1.0	1.0	Fair	Complete
3	0.376	0.4	0.0024	0.8	1.0	Poor	Complete
4	0.580	0.4	0.0024	0.8	1.0	Poor	Complete

a minute, until no further coalescence could be observed. The average droplet sizes were then estimated by comparing with a set of size standards, consisting of polystyrene beads, screened to narrow size fractions averaging 4, 2.5, 1.4, 1.0, 0.7, 0.5, and 0.35 mm.

The amount of Dowex added was calculated in advance by Eq. [2] to give the theoretical drop sizes shown in the table. For these calculations the dry density was taken as 1.44, and the swelling ratio, k, as 1.20.

Owing to the dark brown color of the Dowex, incomplete adsorption at the interface is indicated by a brown color of the water layer after coalescence is complete.

TABLE III

Measured vs. Theoretical Oil Drop Diameters Obtained with Bentonite as Colloid

Bentonite, *grams*	Promoter, % in aqueous phase		Measured oil drop diam. (*mm.*)	Theoretical oil drop diam. (*mm.*)	Drop size uniformity
	$CaCl_2$	Gelatin			
0.0005	0.4	0.001	3.5	4.1	Fair
0.0010	0.4	0.001	1.4	2.05	Fair
0.001	20.0	None	2.0	2.05	Fair
0.002	20.0	None	0.8	1.0	Fair
0.003	20.0	None	0.6	.67	Fair

The data show that the drop size closely approaches the theoretical drop size if the amount of promoter is sufficient to cause complete adsorption. An excess of promoter does not reduce drop size but appears to affect drop size uniformity.

The data also show that the amount of promoter required to cause complete adsorption increases with the amount of Dowex and with decreasing particle size of the Dowex. The latter is to be expected, owing to the greater "escaping tendency" of small particles.

As a further check on Eq. [2], a series of emulsions were prepared, using the same procedure, but with bentonite as the colloid. The results are shown in Table III.

In the calculation of the theoretical drop sizes for Table III, the values $k = 8$, and $d = 2.1$ (J. W. Mellor, Vol. VI, p. 495), and $h = 5 \times 10^{-5}$ cm. (J. P. Chem. 46, 9, p. 1041) were used.

Since the bentonite particles are not spheres, but platelets and clusters of particles of a very wide range of sizes, and since the average size of the clusters may vary with the method of preparation of the suspension, this data can only be regarded as a rough confirmation of Eq. [1]. In fact, the agreement shown in the table is better than one would expect under the circumstances, and may be partly fortuitous.

The validity of Eq. [2] has also been demonstrated with a series of raw starches of varying grain size, and kerosene as the oil phase (26). With corn or rice starch at room temperature no electrolyte or promoter is required, and very uniform droplets are produced in sizes up to 3 mm.

With highly cross-linked, completely sulfonated polystyrene or polyvinyltoluene as the colloid, practically any inorganic acid or salt may be used as promoter. The phenomenon, in this system, sometimes occurs with such speed that no coalescence can be observed, the process being complete within one or two seconds after agitation is stopped. The results, however, vary considerably from batch to batch of the polymer, and with age of the solution, presumably owing to variations in size and size distribution, of the swollen microgels, and in stability of the polymer to age, mechanical agitation, etc.

With inorganic colloidal salts and hydroxides an organic promoter is usually required, especially if prepared by precipitation from pure reagents.

When polyvalent electrolytes, polyelectrolytes, or colloids of opposite electric charge are used as promoters, the oil droplets during coalescence frequently clump or aggregate into a mass resembling frogs' eggs. This condition (also noted by Bennister, King, and Thomas (6)) can usually be remedied either by gentle agitation or by adding a monovalent electrolyte. The reason for this behavior, which occurs also during the homogenization of milk and is overcome by a second, more gentle homogenization (reference 12, p. 345), is not clear.

Another peculiar type of behavior sometimes occurs when the amount of promoter added is insufficient to drive all the colloid to the interface. This consists of typical "limited coalescence" of part of the oil phase, producing some very large oil droplets, but leaving the remainder in the form of very small droplets, thus producing an emulsion having some large droplets, some small ones, with none of intermediate size. The large ones appear to be protected by absorbed colloid, and the small ones by some other mechanism--perhaps a double-layer repulsion. Upon the addition of more promoter, and reshaking, the two peaks in the size distribution approach each other, the small droplets increasing and the large ones decreasing in size, until the distribution becomes sharp. This is especially noticeable with sulfonated polystyrene (cross-linked, "Fish-eye" type) as the colloid, and an electrolyte as promoter.

DISCUSSION

From the standpoint of adsorption theory, with Eqs. [1] and [2], a number of other isolated facts or discrepancies in the field of emulsions and foams seem to be capable of qualitative explanation.

The difficulty of controlling and reproducing results in the use of high molecular weight colloids and finely divided solids as emulsifying agents appears to be due to the difficulty of controlling either the "promoter" action of trace impurities, or the particle size of the colloid, or both.

A scientific basis is provided for the contested (reference 2, p. 104) statement, first made by Pickering (5), that the size of the droplets in certain emulsion systems depends on the size of the particles of the emulsifier.

The behavior of flotation foam bubbles in adsorbing mineral particles (11) is closely correlated with the behavior of oil droplets in adsorbing coarse emulsifier particles. The effect of particle size in both cases is in the direction predicted by Eq. [1], and the "promoter" effect is very similar in both cases. Although no data seem to be available in the literature, one would expect larger bubbles to have a stronger adsorbing capacity per unit surface area than small bubbles, other factors being equal.

This point of view also provides a reasonable explanation of the effect of violent mechanical agitation in producing emulsions of narrow drop size distribution, such as those reported by Bhatnagar (24), for soap-stabilized emulsion, Hohenstein and Mark (20) for suspension polymer beads, and various workers for homogenized milk. Such results cannot be explained on the basis of the mechanics of droplet rupture (27), which should produce only very nonuniform drop sizes. The uniformity is probably due to a coalescence process, in which the rate varies inversely with drop size.

Conclusions

1. "Limited coalescence," with similar phenomena reported in the literature, in which the stability of coarse suspensions and foams increases with increasing radius of curvature of the dispersed phase, is explained by reference to the Kelvin-Gibbs equation.

2. The factors affecting the "limiting size" of the droplets, in the usual case (complete adsorption of the protective colloid), are shown to be related by Eq. [2], derived by assuming "mono-molecular" packing of colloid particles at the interface.

References

1. Hardy, W. B., *Colloid Symposium Monograph* **16,** 8 (1928).
2. Berkman, S., and Egloff, G., "Emulsions and Foams," p. 55. Reinhold Publishing Corporation, New York, 1941.
3. Wright, J., *Western Soc. Engrs.* **3,** 208 (1912).
4. King, A., and Mukherjee, L. N., *J. Soc. Chem. Ind.* (*London*) **59,** 185 (1940).
5. Pickering, S. U., *J. Chem. Soc.*, pp. 91, 2001 (1907).
6. Bennister, H. L., King, A., and Thomas, R. K., *J. Soc. Chem. Ind.* (*London*) **59,** 231 (1941).
7. Kruyt, H. R., "Colloid Science," Vol. 1, p. 296. Elsevier, Amsterdam, 1949.
8. Knapp, W. R., *Trans. Faraday Soc.* **17,** 457 (1922).
9. Rees, A. L. G., *J. Phys. & Colloid Chem.* **55,** 1340 (1951).
10. Verwey, E. J. W., and Overbeek, J. Th. G., "Theory of the Stability of Lyophobic Colloids." Elsevier, 1948.
11. Gaudin, A. M., "Flotation," p. 108. McGraw-Hill Book Company, New York, 1932.
12. Clayton, W., "Theory of Emulsions," 3rd ed., p. 101. Blakiston Company, Philadelphia, 1935.
13. Alexander, Jerome, "Colloid Chemistry," Vol. 6, p. 493. Reinhold Publishing Corporation, New York, 1946.
14. Briggs, T. R., *J. Ind. Eng. Chem.* **13,** 1008 (1921).
15. British Patent 690, 124.
16. Berkman, S., and Egloff, G., "Emulsions and Foams," pp. 80–81. Reinhold Publishing Corporation, New York, 1941.
17. Bechold, A., Dede, L., and Reiner, L., *Kolloid-Z.* **28,** 6 (1921).
18. Stamm, A. J., *Colloid Symposium Monograph* **3,** 257 (1925).
19. Hardy, W. B., *Proc. Royal Soc.* (*London*) **A86,** 627 (1912).
20. Hohenstein, W. P., and Mark, H., *J. Polymer Sci.* **1,** 130–44 (1946).
21. LaMer, V. K., and Gruen, R., *Trans. Faraday Soc.* **48,** p. 410–15 (Part 5, No. 353) 1952.

22. Guggenheim, "Thermodynamics, an Advanced Treatment for Physicists and Chemists," pp. 44–45, 166. Interscience Publishers, New York, 1949.
23. Weiser, H. B., "Colloid Chemistry," 2nd ed., p. 10. John Wiley & Sons, New York, 1949.
24. Bhatnagar, S. S., *J. Chem. Soc.*, pp. 117, 548 (1920).
25. Bauman, W. C., and Eichhorn, J., *J. Am. Chem. Soc.* **69**, 2830 (1947).
26. Unpublished results by the author's son, Richard (Midland, Michigan High School Science Fair Project, 1954).
27. Taylor, G. I., *Proc. Roy. Soc.* (*London*) **A146,** 501 (1934).

THE INFLUENCE OF HIGH POLYMER ON THE RHEOLOGICAL PROPERTIES OF A CARBON BLACK SUSPENSION

Jacob Riseman and Robert C. Harper, Jr.

Research Division, International Resistance Co., Philadelphia, Pennsylvania

Received July 8, 1954

I. Introduction

It is well known that the addition of so-called surface-active agents to a carbon suspension has a profound influence on the rheological properties of the suspension (1).

Examples of such surface-active agents are benzidine, which caused a lowering of the yield value, and Gilsonite (an asphaltite bitumen. See, for example, H. Abraham, "Asphalts and Allied Substances," D. Van Nostrand Co., Inc., New York, 1945), which caused an increase. Recent work (2, 3, 4) on the adsorption by carbon of high polymer molecules from solution suggested the problem of the influence of such materials on the rheological properties of carbon suspensions. In this latter work, there appears to be a polymer molecular weight and a solvent influence on the extent of adsorption. In fact, a major interest in such studies is the possibility of chromatographically fractionating a polydisperse mixture of high polymers. Kolthoff and Gutmacher (3), however, working with GR-S, did not find much of a molecular weight influence.

Differences in the extent of macromolecular adsorption, whether due to solvent or molecular weight, would be expected to appear as differences in the rheological properties. It should also be remembered that solvent adsorption of significant magnitude can occur and has been demonstrated (5). The adsorption studies mentioned above apparently have not taken this into account. Calculations would be affected where concentration of polymer in the supernatant is used as the measure of the extent of adsorption. Solvent adsorption may likewise affect the rheological properties of such systems.

Because of the polymer size, the possibility of inter-particle adsorption could result in interesting effects on the yield stress as a function of the molecular weight. The influence of polymer adsorption on a system which has a yield stress could be such as to interfere initially with the structure responsible for this yield stress. Further adsorption could then build up another structure which would result in a yield stress increase.

Certain differences exist in this work as compared to the adsorption measurements performed in the quoted references (2, 3, 4). The carbon suspensions were all prepared by a much more drastic process (three-roll milling) than that used in the adsorption measurements quoted. It is well known that a carbon suspension prepared by merely stirring carbon into a solvent has rheological properties markedly different from those of one prepared by ball or three-roll milling. It may very well be that in the latter processes a much larger effective surface area is exposed. Electron micrographs have shown that large carbon aggregates break down during dispersion with ultrasonics (6).

It is certainly true that whereas the first case gives a suspension with practically no yield value, the second case gives a suspension whose yield value increases and approaches an asymptotic value. The possible relationship of this fact with an increase in adsorption depending on the processing method will be discussed in the body of this paper.

II. Experimental

A coaxial cylinder viscometer[1] in which the outer cylinder is rotated was constructed with the following features. The drive consists of a 3450 r.p.m. constant speed a.-c. motor coupled to a Graham variable-speed reducer having an output of 0–530 r.p.m. The output of the speed reducer leads through gears, to the speed indicating device. It also leads to the cradle which supports the outer cylinder, passing into the water bath through a mercury seal. The speed is determined by a directly coupled Hasler-Tel tachometer, a revolution counter which, when manually activated, counts the number of revolutions for approximately three seconds and yields a direct reading in revolutions per minute of the average speed during this time interval. Readings of the speed can be made to the nearest 0.1 r.p.m., but since the constancy of the drive is approximately 0.5 r.p.m. over the entire range, readings to the latter precision are taken in practice.

The inner and outer cylinders (hereafter referred to as bob and cup, respectively) were constructed from 303 stainless steel, the surfaces being ground to a diameter uniformity of 0.00025 cm. The nominal dimensions of the cup and bob are given in Fig. 1, where the distribution of the liquid sample is also indicated. By means of the centering pins on the lower side of the cup overflow reservoir and the taper on the side of the cup, snug alignment into the cradle is assured. The brass cradle is slotted so that the water of the surrounding bath flows through the cradle and is directly in

---

[1] This instrument was built by the Process & Instruments Co., Brooklyn, N. Y.

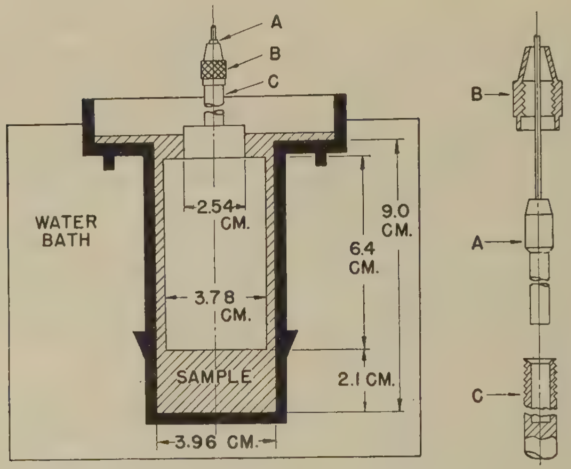

FIG. 1. Schematic representation of cup and bob dimensions and wire suspension system: *A*, chuck jaws; *B*, lock nut collar; *C*, top of bob shaft.

contact with the outer walls of the cup. The cup has a removable bottom to facilitate cleaning. By means of a liquid pump, the water is vigorously circulated. Temperature control (as determined by a calorimeter thermometer) is easily maintained to ±0.02°C. or better with an electrical heater which is controlled by a mercury thermoregulator and electronic relay. In use, the bob is lowered to a fixed depth determined by a mechanical stop. This maintains a constant distance of separation between the bottom of the bob and the bottom of the cup. The slight excess sample used intentionally overflows into the cup reservoir.

The bob and its alignment shaft are an integral piece, being machined from suitable stainless steel stock. The shaft passes through a tube which is attached to a rack and pinion device by which the bob, its upper wire support, and alignment tube are all moved vertically. The bob shaft is aligned in the tube by two rigidly mounted SKF noise-tested precision ball bearings. The alignment of the axis of bob and shaft relative to the axis of the cradled cup was accomplished by proper shimming of the vertical rack.

The bob shaft is suspended from straightened stainless steel music wires by a method which allows easy interchange of wires and permits constancy of the calibration of the torsion constant of the wires. At the top of the bob shaft is a recess into which the base of the chuck jaws of a pin vise fits. After slipping the lock nut collar along the wire, the wire is silver soldered into the base of the chuck jaws. When the chuck jaws are seated into the recess in the bob shaft and the lock nut collar screwed down, the jaws always grasp the wire at the same position. At the top of the suspension, the wire

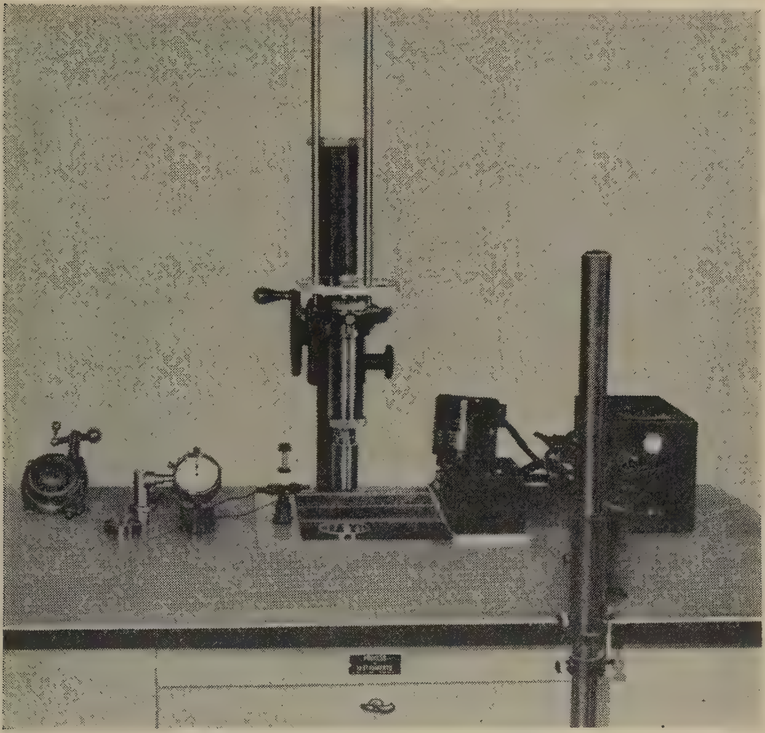

FIG. 2. Photograph of coaxial cylinder viscometer.

is permanently clamped by a pin vise which is an integral part of a bolt which is easily inserted or removed by means of a matching screw clamp. The lower assembly for the suspension wires is illustrated in Fig. 1. By preparing a number of wires (2-ft. lengths) of different diameters according to the method discussed above, a suitable torsion constant may be chosen to study the rheological behavior of materials over a wide range of mechanical properties.

Attached to the bob shaft between the top bearing and pin vise arrangement is a Lucite cylinder 1.3 cm. high and 15 cm. in diameter. In a groove near the edge, a scale having 1000 divisions per revolution is held by a spring wire. This scale is in the form of a paper strip photographically reproduced from a master linear scale. By sighting the scale through a telescope, the deflection of the bob can be determined with a precision of 0.5 division (or 0.18 circular degree). (The over-all construction of the apparatus can be seen in Fig. 2.)

By the use of the suspension wire clamping device described above, the zero point before and after an experimental run remains constant to 0.5 division or better for all wire diameters used to date (maximum wire diameter 0.041 in.). For larger diameter wires, some permanent deformation may result from torsional displacements of about 2 π radians.

Two procedures were used to determine the torsional constants of the suspension wires—the torsion pendulum and weight and pulley methods. Agreement of results from the two methods was generally within 0.3%. If the coupling effects between the bottoms of the cup and bob can be neglected, the concentric cylinder viscometer may be used as an absolute instrument for the determination of the viscosity of liquids in laminar flow, provided the geometry of the cylinders and the torsion constant of the suspension wire are known. In practice, however, the end effects are generally not negligible for an instrument of convenient design. When a liquid of known viscosity was used and the data for torque vs. velocity gradient employed on an absolute basis, an error of about 2% in the viscosity resulted. It was decided to perform an empirical calibration using N.B.S. standard viscosity liquids in order to minimize the end effect error and to eliminate the effect of any fixed errors in angular velocity and/or deflection determinations. A series of experiments were performed using N.B.S. oil L-19, where slopes (as r.p.m. per division) for a given suspension wire were determined at seven temperatures. From the three viscosity-temperature values supplied by the N.B.S., the other temperature-viscosity values necessary were estimated by a graphical procedure. An over-all instrument constant, K, defined as viscosity times slope, could then be evaluated at each temperature. The results are listed in Table I. Thus Newtonian viscosities can be determined with an accuracy of about ±0.5%.

A channel black of 13 mμ mean ultimate particle diameter was heated in a graphite crucible at 1370°C. for 2 hours. A 6.00 wt.% suspension of this conditioned carbon was prepared in No. 10 petroleum oil by three "tight" passes of the mixed components through a three-roll paint mill. Using the same oil, 10.0 wt.% solutions of two commercial polybutene polymers

TABLE I

Calibration with N.B.S. Oil L-19

Temperature (°C.)	Viscosity[a] (*poise*)	K^b (*poise r.p.m. div.*$^{-1}$)
20.00 ± 0.01	0.9754	4.262
23.00 ± 0.01	0.8106	4.252
26.00 ± 0.01	0.6794	4.246
30.00 ± 0.01	0.5448	4.287
32.23 ± 0.01	0.4850	4.291
34.29 ± 0.01	0.4358	4.280
37.17 ± 0.01	0.3765	4.245

Average = 4.268 ± 0.023 (±0.54%)

[a] Relative to the value 0.01002 poise for the absolute viscosity of water at 20°C.

[b] Using a suspension wire having a restoring-force constant of 1459 dyne cm. div.$^{-1}$.

(Vistanex LM-S and LM-H) were prepared. From these initial solutions, two sets of solutions (one for each type of polymer) having the following compositions were prepared.

Component	*Solution A*	*Solution B*
Carbon	3.00 wt. %	3.00 wt. %
Polymer	5.00 wt. %	0.00 wt. %
Petroleum oil	92.00 wt. %	97.00 wt. %

By the proper admixture of solutions *A* and *B*, a polymer concentration ranging from 0–5 wt. % could be prepared with the carbon concentration being fixed at 3.00 wt. %. A similar method of sample preparation was followed for the results at 1.50 wt. % carbon. Using an Ostwald dilution viscometer, relative viscosities of the polymers in benzene at 30°C. were determined at several concentrations. Their intrinsic viscosities (or limiting viscosity numbers) were determined in the conventional manner and found to be 0.24 and 0.425 (100 ml./g.) for Vistanex LM-S and LM-H, respectively. Using the data of Fox and Flory (7) for fractionated polyisobutylenes, these intrinsic viscosities correspond to molecular weights of about 45,000 and 100,000, respectively. Although the use of these data to obtain molecular weights for unfractionated polybutenes is open to question, sufficient characterization for the present purpose is obtained. At 30.00 ± 0.02°C., the concentric cylinder viscometer was employed to obtain the angular velocity vs. torque curves for each solution prepared. In most cases, a solution of the same polymer concentration with no carbon present was also studied for comparison with the samples containing carbon. All solutions not containing carbon were Newtonian. All solutions containing carbon yielded flow curves typical of simple plastic or Bingham flow as characterized by the equation (8)

$$v = \frac{T(r_o^2 - r_i^2)}{4\pi h \omega r_o^2 r_i^2} - \frac{S_0}{\omega} \ln \frac{r_o}{r_i},$$

where v is the plastic viscosity, T the torque experienced by the bob at an angular velocity ω, h the depth of immersion of the bob (or effective length of the bob), S_0 the yield stress, and r_o and r_i the radii of the cup and bob, respectively. For such a flow curve, the plastic viscosity or yield stress may be determined from the slope and extrapolated intercept, respectively, of the linear portion of the angular velocity vs. torque curve. To obtain reproducible results, it was necessary to store the carbon samples at 30°C. for at least 18 hours prior to their evaluation. There are no materials having standardized Bingham flow properties. Hence, although the precision of the measurements can be estimated from their reproducibility, the accuracy can be estimated only by reference to results obtained with Newtonian liquids. In this regard, the precision of the plastic viscosity values reported

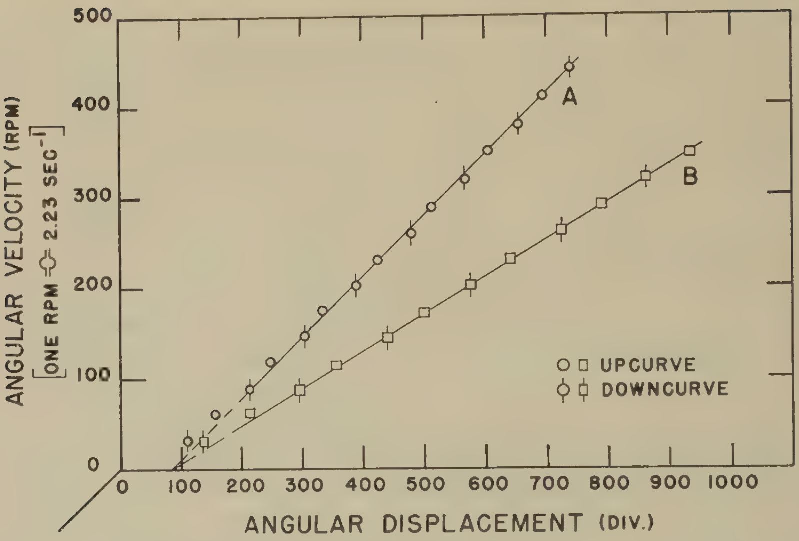

FIG. 3. Angular velocity versus angular displacement for: *A*, 3.00 wt. % carbon plus 0.50 wt. % Vistanex LM-S (one div. ⇔ 302 dyne cm. of torque ⇔ 20.23 dyne cm.$^{-2}$ of shearing stress); *B*, 3.00 wt. % carbon plus 3.0 wt. % Vistanex LM-H (one div. ⇔ 490 dyne cm. of torque ⇔ 32.83 dyne cm.$^{-2}$ of shearing stress.

is about ±1 %, the precision of the yield stress varying with its magnitude and the experimental conditions chosen. Typical primary data for individual determinations on the carbon samples are depicted graphically in Fig. 3. From these representative data, it is clear that the plastic viscosity values are independent of the rate of shear over the range studied.

III. RESULTS AND DISCUSSION

The data obtained in this work are summarized in Tables II and III and in Figures 4, 5, and 6. From these several results are evident:

1. The yield stress initially decreases with the addition of Vistanex (Fig. 5 and 6). The decrease occurs at lower Vistanex concentration and is appreciably more marked with increasing molecular weight. In the case of the 1.5 % carbon concentration, where the initial yield stress is quite low, the uncertainty in the measurement appears to mask this effect. But even here, the addition of 1 % of Vistanex does not appear to influence the yield stress. The second 1 %, however, causes a profound effect, increasing the yield stress by some 60 %.

2. With increasing concentration of Vistanex, the initial decrease of the yield stress is followed by a sharp increase. The nature of the increase again differs markedly with the molecular weight of the polymer. For the 45,000 molecular weight polymer, the increase is smooth. At the higher concentration of Vistanex, the rate of change becomes slow, and the sys-

TABLE II

Experimental Results with Vistanex LM-S

Vistanex LM-S concentration	Newtonian viscosity of LM-S in oil, η	Plastic viscosity of carbon and LM-S in oil, v	Yield stress of carbon and LM-S in oil	Specific viscosity
(*wt. %*)	(*poise* ± 0.5%)[a]	(*poise* ± 1%)[a]	(*dyne cm.*$^{-2}$ ± *2.5%*)[a]	$\left(\frac{v}{\eta} - 1\right)$
3.00 Wt. % Carbon Concentration				
0	0.675	1.18	2065	0.75
0.25	0.723	1.26	1860	0.74
0.50	0.769	1.325	1720	0.72
0.75	0.839	1.46	1840	0.74
1.0	0.902	1.565	1940	0.74
1.5	1.043	1.81	2185	0.73
2.0	1.203	2.115	2560	0.76
3.0	1.527	2.57	3100	0.69
4.0	1.985	3.27	3280	0.65
5.0	2.506	4.14	3410	0.65
1.5 Wt. % Carbon Concentration			(±10%)	
0	0.675	0.890	330	0.32
0.5	0.769	1.024	370	0.33
1.0	0.902	1.207	340	0.34
2.0	1.203	1.566	525	0.30
3.0	1.527	2.02	690	0.32
4.0	1.985	2.58	710	0.30
5.0	2.506	3.20	800	0.28

[a] Average expected error.

TABLE III

Experimental Results with Vistanex LM-H

(3.00 wt. % carbon concentration)

Vistanex LM-H concentration	Newtonian viscosity of LM-H in oil, η	Plastic viscosity of carbon and LM-H in oil, v	Yield stress of carbon and LM-H in oil	Specific viscosity
(*wt. %*)	(*poise* ± 0.5%)[a]	(*poise* ± 1 %)[a]	(*dynes cm*$^{-2}$ ± *2.5%*)[a]	$\left(\frac{v}{\eta} - 1\right)$
0	0.675	1.18	2065	0.75
0.07		1.19	1760	
0.14		1.25	1580	
0.25		1.33	1580	
0.50	0.847	1.48	1840	0.75
1.0	1.061	1.81	2050	0.71
2.0	1.418	2.52	2230	0.78
3.0	1.97	3.50	2800	0.78
4.0	2.70	4.71	3600	0.75
5.0	3.57	6.12	4750	0.72

[a] Average expected error.

tem appears to be approaching a yield stress no longer dependent on Vistanex concentration. The difficulty of obtaining higher concentrations of Vistanex in the procedure used prevented us from examining this point in more detail. With the 100,000 molecular weight Vistanex, the initial in-

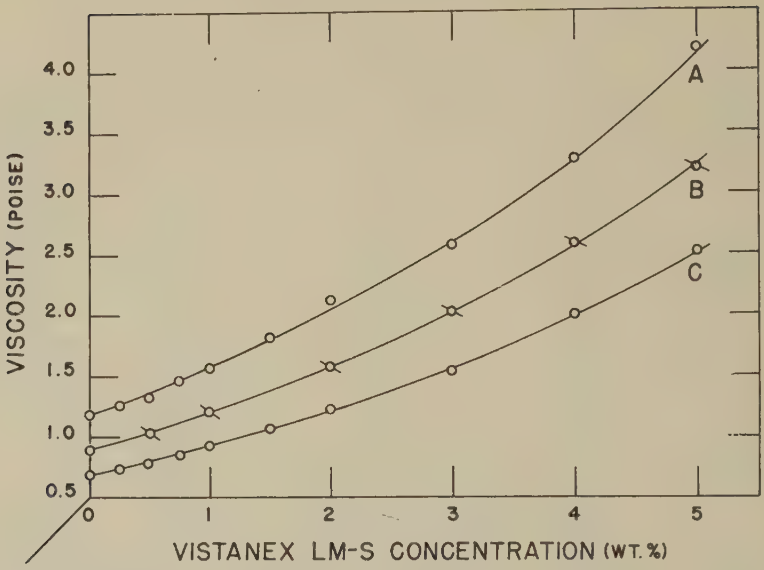

FIG. 4. Dependence of viscosity on Vistanex LM-S concentration at *A*, 3.00 wt. % carbon; *B*, 1.50 wt. % carbon; *C*, 0 wt. % carbon.

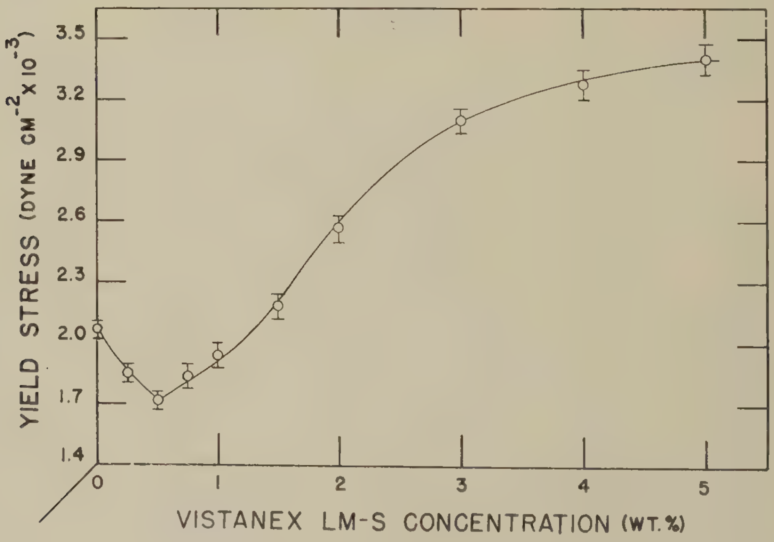

FIG. 5. Dependence of yield stress on Vistanex LM-S concentration at 3.00 wt. % carbon.

crease from the minimum in the yield stress is as sharp as the initial decrease. This is followed by a less steep section which extends to a concentration of about 2% of Vistanex. Following this the yield stress increases very sharply and shows no tendency, over the concentration range studied, to

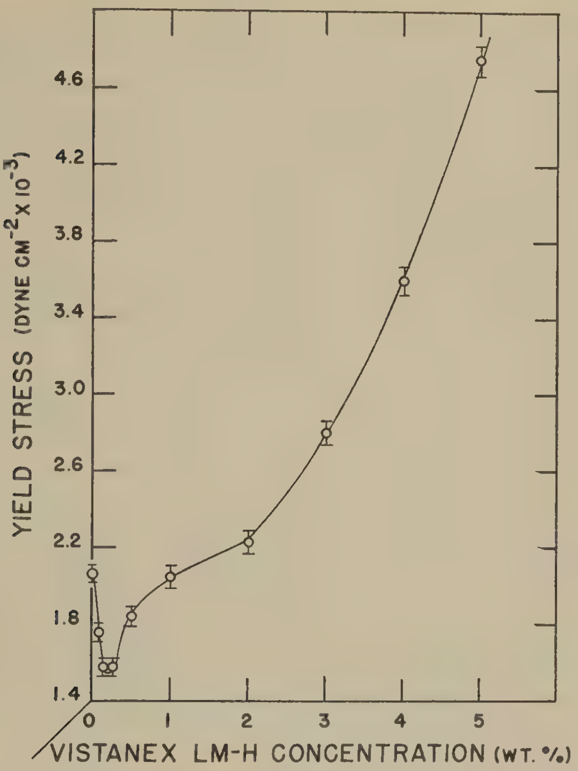

FIG. 6. Dependence of yield stress on Vistanex LM-H concentration at 3.00 wt. % carbon.

approach the approximate constancy manifested with the lower molecular weight polymer. The increase in yield stress is very marked, showing an effect in excess of threefold.

3. The plastic viscosity at each carbon concentration increases, as would be expected, with increase of Vistanex concentration. It was quite surprising, however, to find that the increase in viscosity, relative to the polymer-oil solution, as given by the specific viscosity in Table II, remained practically constant. Not only does it remain constant, but it appears to be sensibly independent of the polymer molecular weight and has the same value as for the two-component system carbon-petroleum oil.

If the influence of polymer concentration and molecular weight on the yield stress is attributed to adsorption effects, discrepancies appear between such an interpretation and the results obtained by others (2, 3, 4) investigating the adsorption of polymer by carbon.

Thus, relative to Jellinek's work (4), saturation would have already occurred at less than 0.5% polymer concentration. This was quite disturbing until the experimental details of Jellinek's work were compared to ours.

At a concentration of 5%, carbon dispersed by shaking in petroleum oil is quite fluid. Upon passing through a three-roll mill or ball milling the system becomes semisolid, so that a beaker containing the mix can be inverted without the occurrence of flow. It may be that the mild dispersing method used in the quoted works is probably such as to leave the carbon in a highly aggregated condition so that, in all probability, the surface area offered for adsorption is much smaller than the 10^7 cm.^{2}/g. mentioned (6). Under the assumption that each monomer element was adsorbed, the experimental adsorption values indicated that only about 7% of the surface was covered at saturation. This type of adsorption would provide for a maximum of coverage. If, however, as is more likely, only a few of the monomer elements of any polymer chain are adsorbed, a much smaller fraction of the surface would be covered. Adsorption studies of decane on carbon (Spheron) indicate that multilayer coverage occurs (9).

The small coverage mentioned above was interpreted (3, 4) as being due to a blocking of the capillaries of the carbon by the high polymer molecule. This extremely small surface coverage as well as the profound differences in flow properties of carbon suspensions with method of dispersion poses the question as to whether the latter may influence the extent of surface available for adsorption. The possibility of a greater extent of adsorption offers itself in our work. Perhaps related to this question is the amount of rubber taken up by carbon when the two are cold-roll milled together (3). Appreciable amounts are "bound" to the carbon as contrasted to the very small amount adsorbed from solution.

Lowering of the yield stress of carbon suspensions by surface-active agents is known (1). The initial lowering of the yield stress with addition of Vistanex is believed to be a similar phenomenon. The relatively slight coverage of the surface at low polymer concentrations is sufficient to interfere with and weaken the normal carbon structure responsible for the yield stress of a carbon-solvent sytsem. The increase of yield stress with both polymer molecular weight and concentration would imply that the polymer molecule does influence the structure formation associated with yield stress phenomena. If this were due only to a viscosity effect, the polymer molecule increasing the viscosity of the medium, then for the same viscosity similar yield values would be expected. That this is not so can be readily seen from the data. Not only is there no relationship between yield values and medium viscosity, but a crossover occurs such that higher yield values occur for lower viscosities depending only on the molecular weight. The effect of the polymer in increasing the yield value is believed to be due to another contribution, namely, binding of the carbon particles through the adsorbed polymer molecules.

The increase of plastic viscosity with polymer concentration and molecular weight is to be expected. If one regards the polymer solution as the dispersing medium, the relative viscosity becomes essentially independent of both polymer concentration and molecular weight. Thus in Table II the specific viscosity for zero Vistanex concentration is in all cases approximately the same as that for the addition of Vistanex. At the higher Vistanex concentrations, there is an apparent decrease, but it is not certain whether this does indeed represent a deviation from the above-mentioned constancy or is due to experimental error.

This effect is all the more interesting in that 3% of Vistanex causes a greater increase in viscosity than does a like amount of carbon. On this basis the Vistanex perturbs the fluid flow lines to a greater extent than does the carbon. Referring the plastic viscosity to the Vistanex solution viscosity effectively treats the latter as the "fluid medium" in which the carbon is dispersed.

IV. CONCLUSIONS

1. A question has been raised as to whether the total surface area of carbon black, or like materials, as determined by gas adsorption is displayed in suspensions, particularly with respect to macromolecular adsorption. The surface available in suspension may very well depend on the method of dispersion. If so, the extent of adsorption of macromolecules from solution will depend on the experimental procedure. We plan, using better defined systems, to examine this point by direct adsorption measurements, over a variety of dispersion methods.

2. The yield stress of a carbon black suspension in petroleum oil is markedly dependent on the concentration and molecular weight of macromolecules present. This effect cannot be explained as due merely to that of changes in medium viscosity. It is proposed that a structure reinforcement occurs because of the binding of carbon particles by adsorbed polymer molecules. There may be an analogy here to the reinforcing action of carbon in rubber.

3. The plastic viscosity, referred to the viscosity of the polymer-oil as "dispersing medium," remains substantially constant, independent of polymer concentration or molecular weight over the range investigated.

ACKNOWLEDGMENTS

The authors are pleased to acknowledge the advice and suggestions of the following persons with regard to the construction and calibration of the viscometer: Professor S. H. Maron of the Case Institute of Technology, Dr. J. Greenspan of the Process and Instruments Company, Dr. J. Bohrer and Mr. A. Pugh of the International Resistance Company.

We are also grateful to Drs. J. Bohrer and S. J. Stein for their encouragement in this work and to the International Resistance Company for permission to publish the results.

References

1. Fischer, E. K., and Jerome, C. W., *Ind. Eng. Chem.* **35,** 336 (1943).
2. Jenckel, E., and Rumbach, B., *Z. Elektrochem.* **55,** 612 (1951).
3. Kolthoff, I. M., and Gutmacher, R. G., *J. Phys. Chem.* **56,** 740 (1952).
4. Hobden, J. F., and Jellinek, H. H. G., *J. Polymer Sci.* **11,** 365 (1953).
5. Bakr, A. M., and McBain, J. W., *J. Am. Chem. Soc.* **46,** 2718 (1924).
6. Garner, F. H., Nutt, C. W., and Mohtadi, M. F., *J. Inst. Petroleum* **39,** 677 (1953).
7. Fox, T. G., Jr., and Flory, P. J., *J. Phys. & Colloid Chem.* **53,** 197 (1949).
8. Reiner, M., and Riwlin, R., *Kolloid-Z.* **43,** 1 (1927).
9. Schaeffer, W. D., Polley, M. H., and Smith, W. R., *J. Phys. & Colloid Chem.* **54,** 227 (1950).

VAN DER WAALS' ATTRACTION BETWEEN ANISOMETRIC PARTICLES

Marjorie J. Vold[1]

Van't Hoff-Laboratory, University of Utrecht, Netherlands

Received May 27, 1954

SUMMARY

Calculations based on additivity of the London-van der Waals' dispersion forces show that for particles of colloidal dimensions the total attractive energy is of the same order of magnitude as thermal energies when the mean diameter ($v^{1/3}$, where v is the volume) is of the order of magnitude of the particle separation, regardless of whether the particles are ball-, rod-, or plate-shaped. At smaller separations the order of attractive energies is plates > rectangular rods > cylinders > spheres. At separations such that $V \sim 10\,kT$ the attraction between spheres varies nearly as r^{-1}, but for rods and cylinders it varies approximately r^{-2} and for platelets r^{-3}.

Likewise, (for rods) parallel orientation is greatly favored over perpendicular orientation at small separations, and (for rectangular rods) orientation with the largest faces opposite each other is favored. These differences diminish as the particle separation increases but remain important so long as the van der Waals' attraction itself is of the order of kT or larger.

Although the essential features of the London-van der Waals' forces of interaction of colloidal particles are widely recognized, actual calculations appear to have been made only for spherical particles and parallel plates whose area is large compared to their separation (3). The result of Dube and Das Gupta (1) for disclike particles does not appear to be useful, because the limitation of infinite thinness for the discs in the beginning of the calculation means that the limiting formula for "small" distances can be valid only for distances large compared to the disc thickness. In fact, for parallel discs perpendicular to the line of centers they find an inverse fourth-power law, which is similar to that found for platelike particles when their separation is large compared to their thickness (5). One factor contributing to the lack of calculations for various shapes of particles is the intractability of the pertinent integral

$$V = -\int_{v_1,v_2} \frac{q^2\lambda\, dv_1\, dv_2}{r^6} \qquad [1]$$

---

[1] Guggenheim Fellow at the University of Utrecht.

Permanent address (after September 1, 1954): Department of Chemistry, University of Southern California, Los Angeles, Calif.

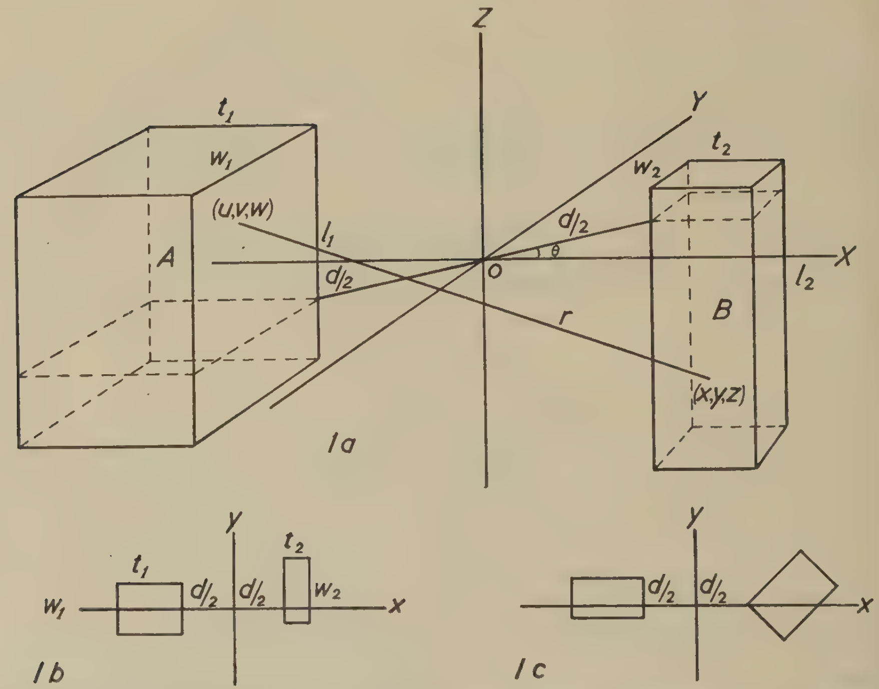

FIG. 1. Nomenclature and co-ordinate system. The two particles A and B are parallel but otherwise unrestricted in relative positions. The origin is always located so as to bisect the shortest distance between them which may be between corners as in Fig. 1a or sides as in Fig. 1b. In the calculations at least one dimension of each particle has been assumed large compared to the others and to the separation. Moreover, the explicit formulas are given for identical particles whose ends (cross section t, w) lie in the same plane. Figure 1c shows the relative orientation which has not been successfully treated.

where V is the total attractive energy, v_1 and v_2 are the volumes of particles containing q atoms per unit volume whose London constant is λ, and r is the distance between a point in one particle and a point in the other.

However, explicit integration of [1] can be carried out for rectangular rods so oriented that the edges are parallel to the x, y, or z axes of a cartesian co-ordinate system, and the resulting attractive energy expressed as a function of the Hamaker constant, $\pi^2 q^2 \lambda$, the dimensions of the particles, and d, the smallest distance between them, provided the rods are long compared to their cross section and their separation. Such a shape is more nearly representative of the actual shape of many real particles (soap fibers in both aqueous gels and greases, linear polymers in extended configurations, rod-shaped protein molecules, etc.) than either of the previously treated cases.

Figure 1 shows two such rectangular particles, the co-ordinate system, and the nomenclature in terms of which Eq. [1] can be written

$$V = -q^2\lambda \iiiint\!\!\iint \frac{dx\,dy\,dz\,du\,dv\,dw}{[(x-u)^2+(y-v)^2+(z-w)^2]^3}. \qquad [1a]$$

Two of the six integrations can be performed at once, leading to the result:

$$V = -\frac{q^2\lambda}{8} \iiiint dx\,dy\,du\,dv \cdot \left[\frac{1}{R^2[R^2+(z-w)^2]} - \frac{3(z-w)}{R^5}\tan^{-1}\frac{z-w}{R} - \frac{3\ln R}{R^4}\right] \qquad [2]$$

where $R^2 = (x-u)^2 + (y-v)^2$. Further progress requires insertion of the limiting values of $(z-w)$. From Fig. 1*a* for identical particles whose ends lie in the same plane, $(z-w) = 0$ or $\pm l$ so that

$$V = -\frac{q^2\lambda}{4} \iiiint dx\,dy\,du\,dv \left[\frac{1}{R^4} - \frac{1}{R^2(R^2+l^2)} + \frac{3l}{R^5}\tan^{-1}\frac{l}{R}\right]. \qquad [2a]$$

Further progress appears to present difficulties unless an expansion be made in powers of $R/l < 1$, which leads to

$$V = -\frac{q^2\lambda}{4} \iiiint dx\,du\,dy\,dv \left[\frac{3\pi l}{2R^5} - \frac{2}{R^4} + \sum_{n=0}^{\infty}(-1)^n\frac{2(n+1)R^{2n}}{(2n+5)l^{2n+4}}\right]. \qquad [2b]$$

The second term here is smaller than the first by a factor of $4R/3\pi l$, and the third is smaller than the second by $\frac{1}{5}(R/l)^4$. Now $R_{\text{max.}}$ is of the order of $(w^2+t^2+d^2)^{1/2}$, where w is the width, t the thickness, and d the separation of the particles. It follows that calculations based on only the first term are valid for particles of mean diameter small compared to their length and separated by distances which are also small compared to their length. Although the calculations of the present paper are based only on this term, the second and higher terms could be included without real difficulty whenever either experimental data or further theoretical developments justify the labor involved.

Keeping only the first term, the next two quadratures lead to

$$V = -\frac{\pi q^2\lambda l}{8} \iint \frac{dy\,dv[2(x-u)^2+(y-v)^2]}{(y-v)^4[(y-v)^2+(x-u)^2]^{\frac{1}{2}}} \qquad [3]$$

in which limiting values of $(x-u)$ are still to be inserted. These will depend upon the mutual orientation of the particles about their long axes. When $(x-u) = 0$ the form taken by Eq. [3] is

$$V = -\frac{\pi q^2\lambda l}{8} \iint \frac{dy\,dv}{(y-v)^3} = \frac{\pi q^2\lambda l}{16(y-v)} \qquad [4a]$$

while for $(x-u) = \text{constant} = k$

$$V = +\frac{\pi q^2\lambda l}{24}\,\frac{[k^2+(y-v)^2]^{3/2}}{k^2(y-v)^2} \qquad [4b]$$

with $(x - u) = k$ very large

$$V = +\frac{\pi q^2 \lambda l k}{24(y - v)^2}. \tag{4c}$$

Formulas for the total potential for various orientations can now be written down by inserting the appropriate limits in Eqs. [4]. For the particle orientation illustrated in Fig. 1*b* the formula is

$$V = -\frac{\pi q^2 \lambda l}{12} \cdot \left\{ \frac{(w^2 + d^2)^{3/2}}{w^2 d^2} + \frac{(w^2 + (d + 2t)^2)^{3/2}}{w^2(d + 2t)^2} - \frac{2[w^2 + (d + t)^2]^{3/2}}{w^2(d + t)^2} \right\} + \frac{\pi q^2 \lambda l}{8}\left[\frac{1}{d} + \frac{1}{d + 2t} - \frac{2}{d + t}\right]. \tag{5}$$

For small values of the separation this formula yields

$$V = -\frac{\pi q^2 \lambda l w}{12 d^2} \tag{5a}$$

and for large values

$$V = -\frac{3\pi q^2 \lambda l w^2 t^2}{8 d^5}. \tag{5b}$$

For case [1*a*], the formula is

$$V = -\frac{\pi q^2 \lambda l}{24}\left\{\frac{1}{d \cos^2\theta \sin^2\theta} + \frac{4[(q + t)^2 + (p + w)^2]^{3/2}}{(q + t)^2(p + w)^2} + \frac{[(q + 2t)^2 + p^2]^{3/2}}{(q + 2t)^2 p^2} \right. + \frac{[(p + 2w)^2 + q^2]^{3/2}}{(p + 2w)^2 q^2} + \frac{[(p + 2w)^2 + (q + 2t)^2]^{3/2}}{(p + 2w)^2(q + 2t)^2} - \frac{2[(q + t)^2 + (p + 2w)^2]^{3/2}}{(q + t)^2(p + 2w)^2} - \frac{2[(p + w)^2 + (q + 2t)^2]^{3/2}}{(p + w)^2(q + 2t)^2} - \frac{2[(p + w)^2 + q^2]^{3/2}}{(p + w)^2 q^2} - \frac{2[(q + t)^2 + p^2]}{(q + t)^2 p^2} \tag{6}$$

where for convenience $p = d \sin\theta$ and $q = d \cos\theta$. For large distances this has the same limit as Eq. [5] but for small distances the limit is

$$V = -\frac{\pi q^2 \lambda l}{24 d \cos^2\theta \sin^2\theta}. \tag{6a}$$

Finally, the interaction energy for two rods crossed perpendicularly with flat sides parallel to each other can be obtained by choosing $z = \pm\infty$ in [2] with $w = \pm w/2$ and $u = \pm\infty$ in [3] with $x = \pm w/2$. This gives

$$V = -\frac{\pi q^2 \lambda w^2}{12}\left[\frac{1}{d^2} + \frac{1}{(d + 2t)^2} - \frac{2}{(d + t)^2}\right]. \tag{7}$$

Formulas [5] through [7] permit discussion of the mutual attraction as a function of particle separation and particle orientation, but the restriction on the length of the particles must not be forgotten.

Particle Orientation

Three cases have been considered: (1) the relative attractive energies between two ribbon-like particles as a function of whether their wide surfaces face each other ($w > t$) or narrow surfaces face each other ($w < t$); (2) the relative attractive energies between two symmetrical rods ($w = t$) as a function of whether their flat sides face each other or their diagonals face each other ($\theta = 45°$ in Eq. [6]); and (3) the relative attractive energies for perpendicular or parallel orientation of the rods.

It can be seen from formula [5*b*] that for ribbon-like particles of constant cross section (w, t) the attraction at large distances is independent of the orientation of the particles about their long axes. For small distances formula [5*a*] shows that the attraction is greater for wide sides facing each other, directly in the ratio of w to t. Intermediate cases can be visualized more easily by numerical examples than by algebraic manipulation of Eq. [5]. Figure 2, curve *A* shows the ratio of V_w (attractive energy for wide sides facing each other) to V_t (narrow sides) for a ratio $w/t = 10$ as a function of a distance parameter $\sigma = (d^2/wt)^{1/2}$. It can be seen that there is a strong preference for orientation with wide sides facing each other which persists out to quite large distances.

Comparison of formula [5*a*] with formula [6*a*] for $\theta = 45°$ shows that at small distances the attractive energy for parallel rather than diagonal orientation is larger by a factor of $w/2d$ ($w/2d \gg 1$ for the validity of these formulas). Figure 2, curve *B*, which was calculated using Eqs. [5] and [6] (with $w = t$, $\theta = 45°$) shows V_p (parallel orientation) / V_d (diagonal orientation) as a function of the distance parameter d/w. It can be seen that V_p is very much larger, even for substantial distances. A somewhat more interesting case, in which the diagonal of one particle cross section is parallel to the edge of the second, can not be easily derived from Eq. [1*a*].

Comparison of formula [5*a*] with [7] shows that parallelism of the rods along their length is favored over perpendicular orientation by a factor of l/w at small distances. Estimates of the rate at which this preference diminishes are not, as in the previous cases, independent of just how long the "infinitely long" particles assumed in the derivation are actually taken to be. Figure 2, curve *C*, which was calculated for a length/width ratio of 20, shows that this preference persists up to a particle separation appreciably larger than the rod diameter.

Particle Separation

The total van der Waals' attraction between spheres depends only on the ratio of the separation to the diameter of the sphere. For large platelets or long rods, this is no longer true. The formula for thin platelets can be put in the form

$$V_P = -\frac{A}{12\pi s^2}\cdot\frac{v}{t^3}\left(1+\frac{s^2}{(s+2)^2}-\frac{2s^2}{(s+1)^2}\right) \qquad [8]$$

where the parameter $s = d/t$, $A = \pi^2 q^2 \lambda$, and v is the volume of the plates. The ratio v/t^3 can be looked on as an asymmetry factor. Hamaker's formula for equal spheres and Eq. [5] of this paper for rods of square cross section, in a similar form are

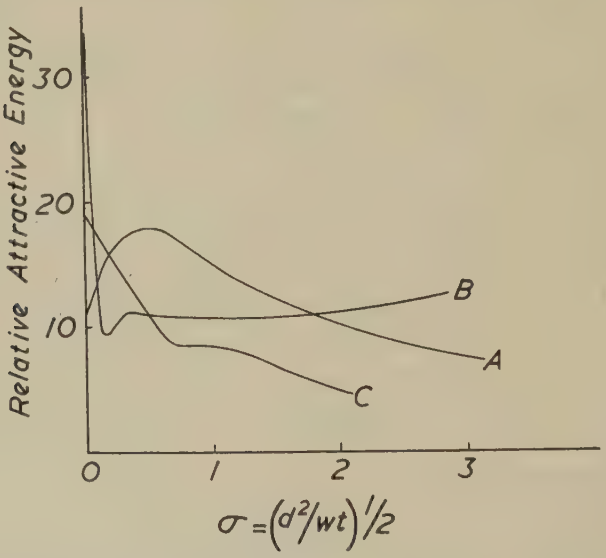

FIG. 2. Relative attractive energy between rod-shaped particles as a function of separation for various orientations. *A*. V_w/V_t for laths for which $w/t = 10$. *B*. V_p/V_d for rods of square cross section with V_p corresponding to Fig. 1*b* and V_d to Fig. 1*a*. *C*. $V_p/V_\perp$ for rods of square cross section with V_p corresponding to long rods parallel and $V_\perp$ to long rods crossed perpendicularly, calculated for a length/width ratio of 20. All curves must approach unity for large enough σ, but V itself is no longer important when σ becomes as large as 2 or 3 where the orientation still produces differences of factors of 5 to 10.

$$V_S = -\frac{Av}{4\pi s D^3}\left(\frac{2}{s+2}+\frac{2s}{(s+1)^2}+4s\ln\frac{s(s+2)}{(s+1)^2}\right) \qquad [9]$$

and

$$V_R = -\frac{A}{12\pi s^2}\cdot\frac{v}{t^3}\left\{(1+s^2)^{3/2}+\frac{s^2[1+(s+2)^2]^{3/2}}{(s+2)^2}-\frac{2s^2[1+(s+1)^2]^{3/2}}{(s+1)^2}\right.$$
$$\left.-\frac{3}{2}s-\frac{3s^2}{2(s+2)}+\frac{3s^2}{s+1}\right\}. \qquad [10]$$

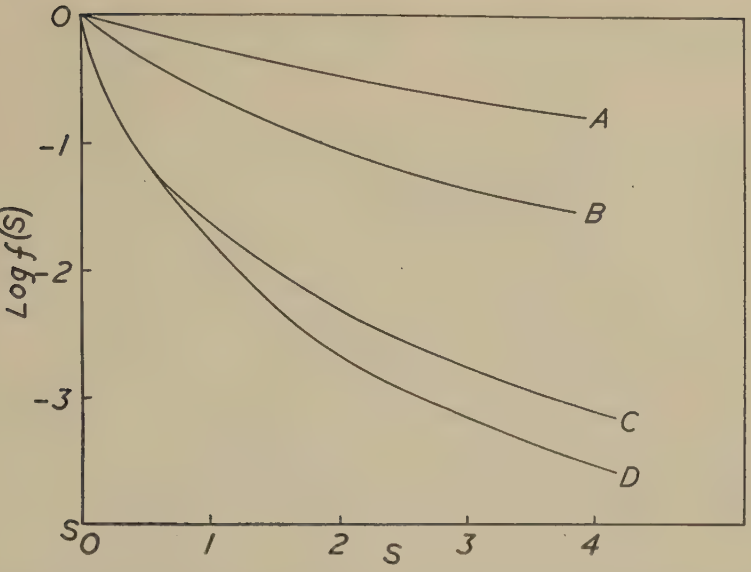

FIG. 3. $f(s)$ for various particle shapes. In every case the van der Waals' attraction can be expressed as a limiting law multiplied by a factor approaching unity at small distances, and decreasing rapidly at large distances, see Eqs. [8]–[11]. Curve *A*s platelets. Curve *B*, rods of square cross section oriented as in Fig. 1*b*. Curve *C*, rod-of square cross section oriented as in Fig. 1*a*. This orientation is regarded as approximating the effect expected for cylindrical particles. Curve *D*, spheres.

Even though the discussion of orientation shows that the rods are more likely to be oriented in such a way as to make Eq. [5] rather than Eq. [6] applicable, Eq. [6] has been cast in the same form and included in the calculations on the grounds that it may represent a fair approximation to the behavior of cylindrical particles. For this case

$$V_C = -\frac{A}{3\pi^2 s}\cdot\frac{2v}{t^3}\left\{1+\frac{s}{s+2}+\frac{4s}{s+1}+\frac{\sqrt{2}}{2}\,\frac{(s^2+(s+2)^2)^{3/2}}{s(s+2)^2} - \frac{\sqrt{2}(s^2+(s+1)^2)^{3/2}}{s(s+1)^2} - \frac{\sqrt{2}\,s[(s+1)^2+(s+2)^2]^{3/2}}{(s+1)^2(s+2)^2}\right\} \qquad [11]$$

where t is now the diameter of the "cylinder" and $s = d/t$. The four functions of the closely related parameters (s) in formulas [8]–[11] have been plotted in Fig. 3, which is quite useful for further calculations.

The relative attractive energies of particles of equal volume at the same distance of closest approach is dependent upon just how large are the "infinite" platelets of formula [8] or how long are the "infinite" rods of formulas [10] and [11]. However, at small separations, when the functions of s are nearly unity, the attraction between the anisometric particles is always larger than for spherical particles of equal volume, because the

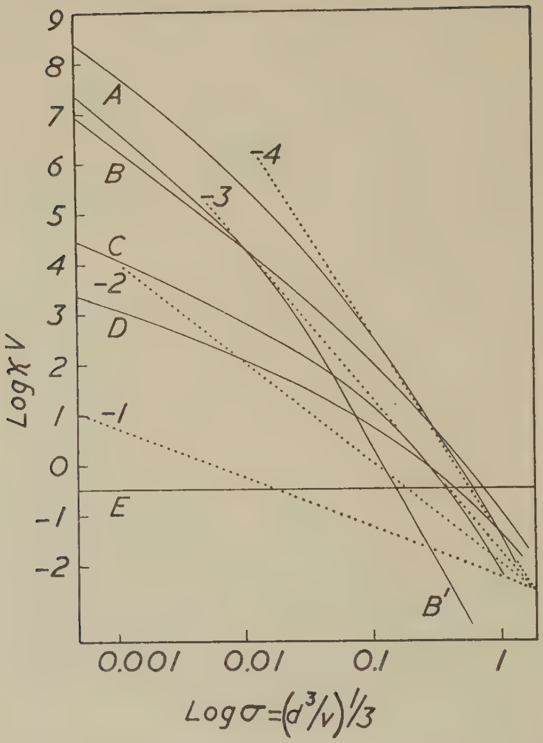

FIG. 4. Van der Waals' attractive energy between colloidal particles of the same volume but different shapes. Curve A, plates with an edge/thickness ratio of 800. B and B', rods of square cross section with length/width ratios of 28 and 316, respectively. Curve C, "cylinders" of length/diameter ratio of 28, i.e., rods of square cross section oriented as in Fig. 1a with length/diagonal ratio of 28. Curve D, spheres. Line E, $V = kT$ for $A = 3 \times 10^{-12}$ and $kT = 4 \times 10^{-14}$. Units: The ordinate is log $24V/A$ where V is the mutual van der Waals' energy in ergs and A is Hamaker's constant. The abscissa (on a logarithmic scale) is the dimensionless ratio of the separation d to the cube root of the volume v. The dotted lines of varying slope show how V is varying with separation. For example, curve A is parallel to the line of slope -2 at very small separations, slope -3 at $\sigma = 0.05$, and slope -4 at $V = kT$.

thickness t is always less than the diameter of the equivalent sphere and occurs in an inverse power. This result is seen to be plausible since, at a given distance of closest approach, a far higher proportion of the total number of atoms in the particles of a flat plate or rod are at or near this separation than is the case with spherical particles.

The order of magnitude of the differences is indicated by Fig. 4, which shows the course of the attractive energy as a function of a separation variable $(d/v^{1/3})$ keeping v constant. The platelets were taken to have an edge/thickness ratio of 800, which is a not unreasonable approximation for bentonite particles, while the rods were taken to have a length/thickness ratio of 28, which is reasonable for soap fibers, as estimated from electron micrographs. An additional curve is plotted for much more asymmetric rods ($l/t = 316$).

All the curves tend to convergence as the separation increases, as indeed they must, for at very large distances all must eventually approach the inverse sixth-power law valid for atoms. The important observation is that this convergence brings the attractive energies to the *same rough order of magnitude, independent of shape and orientation, when the separation approaches* $v^{1/3}$. This observation is, of course, dependent upon arbitrary choices of particle asymmetry, and curve A of Fig. 4 calculated for extremely asymmetric rods illustrates the point that for such cases the attractive energy is of shorter range. However, the choices made are reasonable approximations to the shapes encountered in real systems.

Recently (4) considerable attention has been given to the possible importance for coagulation phenomena of a so-called "secondary" minimum in the total potential energy curve for two particles at fairly large separations. It is not possible to make great progress in considering such minima for anisometric particles without a knowledge of the accompanying repulsive interactions. However, for such a minimum to have appreciable depth, $V_{\text{attr.}}$ must be of the order of at least 10 kT and perhaps larger. For attractive energies of this order of magnitude the form of the dependence of attractive energy on separation is quite different for different particle shapes, being steepest for platelets and most gradual for spheres, with rods and cylinders occupying an intermediate position. It follows that the depth and location of the secondary minimum may be quite dependent upon particle shape.

A second commonly observed phenomenon (2) is that when symmetrical particles aggregate to form flocs, the flocs are often asymmetric, like beads on a string. But the van der Waals' interaction between asymmetric particles is such that they tend on approach to orient themselves to build a more symmetrical double particle, so that it seems unlikely that the explanation of chain building by aggregation of isometric particles is to be found in the attractive term.

The writer wishes to thank Prof. J. Th. G. Overbeek for many helpful suggestions during the course of this development and the John Simon Guggenheim Foundation for financial support.

REFERENCES

1. DUBE, G. P., AND DAS GUPTA, H. K., *Indian J. Phys.* **13**, 411 (1939).
2. FOSTER, M. J., AND MEAD, D. J., *J. Appl. Phys.* **22**, 705 (1951).
3. HAMAKER, H. C., *Physica* **4**, 1058 (1937).
4. OVERBEEK, J. TH. G., *in* Kruyt "Colloid Science," Vol. 1, p. 324. Elsevier, Amsterdam, 1952.
5. VERWEY, E. J. W., AND OVERBEEK, J. TH. G., "Theory of the Stability of Lyophobic Colloids," p. 101. Elsevier, Amsterdam, 1948.

FLOW ELASTICITY OF HYALURONATE SOLUTIONS[1]

C. E. Jensen and Jørgen Koefoed

Universitetets Fysisk-Kemiske Institut, Copenhagen, Denmark

Received June 21, 1954

Abstract

With the oestroscope technique of Scott-Blair (1) solutions of pure potassium hyaluronate have been shown to give a well-defined elastic recoil. Recoil and viscosity were measured at several concentrations, and maximum recoil was found with a 0.25% solution. The stable and well-defined solutions are well suited to examine the phenomena of flow elasticity and elastic recoil, and some preliminary results are reported.

The common raw materials of hyaluronate, human umbilical cord extract and bovine synovial fluid, were also tested and showed elastic recoil, which disappeared on incubation with testicular hyaluronidase.

A model is proposed which ascribes the elasticity to cross-linking and the flow to the fact that the cross-links are the fairly labile hydrogen bonds.

Introduction

Hyaluronic acid according to our present knowledge is a straight-chain polymer (2, 3) of a disaccharide derivative composed of *N*-acetylglucosamine and glucuronic acid. It is found in the connective tissue and in several physiological and pathological secretions (the vitreous body of the eye (4), the synovial fluid (5), the endolymph of the inner ear (6), the contents of pseudo-mucinous ovarian cysts (7), etc.), and it is considered of great importance to many physiological and medical problems, to which rheological properties may be relevant. Being in possession of a sample of very pure (umbilical) potassium hyaluronate of high molecular weight (500,000) (8), we found it of interest to investigate whether its rather viscous solutions had any elasticity, and whether a possible elasticity of the raw materials were connected specifically to their contents of hyaluronic acid.

Experimental

Flow elasticity was detected by means of a 1.6-mm. bore capillary tube, graduated in millimeters, provided with a side hole, and placed in horizontal position. The liquid was sucked up to 100 mm. with an attached syringe and re-expelled to 70 mm., the hole being closed by a finger. Excess liquid was wiped off at the free end and the pressure released through the hole. Recoil of the liquid was measured in millimeters and taken as indication and measure of flow elasticity. This technique was applied by Scott-Blair (1) to detect oestrus in cows through the recoil of cervical mucus, hence the name oestroscope.

---

[1] Hyaluronic Acid.VII. I–VI: refs. 13,9,7,8,2,3.

Earlier applications of the oestroscope have implied only rather qualitative investigations on animal secretions. Working with the well-defined solutions of our pure hyaluronate, we found easily reproducible results, when the tube was kept clean and degreased. The dependence of the recoil on concentration was investigated, and also the dependence on the time in which the column was kept at 70 mm. before being released. The column was kept at 100 mm. for 1 min. in the last-mentioned experiments, but for the more concentrated solutions, this was possibly too short an interval to give maximum recoil. The measurements should not be taken, therefore, as quantitative information on the decay of the structure, but they give an idea of the order of magnitude of the relaxation times involved in the structural "memory" of the liquids.

The viscosities were measured in a modified Ostwald-Sprengler viscometer at 20°C. as in reference 9. The reported relative viscosities should be understood as apparent values, calculated from measurements with the same viscometer, neglecting nonNewtonian behavior.

Results with Pure Solutions

The results of the recoil and viscosity measurements appear from Fig. 1. The nonlinearity of the apparent relative viscosity indicates strong interaction between solute molecules ("cross-linking," see below). Maximum recoil is obtained when the viscosity is 30 to 50 times that of pure water.

The recoiling movement is by no means instantaneous, as appears from the pointed curve in Fig. 2, and the recoil value can first be read after 3 to 5 min.

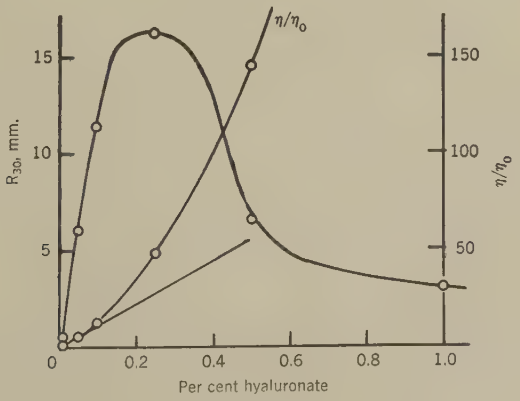

FIG. 1. Recoil on instant release after 30 mm. displacement and relative viscosity at 20°C. versus concentration in grams potassium hyaluronate per 100 ml.

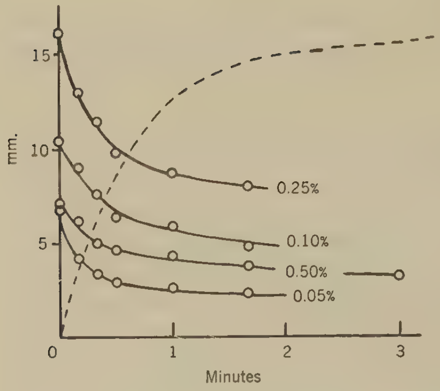

FIG. 2

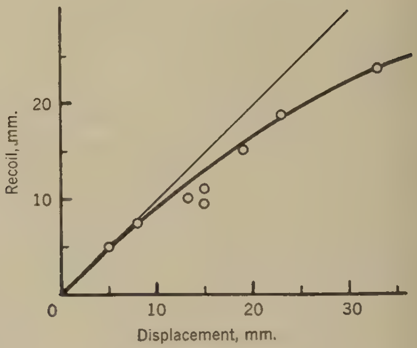

FIG. 3

FIG. 2. Recoiling movement of meniscus after instant release (30 mm. displacement, 0.25% solution) and recoil at various concentrations as function of delay in release in minutes.

FIG. 3. Recoil as function of displacement (0.15% solution of Leo sample).

The decay of that internal structure, which must be responsible for the tendency to recoil, was investigated through delaying the release an increasing number of minutes. Results are also plotted in Fig. 2 and show a peculiar shift from a very rapid decay in the beginning to a very long persistence in the last half or so of the recoil.

We suspected this to be due to a difference in behavior towards smaller and larger displacements. The supplies of our high-molecular preparation being exhausted, the measurements plotted in Fig. 3 were carried out on a 0.15% solution of a sample prepared after Jeanloz and Forchielli (10) and kindly presented to us by A/B Leo, Hälsingborg (Dr. B. Högberg). The molecules of this sample were probably shorter, and it gave a lower viscosity and larger recoil values than our sample. It turned out that displacements up to about 8 mm. are restored to practically 100%, whereas over this limit the recoil increases less than the displacement. In the 10 to 20 mm. region results were less reproducible than usual, probably because they were more sensitive to variations in the velocity impressed during the displacement. Delaying the release, we found that the recoil from a 5 mm. displacement decreased less than 30% with 10 min. delay, while a 15 mm. displacement gave only 4.5 mm. recoil at 1 min. delay against about 11 mm. at instant release, indicating an even quicker initial decay than appears from the results with our own sample in Fig. 2.

RESULTS WITH SECRETIONS AND EXTRACTS

Various fluids, known or suspected to contain hyaluronic acid, were examined and gave recoil as expected. Dilution caused in some cases an increase of the recoil, and incubation with hyaluronidase in all cases gave fluids of low viscosity and without any detectable recoil.

Umbilical Cord Extract. Twenty-five cords were stored 6 to 7 weeks under acetone, chopped, and extracted with 500 ml. of physiological saline for 4 days at room temperature. Recoil of the extract was 14.0 mm; when diluted to double volume, 11.4 mm.; and to four volumes, 8.4 mm.

Umbilical Cord Mucin was precipitated from this extract with one vol.-% acetic acid. Nitrogen content 4.9 % (potassium hyaluronate 3.36 %, protein 16 to 17 %). A "saturated" solution of this mucin in $M/20$ Na_2HPO_4 gave a recoil of 8.4 mm., diluted to double volume 12.8 mm., to four volumes, 13.9 mm., and to eight volumes, 11.1 mm.

Bovine Synovial Fluid. Native fluid gave 7.9 mm. recoil, diluted to two volumes, 3.9 mm., to three volumes, 2.3 mm., and to five volumes, 1.9 mm.

Bovine Synovial Mucin was prepared according to Ropes *et al.* (11). Recoils of solutions in $M/20$ Na_2HPO_4 were:

0.4	0.2	0.1	0.05	0.025	0.013	% mucin
3.8	5.0	5.1	6.0	3.5	0	mm. recoil

The Contents of a Pseudomucinous Ovarian Cyst gave a recoil of 17.4 mm.

TENTATIVE MODEL OF FLOW ELASTICITY

To prove a detailed model of the elastic liquids would need a detailed study of hydrodynamic properties under a great variety of conditions. We will attempt here only to sketch how the phenomenon can be understood in the light of our present knowledge of rubber elasticity and of the structure of hyaluronic acid.

It is well known how the linear hydrocarbon chains in vulcanized rubber with their side chains and sulfur cross-links give the characteristic rubbes elasticity. In hyaluronic acid we have long linear polysaccharide chainr with carboxyl groups and acetylated amino groups as side chains. Both kinds of groups as well as the hydroxyl groups in the chain will be able to provide cross-linking between the coiled chains through hydrogen bond formation. The same groups presumably cause strong hydration of the hyaluronate ion. The low specific density, 1.16(12), indicates a spacious ("icelike"?) configuration of the bound water molecules.

Hyaluronate ions, presumably, adhere to the glass wall and form a three-dimensional lacework all through the liquid. The elastic recoil is brought about by a readjustment of the distorted lacework. The ability to flow is connected to the ease with which hydrogen bonds are broken or rearranged. A valence-bond cross-linking would lead to the formation of gels with no flow-ability. The formerly reported (13) gelatination by copper ions can with great probability be ascribed to cross-linking through complex-formation between copper ions and pairs of acetyl-amino groups from different chains. The concentration of acetyl-amino groups was about $2.5 \cdot 10^{-3}$ and gelatination was observed with cupric ion concentrations between 10^{-4} and $3 \cdot 10^{-3}$ mole per liter.

The possibility of forming permanent peptide-bond cross-links through deacetylation of amino groups and condensation with carboxylic groups may be of significance to the function of hyaluronic acid in physiological and pathological processes.

Any structure depending on hydrogen bonds and preserving the "memory" of past events must eventually be destroyed through thermal rearrangement. It is not surprising that the decay does not in general follow the laws of a first-order reaction, because the more strained loops, which can contribute most to the recoil, will have a greater probability of being broken up. The comparatively very long persistence of the small "perfect" recoils seems to indicate that the elastic free energy at small displacements is established through making the configuration less favorable with respect to the repulsion between the electric charges on the COO^- groups or with respect to thermal movements of the side chains (entropy-elasticity), but without straining the hydrogen bonds. Strained hydrogen bonds appear, then, first at greater displacements, as we approach the yield value and the recoil per cent value begins to fall.

Scott-Blair *et al.* (1), working with secretions, report recoil value considerably lower than 100% and that the per cent values are practically independent of the length of displacement. This difference from our results can probably be explained by a viscous flow of solvent through the loops in the hyaluronate lacework. The protein content in the secretions may very well cause a considerable friction in this flow and hence even at small displacements a loss of energy which is greater than in our system. Increase in hyaluronate concentration over the optimum value leads to decreased recoil for similar reasons, because the loops through which the water moves get more narrow.

Conclusion

It seems likely that the rheological behavior of hyaluronate solutions depends on several parameters in a somewhat complicated way. The reported results indicate that it ought to be possible to sort them out and to correlate them with a fairly simple model of the molecular structure. We hope later to pursue this work with a new sample of high molecular hyaluronate and with a more refined experimental technique, involving, say, control of temperature and of evaporation from the ends.

Acknowledgments

Professor Rydberg, Obstetrical Department of the Rigshospital, Copenhagen, made this work possible by placing extraordinarily well-rinsed human umbilical cords and the contents of ovarian cysts at our disposal. A/B Leo, Hälsingborg, have given us valuable samples of hyaluronic acid and hyaluronidase.

Our thanks are also due to the head of this institute, Professor J. A. Christiansen.

To "Statens almindelige Videnskabsfond", "Carlsberg-fondet," and the University of Copenhagen we are indebted for financial support.

REFERENCES

1. Scott-Blair, G. W., Falley, S. J., Malpress, F. H., and Coppen, F. M. V., *Biochem. J.* **35,** 1039 (1941).
2. Jensen, C. E., *Acta Chem. Scand.* (in press).
3. Jensen, C. E., and Carlsen, Frits, *Acta Chem. Scand.* (in press).
4. Meyer, K., and Palmer, J. W., *J. Biol. Chem.* **107,** 629 (1934).
5. Meyer, K., Smyth, E., and Dawson, M. H., *Science* **88,** 129 (1938).
6. Jensen, C. E., *Acta Chem. Scand.* **8,** 292 (1954).
7. Jensen, C. E., *Acta Pharmacol. Toxicol.* **10,** 83 (1954).
8. Christiansen, J. A., and Jensen, C. E., *Acta Chem. Scand.* **7,** 1247 (1953).
9. Jensen, C. E., *Acta Chem. Scand.* **7,** 603 (1953).
10. Jeanloz, R. W., and Forchielli, E., *J. Biol. Chem.* **186,** 495 (1950).
11. Ropes, M. W., Robertson, W. v. B., Rossmeisl, E. C., Peabody, B., and Bauer, W., *Acta Med. Scand.* **128,** 700 (1947) (Suppl. 196).
12. Jensen, C. E., and Jensen, Robert, *Acta Chem. Scand.* (in press).
13. Jensen, C. E., *Acta Chem. Scand.* **3,** 584 (1949).

VISCOSITIES OF SODIUM POLYACRYLATE IN AQUEOUS SODIUM CHLORIDE

Hiroshi Fujita, Kaoru Mitsuhashi, and Terutake Homma

Department of Fisheries, Faculty of Agriculture, Kyoto University, Maizuru, Japan

Received July 30, 1954

INTRODUCTION

We (12) have recently shown that the reduced viscosity, η_{sp}/C, vs. concentration relationship of sodium carboxy methyl cellulose (Na-CMC) in pure water changes, with increasing the molecular weight (keeping the degree of etherification nearly constant), from type (*a*), in which η_{sp}/C initially increases sharply with polymer concentration, C, reaches a maximum, and then decreases steadily, to type (*b*), in which η_{sp}/C increases steadily with increasing C, exhibiting a rather wide plateau region. The former type of behavior, except for the rapid fall of η_{sp}/C at extremely low concentrations, had been observed in a number of cases by previous investigators, but as regards the latter type we have not yet much information.

The purpose of the present paper is to show that the (*b*) type of behavior can be obtained for other polyelectrolyte of a high enough molecular weight and to explore the effect of an added salt thereon. The polyelectrolyte investigated was a sodium salt of polyacrylic acid having a viscosity-average degree of polymerization of about 1.9×10^4. This polymer salt was chosen in part because of its larger flexibility in contrast to the stiffer nature of Na-CMC investigated previously, and in part because details of the viscosity behavior are well known in a lower molecular weight sample (14).

MATERIALS AND METHODS

The sample of sodium polyacrylate (Na-PAA) was kindly supplied us by Professor M. Nagasawa (Department of Applied Chemistry, Faculty of Engineering, Nagoya University) as a crude aqueous solution of approximately 35 % concentration. After dilution to about 1 % concentration, the solution was filtered through fine sintered-glass filters to remove dust particles. The polymer was then precipitated by addition of alcoholic NaOH and separated by decantation. It was then washed repeatedly with a mixture of methanol and water (80/20 by volume) and finally with acetone until no excess NaOH could be detected with phenolphthalein as indicator. This process was repeated twice for completeness. The precipitate was finally air-dried under reduced pressure at room temperature to remove the volatiles. The master solution for the viscometry was prepared at about 0.1 % concentration by dissolving a weighed amount of the dry product in doubly distilled water. All test solutions were derived by diluting this volumetrically within the viscometer. The concentrations of the test solutions were calculated, assuming no volume change on dilution, from the concentration of the master solution, which was determined, as usual, by careful evaporation of a weighed portion. Sodium chloride which had been purified by recrystallization of a high-grade product was used to study the effects produced by the addition of a simple salt.

The degree of neutralization of the polymer salt (i.e., number of Na-atoms carried per monomer unit) was determined by electroconductometric titration, giving the value of 98.1 %.

The average degree of polymerization or molecular weight of the sample was determined by converting the polymer salt to polyethyl acrylate, for which the viscosity-molecular weight relationship had been established by Sumitomo and Hachihama (19). An approximate degree of polymerization of 1.9×10^4 was found for the converted polyacrylic ester. The corresponding molecular weight of the polymer salt was then calculated to be about 1.8×10^6. In comparison with the PAA sample used by Markovitz and Kimball (14), our sample was considerably higher in molecular weight, thus being suitable for the present purpose of exploring the viscosity behavior of a higher molecular weight polyelectrolyte in dilute solutions.

Two Ubbelohde-type viscometers (suspending level) having flow times of water at 30°C. of about 150 sec. were used. Such relatively short flow times of solvent were needed because it had been found in preliminary trials that the relative viscosity of the sample in pure water was extremely large even at as low a concentration as about 0.05 %. All measurements were made in a double-layer constant temperature bath at 30.000 ± 0.003°C. As shown recently by Flory and his co-workers (9), this temperature is equal to the Flory temperature (8), Θ, for polyacrylic acid. The efflux time was measured with a stopwatch reading to an accuracy of 0.05 sec. Flow times were usually measured at least in duplicate, except for solutions of very low ionic strengths (<0.0005 mole/l.), where duplicate measurements were often discarded because of the extremely long flow times encountered. The reservoirs of the viscometers had been designed to hold approximately 40 ml. of liquid without disturbing the suspended level. This design made it possible to perform successive dilutions within the viscometer. When the capacity of the reservoir was reached, an aliquot of the solution was transferred to another viscometer and the measurements were continued. In this manner, an entire concentration range to be investigated was covered with a single master solution. In order to obtain reproducible data it was necessary to effect complete mixing of the solution in the reservoir of the viscometer, not only immediately after diluent was introduced but also when repeating the measurement at a given concentration. This was done by blowing air gently into the viscometer through a concentrated aqueous NaOH. The kinetic energy correction could be neglected within the accuracy of the present experiments. The drainage error was assumed to be negligible. The correction for shear-rate effects was also ignored, although there is no doubt that the viscosity behavior of such highly viscous solutions as were investigated here should pronouncedly be affected by the velocity gradient of capillary flow (1, 11).

RESULTS AND DISCUSSION

The results of viscosity measurements on dilute aqueous solutions of Na-PAA of molecular weight 1.8×10^6 at different concentrations of NaCl are shown graphically in Figs. 1 and 2, where C is the polymer concentration in grams per 100 ml. solution and x is the added salt concentration in moles per liter of solution. To avoid confusion, curves for high ionic strengths are specifically plotted in Fig. 2 with a magnified scale of the ordinate, wherein the curve for $x = 3$ moles/l. coincides almost completely with the curve for $x = 2$ moles/l. It is seen from the figures that the reduced viscosity varies over a very wide range when the added salt content is diminished from 3 to 0 mole/l. at a fixed polymer concentration; for example, at $C = 0.05$ g./100 ml., the variation is about 140-fold. It may be noted that such an enormous change in η_{sp}/C was not observed in our previous work on Na-CMC (11).

It is first noted from Fig. 1 that the viscosity curve in pure water solutions ($x = 0$) initially rises very steeply and almost linearly with increasing C and then levels off at concentrations higher than about 0.03 g./100 ml. Neither an indication for the appearance of a maximum point nor a tendency for η_{sp}/C to decrease steadily with increasing C can be observed within the concentration range examined. The type of behavior herein observed for a high molecular weight Na-PAA is entirely of the same nature as that which we observed previously with high molecular weight samples of Na-CMC (12). Aside from the difference in absolute value of η_{sp}/C, the only difference to be pointed out between these two cases is the concentration at which the curve begins to level off. Whereas in the present case such concentration is about 0.03 g./100 ml., in the previous case it is smaller than 0.01 g./100 ml. in either of the samples studied. As mentioned in the *Introduction*, the reduced viscosity of polyelectrolytes in solutions containing no added salts has been found in a number of cases to increase markedly with decreasing concentration. Specifically, such

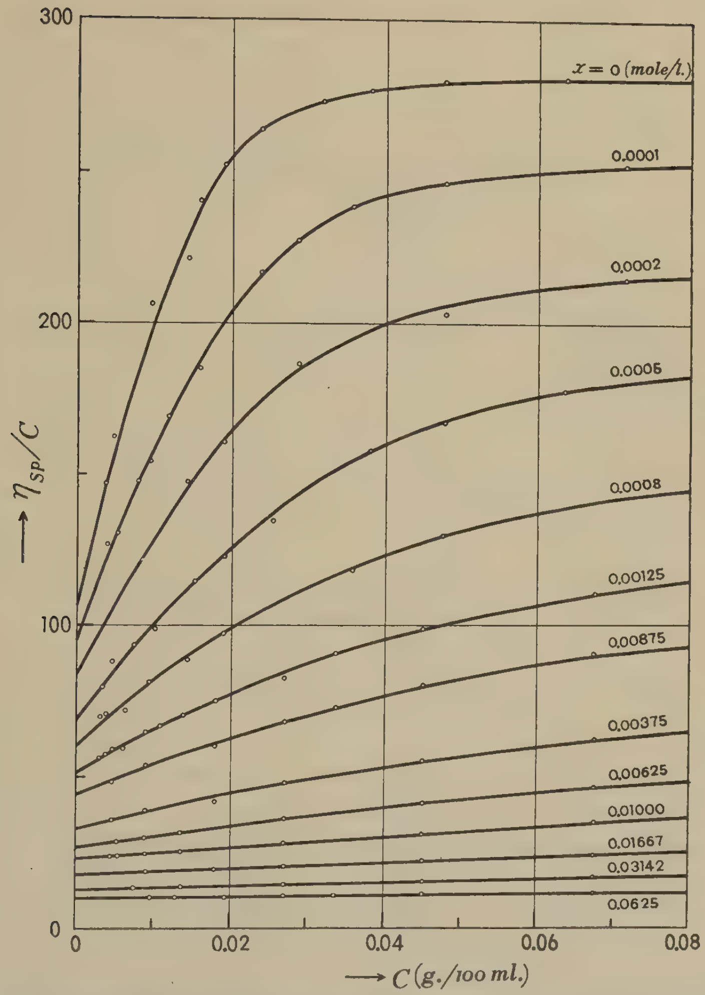

FIG. 1. Reduced viscosity curves of Na-PAA (sodium polyacrylate) in aqueous media of different ionic strengths. x is the concentration of added NaCl in moles per liter.

observations for sodium salts of polyacrylic acid were made by Markovitz and Kimball (14), and others. However, the molecular weights of the Na-PAA samples treated by these previous workers are much lower than that of the one used in this investigation, and no experimental information is yet available in the literature showing the steady increase of η_{sp}/C upon dilution for a Na-PAA sample having a molecular weight as high as that of the present sample. We may thus conclude, for the moment, that the viscosity behavior of Na-PAA also changes its type from (*a*) to (*b*) as the molecular weight is increased, in conformity with our previous observation

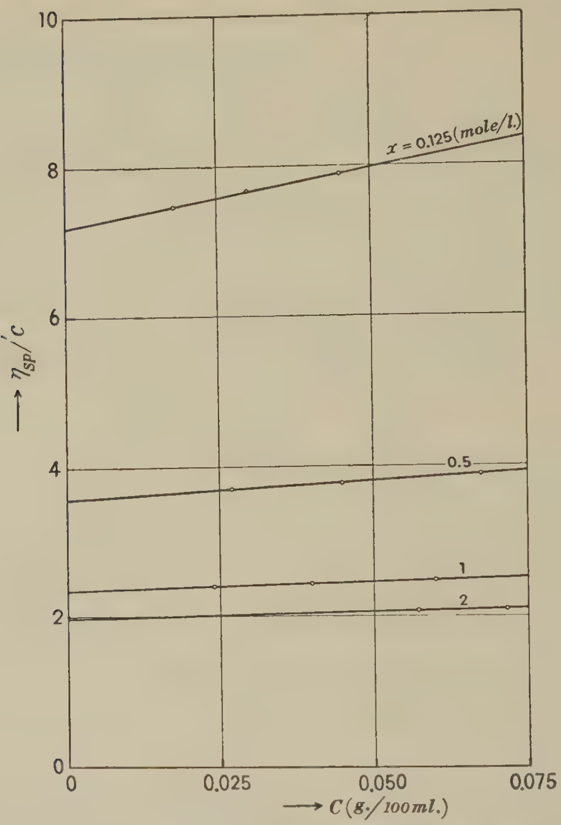

FIG. 2. Reduced viscosity curves of Na-PAA in aqueous media of high ionic strengths.

on Na-CMC. In the course of this study, we became aware of similar results obtained by Butler and his school with samples of partially neutralized polymethyl methacrylate. Butler (6) reported, at the Uppsala Symposium on Macromolecules in 1953, that a sample of polymethacrylic acid of molecular weight of about 2×10^6 gave a reduced viscosity increasing with the concentration (type (*b*) mentioned above), whereas a sample with a lower molecular weight 2×10^5 showed values increasing at low concentrations to a maximum (type (*a*)). This observation is undoubtedly in line with those made by us for other polyelectrolytes. The reason why the change in type of viscosity behavior of a polyelectrolyte in salt-free solution occurs with change in molecular weight has not yet been elucidated, but it has been discussed qualitatively (12) on the basis of electrostatic interactions between polyions and between polyions and their counter-ions, in conjunction with the folding-chain theory of Fuoss and others.

It has been shown for various polyelectrolyte systems that the reduced

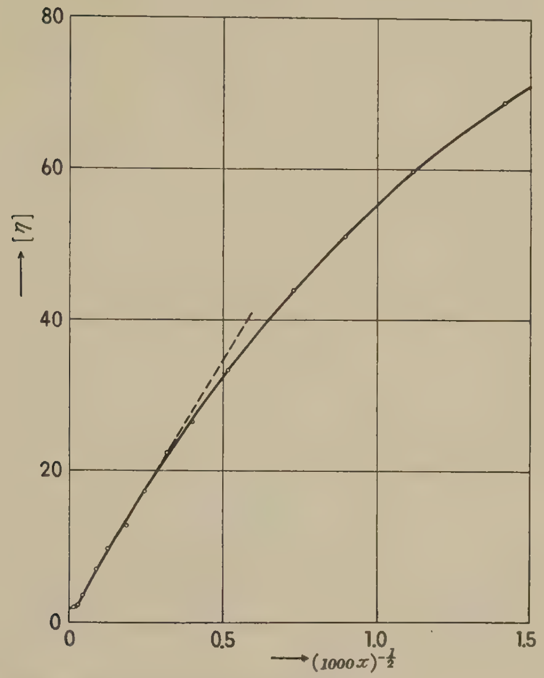

FIG. 3. Intrinsic viscosity, [η], plotted against the reciprocal root of ionic strength, x, of the medium.

viscosities in solutions of low ionic strengths go through a maximum at a polymer concentration where the equivalence of the polyelectrolyte is of the same order of magnitude as that of the added salt, and a plausible interpretation of this phenomenon has been presented (15) in terms of the combination of the folding-chain effect and the normal concentration effect. According to it, the addition of some amount of simple salt is necessary to produce the maximum of reduced viscosity. However, this condition does not always obtain, because, as has recently been demonstrated in several cases (12, 2, 4, 5, 7), the maximum of η_{sp}/C is obtained in salt-free solutions. That the addition of simple salt is not always the sufficient condition to bring about the maximum of η_{sp}/C may be realized from the data plotted in Fig. 1, where no indication for the appearance of a maximum can be observed at any concentration of NaCl studied. The only effect of the addition of NaCl was in reducing pronouncedly the viscosity of the solution.

The intrinsic viscosities, [η], obtained by extrapolating graphically the curves of Figs. 1 and 2 to infinite dilution, are plotted in Fig. 3 against the reciprocal root of the ionic strength, x, of the medium. In Fig. 4, the behavior at very low ionic strengths is shown on a linear plot. The method

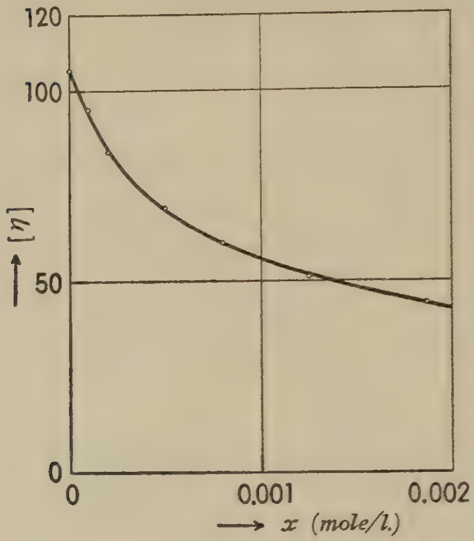

FIG. 4. Intrinsic viscosities at lower ionic strengths.

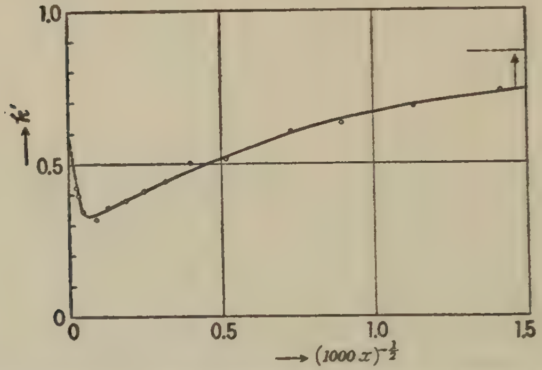

FIG. 5. Huggins' constant, k', plotted against the reciprocal root of ionic strength, x.

of extrapolation employed here is different from the "isoionic" method of Pals and Hermans (15). It is easily shown from the data of Fig. 1 that in this case the isoionic dilution method fails to give a family of straight lines between η_{sp}/C and C, in contrast to the cases of Na-CMC and sodium pectinate (11, 15). This is probably due to the high charge density and high molecular weight of our polyelectrolyte.

The Huggins slope constants, k', calculated from the initial slopes of the curves of Figs. 1 and 2, are plotted in Fig. 5 against $(1000\,x)^{-1/2}$. It should be noted that evaluation of the Huggins constant is generally less reliable than that of the intrinsic viscosity, especially for viscosity curves having

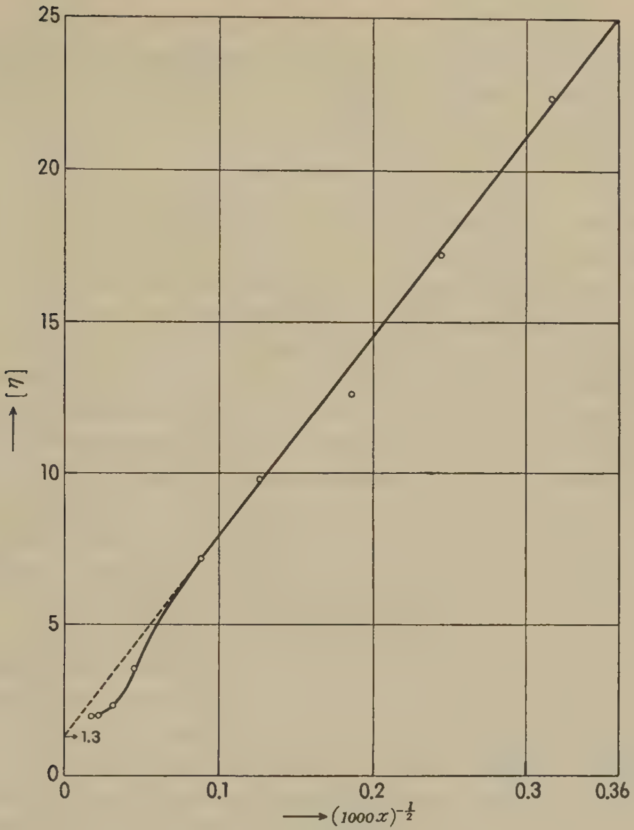

FIG. 6. Intrinsic viscosities at higher ionic strengths.

a limited linear part, as is the case with our curves at low ionic strengths. The k' curve obtained is seen to follow an interesting course. The curve may be extrapolated to $k' \risingdotseq 0.6$ at the limit of very high ionic strength. On decreasing the ionic strength (i.e., on increasing $(1000\ x)^{-1/2}$), the curve falls off sharply, reaches a minimum at a $(1000\ x)^{-1/2}$ value of about 0.07, and rises slowly to tend to a k' value of about 0.85 at the limit of zero ionic strength. The k' value at the minimum is about 0.33. It is interesting to note that this value is in conformity with the values commonly observed for neutral flexible polymers in good solvents. From the k' behavior obtained we may infer the configurational change of the Na-PAA molecule as produced by the change in the ionic strength of the medium.

We assume that experimentally observed k' values are contributed by two factors, one of which is the normal hydrodynamic intermolecular interference, as has recently been discussed in detail by Simha (17, 18), Saito (16), and Brinkman (3); and the other of which is the electrostatic interactions between polyions and between polyions and their counter-ions. The latter factor is, of course, characteristic of polyelectrolytes only. Denote the contribution of the hydrodynamic factor by k_H' and that of the electric factor by k_E'. Then, we have

$$k' = k_H' + k_E'.$$

At low ionic strengths, the values of k_H' are small because the polymer molecule assumes an elongated shape, while the values of k_E' are probably considerable because the molecule is highly ionized. As a result, rather high k' values would be obtained experimentally at low ionic strengths. On increasing the ionic strength, the polyelectrolyte molecule coils, losing asymmetry, and k_H' increases. At the same time, a marked decrease in the degree of ionization should occur, which results in a reduction of the k_E' value. When the latter effect predominates over the former, k' values decreasing with increasing ionic strength should be observed. This is just the case encountered in this experiment. At higher ionic strengths, the contribution of the electric factor is practically masked by the normal hydrodynamic contribution. At this stage, the polymer molecule would be in a randomly but still rather loosely coiled configuration, since the molecule is still ionized to some extent so that some space is open for intramolecular electrostatic forces to expand the coil. Such a configuration of the polyelectrolyte molecule may be compared to that of uncharged flexible polymers in good solvents. Consequently, it is expected that k' values at moderately high ionic strengths will be in a range from about 0.3 to 0.35, which is typical for uncharged flexible polymers in good solvents. This is well borne out by our experimental data. As the ionic strength is increased further, the counter-ions are more and more absorbed into the coil to suppress the ionization; this in turn causes the molecule to coil up more and more tightly. This hypercoiling is possible only for polyelectrolytes having flexible chains, as is the case with the polymer used in this investigation. With increase in hypercoiling, the molecule behaves as a hard sphere in the sense that its permeability to the flow of solvent is diminished owing to the increasing average density of the chain elements. One may be tempted to suppose that such a configurational change of a polyelectrolyte molecule as well as the accompanying change in the permeability to solvent flow resembles closely those appearing when an uncharged flexible polymer in a good solvent is transferred into a poor solvent. It is now generally accepted that k' values for uncharged flexible polymers in poor solvents are larger than in good solvents. Simha (17, 18), Brinkman (3), and others have shown theoretically that the k' value of the uncharged hard sphere is of the order of 0.7. It is expected, therefore, that k' values for our Na-PAA increase again with increasing ionic strength, after passing through a minimum with $k' = 0.3 \sim 0.35$, to this theoretical value at the limit of very high ionic strength. This expectation is also well confirmed by the experimental data presented. In this manner, the general trend of the k' curve for our Na-PAA sample may be explained qualitatively.

Finally, we remark that, in the cellulosic polyelectrolytes as investigated previously (11, 15), the k' values became linear against the reciprocal of the added salt concentration over the range studied, and no indication for the minimum could be observed. The absence of the minimum in those polymers may, according to the above interpretation, be ascribed to the stiff nature of their chains which does not allow the molecule to coil up tightly even at high ionic strength.

Calculations of the Molecular Dimensions

We first attempt to calculate the dimensions of the molecule at sufficiently high ionic strength on the basis of the method of Pals and Hermans (15), which was successfully applied for Na-CMC and for sodium pectinate (11, 15). To this end we must first find a linear part on the experimentally obtained $[\eta]$ vs. $(x)^{-1/2}$ curve in the region of sufficiently high values of x. This linear part may be taken as shown in Fig. 3 by the broken line. To confirm this a magnified graph of the $[\eta]$ vs. $(x)^{-1/2}$ curve in the neighborhood of the origin is given in Fig. 6. Here, the straight-line relationship is evident, except in the region of $(1000\ x)^{-1/2}$ below about 0.07. According to the theory of Hermans and Overbeek (13) of polyelectrolyte molecules in dilute solutions, on which the method of Pals and Hermans (15) is based, the $[\eta]$ vs. $(x)^{-1/2}$ curve should deviate slightly above the straight line in the vicinity of the origin, in contrast to the present data. The reason for the discrepancy encountered may be inferred as follows:

The theory of Hermans and Overbeek assumes the molecule to be completely permeable to the flow of solvent at any state of coiling (hence, at any ionic strength of the medium). This assumption may hold with good approximation for polymers having stiff chains or for polyions in media of not so high ionic strength. However, as found in the preceding section through the behavior of the Huggins constant, the polyelectrolyte under consideration becomes impermeable to the flow of solvent as a result of hypercoiling when the added salt concentration becomes sufficiently large, thus violating the assumption of Hermans and Overbeek's theory. It can be shown generally that for a polymer coil of a given molecular weight in a given solvent the intrinsic viscosity calculated assuming no penetration of the solvent is smaller than that for the completely permeable coil. Therefore, it is expected that the experimental $[\eta]$ vs. $(x)^{-1/2}$ curve for our polyelectrolyte would be gradually deviated downward from the theoretical curve derived on the permeable molecular model, beyond the ionic strength where the coil ceases to be completely penetrable. The experimental curve well conforms to this consideration. In agreement with the prediction, the x value at which the $[\eta]$ vs. $(x)^{-1/2}$ begins to deviate from the straight line is nearly equal to the x value corresponding to the minimum point in the

k' curve. The curve of Fig. 6 appears to level off in the region of very high ionic strength, yielding an $[\eta]$ value of 1.95 at the limit. This leveling off of $[\eta]$ may be an indication that the molecule attains the limit of hypercoiling at this order of ionic strength.

Based on the straight line settled in this way, the analysis was carried out in accordance with the procedure as described by Pals and Hermans (15). The effective bond length, b, obtained is

$$b = 22 \text{ A.}$$

The end-to-end distance, h, and the effective radius, R, of the coil at high ionic strengths of the solution are calculated, respectively, to be

$$h = 3040 \text{ A.,}$$

$$R = 1610 \text{ A.}$$

The fully extended length of the molecule, L, is

$$L = 47{,}000 \text{ A.}$$

Comparison of these values of h and L indicates that the degree of coiling in our Na-PAA molecule at high ionic strengths is sufficiently large, in harmony with the flexible nature of the molecular chain. However, if, as has been discussed above, the molecular configuration of our polyelectrolyte in solutions of moderately high ionic strengths resembles those of uncharged flexible polymers in good solvents, the b value obtained appears to be too large. In fact, this b value leads to as large a value as about 200 A. for the length of a statistical segment in Kuhn's sense. The usual lengths of the statistical segment of vinyl polymers derived from various measurements are of the order of 20 to 40 A. Although this large difference may in part be due to the fact that the character of Na-PAA is still considerably polyelectrolytic even at high ionic strengths, it appears that it cannot be satisfactorily accounted for solely by this effect.

Next, we use the Flory-Fox equation (8):

$$h = \left(\frac{[\eta]M}{\Phi}\right)^{1/3},$$

which relates the end-to-end distance, h, of an uncharged coil to its molecular weight, M, and intrinsic viscosity $[\eta]$. In this equation, Φ is a universal constant of the order of 2.1×10^{21}. The above equation with this Φ value may be strictly applied only for completely impermeable coils. Accordingly, in order to apply this equation to our data, the value at the limit of very high ionic strength must be inserted for $[\eta]$. Simple calculations give

$$h = 1200 \text{ A.,}$$

$$R = 540 \text{ A.,}$$

$$b = 8.7 \text{ A.}$$

This b value leads to a length of 38 A. for the statistical segment, which is a reasonable value for vinyl polymers as noted above. Thus, it proves that, so far as the present data are concerned, the Flory-Fox theory is preferable to the Hermans-Overbeek theory to determine the molecular dimensions.

ACKNOWLEDGMENT

We wish to thank Professor M. Nagasawa, of the Department of Applied Chemistry, Faculty of Engineering, Nagoya University, for his kindness in supplying us with the sample of sodium polyacrylate.

SUMMARY

Dilute solution viscosity data were obtained for a 98.1% neutralized sodium salt of polyacrylic acid having a viscosity-average degree of polymerization of about 1.9×10^4, over a wide range of added salt (NaCl) concentrations. It was found that:

1. The shape of the η_{sp}/C curve in pure water is of an entirely different type from that expected from the folding-chain theory of Fuoss and others, but is essentially similar to that which we observed with sodium carboxy methyl celluloses of high degrees of polymerization. The curve increases steadily with increasing C, exhibiting a rather wide plateau region.

2. A marked decrease of the reduced viscosity is brought about by the addition of NaCl, but no indication for the appearance of a maximum in η_{sp}/C is observed for the added salt concentration ranges studied.

3. With increasing ionic strength of the medium, the Huggins constant, starting with a value of about 0.6, initially decreases, reaches a minimum with a value of about 0.33, increases again, and tends to 0.85 at the limit of zero ionic strength. This behavior is discussed in connection with the change in degree of coiling of the polyelectrolyte molecule as caused by the change in the ionic strength. In particular, the behavior at sufficiently high ionic strengths is interpreted as a result of hypercoiling of the molecule.

4. The application of the method of Pals and Hermans to our data leads to too high a value for the length of a statistical segment in Kuhn's sense. In contrast to this, the Flory-Fox equation, when applied at the limit of very high ionic strength, gives a very reasonable value for this length, being about 38 A.

REFERENCES

1. AKKERMAN, F., PALS, D. T.F., AND HERMANS, J. J., *Rec. trav. chim.* **71,** 56 (1952).
2. ALEXANDER, P., AND HITCH, S. F., *Biochim. et Biophys. Acta* **9,** 229 (1952).
3. BRINKMAN, H. C., *J. Chem. Phys.* **20,** 571 (1952).
4. CONWAY, B. E., AND BUTLER, J. A. V., *J. Chem. Soc.* **1952,** 3075.
5. CONWAY, B. E., AND BUTLER, J. A. V., *J. Polymer Sci.* **11,** 277 (1953).
6. CONWAY, B. E., AND BUTLER, J. A. V., *J. Polymer Sci.* **12,** 199 (1954).

7. Eisenberg, H., and Pouyet, J., *J. Polymer Sci.* **13,** 85 (1954).
8. Flory, P. J., and Fox, T. G., *J. Polymer Sci.* **5,** 745 (1950).
9. Flory, P. J., Krigbaum, W. R., and Shultz, J., *J. Chem. Phys.* **21,** 164 (1953).
10. Fuoss, R. M., *J. Polymer Sci.* **12,** 633 (1954).
11. Fujita, H., and Homma, T., *J. Polymer Sci.*, in press.
12. Fujita, H., and Homma, T., unpublished paper.
13. Hermans, J. J., and Overbeek, J. Th. G., *Rec. trav. chim.* **67,** 761 (1948).
14. Markovitz, H., and Kimball, G. E., *J. Colloid Sci.* **5,** 115 (1950).
15. Pals, D. T. F., and Hermans, J. J., *Rec. trav. chim.* **71,** 433 (1952).
16. Saito, N., *J. Phys. Soc. Japan* **4,** 85 (1949).
17. Simha, R., *J. Research Natl. Bur. Standards* **42,** 409 (1949).
18. Simha, R., *J. Colloid Sci.* **5,** 386 (1950).
19. Sumitomo, H., and Hachihama, Y., *Chem. High Polymers (Japan)* **11,** 65 (1954).

DYNAMIC MECHANICAL PROPERTIES OF POLYVINYL ACETATE[1]

Malcolm L. Williams[2] and John D. Ferry

Department of Chemistry, University of Wisconsin, Madison, Wisconsin

Received August 5, 1954

INTRODUCTION

Dynamic mechanical properties in the lower audio-frequency range, carried through the transition from rubberlike to glasslike consistency, have been previously reported from this laboratory for polyisobutylene (1) and polystyrene (2). Similar measurements on polyvinyl acetate are now presented. The extensive dielectric measurements of Mead and Fuoss (3) on this polymer permit a comparison of mechanical and electrical relaxation distributions and their temperature dependence.

MATERIALS AND METHODS

The polyvinyl acetate was an unfractionated sample of grade AYAX, lot 1232, furnished through the kindness of Mr. A. K. Doolittle of Carbide and Carbon Chemicals Company. Its intrinsic viscosity in methyl ethyl ketone at 25°C. was 0.96 deciliter per gram, its number-average molecular weight 140,000 (4), and its weight-average molecular weight[3] 420,000. The wide distribution of molecular weights in this sample is probably accompanied by branching. However, this should not have much effect on the mechanical properties in the transition region. This polyvinyl acetate has been extensively studied in solution (5–8).

Measurements of the complex shear compliance ($J^* = J' - iJ''$) were made with the double transducer of Fitzgerald and Ferry (9). Some minor changes in this apparatus had been introduced by Dr. Fitzgerald[4] since its original description (9). A new driving tube, with a mass of 31.03 g., was constructed without splitting the metal section, and carried coils 1A and 2A wound with two layers of No. 36 enameled copper wire, increasing the transducer constant K^2 to 3.47×10^5. Subsequently, a magnet core of smaller diameter was used to provide larger clearance (0.050 in.) between it and the driving tube. This change diminished K^2 to 3.10×10^5 but made alignment of the driving tube in the annular gap much less critical.

---

[1] Part XVI of a Series on Mechanical Properties of Substances of High Molecular Weight.

[2] Union Carbide and Carbon Fellow in Physical Chemistry, 1952–54.

[3] We are greatly indebted to Dr. E. F. Casassa for determining this value from light-scattering measurements in methyl ethyl ketone. Measurements of absolute intensity at 45°, 90°, and 135° were made in semioctagonal cells, and the molecular weight was corrected for the observed dissymmetry on the basis of polydisperse random coils with a polyester type of distribution. The value of dn/dc was taken as 0.0848 ml./g. (private communication from Prof. W. H. Stockmayer).

[4] The assistance of Dr. Fitzgerald, now at Pennsylvania State University, in supervising maintenance of the apparatus is gratefully acknowledged. We are especially indebted also to Mr. Russell Riley and the other mechanicians of the Department of Chemistry for their co-operation.

Five pairs of disc-shaped samples were employed, three (Nos. 38, 43, and 44) molded directly from the granular polymer as supplied by the manufacturer, and two from the product obtained by drying from a frozen benzene solution. The samples were annealed, after molding, for at least 18 hr. at 85°C. and in some cases considerably longer. The samples were attached to the cylinders of the floating mass by warming the latter to about 70°C., and their adhesion to the driving tube was facilitated by blowing hot dry air into the apparatus.

Samples 43 had dimensions of $1\frac{1}{16}$ in. (diameter) by $\frac{3}{32}$ in. (thickness) and, after compression, a sample coefficient ($A_1/h_1 + A_2/h_2$, where the A's and h's are the respective face areas and thicknesses) of 21.7 cm. at 25°C. Samples 44,$1\frac{1}{32}$ in. by $\frac{3}{16}$ in., had a coefficient of 2.98 cm. Values of J' and J'' measured on these two pairs agreed where the measurements overlapped (64.9°C. and 69.8°C.). Samples 29, also $1\frac{1}{32}$ in. by $\frac{3}{16}$ in., had a nominal sample coefficient of 2.76, but it was necessary to apply an empirical correction of 35% to bring the values of J' and J'' into agreement with those measured for the other samples; this was attributed to an obvious incomplete attachment of the inner surface of each of the pair to the driving tube. Samples 32 and 38 had nominal sample coefficients of 4.90 and 30.3, respectively; values of J'' calculated from the latter agreed with the other data, but the values for samples 32 were corrected by a bulging correction of 25% (in principle calculable from measurements of bulging (9), but in practice determined empirically). Because of experimental difficulties, the data for these last two pairs of samples are less extensive than for the others.

Sample coefficients at temperatures other than 25°C. were calculated, as usual, from the thermal expansion coefficient, 0.57×10^{-3} deg.$^{-1}$ (10), assuming that the sample thickness remained constant.

RESULTS

Values of J' and J'' at temperatures from 50°C. to 90°C. are shown as double logarithmic plots against frequency (from 30 to 5100 cycles/sec.) in Figs. 1 and 2. Where data on different samples were taken at the same frequencies and temperatures, the values have been averaged. Complete numerical data are recorded elsewhere (11). Over this range of temperatures and frequencies, J' varies from $10^{-6.7}$, characteristic of a rubbery solid, to 10^{-10}, characteristic of a hard glass; J'' varies from $10^{-7.0}$ to $10^{-10.7}$.

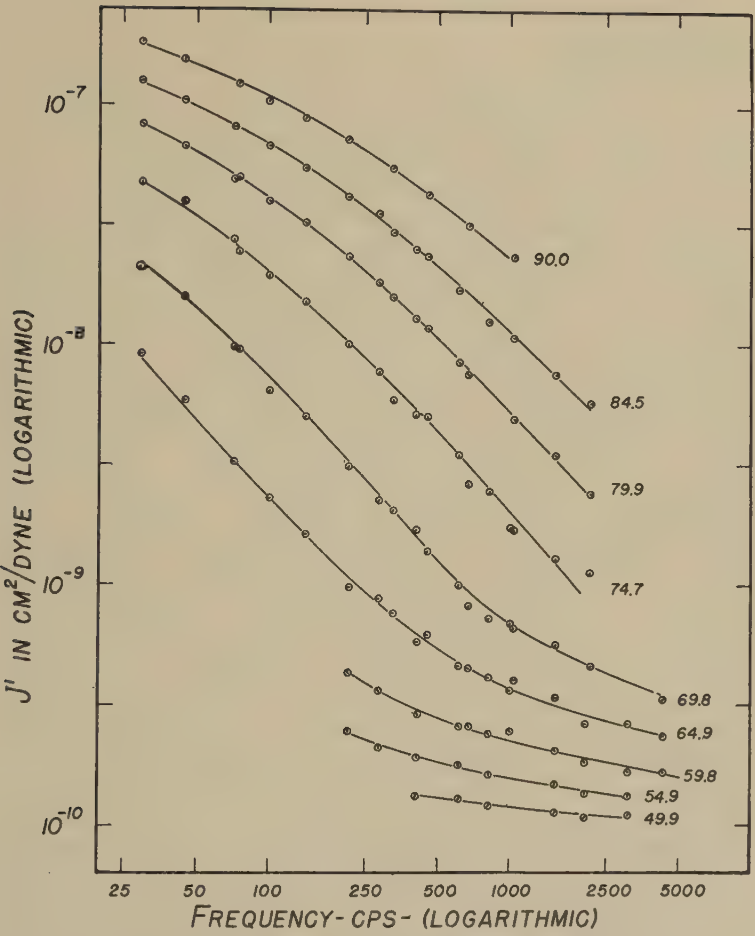

FIG. 1. Variation of the real part of the dynamic shear compliance, J', with frequency for polyvinyl acetate AYAX at nine temperatures as indicated.

For application of the method of reduced variables, double logarithmic plots of $J'_p = J'[T\rho/T_0\rho_0 + (J_\infty/J')(1 - T\rho/T_0\rho_0)]$ and $J''_p = J''(T\rho/T_0\rho_0)$ were prepared. Here ρ and ρ_0 are the densities at the absolute temperature of measurement, T, and a standard temperature, T_0, chosen as 348°K. The limiting high-frequency compliance, J_∞, was estimated to be 1.0×10^{-10} cm.²/dyne. Values of log a_T, the reduction factor expressing the change of all retardation times with temperature, were obtained from these plots, and those from J'_p and J''_p were in good agreement; they are listed in Table I.

Reduced double logarithmic plots of J'_p and J''_p against ωa_T (where ω is the circular frequency) are shown in Figs. 3 and 4; the data at all temperatures and frequencies superpose well, indicating that the assumption of equal temperature dependence of all retardation times holds for this polymer

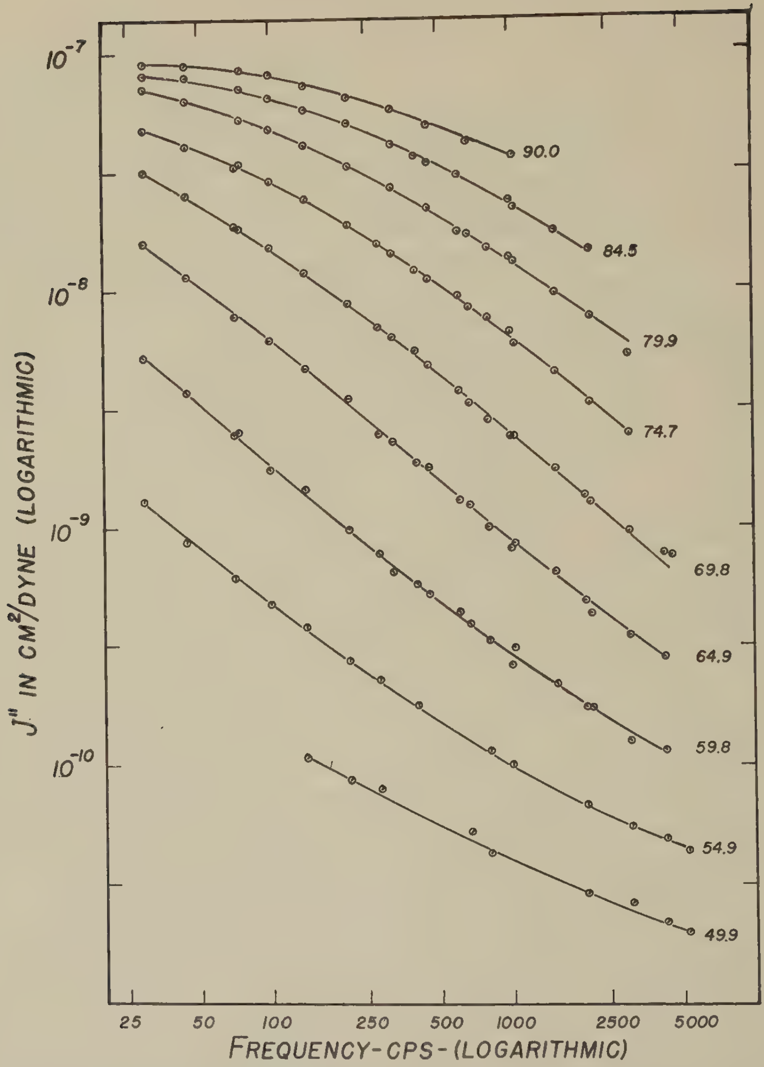

FIG. 2. Variation of the imaginary part of the dynamic shear compliance, J'', with frequency for polyvinyl acetate AYAX at nine temperatures as indicated.

as it does for numerous other systems investigated in the transition from rubberlike to glasslike consistency (1, 2, 12). The composite curves represent J'_p and J''_p over an extended frequency range at 75°C. From these curves, the components of the complex rigidity, G'_p and G''_p, and the real part of the complex viscosity, η'_p, have been calculated and are plotted logarithmically in Fig. 5, also reduced, of course, to 75°C. The shapes of all these curves are similar to those of polymers previously investigated,

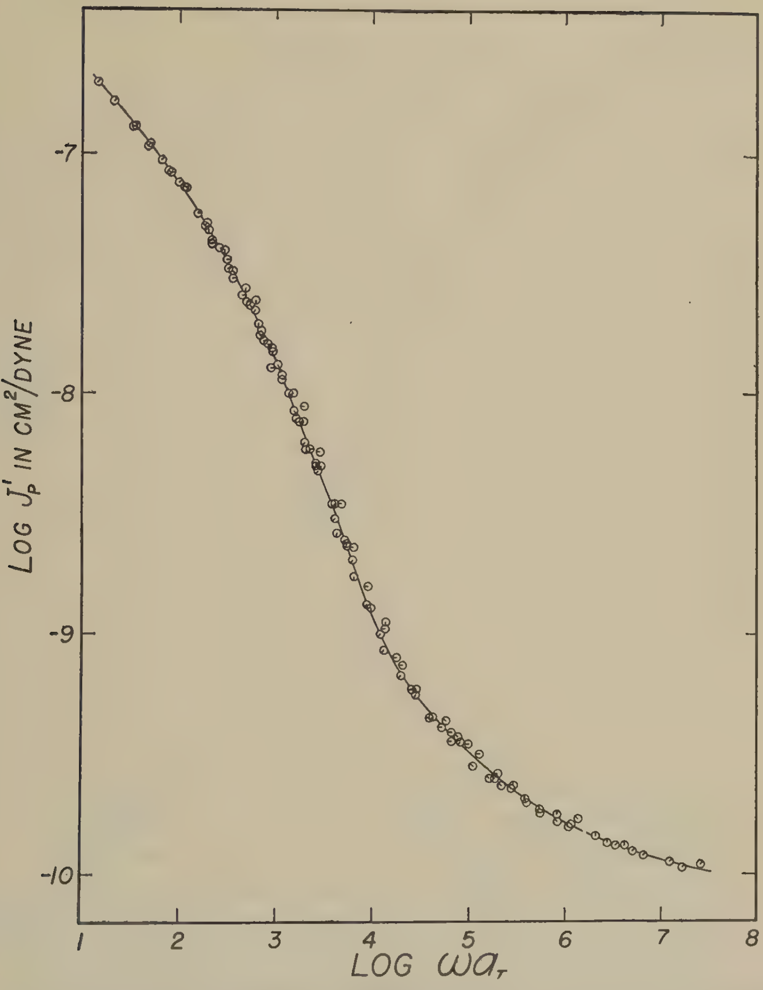

FIG. 3. Real part of the complex compliance reduced to 75°C., plotted logarithmically against reduced frequency. Temperature key same as in Figs. 1 and 2.

although the dispersion is somewhat sharper than in polystyrene (2) and considerably sharper than in polyisobutylene (1); the maxima in the loss tangents ($G''/G' = J''/J'$) for these three polymers are 3.55, 2.75, and 1.65, respectively.

TREATMENT OF DIELECTRIC DATA

For comparison with the dispersion of mechanical properties, the dielectric data of Mead and Fuoss (3) may be subjected to a similar reduction treatment to provide the components of the complex dielectric constant over an extended frequency range. The method previously used for di-

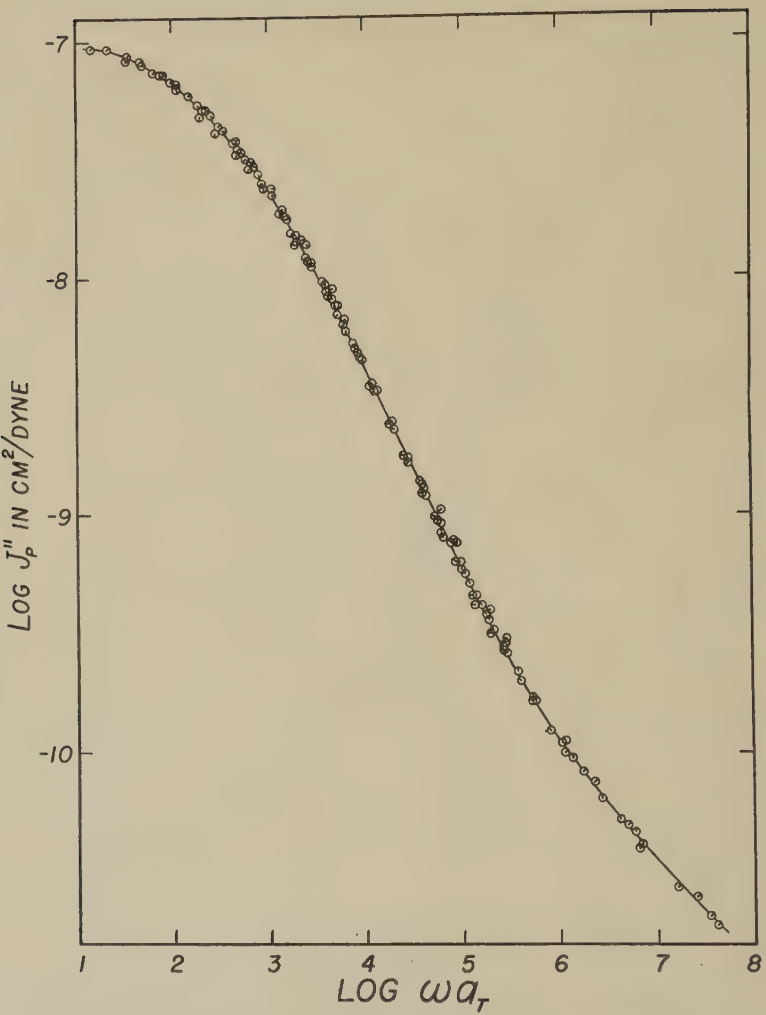

FIG. 4. Imaginary part of the complex compliance reduced to 75°C., plotted logarithmically against reduced frequency. Temperature key same as in Figs. 1 and 2.

electric data of polyvinyl chloride compositions (11)—identical with the reduction formulas for J' and J'' except for the interchange of ρ and ρ_0—turns out to be inapplicable in this case because ϵ_0, the low-frequency limiting value of ϵ', falls with increasing temperature faster than proportional to ρ/T. (This fact led, for example, to values of dipole moment calculated by Mead and Fuoss which decreased substantially with increasing temperature.) For the present purpose, the temperature dependence of ϵ_0 will be circumvented by normalizing both components of $\epsilon^{\pm}$ at each temperature, using as variables $(\epsilon' - \epsilon_\infty)/(\epsilon_0 - \epsilon_\infty)$ and $\epsilon''/(\epsilon_0 - \epsilon_\infty)$. The

TABLE I

Reduction Factors

Mechanical		Electrical		
Temp., °C.	Log a_T AYAX 1232	Temp., °C.	Log b_T	
			Gelva 60	Gelva 15
49.9	3.12	40		4.86
54.9	2.34	45	4.06	3.85
59.8	1.64	48	3.50	3.31
64.9	1.02	51	2.99	2.85
69.8	0.50	54	2.49	2.40
74.7	0.02	57	2.05	1.99
79.9	−0.39	60	1.64	1.63
84.5	−0.75	63	1.28	1.26
90.0	−1.12	66	0.91	0.94
		69	0.59	0.58
		71		0.35
		72	0.29	
		75	0.00	0.00
		80	−0.41	−0.42
		85	−0.80	
		90	−1.19	
		95	−1.53	
		100	−1.83	
		105	−2.08	

value of ϵ_∞ is taken as the square of the refractive index, 2.16 (3); ϵ_0 is taken as the limiting value of ϵ' from 72°C. to 105°C., and at other temperatures, where the dispersion data are incomplete, it is extrapolated from a plot of ϵ_0 against temperature, which fits the empirical equation $\epsilon_0 = 8.28 - 0.039(T - 348)$.

From plots of the above normalized variables against frequency, values of log b_T, the factor expressing the change of all *electrical* relaxation times with temperature, were obtained, and those from the real and imaginary components were found to be in good agreement. Values of log b_T obtained in this way from data for two samples of polyvinyl acetate (Gelva 15, intrinsic viscosity in cyclohexanone at 25°C., 4.25, and Gelva 60, intrinsic viscosity, 9.25) are given also in Table I, and are plotted together with log a_T in Fig. 6. There is good agreement in b_T for the two samples, although below 55°C. those for Gelva 60 are slightly higher. The values of a_T for our sample AYAX also agree very well with the others, though its molecular weight as judged from intrinsic viscosity is considerably less. Thus the expectation that the temperature dependence of relaxation times should be scarcely affected by molecular weight, and that a_T and b_T should be identical (12), is confirmed. The observation has also been made by Sack

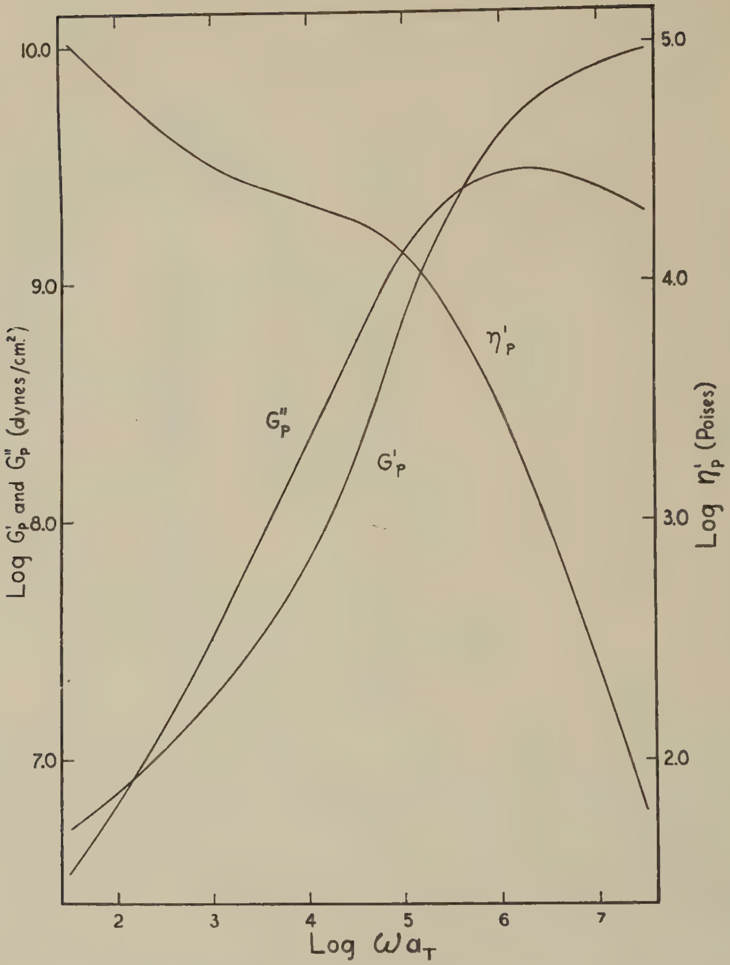

FIG. 5. Real and imaginary parts of the complex shear modulus and real part of the complex viscosity, reduced to 25°C., plotted logarithmically against reduced frequency.

et al. (13) that the temperature dependences of mechanical and electrical relaxations are identical, although apparently over a temperature range where the variation of ΔH_a was not detected.

Finally, $(\epsilon' - \epsilon_\infty)/(\epsilon_0 - \epsilon_\infty)$ and $\epsilon''/(\epsilon_0 - \epsilon_\infty)$ were plotted logarithmically against ωb_T for both the Gelva samples, and in each case data at all frequencies and temperatures superposed to give a composite curve reduced to 75°C. The pair of curves for Gelva 60 are shown in Fig. 7; the others will be published elsewhere (14). (The points lying below the ϵ' curve in Fig. 7 are nearly all from measurements at 10,000 cycles, and perhaps reflect a systematic error at this frequency. Values of ϵ'' below a reduced frequency

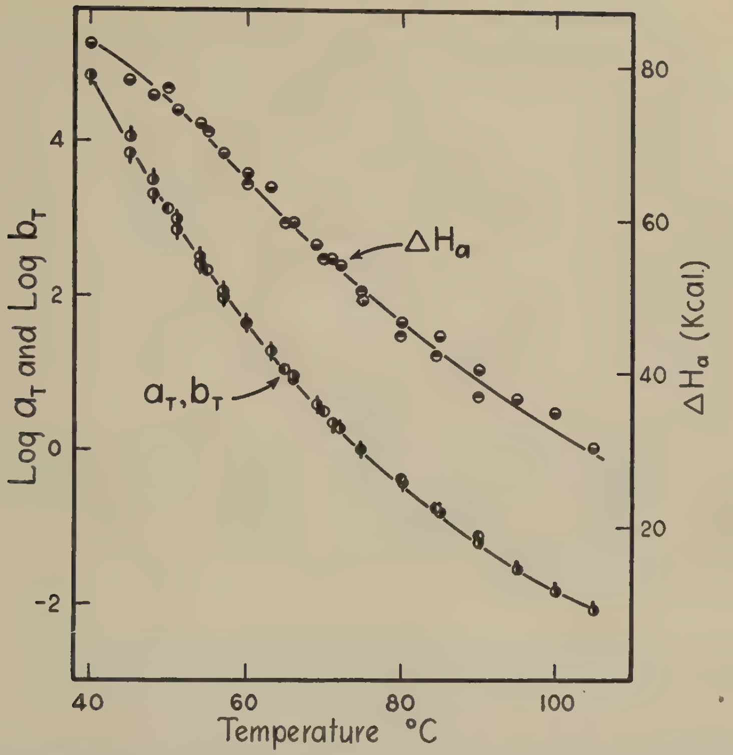

FIG. 6. Logarithm of reduction factors a_T and b_T and the apparent activation energy for relaxation plotted against temperature. Key to circles: left black, a_T from polyvinyl acetate AYAX; right black, pip up, b_T from Gelva 60; right black, pip down, b_T from Gelva 15; top black, ΔH_a from a_T; bottom black, from b_T.

of 10^2 are not included, because they are influenced by high temperature conductance.)

DISTRIBUTION FUNCTIONS

The mechanical distribution functions, $\Phi\, d \ln \tau$ and $L\, d \ln \tau$, represent the differential contributions to instantaneous rigidity and steady-state compliance, respectively, associated with relaxation and retardation times whose logarithms lie between $\ln \tau$ and $\ln \tau + d \ln \tau$. The function Φ can be calculated from G' or G'', and L from J' or J'', by second approximation formulas previously given (15). Values thus derived from the data of Figs. 3 and 4 are listed in Table II and plotted with logarithmic scales in Fig. 8. In each case the value derived from the real component (G' or J') agrees well with that from the imaginary (G'' or J''), except at the low end of the time scale, where the calculation becomes somewhat uncertain. As in previous tests of the second approximation formulas, the agreement be-

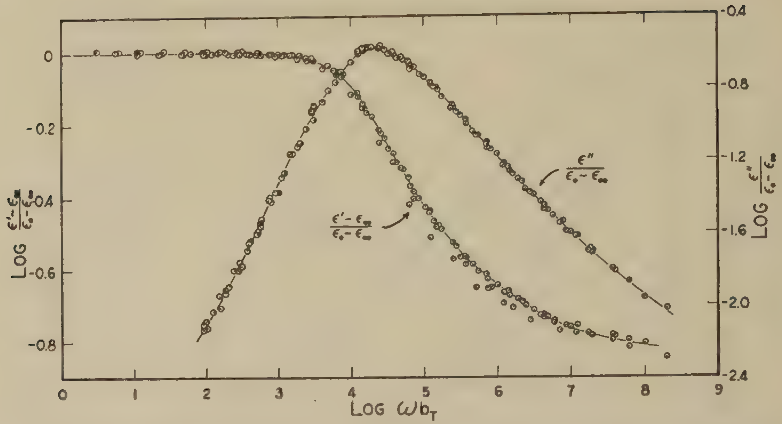

FIG. 7. Real and imaginary parts of the dielectric constant (data of Mead and Fuoss), normalized and reduced to 75°C., plotted logarithmically against reduced frequency for Gelva 60. Temperature key: pip left, 45°C. (at highest reduced frequency); succeeding 45° rotations of pip counterclockwise correspond to 48°, 51°, 54°, 57°, 60°, 63°, 66°, 69°, 72°, 75°, 80°, 85°, 90°, 95°, 100°, 105°C., ending with pip left (at lowest reduced frequency).

tween real and imaginary sources is better than when the earlier first approximation formulas are used. The agreement is an excellent confirmation of the internal consistency of the experimental data.

An alternative higher approximation method, given by Schwarzl and Staverman (16), provides the following formulas for determining Φ, in our notation:

$$\Phi_{\tau=1/\omega} = G' \frac{d \log G'}{d \log \omega} - \frac{G'}{4}\left[\frac{d^3 \log G'}{d(\log \omega)^3} + 3\,\frac{d^2 \log G'}{d(\log \omega)^2}\,\frac{d \log G'}{d \log \omega} + \left(\frac{d \log G'}{d \log \omega}\right)^3\right]$$

$$\Phi_{\tau=1/\omega} = \frac{2G''}{\pi}\left\{1 - \left[\frac{d^2 \log G''}{d(\log \omega)^2} + \left(\frac{d \log G''}{d \log \omega}\right)^2\right]\right\}$$

Calculations of Φ from these formulas are also given in Table II. Here, also, there is good agreement between the values from the real and imaginary components, and the two approximation methods yield essentially equivalent results. Another method of calculation, which is exact but laborious to apply, has been described by Roesler and Pearson (17).

A distribution function of electrical relaxation times can be calculated in the same way from ϵ' and ϵ''. Application of our formulas (15) to the normalized variables of Fig. 7 yields a normalized distribution function, Ψ_n; the function Ψ previously calculated for polyvinyl chloride compositions (12) is $\Psi_n(\epsilon_0 - \epsilon_\infty)$. The distribution Ψ_n is also plotted in Fig. 8, and

TABLE II

Relaxation and Retardation Distribution Functions, Reduced to 75°C.

log τ	log Φ (relaxation), dyne/cm.^{2}				log L (retardation), cm.^{2}/dyne, W-F Appx.[a]	
	W-F Appx.[a]		S-S Appx.[b]			
	From G'	From G''	From G'	From G''	From J'	From J''
−1.5	6.14	6.08	6.12	6.05	−7.22	−7.23
−2.0	6.33	6.33	6.30	6.29	−7.42	−7.37
−2.5	6.59	6.56	6.57	6.54	−7.60	−7.63
−3.0	6.84	6.85	6.89	6.81	−8.05	−8.15
−3.5	7.10	7.22	7.04	7.17	−8.55	−8.54
−4.0	7.50	7.57	7.13	7.60	−9.10	−9.12
−4.5	8.07	7.96	7.97	8.03	−9.71	−9.52
−5.0	8.55	8.69	8.86	8.99	−10.00	−9.94
−5.5	9.08	9.18	9.28	9.31	−10.29	−10.17
−6.0	9.30	9.26	9.44	9.40	−10.52	−10.38
−6.5	9.18	9.30	9.06	9.38	−10.80	−10.57
−7.0	9.07	9.21	8.90	9.26	−10.92	−10.77
−7.5	9.11	9.09	9.01	9.13	−11.17	−10.98

[a] Williams and Ferry approximation (15).

[b] Schwarzl and Staverman approximation (16).

shows excellent agreement between real and imaginary sources except just at the right of the maximum.

In comparing L with Ψ_n, it is noted, as for polyvinyl chloride compositions, that Ψ_n is flatter and its maximum lies at shorter times by several powers of ten. The displacement of the time scale would no doubt be further enhanced if measurements on the same polymer sample were being compared; Gelva 60 has about ten times the intrinsic viscosity of AYAX, and in accordance with Fuoss's observations (3, 18) the electrical distribution of the latter should lie about one power of ten to the left of that of the former. The difference between L and Ψ_n is attributed, as before (12), primarily to the fact that the maximum compliance is inversely proportional to the number of molecules per unit volume but the maximum polarization depends on their mass and is therefore practically independent of molecular weight; qualitatively, the short-time contributions are weighted more heavily in Ψ_n than in L. A further complication, of course, may arise from the ability of the side-chain dipole in polyvinyl acetate to orient without co-operation of the chain backbone. Nevertheless, the identity of a_T and b_T suggests that in the region of time scale shown in Fig. 8 the electrical, like the mechanical, responses involve largely backbone motions.

TEMPERATURE DEPENDENCE OF RELAXATIONS

From the values of a_T and b_T plotted in Fig. 6, the apparent activation energies for mechanical relaxation (or retardation) and electrical relaxation

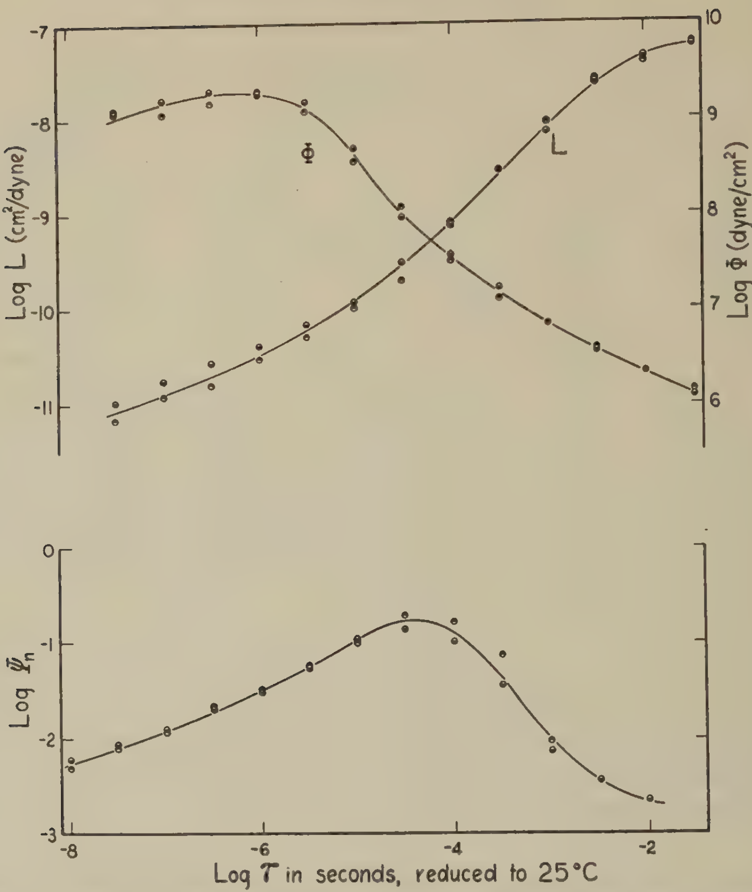

FIG. 8. Distribution functions of mechanical relaxation times (Φ), mechanical retardation times (L), and electrical relaxation times (Ψ_n), plotted logarithmically, reduced to 75°C. Key to points: top black, calculated from G'_p, J'_p, or $(\epsilon' - \epsilon_\infty)/(\epsilon_0 - \epsilon_\infty)$; bottom black, from G''_p, J''_p, or $\epsilon''/(\epsilon_0 - \epsilon_\infty)$.

may be calculated by the usual differentiation procedure. These values are also plotted in Fig. 6. The activation energy increases from 30 kcal. at 105°C. to 82 kcal. at 40°C., rising steeply with decreasing temperature as the glass transition (28°C.) is approached, as observed in other polymers. This behavior, like that of the temperature dependence of steady-flow viscosity, reflects primarily changes in a segmental or monomeric friction coefficient (19), which involves volume and energy requirements for local co-operative motions (19, 20).

ACKNOWLEDGMENTS

This work was part of a program of research on the physical structure and properties of cellulose derivatives and other polymers supported by the Allegany Ballistics

Laboratory, Cumberland, Maryland, an establishment owned by the United States Navy and operated by the Hercules Powder Company under Contract NOrd 10431. It was also supported in part by a grant from Research Corporation and by the Research Committee of the Graduate School of the University of Wisconsin from funds supplied by the Wisconsin Alumni Research Foundation. The fellowship in Physical Chemistry given by Union Carbide and Carbon Corporation is gratefully acknowledged. We are much indebted to Mrs. J. C. Alexander for assistance in calculations.

SUMMARY

The real and imaginary components of the complex compliance have been measured between 30 and 5100 cycles/sec. at nine temperatures between 50°C. and 90°C. on an unfractionated sample of polyvinyl acetate (M_n = 140,000, M_w = 420,000). The results superpose by the method of reduced variables to give composite curves covering the transition from rubberlike to glasslike consistency as a function of frequency at 75°C. From these, the reduced curves for the real and imaginary parts of the complex shear modulus, and the real part of the complex viscosity, have been calculated. Earlier data of Mead and Fuoss on dielectric dispersion and dielectric loss of polyvinyl acetate have been reduced to 75°C. in the same manner, and the mechanical and electrical reduction factors are found to be identical. The apparent activation energy for mechanical and electrical relaxation increases sharply with decreasing temperature, as observed for other polymers. Distribution functions of mechanical relaxation and retardation times, and of electrical relaxation times, have been calculated from both real and imaginary components of modulus, compliance, and dielectric constant, respectively. The results of the approximation formulas of Williams and Ferry and of Schwarzl and Staverman are found to be closely similar. The electrical relaxation spectrum is somewhat flatter, and lies at shorter times, than the mechanical retardation spectrum.

REFERENCES

1. FITZGERALD, E. R., GRANDINE, L. D., JR., AND FERRY, J. D., *J. Applied Phys.* **24,** 650 (1953).
2. GRANDINE, L. D., JR., AND FERRY, J. D., *J. Applied Phys.* **24,** 679 (1953).
3. MEAD, D. J., AND FUOSS, R. M., *J. Am. Chem. Soc.* **63,** 2832 (1941).
4. BROWNING, G. V., AND FERRY, J. D., *J. Chem. Phys.* **17,** 1107 (1949).
5. SAWYER, W. M., AND FERRY, J. D., *J. Am. Chem. Soc.* **72,** 5030 (1950).
6. FERRY, J. D., SAWYER, W. M., BROWNING, G. V., AND GROTH, A. H., JR., *J. Applied Phys.* **21,** 513 (1950).
7. FERRY, J. D., FOSTER, E. L., BROWNING, G. V., AND SAWYER, W. M., *J. Colloid Sci.* **6,** 377 (1951).
8. WILLIAMS, M. L., AND FERRY, J. D., *J. Colloid Sci.* (to be submitted).
9. FITZGERALD, E. R., AND FERRY, J. D., *J. Colloid Sci.* **8,** 1 (1953).
10. WILEY, R. H., AND BRAUER, G. M., *J. Polymer Sci.* **4,** 351 (1949).
11. WILLIAMS, M. L., Ph.D. Thesis, University of Wisconsin, 1954.
12. FERRY, J. D., AND FITZGERALD, E. R., *J. Colloid Sci.* **8,** 224 (1954).

13. Sack, H. S., Cuykendall, T. R., and Woods, T. J., *Phys. Rev.* **94,** 1414 (1954).
14. Ferry, J. D., Williams, M. L., and Fitzgerald, E. R., *J. Am. Chem. Soc.* (to be submitted).
15. Williams, M. L., and Ferry, J. D., *J. Polymer Sci.* **11,** 169 (1953).
16. Schwarzl, F., and Staverman, A. J., *Appl. Sci. Research* **A4,** 127 (1953).
17. Roesler, F. C., and Pearson, J. R. A., *Proc. Phys. Soc. (London)* **B67,** 338 (1954).
18. Fuoss, R. M., *J. Am. Chem. Soc.* **63,** 2401 (1941).
19. Bueche, F., *J. Chem. Phys.* **21,** 1850 (1953).
20. Fox, T. G., Jr., and Flory, P. J., *J. Applied Phys.* **21,** 581 (1950).

BOOK REVIEWS

Proceedings of the Second International Congress on Rheology. Edited by V. G. W. Harrison. Academic Press Inc., New York 10, N. Y., 1954. 451 pp. Price $10.

Some 245 members from 15 countries and 50 guests comprised this Congress held in Oxford in July, 1953. The aim of the Congress was to cover the extended field of the "study of the deformation and flow of matter" as widely as possible. The present volume reflects that objective.

The volume opens with the Presidential address, "Rheology for Mathematicians," by Sir Geoffrey Taylor, F.R.S., given in a light vein but nonetheless interesting, informative, and orienting in respect to modern developments. Then follow 55 contributions by well-known authors; 47 are in English, 5 in French, and 3 in German; under the subheadings of General Lectures, High Polymers, Viscosity and Plasticity, Biology, Oils and Greases. There is a Table of Contents and a Subject Index. An author index would have been helpful, especially as an aid in finding the names of the contributors to the printed discussions which follow the majority of the papers. Aside from this omission, one can speak only in high praise of this volume.

The Congress gives evidence of being well organized; the printed record is one which every serious student of Rheology will need on his shelf for ready reference. The format of the book is excellent.

Victor K. La Mer, New York, New York

Chemistry of the Lanthanons. By R. C. Vickery, D.Sc., Ph.D. Butterworths Scientific Publications, London, and Academic Press, Inc. New York, 1953. viii + 296 pp. Price $6.

To produce a complete text on the chemistry of the lanthanides (called lanthanons by the author) is indeed a formidable task. The 1928/32 edition of Gmelin's Handbook devoted 1109 pages to the subject. Mellor (1924) covered it in a mere 215 pages. Of the new Gmelin volume (1938) only the first part (history and occurrence) has appeared. It alone takes 122 pages.

The present monograph is apparently designed to meet the demand until the larger handbooks are brought up to date. It covers the subject far more extensively than the recent book by Yost, Garner, and Russell, exceeding the latter work more than three times in length. The literature is said to have been abstracted through December 1951, though many references dating from 1952 and 1953 will be found as well.

About one-half of the book is devoted to analytical methods. The compounds occupy nearly one-fifth of the book, and the remainder is divided into chapters dealing with the history, occurrence, physical properties, and uses of the elements.

The book contains a wealth of up-to-date information, and being by far the most complete treatise written on the subject in recent years, will certainly arouse wide interest. It is regrettable that this very praiseworthy effort of an experienced worker in the field has not been a complete success.

Throughout the book, one is constantly disturbed by the author's partiality. All too often does he overlook priority rights, failing to give credit where credit is due. References to the work of others are often omitted, so that one easily mistakes the author for the discoverer (e.g., pp. 82, 83, 125, 126, etc.). In many cases, no references on the origin of tables and graphs are given.

One might also disagree with the author's way of deciding controversial issues, such as the existence of bipositive neodymium (pp. 62, 76, 133, 134) or the color of CeO_2 (p. 209). His high esteem for the excellent work of J. K. Marsh, as manifested on nearly every page in the book, is quite understandable; however, it should not lead to extremes such as the postulation of an untenable mechanism (e.g., p. 133) for the sole purpose of backing an accidental, and possibly erroneous, observation by the latter author.

People who like to separate lanthanides by ion exchange (as is the trend these days) will search the subject index in vain. True, the matter is taken up twice in the text (pp. 147, 148 being an almost verbatim repetition of p. 82, oddly enough), but except for occasional passing remarks, the subject is ignored almost completely. In the "Complete Separational Scheme," ion exchange is used only in the final purification of the individual elements, the separation having been accomplished by conventional methods. Statements like: "James crystallized thulium fractions 15000 times before attaining any reasonable purity"; ". . . after 7 months' work most of the Dy had been separated"; ". . . it will require approximately a year to reach this point"; sound like reports of Columbus' voyage in an age of trans-Atlantic flights.

Many inaccurate or outmoded statements have found their way into the book (e.g., pp. 9, 10, 11, 14, 23, 30, 41, 42, 72, 73, 74, 75, 76, 77, 80, 124, 128, 135, 185, 215, 233, 242). Mistakes of this kind are particularly dangerous because of their tendency to perpetuate themselves.

One must hope that these shortcomings will be eliminated in a future edition, and that this book, containing the vast fund of the author's experience, will then be ready to fill the long-standing need for a textbook on the lanthanides.

EDWARD A. ALPEROVITCH, Urbana, Illinois

Interscience Manuals. Interscience Publ., Inc., New York, and Interscience Publ., Ltd., London, 1952–1954.

Manual No. 1: *Statistical Methods for Chemical Experimentation*, by W. L. Gore, 1952, $3.50.

Manual No. 2: *Fiber Microscopy*, by A. N. J. Heyn, 1954, 407 pp. plus 12 plates, $5.50.

Manual No. 3: *Chemical Methods in Industrial Hygiene*, by F. H. Goldman and M. B. Jacobs, 1953, 274 pp. $3.75.

Manual No. 4: *Detergency Evaluation and Testing*, by Jay C. Harris, 1954, 210 pp., $3.75.

To date four manuals have appeared in this series. They will be of value to readers of this Journal interested in special industrial applications.

The principal feature of the series is the assembling in compact form of laboratory procedures which have appeared in a scattered literature. The manual on detergents, in particular, brings to light the complex character of the subject, the provisional nature of the tests, and the need for more fundamental investigations into the mode of action of detergents—a problem which is a primary objective of this Journal.

VICTOR K. LA MER, New York, New York

FOAMINESS OF AQUEOUS SOLUTIONS OF SODIUM ACETATE, SODIUM PROPIONATE, AND SODIUM BUTYRATE, AND OF DILUTE SILICA SUSPENSIONS

Leonard Topper and Eric Baer

The Johns Hopkins University, Baltimore, Maryland

Received September 30, 1954

Introduction

The foaminess of aqueous solutions of soaps and of suspensions of fine solids in these solutions has both theoretical and practical interest. In this paper, the results of pneumatic testing of solutions of sodium acetate, sodium *n*-propionate, and sodium *n*-butyrate, and of very dilute suspensions of 30 mμ silica particles are presented.

Experimental

An apparatus for the pneumatic testing of foaminess was constructed by fitting a 500-cc. round-bottomed flask with a tall tube of ¾-inch diameter. A glass bubbler tube, its open end covered with a cotton gauze, was installed directly below the foam tube. The flask was filled with solution to a height of 10 cm. above the bubbler, and air was admitted at the rate of 900 cc./minute. After 30 minutes, seven measurements of the foam height (difference in level between the top of the foam and the upper boundary of the liquid before frothing) were made at 15-second intervals, and these were averaged. The injection of gas was discontinued, and the collapse time (time from end of bubbling until only one bubble remains) was recorded. When distilled water was used in place of a solution, the foam height was 6.5 cm. and the collapse time 2.0 seconds. The solutions were always at 26°–28°C. The materials used included research–grade sodium acetate, sodium *n*-propionate, and sodium *n*-butyrate from Eimer and Amend Company and a nonporous research sample of 30 mμ nonporous spheroidal silica from The Davison Chemical Company. The initial volume of the solution was 1000 cc.; when silica was added, its mass was 0.025 g.

Results

See Figs. 1 and 2. The foam heights and collapse times of the solutions exhibit maxima at characteristic concentrations. These concentrations were approximately the same for both the foam height and the collapse time.

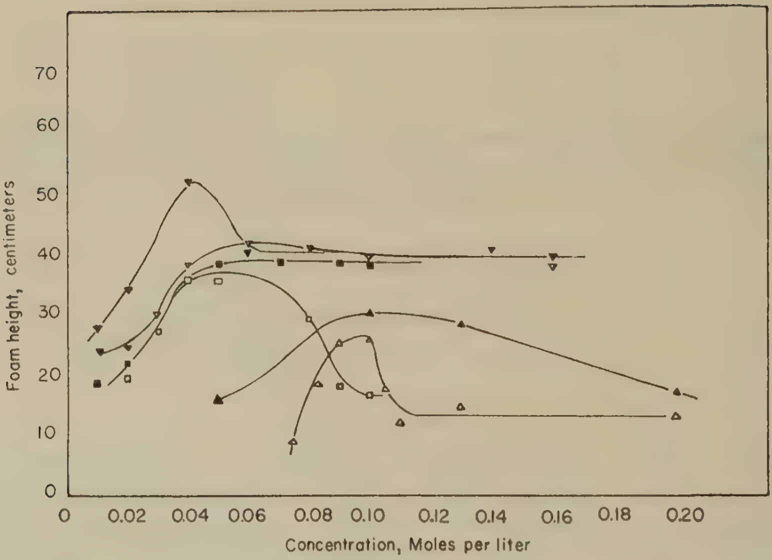

FIG. 1. Foam height of solutions. ▽, sodium *n*-butyrate; □, sodium *n*-propionate; △, sodium acetate. Solid symbols, as above, 0.0025% silica added.

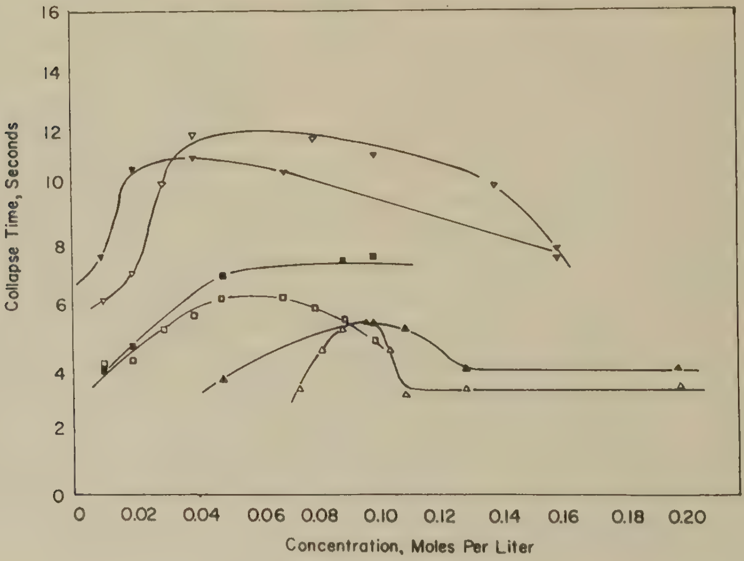

FIG. 2. Collapse time of solutions.

This characteristic concentration increased in the order butyrate, propionate, acetate; both foam height and collapse time decreased when the concentration of the salt was higher than this value, but the decrease was most rapid with the lower members of the series.

The addition of hydrophilic silica particles to the extent of 0.0025% of the weight of the solution increased the foam height of the solutions, particularly at concentrations close to that characteristic of the best foaming solid-free solution. It also extended the range of salt concentrations capable of substantial foam heights. The effect of solids on the foam stability was similar, except that the stability of sodium butyrate solutions more concentrated that 0.035 mole per liter was impaired.

Discussion

The relation of foam height and collapse time to salt concentration is of the same form as was observed by Burcik (1) with sodium laurate solutions, except that the foam heights of sodium acetate and sodium propionate solutions are more sensitive to concentration than are those of higher molecular weight soaps. It appears that the silica particles are effective in improving the foam only in the range of concentrations where the rate of change of foam height (or of collapse time) with concentration is substantial. This range is probably one where surface tension also varies rapidly with concentration (1), so that absorption of solute on the dispersed solid may be important in explaining this effect.

Bartsch (2) found that the maximum collapse time of aqueous isoamyl alcohol solutions containing finely powdered solids was at a concentration near that corresponding to most stable foam without added solids; the present work is in harmony with his experience.

Acknowledgment

The authors are grateful to the Research Corporation for a grant in aid of this work.

Summary

The foaminess of aqueous solutions of sodium acetate, sodium *n*-propionate, and sodium *n*-butyrate, and of an 0.025% suspension of 30 mμ silica particles was studied by the pneumatic method.

Both the maximum foam height and the maximum collapse time of solutions of each salt were associated with the same concentration of solute, and the addition of silica did not shift this concentration appreciably, but did extend the concentration range of good foam height and stability.

References

1. Burcik, E. J., *J. Colloid Sci.* **5**, 421 (1950).
2. Bartsch, O., *Kolloidchem. Beih.* **20**, 1 (1924).

THE EFFECT OF ORGANIC ADDITIVES ON THE RATE OF SURFACE TENSION LOWERING OF SODIUM DODECYL SULFATE SOLUTIONS[1]

Emil J. Burcik and Robert C. Newman

The Pennsylvania State University, College of Mineral Industries, State College, Pennsylvania

Received August 9, 1954; revised received September 20, 1954

INTRODUCTION

Solutions containing a dissolved surface-active agent capable of reducing the surface tension of a solvent have a higher concentration in the solution surface than in the bulk liquid. When the surface equilibrium is disturbed, a finite time is required for the surface-active agent to diffuse to the interface and re-establish equilibrium. The time rate at which the surface tension decreases to its static equilibrium value is determined by a number of variables. This rate is a function of the structure and concentration of the surface-active agent, the temperature, the *p*H of the solution when the surface-active agent hydrolyzes, and the concentration of added electrolytes when the surfactant is ionic (2, 3, 4).

In the past, evidence has been presented which indicates that the rate of surface equilibrium attainment is a factor in foaming and detergency (2, 4). Indeed, this rate should be important in all processes which involve surface energies under nonequilibrium conditions, that is, in processes where dynamic surface energies, rather than static, equilibrium surface energies, are manifest. In view of these concepts, investigations to determine other variables which affect the rate of surface tension lowering are of importance. It will be shown below that certain organic additives have the ability to alter the rate of surface tension lowering of sodium dodecyl sulfate solutions. The additives tested were dodecanol, dodecanoic acid, and decane. The dodecanol and the dodecanoic acid appear to associate with the surfactant. The results show that, in so far as the rate of surface tension lowering is concerned, these association aggregates behave like the acid soaps which form on hydrolysis of an alkali metal soap.

EXPERIMENTAL

Techniques

The vibrating jet method was employed in a previously described manner (2) to measure the rate of surface tension lowering. This method

---

[1] This investigation is a joint undertaking of The Pennsylvania State University Mineral Industries Experiment Station and the Office of Naval Research.

is based on the fact that a liquid jet issuing from a noncircular orifice will produce a series of standing waves along the jet whose wave length is a function of the surface tension. A solution containing a surface-active agent produces a jet for which the wave length of successive waves increases because the surface tension of the liquid is decreasing as it moves outward from the orifice. From the measured wave lengths and the known velocity of the jet, the surface tension can be determined as a function of time.

In these experiments, which were all conducted at 25°C., a constant rate of flow of 83.5 cc./min. was employed. The experimental results reported are the averages of at least two separate determinations. The mean deviation of these determinations was 1.6%.

Static, equilibrium surface tensions were determined with a du Noüy Interfacial Tensiometer. The values reported were corrected by the method of Zuidema and Waters (8).

To determine the effects of organic additives on the rate of surface tension lowering, a solution of sodium dodecyl sulfate was prepared and divided into several parts. One part was used directly to determine the rate of surface tension lowering of the pure surfactants. To each of the other parts a certain percentage by weight (based on the weight of sodium dodecyl sulfate in solution) of different organic additives was introduced and the solution heated to dissolve the additive. After cooling to 25°C. the rate of surface tension lowering was determined. In this way, each solution contained the same concentration of sodium dodecyl sulfate, and any differences observed in their behavior can be attributed to the presence of the organic additive.

Materials

The sodium dodecyl sulfate was prepared from Eastman White Label Lauryl Alcohol (m.p. = 22.2°–22.6°C., Theory = 22.6°C.) by treatment with a mixture of acetic and chlorosulfonic acids. Butanol and water were added and the acid neutralized with $NaHCO_3$ and Na_2CO_3. The sodium dodecyl sulfate was extracted with butanol and the extract boiled to precipitate the inorganic salts and then filtered. After chilling, the addition of ether precipitated the crude product which was filtered and washed with cold ether. The sodium dodecyl sulfate was redissolved in hot butanol and recrystallized as before. It was then extracted with ether in a Soxhlet extractor for 24 hours. A final recrystallization from ethanol yielded the purified sodium dodecyl sulfate (%S = 11.09%, Theory, 11.10%). The surface tension versus concentration curve for this material showed no minimum.

The dodecanoic acid used as an additive was purchased from Eimer and Amend and used as received (m.p. 41.2°–41.9°C.).

The 95% *n*-decane was purchased from Humphrey-Wilkinson, Inc., and used as received.

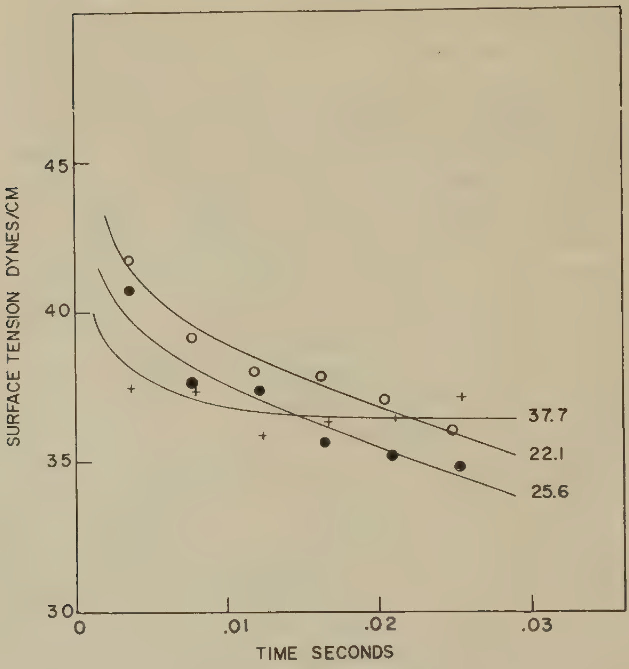

FIG. 1. Surface tension versus time for 0.015 N sodium dodecyl sulfate containing organic additives. Temperature 25°C. + no additive, ○ 7% dodecanol, ● 7% dodecanoic acid. Figures beside the curves represent the static surface tension.

Results

The effect of dodecyl alcohol on the rate of surface tension lowering of 0.015 N sodium dodecyl sulfate at 25°C. is shown in Fig. 1. In this case 7.0% by weight (based on the weight of the sodium dodecyl sulfate) of the alcohol resulted in a decrease of the static surface tension from 37.7 to 22.1 dynes/cm. Furthermore, the addition of the alcohol *decreased* the rate of surface tension lowering, as is shown by the fact that the solution containing only the pure sodium dodecyl sulfate has essentially reached its static surface tension value in less than 0.01 second, whereas the tension of the solution containing the added alcohol becomes equal to that of the pure surfactant after about 0.022 second and is still considerably above its static value after 0.03 second.

Similar results were observed when lauric acid was added to 0.015 N sodium dodecyl sulfate, as shown in the same figure (Fig. 1). In this case 7.0% by weight of dodecanoic acid was added. These results indicate that lauric acid is not as effective as dodecanol in reducing the rate of surface tension equilibrium attainment.

The effect of 7.0% n-decane on the rate of surface tension lowering of 0.015 N sodium dodecyl sulfate is shown in Fig. 2. Since the rates of

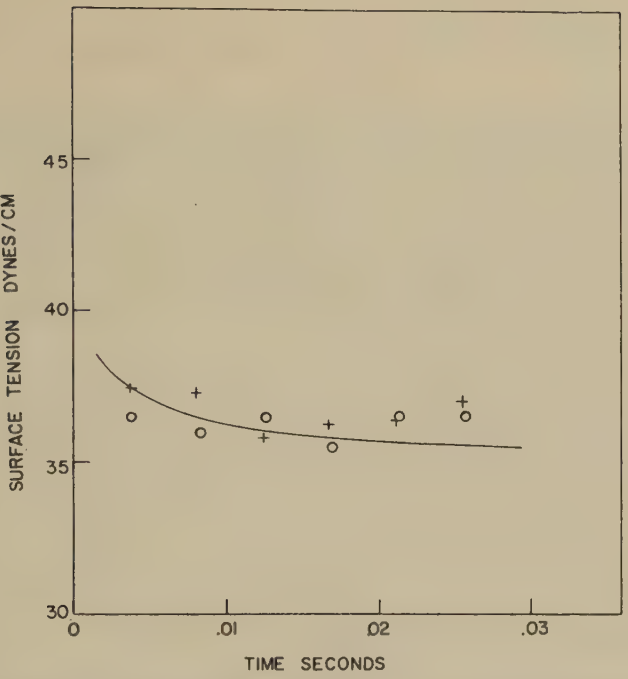

FIG. 2. Surface tension versus time for 0.015 *N* sodium dodecyl sulfate containing decane. Temperature = 25°C. + no additive, static surface tension = 37.7 dynes/cm., ○ 7% decane, static surface tension = 38.2 dynes/cm.

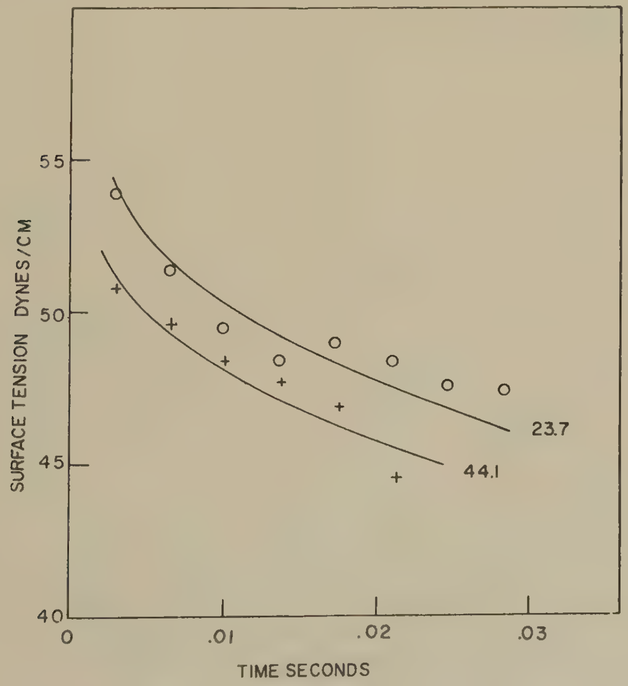

FIG. 3. Surface tension versus time for 0.005 *N* sodium dodecyl sulfate containing dodecanol. Temperature = 25°C. + no additive, ○ 7% dodecanol. Figures beside the curves represent the static surface tension.

surface tension lowering of the two solutions with and without added decane are nearly equal, it can be concluded that the hydrocarbon has no effect on the rate. It is also noteworthy that the added decane has little or no effect on the static surface tension value. The appearance of this solution was also different from those containing added dodecanoic acid and dodecanol. The latter solutions appeared to be colloidally dispersed, but when decane was added some of the hydrocarbon remained undispersed as droplets on the solution surface.

Results with 0.005 *N* sodium dodecyl sulfate and 0.005 *N* sodium dodecyl sulfate containing 7.0% dodecanol-1 are shown in Fig. 3. Here again the solutions were essentially clear and appeared to be colloidally dispersed. The effectiveness of added dodecanol in reducing the rate of surface tension lowering in this relatively dilute solution is apparent. A qualitative test, by the pinacyanole dye method, showed that the 0.005 *N* solution is below the critical micelle concentration, but the solution containing the added dodecanol is above the critical. (Critical micelle concentration for pure sodium dodecyl sulfate = 0.008 *N* (5).)

DISCUSSION

Other investigators have reported strong interactions in surfaces of systems containing a long-chain alcohol and an alkyl sulfate. Brown, Thuman, and McBain (1) have shown that these systems exhibit marked surface plasticity, and Epstein *et al.* (5) report that these systems form slow-draining foams and single films. The latter investigators have also isolated and analyzed several crystalline adducts of sodium alkyl sulfates and long-chain alcohols. Earlier work by Schulman and Rideal (7), using their film penetration technique, indicated strong interactions when sodium cetyl sulfate was introduced beneath a monolayer of cetyl alcohol. They also found that systems which show strong association in surface films are likely to form complexes in solution as well.

The results reported in this paper provide further experimental evidence that dodecanol and dodecanoic acid associate with sodium dodecyl sulfate. When this association occurs, the more mobile ions of the pure surface-active agent are partially replaced by highly surface-active aggregates. The increased molecular weight reduces the rate of diffusion and the increased surface activity reduces the critical micelle concentration, which causes a reduction in the ion concentration. Both of these effects tend to reduce the rate of surface tension lowering. It is suggested that this association is the result of hydrogen bond formation between the alcohol or carboxyl group and the oxygen atoms in the sulfate group. This accounts for the absence of any effect on the rate of surface tension lowering by the addition of decane, since hydrogen bond formation would not be possible in this case.

The behavior of sodium dodecyl sulfate with an organic additive which associates is analogous to the behavior of sodium soaps. The acid soap formed by hydrolysis of sodium myristate, for example, is analogous to the aggregates which form when dodecanol is added to sodium dodecyl sulfate. Repression of hydrolysis in sodium myristate solutions by the addition of alkali causes an increase in surface tension (6) which is similar to the behavior of sodium dodecyl sulfate when the organic additive is removed. The effects on the rate of surface tension lowering are also analogous. Repression of hydrolysis in sodium myristate solutions results in a marked increase in the rate of surface tension lowering while addition of free myristic acid results in the formation of more acid soap so that a decrease in rate of surface tension lowering is observed (3). This behavior is again comparable to the behavior of sodium dodecyl sulfate described herein.

SUMMARY

1. Addition of dodecanol-1 or dodecanoic acid to solutions of sodium dodecyl sulfate lowers the static surface tension of the solution and causes a *decrease* in the rate of surface tension lowering.

2. Addition of *n*-decane to solutions of sodium dodecyl sulfate does not cause these effects.

3. These results suggest that dodecanol-1 and dodecanoic acid associate with the sodium dodecyl sulfate. These association aggregates behave similarly to acid soaps with regard to their effects on the static and dynamic surface tensions.

REFERENCES

1. BROWN, A. G., THUMAN, W. C., AND MCBAIN, J. W., *J. Colloid Sci.* **8,** 491 (1953).
2. BURCIK, E. J., *J. Colloid Sci.* **5,** 421 (1950).
3. BURCIK, E. J., AND VAUGHN, C. R., *J. Colloid Sci.* **6,** 522 (1951).
4. BURCIK, E. J., *J. Colloid Sci.* **8,** 520 (1953).
5. EPSTEIN, M. B., WILSON, A., JACOB, C. W., CONROY, L. E., AND ROSS, J., *28th. National Colloid Symposium* (1954).
6. POWNEY, J., *Trans. Faraday Soc.* **31,** 1510 (1935).
7. SCHULMAN, J. H., AND RIDEAL, E. K., *Proc. Roy. Soc.* (*London*) **B122,** 29 (1937).
8. ZUIDEMA, H. H., AND WATERS, G. W., *Ind. Eng. Chem.* **13,** 312 (1941).

THE BEHAVIOR OF LINEAR POLYMERS AT INTERFACES

Hiroshi Hotta

The Institute of Scientific and Industrial Research, Osaka University, Sakai,
Osaka, Japan

Received July 30, 1954

Abstract

Monolayers of synthetic linear polymers were studied by means of measurements of interfacial pressure and potential at air/water and oil/water interfaces. The polymers examined were: poly-*N*-vinyl pyrrolidone, polyvinyl acetate, polyvinyl stearate, polymethyl methacrylate, polymethacrylic acid, copolymers of polymethacrylic acid and diethylaminoethyl vinyl ether, poly-ϵ-caproamide, polyethylene terephthalate, and polyacrylonitrile. All the polymers except polyvinyl acetate give films of the condensed type at the air/water interface, whereas all the polymers except polyethylene terephthalate and polyacrylonitrile give films of the expanded type at the oil/water interface. The film of the condensed type gives a constant surface moment up to a collapse point, and the true molecular weight can be obtained from the surface pressure. The film of the expanded type gives a constant surface moment at larger areas, but the moment changes at a certain area. In this case, a smaller molecular weight than the true one is obtained from the surface pressure. The film of the expanded type at the oil/water interface has segments in the main chain as a statistical kinetic unit, each consisting of about 48 skeletal atoms, and is discussed in the light of the Singer equation of state. The value of surface moment is determined chiefly by the orientation of the C=O bond. The behavior of an ampholyte was studied by the measurement of interfacial potential. The results showed that the amine groups could not be ionized more than about 20 mole per cent owing to the strong cohesion between major nonionized carboxyl groups at the air/water interface, but such a restriction was not found at the oil/water interface owing to the sufficiently expanded state. The extension of these conclusions to proteins is suggested.

Introduction

Surface films of synthetic high polymers were studied systematically first by Crisp in 1946 (1, 2). As the constitutions of synthetic high polymers are not only generally well known but also can be varied as desired, they are well suited to an investigation of surface behavior. Furthermore, their study may provide a useful key to the behavior of organic substances in nature.

We have carried out for some years a series of studies of synthetic linear polymers by means of measurements of interfacial pressure and potential at air/water and oil/water interfaces to obtain information on the general behavior of linear polymers at interfaces. The copolymers especially gave many interesting results. Although the results for each polymer have been published (3, 4, 5, 6, 7, 8), we will discuss the relationships between all these results in the present paper.

EXPERIMENTAL

The surface pressure and potential of films spread at the air/water interface were measured simultaneously by the hanging plate method and the vibrating electrode method, respectively, using standard techniques. The low surface pressure associated with the determination of molecular weight was measured by a surface balance of the Langmuir-Adam type (3).

Films were spread at a petroleum ether (b.p. 100°–140°C.)/water interface, using a micrometer syringe according to Alexander and Teorell's method (9). Only a film of polyethylene terephthalate was spread at the benzene/water interface. The interfacial pressure and potential were measured by the ring method (4, 10) and the vibrating electrode method (7, 11), respectively.

Measurements were made at room temperature without any special temperature regulation, but the variation of temperature during the determination of a single curve never exceeded one degree. Distilled water was used as the substrate for nonelectrolyte. The *p*H for the polyelectrolyte was adjusted with hydrochloric acid or sodium hydroxide, and measured with *p*H test paper. Detailed descriptions of apparatus and procedure were given in the previous papers (3, 4, 7).

The polymers and the solvents used for spreading are shown in Table I.

TABLE I

Principal Polymers Used in the Present Paper

Abbreviations	Polymers	Spreading solvents	References At A/W	References At O/W
PVP	Poly-*N*-vinyl pyrrolidone	Water + pyridine (4/1)	8	8
PVAc	Polyvinyl acetate	Benzene	3	4
PVS	Polyvinyl stearate	Benzene	3	4
PMM	Polymethyl methacrylate	Benzene	5	5
Amilan	Poly-ϵ-caproamide	Water + conc. H_2SO_4 + isopropyl alcohol (5/1/4)	4, 5	4, 5
PMA	Polymethacrylic acid	Water + pyridine (4/1)	5, 6	7
PMA-DAV	Copolymers of PMA with diethylaminoethyl vinyl ether	Water + pyridine (4/1)	6	7
PET	Polyethylene terephthalate	Benzene + cresol (4/1)	8	8
PAN	Polyacrylonitrile	Dimethylformamide	—	5

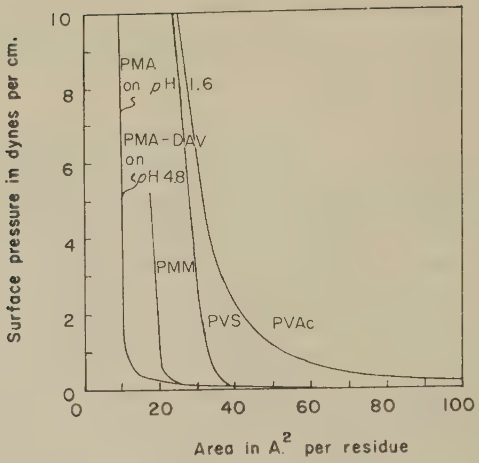

Fig. 1. The surface pressure-area curve of various polymers at the air/water interface.

The abbreviation for each polymer in Table I is used throughout in the present paper. The detailed precautions for each polymer are given in the references listed in Table I. The compositions of copolymers were evaluated from the results of elemental analyses. The air/water and oil/water interfaces are abbreviated hereafter as A/W and O/W interfaces, respectively.

Results

The interfacial pressure (π)-area (A) curves of the nonelectrolytic linear polymers of the type of 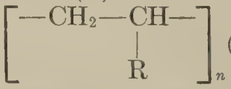 $\left[\begin{array}{c}\text{—CH}_2\text{—}\underset{\displaystyle\text{R}}{\underset{|}{\text{CH}}}\text{—}\end{array}\right]_n$ (R representing a side chain) at the A/W and O/W interfaces are shown in Figs. 1 and 4, respectively. In the case of the polyelectrolyte, only the result under the condition of no effective charge is shown in these figures. In Fig. 4, kink points are shown by arrows. The characteristics of each polymer are described in full in the references shown in Table I. The area for copolymers was calculated as the mean area per vinyl unit from their composition. The surface moment was calculated from the observed surface potential using Helmholtz's formula in the usual manner (3).

Discussion

When we investigate the conditions under which polymers can be spread as a monomolecular film at an interface, the interaction between polymer and upper or lower phase, chiefly the hydrophility and oleophility of the polymer, should be considered first. However, once molecules are spread at the interface as the result of a counterbalance between such interactions with the phases and the intra- and intermolecular forces, the state of the film is chiefly determined by the latter. The various factors may be classified as follows: the effects of medium include (1) the effect of aqueous phase, and (2) the effect of oil phase; and the effects of intra- and intermolecular actions include (3) the cohesion between nonpolar groups, (4) the steric effect of a side chain, (5) the interaction between polar groups, and (6) the interaction between ionized groups. To interpret how the state of the film is influenced by these various effects, we shall discuss first the behavior of nonelectrolytic linear polymers in Sections A and B and then that of polyelectrolytes in Section C.

A. The Behavior of Nonelectrolytic Polymers at the Air/Water Interface

(*a*) *Surface Pressure.* As shown in Fig. 1, most of the linear polymers give films of the condensed type. They have a specific limiting area depending on the nature of the side chain lying at the interface, although the main chain is constant $(\text{—CH}_2\text{—}\underset{|}{\text{CH}}\text{—})$. They have a common limiting area (about 10 A.^{2} per residue) in the case of no side chain lying at the interface. The disposition of the side chain, whether at the interface or not, is more important with copolymers than with homopolymers. That is, the copolymers of vinyl acetate and vinyl stearate (VS), which lay their side chains at the interface, give irregular results and have a smaller limiting area than that of PVS (3), whereas the PMA-DAV copolymers, which lay no side chain at the interface, give reproducible results and have the same limiting area as that of PMA under the condition of no effective charge (6). The latter area is also nearly equal to that of PAN at the O/W interface, as shown later in Fig. 4. On the other hand, PVAc gives a film of the expanded type, but the film of its copolymers with VS is considerably condensed even if it contains only 10 mole per cent VS (3). It is clear in such a case that the cohesion between nonpolar groups makes a film condensed. But, in the case of PMA, the action of hydrogen bonds between the nonionized carboxylic groups contributes considerably to condensation (6, 25). It will be clear later why the film of PVAc is of the expanded type.

It has been confirmed by many investigators that the molecular weight of high polymers determined from surface pressure at the A/W interface agrees satisfactorily with that determined by other methods in the case of natural materials such as protein (12). On the other hand, it has been reported that the monolayer method is unsuitable for some synthetic polymers such as PVAc (13). We obtained the experimental results shown in Table II, that the monolayer method gives fairly good agreement with

TABLE II

Molecular Weight of PVAc and PVS

Polymer	Sample	Molecular weight from		
		Surface pressure	Viscosity	Osmotic pressure
PVAc	a	10,000	58,820	—
	b	7,020	69,350	—
	c	7,920	110,500	—
	d	9,240	—	110,000 ± 5,000
PVS	e	41,000	—	70,000

the bulk method in the case of PVS, whereas it gives a far smaller result than the bulk method in the case of PVAc (3). The reason for the disagreement with PVAc is as follows.

The molecule of PVS is considered to behave as a rigid island in the film of the condensed type at the A/W interface, because of the strong cohesion between the long side chains of the stearyl group (as shown later in Table III). In such a case, where one molecule corresponds to one rigid aggregate, the molecular weight can be determined by the monolayer method, and the result agrees satisfactorily with that by other methods. The good agreement between the monolayer and bulk methods with proteins is because of some rigid structure in the protein, arising from intramolecular hydrogen bonding, interaction between polar groups, or other chemical bonds.

On the other hand, the molecule of PVAc is considered to be fairly loosely packed and is subject to micro-Brownian motion owing to its weak intramolecular cohesion (Table III). Therefore, the film is of the expanded type. In such a case, where one molecule corresponds to more than one kinetic unit, only the molecular weight of the submolecule is determined by the monolayer method, and the result is far smaller than the true one, as shown in Table II.

(b) *Surface Moment.* The observed value of the surface moment of polymers varies with area up to a certain area, shown as $A_{\max}$ in Table III. PVP is the extreme example for a small $A_{\max}$, and does not give a reliable surface moment nearly up to its kink point of surface pressure (8). The maximum area obtainable for a reliable value is denoted hereafter by $A_{\max}$. When we notice the surface moments in the range of area for reliable potentials shown in Fig. 2, they are constant up to the kink point of surface pressure except for PVAc. The case of PVS is somewhat different because there is no constant region but a continuous linear change.

In Fig. 3 for Amilan, the surface viscosity, measured by the oscillating disc method in our laboratory, also varies up to $A_{\max}$ and rises rapidly below $A_{\max}$ (14). It is supposed from these facts that the film of polymer is not always compressed uniformly in all parts of a trough, with a moving barrier, at areas larger than $A_{\max}$ but that compression becomes uniform

TABLE III

Surface Moment and Corresponding Model at the Air/Water Interface

Polymer	Model	Surface moment (*mD.*)	A_{max} (*A.*^{2} *per residue*)
Polyvinyl[a] alcohol	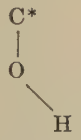	40	50
PMA[b]	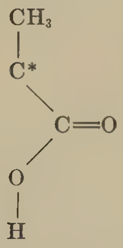	90	65
PET	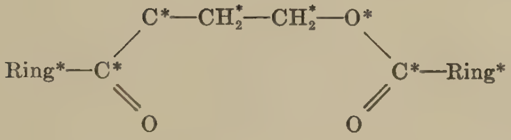	175 × 2	115
PMM	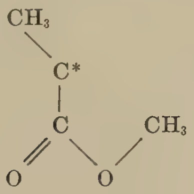	250	25
PVAc	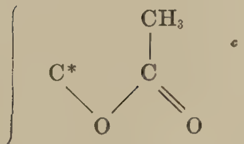	280[c]	—
	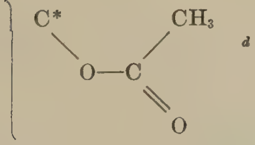	340[d]	70
PVS	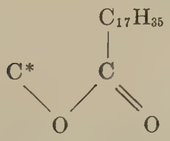	280[c]	55
Polyoctadecyl methacrylate[a]	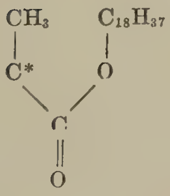	460	45

[a] From Ref. 2.
[b] In the nonionized state.
[c] At 25 A.^{2} per residue.
[d] In the expanded state.

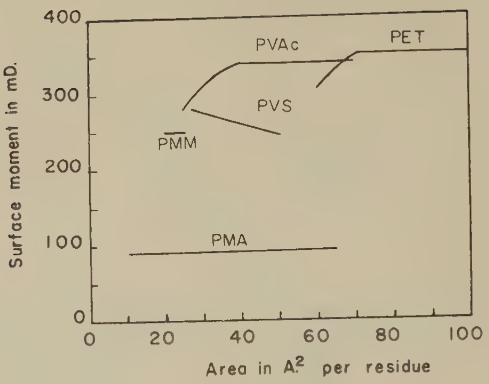

Fig. 2

FIG. 2. The surface moment-area curve of various polymers at the air/water interface.

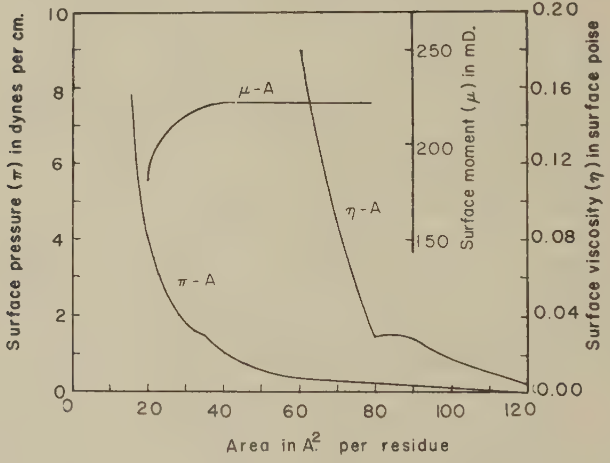

FIG. 3. The surface pressure, moment, and viscosity of Amilan at the air/water interface as the function of area per residue.

at $A_{\max}$. Then, the reproducible surface moment and viscosity can be obtained at $A_{\max}$. Therefore, $A_{\max}$ is also the appropriate measure to study the surface behavior of polymers, which may be affected not only by the specific property of the residue but also by its degree of polymerization. Since the polymer molecule has a rigid structure in a film of the condensed type, as mentioned above, the form of each residue is unchanged with compression. Therefore, they have their surface moment as shown in Figs. 2 and 3. On the other hand, since the polymer molecule has a loosely packed structure in a film of the expanded type, such as PVAc as mentioned above, the form of each residue is transformed to a more packed form from a certain area as compression occurs. Therefore, the surface moment has a bending point in the curve as shown in the case of PVAc in Fig. 2, even if a kink point does not appear in the case of surface pressure. This is also confirmed by the fact that the area at this bending point for PVAc agrees closely with that for the kink point of interfacial pressure for PVS shown in Fig. 4.

In spite of their similar polar groups, the polymers shown in Fig. 2 have different surface moments, as shown in Table III, in which Crisp's data are also included (2). On the other hand, the bond moments of C═O and C—O bonds *in vacuo* are 2.5 and 0.86 D., respectively (15). In the light of the moment and the orientation of these polar bonds at the A/W interface, the most plausible models consistent with the observed surface moments are proposed in Table III, in which the atom of the main chain is shown by a star. In these models polyvinyl alcohol, which has no C═O bond, has the lowest value, and the polymers which have a C═O bond have a higher value with increasing inclination of the C═O. Furthermore, the various limiting areas shown in Fig. 1 and the surface properties of PVAc mentioned above are also understood in the light of these models (5). Therefore, this table would be useful for estimating the inclination of the C═O bond for an unknown polymer.

The interaction between polar groups is a function of the magnitude and direction of dipole moment and of the distance between the groups. But these variables at the interfaces cannot be estimated directly from the data in bulk phase owing to the specific orientation at the interfaces. Furthermore, the orientation is different even between the A/W and O/W interfaces (7, 16). For example, according to Wesson's Table, the dipole moment of all carboxylic acids and their esters is about 1.7 D. (17), while they have different surface moments as mentioned above. On the other hand, polyacrylate and polymethacrylate show a quite different surface behavior (1, 2). The expanding property of PVAc is due not only to the short side chain but also to the large distance between polar groups as shown in Table III. With PAN the dipoles can approach closely parallel to each other because there is no side chain and, in addition, the bond moments are large, 3.6 D. (15, 17). Consequently, it cannot be spread at the A/W interface, and is spread as a film of the condensed type even at the O/W interface, as shown in Fig. 4.

B. The Behavior of Nonelectrolytic Polymers at the Oil/Water Interface

Since the effect of cohesion between nonpolar groups is predominant in most cases at the A/W interface, we investigated behavior at the O/W interface in order to bring out other effects. That is, on dissolving hydrocarbon chains in a hydrocarbon phase, the nonpolar main chain can move

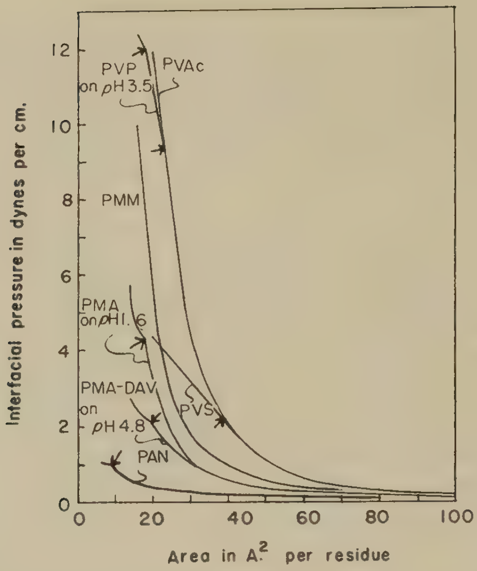

Fig. 4

FIG. 4. The interfacial pressure-area curve of various polymers at the petroleum ether/water interface.

freely at the interface owing to liberation from lateral cohesion. For example, whereas the different behavior between PVAc and PVS at the A/W interface might be attributed to different cohesion of side chains as mentioned above, this cohesion would be eliminated at the O/W interface. In fact, both polymers show entirely identical pressure-area curves up to 2 dynes per cm. at the O/W interface, as shown in Fig. 4.

In such a case, the Flory-Huggins' treatment of flexible linear polymers in bulk solution may be applied to the behavior at the interface. Singer has made the necessary calculation (18), the equation of state at the interface being given to a close approximation by:

$$\pi = \frac{kT}{A}\left\{\frac{x-1}{x}\,\frac{z}{2}\ln\left(1-\frac{2A_0}{zA}\right)-\ln\left(1-\frac{A_0}{A}\right)\right\}, \qquad [1]$$

where π, A, x, A_0, and z are interfacial pressure, apparent area per residue, the degree of polymerization, the actual area occupied by each residue (the size of a surface site), and the co-ordination number around a surface site, respectively. Since z should be 2 in the case of a rigid molecule, Davies defined the increment of z from 2 as surface flexibility (19). His results for synthetic polyamino-acid and protein are shown for comparison in Table IV.

TABLE IV

Polymer	n in Eq. [4]	n_{atom} in Eq. [5]	a_s in Eq. [6]	z^a	
				At O/W	At A/W
PVP[b]	18.5	37	0.6	3.60	—
PVAc	19	38	0.5	3.60	2.20
PVS	19	38	0.5	3.60	2.02
PMM	23.5	47	0	3.75	—
Amilan	6.9	48	0	3.75	—
PMA-DAV[c]	23.5	47	0	3.75	—
PMA[d]	26.5	53	−0.2	3.75	—
PAN	36.5	73	−0.7	2.05	—
PET	13	123.5[e]	−5.8	2.02	—
Polyamino-acid[f]	—	—	—	3.33	—
Human methemoglobin[f]	—	—	—	2.12	2.015

[a] At 0.1 dyne per cm. (A_0 = 5 A.^{2} per skeletal atom).

[b] On the acidic substrate.

[c] At *p*H 5.

[d] At *p*H 1.6.

[e] Assumed on the basis of a ring group being equivalent to 3.5 straight chain atoms in a.

[f] From Ref. 20.

In the limit where $A \gg A_0$, Eq. [1] can be rewritten as

$$\pi A = \frac{kT}{x}\left(1 + \frac{b}{A}\right), \qquad [2]$$

where

$$b = A_0\left(\frac{2 - 2x + zx}{2z}\right) \qquad [3]$$

In fact, when we plot the product of π and A against the reciprocal of A, a curve as shown in Fig. 5 can be obtained. Then, on putting

$$n = (x)_{A=\infty} = \left(\frac{kT}{\pi A}\right)_{A=\infty}, \qquad [4]$$

we can determine the value of n by the extrapolation of such a curve to an infinite area. However, this value is far smaller than that at the A/W interface as well as the true value of x. For example, the values of n and x for PVAc are 19 and about 10^3, respectively (see Tables II and IV). It is concluded from this fact that we must consider a n-mer segment as a statistical kinetic unit at the O/W interface instead of x. The values of n for various polymers obtained by us are shown in Table IV together with the values of n_{atom}, which is defined as

$$n_{\text{atom}} = a\,n, \qquad [5]$$

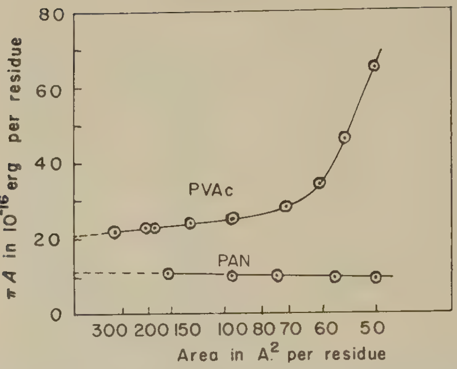

FIG. 5. The product of interfacial pressure (π) and area per residue (A) plotted against the reciprocal of A at the petroleum ether/water interface.

where a is the number of atoms constituting the skeleton of the main chain per residue. In this case, the length of this segment can be expressed on a universal scale. In respect to a, a question rises how many carbon atoms of straight chain might be equivalent to a benzene ring in PET. Since it is reported that a benzene ring is equivalent to 3.5 straight-chain carbon atoms in the effect on the critical micelle concentration for micelle formation (20), we used for convenience this value in Table IV. Flory had estimated from the activation energy for viscous flow that there are approximately 32 atoms in each segment of flow of polyesters (21).

Then, when it is assumed in Eq. [1] that there are segments consisting of n_{atom} skeletal atoms in the very dilute state, and that each skeletal atom occupies apparently one-a'th of the area per residue (A) and actually 5A^2 as the size of a surface site (A_0), we can obtain the value of z at 0.1 dyne per cm., as shown in Table IV. If the side chain affects the behavior of the main chain, the effect may appear in z. For comparison, the values of z for PVAc and PVS at the A/W interface were calculated from the data for Table II (3), and are shown together in Table IV. On the other hand, to estimate the contribution of a side chain to n_{atom}, we calculate the value of a_s shown in Table IV, which is defined by

$$a_s = \frac{48}{n} - a, \qquad [6]$$

on assuming that all segments in the perfectly expanded state should have the length of 48 skeletal atoms. Negative values of a_s occur with larger values of n_{atom} and correspond to the degree of condensation of the monolayer.

On summarizing these results, it is concluded that there is no serious effect of the side chain on z in the sufficiently expanded state. In other words, the above assumptions in our theory are correct for this state. The value of a_s in this state is also equal to about 0.5 for a massive side chain independent of its structure. On the other hand, a low value of z corresponds with a negative value of a_s. The low value of z for PET is due to the complete rigidity of the benzene ring, which is assumed to be equivalent to a flexible chain consisting of 3.5 atoms. From the viewpoint of a_s, the group 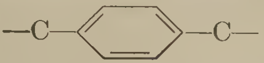 should be considered to be kinetically a rigid unit of flexibility equivalent to -0.3 ($= 5.5 - 5.8$) carbon atoms instead of 5.5 ($= 3.5 + 2$). The behavior of PAN has been already interpreted in terms of the strong interaction between polar groups. However, its film may be expanded if we can select a suitable solvent having a higher dielectric constant, as the oil phase. Proteins show the very condensed behavior even at the O/W interface (22), but to some extent are more expanded than at the A/W interface (19). This difference is shown in z in Table IV. This fact shows, as pointed out already by Davies and also by us, that the links holding the native protein in its characteristic configuration are due not only to cohesion between nonpolar parts, but also, mainly, to interaction between polar groups and intramolecular chemical bonds. The difference between PVAc and PVS at the A/W interface is also shown in Table IV. When we compare them with human methemoglobin at both interfaces, on the basis of z, the degree of expansion of PVAc at the A/W interface becomes clear. Although Davies' results are quoted in the same table, we must remember the difference between n_{atom} and x on comparing all values in Table IV.

Although we have hitherto tried various quantitative interpretations of the "expanded" and "condensed" states, surface elasticity seems to be also the appropriate measure. Bateman and Chambers defined the quantity

$$M = -A\frac{d\pi}{dA} \qquad [7]$$

as surface elasticity (23) and we calculate it at 0.5 dyne per cm., using the data in Fig. 4. For a plot of log M versus log n_{atom}, the points lie perfectly on a straight line expressed by the equation

$$M = \frac{303}{(n_{\text{atom}})^{1.5}}, \qquad [8]$$

as shown in Fig. 6, except for the polymers containing a ring group. However, we must bear in mind that the value of M reflects the uncertainty in the determination of $\frac{d\pi}{dA}$. When the values of n_{atom} for polymers deviating from the straight line are calculated by Eq. [8], a ring group in PET and PVP becomes equivalent to -1.4 and 0.5 skeletal atom of the main

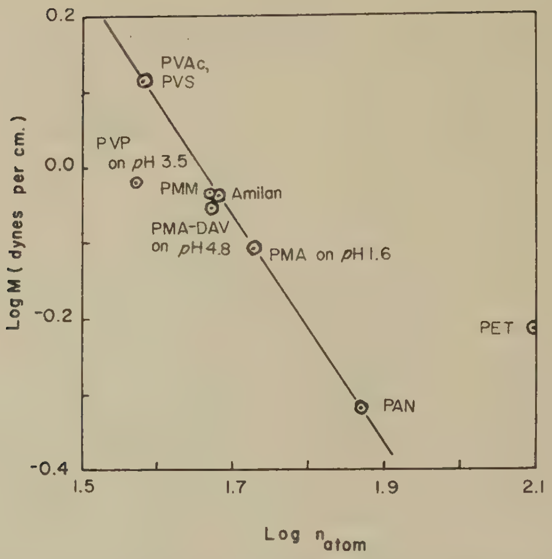

FIG. 6. The log of M at 0.5 dyne per cm. in Eq. [7] plotted against the log of n_{atom} for various polymers at the oil/water interface. The straight line is expressed by Eq. [8].

chain respectively. It is concluded that the ring group in a main chain should be considered in a different way from the ring group in a side chain.

When the kink points in Fig. 4 are compared with the corresponding points in Fig. 1, it is found that a classification can be drawn up in terms of vinyl units: that is, (1) polymers which lay no side chain at the interface have a kink point at 9 ∼ 10 A.^{2}, per vinyl unit as mentioned in Section A; (2) polymers which lay a side chain, consisting of a chain group alone, at the interface have a kink point at about 19 A.^{2} per vinyl unit, which is equal to the second kink point of PVP; (3) polymers which lay a ring group as the side chain at the interface have a kink point at about 24 A.^{2} per vinyl unit. However, these values hold for a condensed structure, and not always for a structure at a larger area. Therefore, it is easily understood by comparison with the model of PVAc at the larger area in Table III that PVS has a kink point at 38 A.^{2} in spite of its being in group II. That is, there is a transformation not accompanied with a kink point of surface pressure as mentioned in the case of the surface moment of PVAc. On the other hand, PVP has a second kink point. The appearance of a kink point depends on the degree of hydrophility of the group, which is transformed at this point. The degree of hydrophility of a polar group may be measured by a study of the adsorption of water on the polymer (24).

C. The Effect of Substrate (*p*H)

Now, we shall consider the effect of substrate. Although there are various problems concerned with some primary or secondary chemical reaction, namely, oxidation, hydrolysis, complex formation, penetration, and adsorption, the most fundamental problem for physical chemistry is the effect of hydrogen ion and neutral salt in a substrate. Among these, only the effect of the *p*H of the substrate on a polyampholyte, namely, the effect of ionization on its surface behavior will be discussed here.

To make this effect clear, we studied the monolayer of PMA and of the copolymers of methacrylic acid with diethylaminoethyl vinyl ether (DAV) at the A/W (6) and O/W (7) interfaces. The mole percentage of DAV for the copolymers K and L is given in Table V. The surface moment of copolymer L at both interfaces is shown in Fig. 7. When we plot the interfacial moment of all samples in the constant range at the larger area at both interfaces against the *p*H of the substrate, the relationship between them becomes as shown in Fig. 8. The trend of PMA in Fig. 8 corresponds closely to the change of the ionization and viscosity of its solution with *p*H, which was interpreted in detail by Katchalsky (25). Therefore, the surface behavior can also be entirely understood by his interpretation of the relationship between the shape of the molecule and the degree of ionization in solution. The constant range of interfacial moment corresponds to the nonionized state, and the range of decreasing moment is due to the ionization of carboxylic groups. In the case of copolymers, it is considered that their carboxylic groups are in the nonionized state in the constant range of interfacial moments, that the degree of ionization of DAV groups is not changed in the same range, and that their interfacial moments decrease with the ionization of carboxylic groups. The ionization of carboxylic groups, which is pronounced even in sample K, is so predominant in the high *p*H range that the interfacial moment becomes negative, but we cannot determine its exact magnitude owing to partial dissolution into the substrate. Therefore, the points in the negative area in Fig. 8 indicate no absolute value but only qualitatively the inversion of sign. The molecular interpretation of this behavior was given in detail in the previous papers (6, 7). On assuming the perfect ionization of DAV groups and the perfect nonionization of carboxylic groups in the constant range, the interfacial moments of DAV groups are calculated as shown in Table V from the mole percentage of DAV and the interfacial moment of nonionized carboxylic groups at the corresponding interface shown in the same table. On the other hand, the interfacial moment of $C_{18}H_{37}N(CH_3)_3^+$ was reported to be 600 mD. or more and equal at both interfaces (11). Therefore, only the value of sample K at the A/W interface in Table V might be inconsistent with the above fact, owing to the incorrect assumption of the perfect ionization of DAV groups. It is concluded from these facts

TABLE V

The Interfacial Moments of Nonionized Carboxylic Group and Ionized DAV Group in PMA and Its Copolymers with DAV at Both Interfaces Estimated from the Data in Fig. 8

		Interfacial moment in mD. of			
		Nonionized carboxylic group		Ionized DAV group	
Sample	Mole percentage of DAV in copolymer	At A/W	At O/W	At A/W	At O/W
K	31	(90)[a]	(15)[a]	450	600
L	20	(90)[a]	(15)[a]	600	600
PMA	0	90	15	—	—

[a] The assumed value used for the estimation of the DAV group.

that the DAV groups of both copolymers are perfectly ionized to the expanded state at the O/W interface, whereas they cannot be ionized more than about 20 mole per cent of total ionizable groups in the condensed state at the A/W interface. That is, there exists a certain minimum distance to which ionized groups can approach in the condensed state of the polyampholyte, owing to the mutual repression of ionization by any closer approach. The residual nonionized DAV groups appear to have a surface moment of about 90 mD. at the A/W interface. Since such a restriction is due to the strong cohesion between nonionized carboxylic groups mentioned already, this is not found for PMA owing to the absence of such a nonionized opposite component. McBain and Peaker have already suggested that the film of stearic acid cannot be much ionized in the solid state (26).

The interfacial moment-area curves of three samples at both interfaces converge to about 90 $\sim$ 100 mD. at 10A.^{2} per residue with a few exceptions as shown in Fig. 7. The trend of curves is also understood in the light of the above conclusion. As the mutual repression of ionization by the approach of already ionized groups takes place with compression, the apparent mean interfacial moment per residue decreases and the difference in all cases disappears at the collapse point, at which the state of the molecules becomes identical with that at the A/W interface. However, the surface moment of sample L at *p*H 4.9 is constant up to the collapse point in Fig. 7. The reason is that a repression does not take place at this *p*H, which corresponds to the isoelectric point of this polyampholyte. This is also concluded from the fact that the value of n_{atom} at this *p*H is identical to that of other similar nonelectrolytic linear polymers in Table IV. All the conclusions from the results of interfacial moment are perfectly consistent with those from the interfacial pressure at both interfaces (6, 7).

The *p*H (*p*H 3.5), from which the interfacial moment of PMA begins to decrease at the O/W interface, is lower than that (*p*H 4.0) at the A/W interface in Fig. 8. Furthermore, the change is sharper at the latter than at the former because the cohesive force connecting ionizable groups is stronger at the latter.

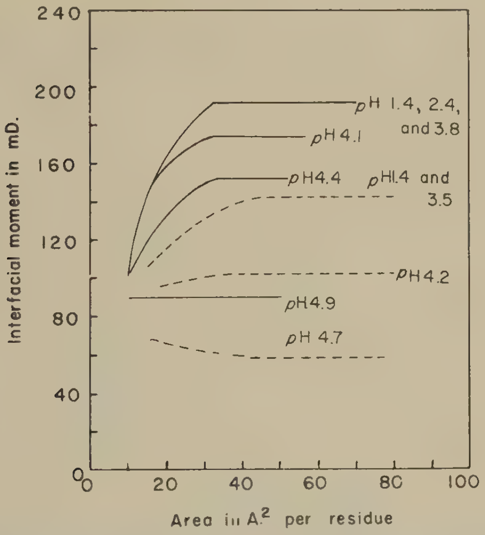

FIG. 7. The interfacial moment-area curve of sample L at the air/water (——) and oil/water (– – –) interfaces on the substrate of various pH's.

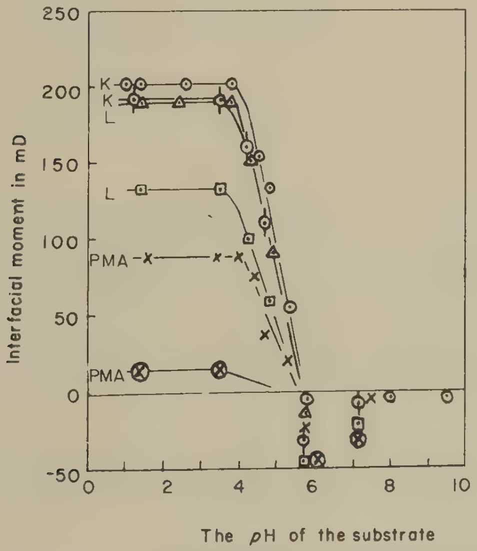

FIG. 8. The interfacial moment of copolymers at the larger area at both interfaces plotted against the pH of the substrate. Symbols in the figure are as follows:

Sample	At A/W	At O/W
K	⊙	⦶
L	△	⊡
PMA	×	⊗

Glazer and Dogan investigated the state of ionization of an insoluble monolayer by the measurement of maximum surface potential at the A/W interface (27). Although they found that the value of *p*K from their surface technique agrees fairly well with that from the measurement in bulk solution in the case of proteins, but not in the case of small molecules such as stearic acid and octadecylamine, they could not explain the latter disagreement satisfactorily. Nevertheless, these facts may be understood in the light of our present investigation. That is, the method of maximum surface potential is applicable to those compounds that have a constant interfacial moment up to a collapse point, owing to a rigid structure. It is unsuitable, however, for such compounds as stearic acid, which have a varying interfacial moment up to the collapse point, owing to a loosely packed structure. For the latter, we must consider the interfacial moment at the larger area instead of that at a collapse point as shown in Fig. 8. The value of *p*K from the measurement in bulk solution in such a case corresponds to that for an expanded film.

Some investigators consider that the *p*H under the interface is different from that in bulk solution (28). Nevertheless, the trend in bulk solution is almost directly applicable to that at the interface as mentioned above. It is because conditions for both cases are identical in respect to the atmosphere in the vicinity of the ionizable groups, except for the characteristic orientation and concentration at the interface. In this case, we must of course keep the difference between expanded and condensed films in mind.

SUMMARY

We now summarize the above discussion according to the classification mentioned at the outset. For the effects of medium:

(1) The most important effect of the aqueous phase is due to hydrogen ion and neutral salt; and

(2) The most important effect of the oil phase is the liberation of the cohesive forces between nonpolar parts. For the effects of intra- and intermolecular actions:

(3) The cohesion between nonpolar groups is predominant in most cases at the air/water interface and is absent at the oil/water interface.

(4) The steric effect of side chains is very effective when they lie at the interface.

(5) The interaction between polar groups is not relieved by the petroleum ether phase, and cannot be estimated directly from the magnitude of the dipole moment in the bulk phase alone.

(6) The interaction between ionized groups should not be considered without considering the type of film.

Acknowledgments

The author expresses his hearty thanks to Professor T. Isemura for his kind guidance throughout the present work, and to Professor S. Murahashi and Mr. S. Otsuka in the Institute, who kindly supplied valuable samples to him.

References

1. Crisp, D. J., *J. Colloid Sci.* **1,** 49 (1946).
2. Crisp, D. J., *J. Colloid Sci.* **1,** 161 (1946).
3. Isemura, T., Hotta, H., and Miwa, T., *Bull. Chem. Soc. Japan* **26,** 380 (1953).
4. Hotta, H., *Bull. Chem. Soc. Japan* **26,** 386 (1953).
5. Hotta, H., *Bull. Chem. Soc. Japan* **27,** 80 (1954).
6. Isemura, T., Hotta, H., and Otsuka, S., *Bull. Chem. Soc. Japan* **27,** 93 (1954).
7. Hotta, H., *Bull. Chem. Soc. Japan* **27,** 412 (1954).
8. Hotta, H., *Bull. Chem. Soc. Japan*, in press.
9. Alexander, A. E., and Teorell, T., *Trans. Faraday Soc.* **35,** 727 (1939).
10. Alexander, A. E., "Surface Chemistry" [Supplement of *Research* (*London*)], p. 123 (1949).
11. Davies, J. T., *Nature* **167,** 193 (1951); *Z. Elektrochem.* **55,** 559 (1951).
12. Abribat, M., and Pouradier, J., *Compt. rend.* **227,** 1101 (1948); Bull, H. B., *J. Biol. Chem.* **185,** 27 (1950).
13. Benson, G. C., and McIntosh, R. L., *J. Colloid Sci.* **3,** 323 (1948).
14. Isemura, T., and Hamaguchi, K., *Bull. Chem. Soc. Japan* **27,** 125 (1954).
15. Smyth, C. P., *J. Am. Chem. Soc.* **60,** 183 (1938).
16. Davies, J. T., *Trans. Faraday Soc.* **49,** 949 (1953).
17. Wesson, L. G., "Table of Electric Dipole Moment," The Technology Press, M.I.T., 1948.
18. Singer, S. J., *J. Chem. Phys.* **16,** 872 (1948).
19. Davies, J. T., *Biochim. et Biophys. Acta* **11,** 165 (1953).
20. Paquette, R. G., Lingafelter, E. C., and Tartar, H. V., *J. Am. Chem. Soc.* **65,** 686 (1943).
21. Flory, P. J., *J. Am. Chem. Soc.* **62,** 1057 (1940).
22. Cheesman, D. F., *Biochem. J.* **50,** 667 (1952).
23. Bateman, J. B., and Chambers, L. A., *J. Chem. Phys.* **7,** 244 (1939).
24. McLaren, A. D., and Rowen, J. W., *J. Polymer Sci.* **7,** 289 (1951).
25. Katchalsky, A., *J. Polymer Sci.* **7,** 393 (1951).
26. McBain, J. W., and Peaker, C. R., *Proc. Roy. Soc.* (*London*) **125A,** 394 (1929).
27. Glazer, J., and Dogan, M. Z., *Trans. Faraday Soc.* **49,** 448 (1953).
28. Havinga, E., and Hertog-Polak, M. Den, *Rec. trav. chim.* **71,** 64 (1952).

THE PROPERTIES OF INSULIN FILMS, SPREAD AT THE AIR-WATER INTERFACE

B. S. Harrap

Biochemistry Unit, Wool Textile Research Laboratory, Commonwealth Scientific and Industrial Research Organization, Melbourne, Australia

Received August 6, 1954

ABSTRACT

The pressure-area and surface potential-area curves for insulin at the air-water interface have been determined over a considerable range of subsolution *p*H and ionic strength. The area of first collapse of the protein has been found independent of either of these factors, indicating that complete spreading has been achieved over the range studied. This area corresponds to the area per residue for a crystalline protein in the β configuration. The surface pressure is shown to be a minimum at the isoelectric point of the protein (*p*H 5.7), providing a method for determining the latter for proteins insoluble at this point. The balance between Coulombic and non-Coulombic bonding is considered in an attempt to explain the effects of *p*H and ionic strength on the surface pressure- and surface potential-area curves. The curve of *p*H vs. surface potential at constant area is shown to be analogous to the usual electrometric titration curves for proteins.

INTRODUCTION

During the past 20 years a considerable number of investigations have been made on the properties of proteins spread as insoluble films at the air-water interface. Although the general characteristics of the surface pressure-area curves for proteins have been established, considerable disagreement exists between the results of different workers on the finer details of these curves.

Undoubtedly, many of the earlier results are vitiated because the conditions under which protein films may be completely spread had not then been established. Even now the fundamental investigations of Guastalla (1), Joly (2), Dervichian (3), and Bull (4) do not seem to be appreciated, and the value of the results in some recent papers is lessened because of the poor spreading techniques used. From a review of previous results, it is now clear that spreading of a protein film is most easily achieved if drops of a dilute protein solution are gently touched against the surface of a subsolution of considerably higher surface tension than the spreading solution. Spontaneous spreading of the drops occurs and the protein is dispersed over the complete surface of the subsolution. These conditions may be realized (*a*) by lowering the surface tension of the dilute spreading solution, or (*b*) by raising the surface tension of the subsolution. For method (*a*) Dervichian (3) added isoamyl alcohol to the protein solution to the extent of 0.2–0.3 %, whereas Ställberg and Teorell (5) have proposed the use of 60 % (by volume) isopropanol solution, 0.5 molar with respect to sodium acetate, as a solvent for the protein. Most proteins may be quantitatively spread, even on distilled water, from either of these solutions. Method (*b*) has been applied by Bull (4), who used concentrated salt solutions (e.g., 35 % ammonium sulfate) as subsolution, thereby considerably increasing its surface tension above that of water. In this way proteins may be completely spread from distilled water solutions.

Apart from the question of solvent and subsolution, Joly's (2) important experiments on the effect of the initial surface concentration on the characteristics of the protein at the surface have also been largely overlooked. Joly observed that a protein spread at an initial surface concentration corresponding to a surface pressure greater than a few tenths of a dyne per centimeter (type B film) has quite different surface properties from those of one spread at lower initial surface concentrations (type A film). The former are characterized by a much higher surface viscosity than type A films and by the fact that they age with time (indicated by an increase in surface pressure at constant area); they cannot be reversibly compressed and expanded, nor can they be spread reproducibly. On the other hand, type A films seem to be equilibrium films: they show no aging effect, may be reproducibly spread, and may be reversibly compressed and expanded up to the point where collapse of the film occurs. Clearly, type A films are the more useful for examining the finer details of the variation of surface properties with surface concentration.

Little information is available on the effects of *p*H and ionic strength of the subsolution on the characteristics of protein monolayers. A knowledge of the second of these factors is particularly important in order to compare the results obtained by spreading methods (*a*) and (*b*). The present paper reports an examination of the effects of these two factors on both surface pressure and surface potential as functions of surface concentration for insulin spread at the air-water interface.

Experimental Methods

The surface pressures of the protein films were determined with the use of a standard Langmuir-Adam type surface balance. This was used as a null instrument, and surface pressures could be measured to ±0.05 dyne/cm. Surface potentials were measured by means of a polonium-tipped air electrode, together with a silver-silver chloride reference electrode and a valve electrometer similar to that described by Few and Pethica (6). The subsolutions were contained in a shallow Pyrex-glass trough and all measurements were made at room temperature (18°–20°C.). The balance and electrode system were enclosed in a wooden box lined with earthed aluminum foil, the latter providing both an electrostatic shielding system and a protection for the liquid-air interface from contamination and draughts. The air electrode could be moved over a considerable area of the interface, provision being made for the operation of this, together with the compression barrier and the torsion balance, from outside the box.

Two samples of crystalline zinc insulin were used, one supplied by the Commonwealth Serum Laboratories, Melbourne, and the other by Boots and Co., London. So far as could be ascertained, both samples behaved identically at the air-water interface. The insulin was exhaustively dialyzed against 0.033 *N* hydrochloric acid to free it from zinc (Oncley and Ellenbogen (7)) to give a stock solution of concentration about 0.1%. Its concentration was determined by the micro-Kjeldahl nitrogen procedure and the stock solution diluted tenfold with approximately 0.25% isoamyl alcohol solution to give the spreading solution. The insulin films were spread using an "Agla" all-glass micrometer syringe and were allowed to stand for 10 minutes before compression.

Because of the profound effect of heavy metal ions on protein monolayers observed by Schulman and Dogan (8), all solutions were prepared with doubly distilled water, the second time from alkaline permanganate in a well-steamed, all-Pyrex-glass still. All salts used were of Analar quality and the isoamyl alcohol was redistilled. A glass electrode system was used to measure *p*H values.

RESULTS

Curves showing the variation of surface pressure (π) and surface potential (ΔV) with area for insulin spread on subsolutions of ionic strength $\Gamma/2 = 0.01$ are plotted in Figs. 1–9. Figures 1, 4, and 8 (*p*H values 2.1, 5.45, and 8.95, respectively) also show π-A and ΔV-A curves for subsolutions with the same concentrations of buffer salts, but containing sufficient potassium chloride to raise the ionic strength to $\Gamma/2 = 1$. Because of complicating effects due to interaction, multivalent ions were avoided, the buffers used being hydrochloric acid, glycine, borate, and acetate. Moreover, whenever *p*H requirements necessitated a change in the buffer anion used, measurements were made with the two overlapping buffer systems at a common *p*H. In each case the same results within experimental error were obtained with both buffer systems at these points, demonstrating the continuity of results obtained over the whole range of *p*H from 2.1 to 9.7. At each point on the compression curve 5 minutes were allowed to elapse and any changes in surface pressure and surface potential with time due to collapse of the film were noted. The areas at which such changes first oc-

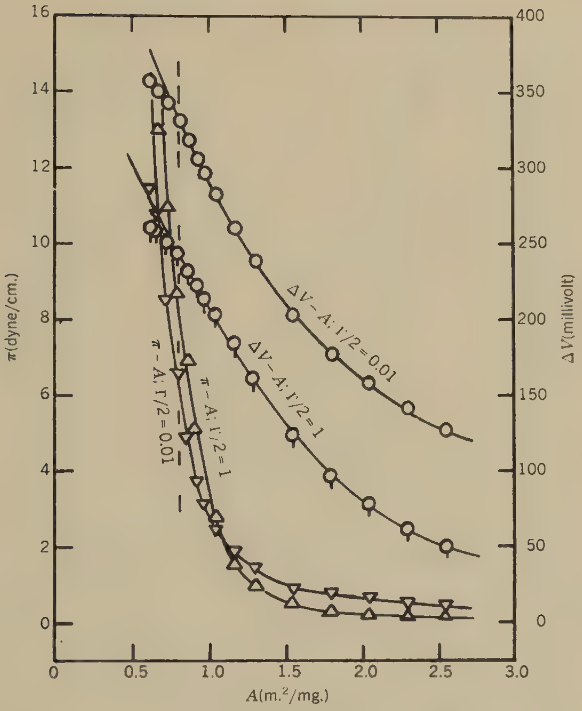

FIG. 1. π-A and ΔV-A curves for insulin films on subsolutions of pH 2.10.

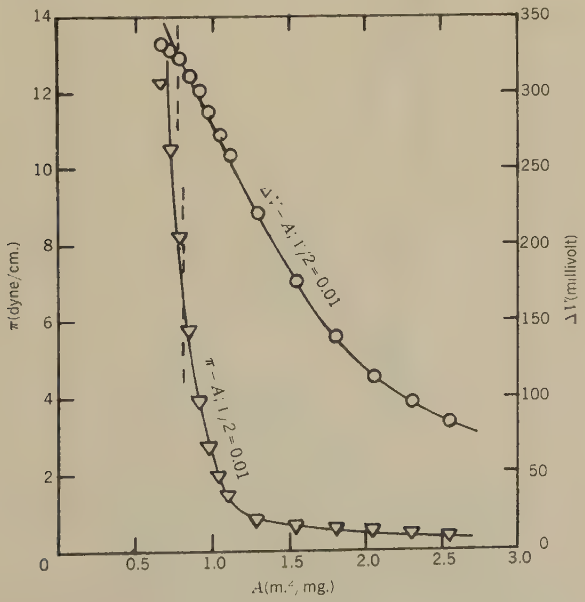

FIG. 2. π-A and ΔV-A curves for insulin films on subsolutions of pH 3.33.

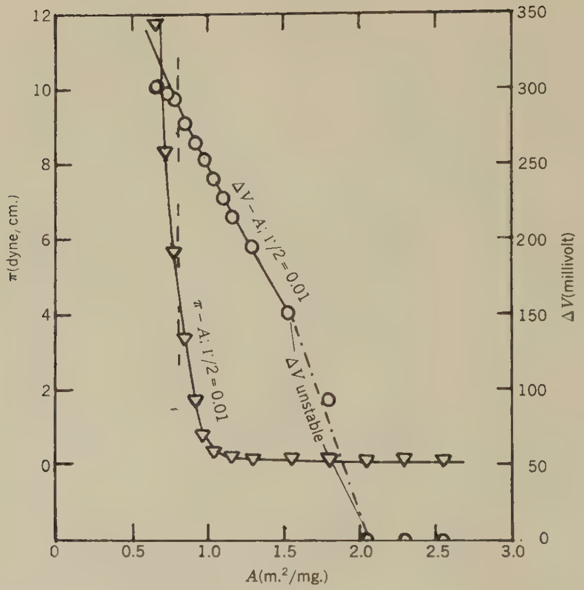

FIG. 3. π-A and ΔV-A curves for insulin films on subsolutions of pH 4.65.

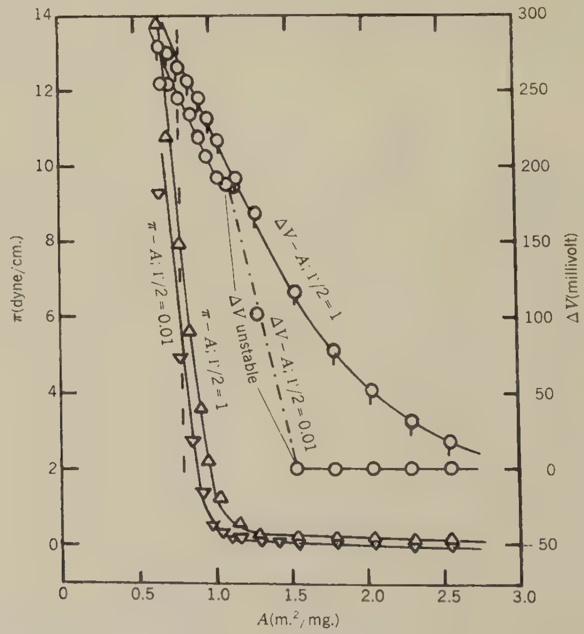

FIG. 4. π-A and ΔV-A curves for insulin films on subsolutions of pH 5.45.

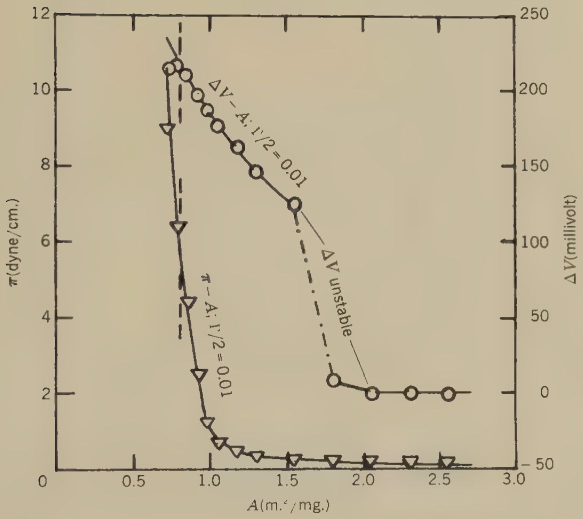

FIG. 5. π-A and ΔV-A curves for insulin films on subsolutions of pH 6.86.

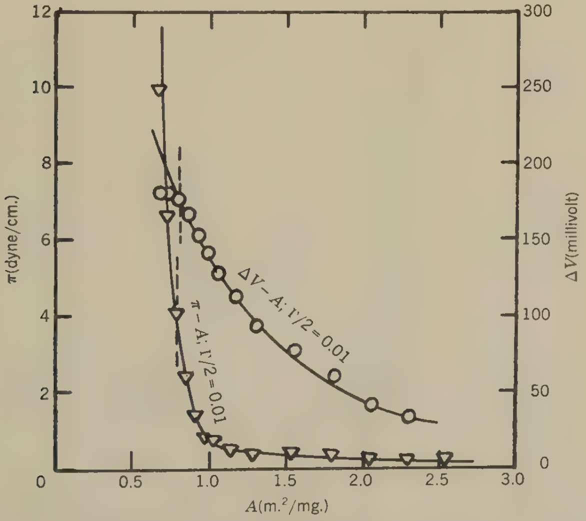

FIG. 6. π-A and ΔV-A curves for insulin films on subsolutions of pH 7.67.

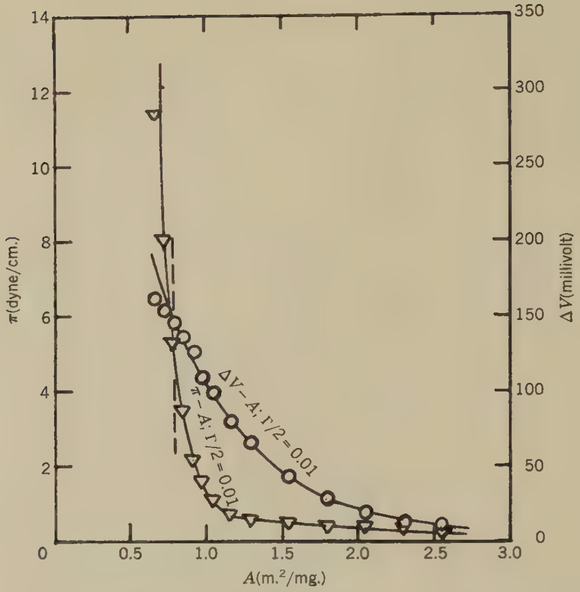

FIG. 7. π-A and ΔV-A curves for insulin films on subsolutions of pH 8.34.

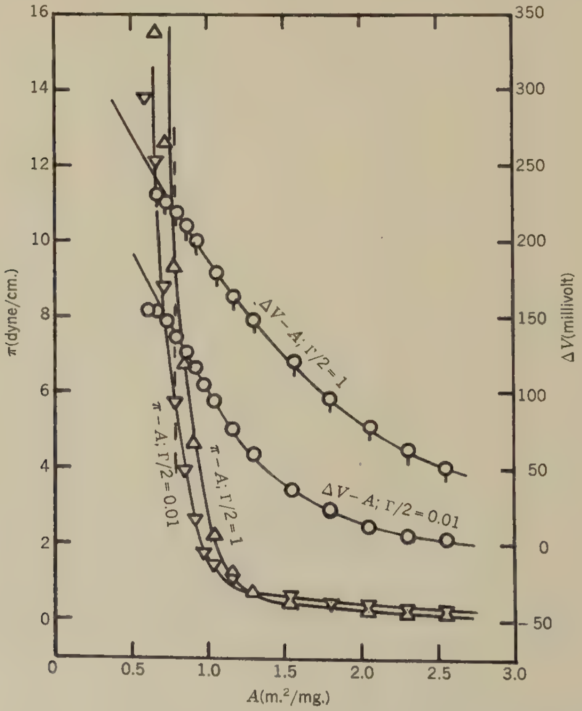

FIG. 8. π-A and ΔV-A curves for insulin films on subsolutions of pH 8.95.

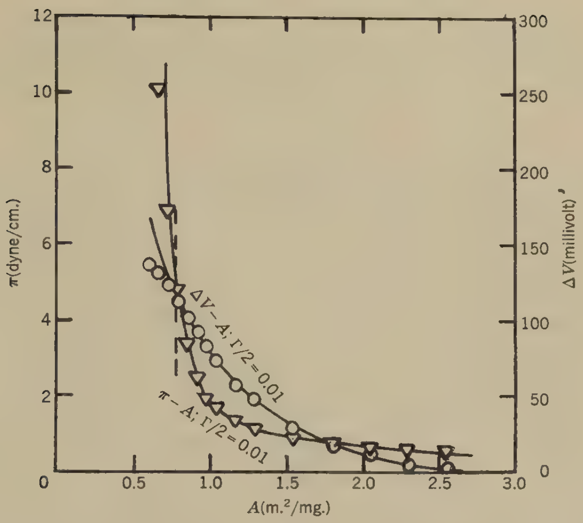

FIG. 9. π-A and ΔV-A curves for insulin films on subsolutions of pH 9.70.

curred (0.79–0.85 m.²/mg.) are indicated by vertical dotted lines on Figs. 1–9. Qualitative estimates of the surface viscosity of the films were also made by gently blowing a few grains of talc sprinkled on the surface.

DISCUSSION

It is clear from Figs. 1–9 that, although the π-A and ΔV-A curves for insulin vary considerably with pH and ionic strength, the point at which the first collapse of the film occurs varies only slightly with these factors. This point is therefore not characteristic of any inter- or intramolecular interaction due to the ionic charge on the molecule. It is the smallest area to which the protein film may be reversibly compressed and expanded and is preceded by a sharp rise in surface viscosity.[1] It is suggested that at this area a two-dimensional crystallization of the protein film occurs and that the molecules, in the β form, are in a configuration and state of packing similar to that in the bulk phase.

The area of first collapse (approximately 0.82 m.²/mg.), calculated for a mean residue weight of 114 (Tristram (9)), gives an area of about 15.5 A.² per mean residue. This value corresponds closely with the area of 15.2 A.² calculated using the values for the mean residue repeat distance (3.3 A.) and backbone spacing (4.65 A.) obtained by Astbury, Dickinson, and Bailey (10) from an X-ray analysis of several proteins in the β configuration. Furthermore, if we assume that the density of the protein in the monolayer is equal to that in the bulk (1.31 g./cm.³), the thickness of the film at the point of first collapse is 9.4 A. This value corresponds very closely to the X-ray mean side-chain spacing found by Astbury *et al.* (10). These results are further evidence for the correctness of Bull's hypothesis (4) that protein molecules are oriented at the air-water interface in the unfolded, β configuration with their side chains perpendicular to the plane of the interface.

---

[1] This area also corresponds to the area of minimum compressibility of Bull (4).

It has frequently been stated in the past (Gorter (11); Glazer and Dogan (12)) that complete spreading of proteins does not occur over the whole *p*H range, but only on strongly acid or alkaline subsolutions or on those in the vicinity of the isoelectric point of the protein. This was based on the shape of the curves of *p*H vs. the so-called limiting area. However, this interpretation is not substantiated by the present results since the collapse area is independent of *p*H, showing that complete spreading occurs, for this protein at least, over the whole *p*H range. The variations in surface pressure with *p*H at this point, or at any other constant area, are more likely to be indicative of changes in inter- and intra-molecular interaction due to changes in the net charge on the molecule. Thus, it seems preferable to compare π and ΔV values at fixed surface areas rather than at fixed surface pressures, as was done by Glazer and Dogan. Moreover, since the collapse area does not vary significantly with ionic strength, it is clear that complete spreading occurs whether method (*a*) or (*b*) above is used.

Having established that the extent of spreading is independent of the ionic strength and *p*H of the subsolution, we may now consider the π-A and ΔV-A curves at areas above the collapse area. To consider first the influence of *p*H on the π-A curves at low ionic strength, it is clear from Figs. 1–9 that at any particular area the surface pressure increases as the *p*H moves above or below the isoelectric region. This may be ascribed to the increased Coulombic repulsion between the molecules as their net charge increases. If the surface pressure at constant area is plotted against *p*H as in Fig. 10 (area = 1 m.^{2}/mg.), a curve with a minimum at approximately *p*H 5.7 is obtained. This compares very favorably with the isoelectric point of 5.6 obtained recently by Tanford and Epstein (13) from the electrometric titration curve for Zn-free insulin. The surface chemical technique should provide, then, a very useful and simple method for the determination of the isoelectric points of proteins which are insoluble in this region.

The influence of *p*H on the ΔV-A curves is also very marked. In the vicinity of the isoelectric point and at high areas the surface potential fluctuates violently as the electrode is moved across the surface of the interface. A similar effect has been observed for gliadin films by Cockbain and Schulman (14), who suggested that the protein molecules are clustered together in discreet "islands" on the surface. It seems likely to us that this occurs because the net charge on the molecules in this *p*H region is so low that there is a high probability of their approaching within the distance over which hydrogen bonding and van der Waals' forces may operate to stabilize the molecules in clusters. The gaseous film between these clusters

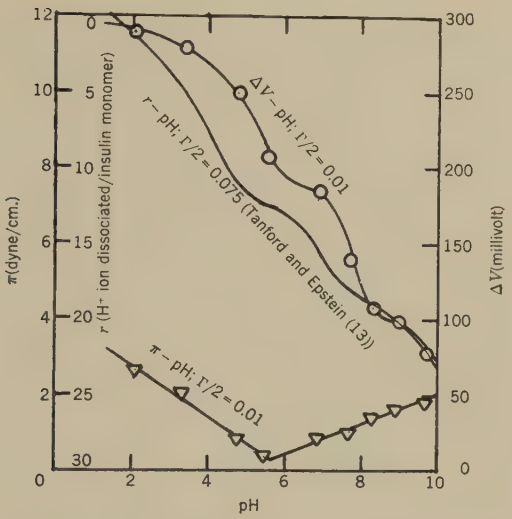

FIG. 10. π-*p*H and ΔV-*p*H curves for insulin films on subsolutions of ionic strength. $\Gamma/2 = 0.01$, together with the electrometric titration curve taken from Tanford and Epstein (13).

will contribute little to the surface potential and, as observed, it is to be expected that the surface pressure would be low and the compressibility high. As the net charge increases, so the probability of two molecules coalescing decreases, in accord with the observation that the surface potential becomes uniform over the whole interface at higher areas as the *p*H moves away from the isoelectric point. At *p*H 2.1 the surface potential is uniform even at the highest area investigated (2.5 m.^{2}/mg.). The net charge is so high at this *p*H that the protein probably exists as a gaseous film of single molecules at the surface, and it is not until the film is considerably compressed that molecules approach sufficiently close for hydrogen- and van der Waals'-bonding to occur, as a prelude to the two-dimensional crystallization of the film. This large Coulombic repulsion explains the high collapse pressures at high and low *p*H. This argument is borne out by the qualitative observations on the surface viscosity of the films. It was noted that sharp increases in the surface viscosity and gel formation occurred at higher areas in the isoelectric region than when the molecule had a high net charge. Since gel formation is due to the operation of non-Coulombic forces, this is to be expected. At *p*H 2.1 there was no tendency to gel formation until the collapse area was almost reached, owing to the high net charge on the molecules.

Glazer and Dogan (12) have investigated the variation of surface potential with *p*H for certain polypeptides and proteins, and have shown that it is the contribution of the ionogenic side chains which is *p*H-dependent. They have plotted ΔV as a function of *p*H, the former quantity being taken either at fixed surface pressures or at the collapse point. We have already shown that constant area is preferable to constant pressure as a basis for comparison. Although comparison at the collapse point is in effect a comparison at constant area, in practice it is found that the film is in such a gelatinous state at this point that equilibrium values for ΔV are reached only slowly, especially in the isoelectric region. We have therefore constructed the ΔV-pH curve for insulin shown in Fig. 10, taking ΔV at an area of 1 m.^{2}/mg., considerably above the collapse area. This is of the same general shape as the electrometric titration curve for insulin obtained by Tanford and Epstein (13), also shown in Fig. 10, and, in contrast to the constant pressure curves of Glazer and Dogan, it clearly separates the neutralization of the imidazole and α-NH_2 groups (pH 6–8) from that of the more basic or acidic groups. It is seen that titration of the more basic groups is just commencing at the highest pH investigated. It was found impossible to obtain reliable values using more alkaline subsolutions with the present apparatus, owing to the fast absorption of atmospheric carbon dioxide by the large surface of buffer exposed. It is hoped to investigate later the high pH region by means of an apparatus from which carbon dioxide is excluded.

On turning to the effect of ionic strength on the properties of the protein film, it is seen from Figs. 1, 4, and 8 that its influence varies according to the area of the film and the pH of the subsolution. To consider first areas greater than approximately 1.3 m.^{2}/mg., it is seen that at both high and low pH the surface pressure at constant area decreases as the ionic strength increases. At these pH values the protein molecules carry a high net charge, and an increase in ionic strength may be expected to decrease the Coulombic interaction, leading to the low surface pressure observed. On the other hand, Figs. 1 and 8 show that at low pH the surface potential at constant area decreases, whereas in the alkaline region the surface potential increases as the ionic strength increases. That is, on the acid side of the isoelectric point, addition of salt lowers the surface potential to a value it would have at a higher pH at low ionic strength, whereas on the alkaline side of the isoelectric point the reverse occurs. This is simply a further example of the well-known phenomenon of increasing salt concentration causing protein titration curves to rotate around the isoionic point (see Cohn and Edsall (15)) and is additional evidence for the assumption that the change in surface potential at constant area with pH reflects, at least in part, the dissociation of the various basic and acidic groups on the protein molecule.

In the isoelectric region the increased ionic strength has little effect on the surface pressure at high areas. This is to be expected since the net charge on the protein is very low. Closer inspection of Fig. 4 reveals that there is actually a very slight but significant increase in surface pressure on addition of salt. The explanation for this effect is clearer when we consider the considerably more marked influence of ionic strength on the surface potential. Here we find that a high areas, ΔV is now uniform over the surface of the film. Apparently the high salt concentration inhibits the clustering of the protein molecules into "islands" as was observed at low ionic strength. It is likely that the breaking-up of these clusters accounts for the small increase in surface pressure with increase in ionic strength in this *p*H region.

As the film is compressed to areas less than 1.3 m.^{2}/mg., it is seen that an increase in ionic strength results in a considerable increase in surface pressure at constant area, this effect being maintained right to the collapse area. The magnitude of this surface pressure increase varies little with *p*H, suggesting that its origin is not due to any change in the Coulombic forces between the molecules but rather to changes in the van der Waals' or non-ionogenic hydrogen bonding in the system. Although the nature of this interaction is somewhat obscure, it is probably connected with the formation of clusters already noted, and with the dissociating effect on them of the addition of salt. Moreover, although only qualitative observations were made, it seemed clear that, with the addition of salt, the sharp increase in surface viscosity and gel formation did not occur until smaller areas were reached, again pointing to the breaking-down effect of higher ionic strength. If the proposed cluster or gel formation results from interaction with water molecules, possibly to form some manner of a two-dimensional hydrogen-bonded lattice structure, it is readily understandable that an increase in salt concentration would break down such a structure because of competition by the salt ions for the water molecules.

The effect of ionic strength on the surface potential at these areas corresponds with that at higher areas. In the isoelectric region the ΔV-A curves for the two salt concentrations merge at lower areas (Fig. 4), again suggesting that the change in surface pressure in this region is due to factors other than ionic effects. The values of ΔV at high and low *p*H provide a further example of the clockwise rotation of protein titration curves around the isoelectric point with increase in ionic strength.

ACKNOWLEDGMENT

The author wishes to thank Mr. K. Wood of this Unit for assistance in the construction and operation of the electrometer.

REFERENCES

1. GUASTALLA, J., *Cahiers phys.* **13,** 5 (1943).
2. JOLY, M., *Compt. rend.* **208,** 975 (1939).
3. DERVICHIAN, D., *Nature* **144,** 629 (1939).
4. BULL, H. B., *Advances in Protein Chem.* **3,** 95 (1947).
5. STÄLLBERG, S., AND TEORELL, T., *Trans. Faraday Soc.* **35,** 1413 (1939).
6. FEW, A. V., AND PETHICA, B. A., *Research* (*London*) **5,** 291 (1952).

7. Oncley, J. L., and Ellenbogen, E., *J. Phys. Chem.* **56,** 85 (1952).
8. Schulman, J. H., and Dogan, M. Z., *Nature* **170,** 31 (1952).
9. Tristram, G. R., *Advances in Protein Chem.* **5,** 85 (1949).
10. Astbury, W. T., Dickinson, S., and Bailey, K., *Biochem. J.* **29,** 2351 (1939).
11. Gorter, E., *Ann. Rev. Biochem.* **10,** 619 (1941).
12. Glazer, J., and Dogan, M. Z., *Trans. Faraday Soc.* **49,** 448 (1953).
13. Tanford, C., and Epstein, J., *J. Am. Chem. Soc.* **76,** 2163 (1954).
14. Cockbain, E. G., and Schulman, J. H., *Trans. Faraday Soc.* **35,** 1266 (1939).
15. Cohn, E. J., and Edsall, J. T., "Proteins, Amino Acids, and Peptides," p. 468. Reinhold Publishing Corporation, New York, 1943.

MONOMOLECULAR FILMS OF MIXTURES.

I. STEARIC ACID WITH ISOSTEARIC ACID AND WITH TRI-*p*-CRESYL PHOSPHATE. COMPARISON OF COMPONENTS WITH OCTADECYLPHOSPHONIC ACID AND WITH TRI-*o*-XENYL PHOSPHATE

Herman E. Ries, Jr., and Hurley D. Cook

Research Department, Standard Oil Company (Indiana), Whiting, Indiana

Received May 24, 1954; revised, received September 2, 1954

Abstract

Pressure-area isotherms have been obtained for mixed monolayers of pure compounds whose structures are related to those of lubricant additives. Individually, stearic acid and octadecylphosphonic acid with long unbranched chains form strong films. Isostearic acid has a larger molecular area and a much lower collapse pressure than stearic acid. This difference demonstrates the great sensitivity of monolayers to a single methyl side chain. Tri-*p*-cresyl phosphate and tri-*o*-xenyl phosphate have much larger areas and lower collapse pressures.

An equimolar mixture of two similar compounds, stearic acid and isostearic acid, has monolayer properties close to the calculated average. An equimolar mixture of dissimilar compounds, stearic acid and tri-*p*-cresyl phosphate, shows film properties of the phosphate at low pressures, expulsion of the phosphate from the monolayer at intermediate pressures, and properties of stearic acid at high pressures.

Introduction

Many additives in lubricating oils are effective because they form adsorbed films (1, 2, 3). In most cases the monomolecular film, or monolayer, at an interface is responsible for the effects of such additives on friction, wear, corrosion, and detergency. Nevertheless, much remains to be learned about molecules in adsorbed films and the nature of adsorption processes.

A reliable and versatile technique for studying monolayers is the determination of pressure-area isotherms on the Langmuir-Adam-Harkins film balance (4, 5). Such isotherms are sensitive to small differences in molecular structure, orientation, and packing. They fingerprint molecular structure and can be used to characterize a wide variety of compounds. Most organic compounds with 12 or more carbon atoms and a polar group can be studied by this technique. The study of pure compounds, alone and in mixtures, provides a basis for interpreting the behavior of complex lubricant additives. Because mixtures almost always occur in practice, they warrant the most attention. Of primary importance are the effects of additives on each other and the effects of diluent hydrocarbons upon them. Little detailed information on mixed monolayers is available (4, 5, 6, 7).

A fundamental study of adsorbed films is in progress in our laboratories. The present work deals primarily with monolayer properties of two binary mixtures. One mixture, stearic acid and isostearic acid, contains compounds of similar structure. The other, stearic acid and tri-*p*-cresyl phosphate, contains compounds of widely different structure. These compounds represent structural types often found together in lubricants: straight chains with branched chains, and aliphatics with aromatics. For further comparisons, two related compounds were studied: octadecylphosphonic acid and tri-*o*-xenyl phosphate.

EXPERIMENTAL

Pressure-area isotherms have been determined for five compounds and two binary mixtures. The basic apparatus and techniques (4, 5) have been modified to improve the reliability of measurements.

Materials

All materials were of the highest purity available. Special preparations of stearic acid (m.p. 69.61°C.) and octadecylphosphonic acid (m.p. 97.2°–98.2°C.) were obtained from the Research Division of Armour and Company. Isostearic, or 16-methylheptadecanoic, acid (m.p. 69.5°C.) was prepared in our laboratories (8).

Tri-*p*-cresyl phosphate was obtained from the Eastman Kodak Company. A part of the sample fractionated under high vacuum showed the same film properties as the original material. Analysis of the original material showed 8.43% phosphorus, compared with a theoretical value of 8.41%. Tri-*o*-xenyl phosphate, or Phosphen 9 (m.p. 113°–115°C.), was supplied by the Dow Chemical Company. Analysis showed 5.54% phosphorus, compared with a theoretical value of 5.60%.

The volatile solvent for the film-forming compounds was C.P. benzene, twice distilled to remove nonvolatile impurities. Film experiments on the benzene alone showed that remaining impurities were negligible.

Apparatus

The apparatus is a modified Cenco Hydrophil Balance of the Langmuir-Adam-Harkins type (4, 5). It is housed in a double-walled cabinet; both pressure and area adjustments are made with the cabinet closed. The entire apparatus stands on a stainless steel plate imbedded in a 3000-pound concrete base; the base reduces vibration and improves reproducibility of measurements. A glass weighing pipet is used for spreading the film-forming materials in a few drops of volatile solvent.

Procedure

Before each experiment, the trough, barriers, float, and platinum foils of the film balance were thoroughly cleaned and coated with high-melting paraffin wax dissolved in hot *n*-hexane. The wax was Eimer and Amend "Hard" (m.p. 68°–70°C.), and the *n*-hexane was distilled from Phillips Pure Grade. A concentrated solution was used for the trough and barriers to provide a heavy coating and prevent metal ions from contaminating the water; a dilute solution was used for the float and foils. The coated trough was filled with deionized water to about 2½ mm. above the edge. The water, which was deionized and equilibrated with atmospheric carbon dioxide, had a conductivity of about 0.5 micromhos and a *p*H of 6.

The large area in front of the float was swept at least five times by five small barriers; the small area behind the float, three times. The film was spread, and 10 minutes were allowed for evaporation of the solvent. About 0.01 mg. of the compound under study remained on the water surface. Surface pressures were read, usually at intervals of 2 minutes, as the film area was reduced in small decrements. One-minute intervals were used for extremely small decrements. The film was compressed until the pressure remained constant or fell.

At the completion of an experiment, the surface behind the float was examined for cleanliness by moving a barrier across it to the float. Movement of the float indicated leakage of the film or possibly contamination. Directing a beam of light at a small angle of incidence across the film sometimes revealed characteristic patterns. Finally, lycopodium powder, an extremely fine pollen, was sprinkled over the film and a small stream of air was directed across the surface; the more rigid the underlying film, the less the powder moved.

Temperatures were measured by a thermometer fully immersed in the shallow water of the trough. The experiments of this series were conducted at 21° to 25°C. In this range, temperature had little effect on the films studied. During a single experiment, it rarely varied more than 0.1°C.

RESULTS

Film properties calculated from the isotherms are shown in Table I. These include cross-sectional area per molecule, collapse pressure, and compressibility. Areas given are obtained by extrapolating the steepest part of the isotherm, usually near the collapse pressure, to the area axis at zero pressure.[1] Film thickness, which is the vertical dimension of the oriented molecule, can be calculated from the area and volume of the film. The volume is obtained by assuming that the monolayer has the same density as the bulk material.

[1] Extrapolation is illustrated in Fig. 5.

TABLE I

Monolayer Properties of Compounds and Mixtures

	Area, square Angstroms per molecule[a]	Collapse pressure, dynes per cm.	Compressibility $\frac{a_0 - a_1}{a_0 f_1}$
Individual Compounds			
Stearic acid	20.3	42	0.0019
Octadecylphosphonic acid	22.2	53	.0035
Isostearic acid	31.6	15	.0069
Tri-*p*-cresyl phosphate	95.0	9	.0538
Tri-*o*-xenyl phosphate	96.0	3	.0142
Equimolar Mixtures			
Stearic acid and isostearic acid	27.5	31	.0061
Stearic acid and tri-*p*-cresyl phosphate			
Low-pressure region	72.0	11	.0404
High-pressure region	14.5	38	.0033

[a] At the extrapolated zero pressure.

Collapse pressure is sometimes referred to as maximum film pressure. Rigid or solid-like films usually collapse abruptly; mobile or liquid-like films gradually approach constant pressure. In the latter case, the molecules move less suddenly from the monolayer into the upper layers. Film compressibility is the change in area with pressure:

$$\frac{a_0 - a_1}{a_0 f_1}$$

where a_0 is the extrapolated area at zero pressure, and a_1 is a smaller area at pressure f_1.

Each point on an isotherm represents a pressure and an area calculated directly from measurements on the film. Repeated determinations of the isotherms are in good agreement. Although abrupt collapse is a "weakest link" phenomenon and should be difficult to duplicate, good reproducibility has been obtained.

DISCUSSION

Isotherm characteristics are intimately related to molecular geometry, molecular cohesion and adhesion, the location of polar groups, and the compatibility and packing behavior of molecules in mixtures. The schematic drawings of Fig. 1 show the three most important structures of this study and their orientation at the air-water interface. Molecular models of stearic and isostearic acids show cross-sectional areas in about the same ratio as the extrapolated values obtained in monolayer measurements. However, to account for observed periodicities in melting points and long crystal spacings in a series of iso acids, Weitkamp (8) and Velick (10) have

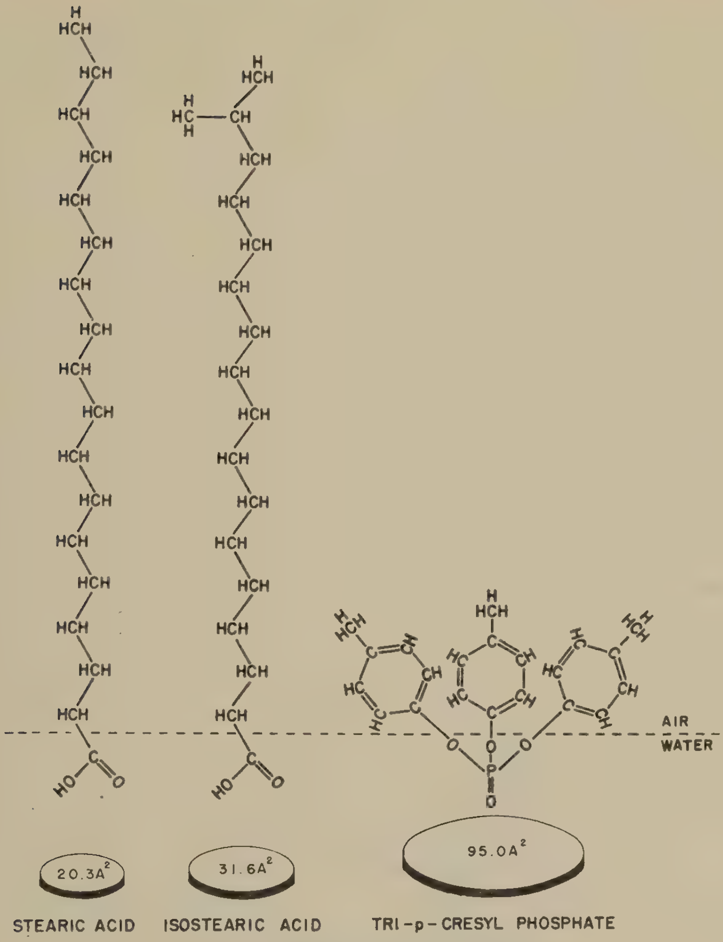

FIG. 1. Molecular orientation.

suggested that the iso acids may have a spiral rather than the usual zigzag structure.

Films of Individual Compounds

Film properties of the individual components of the mixtures were needed for comparison with those of the mixtures. Two additional compounds were studied for comparison of polar groups and hydrocarbon structures. Stearic acid and octadecylphosphonic acid have the same hydrocarbon structure and different polar groups. Stearic acid and isostearic acid have the same polar group and slightly different hydrocarbon structures. Tri-*p*-cresyl phosphate and tri-*o*-xenyl phosphate have the same polar group and greatly different hydrocarbon structures.

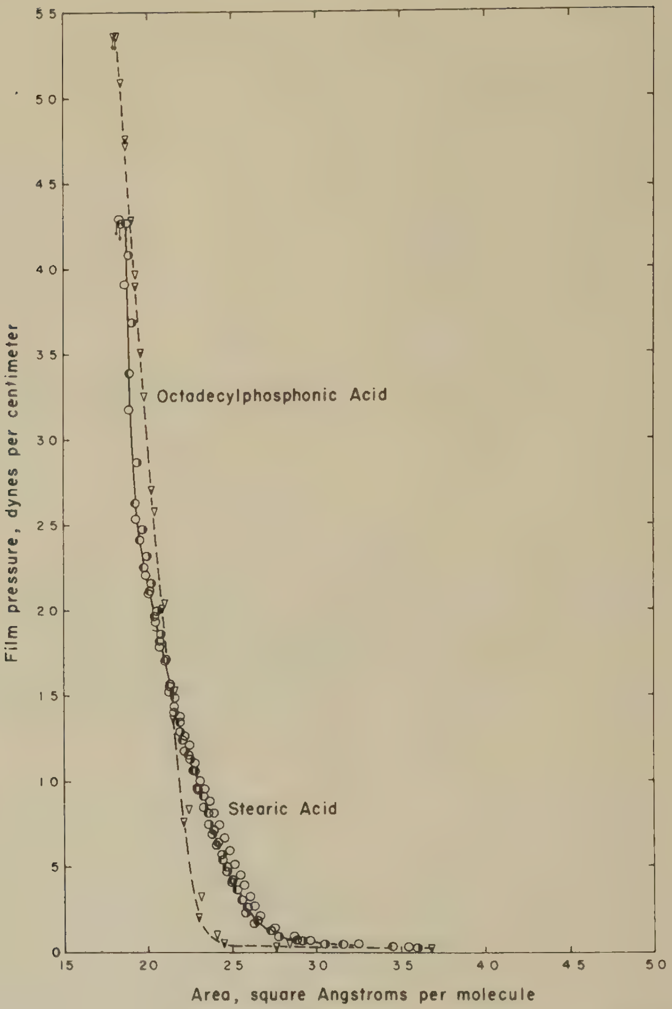

FIG. 2. Pressure-area isotherms for stearic acid and octadecylphosphonic acid.

Stearic Acid. At zero pressure, the cross-sectional area of the stearic acid molecule is 20.3 A.^{2}. This is obtained by the usual extrapolation of the steep upper portion of the isotherm in Fig. 2.[2] The film thickness or the vertical length of the molecule, calulated from the area, is about 27 A.

---

[2] Only small differences have been observed in our laboratory when twice-distilled *n*-hexane is substituted for benzene as the volatile solvent for stearic acid. Isotherms obtained with *n*-hexane are displaced slightly to the left at pressures below 10 dynes per cm., but the two isotherms agree within experimental error at higher pressures. The difference at low pressures may be due to benzene held in the film, wax dissolved from the apparatus by the benzene, or both. In any case, the contaminating component is apparently squeezed out of the monolayer as the film is compressed.

In the case of stearic acid, another area value is obtained by extrapolating the straight-line portion of the isotherm just below the steepest region. This lower portion yields a value of 25.0 A.^{2}. Both values are in good agreement with earlier measurements made on substrates of freshly distilled water and of dilute acids (4, 5, 9). The two extrapolated areas, 20.3 and 25.0 A.^{2}, obtained in the present study are in particularly good agreement with the corresponding calculated values, 20.5 and 25.2 A.^{2}, reported by Vold (11). The value of 20.5 A.^{2} is calculated by assuming efficient packing of vertically oriented stearic acid molecules that are elliptical in cross section and that do not rotate on the vertical axis. The greater area, 25.2 A.^{2}, is obtained by assuming free rotation on the vertical axis and a cylindrical close packing. More recent calculations by Kipling and Norris (12), based on a "closed" and an "open" configuration of the carboxyl group, give values in agreement with those of Vold.

Stearic acid monolayers have a high collapse pressure. Five experiments show abrupt collapse between 41 and 43 dynes per centimeter. Reported collapse pressures (4, 5, 9) are lower. A low compressibility, 0.0019, is apparent in the steeply rising isotherm. At small areas, the films are extremely rigid. Collapsed stearic acid films appear to contain long thin crystallites or fibers that may be related to the fiber structure of similar compounds in grease (13).

Octadecylphosphonic Acid. The data plotted in Fig. 2 demonstrate the strong film-forming properties of octadecylphosphonic acid. The isotherm is similar to that for stearic acid. The extrapolated area, 22.2 A.^{2}, is slightly greater than for stearic acid, 20.3 A.^{2}. This difference may be related to the larger polar group of the phosphonic acid. At the highest pressure, however, the cross-sectional area of the hydrocarbon chain is probably the limiting factor in packing for both compounds.

Four determinations of collapse pressure give an average value of 53 dynes per centimeter, about 11 dynes higher than for stearic acid. The higher collapse pressure and the steeper slope of the low-pressure portion of the isotherm may be related to the tighter binding or association of the phosphonic polar groups with the water or with themselves. The high polarity of the phosphonic group is indicated also by the limited solubility in benzene of the compound compared with stearic acid; even at extremely low concentrations, it was necessary to warm the solution. Nevertheless, identical collapse pressures and almost complete coincidence were obtained in the two experiments of Fig. 2.

Isostearic Acid. The sensitivity of monolayers to branching is illustrated by comparing isostearic acid with stearic acid. The methyl side chain of isostearic acid should have the minimum effect on packing and film strength because it is small and at the remote end of the long molecule. Furthermore, the melting points of the isostearic and stearic compounds are almost identical.

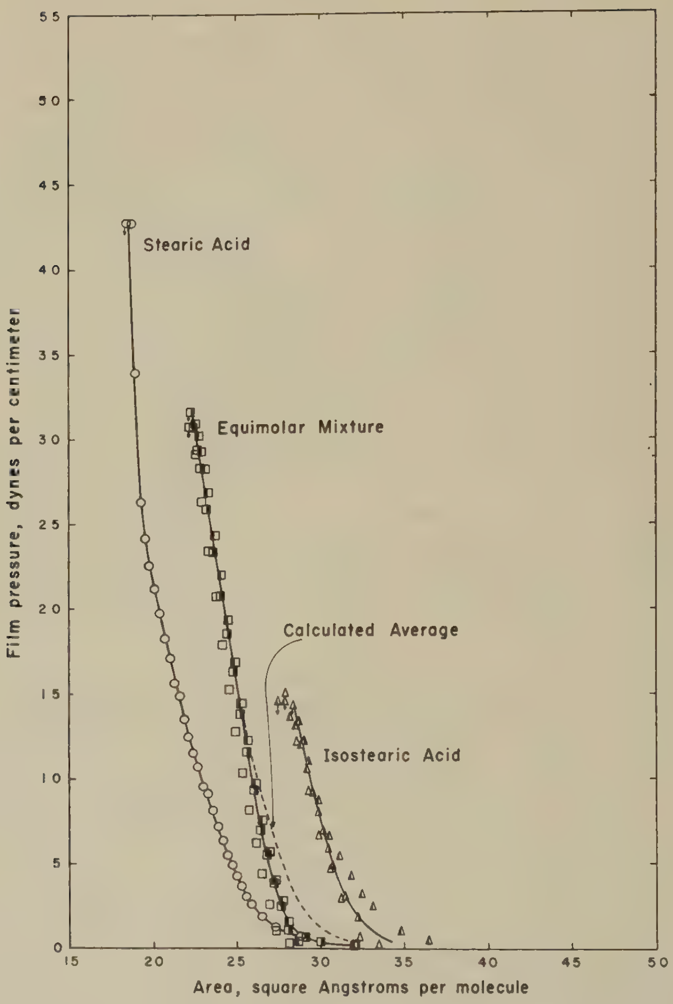

FIG. 3. Pressure-area isotherms for stearic acid, isostearic acid, and an equimolar mixture.

Isotherms for stearic and isostearic acids are presented in Fig. 3. A marked difference is evident. The extrapolated area for isostearic acid is 31.6 A.^{2}, compared with 20.3 A.^{2} for the straight-chain acid. At collapse, the minimum area for the isostearic molecule is 28.0 A.^{2}. The collapse pressure for isostearic acid is 15 dynes per centimeter (14.3, 14.5, and 15.0 in three experiments), only a third of that for stearic acid. The compressibility of the isostearic film, 0.0069, is more than three times as large. The increase in area and the threefold difference in collapse pressure and

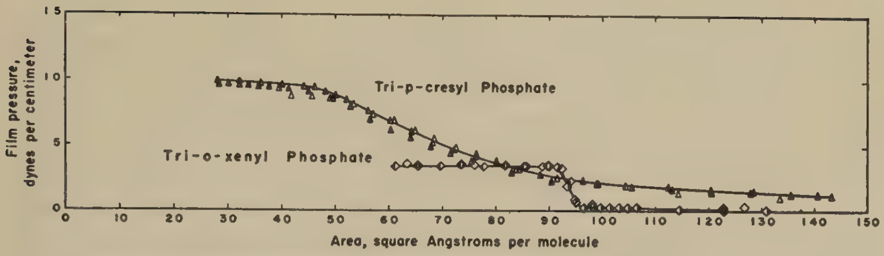

FIG. 4. Pressure-area isotherms for tri-*p*-cresyl phosphate and tri-*o*-xenyl phosphate

compressibility demonstrate the extreme sensitivity of monolayers to small changes in structure. Area data obtained under slightly different conditions by Sobotka, Rosenberg, and Birnbaum (14) on another preparation of isostearic acid are in qualitative agreement.

The isostearic acid data may be interpreted by assuming either vertical or sloping orientation. If the molecules are vertically oriented and the branched methyl group sweeps out a wide area to give a film of low density, intermolecular cohesion and film strength are reduced. If the orientation angle of the molecules is considerably less than 90° and the packing is relatively close, intermolecular slippage is allowed and film strength is reduced. The first interpretation implies a greater film thickness than the latter.

Tri-p-cresyl Phosphate. Tri-*p*-cresyl phosphate has a squat bulky structure, in sharp contrast with that of stearic acid. The extrapolated area for tri-*p*-cresyl phosphate is 95.0 A.^{2}. The thickness of the film, or vertical dimension of the molecule, is about 6 A.

Tri-*p*-cresyl phosphate has a low collapse pressure, 9 dynes per centimeter. The isotherms of Fig. 4 show the gradual collapse or slow approach to constant pressure. The film has high mobility, in contrast with the rigidity of stearic acid. Its compressibility of 0.0538 is more than 25 times that of stearic acid. Nevertheless, the phosphorus-oxygen group is strongly polar, as indicated by the films of octadecylphosphonic acid. Therefore, the low collapse pressure and high compressibility of tri-*p*-cresyl phosphate are undoubtedly due to poor packing, both intra- and intermolecular, of the three bulky ring groups.

A marked difference exists between molecules in oriented monolayers and in the bulk phase. Tri-*p*-cresyl phosphate, which melts at 77°C., gives a mobile, liquid-like film. Stearic acid, which has a lower melting point, 69°C., gives a rigid, solid-like film. The higher melting solid behaves as a liquid in monolayers, whereas the lower melting solid is extremely rigid in two dimensions.

Tri-o-xenyl Phosphate. The hydrocarbon portion of tri-*o*-xenyl phosphate, which consists of three biphenylyl groups, is much larger than that of tri-*p*-cresyl phosphate. Nevertheless, the geometry and orientation of the multiple-ring structure give a molecular area of only 96.0 A.². This value is almost identical to the extrapolated area of tri-*p*-cresyl phosphate. However, an area value for tri-*p*-cresyl phosphate taken at the point of discontinuity near the maximum pressure, as shown in Fig. 4, is only about half that of tri-*o*-xenyl phosphate. Under compression, the three rings of tri-*p*-cresyl phosphate perhaps become closely packed, whereas the xenyl structures do not. The tri-*o*-xenyl phosphate monolayer collapses at a low pressure, 3.4 dynes per centimeter, but moderate rigidity is indicated by its compressibility, 0.0142. These data indicate a dominating effect of hydrocarbon structure in a molecule containing a strong phosphorus-oxygen polar group.

Interestingly, the structures of the three principal compounds of this study, drawn in Fig. 1, suggest the corresponding isotherms of Figs. 3 and 4. The horizontal cross sections are reflected in the displacement of the isotherms from the origin. Moreover, the tall stearic acid structure suggests a steep isotherm with a high collapse pressure; the squat tri-*p*-cresyl phosphate suggests a low collapse pressure. Isostearic acid is intermediate in both respects.

Films of Mixtures

Experimental isotherms for two equimolar mixtures, stearic acid with isostearic acid, and stearic acid with tri-*p*-cresyl phosphate, have been compared with the calculated average isotherms. The first mixture, which contains similar compounds, has monolayer properties close to the average. The second mixture, which contains dissimilar compounds, shows properties of the individual components and an isotherm differing markedly from the calculated average.

Stearic Acid and Isostearic Acid. The isotherm for an equimolar mixture of stearic acid and isostearic acid is presented in Fig. 3. At the lowest pressures, it lies close to stearic acid alone, but on compression the divergence becomes greater. The extrapolated area for the mixed film is 27.5 A.² per average molecule, compared with a calculated average of 26.0 A.². The calculated average curve, based on simple additivity of the two individual monolayers, is nearly within experimental error of the data for the mixed film. Apparently there is little interference or co-operation between the two molecules in the monolayer.

The collapse pressure for the mixed film is near the mean of those of its components. The mixture has a collapse pressure of 31 dynes per centimeter (30.7, 30.9, and 31.6 in three successive experiments), not far from the average, 28.5 dynes, for the two components. If any microscopic area of the mixed film had the weakness of isostearic molecules alone, a much lower collapse pressure would be expected. Evidently there is uniform

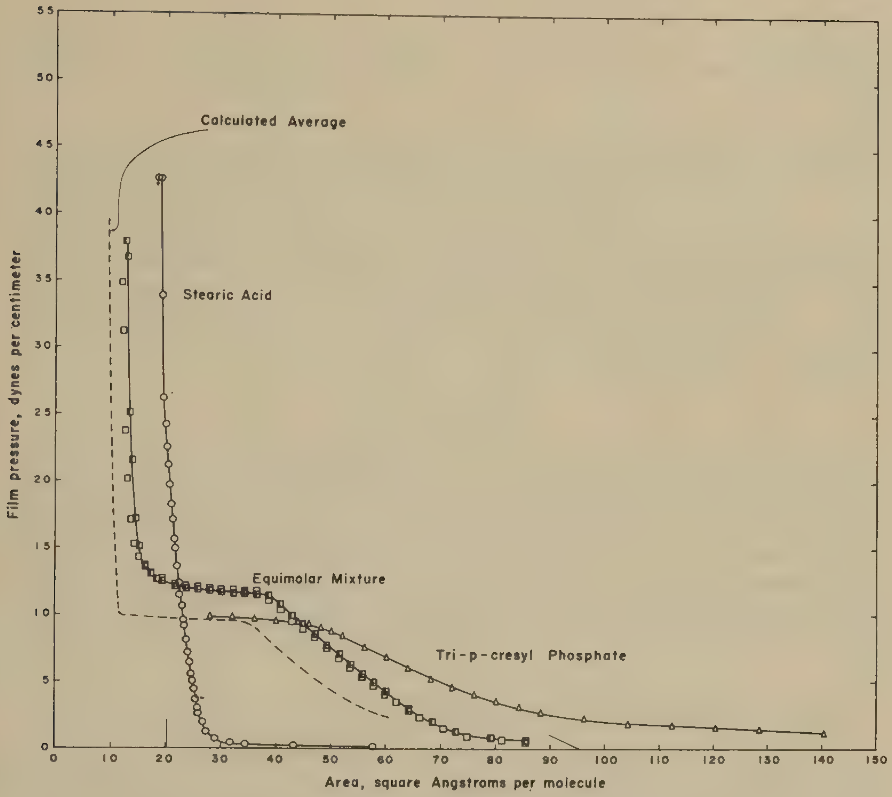

FIG. 5. Pressure-area isotherms for stearic acid, tri-*p*-cresyl phosphate, and an equimolar mixture.

distribution or mixing of the isomers in the monolayer. Certainly no domination of the film by the weaker member of the pair is indicated.

Stearic Acid and Tri-p-cresyl Phosphate. The isotherm for an equimolar mixture of two widely different compounds, stearic acid and tri-*p*-cresyl phosphate, is plotted in Fig. 5. In the high-area or low-pressure region, the tri-*p*-cresyl phosphate molecules dominate the film structure. In the low-area region, stearic acid apparently controls the film. The horizontal plateau between these two parts of the isotherm appears to be a region in which the tri-*p*-cresyl phosphate molecules are squeezed out of the monolayer.

Throughout the entire isotherm, there are effects considerably greater than would be predicted by simple additivity. In the high-area region, the mixed molecules do not pack as closely as they do separately. Nevertheless, the compressibility in this region, 0.0404, is less than for tri-*p*-cresyl phosphate alone, 0.0538. The influence of the stearic acid at high areas is thus apparent. The isotherm then rises to a plateau about 2 dynes per centimeter above that for the tri-*p*-cresyl phosphate alone. Possibly the tall stearic acid molecules interfere with the escape of the phosphate molecules from the monolayer.

Although stearic acid apparently dominates the mixed film in the low-area region, the area is greater than predicted by the calculated average curve. Perhaps not all of the tri-*p*-cresyl phosphate has been forced out of the monolayer. Possibly the phosphate molecules have some effect on the monolayer packing even after they have been displaced to a second-layer position. However, little is known about the state of such partially collapsed films, that is, the state between the monolayer and the bulk aggregate.

Conclusion

Monolayers of mixtures reflect structure characteristics and interaction effects not obtained with films of individual compounds. Mixed films are of basic importance in studying lubricant additives, emulsions, foams, micelles, detergents, biological systems, and heterogeneous catalysis of large molecules. The present work and investigations in progress should not only improve our understanding of surfaces and interfaces but provide a basis for designing molecular structures having specific film properties.

Acknowledgments

The authors are grateful to C. M. Loane for valuable advice during these studies and to Joseph Gabor for assistance in the experimental work. The authors also thank H. J. Harwood of Armour and Company for the stearic acid and octadecyl phosphonic acid, and A. W. Weitkamp of our laboratories for the isostearic acid.

References

1. Bondi, A., "Physical Chemistry of Lubricating Oils." Reinhold Publishing Corporation, New York, 1951.
2. Bowden, F. P., and Tabor, D., "The Friction and Lubrication of Solids." Oxford University Press, Oxford, 1950.
3. Brophy, J. E., and Zisman, W. A., *Ann. N. Y. Acad. Sci.* **53,** 836 (1951).
4. Adam, N. K., "The Physics and Chemistry of Surfaces," 3rd ed. Oxford University Press, Oxford, 1941.
5. Harkins, W. D., "The Physical Chemistry of Surface Films." Reinhold Publishing Corporation, New York, 1952.
6. Clowes, G. H. A., "Surface Chemistry," ed. by F. R. Moulton. *Publ. Am. Assoc. Advance. Sci.* **21,** 1 (1943).
7. Goddard, E. D., and Schulman, J. H., *J. Colloid Sci.* **8,** 309 (1953).
8. Weitkamp, A. W., *J. Am. Chem. Soc.* **67,** 447 (1945).
9. Porter, E. F., *J. Am. Chem. Soc.* **59,** 1883 (1937).
10. Velick, S. F., *J. Am. Chem. Soc.* **69,** 2317 (1947).
11. Vold, M. J., *J. Colloid Sci.* **7,** 196 (1952).
12. Kipling, J. J., and Norris, A. D., *J. Colloid Sci.* **8,** 547 (1953).
13. Hotten, B. W., and Birdsall, D. H., *J. Colloid Sci.* **7,** 284 (1952).
14. Sobotka, H., Rosenberg, S., and Birnbaum, A., *J. Colloid Sci.* **5,** 567 (1950).

TREATMENT OF VISCOSITY DATA ON POLYMER SOLUTIONS[1] (AN ANALYSIS OF EQUATIONS AND PROCEDURES).

I. INTRINSIC VISCOSITY AND LIMITING SLOPE CONSTANTS

Wilfried Heller

Chemistry Department, Wayne University, Detroit, Michigan

Received August 4, 1954

INTRODUCTION

Whatever the ultimate purpose of viscosity measurements on polymer solutions, the primary quantities of interest are, in general, (1) the intrinsic viscosity, $[\eta]$, (2) the limiting slope constants of $f(c)$ plots, where c is the concentration of polymer in grams per 100 ml. and f is the directly measured viscosity η, (3) the relative viscosity, η_r, (4) the specific viscosity, η_{sp}, (5) the reduced viscosity, η_{sp}/c—or the logarithm of any of these quantities.

Intrinsic viscosity and limiting slope constants are obtained by means of simple and well-known graphical procedures which are satisfactory as long as neither high accuracy nor high precision is needed. Whenever either or both are desirable, most of the procedures break down, although this is often not realized. In part, inadequacies in the equations underlying the plots are responsible. It is the purpose of this paper to analyze the conventional procedures and the respective equations and to point out a few possibilities for improvement. A subsequent paper will, similarly, deal with the explicit concentration function of the measured viscosity and of the various derived quantities.

The analysis will be based entirely upon recent data by Streeter and Boyer (1). They were obtained on a single sample of polystyrene ($\bar{M}_w = 370{,}000$) dissolved in a large variety of nonpolar solvents. Many of the data covered a rather wide range of concentrations. The rate of shear was apparently close to zero. All this seemed to make these data particularly suitable for the present purpose in spite of the regrettable choice of a geometric progression for concentrations below 2%. The choice of these systems will limit part of the conclusions, arrived at in the following, to solutions of nonpolar flexible macromolecules of large $\bar{M}$ in organic

---

[1] Paper presented at the 1954 March meeting of the American Physical Society at Detroit and Ann Arbor, *Phys. Rev.* **94,** 1426 (1954).

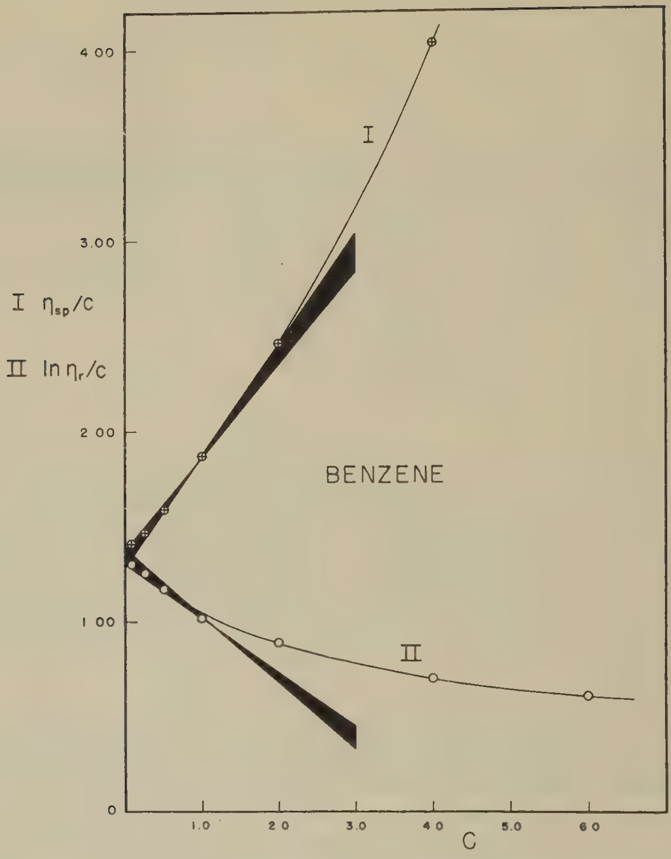

FIG. 1. Illustration of uncertainties in conventional determinations of $k_1[\eta]^2$ and $k_2[\eta]^2$.

Equations used: I: [2]; II: [3]

solvents. An extension of the analysis particularly to solutions of rigid nonspherical macromolecules in organic solvents, and to ionogenic macromolecules in aqueous solution, would be desirable but is not intended by this author.

I. EXTRAPOLATIONS TO INTRINSIC VISCOSITY

1. *Definition of the Problem*

The equation most generally used for obtaining $[\eta]$ graphically is

$$\frac{\eta_{sp}}{c} = a + bc \cdots \qquad [1]$$

where a is $[\eta]$ by definition. The interrelation between slope and intercept found by Schultz and Blaschke (2) and the subsequent theoretical argument offered by Huggins (3), led to a replacement of b by $k_1[\eta]^2$ so that the now generally adopted form of this equation is

$$\eta_{sp}/c = [\eta] + k_1[\eta]^2c + \cdots \qquad [2]$$

The alternate relationship

$$\ln \eta_r/c = [\eta] - k_2[\eta]^2c + \cdots, \qquad [3]$$

generally attributed to H. Staudinger[2], obviously yields the same extrapolated value of $[\eta]$. It has therefore become common practice to make extrapolations to $[\eta]$ more secure by combining plots of Eqs. [2] and [3]. Although this combination may be relied upon for poor solvents, the precision obtainable for good solvents leaves much to be desired, since neither linear relationship applies then in satisfactory approximation. The situation is illustrated by Fig. 1. Neither Eq. [2] nor Eq. [3] is strictly valid at any of the experimental concentrations. The resulting uncertainty of the limiting slope is expressed by the contour lines of the two black areas, and the uncertainty of $[\eta]$ follows from the vertical range of possible common intercepts.

It is apparent that alternate methods are necessary in order to increase the number of significant figures possible for $[\eta]$-values. Two types of methods suggest themselves. They will be discussed in succession.

2. Extrapolations from Limiting Slopes of Alternate Equations

The first step consists of exploring the various possible functions of which the right hand side of Equations [2] or [3] may be considered as the first terms of expansion, selecting that or those among them which can be brought into a graphically useful form. The only additional requirement is that the third and higher terms selected for either of the two infinite series become negligible at concentrations $\leqslant$ 2 g./100 ml., so that a straight-line plot will result within a reasonably extended range of low concentration on applying the new equations. It is, on the other hand, quite immaterial for the present purpose how well or how poorly the same equations perform at higher concentrations.

One equation meeting these requirements can be obtained by extending Eq. [2] in the following manner

$$\eta_{sp}/c = [\eta] + k_1[\eta]^2c + k_1^2[\eta]^3c^2 + k_1^3[\eta]^4c^3 + \cdots \qquad [2a]$$

---

[2] Except for the substitution of c by the weight fraction, w, it is identical with the repeatedly tested equation

$$\log \eta_r = a'w + b'w^2$$

or the theoretically justified analog

$$\ln \eta_r = a''\phi + b''\phi^2$$

[ϕ: volume fraction. See e. g. "Natural and Synthetic High Polymers," Vol. 4, p. 780, Interscience Publishers, New York, 1950. See also Mead, D., and Fuoss, R. M., *J. Am. Chem. Soc.* **64,** 277 (1942)].

This equation, in graphically useful form, is

$$c/\eta_{sp} = 1/[\eta] - k_1c. \qquad [4]$$

In order to take full advantage of this equation for graphical extrapolations to $1/[\eta]$,[3] it is desirable to find an auxiliary equation which also reduces to $1/[\eta]$ as $c \rightarrow 0$. This will reduce the considerable uncertainty of graphical extrapolation from one curve.

On extending the infinite series [3] in the following manner

$$\ln\eta_r/c = [\eta] - k_2[\eta]^2c + \tfrac{4}{3}k_2^2[\eta]^3c^2 - 2k_2^3[\eta]^4c^3 + \cdots \qquad [5]$$

the function

$$\eta_r = (1 + 2k_2[\eta]c)^{1/(2k_2)} \qquad [6]$$

is obtained, which is identical with the "Baker" equation (4), on replacing $1/2k_2$ by a single constant n. (Equation [3] may therefore be considered as a two-term expansion of the Baker equation.) Equation [6] is, unfortunately, not useful graphically for the present purpose. It may, however, be brought into such a form by considering the following of its various possible alternate forms

$$\ln \eta_r = \frac{\ln\left(\frac{1}{2k_2} + [\eta]c\right)}{2k_2} - \frac{\ln\left(\frac{1}{2k_2}\right)}{2k_2}. \qquad [7]$$

This equation, on expansion of the first term and subsequent simple transformation, yields

$$\frac{c}{\ln \eta_r} = \frac{1}{[\eta]} + k_2 c, \qquad [8]$$

which is a suitable auxiliary equation to be combined with Eq. [4].

Joint use of these two equations furnishes an independent method of extrapolations to $[\eta]$ for two reasons: (1) The difference in slope constants compared to Eqs. [2] and [3] excludes any symmetry between the new and the old double plot. The lack of symmetry is enhanced by the difference in the concentration dependence of the slope constants, outside of the range of validity of the four equations. (2) The extrapolations yield $1/[\eta]$ so that any, though unconscious, arbitrariness in carrying the two curves to their common intercept is excluded in such cases where an extrapolation to $[\eta]$, by the conventional double plot, has preceded the new double plot.

The new method of extrapolation, combined with the conventional method, is illustrated in Fig. 2 for the case of a moderately poor solvent.

---

[3] The application of this equation must obviously be limited to graphical extrapolations of $1/[\eta]$ since the factors, μ, ν, . . . , omitted in the third and higher terms of [2a] are <1.0.

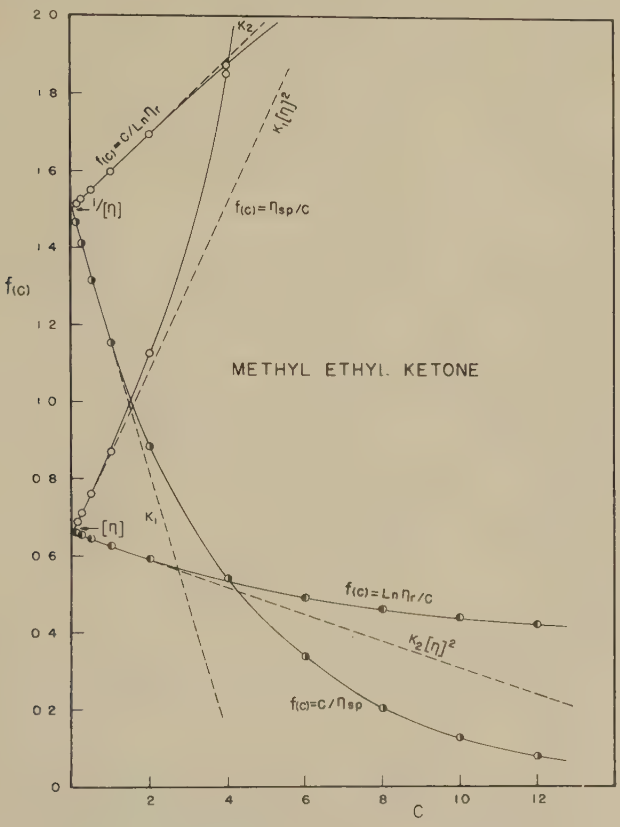

FIG. 2. The conventional double plot and the new double plot for determining $[\eta]$ (The four limiting slopes give k_1, $k_1[\eta]^2$, k_2 and $k_2[\eta]^2$.)

Equations used: [2], [3], [4] and [8]

The numerical values of $[\eta]$ obtained are 0.66_1 (old double plot) and 0.66_4 (new double plot). Thus, it is likely that the true value of $[\eta]$ is 0.6625 ± 0.0015. This will be verified below. To be discussed later is the fact, also apparent from Fig. 2, that the combination of the four plots gives directly the values of k_1, k_2, $k_1[\eta]^2$, and $k_2[\eta]^2$.

On applying the new double plot to a good solvent, (Fig. 3), one faces, in principle, the same situation as illustrated in Fig. 1 for the old double plot. The uncertainty is here smaller, however, for apparent reasons of symmetry. Either of two measures allows a further reduction in this uncertainty of $[\eta]$. One consists of ascertaining the extreme range of possible intercepts (see Fig. 1) for both double plots. The most probable value of $[\eta]$ and the remaining uncertainty will be defined by the overlap of the two ranges, it being understood that the values of one range are inverted prior

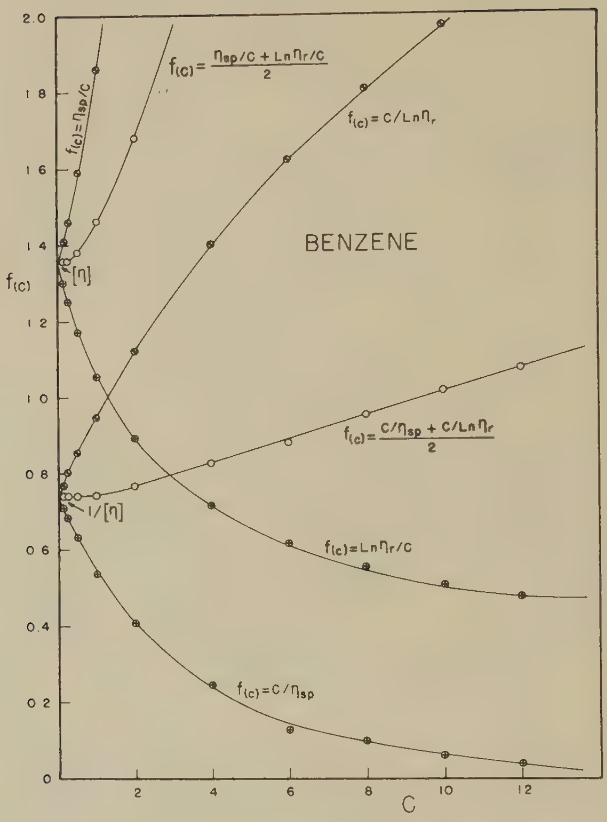

FIG. 3. The determination of $[\eta]$ from triple plots.
Equations used: [2], [3], [4], [8], [9] and [10]

to comparison. Simpler and more effective is an alternate procedure, which takes advantage of the fact that

$$\left(\frac{c}{\eta_{sp}} + \frac{c}{\ln \eta_r}\right) \Big/ 2 = \frac{1}{[\eta]} - \left(\frac{k_1 - k_2}{2}\right) c. \qquad [9]$$

A plot based upon this equation will therefore yield a straight, nearly horizontal line at low concentrations, provided k_1 and k_2 have similar values. It is now precisely in good solvents that the two constants differ the least (see Tables III and IV). On converting the new double plot into a triple plot, virtually any uncertainty of the intercept is therefore removed in good solvents. Figure 3 shows, in fact, that the third plot (Eq. [9]) yields a practically horizontal line for all concentrations below 2%. This alternate procedure allows one to dispense with the old double plot entirely.

TABLE I

Intrinsic Viscosities of Polystyrene

Method	Solvent					
	Benzene	Toluene	o-Dichlorobenzene	x-Dichloro x-diethyl benzene	Methyl ethyl ketone	Decalin
1	1.34–1.36	1.23_2	1.11_3	0.90_3	0.66_1	0.560–0.565
2	1.35_1^{T}	1.23_0^{D}	1.11_7^{D}	0.90_5^{D}	0.66_4^{T}	0.56_2^{T}
3	1.35_0	1.231 ± 0.001*	1.115 ± 0.002*	0.904 ± 0.001*	0.6625 ± 0.0015	0.56_{25}
4	1.356 ± 0.001*	—	—	—	0.663 ± 0.001*	0.5625 ± 0.0005*
5	1.3_5	1.2_3	1.1_0	0.9_0	0.65_5	0.56_8
6	1.75	1.60	1.50	—	0.72	0.53

Methods:

1. Conventional double plot (Eqs. [2] and [3]; see Fig. 1).
2. New double plot (D) (Eqs. [4] and [8]) or triple plot (T) using, in addition, Eq. [9]; see Figs. 2 and 3.
3. Mean of lines (1) and (2).
4. Extrapolation of $[\eta]_a(c)$-curves; see Figs. 5 and 6.
5. Correct extrapolation of $\log(\eta_{sp}/c)(c)$-plots (Eq. [12], Fig. 7).
6. Conventional (Incorrect) extrapolation of same (Fig. 7).

* Values used in later calculations, Tables, and Figures.

Equations [2] and [3] also may be combined to give

$$\left(\frac{\eta_{sp}}{c} - \frac{\ln \eta_r}{c}\right) \Big/ 2 = [\eta] + \left(\frac{k_1 - k_2}{2}\right)[\eta]^2 c. \qquad [10]$$

It is thus possible, in principle, to convert the conventional double plot also into a triple plot. Clearly, this has much less interest, since the horizontal section of the third plot is limited to far too narrow a concentration range.

Numerical data obtained for six solvents are given in Table I. Line 1 gives the values obtained by means of the conventional double plot. For benzene and decalin the entire range of possible values is given (see Fig. 1); for the other solvents only the mean $[\eta]$ is indicated. Line 2 contains the values obtained by means of the new double plot (three cases) and triple plot (three cases), respectively. Line 3 gives the mean of the values obtained by the conventional and new plots, respectively. In four of the six cases considered, the comparison of the values obtained by the new

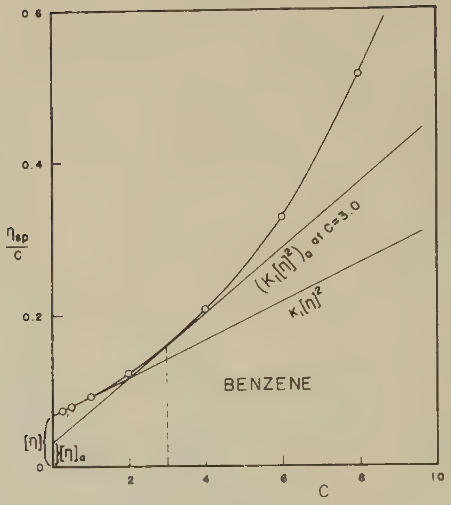

Fig. 4. Principle of precision method for determining $[\eta]$.

and old procedure, respectively, allows an approximate definition of the accuracy of the $[\eta]$-values obtained. In the two remaining cases, preference must be given to the values obtained by the new procedure rather than to the mean. This is borne out by the results given in the following section.

3. Extrapolations of the "Apparent" Intrinsic Viscosity

Equation [2] may be substituted by the following equation, outside of its very limited range of approximate validity:

$$\frac{\eta_{sp}}{c} = [\eta]_a(c) + (k_1[\eta]^2)_a(c)c \qquad [2b]$$

where $[\eta]_a \underset{c\to 0}{=} [\eta]$ and $(k_1[\eta]^2)_a \underset{c\to 0}{=} k_1[\eta]^2$. The meaning of these terms is illustrated by Fig. 4.[4]

Similarly,

$$\frac{c}{\eta_{sp}} = \frac{1}{[\eta]_a}(c) - (k_1)_a(c)c. \qquad [4a]$$

Applying the same principle to Eqs. [3] and [8], two $[\eta]_a(c)$ and two $1/[\eta]_a(c)$ curves can be obtained once the concentration function of the slopes is known in sufficient approximation. The latter information can easily be obtained by a graphical method discussed in the following section.

The four curves thus obtained are given in Fig. 5 for the solvent benzene. All $1/[\eta]_a$-values are inverted, prior to plotting, in order to produce a com-

---

[4] The subscript "a" defines an apparent value.

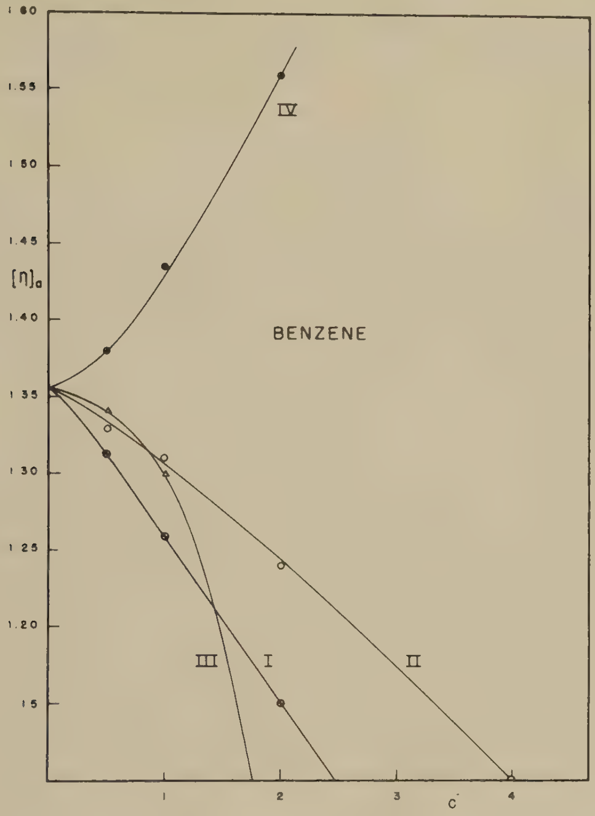

FIG. 5. Precision method for determining $[\eta]$ (quadruple plot).

$$\text{I: } [\eta]_a = \ln \eta_r/c + (k_2[\eta]^2)_a\,(c)c$$
$$\text{II: } [\eta]_a = 1/\{(c/\ln\eta_r) - (k_2)_a(c)c\}$$
$$\text{III: } [\eta]_a = \eta_{sp}/c - (k_1[\eta]^2)_a(c)c$$
$$\text{IV: } [\eta]_a = 1/\{c/\eta_{sp} + (k_1)_a(c)c\}$$

mon intercept. (Obviously, all the plotted $[\eta]_a$-values are calculated values.) It is apparent that the quadruple plot has no advantage over the double plot based upon Eqs. (2*b*) and (4*a*) (curves III and IV, respectively). This double plot exhibits the desirable feature that both slopes approach, of necessity, the value of 0 as $c \rightarrow 0$. Thus, there exists virtually no uncertainty about the intercept. An additional important factor is the fact that uncertainties due to the scattering of experimental data at low concentrations are removed in the preceding process of obtaining the approximate concentration function of $(k_1[\eta]^2)_a$ and $(k_1)_a$, respectively. A more detailed illustration of the proposed double plot of $[\eta]_a$-values is given in Fig. 6 for the solvent methyl ethyl ketone.

This method is more laborious than that of the triple plot described in

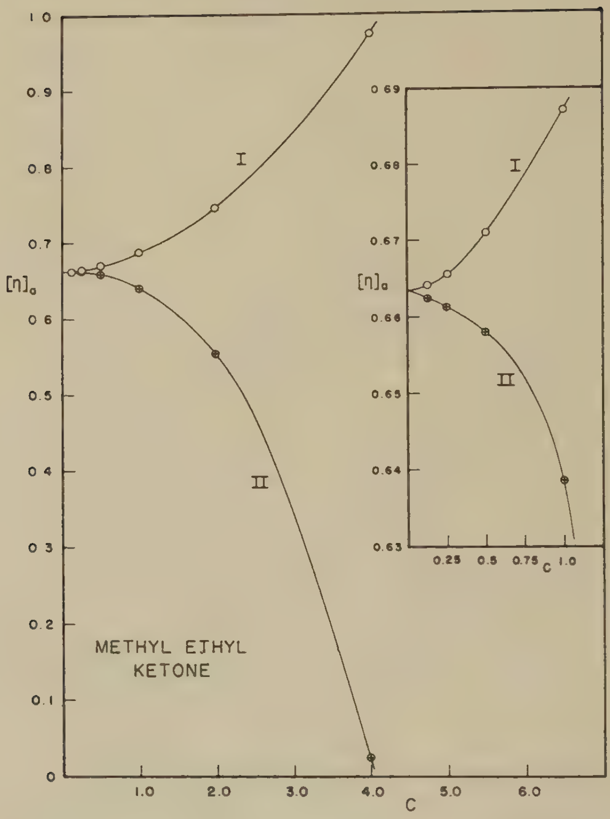

FIG. 6. Precision method for determining $[\eta]$ (double plot).

Equations used for calculation of $[\eta]_a$:
I: same as for IV in Fig. [5]
II: same as for III in Fig. [5]

the preceding section. It furnishes, on the other hand, undoubtedly the most precise $[\eta]$-values. Its use is indicated primarily in those cases where a check of $[\eta]$-values obtained by the alternate new procedure discussed in Section I, 2 appears desirable. Data obtained in the three cases tested are given in line 4 of Table I.

4. *Extrapolations from Logarithmic Plots*

A few comments may be in order with regard to a method of $[\eta]$-extrapolation used by a number of authors.

On replacing b in Eq. [1] by $k_3[\eta]$ rather than by $k_1[\eta]^2$, one arrives at

$$\frac{\eta_{sp}}{c} = [\eta]e^{k_3 c} \qquad [11]$$

as a possible function assuming, again, suitable higher terms in [1]. This function, proposed by several authors,[5] is generally referred to as the "Martin" equation. Its form

$$\ln\left(\frac{\eta_{sp}}{c}\right) = \ln\,[\eta] + k_3c \tag{12}$$

invites graphical application.

It is now clear from the outset that a straight line obtained from such a log plot with $c = 0$ as the origin, cannot extend over the same range of low concentrations as the straight-line portion of a plot of Eq. [2] except for the rare case that the third term in the logarithmic equivalent of Eq. [2]

$$\ln\left(\frac{\eta_{sp}}{c}\right) = \ln\,[\eta] + k_1[\eta]c - \tfrac{1}{2}k_1^2[\eta]^2c^2 + \cdots \tag{13}$$

is negligible, at any value of c.[6] The virtual absence of a limiting straight line follows from Fig. 10. An extrapolation to a precise $[\eta]$-value is therefore not possible. Values obtained from the "best possible straight line" at very low concentrations are given in line 5 of Table I.

The procedure commonly used in connection with these log plots consists, however, of extrapolating a quasi straight line found at $c > 4\%$, with omission of experiments at lower concentrations. In this manner fairly precise but outright inaccurate $[\eta]$-values are obtained. They are generally far too large (line 6 of Table I, and Fig. 7). (For a further discussion of these log plots see Section II, 4 and also the subsequent paper.)

II. Determination of Limiting Slopes

1. The Limiting Slope $k_1[\eta]^2$

The direct graphical determination of the limiting slope, $k_1[\eta]^2$, yields quite uncertain numerical values if a strong curvature of the $\eta_{sp}/c(c)$-curves begins at very low concentrations (good solvents). The situation is illustrated by Fig. 1. The use of a different procedure is then particularly important.

Such a procedure may be based upon differentiation, with respect to c, of Eq. [2*b*].

In order to simplify, the first term may be replaced by $[\eta]$. This will,

---

[5] The first reference to this equation is found in: Bungenberg de Jong, H. G., Kruyt, H. R., and Lens, J., *Kolloid Beih.* **36**, 429 (1932); for the unpublished contribution of Martin, A. F., see Abstracts of A.C.S. Meeting, Memphis, Tennessee, April, 1942.

[6] Since it is negligible as $c \to 0$, it follows that the limiting value of the "Martin" constant

$$\underset{c\to 0}{k_3 =} (k_3)_0 = k_1[\eta]$$

as already known.

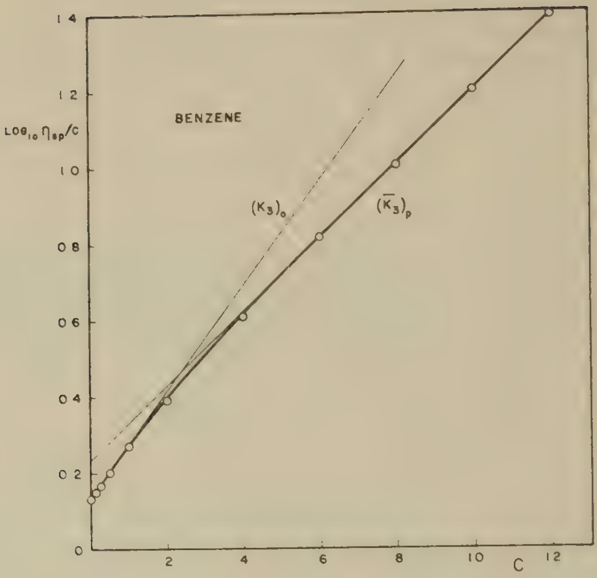

FIG. 7. The two characteristic slopes in "Martin" plots.

obviously, lead to quite incorrect values of the slope $(k_1[\eta]^2)_a$ at large c-values, but it cannot affect the value of the limiting slope.

Chord plots are the most rapid and convenient procedure for the problem at hand. They cannot be used to fullest advantage here because Streeter and Boyer unfortunately chose a geometrical progression for concentrations below 2%. Figure 8 illustrates the procedure for three solvents, with omission of the chords in the main curve of decalin in order to avoid crowding. The intercept of these curves represents the limiting slope $k_1[\eta]^2$.

In addition to illustrating the method proposed, this figure reveals clearly two facts which are more difficult to discern in a direct plot of Eq. [2]: First of all, it is apparent that Eq. [2] does not hold strictly at any finite concentration, not even in poor solvents. It follows implicitly that it is really impossible to obtain a true value of the limiting slope from a direct plot of $\eta_{sp}/c(c)$. Secondly, the chord plot reveals quite strikingly anomalous changes in slope for all solvents, but particularly for benzene, at concentrations of 0.5% and less. Whether these anomalies are due to experimental errors or are real—as recent work of Streeter and Boyer at very low concentrations may possibly indicate (5)—is immaterial. For, the search for a limiting slope would obviously be futile—irrespective of the method used—unless the basic concentration function is assumed to be monotonic and is considered apart from any possible anomalies at very low concentrations.

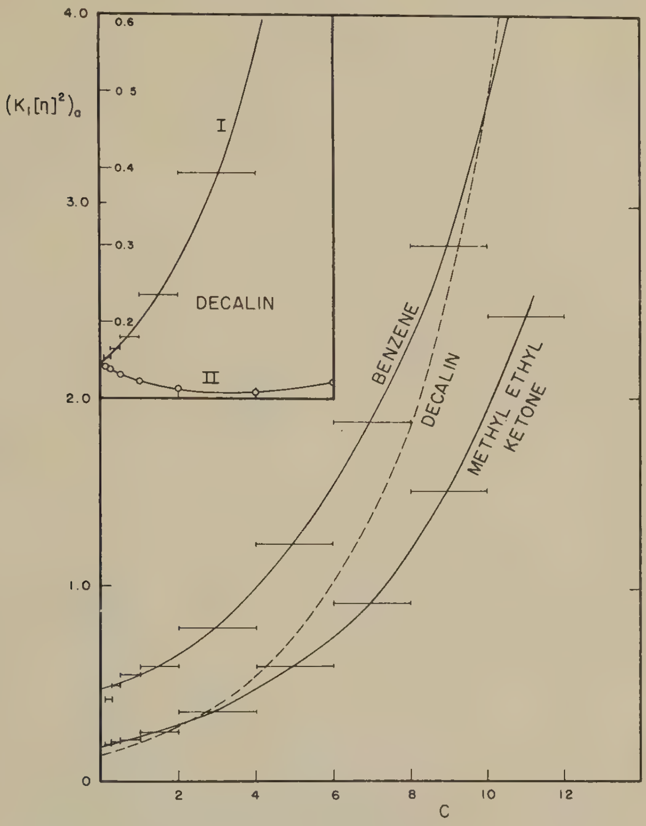

FIG. 8. Precision method for determining $k_1[\eta]^2$.

$$\text{II: } (k_1[\eta]^2)_a = \frac{d(c/\eta_{sp})}{dc}[\eta]_a^2 c$$

all other curves:

$$(k_1[\eta]^2)_a = d(\eta_{sp}/c)/dc$$

These anomalies, or experimental uncertainties, at low concentration make it desirable, however, to fix the intercept more securely than is possible by means of single plots. Fortunately, Eq. [4*a*] allows one to obtain an independent second (or third) value of $k_1[\eta]^2$, based upon multiplying the slope values $(k_1)_a(c)$ discussed below, by either $[\eta]^2$ or $[\eta]_a{}^2(c)$. A double (or triple) plot is thus obtained in which (at least two of) the converging curves have slopes of opposite sign at all concentrations. It is illustrated, for decalin, in the inset to Fig. 8. (The use of $[\eta]_a$, as a multiplier, leads here to a minimum (curve II), at moderate concentrations. This is absent if $[\eta]$ is used instead.)

Numerical values obtained by the various procedures are given in Table II. Line 1 gives the data obtained by the conventional method

TABLE II

Limiting Values of $k_1[\eta]^2$

Method	Solvent		
	Benzene	Toluene	*o*-Dichlorobenzene
1	0.48–0.58	0.53–0.57	.047–0.48
2	0.50 ± 0.025	—	—
3	$0.47_5{}^{*a}$	—	—
4	0.43_2	$0.48_9{}^{*}$	$0.42_3{}^{*}$

Method	Solvent		
	x-Dichloro *x*-diethyl benzene	Methyl ethyl ketone	Decalin
1	0.33_6	0.21_5	0.17_4
2	—	0.19_0	0.14_5
3	—	$0.18_7{}^{*a}$	$0.14_7{}^{*b}$
4	$0.30_5{}^{*}$	0.18_5	0.14_6

Methods:

1. Conventional tracing of limiting tangent (Figs. 1 and 2).
2. Single plot extrapolation of $(k_1[\eta]^2)_a(c)$-curve (Fig. 8).
3. Double plot extrapolation using for second plot $(k_1)_a(c)$-curves and multiplying all values by $(a)\ [\eta]^2$ or $(b)\ [\eta]^2{}_a(c)$.
4. Multiplying limiting values of k_1 (Table IV) by $[\eta]^2$ (Table I).

(plot of Eq. [2]). These data are too high compared to those obtained with the alternate methods proposed here (lines 2 and 3). This has a good reason explained shortly. A comparison of lines 2 and 3 shows that a single plot of $(k_1[\eta]^2)_a(c)$ may be sufficient to obtain acceptable values of $k_1[\eta]^2$, but that a double (or triple) plot is desirable for good solvents. Line 4, finally, gives data obtained by multiplying, by $[\eta]^2$, the "mean values" of k_1 discussed in the following section. Because of the amplification of errors by multiplication, the latter values are only second best, by comparison, to those in line 3.

2. *The Limiting Values of* k_1

The conventional method of obtaining k_1 consists of dividing the slope $k_1[\eta]^2$ of the η_{sp}/c-plot by $[\eta]^2$. The resulting appreciable uncertainty is defined by the ratio of two errors, of which one is significant in itself and the other is amplified by squaring. Apart from the inherent nonsystematic errors, such k_1-values are bound to be too large, since the $k_1[\eta]^2$-values are too large.[7] They are given in line 2 of Table III.

---

[7] The reason is that none of the slopes becomes really constant at small c, but keeps on decreasing or increasing respectively as $c \to 0$. While this is quite evident from appropriate figures, such as Figs. 8 and 9, it is difficult to detect visually in primary plots (Figs. 2 and 3). The strong curvature at intermediate concentrations overshadows here the comparatively slight curvature at low concentrations to an

TABLE III

Limiting Values of k_1

Method	Solvent		
	Benzene	Toluene	*o*-Dichlorobenzene
1	0.20_8	0.28_3	0.29_7
2	0.2_{88}	0.36_3	0.38_2
3	0.2_{48}	0.32_3*	0.34_0*
4	0.235 ± 0.0025*	—	—
5	0.25_8	—	—

Method	Solvent		
	x-Dichloro *x*-diethyl benzene	Methyl ethyl ketone	Decalin
1	0.33_5	0.34_6	0.45_7
2	0.41_1	0.48_9	0.55_0
3	0.37_3*	0.41_8	0.50_4
4	—	0.420 ± 0.0025*	0.46 ± 0.01*
5	—	0.42_5	0.46_5

Methods:

1. Limiting tangent from plot of Eq. [4] (Fig. 2).
2. Limiting tangent from plot of Eq. [2], divided by $[\eta]^2$ (conventional method).
3. Means of lines (1) and (2).
4. New double (triple) plot (see Fig. 9).
5. Calculated from $k_1[\eta]^2$ (line 3, Table II).

Equation [4] offers now the possibility of determining the limiting value of k_1 by direct graphical method (see Fig. 2). Data thus obtained for the five solvents tested are given in line 1 of Table III. It must be suspected at once that these values are too small. The two sets of k_1-values in lines 1 and 2 of Table III differ in fact as anticipated. Inspection of the character of the (c/η_{sp}) (c)- and $(\eta_{sp}/c)(c)$-curves in Figs. 2 and 3 makes it likely that the systematic errors inherent in the k_1-values of lines 1 and 2 are very similar though opposite in sign. Granting this—which will have to be verified in the following—the mean values given in line 3 should come very close to the true k_1-values.

A precision method, similar to that used for obtaining the best $k_1[\eta]^2$-

---

extent sufficient to make the latter appear nonexistent. Consequently, limiting tangents fitted to the curves are bound to have values too small if the rate of change in the slope with c is negative, and values too large if the rate of change is positive. Inspection of Fig. 2 will show that the values of k_1, k_2 and k_2 $[\eta]^2$ will therefore be too small, while those of $k_1[\eta]^2$ and those of k_1 derived from it, will be too large. It is noteworthy that this psychological error is perfectly reproducible, as the fairly good agreement between our respective data and those given by Streeter and Boyer (1) indicates. Since the rate of change of the various slopes varies with the quality of the solvent, and therefore with $[\eta]$, it is clear that the change of this error with $[\eta]$ can lead to freak relationships (see Sections III, 2 and III, 4).

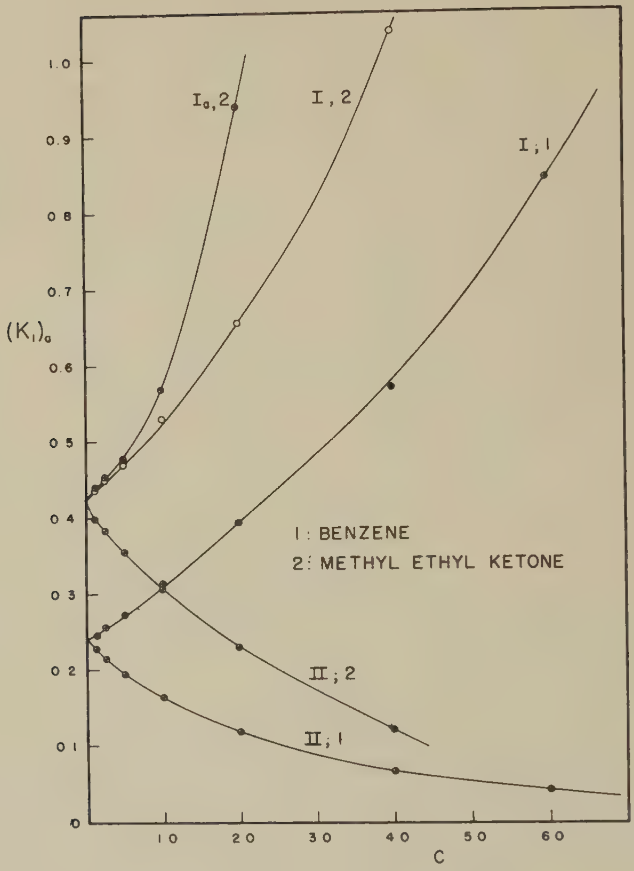

FIG. 9. Precision method for determining k_1.

I: $(k_1)_a = (k_1[\eta]^2)_a(c)/[\eta]^2$
Ia: $(k_1)_a = (k_1[\eta]^2)_a(c)/[\eta]_a^2$
II: $(k_1)_a = d(c/\eta_{sp})/dc$

values, is based upon Eq. [4*a*]. The first derivative of this equation gives the true limiting k_1-value on extrapolating the $(k_1)_a(c)$-curve to $c = 0$. Again, $1/[\eta]$ may be substituted for $1/[\eta]_a$, since the slope at finite concentration is of only minor interest here. The curves II, 1 and II, 2 in Fig. 9 illustrate the procedure for two solvents. The points given are, again, values interpolated from chord plots. In order to obtain a double plot, independently obtained $(k_1[\eta]^2)_a$-values (Fig. 8) are divided by $[\eta]^2$ (curves I, 1 and I, 2); a triple plot follows on dividing by $[\eta]_a^2$ (curve I*a*). There is, however, no material advantage in using a triple plot here. Numerical values of the intercepts are given in line 4 of Table III, for three solvents tested. These precision data do not differ by more than 8 % at the most from the mean of the alternate k_1-values given in line 3. Unless optimum accuracy is desired, such mean values may therefore be used instead of the values derived by the precision method.

An alternate method of obtaining precision values consists, of course, of using the precision values of $k_1[\eta]^2$ (line 3 of Table II) and dividing these by the square of the precision values of $[\eta]$ (line 4 of Table I). These values are given in line 5 of Table III. In two of the three cases tested, the agreement is excellent, the deviation being less than 2%.

3. *The Limiting Values of* k_2

The procedures for a determination of the limiting values of k_2 are completely analogous to those described for k_1. The values in line 1 of Table IV are obtained by fitting a limiting tangent to plots of Eq. [8]. The values in line 2 pertain to the limiting tangents of graphs according to Eq. [3], dividing the result by $[\eta]^2$. Both sets of values are bound to be somewhat too small. Taking their mean, in line 3, has therefore here only one advantage, that of reducing the nonsystematic error.

Data obtained by the analog of the precision method used for k_1 are given, for two cases tested, in line 4. The intercepts of double plots

TABLE IV

Limiting Values of k_2

Method	Solvent Benzene	 Toluene	 *o*-Dichlorobenzene
1	0.24_7	0.16_9	0.14_4
2	0.20_7	0.16_2	0.12_5
3	0.22_7	0.16_6*	0.13_5*
4	0.23_6*	—	—
5	0.26_5	0.17_7	0.16_0

Method	Solvent *x*-Dichloro *x*-diethyl benzene	 Methyl ethyl ketone	 Decalin
1	0.13_8	0.096_9	0.033_2
2	0.12_6	0.080_7	0.028_8
3	0.13_2*	0.088_8	0.031_0*
4	—	0.083 ± 0.005*	—
5	0.12_7	0.08_0	0.0_4

Methods:

1. Limiting tangent from plot of Eq. [8] (Fig. 2).
2. Limiting tangent from plot of Eq. [3], divided by $[\eta]^2$ (conventional method).
3. Mean of lines (1) and (2).
4. New double (triple) plot.
5. Calculated from Eq. [15*a*].

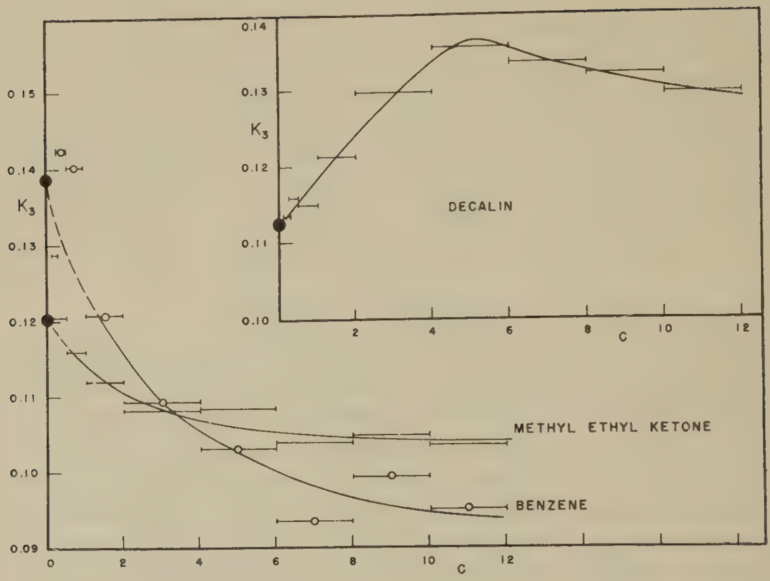

FIG. 10. The slope in "Martin" plots.

$k_3 = d \log_{10} \eta_{sp}/dc$

cannot be obtained here with a precision approaching that in the case of k_1, owing to unfavorable similarities of $(\ln\eta_r/c)(c)$ and $(c/\ln\eta_r)(c)$ curves. The method is therefore here of minor usefulness only and hardly warrants the time spent with applications. The data in line 4 do not, however, contain any systematic error.

In view of the difference in precision and accuracy of k_1- and k_2-values it may be preferable to obtain k_2-values—for good solvents—indirectly, by means of a simple relation existing between these values and the k_1-values (see Section III, 1). Such indirect k_2-values are given in line 5 of Table IV.

The interest in the limiting slope $k_2[\eta]^2$ is minor. The possible methods for its determination are now obvious.

4. The Limiting and Principal Values of k_3

The $\left(\frac{d\log_{10}\eta_{sp}}{dc}\right)(c)$-curves in Fig. 10 show that the slope k_3 (Eq. [12]) increases continuously with decreasing concentration, with the exception of decalin, where the behavior is quite complex. This increase—directly opposite to the behavior of other slopes discussed previously—becomes so strong at the lowest concentrations that a reliable direct extrapolation of the limiting slope, $(k_3)_0$, is not possible. (This amplifies the earlier statement that these plots are unsuitable for determinations of $[\eta]$.) The values of $k_1[\eta]$ (line 1, Table V) drawn into the ordinate,[8] at $c = 0$, represent

---

[8] The values were, to this effect, multiplied by 0.4343.

TABLE V

The Limiting Values of $k_1[\eta] \equiv (k_3)_0$ *and the Value of* $(k_3)_p$

(Valid for $\log_e$ plots)

Quantity considered	Solvent Benzene	 Toluene	 *o*-Dichlorobenzene
$k_1[\eta] \equiv (k_3)_0$ (1)	0.31_9	0.39_7	0.37_9
$(\bar{k}_3)_p$ (2)	0.221_1	0.222_4	0.211_8
$(\bar{k}_3)_p - (k_3)_0$ (3)	-0.09_8	-0.17_5	-0.16_7

Quantity considered	Solvent *x*-Dichloro *x*-diethyl benzene	 Methyl ethyl ketone	 Decalin
$k_1[\eta] \equiv (k_3)_0$ (1)	0.33_7	0.27_8	0.25_9
$(\bar{k}_3)_p$ (2)	—	0.241_1	0.305_4
$(\bar{k}_3)_p - (k_3)_0$ (3)	—	-0.03_7	$+0.04_6$

Methods:

1. Calculated from Tables I and III.
2. Mean slope between 6% and 12%.
3. Using the values of lines 1 and 2.

a plausible intercept for these curves. These values were calculated from those in Tables I and III. Since $(k_3)_0 = k_1[\eta]$, as shown earlier, the acceptable fit of the calculated intercepts may be considered as a preliminary and satisfactory check of the accuracy of the k_1 and $[\eta]$-values involved.

Between $c \cong 6$ and $c = 12$, the rate of change in the slope value is so slow that these log plots approximate a straight line within this range (see Fig. 7). There is therefore some justification for replacing $k_3(c)$ within this range by a mean value, $(\bar{k}_3)_p$, the principal slope constant of Martin plots. Values of $(\bar{k}_3)_p$ for the five solvents considered are given in line 2 of Table V. Line 3 gives the difference between $(\bar{k}_3)_p$ and $(\bar{k}_3)_0$. This difference allows a quantitative definition of the error committed on extrapolating the quasi-straight portion of a Martin plot, *i.e.*, $(\bar{k}_3)_p$, to zero concentration for the purpose of obtaining the intrinsic viscosity. The error inherent in the incorrect value, $[\eta]_M$, thus obtained can be calculated from the following obvious relation

$$\frac{[\eta]}{[\eta]_M} = \exp \{[(\bar{k}_3)_p - (k_3)_0]c_i\} \tag{14}$$

where c_i is the concentration at which the two slopes intersect (see Fig. 7). Since this intersection generally occurs in the neighborhood of $c = 2$, Eq. [14*a*]

$$\frac{[\eta]}{[\eta]_M} \sim \exp \{2[(\bar{k}_3)_p - (k_3)_0]\} \tag{14a}$$

is sufficient for a rapid evaluation of the error. There is, in fact, a satisfactory agreement between the error thus calculated and that obtained from comparing directly the $[\eta]$-values in lines 4 or 3 with those in lines 6 in Table I.

It is of interest to inquire into the relationship of the two slope constants, $(k_3)_0$ and $(\bar{k}_3)_p$ and also into the cause of peculiarities of $\log(\eta_{sp}/c)(c)$-curves such as that illustrated for decalin in Fig. 10. These matters, being outside of the scope of the subject matter treated here, will be discussed in the subsequent paper. It should be mentioned, however, that some unjustified criticism of "Martin plots" in the recent literature is due to failure of the authors to differentiate properly between $(k_3)_0$ and $(\bar{k}_3)_p$.

III. Check of the Data

The preceding discussion has shown that it is now possible to obtain more precise $[\eta]$-values and limiting slope constants. It also became probable that these values are, in addition, more accurate. It is important to prove the latter point and also to verify the precision.

1. Direct Mutual Check of k_1 and k_2

Equation [3] may be transformed to

$$\eta_{sp} = -1 + \exp\{[\eta]c - (k_2)_a[\eta]^2c^2 + \cdots\}. \tag{3a}$$

On expanding, neglecting quartic and higher concentration terms in the result, and equating with

$$\eta_{sp} = [\eta]c + (k_1)_a[\eta]^2c^2, \tag{2c}$$

the relation

$$(k_1)_a = 0.5 - (k_2)_a + \{1/6 - (k_2)_a\}[\eta]c \tag{15}$$

is obtained. A $(k_1)_a$ (c)-plot should therefore approach a straight line at low concentrations as $(k_2)_a \rightarrow k_2$, and the intercept should have a numerical value of $(0.5\text{-}k_2)$. The pertinent curves in Fig. 9 agree with these deductions.

Of primary interest here is the fact that the limiting slope constants obviously and necessarily are connected by the simple relation

$$k_1 + k_2 = 0.5, \tag{15a}$$

which had already been pointed out by Ewart (6) and criticism of which by a few authors has no foundation.

This relation provides an excellent and very severe test for the k_1- and k_2-values obtained with the new procedures. This test is carried out in Fig. 11. Its result is very satisfactory considering that the deviations observed are the composite of the deviations of both k_1 and k_2. The major part of the deviations goes to the account of the k_2-values, as will become apparent shortly.

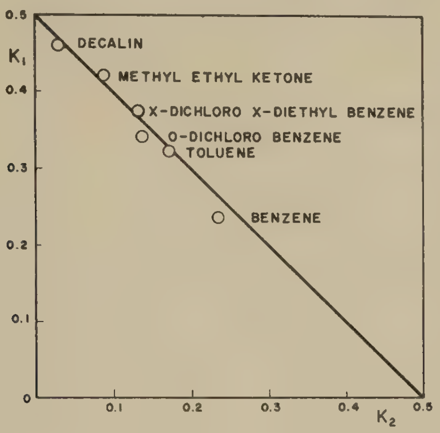

FIG. 11. Test of the Ewart relation $k_1 + k_2 = 0.5$.

2. Indirect Mutual Check of k_1 and k_2

An intimately related check which is still more sensitive to deviations than the preceding one, may be based upon the relationship between k_1 and the Baker constant n. On transforming the Baker equation

$$\eta_r = \left(1 + \frac{[\eta]c}{n}\right)^n \qquad [6a]$$

to

$$\frac{\eta_{sp}}{c} = [\eta] + \frac{(n-1)[\eta]^2c}{2n} + \cdots \qquad [6b]$$

and equating it to Eq. [2], the $n(k_1)$ relation[9]

$$n = \frac{0.5}{0.5 - k_1}; \qquad k_1 = \frac{n-1}{2n} \qquad [16]$$

is obtained, which leads back to Eq. [15a] on substituting n by $1/2k_2$. The theoretical $k_1(n)$ plot is given in Fig. 12. The $k_1 -$ values of Table III and the n-values, derived from the k_2-values of Table IV, appear again as satisfactory. In contradistinction, the corresponding values, obtained by Streeter and Boyer (1) by means of the conventional procedures, are satisfactory only for k_1-values within the limited range of 0.3 to 0.4. On either

---

[9] The $n(k_3)_0$ relation

$$n = \frac{[\eta]}{[\eta] - 2(k_3)_0}; \qquad (k_3)_0 = \frac{[\eta]}{2}\left(\frac{n-1}{n}\right) \qquad [16a]$$

is also obtained. Although such an equation is found in the literature, it should be emphasized that there exists no simple relation between n and $(\bar{k}_3)_p$.

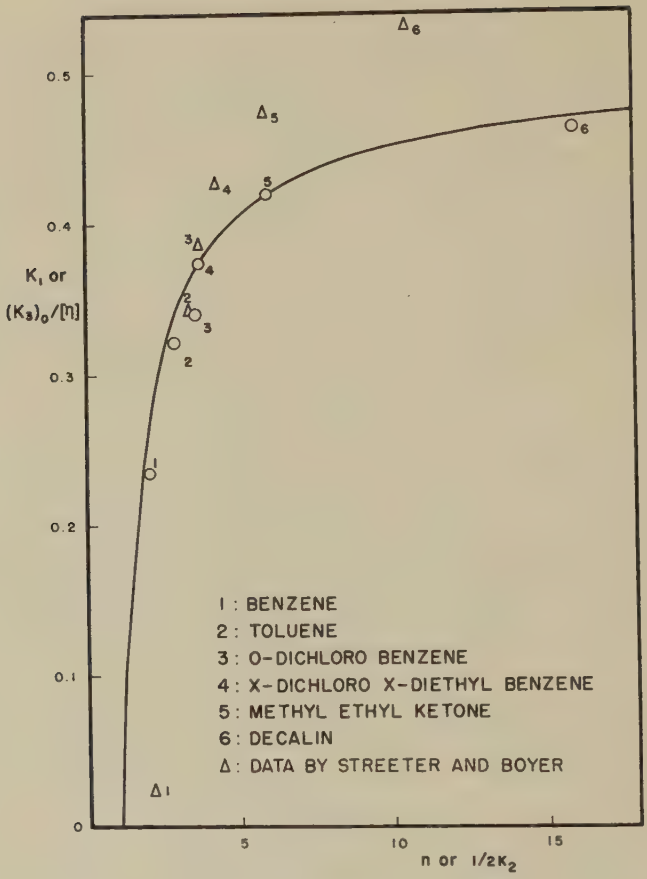

FIG. 12. Test of the $k_1(\eta)$ relationship.

side of this limit, the error increases rapidly in a systematic manner. The insertion of additional data collected by Streeter and Boyer on solvents not considered here, would strengthen further the latter statement; so would also the insertion of our own data obtained with the approximate graphical methods (line 1 of Table III and line 1 of Table IV). The respective approximate procedures are herewith conclusively recognized as inadequate.[10]

A brief reference may be made here to the fact that the relation shown in Fig. 12 provides the fastest and most accurate method of determining n-values if the Baker equation is to be used for calculating the concentra-

---

[10] On plotting the constants of Streeter and Boyer into Fig. 11, a sigmoid curve is obtained which crosses the straight line at $k_1 \sim 0.35$. The variation in the systematic error with the magnitude of k_1 and k_2 is such that a fictitious relation is obtained on plotting $(k_1 + k_2)$ vs. k_1 (Fig. 2, *loc. cit.*).

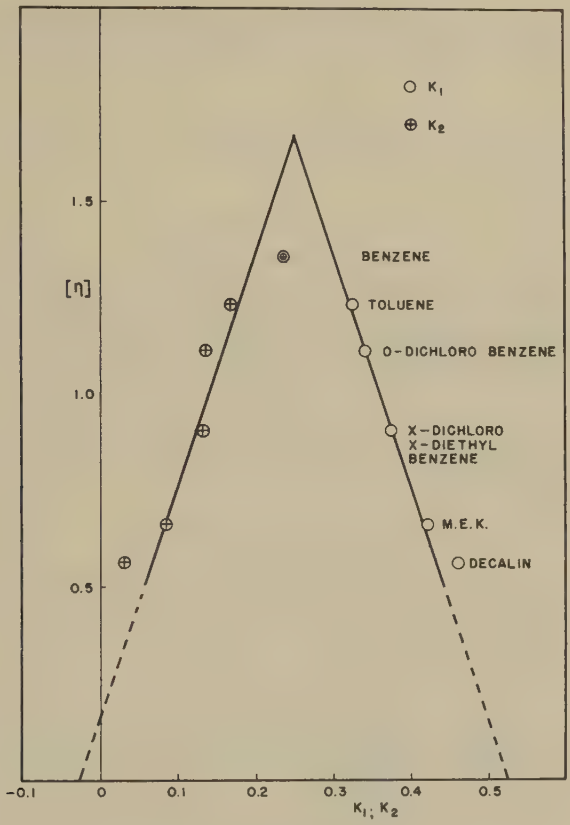

FIG. 13. The $k_1([\eta])$ and $k_2([\eta])$ relations.

tion dependence of viscosity. For other methods see the subsequent paper and also (11).

3. Independent Check of k_1 and k_2

The value of k_1 increases and k_2 decreases with decreasing $[\eta]$. Nothing too definite can be predicted for the respective relationships, k_1 $([\eta])$ and $k_2([\eta])$ except that they have to be antisymmetrical in view of Eq. [15*a*]. Whereas any empirical relation to be found can therefore not be used as a criterion of the accuracy of either k_1 or k_2-values (or, instead, of the respective $[\eta]$-values), it should show which values are more precise, those of k_1 or those of k_2.

Plots of $k_1([\eta])$ and $k_2([\eta])$ are given in Fig. 13. The $k_1([\eta])$ plot yields a straight line within the range of $[\eta]$-values considered here, so that

$$[\eta] = a - bk_1 \qquad [17]$$

where the constants a and b have the values 3.18 and 6.05_7, respectively. Consequently, within the same range of $[\eta]$-values,

$$[\eta] = a' + bk_2 \tag{18}$$

where a' has the value of 0.155, as it should. In view of Eq. [15a] it is, in fact, necessary that

$$a - a' = 0.5b; \tag{19}$$

it is also necessary that the bisectrice of the two straight lines intersect the abscissa at the value of 0.25 and that the sum of the actually drawn two intercepts with the abscissa amounts to 0.5. The figure shows, as suspected, that the scattering of the k_2-values is stronger than that of the k_1-values.

The lack of scattering (except for benzene and decalin) of the $k_1([\eta])$ data implicitly attests to the high precision of the $[\eta]$-values obtained by the new procedures.

4. Check of the $k_1[\eta]^2$-Values

In view of the preceding checks, it is, not necessary to test the $k_1[\eta]^2$-values obtained separately. It is, of interest, however, to use those data for a test of the relationship

$$k_1[\eta]^2 = \alpha + \sigma[\eta] \tag{20}$$

proposed by Eirich and Riseman (7). Fig. 14 shows that this relation approximates the facts sufficiently well within the narrow range of $[\eta]$-

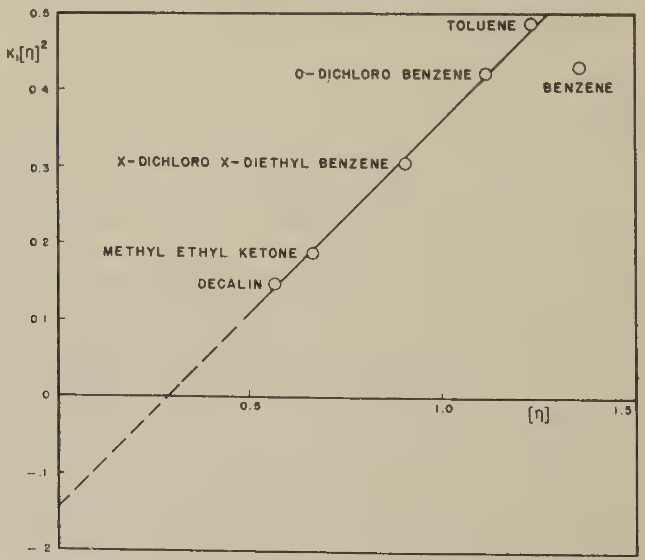

FIG. 14. Test of the Eirich-Riseman relation: $k_1[\eta]^2 = \alpha + \sigma[\eta]$.

values considered here. Slope and intercept have the values 0.50_7 and -0.14_6, respectively.[11]

According to [20]

$$k_1 = \frac{\alpha}{[\eta]^2} + \frac{\sigma}{[\eta]} \tag{20a}$$

whereas, according to [17]

$$k_1 = \frac{a - [\eta]}{b} \tag{17a}$$

Apparently, the range of $[\eta]$-values in the solvents discussed is small enough (0.56 to 1.36) and the absolute values are close enough to 1.0 to make both slopes practically constant, viz.,

$$\sigma = \frac{[\eta]a - [\eta]^2}{b} - \frac{\alpha}{[\eta]} \sim \text{constant} \tag{21}$$

or

$$b = \frac{[\eta]^2 a - [\eta]^3}{[\eta]\sigma + \alpha} \sim \text{constant} \tag{21a}$$

respectively. Strict relationships of which [20] and [17] are approximations will be discussed elsewhere.

IV. Application of the Results to Other Types of Measurements

Some of the new equations and procedures discussed above may be useful also in connection with other types of investigations, such as measurements of osmotic pressure and light scattering. It is not intended to attempt here a systematic survey of the possibilities. One example will suffice. On selecting for the well-known osmotic pressure equation

$$\frac{\pi}{c} = \frac{RT}{M} + Bc + \cdots \tag{22}$$

the following higher terms

$$\frac{\pi}{c} = \frac{RT}{M} + Bc + \left(\frac{M}{RT}\right) B^2 c^2 + \left(\frac{M}{RT}\right)^2 B^3 c^3 + \cdots, \tag{22a}$$

the graphically useful function of the above series results as

---

[11] Using their different $k_1[\eta]^2$-data, obtained by the conventional procedure, Streeter and Boyer (1) also confirmed Eq. [20]. The slope and intercept of the respective straight line are 0.53 and -0.12, respectively. This may suggest that, here again, the systematic error inherent in conventional slope determinations varies linearly with $[\eta]$.

$$\frac{c}{\pi} = \left(\frac{c}{\pi}\right)_0 - \left(\frac{c}{\pi}\right)_0^2 Bc \qquad [23]$$

This is the osmometric analog of Eq. [4][12]. Of interest is the fact that a slight transformation yields

$$\pi = \frac{RT}{M} \frac{c}{\left(1 - \frac{M}{RT} Bc\right)} \qquad [24]$$

which, upon substituting

$$\frac{MB}{RT} \longrightarrow s \qquad [25]$$

reduces to the Sackur (8) equation as used by Schultz (9)

$$\pi = \frac{RT}{M} \frac{c}{1 - cs} \qquad [24a]$$

In view of the well known relationship between B and the Huggins interaction constant, μ, it is now possible to give to s, defined by Schultz as the ratio of the so-called "co-volume" to the concentration, a modern meaning. Because of [25], it is, in particular, no longer surprising that s increases with molecular weight (10).

SUMMARY

1. Existing equations and conventional procedures for the graphical determination of intrinsic viscosity and slope constants are analyzed. It is shown that slope constants obtained by the conventional procedures contain a systematic error which varies with the intrinsic viscosity.

2. Several new equations and procedures are proposed which allow a more precise and more accurate determination of intrinsic viscosity and slope constants.

3. Accuracy and precision of the latter data are checked by means of relationships existing between the various quantities.

4. Several new relationships between the various quantities are established and tested.

5. Attention is drawn to the possible application of the new equations and procedures to the evaluation of measurements of osmotic pressure and of light scattering.

REFERENCES

1. STREETER, D. J., AND BOYER, R. F., *Ind. Eng. Chem.* **43**, 1790 (1951).
2. SCHULTZ, G. V., AND BLASCHKE, F., *J. prakt. Chem.* **158**, 130 (1941).

---

[12] The limitations of this equation and their cause are analogous to those of Equation [4]; see Footnote 3.

3. Huggins, M. L., *J. Am. Chem. Soc.* **64,** 2716 (1942).
4. Baker, F., *J. Chem. Soc.* **103,** 1653 (1913).
5. Streeter, D. J., and Boyer, R. F., *J. Polymer Sci.* **14,** 5 (1954).
6. Ewart, R. H., *Advances in Colloid Sci.* **2,** 211 (1946).
7. Eirich, F., and Riseman, J., *J. Polymer Sci.* **4,** 417 (1949).
8. Sackur, O., *Z. physik. Chem.* **70,** 477 (1910).
9. Schultz, G. V., *Z. physik. Chem.* **A158,** 237 (1932) (and later papers).
10. Schultz, G. V., *Z. physik. Chem.* **A176,** 317 (1936).
11. Weissberg, S. G., Simha, R., and Rothman, S. *J. Research Natl. Bur. Standards* **47,** No. 4 (October 1951).

STUDIES ON POLYELECTROLYTES.

VI. GUM AGAR

Sadhan Basu and Anil K. Sircar

Indian Association for the Cultivation of Science, Calcutta, India

Received August 31, 1954

INTRODUCTION

In a previous communication it has been shown by Basu *et al.* (1) that the sodium salt of arabic acid behaves as a polyelectrolyte; this has been taken to indicate a linear structure of the gum arabate molecule. The work has been extended to other gums, and the present paper reports the results of similar studies on gum agar. The difference between the acidic character of arabic acid and agar acid lies in the fact that whereas the acidity in arabic acid is due to the COOH group of the uronic acid segment of the molecule, in agar acid this is due to the SO_3H group, agar being a calcium salt of the sulfuric acid ester of a complex polycarbohydrate. The present study has been confined to the free acid and its sodium salt and is expected to throw some light on the nature of the molecule and the physical properties of its solution.

EXPERIMENTAL

Preparation of Free Agar Acid and Its Sodium Salt

The usual method of liberating agar acid from the gum is to treat the aqueous dispersion with hydrochloric acid when the gum is decomposed into calcium chloride and free agar acid which can be precipitated out by alcohol or acetone. It has, however, been shown by Fairbrother and Mastin (2) that the reaction reaches an equilibrium; hence in order to effect a complete removal of calcium the gum solution must be made rather strongly acidic, which introduces the chance of extensive degradation. In order to avoid this complication the gum solution was treated with a solution of sodium oxalate when calcium precipitated out as oxalate. The solution was filtered and then dialyzed free of sodium oxalate. The dialyzed solution was made acidic with HCl and the agar acid precipitated with alcohol. The acid was again dissolved in water and dialyzed free of chloride ions. The equivalent weight, obtained by electrometric titration with alkali, was 2213. The ash content of the free acid was 0.7%.

The free acid was converted into its sodium salt by treating it with a solution of sodium hydroxide, somewhat in excess of the equivalent amount, precipitated with alcohol, again dissolved in water, and dialyzed until neutral.

The molecular weight of the sodium salt, determined osmometrically in a NaCl solution, was about 30,000. It is evident, therefore, that even in this operation the molecule has undergone degradation. On an average there are about 14 acidic groups distributed along the chain per molecule.

The solutions of free acid and its sodium salt in water were stable for at least two weeks when preserved at 15°C.

Measurement of Viscosity

The viscosity measurements were done with two Ostwald capillary viscometers of flow times 3 minutes 22 seconds and 4 minutes 37 seconds, respectively, with water at 35° ± 0.1°C. The specific and relative viscosities were calculated with the use of the following relations:

$$\text{relative viscosity} = \eta/\eta_0 = \frac{\rho_1 t_1}{\rho t}$$

$$\text{specific viscosity} = \eta_{sp} = \frac{\eta}{\eta_C} - 1$$

where η and η_0 are the viscosities, ρ_1 and ρ the densities, and t_1 and t the time of efflux (in seconds) for the solution and solvent, respectively. In the range of dilute solutions used, the difference in densities between solution and water was insignificant and no density measurements were made.

The results of viscosity measurements with and without added electrolytes and also at various *p*H's are shown graphically in Figs. 1–3.

DISCUSSION

It may be observed from Figs. 1 and 2 that the η_{sp}/c versus c plot for both free acid and its sodium salt in solution increases rapidly with dilution, which evidently indicates an increase in hydrodynamic volume unit. This observation may reasonably be explained from the consideration of folding-unfolding properties of high molecular chain compounds, *i.e.*, repulsion between similarly charged centers on the agar chain causing the molecule to extend, which evidently increases with an increase in the extent of electrolytic dissociation, *i.e.*, with increased dilution.

Various η_{sp}/c versus c curves for agar acid in the presence of different amounts of H_2SO_4 and for sodium salt in the presence of different amounts of NaCl are also given in Figs. 1 and 2. It may be observed that the sharp rise at lower concentration disappears and is replaced by a bell-shaped curve with a well-defined maximum which shifts towards higher concen-

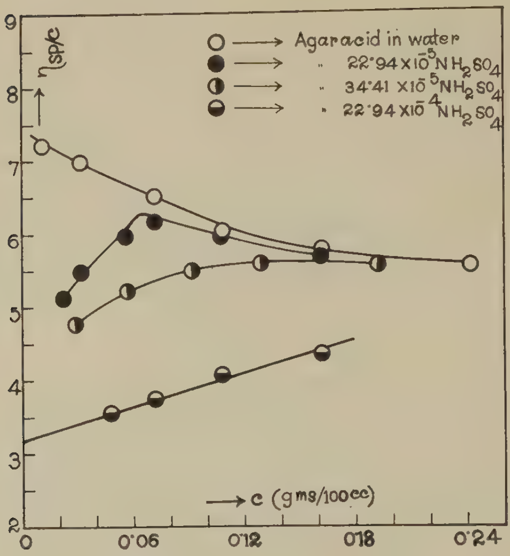

FIG. 1. Viscosity of agar acid in presence of H_2SO_4 .

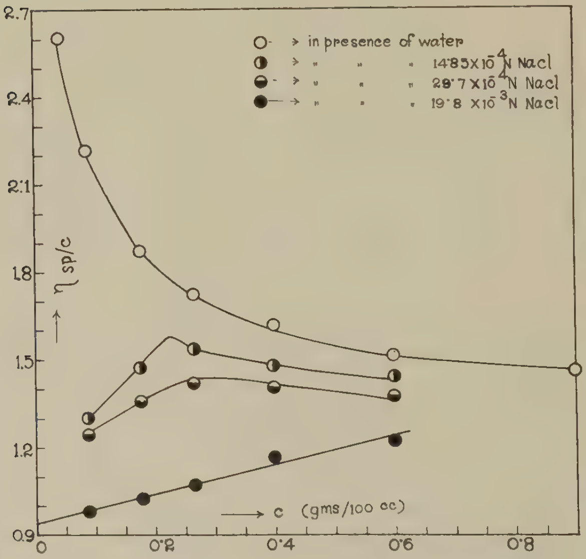

FIG. 2. Viscosity of Na-agarate in presence of NaCl.

tration of solute as the added electrolyte concentration is increased. At sufficiently high concentrations of electrolyte the curves in both cases are perfectly linear, resembling those of a neutral polymer. This type of viscosity behavior has been noticed in the case of a large number of high

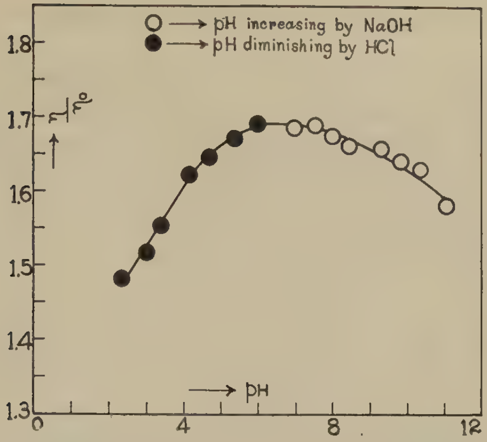

FIG. 3. Effect of pH on the viscosity of Na-agarate solution.

molecular weight ionic compounds and fits the general behavior of polyelectrolytes.

Although both free agar acid and its sodium salt behave as polyelectrolytes, signifying a chainlike character of the agar molecule, there is a characteristic difference in the structural details of the free acid and its sodium salt in solution. Although the reduced viscosity rises with dilution in both cases, the absolute value of reduced viscosity for free acid is much higher than that for its sodium salt. We may explain this on the assumption of the formation of hydrogen bonds in free acid, but there is no way of establishing this point unequivocally.

The variation of relative viscosity of a solution of the sodium salt of agar acid with pH also follows a course similar to that of the sodium salt of arabic acid (Fig. 3). Over a pH range of 6 to 8, η/η_0 stays almost constant and drops rather sharply on either side of the range. The curves could not be retracted by neutralizing the acid or alkali, but could be by dialysis. Substantial part of this curve can therefore be explained by the folding-unfolding phenomenon of the chain molecule in the presence of electrolyte—an explanation that has also been suggested for arabic acid.

Incidentally it may be noted that the variation of relative viscosity with pH is exactly similar to the variation of relative swelling with the pH of gum agar (2). If we are permitted to draw a conclusion by analogy, the swelling may be explained as the expansion-contraction of the cross-linked polyelectrolyte in a medium of different pH's. In fact it has been shown by Katchalsky (3) that a network of a cross-linked synthetic polyelectrolyte does expand and contract reversibly on changing the degree of ionization. Our present interpretation receives further support from the fact that free agar acid does not form gel, while its calcium salt, in which interchain cross-linkings may be established through the calcium atoms, does.

An important fact emerges from our studies on arabic and agar gums: the polyelectrolyte character is dependent on the charge on the chain molecule and not on the chemical nature of the group contributing the charge, because both arabic and agar gums show similar physical characteristics, although in one case the charge-producing group is the COOH group, whereas in the other it is the SO_3H group.

ACKNOWLEDGEMENTS

Thanks are due to Dr. S. R. Palit for laboratory facilities and to the Council of Scientific & Industrial Research, India, for a fellowship to one of us (A. K. S.).

SUMMARY

Measurements of viscosity with varying concentration of solute, with and without added electrolyte, and at different *p*H's of solutions of agar acid and its sodium salt are reported. A connected explanation of the observations has been formulated on the assumption of the polyelectrolytic character of the molecule. A tentative explanation has been put forward for the phenomenon of the swelling of agar gum in water at different *p*H's.

REFERENCES

1. BASU, S., DASGUPTA, P., AND SIRCAR, A. K., *J. Colloid Sci.* **6**, 539 (1951).
2. FAIRBROTHER, F., AND MASTIN, H., *J. Chem. Soc.* **123**, 1412 (1923).
3. KATCHALSKY, A., *J. Polymer. Sci.* **7**, 571 (1951).

PROPERTIES OF POLYELECTROLYTE MONOLAYERS

Israel R. Miller

The Weizmann Institute of Science, Rehovot, Israel

Received September 7, 1954

Abstract

1. Monolayers of polyvinyl benzoic acid (P.V.B.A.), of poly *ortho*- vinyl pyridine, and poly *para*- vinyl pyridine as well as of copolymers containing varying proportions of vinyl benzoic acid (V.B.A.) and 2-vinyl pyridine (2-V.P.) were investigated. These polymers were spread on the air-water interface of buffer solutions of constant ionic strength and of various *p*H values, and their surface pressure and potentials were measured.

2. The measured surface potentials and pressures of poly 4-vinyl pyridine (4 P.V.P.) were smaller than the corresponding potentials and pressures of poly 2-vinyl pyridine (2 P.V.P.) at the same surface concentration. From these results it was concluded that there is a higher probability for the *trans*- than for the *cis*-configuration of the pyridine residues in the polymeric chain.

3. In the case of polyvinyl benzoic acid and the polyampholytes, strong intermolecular forces are evident. As a result, equilibrium pressure values were reached very slowly after a certain surface area was established. The forces acting in the case of P.V.B.A. are due to hydrogen bonds and, in the case of the polyampholytes, in the neighborhood of the isoelectric point, are due to both hydrogen bonds and electrostatic attraction of oppositely charged monomeric residues.

4. The *p*H of the solution has only negligible influence on the surface pressures and potentials of 2-P.V.P. and 4-P.V.P. until a *p*H value is reached where the film starts to dissolve. At this point both the pressure and the potential drop suddenly. The influence of *p*H is more pronounced in the case of P.V.B.A. and is quite striking in the case of polyampholyte films. The contractive forces prevent the dissolution of the hydrophilic units in the surface. They are balanced by repulsive forces which arise from the net charge of the surface film.

Introduction

The investigation of the surface behavior of polyelectrolytes may be considered as a means for understanding part at least of the possible biological processes at interfaces. The behavior of synthetic and natural polyelectrolytes at water interfaces is therefore of considerable interest.

Protein monolayers have been extensively studied during the last 20 years (1), and a great deal of information about their structure and properties has been obtained. Recently ionization studies of protein monolayers spread on buffer solutions at various *p*H values have been carried out (2).

Relations between surface potential of polypeptide monolayers and the orientation of their functional groups in the surface have recently been discussed by Davies (3). Special consideration has been given to the orientation of the NH_2-groups of polypeptide and protein monolayers containing lysine. These groups are known to play an important part in biological activity.

During the last five years various attempts at understanding the behavior of adsorbed as well as of spread synthetic polyelectrolytes on water interfaces have been made (1, 4, 5, 6).

This paper deals with spread monolayers of polymers and copolymers containing 2- and 4-vinyl pyridine (2-V.P. and 4-V.P.) and 4-vinyl benzoic acid (4-V.B.A.). One can draw conclusions about the composition and orientation of the polymers in the surface from surface pressure and potential measurements. From such results the relation between the behavior of these polyelectrolytes in surface monolayers and in water solutions can be derived. This behavior is in both cases a function of electrostatic and van der Waals' forces, as well as of hydrogen bonding. These forces cause intra- and inter-molecular interactions. The amount of hydrogen bonding and the strength of the interacting forces are a function of the *p*H and of the ionic strength of the substratum.

EXPERIMENTAL

1. Synthesis of the Polyelectrolytes

a. Monomers. The 2-V.P. and 4-V.P. used for the polymerization were obtained by the distillation of commercial vinyl pyridines at reduced pressure. The 4-V.B.A. was prepared by the method of Marvel and Overberger (7).

b. Polymers. The polymerizations were carried out at 50°C. in alcohol solution with 0.5 % H_2O_2 as a polymerization initiator.

The two types of P.V.P. were subjected to a rough fractionation. The fractionation was done by precipitation of the polymers with ethyl ether from an alcoholic solution. Only two fractions from each polymer were collected. The molecular weights were determined by light scattering of alcoholic solutions of the polymers. In the case of 4-P.V.P. the degrees of polymerization of the two fractions were about 450 and 800, and for 2-P.V.P. they were about 350 and 600 monomeric units.

As no molecular-weight–dependent differences in the measured surface properties of the polymers could be detected, no further fractionations were done.

The degree of polymerization of P.V.B.A. was found to be about 320 monomeric units.

In order to obtain the copolymer, benzoic acid and 2 vinyl-pyridine of different proportions were dissolved in alcohol. H_2O_2 was added as an initiator. The polymerization was carried out until about 30 % conversion was achieved. The polymer composition was determined by elementary analysis and by titration of the carboxyl groups.

TABLE I

Copolymerization of 2-V.P. with V.B.A.

Copolymer	Monomer composition (*weight % in alcohol*)		% Conversion	Polymer composition (*weight %*)		Polymer composition (*molecular units, %*)	
	2-V.P.	V.B.A.		2-V.P.	V.B.A.	2-V.P.	V.B.A.
I	4	16	26	29.2	70.8	35.6	64.4
II	8	12	33	47.5	52.5	55.7	44.3
III	12	8	30	60.6	39.4	68	32
IV	16	4	31	76.5	23.5	82.3	17.7

All the data concerning the preparation and the composition of the copolymer are given in Table I.

2. Measurements

The pressure-area measurements were made on a modified (8) Langmuir-type surface balance which was enclosed in a Faraday cage in order to permit taking simultaneous surface-potential measurements. The surface potential was obtained by measuring with a Cambridge potentiometer, the potential between a polonium-coated silver "air electrode" and two calomel electrodes immersed in the solution at different parts of the tray.

In order to obtain monolayers the polymers were dissolved in a 50% alcohol-benzene solution. A measured amount of this solution was spread on the surface of a buffered water solution of ionic strength 0.02. Care was taken to avoid having polyvalent ions in the bulk solution of sign opposite to the net charge of the polymers in the monolayer (cf. reference 6). Organic ions were not used for buffering the solution.

Results and Discussion

1. Polyvinyl Pyridine

Surface pressure (P) and surface potential of 2- and 4-P.V.P. films were measured as a function of area (A) per monomeric unit. The measurements were performed on films spread on solutions buffered to pH values of 3.7, 4.4, 6.5, and 10.5. It was observed that in the presence of CO_2 films which were spread at higher starting surface concentrations reached a higher final potential after compression than those spread at lower surface concentrations. This was avoided by passing a CO_2-free air stream through the cage which enclosed the tray carrying the film.

The surface pressure and potential values of 2-P.V.P. and 4-P.V.P. at pH 10.5 and 3.7 are given in Fig. 1*A* and 1*B*, respectively. From the figures it is evident that of these two polymers 2-P.V.P. has a higher surface potential and surface pressure than its isomer. The higher surface potential of the 2-P.V.P. as compared with 4-P.V.P. at equal surface area is out of line when compared with dipole moments of analogous monomeric

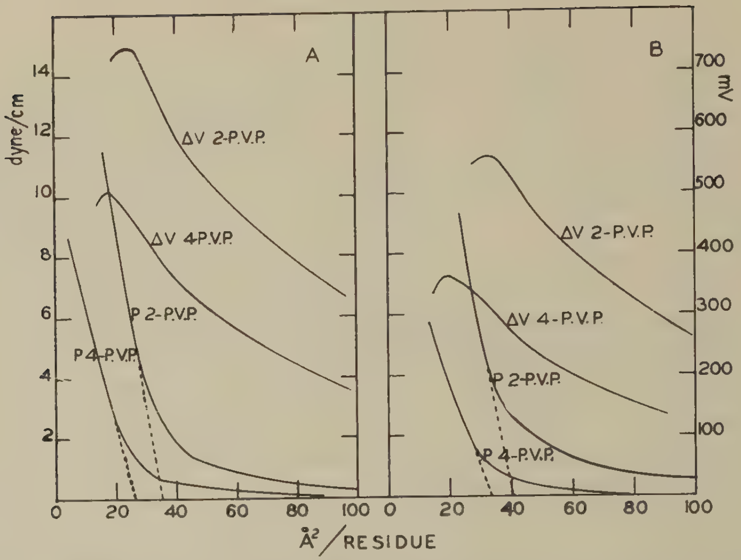

FIG. 1. Change of surface pressure and surface potential with area per monomeric residue in monolayers of 2-P.V.P. and 4-P.V.P. *A*, substratum at *p*H 3.7; *B*, substratum at *p*H 10.5.

P = surface pressure. *V* = Differences between potentials measured in absence and presence of the monolayer.

compounds: *e.g.*, 4-picoline (2.57 Debye units) and 2-picoline (1.72 Debye units) (9). The surface orientation of the polymers provides the only explanation for this behavior. Assuming a true dipole moment μ of 2.57 Debye units for a monomer residue of 4-P.V.P. and 1.72 Debye units for a residue of 2-P.V.P., we are able to calculate by means of the Hemholtz equation, $\Delta V = 4\pi n\mu \cos \theta$, the mean values of $\cos \theta$, where θ is the angle between the dipole and the vertical to the surface and n is the number of dipoles per square centimeter. For example, when the surface area is 40 A.^{2} per residue, the surface potentials of 4-P.V.P. and 2-P.V.P. on a basis substratum are 275 mv. and 520 mv., respectively. In this case the calculated angles between the dipoles and the vertical to the surface are 83.3° for 4-P.V.P. and 71° for 2-P.V.P. The interpretation of the higher degree of orientation in the case of 2-P.V.P. is thus as follows: In order to obtain the maximal surface potential all the polar ground should point perpendicularly toward the surface. This orientation requires in the case of 4-P.V.P. that the pyridine groups all be in *cis*-position to each other. Each deviation from the "*cis*" position alters the angles between the direction of the dipole and the vertical to the surface from 0°, and diminishes the observed surface dipole moment. However, the *cis* configuration is statistically highly improbable, especially when taking into account that

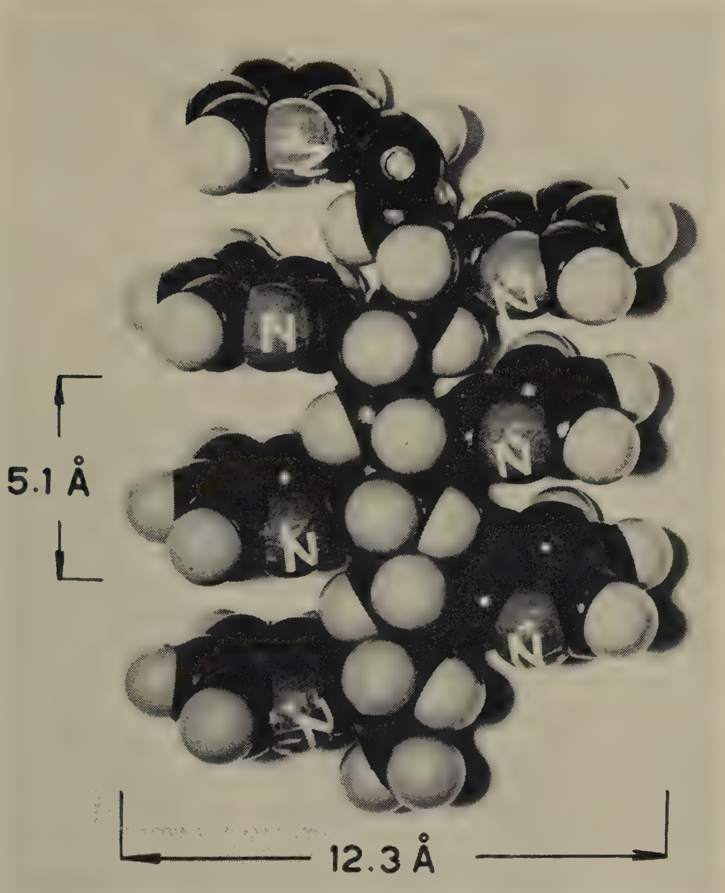

FIG. 2. Model of a segment of 2-P.V.P. lying in the surface, viewed from the water phase. Dimensions of the area covered by a pair of monomers in the surface are given in the figure.

parallel dipoles repel each other. The energy due to repulsion between two parallel dipoles having a dipole moment of 2.5 Debye units at a distance of 5.1 A. is about 2.5 kT. On the other hand, the antiparallel configuration, which is energetically very probable, does not contribute anything to the surface potential.

In the case of 2-P.V.P. the situation is quite different. Owing to the free rotation around the link which connects the pyridine group to the main chain, the dipole moment can always be oriented in the direction of maximal contact of the polar group with the water surface. The pyridine groups may for instance be all in *trans* position to each other and at the same time the dipoles may point perpendicularly toward the surface (Fig. 2).

The limiting surface area is smaller for 4-P.V.P. (34 A.^{2}) than for 2-P.V.P. (41 A.^{2}). The calculated net area per vinyl pyridine residue, when pointing perpendicularly toward the surface, is about 10.5 A.^{2}. The net area per pair of neighboring vinyl pyridines, lying in the surface in the *trans* position, is about 63 A.^{2}, or 31.5 A.^{2} per residue. Ascribing to both polymers a similar rigidity along the main chain, one would have to expect the mutual orientation of the side groups to determine the surface areas at equal potentials. Hence if 4-P.V.P. were to preserve the *cis* and 2-P.V.P. the *trans* configuration, the difference between their limiting areas should be larger then actually measured. Consequently a random constellation of the residues in both cases has to be assumed. There is only a trend toward the *cis* configuration in the case of 4-P.V.P. and toward the *trans* configuration in the case of 2-P.V.P.

With regard to the behavior of the surface films at different *p*H values, it was found that there is an increase in the surface potential and a decrease in surface pressure for constant area with decreasing *p*H. The increase in surface potential comes from the electrostatic field of the electrical double layer created by the ionization which acts parallel to the field of the dipoles in the surface. Although the potential changes continuously for the *p*H values 10.5, 6.5, 4.4, and 3.7 (at a lower *p*H the film dissolves), the main change in the surface pressure occurs between *p*H 10.5 and 6.5, the surface pressure at *p*H lower than 6.5 remaining constant.

The fact that the surface pressure is at first constant and then decreases as the *p*H of the substrate is decreased is not obvious. What would actually be expected is that the pressure should increase owing to the increase of repulsive forces between the charged segments. The behavior described above indicates, therefore, that the ionized monomers tend to dissolve in the water. This gives a picture of a floating polymer chain attached to the water surface by the more hydrophobic unionized residues, whereas the soluble ionized monomeric units tend to enter the water phase. As will be seen later, the picture is slightly different when there are intra- and intermolecular attractive forces.

2. Poly 4 Vinylbenzoic Acid (*P.V.B.A.*)

The carboxylic groups of P.V.B.A. interact by hydrogen bonding. This interaction is strongly evidenced by the surface films. After compression or expansion at pressures of about 1 dyne/cm. or higher the final pressure is not instantaneously established. With compression a sudden increase in the surface pressure occurs which at first decreases very rapidly and reaches a final value after about 40 to 60 minutes. The same surface pressure as with compression is reached after a similar time interval by expanding the film from a lower surface area to the area at which the pressure is to be measured. Immediately after expansion the surface pressure drops to zero and then rises asymptotically to the final value. In order to perform the measurements faster the final surface-pressure values were obtained through interpolation of values taken at different times after expansion and compression of the film to the same area. The same procedure was followed in the case of the polyampholytes, where the intramolecular forces and, therefore, the time effect were also very pronounced.

The time effect is a consequence of a slow rearrangement process after expansion or compression. We assume that the rate of this process is determined by an activation energy which must be supplied in order to break intramolecular bonding—in this case, presumably, hydrogen bonding—before a new surface configuration corresponding to the new area can be established. A time effect is expected in polymer films generally because the molecular rearrangements corresponding to the change of area take a finite time. As is made evident from the behavior of films of polyvinyl pyridine and other polymers lacking specific intramolecular interactions, however, the time effect from this source is negligible.

As is seen from Fig. 3, the limiting area on an acid substrate is about

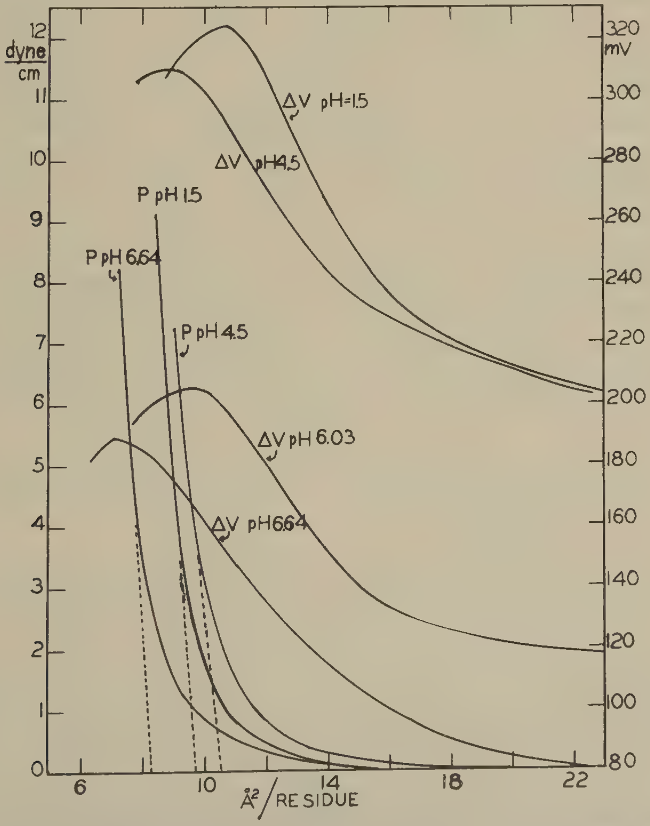

FIG. 3. *P* and *V* versus area per monomeric unit of P.V.B.A. Monolayer for various *p*H values of the substratum.

9.6 A.^{2}, which is considerably lower than in the case of both 2-P.V.P. and 4-P.V.P. The limiting area increases slightly with increasing *p*H of the substratum, probably owing to electrostatic repulsion, until it reaches a maximum at about *p*H 5. At still higher *p*H values dissolution of the polymeric film begins to take place. At *p*H 6.7, for instance, the polymer molecules seem to be partly submerged in the water and the limiting area drops to about 8.3 A.

The exceptionally low areas indicate that the polymer molecules are not fully spread in the surface. The picture at low pressures is probably that of separate polymer molecules of a thickness of more than the length of one monomeric unit floating on the surface. The slightly bulky configuration of the P.V.B.A. in the surface can be attributed to intramolecular interactions through van der Waals' forces and hydrogen bonds. The state in which the P.V.B.A. molecule persists cannot therefore be considered as a nonequilibrium state and spreading is complete. There exist in all the kinds of polymeric molecules interaction forces which oppose the spreading or which tend to cause parts of the molecules to submerge into the solution. The assumption consequently of a freely coiled chain floating flat in the surface is in all cases an idealization. The deviation from that ideal state depends on the intramolecular forces. At higher pressures, obviously, when the different segments of the molecule are forced close together and the interactions increase, the deviation from the ideal monomolecular layer increases too.

The surface potential also is influenced by the *p*H of the substratum. The maximum potential decreases continuously from about 325 mv. at *p*H 1.5 to about 190 mv. at *p*H 6.7. The change in the surface potential may be attributed to three factors: (1) to the change of the dipole moment of the ionized group; (2) to the change in the electrical double layer; and (3) to the partial dissolution of the ionized groups. The electrical field created by the ionized carboxylic groups in the surface and their counter ions 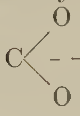 $\mathrm{C}\overset{\mathrm{O}}{\underset{\mathrm{O}}{<}}$ - → M^+ is opposite in direction to the field of the dipoles of the unionized groups 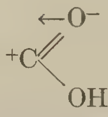 $^{+}\mathrm{C}\overset{\leftarrow \mathrm{O}^{-}}{\underset{\mathrm{OH}}{<}}$. Consequently the surface potential decreases with increasing *p*H. The solution of the carboxylic group would cancel the effect of ionization, because the carboxylic group would be symmetrically surrounded by the counter ions. It seems, therefore, that the partial dissolution of the ionized groups plays an important part at high *p*H values only. In order to obtain a more definite idea about the contribution of each of the above factors to the surface potential, potential measurements should be made for different ionic strengths of the substrate.

3. The Polyampholytes

The copolymers of 2-V.P. and V.B.A. give good monomolecular films at *p*H values close to the isoelectric point. In very acid or very alkaline solutions the ampholytic monolayers dissolve. The surface potentials at different *p*H values are even more complicated than in the case of monolytic polymers. Since no measurements at varying salt concentration of the bulk solution have yet been made, the results of the potential measurements are not given in this paper.

In the neighborhood of the isoelectric point, charges of both signs are present on the polymeric chain and long-range attractive forces are added to the short-range hydrogen bonds and van der Waals' forces. By changing the *p*H of the solution in both directions, we get superposition of repulsive and attractive forces. Charges of opposite signs tend to form zwitterions. The zwitterions formed, as well as the hydrogen bonds, increase the rigidity of the polymeric molecule in their immediate vicinity. The net effect is thus a masking of the hydrophilic groups and a restriction upon their dissolution. On the other hand, the presence of an excess (or net) charge, which is positive on the acidic and negative on the basic side of the isoelectric point, tends to increase the dimensions of the polymeric molecule in the surface. Hence at equal pressures the areas are smallest at the isoelectric point and should increase with both decreasing and increasing *p*H. As shown in Fig. 4 for copolymer II containing 47.5% V.P., this is found to be the case. From the figure it can be seen that at *p*H 2.3

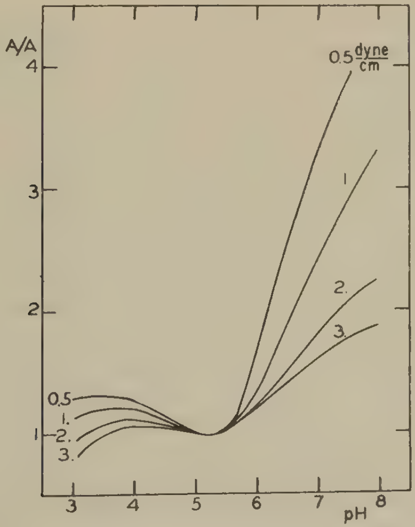

FIG. 4. Pressure as a function of reduced area A/A_i (ratio of the area at a given *p*H to the area at the isoelectric point) for monolayers of copolymer II containing 47.5% 2-V.P. Substratum at various *p*H's.

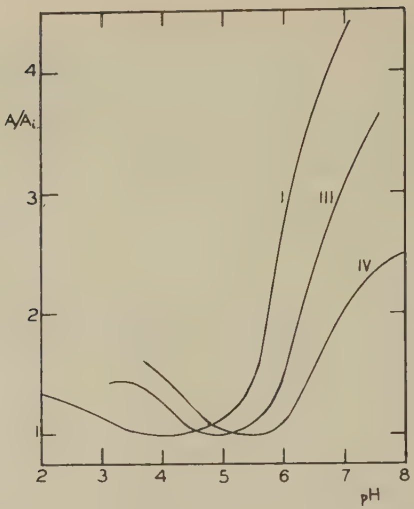

FIG. 5. Reduced area A/A_i (ratio of the area at a given pH to the area at the isoelectric point) versus pH at P = 0.5 dyne/cm. for three different copolymers:

I Containing 35.6% 2-V.P.
III Containing 68% 2-V.P.
IV Containing 82.3% 2-V.P.

and 7.25, at all surface pressures, the area per residue is greater than at pH 4.5, which is roughly the isoelectric point. Above pH 7.25 and below 2.3 dissolution of the monolayer starts.

The increase of surface area per monomer is not symmetrical about the isoelectric point. As shown in Fig. 5, it is in all cases larger on the alkaline than on the acid side. This can be understood by taking into consideration the hydrogen bonding between the carboxyl groups. The number of these hydrogen bonds diminishes very fast on the alkaline side where the carboxyl groups are ionized. On the acid side the positive charge density on the polymeric chains has to be high enough to break the hydrogen bonding by electrostatic repulsion. (In principle the behavior in the surface is analogous to that in the bulk (cf. reference 10)). When this charge density is reached, however, the polymer film starts to dissolve. The reduced area A/A_i (A_i indicates the area at the isoelectric point) is influenced not only by the pH of the solution but also by the surface pressure. A/A_i decreases with increasing surface pressure (Fig. 6). This behavior is in agreement with the decreasing compressibility $-\frac{1}{A}\frac{dA}{dp}$ of the film at higher surface pressures. The compressibility reaches a minimum before the film is dissolved or is expelled from the surface.

From Fig. 7, it is evident that the surface area per residue is a function of the composition. It is plausible that the increase of hydrogen bonding

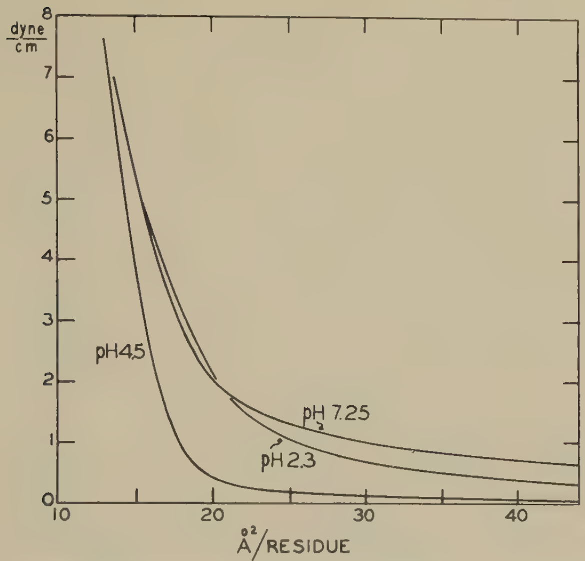

FIG. 6. A/A_i versus pH as a function of surface pressure. Copolymer III containing 68% 2-V.P.

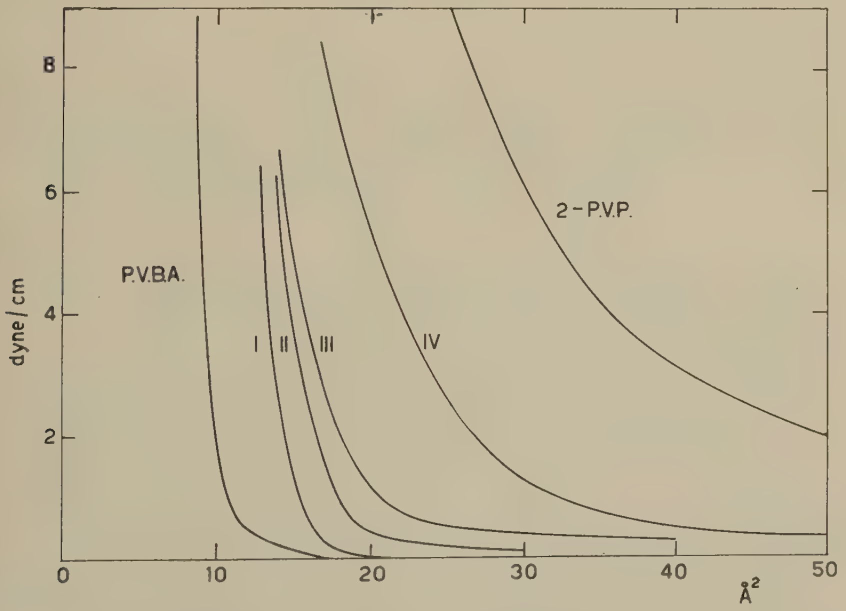

FIG. 7. Pressure-area curves of monolayers of different polyampholytes at the isoelectric point compared with 2-P.V.P. and P.V.B.A.

Polymer compositions:

I 35.6% 2-V.P.; 64.4% V.B.A.
II 55.7% 2-V.P.; 44.3% V.B.A.
III 68% 2-V.P.; 32% V.B.A.
IV 82.3% 2-V.P.; 17.7% V.B.A.

with increasing vinyl benzoic acid content of the polyampholyte plays a great part in the change of the surface area with polymer composition, although the influence of zwitterions and to a smaller extent of the *ortho* and *para* compositions should not be neglected. These changes are moderate when the 2-V.P. content in the copolymer changes from 35.6 to 68 mole per cent. When however, the 2-V.P. content increases from 68% to 82.3% and 100%, the change in surface area per monomeric unit is considerably higher. The following consideration is intended as a qualitative explanation of this behavior:

The comparison of the pressure-area curves of the different polymers was made at their isoelectric point. In the monolytic polymers the isoelectric point corresponds to the undissociated state, and the number of zwitterions is zero. The total number of zwitterions is highest in the copolymers in which the content of both groups (2-V.P. and V.B.A.) is about equal (10). At this composition the contraction due to electrostatic interaction is maximal. The contraction due to hydrogen bonding increases with increasing content of vinylbenzoic acid in the copolymer and reaches its maximum for pure P.V.B.A. The combined effect of both kinds of interactions satisfactorily explains the measured surface areas of the various copolymers.

ACKNOWLEDGMENTS

I want to thank Prof. Aharon Katchalsky for his helpful discussion of the problem. I am also thankful to the Research Laboratory of A.K.U., Arnhem, Holland, for the design of the surface balance built by J. W. Y. Heynis and L. Maaskant, and to Mr. Saul Gassner for his technical assistance in building our apparatus.

REFERENCES

1. BULL, H., *Advances in Protein Chem.* **3,** 53 (1943).
2. GLAZER, J., AND DOGAN, M. Z., *Trans. Faraday Soc.* **49,** 448 (1953).
3. DAVIES, Y. T., *Trans. Faraday Soc.* **49,** 949 (1953).
   DAVIES, Y. T., *Biochem. J.* **56,** 509 (1954).
4. KATCHALSKY, A., AND MILLER, I. R., *J. Phys. & Colloid Chem.* **55,** 1182 (1951).
5. CUMPER, C. W. N., AND ALEXANDER, A. E., *Trans. Faraday Soc.* **46,** 236 (1950).
   POWELL, B. D., AND ALEXANDER, A. E., *J. Colloid Sci.* **7,** 482 (1952).
6. MILLER, I. R., Thesis submitted to the University of Jerusalem, July, 1952.
   MILLER, I. R., AND KATCHALSKY, A., *Bull. Research Council Israel* **2**(No. 3) (1952).
7. MARVEL, C. S., AND OVERBERGER, C. G., *J. Am. Chem. Soc.* **67,** 2250 (1945).
8. HEYNIS, J. W. Y., AND MAASKANT, L., *J. Phys. & Colloid Chem.* **54,** 1222 (1950).
9. WESSON, I. G., "Tables of Electric Dipole Moments." The Technology Press, M.I.T.
10. KATCHALSKY, A., AND MILLER, I. R., *J. Polymer Sci.* **13,** 57 (1954).

VISCOSITY BEHAVIOR OF SODIUM CARBOXY METHYL CELLULOSE IN WATER AT HIGH DILUTIONS

Hiroshi Fujita and Terutake Homma

Department of Fisheries, Faculty of Agriculture, Kyoto University, Maizuru, Japan

Received September 14, 1954

INTRODUCTION

The reduced viscosity of polyelectrolytes in solutions containing no added salts has been found in a number of cases to increase markedly with increasing dilution, but it appears that no confirmative information has yet been obtained as to whether such an increase of reduced viscosity persists up to the limit of infinite dilution, or whether, even if this is the case, the curve can be extrapolated to give a finite intrinsic viscosity. If we consider the fact that most of the reported data on the reduced viscosity of polyelectrolyte solutions in the absence of added salts can be satisfactorily fitted, at least to the lowest concentrations used in the particular experiments, by the so-called Fuoss viscosity equation (1), it appears reasonable to expect that the rising trend of the curve may actually be maintained to zero concentration in accordance with the Fuoss equation.

In the course of a recent investigation on the viscosities of dilute aqueous solutions of a sample of sodium carboxy methyl cellulose (Na-CMC) whose average degree of polymerization and degree of etherification were, respectively, about 400 and 0.7, we observed that the reduced viscosity in the absence of added salt reached a maximum in the vicinity of a concentration of 0.005 g./100 ml. and then fell off rapidly with further decrease in concentration. This behavior is different from the type which may be expected on the basis of previous experimental data or of the Fuoss viscosity equation. Moreover, it is difficult to interpret it in terms of the current theory of linear polyelectrolyte molecules in dilute solutions. According to this theory, the diminishing of the polymer concentration causes an uncoiling of the polyelectrolyte chain owing to an increase in the repulsive forces of its charges, thus giving rise to a steady increase of the reduced viscosity with increasing dilution.

It seemed interesting and desirable to investigate whether there is really a maximum point in the reduced viscosity plot of a polyelectrolyte in solution containing no added salt or whether our finding on Na-CMC was only an apparent one brought about by our experimental errors. We have therefore undertaken a series of careful viscosity measurements in capillary viscometers with four samples of Na-CMC, down to the lowest concentrations where reasonably reproducible data could be obtained. Thus, the lowest concentrations used were about 0.0003 g./100 ml. for the two higher molecular weight samples, and about 0.0005 g./100 ml. for the other two samples of lower molecular weights. The results of these viscosity measurements are reported in this paper.

EXPERIMENTAL

1. Materials

Four samples of sodium carboxy methyl cellulose (Hercules Powder Co.) were kindly given us by Mr. H. Inagaki (Department of Textile-Chemistry, Faculty of Engineering, Kyoto University); these were designated, respectively, as "Superhigh Viscosity Type," "Premium High Viscosity Type," "Premium Medium Viscosity Type," and "Premium Low Viscosity Type." They were thoroughly purified by alcohol precipitation as described by Pals and Hermans (2), and also used in our previous work (3) on a sample of Na-CMC. All solutions were prepared with water doubly distilled in alkaline solution over potassium permanganate. Great precaution was always taken to avoid leaching alkali from the glassware into the test solutions. The stock solutions, except for the case of the lowest molecular weight sample, *i.e.*, "Premium Low Viscosity Type," were made up at low concentrations of about 0.05 g./100 ml., since otherwise a serious drainage error might have been introduced in diluting them with the pipet owing to their high viscosities. They were filtered successively through finely sintered glass filters before use, and care was always taken to prevent contamination with dust particles as much as possible. The concentrations of each set of solutions were calculated, on the assumption of no volume change on dilution, from the concentration of the most concentrated (*i.e.*, stock solution), which was determined by careful evaporation of a weighed portion.

2. Viscometry

The three Ostwald type viscometers used in our previous work (3) were also used, the dimensions and flow times for water at 25°C. of which are recorded in the previous paper (3). The free-fall method was employed throughout, so that no account was taken here of the correction for shear-rate effects. However, there is no doubt that such highly viscous solutions of polymer as dealt with in this work should exhibit a marked non-Newtonian behavior, as may be inferred, for example, from recent investigations on some Na-CMC samples by Akkerman, Pals, and Hermans (4) and by us (3). Our present study therefore has only relative rather than absolute value. The kinetic energy correction was unnecessary in all cases examined. The drainage error was assumed to be negligible.

All measurements were made at 25.000° ± 0.001°C. in a specially designed constant-temperature bath. A double-layer thermostated water bath was enclosed by a thick-walled air-thermostated bath, maintaining vigorous agitation in each. Each section of the thermostat was controlled with sensitive thermoregulators connected with electronic relays and suitable heaters. The agitation system was constructed so that the bath might be freed of any mechanical disturbance from the driving motors. When the temperature in each bath was appropriately adjusted, the variation was not readable on a Beckmann thermometer mounted in the inner bath over the whole period of a particular set of measurements. The viscometer was clamped to the side wall of the water bath with a special clamp so as to ensure that the position was always exactly the same. The efflux time was measured with a stop-watch reading to an accuracy of 0.1 sec. At each concentration the flow times were repeatedly measured until at least duplicate runs checked within a desired accuracy (generally 0.3 sec., but for $\eta_{sp} < 0.1$, 0.1 sec. or more). Flow times decreasing regularly with the repetition of the measurements were occasionally obtained, generally at high specific viscosities. When such occurred, the viscometer was carefully cleaned, the new solution was prepared and pipeted into it, and the viscosity run was repeated. Each set of measurements for a given sample was started after the solution was allowed to stand generally for one day. This period of standing may have been too short to stabilize the solution fully.

Successive dilutions of the stock solution were made volumetrically, measuring all volumes with a single pipet. In order to prevent the ambiguity arising from dilution errors, each concentration was prepared from the stock solution through two or three different dilution steps, and the viscosities of such differently prepared solutions were individually determined, with the desired value obtained by averaging them when they were in accord with each other within the demanded degree of accuracy. Although in this way care was taken to avoid the concentration error due to dilution, flow times were occasionally obtained such that the reduced viscosities derived from them were far out of line with the other results. In such instances the experiment was repeated as mentioned above. Such repetition of the measurement was frequent at concentrations below 0.002 g./100 ml. where data deviating by a factor of several per cent or even of 10 per cent were sometimes found; but, in contrast, such abnormality was hardly ever encountered at concentrations above 0.005 g./100 ml. in all samples studied. Although it is not clear to us why the measurements were not very reproducible at small concentrations below the order of 0.002 g./100 ml., we suppose that it is a consequence associated with a very unstable state of polyelectrolyte molecules in solutions of very low ionic strengths. The adsorption effect may also play an important role in making the reproducible measurements difficult in such a region of very small concentrations. It must be remarked, however, that the capillary viscometers used were not always suitable for accurate viscosity measurements at such low concentrations owing to their relatively short efflux times for water at the desired temperature (about 300 sec.). We are planning a viscometry of higher precision, along with an elaboration of the shear-rate correction which was neglected completely in this work.

3. Determination of Degrees of Polymerization

As in the previous study (3), we estimated the average degrees of polymerization ($\overline{\mathrm{DP}}$) of the samples from the intrinsic viscosities, $[\eta]_{2N\text{-NaOH}}$, in $2N$-NaOH, using the Kagawa-Fukuda formula (5), although it is doubtful whether this formula can be applied with reliability to such fairly high molecular weight samples as those investigated here. Osmotic pressure measurements are in progress in a modified Zimm-Myerson type osmometer to obtain more direct information about the sizes of the polyelectrolyte samples used, but we have not yet had much to report here. It seems rather immaterial at the present stage of our viscometric investigation to know the exact values of the molecular weights of the samples, because the viscosity data presented here are not corrected for the shear-rate effect, and therefore we are not yet in a position to be able to discuss the intrinsic viscosity–molecular weight relation in detail.

4. Determination of Degrees of Etherification

The degree of etherification of each polymer salt was determined by dissolving its ash into a 0.3 N-H_2SO_4 solution and titrating the mixture with a 0.3 N-NaOH. The analysis was repeated at least twice, and the values obtained were averaged to give a final result.

RESULTS

1. Characteristics of the Na-CMC Samples

The viscosity average degrees of polymerization, $\overline{\mathrm{DP}}$, the intrinsic viscosities, $[\eta]_{2N\text{-NaOH}}$, in $2N$-NaOH solution, and the degrees of etherification, $\overline{\mathrm{DE}}$, of the four Na-CMC samples used are recorded in Table I. It

TABLE I

Some Characteristics of the Na-CMC Samples Investigated

Sample	$\overline{\mathrm{DP}}$	$\overline{\mathrm{DE}}$	$[\eta]_{2N\text{-NaOH}}$
PL	180	0.71	1.44
PM	320	0.60	2.38
PH	760	0.64	5.75
SH	1050	0.78	9.05

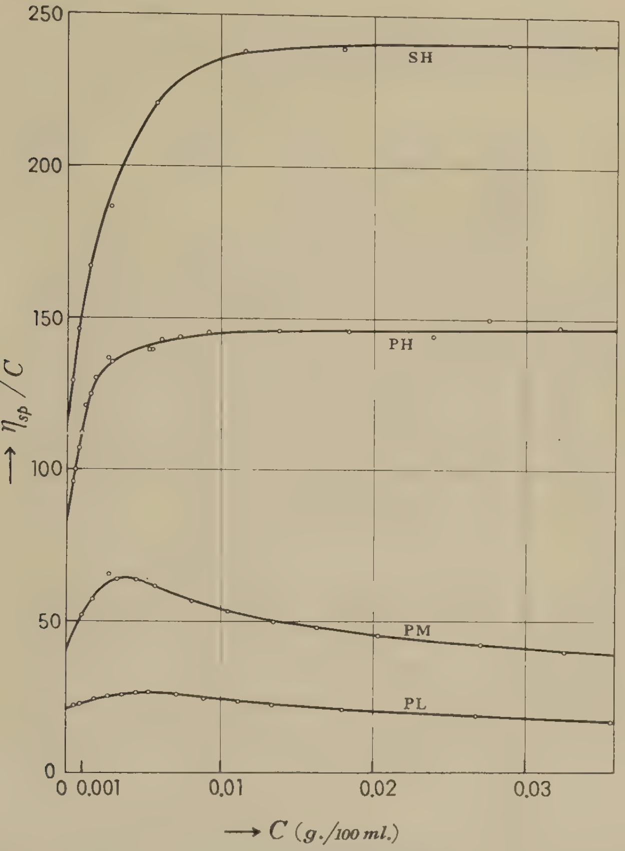

FIG. 1. Reduced viscosity, η_{sp}/c, vs. concentration, c, curves for four Na-CMC samples at 30°C. As to the sample designation attached to the curves, see Table I.

proves from the table that the $\overline{\text{DE}}$ values are nearly equal for the four samples, whereas their $\overline{\text{DP}}$ values are extended over a fivefold range. The abbreviations, PL, PM, PH, and SH, used in the table represent the exact designations, "Premium Low Viscosity Type," "Premium Medium Viscosity Type," "Premium High Viscosity Type," and "Superhigh Viscosity Type." These abbreviations will be used throughout the presentation given below.

2. Viscosity

The viscosity data obtained in aqueous solutions are shown graphically in Fig. 1, wherein the reduced viscosity, η_{sp}/c, is plotted against the polymer concentration, c (in grams of solute molecules per 100 ml. solution), for the four samples studied.

As can be seen from the figure, the reduced viscosities of samples PL and PM initially increase with dilution, as usually reported in the literature,

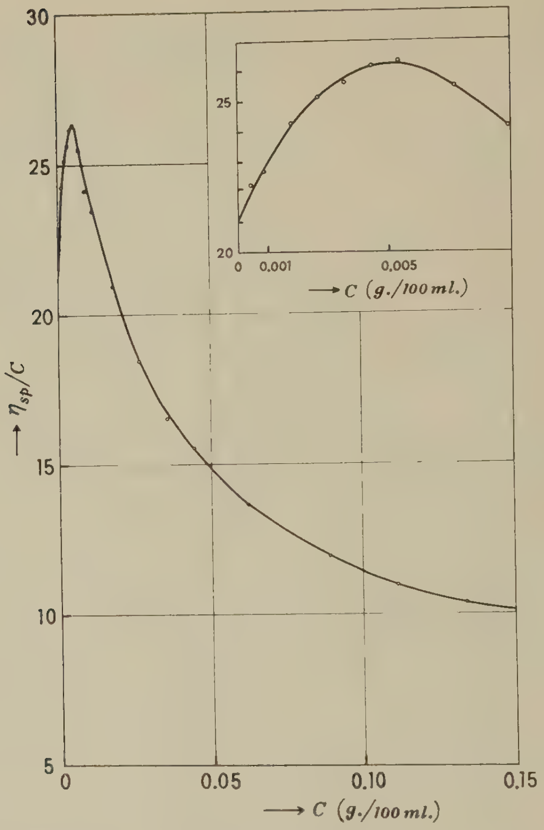

FIG. 2. Reduced viscosity vs. concentration curves for samples PL in two different concentration ranges.

but reach a maximum at a concentration of about 0.005 g./100 ml., and then fall off rather rapidly with further decrease of concentration to give a definite intrinsic viscosity value. The maximum point is shifted somewhat to a lower concentration as the molecular weight increases. The initial slope of the plot is also steeper as the molecular weight becomes large. Figure 2 illustrates the reduced viscosities of sample PL over a wider concentration range, with a magnified ordinate axis. A graph showing the details at concentrations below about 0.008 g./100 ml. is also inserted in the figure. The upward curvature of the curve in the region above $c =$ 0.005 g./100 ml. is markedly similar to those which were found by previous workers for various polyelectrolytes, but at the same time we can confirm with reliability a maximum of η_{sp}/c appearing really at a finite but very small concentration. This justifies the validity of our previous finding mentioned in the introduction of this paper. From the upper graph in Fig. 2 the plot can be extrapolated to give an intrinsic viscosity $[\eta]$ of about

21. However, this [η] value has to be accepted with reservation because values of η_{sp}/c at concentrations below about 0.002 g./100 ml. were not always reproducible, and therefore the plotted experimental points may involve considerable errors. That the points so regularly arranged up to as low concentrations as 0.0005 g./100 ml. (where the value of η_{sp} was of the order of 0.01) were obtained as can be seen in the figure is considered rather fortuitous. A graph similar to Fig. 2 was prepared with the data of sample PM, with the [η] value found to be about 41.

The reduced viscosities of both PH and SH are seen to exhibit a type of behavior markedly different from that for the lower molecular weight samples as mentioned above. The viscosity plots of these higher molecular weight samples show neither a maximum nor the usual upward curvature with dilution, but are nearly horizontal over most of the concentration range examined, except at very small concentrations where each curve falls off so rapidly as to render the reliable extrapolation to infinite dilution practically impossible. A drastic extrapolation of each to infinite dilution yields: [η] = 83 for sample PH, and [η] = 115 for sample SH. It is apparent, however, that these values have to be accepted with more reservation than in the case of the lower molecular weight samples, because the influence of the rate of shear should be much more pronounced for such extremely high intrinsic viscosities. If these values were corrected to zero shear rate by means of a suitable method of extrapolation, values would be obtained which are far higher than those determined at finite rates of shear. For this and other reasons (for example, the difficulty of making reliable experiments at high dilutions), all the [η] values recorded here have a relative rather than absolute value. Nevertheless, we believe that the relative behavior of the viscosity curves presented would not be changed substantially even if the correction for rate of shear were applied. In Fig. 3 the [η] values are plotted against the $\overline{DP}$ values on a log-log graph,

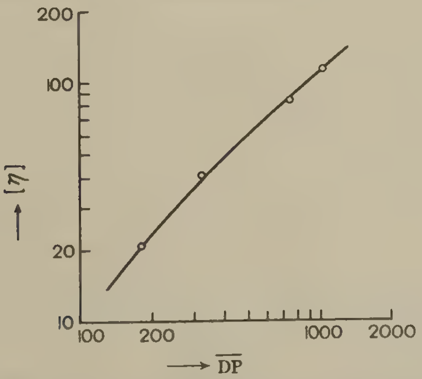

FIG. 3. The intrinsic viscosities in pure water plotted against the viscosity average degrees of polymerization calculated from the intrinsic viscosities in 2 N—NaOH.

although it is apparent that this plot is of relative value because the degree of etherification was not exactly the same for the samples and because no correction of the shear rate was applied.

Discussion

Our experiments have demonstrated a large decrease of η_{sp}/c occurring, irrespective of the molecular weights of the samples used, at concentrations below about 0.008 g./100 ml. It is difficult to explain this behavior on the basis of the current theory of linear polyelectrolytes, according to which only a steady increase of η_{sp}/c with decreasing c should be expected in the absence of added extraneous salt. One must therefore attribute this to an interaction effect between dissolved polymer molecules. The normal concentration effect leading to the Huggins constant values of the order of 0.3 to 0.7 (6, 7) is insufficient to account for the abnormally high values of these slopes, which, on rough estimate, yield the Huggins constants of 3 to 5 (decreasing with increasing molecular weight). Another source of interaction which is possible in the present case is the interionic forces acting between polyions and/or between polyions and their counterions. It seems likely that a considerable degree of such kind of interaction is present even at high dilutions owing to their long-range nature, thus bringing about an abnormally high value of the Huggins slope constant. Whatever the mechanism may be, it would be difficult to explain the observed rapid falls of η_{sp}/c in the region of very small concentrations, except on the basis of electrical interaction.

Our results of Fig. 1 indicate that the type of behavior at concentrations above those where the rapid fall of η_{sp}/c occurs depends on the molecular weight of the polymer. When the molecular weight is relatively low (PL and PM), the reduced viscosity, after reaching a maximum at about 0.005 g./100 ml., decreases steadily with increasing concentration until a minimum (not revealed in the concentration ranges herein studied) is reached. On the other hand, when the molecular weight is fairly high (PH and SH), such a decreasing trend is no longer realized, but the plot becomes nearly horizontal over a wider range of concentration. It is, therefore, expected that for samples of much higher molecular weights plots increasing steadily with increasing concentration would be obtained. A qualitative interpretation of these facts may be made by combining the usual shape theory with the effect of intermolecular electrical interaction. For a given polyelectrolyte species the relative degree of these two effects upon the reduced viscosity of the solution may vary with molecular weight, concentration, and many other factors, such as the amount of salt, if added. Whatever the mechanism and fashion may be, the interaction effect is considered to increase the reduced viscosity with concentration, whereas the shape effect, as is well known, causes the reduced viscosity to decrease with increasing concentration. It is impossible to exclude the normal concentration effect, which, however, is considered as being less important compared with the electrical interaction effect, so far as the region of small concentrations is concerned. On the basis of this idea, we may explain our experimental results as follows: At sufficiently low concentrations, practically less than about 0.005 g./100 ml., the electrical interaction effect predominates over the other effects, regardless of molecular weight, thus causing the reduced viscosity to increase sharply with increasing concentration. When the molecular weight of the polymer is relatively low, this effect is gradually overcome by the shape effect with increasing concentration, thus leading to a curve decreasing steadily with concentration. The appearance of a maximum point of η_{sp}/c is thus considered as a natural consequence. The nearly horizontal viscosity curves as observed with samples PH and SH may analogously be interpreted as a consequence of the two effects canceling each other.

While we were investigating these types of viscosity behavior with aqueous solutions of Na-CMC, we learned that Conway and Butler had observed, somewhat earlier, types of behavior similar to those we noted with samples PH and SH, in their studies of thymonucleate, deoxyribonucleate, and highly polymerized polymethacrylate solutions (8, 9). Most of their measurements were conducted in a Couette viscometer, but some were in capillary viscometers. Their data obtained in the Couette apparatus give exclusively values of η_{sp}/c increasing with increasing concentration over the whole concentration range examined. It is to be noted that their measurements, in almost all cases, were extended to as extremely low a concentration as 0.00025 g./100 ml. The upper limits examined were 0.1 g./100 ml. in the case of thymonucleate, 0.025 g./100 ml. in the case of deoxyribonucleate, and 0.025 g./100 ml. in the case of polymethacrylate. The general trend of their viscosity curves is markedly similar to that of our results for samples PH and SH, except that the absolute values of η_{sp}/c of their polyelectrolytes, when compared at equivalent concentrations, were much higher than those of our polyelectrolytes and that their curve on polymethacrylate showed again a nearly horizontal region at concentrations below those where the rapid fall of η_{sp}/c occurred. They found, however, with thymonucleate solutions, that the trend obtained in the Couette viscometer was no longer realized in the capillary viscometers. In this case, a type of behavior similar to that we noted with samples PM and PL was observed. Namely, they confirmed a maximum in η_{sp}/c. It is cited in their papers (8, 9) that Alexander and Hitch (11) have observed also a maximum in η_{sp}/c of aqueous polymethacrylate solutions at $c = 0.05$ g./100 ml., but we do not know the details since their paper is not available. The reason why the discrepancy of the viscosity behavior occurs in both the Couette and capillary viscometers has not yet been elucidated. Conway and Butler (9) have supposed that the values measured in the Couette viscometer, owing to the simple geometric conditions obtaining therein, are the more reliable. As an origin of the discrepancy, one may raise the question about the difference of mean rates of shear obtaining in both viscometers. However, this does not offer particular difficulty so far as their data are concerned, because their capillary and Couette results have been compared at equal mean rates of shear. In connection with this situation, it may be of interest to note that the type that Conway and Butler were able to observe only in the Couette viscometer has been revealed herein even in the capillary viscometer with aqueous Na-CMC solutions.

It has been shown for various polyelectrolytes that the reduced viscosities in salt solutions exhibit a maximum at a concentration where the equivalent concentration of the polyelectrolyte is of the same order of magnitude as that of the added salt, and some qualitative interpretations of this phenomenon have been given (2). These indicate that the addition of salt is necessary in order to bring about the maximum of the reduced viscosity. That this condition is not always necessary, *i.e.*, that the maximum can be obtained even in the salt-free solution, is realized from our experimental results presented above. In addition, our recent measurements (10) with sodium polyacrylate solutions have shown that the addition of neutral salt does not necessarily result in a curve of η_{sp}/c containing a maximum, when the viscosity curve in the salt-free solution is of the type noted with the high molecular weight Na-CMC samples PH and SH. These facts would appear to require reconsideration of the viscous behavior of polyelectrolyte solutions with and without added salts.

ACKNOWLEDGMENTS

We wish to thank Mr. H. Inagaki (Department of Textile-chemistry, Faculty of Engineering, Kyoto University) for samples of Na-CMC, and members of the Kyoto High-Polymer Research Group for their interest in this work.

SUMMARY

Reduced viscosity vs. concentration curves for four samples of sodium carboxy methyl cellulose in pure water solutions at sufficiently high dilutions were measured at 30°C. in Ostwald-type viscometers. The viscosity-average degrees of polymerization ($\overline{\text{DP}}$) of the samples used covered about fivefold range, keeping the degrees of etherification nearly constant (about 0.7). It was found that:

1. For two low $\overline{\text{DP}}$ samples, η_{sp}/c first increases very sharply, reaches a maximum at a concentration of about 0.005 g./100 ml., and then decreases steadily as the concentration is increased.

2. For other high $\overline{\text{DP}}$ samples, η_{sp}/c increases more sharply at very low concentrations and gradually levels off at higher concentrations.

The steady decrease of η_{sp}/c with concentration obtained with the low $\overline{DP}$ samples is of the familiar type and may be interpreted in terms of the folding-chain theory of Fuoss and others. However, all other behaviors observed can not be explained without introducing the effects of interionic interactions between polyions and/or between polyions and their counter-ions. A comparative discussion of our experimental data with recent similar observations for other polyelectrolytes was made, leading to the importance of intermolecular electric interactions which play a predominant role in the viscosity behavior of polyelectrolytes in pure water at very low concentrations.

REFERENCES

1. FUOSS, R. M., *J. Polymer Sci.* **3,** 603 (1948).
2. PALS, D. T. F., AND HERMANS, J. J., *Rec. trav. chim.* **71,** 433 (1952).
3. FUJITA, H., AND HOMMA, T., *J. Polymer Sci.*, in press.
4. AKKERMAN, F., PALS, D. T. F., AND HERMANS, J. J., *Rec. trav. chim.* **71,** 56 (1952).
5. KAGAWA, I., AND FUKUDA, M., *J. Chem. Soc. Japan (Ind. Chem. Sect.)* **54,** 97 (1951).
6. SIMHA, R., *J.Research Natl. Bur. Standards* **42,** 409 (1949).
7. SAITO, N., *J. Phys. Soc. Japan* **5,** 4 (1950).
8. BUTLER, J. A. V., AND CONWAY, B. E., *Nature* **172,** 153 (1953).
9. CONWAY, B. E., AND BUTLER, J. A. V., *J. Polymer Sci.* **11,** 277 (1953).
10. FUJITA, H., MITSUHASHI, K., AND HOMMA, T., unpublished work.
11. ALEXANDER, P., AND HITCH S. F., [cited by J. A. V. Butler and B. E. Conway (8, 9), *Biochim. et Biophys. Acta* **9,** 229 (1952)].

INTERFACIAL TENSIONS FROM THE SWELLING OF LATEX PARTICLES

Letter to the Editor

In a recently published paper entitled "Swelling of Latex Particles" by Morton, Kaizerman, and Altier, *Journal of Colloid Science* **9,** 300 (1954), certain observations concerning interfacial tension measurements appear to call for comment.

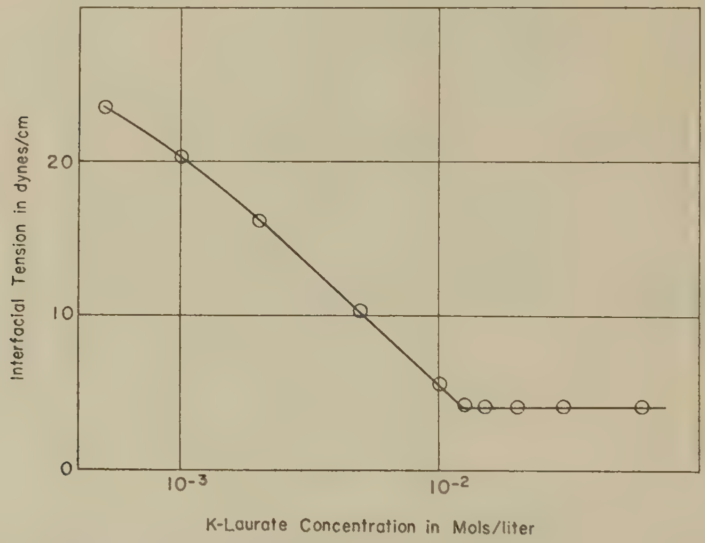

Fig. 1. Tension at interface between toluene and aqueous potassium laurate solutions in which total $[K^+] = 0.1$ Mol/Liter and pH = 10.

Swelling data lead the authors to conclude that the actual tension at the interface between a swollen latex particle and its environing soap solution is much lower than the tension at a plane interface separating phases of the same composition. We believe that the value estimated from swelling experiments is reliable, and that the apparent discrepancy is due to error in the direct measurement of the interfacial tension by the ring method.

Some time ago we made careful measurements of tension at the interface between toluene and potassium laurate solutions, using the drop volume method with corrections published by Harkins and Brown (1). Our work was done in solutions in which the total K^+ was held constant at 0.1 molar. The results are shown in Fig. 1, from which it may be seen that a minimum tension of about 4 dynes per centimeter is obtained. This is in good agreement with the value of 3.5 dynes per centimeter expected according to Morton, Kaizerman, and Altier.

In carrying out this work we attempted to make use of the ring method but finally abandoned it as unreliable in dealing with aqueous surfactant solutions. With the aid of the drop weight and drop volume methods, which are more laborious but very reliable, we had no trouble in securing precise and reproducible results.

REFERENCES

1. HARKINS, W. D., AND BROWN, F. E., *J. Am. Chem. Soc.* **41**, 499 (1919).

United States Rubber Company,
General Laboratories,
Passaic, New Jersey

CHARLES P. ROE
P. D. BRASS

Received November 4, 1954

Book Reviews

Crystal Growth and Dislocations. By Ajit Ram Verma. Academic Press Inc., New York, and Butterworths Scientific Publications, London, 1953. 182 pp. Price $5.00.

"The early crystallographers used to be enchanted by what they termed the perfection of crystals, calling their forms perfect in symmetry, imagining the angles between faces to be exactly repeated on different samples, and thinking that many crystals had extremely plane surfaces. But now our modern techniques (x-ray analysis, electron microscopy, multiple-beam interferometry and phase-contrast microscopy) sadly destroy this illusion and we find crystals to be highly irregular, to contain masses of imperfections, to exhibit astonishing varieties of surface microtopographies, and to be tantalizingly difficult to explain because of their contrary variety."

"X-ray diffraction methods do not reveal information about the very outer layers of atoms, where the strain related to surface tension produces some variation in the spacing of atomic planes. Surface layers play a very important part in the growth of crystals because they act as collectors for fresh material. The electron diffraction technique has provided much information in this direction, and has also been used for the study of the problem of oriented overgrowth."

These quotations outlined the objectives of this book. The author is an expert in this field and, by marshalling supporting evidence for the spiral dislocation theory of F. C. Frank, he has assembled striking and important contributions toward an intelligible and comprehensive theory of crystal growth.

The clear and convincing presentation is illustrated by many excellent half-tones. The format is open to no criticism. Anyone interested in crystals should read this compactly written monograph.

Victor K. La Mer, New York, New York

The Optical Properties of Organic Compounds. By Alexander N. Winchell. Academic Press Inc., New York 10, New York, 2nd edition, 1954. 318 pp. text, 56 pp. tables. $12.00.

This volume and the older companion volume on inorganic compounds also by the same author form the two best sources of information for the analytical chemist who wishes to use crystallographic properties for identification of unknowns. The usefulness of such methods always depends upon the availability of tabulations of data, and Dr. Winchell has done an excellent job of collecting, arranging, and editing the available data. The compounds covered are arranged according to the Beilstein system and a good index facilitates discovery of the data for a given compound. The optical data are also tabulated by refractive index, and two graphs plotting simple relationships between the refractive indices, birefringence, and optic axial angles are quite useful as analytical tools.

W. C. McCrone, Chicago, Illinois

AUTHOR INDEX

A

Altier, Mary W. See Morton, 300
Andrews, D. H. See Kaplan, 203

B

Baer, Eric. See Topper, 495
Basu, Sadhan and Sircar, Anil K. Studies of polyelectrolytes. VI. Gum agar, 574
Bender, Max. Some considerations on the interactions between particles in the presence of a wall-flocculation and adhesion as influenced by the cumulative net weight of the particles, 359
 The electric charge on macroscopic glass surface, 400
Biefer, G. J. and Mason, S. G. Electro-osmosis and streaming in natural and synthetic fibers, 20
Bielak, E. B. and Mardles, E. W. J. The rate of spread of liquid pools over horizontal solid surfaces and between approaching parallel flat plates, 233
Blanchard, Duncan C. A simple method for the production of homogeneous water drops down to 1 micron radius, 321
Boyle, Albert J. See Ressler, 122
Brass, P. D. See Roe, 602
Burcik, Emil J. and Newman, Robert C. The effect of organic additives on the rate of surface tension lowering of sodium dodecyl sulfate solutions, 498
Burcik, Emil J., Sears, James R., and Tillotson, Albert. The surface plasticity of sodium myristate solutions, 281

C

Cheesman, D. F. and Schuller, H. On the surface inactivation of pepsin, 113
Cohen, Irving, Hiskey, Clarence F., and Oster, Gerald. Critical phenomena in aqueous solutions of long-chain quaternary ammonium salts, 243
Cook, Hurley D. See Ries, Jr., 535
Crampsey, Edward, Gordon, Manfred, and Sharpe, John W. Electron microscope study of the locus of a latex reaction, 185

D

DallaValle, J. M. See Hinkle, 70

E

Elder, Max E. See Maron, 89, 104, 263, 347, 353, 382
Epstein, Morton B., Ross, John, and Jakob, Conrad W. The observation of foam drainage transitions, 50
Evans, D. and Matthews, J. B. The structure of aluminum stearate grease, 60

F

Ferry, John D. See Williams, 479
Fraser, M. J. See Kaplan, 203
Fujita, Hiroshi. The analytical solution of the fick equation with a concentration-dependent diffusion coefficient in one dimension having infinite vessel limits, 269
 Mitsuhashi, Kaoru, and Homma, Terutake. Viscosities of sodium polyacrylate in aqueous sodium chloride, 466
 and Homma Terutake. Viscosity behavior of sodium carboxy methyl cellulose in water at high dilutions, 591

G

Gordon, Mandred. See Crampsey, 185
Goring, D. A. I. The effect of hydrogen ion concentration on the viscosity and electrophoretic mobility of solutions of sodium carrageenate, 141

H

Hansen, Robert D. and Hansen, Robert S. Adsorption of both components from binary solution on porous adsorbents, 1
Hansen, Robert S. See Hansen, Robert D., 1
Harper, Robert C., Jr. and Riseman, Jacob. Interpretation of plastic viscosities in terms of newtonian viscosities, 81
  See Riseman, 438
Harrap, B. S. The properties of insulin films, spread at the air-water interface, 522
Heller, Wilfried. Treatment of viscosity data on polymer solutions (an analysis of equations and procedures). I. Intrinsic viscosity and limiting slope constants, 547
Hinkle, B. L., Orr, Clyde, Jr., and DallaValle, J. M. A new method for the measurement of aerosol electrification, 70
Hiskey, Clarence F. See Cohen, 243
Holt, L. Emmet, Jr., Pierce, Jerry A., and Kajdi, Charlotte N. The solubility of the phosphates of strontium, barium, and magnesium and their relation to the problem of calcification, 409
Homma, Terutake. See Fujita, 466, 501
Hotta, Hiroshi. The behavior of linear polymers at interfaces, 504
Howard, Edgar, Jr. See Spring, 371
Hutchinson, Eric. The properties of detergent solutions. I. Molecular weights determined by light-scattering measurements, 191

J

Jacobson, B. and Laurent, T. C. Streaming dielectric data of hyaluronic acid, 36
Jakob, Conrad W. See Epstein, 50
Jensen, C. E. and Koefoed, Jørgen. Flow elasticity of hyaluronate solutions, 460
Joseph, M. and Morawetz, H. Reaction rates in polyelectrolyte solutions. I. The decomposition of ethyl diazoacetate in aqueous polymethacrylic acid solution, 197

K

Kaizerman, Samuel. See Morton, 300
Kajdi, Charlotte N. See Holt, 409
Kaplan, J. Gordin, Andrews, D. H., and Fraser, M. J. Ultraviolet irradiation of dilute solutions of ovalbumin, 203
Koefoed, Jørgen. See Jensen, 460

L

Laurent, T. C. See Jacobson, 36
Layton, Lionel P. and Strauss, Ulrich P. A comparison of the solubilization of several paraffin hydrocarbons by a polysoap, 149
Livingston, H. K. Factors limiting the solubility of nonionic detergents in water, 365

M

Mardles, E. W. J. See Bielak, 233
Maron, Samuel H., Elder, Max E., and Ulevitch, I. N. Determination of surface area and particle size of synthetic latex by adsorption. I. Latices containing fatty acid soaps, 89
  Elder, Max E., and Moore, Carl. Determination of surface area and particle size of synthetic latex by adsorption. II. Latices containing rosin acid soaps, 104
  and Elder, Max E. Determination of surface area and particle size of synthetic latex by adsorption. III. Latices of high initial soap content, 263
  Determination of surface area and particle size of synthetic latex by adsorption. IV. Latices containing daxad 11, 347
  Determination of surface area and particle size of synthetic latex by adsorption. V. Latices emulsified with laurylamine hydrochloride, 353
  Elder, Max E., and Ulevitch, Irwin N. Determination of surface area and particle size of synthetic latex by adsorption. VI. Critical micelle concentrations of various emulsifiers in latex, 382
Mason, S. G. See Biefer, 20
Matsumoto, A. See Nakaya, 41
Matthews, J. B. See Evans, 60
Merrill, Edward W. A coaxial cylinder

viscometer for the study of fluids under high velocity gradients, 7
Flow properties of some buna-N solutions under high velocity gradients, 132
Miller, Israel R. Properties of Polyelectrolyte monolayers, 579
Mitsuhashi, Hiroshi. See Fujita, 466
Moore, Carl. See Maron, 104
Moore, W. R. and Russell, J. Viscosities of dilute solutions of cellulose acetate, 338
Morawetz, H. See Joseph, 197
Morton, Maurice, Kaizerman, Samuel, and Altier, Mary W. Swelling of latex particles, 300

N

Naik, Y. G., Correlation between optical and dynamic methods of measuring size of water drops in a cloud, 393
Nakaya, U. and Matsumoto, A. Simple experiment showing the existence of "liquid water" film on the ice surface, 41
Newman, Robert C. See Burcik, 498
Nilsson, Erik. See Wiklander, 223

O

Ooshika, Yuzuru. A theory of critical micelle concentration of colloidal electrolyte solutions, 254
Orr, Clyde, Jr. See Hinkle, 70
Oster, Gerald. See Cohen, 243

P

Pierce, Jerry A. See Holt, 409
Pilpel, N. On gel formation in soaps, 285

R

Ressler, Newton, Uhl, Henry, and Boyle, Albert J. The relation between the second ionization potential of a metal ion to its interaction with serum, 122
Ries, Herman E., Jr. and Cook, Hurley D. Monomolecular films of mixtures. I. Stearic acid with isostearic acid and with tri-p-cresyl phosphate. Comparison of components with octadecylphosphonic acid and with tri-o-xenyl phosphate, 535
Riseman, Jacob and Harper, Robert C., Jr. The influence of high polymer on the rheological properties of a carbon black suspension, 438
Roe, Charles P. and Brass, P. D. Interfacial tensions from the swelling of latex particles, 602
Romo, Luis. Role of lattice hydroxyls of kaolinite 385
Ross, John. See Epstein, 50
Ross, Sydney and Silverstein, Arthur M. Hemolysis by colloidal electrolytes, 157
Russell, J. See Moore, 338

S

Schaeffer, Vincent J. Ice crystals formed spontaneously by the rapid expansion of moist air, 175
Schuller, H. See Cheesman, 113
Sears, James R. See Burcik, 281
Sharpe, John W. See Crampsey, 185
Silverstein, Arthur M. See Ross, 157
Sircar, Anil K. See Basu, 574
Spring, Samuel and Howard, Edgar, Jr. Solubilization by potassium laurate solutions containing lauric acid, 371
Steele, F. A. Another form of alpha ferric oxide, 166
Stern, Kurt H. Liesegang rings in inhomogeneous media. Partially coagulated gelatin, 329
Strauss, Ulrich P. See Layton, 149

T

Takahashi, S. Cole-cole's circular arc rule on dynamic properties of visco-elastic materials, 313
Tillotson, Albert. See Burcik, 281
Topper, Leonard and Baer, Eric. Foaminess of aqueous solutions of sodium acetate, sodium propionate, and sodium butyrate, and of dilute silica suspension, 495

U

Uhl, Henry. See Ressler, 122
Ulevitch, I. N. See Maron, 89, 382

V

van der Waarden, M. Viscosity and electroviscous effect of emulsions, 215

VOLD, MARJORIE J. Van Der Waals' attraction between anisometric particles, 451

W

WIKLANDER, LAMBERT AND NILSSON, ERIK. Ion release as influenced by the mode of exchange, 223

WILEY, R. M. Limited coalescence of oil droplets in coarse oil—in water emulsions, 427

WILLIAMS, M. L. AND FERRY, JOHN D. Dynamic mechanical properties of polyvinyl acetate, 479

SUBJECT INDEX

A

Acetate, see *Foam*
Adhesion, — and flocculation of particles, BENDER, 359
Adsorption, from binary solution, HANSEN AND HANSEN, 1
Aerosol, measurement of — electrification, HINKLE *et al.*, 70
Air, see *Ice*
Albumin, see *Ovalbumin*
Aluminum stearate, structure of — — grease, EVANS AND MATTHEWS, 60
Ammonium salts, critical micelle phenomena on long-chain quaternary — —, hyamine-NaCl-mixtures, COHEN *et al.*, 243
Attraction, — between anisometric particles, VOLD, 451

B

Barium, see *Phosphates*
Blood, see *Hemolysis*
Buna, see *Circular arc rule*, *Rubber*
Butyrate, see *Foam*

C

Calcification, see *Phosphates*
Carbon black, rheological properties of a — — suspension, RISEMAN AND HARPER, 438
Carrageenate, viscosity and electrophoresis of sodium —, GORING, 141
Cellulose acetate, viscosities of solutions, MOORE AND RUSSELL, 338
Circular arc rule, — — and viscoelasticity, Buna N and other latices, TAKAHASHI, 313
Coalescence, see *Emulsion*
Colloidal electrolyte, see *Critical*, *Hemolysis*
Critical, — micelle concentration of colloidal electrolyte solutions, OOSHIKA, 254
Critical phenomena, see *Ammonium salts*

D

Daxad, see *Latex*
Detergents, (see also *Soaps*) light-scattering measurements, HUTCHINSON, 191; solubility of nonionic — in water, latices and —, LIVINGSTON, 365
Diffusion, Fick equation solution and concentration-dependent — coefficient, FUJITA, 269
Dodecyl sulfate, see *Surface*

E

Electrolytes, see *Hemolysis*, *Polyelectrolytes*
Electroosmosis, — and streaming in fibers, BIEFER AND MASON, 20
Emulsion(s), viscosity and electroviscous effect, VAN DER WAARDEN, 215; coalescence of — droplets, WILEY, 427
Errata, 88, 370
Ethyl diazoacetate, see *Polyelectrolyte*
Exchange, see *Ion*

F

Ferric oxide, another form of alpha — —, STEELE, 166
Fibers, see *Electroosmosis*
Fick equation, see *Diffusion*
Flocculation, see *Adhesion*
Fluoride, see *Kaolinite*
Foam, — drainage transitions, EPSTEIN *et al.*, 50; foaminess of solutions of sodium acetate, sodium propionate, and sodium butyrate, and of silica suspensions, TOPPER AND BAER, 495

G

Gel, see *Soaps*
Gelatin, see *Liesegang*
Glass, electric charge on surface, BENDER, 400
Grease, see *Aluminum stearate*
Gum agar, BASU AND SIRCAR, 574

H

Hemolysis, — by colloidal electrolytes, Ross and Silverstein, 157
Hyaluronate, flow elasticity of — solutions. Jensen and Koefoed, 460
Hyaluronic acid, streaming dielectric data, Jacobson and Laurent, 36
Hyamine, see *Ammonium salts*
Hydrocarbons, solubilization of paraffin — by a polysoap, Layton and Strauss, 149
Hydrochorination, see *Latex*

I

Ice (see also *Water*); — crystals formed by expansion of moist air, Schaefer, 175
Insulin, — films, at air-water interface, Harrap, 522
Interface, see *Insulin, Polymers, Surface*
Ion, release and exchange, Wiklander and Nilsson, 223
Ionization potential, see *Metal*
Iron, see *Ferric*

K

Kaolinite, lattice hydroxyls in phosphate fixation and fluoride, Romo, 385

L

Latex, (see also *Circular arc rule, Detergents*); surface area and particle size of synthetic —, latices containing fatty acid soaps, Maron *et al.*, 89; latices containing rosin acid soaps, Maron *et al.*, 104; electron microscopic study of hydrochlorination reaction, Crampsey *et al.*, 185; surface and particle size, latices with high soap content, Maron and Elder, 263; swelling of — particles, Morton *et al.*, 300; surface area and particle size, latices containing Daxad 11, Maron and Elder, 347; latices with laurylamine hydrochloride, Maron and Elder, 353; critical micelle concentration of emulsifiers in —, Maron *et al.*, 382
Lauric acid, solubilization by potassium laurate solutions containing — —, Spring and Howard, 371
Laurylamine, see *Latex*
Liesegang rings, — —in inhomogeneous media, partially coagulated gelatin, Stern, 329
Light, see *Detergents, Ovalbumin*
Liquid, see *Spreading*

M

Magnesium, see *Phosphates*
Metals (see also *Ion*); ionization potentials and interaction with serum, Ressler *et al.*, 122
Micelle, critical, see *Ammonium salts, Critical*
Mixtures, monomolecular films of —, pressure-area isotherms, stearic acid and phosphates, Ries and Cook, 535
Myristate, see *Surface*

O

Ovalbumin, ultraviolet irradiation, Kaplan *et al.*, 203

P

Paraffin, see *Hydrocarbons*
Particles, see *Adhesion*
Pepsin, surface inactivation, Cheesman and Schuller, 113
Phosphate(s) (see also *Kaolinite, Mixtures*); solubility of the — of strontium, barium, magnesium, and calcification, Holt *et al.*, 409
Polyacrylate, viscosity of sodium — in sodium chloride, Fujita *et al.*, 466
Polyelectrolytes, reaction rates in — solutions, ethyl diazoacetate decomposition in polymethacrylic acid, Joseph and Morawetz, 197; gum agar, Basu and Sircar, 574; properties of — monolayers, Miller, 579
Polymer(s), viscosity and — solutions, Heller, 547; behavior of linear — at interfaces, Hotta, 504
Polymethacrylic acid, see *Polyelectrolyte*
Polyvinyl acetate, properties, Williams and Ferry, 479
Pressure, see *Mixtures*
Propionate, see *Foam*

R

Release, see *Ion*
Rubber (see also *Latex*); flow properties of Buna-N-solutions, MERRILL, 132

S

Serum, see *Metal*
Silica, see *Foam*
Soaps (see also *Detergents*, *Hydrocarbons*, *Latex*); gel formation in —, PILPEL, 285
Solubilization, see *Hydrocarbons*
Solution, see *Adsorption*
Spreading, liquid — on a horizontal surface, BIELAK AND MARDLES, 233
STEARATE, see *Aluminum*
Stearic acid, see *Mixtures*
Streaming, see *Electroosmosis*
Strontium, see *Phosphates*
Surface (see also *Interface*, *Spreading*); — plasticity of sodium myristate solutions, BURCIK *et al.*, 281; — tension lowering of sodium dodecyl sulfate solutions, BURCIK AND NEWMAN, 498

V

Viscoelasticity, see *Circular arc rule*
Viscometer, coaxial cylinder —, MERRILL, 7
Viscosity (see also *Polymer*); plastic and Newtonian —, HARPER AND RISEMAN, 81

W

Water (see also *Ice*); liquid — film on the ice surface, NAKAYA AND MATSUMOTO, 41; production of homogeneous — drops, BLANCHARD, 321; size of — drops in a cloud, NAIK, 393

INDEX OF BOOK REVIEWS

BAILEY, K., AND NEURATH, H. (ed.). The Proteins. Chemistry, Biological Activity and Methods. Vol. 1, part B (Steinhardt, J.) 182
—The Proteins. Chemistry, Biological Activity and Methods. Vol. 2, part A. (STEINHARDT, J.), 369
Current Chemical Papers (LAMER, V. K.), 369
HARRISON, V. G. W. (ed.), Proceedings of the Second International Congress on Rheology (LAMER, V. K.), 493
Interscience Manuals (LAMER, V. K.), 494
SQUIRE, C. F., Low Temperature Physics (ZEMANSKY, M. W.), 87
VERMA, A. R., Crystals Growth and Dislocations (LAMER, V. K.), 604
VICKERY, R. C., Chemistry of the Lanthanons (ALPEROVITCH, E. A.), 493
WINCHELL, A. N., The Optical Properties of Organic Compounds (MCCRONE, W. C.), 604

JOURNAL OF
COLLOID SCIENCE

Editor-in-Chief
Victor K. La Mer, Columbia University, New York

Advisory Board

C. O. Beckmann
K. F. Bonhoeffer
J. A. Christiansen
M. L. Corrin
P. J. W. Debye
John T. Edsall
I. Fankuchen
John D. Ferry
Wilfried Heller
John G. Kirkwood
E. C. Lingafelter
L. G. Longsworth
S. G. Mason
J. Th. G. Overbeek
R. Ruyssen
E. K. Rideal
William Seifriz
Leo Shedlovsky
Theodore Shedlovsky
Robert Simha
R. H. Smellie
Jacinto Steinhardt
The Svedberg
Hugh S. Taylor
Arne Tiselius
Robert D. Vold
Bernard Vonnegut
Ralph W. G. Wyckoff
Bruno H. Zimm

VOLUME 9
1954

ACADEMIC PRESS INC.—PUBLISHERS
NEW YORK, N. Y.

Copyright 1955, by Academic Press Inc.
Made in United States of America

CONTENTS OF VOLUME 9

NUMBER 1, FEBRUARY, 1954

ROBERT D. HANSEN AND ROBERT S. HANSEN. Adsorption of Both Components from Binary Solution on Porous Adsorbents 1
EDWARD W. MERRILL. A Coaxial Cylinder Viscometer for the Study of Fluids Under High Velocity Gradients 7
G. J. BIEFER AND S. G. MASON. Electroosmosis and Streaming in Natural and Synthetic Fibers 20
B. JACOBSON AND T. C. LAURENT. Streaming Dielectric Data of Hyaluronic Acid 36
U. NAKAYA AND A. MATSUMOTO. Simple Experiment Showing the Existence of "Liquid Water" Film on the Ice Surface 41
MORTON B. EPSTEIN, JOHN ROSS, AND CONRAD W. JAKOB. The Observation of Foam Drainage Transitions 50
D. EVANS AND J. B. MATTHEWS. The Structure of Aluminum Stearate Grease 60
B. L. HINKLE, CLYDE ORR, JR., AND J. M. DALLAVALLE. A New Method for the Measurement of Aerosol Electrification 70
ROBERT C. HARPER, JR., AND JACOB RISEMAN. Interpretation of Plastic Viscosities in Terms of Newtonian Viscosities 81

BOOK REVIEW:

MARK W. ZEMANSKY. Low Temperature Physics 87

NUMBER 2, APRIL, 1954

SAMUEL H. MARON, MAX E. ELDER, AND I. N. ULEVITCH. Determination of Surface Area and Particle Size of Synthetic Latex by Adsorption. I. Latices Containing Fatty Acid Soaps 89
SAMUEL H. MARON, MAX E. ELDER, AND CARL MOORE. Determination of Surface Area and Particle Size of Synthetic Latex by Adsorption. II. Latices Containing Rosin Acid Soaps 104
D. F. CHEESMAN AND H. SCHULLER. On the Surface Inactivation of Pepsin 113
NEWTON RESSLER, HENRY UHL, AND ALBERT J. BOYLE. The Relation between the Second Ionization Potential of a Metal Ion to its Interaction with Serum 122
E. W. MERRILL. Flow Properties of Some Buna-N Solutions under High Velocity Gradients 132
D. A. I. GORING. The Effect of Hydrogen Ion Concentration on the

Viscosity and Electrophoretic Mobility of Solutions of Sodium Carrageenate.......... 141
LIONEL H. LAYTON AND ULRICH P. STRAUSS. A Comparison of the Solubilization of Several Paraffin Hydrocarbons by a Polysoap.... 149
SYDNEY ROSS AND ARTHUR M. SILVERSTEIN. Hemolysis by Colloidal Electrolytes.......... 157
F. A. STEELE. Another Form of Alpha Ferric Oxide.......... 166
VINCENT J. SCHAEFFER. Ice Crystals Formed Spontaneously by the Rapid Expansion of Moist Air.......... 175

BOOK REVIEW

JACINTO STEINHARDT. The Proteins. Chemistry, Biological Activity and Methods. Volume I, Part A.......... 182

NUMBER 3, JUNE, 1954

EDWARD CRAMPSEY, MANFRED GORDON, AND JOHN W. SHARPE. Electron Microscope Study of the Locus of a Latex Reaction....... 185
ERIC HUTCHINSON. The Properties of Detergent Solutions. I. Molecular Weights Determined by Light-Scattering Measurements..... 191
M. JOSEPH AND H. MORAWETZ. Reaction Rates in Polyelectrolyte Solutions. I. The Decomposition of Ethyl Diazoacetate in Aqueous Polymethacrylic Acid Solution.......... 197
J. GORDIN KAPLAN, D. H. ANDREWS, AND M. J. FRASER. Ultraviolet Irradiation of Dilute Solutions of Ovalbumin.......... 203
M. VAN DER WAARDEN. Viscosity and Electroviscous Effect of Emulsions.......... 215
LAMBERT WIKLANDER AND ERIK NILSSON. Ion Release as Influenced by the Mode of Exchange.......... 223
E. B. BIELAK AND E. W. J. MARDLES. The Rate of Spread of Liquid Pools over Horizontal Solid Surfaces and Between Approaching Parallel Flat Plates.......... 233
IRVING COHEN, CLARENCE F. HISKEY AND GERALD OSTER. Critical Phenomena in Aqueous Solutions of Long-Chain Quaternary Ammonium Salts.......... 243
YUZURU OOSHIKA. A Theory of Critical Micelle Concentration of Colloidal Electrolyte Solutions.......... 254
SAMUEL H. MARON AND MAX E. ELDER. Determination of Surface Area and Particle Size of Synthetic Latex by Adsorption. III. Latices of High Initial Soap Content.......... 263
HIROSHI FUJITA. The Analytical Solution of the Fick Equation with a Concentration-Dependent Diffusion Coefficient in One Dimension Having Infinite Vessel Limits.......... 269

LETTER TO THE EDITORS:

EMIL J. BURCIK, JAMES R. SEARS AND ALBERT TILLOTSON. The Surface Plasticity of Sodium Myristate Solutions.......... 281

NUMBER 4, AUGUST, 1954

N. PILPEL. On Gel Formation in Soaps 285
MAURICE MORTON, SAMUEL KAIZERMAN AND MARY W. ALTIER. Swelling of Latex Particles 300
S. TAKAHASHI. Cole-Cole's Circular Arc Rule on Dynamic Properties of Viscoelastic Materials 313
DUNCAN C. BLANCHARD. A Simple Method for the Production of Homogeneous Water Drops Down to 1 Micron Radius 321
KURT H. STERN. Liesegang Rings in Inhomogeneous Media. Partially Coagulated Gelatin 329
W. R. MOORE AND J. RUSSELL. Viscosities of Dilute Solutions of Cellulose Acetate 338
SAMUEL H. MARON AND MAX E. ELDER. Determination of Surface Area and Particle Size of Synthetic Latex by Adsorption. IV. Latices Containing Daxad 11 347
SAMUEL H. MARON AND MAX E. ELDER. Determination of Surface Area and Particle Size of Synthetic Latex by Adsorption. V. Latices Emulsified with Laurylamine Hydrochloride 353
MAX BENDER. Some Considerations on the Interactions Between Particles in the Presence of a Wall-Flocculation and Adhesion as Influenced by the Cumulative Net Weight of the Particles 359
LETTER TO THE EDITOR:
H. K. LIVINGSTON. Factors Limiting the Solubility of Nonionic Detergents in Water 365
BOOK REVIEWS:
VICTOR K. LA MER. Current Chemical Papers 369
JACINTO STEINHARDT. The Proteins. Chemistry, Biological Activity and Methods 369
Errata 370

NUMBER 5, OCTOBER, 1954

SAMUEL SPRING AND EDGAR HOWARD, JR. Solubilization by Potassium Laurate Solutions Containing Lauric Acid 371
SAMUEL H. MARON, MAX E. ELDER, AND IRWIN N. ULEVITCH. Determination of Surface Area and Particle Size of Synthetic Latex by Adsorption. VI. Critical Micelle Concentrations of Various Emulsifiers in Latex 382
LUIS A. ROMO. Role of Lattice Hydroxyls of Kaolinite in Phosphate Fixation and their Replacement by Fluoride 385
Y. G. NAIK. Correlation Between Optical and Dynamic Methods of Measuring Size of Water Drops in a Cloud 393
MAX BENDER. The Electric Charge on Macroscopic Glass Surface 400
L. EMMETT HOLT, JR., JERRY A. PIERCE AND CHARLOTTE N. KAJDI.

The Solubility of the Phosphates of Strontium, Barium, and Magnesium and their Relation to the Problem of Calcification 409
R. M. Wiley. Limited Coalescence of Oil Droplets in Coarse Oil-in-Water Emulsions 427
Jacob Riseman and Robert C. Harper, Jr. The Influence of High Polymer on the Rheological Properties of a Carbon Black Suspension 438
Marjorie J. Vold. Van Der Waals' Attraction Between Anisometric Particles 451
C. E. Jensen and Jørgen Koefoed. Flow Elasticity of Hyaluronate Solutions 460
Hiroshi Fujita, Kaoru Mitsuhashi, and Terutake Homma. Viscosities of Sodium Polyacrylate in Aqueous Sodium Chloride 466
M. L. Williams and John D. Ferry. Dynamic Mechanical Properties of Polyvinyl Acetate 479

BOOK REVIEWS

Victor K. La Mer. Proceedings of the Second International Congress on Rheology 493
Edward A. Alperovitch. Chemistry of the Lanthanons 493
Victor K. La Mer. Interscience Manuals 494

Number 6, December, 1954

Leonard Topper and Eric Baer. Foaminess of Aqueous Solutions of Sodium Acetate, Sodium Propionate, and Sodium Butyrate, and of Dilute Silica Suspension 495
Emil J. Burcik and Robert C. Newman. The Effect of Organic Additives on the Rate of Surface Tension Lowering of Sodium Dodecyl Sulfate Solutions 498
Hiroshi Hotta. The Behavior of Linear Polymers at Interfaces 504
B. S. Harrap. The Properties of Insulin Films, Spread at the Air-Water Interface 522
Herman E. Ries, Jr., and Hurley D. Cook. Monomolecular Films of Mixtures I. Stearic Acid With Isostearic Acid and With Tri-ρ-Cresyl Phosphate. Comparison of Components With Octadecylphosphonic Acid and With Tri-o-Xenyl Phosphate 535
Wilfried Heller. Treatment of Viscosity Data on Polymer Solutions (An Analysis of Equations and Procedures) I. Intrinsic Viscosity and Limiting Slope Constants 547
Sadhan Basu and Anil K. Sircar. Studies of Polyelectrolytes. VI. Gum Agar 574
Israel R. Miller. Properties of Polyelectrolyte Monolayers 579
Hiroshi Fujita and Terutake Homma. Viscosity Behavior of Sodium Carboxy Methyl Cellulose in Water at High Dilutions 591

LETTER TO THE EDITOR:

Charles P. Roe and P. D. Brass. Interfacial Tensions from the Swelling of Latex Particles 602

BOOK REVIEW:

John Mandel. Statistical Analysis in Chemistry and the Chemical Industry 604
W. C. McCrone. The Optical Properties of Organic Compounds 604
Author Index 605
Subject Index 609
Index of Book Reviews 611